

Universidade Federal do Rio Grande do Sul

Escola de Engenharia

Programa de Pós-Graduação em Engenharia Civil - PPGEC

BRAZILIAN EXTREME WIND CLIMATE

Matthew Bruce Vallis

Porto Alegre

Maio de 2019

Matthew Bruce Vallis

BRAZILIAN EXTREME WIND CLIMATE

Tese apresentada ao Programa de Pós-Graduação em
Engenharia Civil da Universidade Federal do Rio Grande do Sul,
como parte dos requisitos para obtenção do título de
Doutor em Engenharia.

Porto Alegre

Maio de 2019

Matthew Bruce Vallis

BRAZILIAN EXTREME WIND CLIMATE

Esta tese de doutorado foi julgada adequada e aprovada pelos professores orientadores e pelo Programa de Pós-Graduação em Engenharia Civil da Universidade Federal do Rio Grande do Sul.

Prof. Acir Mércio Loredou-Souza
Ph.D. pela University of Western Ontario,
Canadá
Orientador

Prof. Marcelo Maia Rocha
Dr. Techn. pela Universität Innsbruck,
Áustria
Co-orientador

Prof. Nilo César Consoli
Coordenador do PPGEC/UFRGS

BANCA EXAMINADORA

Dr. John D. Holmes (JDH Consulting)
PhD. pela Monash University, Austrália

Prof. Jorge Daniel Riera (UFRGS)
PhD. pela Princeton University, EUA

Prof. Gilberto Fernando Fisch (IAE)
D. Sc. pelo Instituto Nacional de Pesquisas Espaciais, Brasil

Prof. Ernani de Lima Nascimento (UFMS)
PhD. pela The University of Oklahoma, EUA

Prof. Gustavo Javier Zani Núñez (UFRGS)
D. Sc. pela Universidade Federal do Rio Grande do Sul, Brasil

ACKNOWLEDGEMENTS

Prof. Acir Mércio Loredou-Souza – for guidance, patience, belief and for continually going above and beyond the traditional supervisor role in order to make this happen

PPGEC professors and staff – for administrative support and the gift of education

CNPq – for financial support in the form of scholarship

Entire LAC team – for daily support, encouragement and friendship

Dr. Mario Gustavo Klaus Oliveira, Paulo Francisco Bueno, Arthur Bones, Roges de Mari Leopoldo, Marcelo Zanfêlice Cavalcante, Théa Louise Sequeira Pessoa, Gustavo Schneider Borges, Juarez Paulo Calvi Filho, Josiane Anderle Scotton Marodin, Pedro Grala, Ana Luisa Mércio Loredou Souza, and M.A.Z.I.

Experts and professionals – for essential consultations, technical support and co-operation

Prof. Ernani de Lima Nascimento, Prof. Gilberto Fisch, Prof. Jorge D. Riera, Prof. Gustavo Javier Zani Nuñez, Prof.^a Valeria Durañona, Prof. Marcelo Maia Rocha, Prof. Adrián Roberto Witter, Cel. Cleber Souza Corrêa, Prof. Ruy Menezes, Prof. Enio Bueno Pereira, Dr. John D. Holmes, Dr. Nicholas Khang Truong, Dr. Maryam Refan, Dr. Anderson Tavares, Dr. Ricardo Grunitzki, Dr. Marcelo Pizzuti Pes, Vanessa Ferreira, Amir Ali Safaei Pirooz, Vinícius Couto, Antônio Luís Cardoso Neto, Adam Brownnett, Eric Haddad Parker Guterres, Sergio Montazzolli, Pedro Heleno Isolani, Cody Jaxxon, Jason Ng, and those who prefer to be unnamed.

Institutional support – for the provision of data, metadata or other pertinent information

ICEA, Infraero-Belém, Infraero-Manaus, Infraero-Porto Alegre, Infraero-Belo Horizonte, Infraero-São Paulo, Infraero-Recife, CINDACTA II, CINDACTA IV, various aerodromes (Aracaju, Bauru, Barra do Garças, Cascavel, Chapecó, Fortaleza, Joinville, Campinas, Londrina, Maringá, Palmas, Santa Maria), INMET, various DISMEs, NCEI/NCDC, INUMET (Uruguay), Met Office (UK) and Météo France.

Larissa Cassol Watrin Juarez – for the hard work and dedication in researching aerodrome metadata. It is hoped that your efforts will go a long way to improving future availability of important metadata.

Maria Cristina Dolz Bênia (Titi) and Henrique Falck Grimm (Bomba H) – for gracious translations and review of texts

Sr.^a Lygia Blessmann – for friendship and the gift of several books written by the esteemed and pioneering Prof. Joaquim Blessmann.

Family – for unwavering love, support, belief, patience and joy

Wolverine (R.I.P), Débora, Paul, Sally, Ashleigh + Kaan, my babies Tippi + Luka, Clóvis + Marta, Renata + Renato, Clarissa + André and Bruna + Jessica.

RESUMO

VALLIS, M.B. – **Modelo Climático para Ventos Extremos no Brasil**. Tese de Doutorado – Programa de Pós Graduação em Engenharia Civil, UFRGS, Porto Alegre, 2019.

Uma característica importante da otimização dos processos de projeto em engenharia civil é a demanda pelo aperfeiçoamento da precisão das estimativas das cargas de projeto. As cargas de projeto devidas ao vento são baseadas em análises de registros de dados climatológicos para as quais modelos estatísticos são desenvolvidos. Tais modelos propõem níveis de carga com certas probabilidades de ocorrência durante um determinado período de retorno, ou intervalo médio de recorrência. Desde 1988, a NBR 6123: Forças devidas ao vento em edificações, a norma brasileira de cargas de vento, tem equilibrado a competição das necessidades de segurança e de conforto do usuário contra os custos de construção da cada vez mais alta silhueta urbana da nação. O mapa de isopletras do parâmetro de velocidade básica regional é o ponto inicial para todos os cálculos de cargas de projeto devidas ao vento na maior nação da América do Sul, com velocidades de vento regionais derivadas da distribuição de Fréchet, utilizando as máximas velocidades de rajada anuais equivalentes de 1950 a 1975 observadas, em aeródromos brasileiros. Além do potencial de utilizar mais de 40 anos de novos dados, incluindo dados da rede de observação automatizada do INMET, avanços nas comunidades científicas de engenharia do vento, meteorologia e estatística permitem o desenvolvimento de modelos climáticos mais detalhados e robustos. Há, também, uma crescente necessidade de separar os eventos de tempestades de vento em eventos não-sinóticos e sinóticos, devido às suas diferentes características.

O estudo produz modelos climáticos regionais de ventos extremos atualizados em todo o Brasil, para serem usados tanto em casos de estados limite último e de serviço do projeto. Dados meteorológicos das duas maiores redes meteorológicas brasileiras, adquiridos de diversas fontes, foram utilizados, mas apenas após um exame completo da qualidade de cada fonte. Investigações foram feitas com relação a metadados históricos e atuais (altura, localização, tipo de anemômetro) de cada estação, com resultados variados. Correções de velocidades do vento foram feitas para terreno e altura, onde necessário. Algoritmos robustos para a separação de velocidades de vento pico não-sinóticas, sinóticas e duvidosas foram desenvolvidos e aplicados a uma série histórica de dados de 692 estações meteorológicas de superfície para gerar conjuntos de valores extremos para uma análise de valor extremo com Método de Tempestades Independentes modificado. Constatou-se que os ventos não-sinóticos são dominantes na maioria do Brasil para todos os períodos de retorno. Parâmetros meteorológicos relacionados a ventos extremos não-sinóticos e sinóticos foram mapeados por todo o país. Um mapa de isopletras de velocidades básicas do vento foi proposto para uma versão atualizada da NBR 6123, acompanhado dos fatores probabilísticos atualizados para uma DGVE Tipo I – Distribuição de Gumbel. Recomendações chave incluem a necessidade de maiores investigações sobre as características de ventos não-sinóticos no Brasil e o melhoramento dos registros de metadados por parte das organizações meteorológicas.

Palavras-chave: velocidade básica do vento, NBR 6123, vento extremo, tempestade, INMET, ICEA.

ABSTRACT

VALLIS, M.B. – **Brazilian Extreme Wind Climate**. Doctoral Thesis – Civil Engineering Postgraduate Program, UFRGS, Porto Alegre, 2019.

A critical feature of the continual optimisation of civil engineering design processes is the demand to improve accuracy of design load estimations. Design wind loads are based on analyses of recorded historical meteorological data for which statistical models are developed. Such models propose load levels of certain probabilities of occurrence over a particular return period, or mean recurrence interval. Since 1988, NBR 6123: *Forças devidas ao vento em edificações*, Brazil's wind loading code, has balanced the competing needs of public safety and tenant comfort against construction costs of the nation's ever-growing skyline. The isopleth map of the regional basic velocity parameter is the basis for all wind design load calculations in South America's largest nation, with regional wind speeds derived from the Fréchet distribution of annual maxima equivalent gust speeds from 1950 to 1975 observed at Brazilian aerodromes. Besides the potential to utilise more than 40 years of new data, including data from INMET's automated observing network, advances across the scientific communities of wind engineering, meteorology and statistics allow for the development of more detailed and robust climatic models. There is also a growing need to separate wind storm events into non-synoptic and synoptic events due to their different characteristics.

The study produces updated regional extreme wind climate models across Brazil to be used for both serviceability and ultimate design load cases. Meteorological data from the two Brazilian meteorological networks acquired from several sources were utilised, but only after thorough examination of the quality of each source. Investigations were made regarding historical and current metadata (height, location, anemometer type) of each station with mixed success. Corrections to wind speeds were made for terrain and height where necessary. Robust algorithms for the separation of non-synoptic, synoptic and suspicious peak wind speeds were developed and applied to time-series data from 692 surface weather stations to generate sets of extreme values for a modified Method of Independent Storms extreme value analysis. Non-synoptic winds were found to dominant the majority of Brazil for all return periods. Meteorological parameters relating to non-synoptic and synoptic extreme winds were mapped across the country. An isopleth map of basic wind speeds was proposed for an updated version of NBR 6123, with accompanying updated probabilistic factors for a GEVD Type I – Gumbel distribution. Key recommendations include the need for further investigations into non-synoptic wind characteristics in Brazil and the improvement of metadata records by meteorological organisations.

Keywords: basic wind speed, NBR 6123, extreme wind, storm, INMET, ICEA.

 TABLE OF CONTENTS

LIST OF FIGURES.....	xi
LIST OF TABLES.....	xxiii
LIST OF SYMBOLS.....	xxv
LIST OF ABBREVIATIONS AND ACRONYMS.....	xxxiv
1 INTRODUCTION.....	1
1.1 Relevance of the study.....	1
1.2 Objectives.....	6
2 EXTREME WINDS.....	7
2.1 Fundamentals.....	7
2.2 Classification of extreme winds.....	10
2.2.1 Synoptic winds.....	12
2.2.1.1 <i>Extra-tropical cyclones</i>	13
2.2.1.2 <i>Tropical and subtropical cyclones</i>	18
2.2.2 Non-synoptic winds.....	23
2.2.2.1 <i>Deep, moist convection</i>	23
2.2.2.2 <i>Convective storm straight-line winds</i>	28
2.3 Codification of extreme winds.....	32
2.3.1 NBR 6123.....	33
2.3.1.1 <i>Basic wind speed</i>	33
2.3.1.2 <i>Return periods and risk categories</i>	35
2.3.1.3 <i>Wind characteristics</i>	35
2.3.1.4 <i>Structural wind loads</i>	39
2.3.2 Comparisons with other international wind codes.....	41
2.3.3 Codification of non-synoptic winds.....	44

3 MEASUREMENT OF WIND.....	49
3.1 Organisations and protocols.....	49
3.1.1 Aerodrome SWS.....	52
3.1.1.1 <i>METAR/SPECI</i>	55
3.1.1.2 <i>SYNOP</i>	57
3.1.2 INMET ASWS.....	59
3.2 Homogenisation of wind speeds.....	60
3.2.1 Gusts and instrumentation.....	60
3.2.2 Exposure.....	70
3.2.3 Metadata at study locations.....	79
3.2.3.1 <i>Aerodrome SWS</i>	81
3.2.3.2 <i>INMET ASWS</i>	86
4 EVALUTATION OF SURFACE WIND DATA SOURCES.....	89
4.1 Aerodrome SWS.....	89
4.1.1 METAR, SPECI and SYNOP (MSS).....	89
4.1.2 ICEA-BDC.....	93
4.1.2.1 <i>ICEA web portal</i>	93
4.1.2.2 <i>PSEC-46</i>	94
4.1.2.3 <i>PAS-31</i>	97
4.1.3 Third-party databases.....	98
4.1.3.1 <i>NCEI/NCDC</i>	100
4.1.3.2 <i>Wolfram</i>	102
4.1.3.3 <i>Weather Underground</i>	102
4.1.3.4 <i>CPTEC-INPE</i>	103
4.2 INMET ASWS.....	103
4.2.1 INMET web portal.....	105
4.2.2 SADMET.....	107
4.2.3 DISME.....	110

4.2.4 Restricted INMET Database.....	111
5 EXTREME VALUE ANALYSIS.....	115
5.1 Parent Distribution.....	115
5.2 Generalised Extreme Value Distribution.....	116
5.2.1 Selection of extreme values.....	121
5.2.2 Estimators and determination of model parameters.....	124
5.3 Peaks Over Threshold.....	129
6 METHODOLOGY FOR THE DETERMINATION OF EXTREME WIND CLIMATE.....	132
6.1 Selection of raw data.....	132
6.2 Preparation of time-series.....	134
6.2.1 Aerodromes/MSS.....	135
6.2.2 Aerodromes/PAS-31.....	141
6.2.3 INMET/WRDS.....	143
6.3 Homogenisation of wind speed time-series.....	145
6.4 Selection of contributing sampling periods.....	147
6.5 Identification of synoptic, non-synoptic and suspected false extreme wind events.....	157
6.5.1 Changes in temperature and atmospheric pressure.....	160
6.5.2 Development of classifying algorithms.....	168
6.5.3 Verification of classifying algorithms.....	174
6.5.4 Application of algorithms to study SWS.....	176
6.6 Development of BR-MIS extreme value analysis.....	179
7 RESULTS AND DISCUSSION.....	188
7.1 General wind trends.....	189
7.2 Extreme wind trends.....	189

7.3 Determination of regional basic wind speeds.....	196
8 CONCLUSIONS AND RECOMMENDATIONS.....	218
8.1 Summary.....	218
8.2 Extended Conclusions.....	219
8.3 Recommendations.....	223
8.3.1 NBR 6123	223
8.3.2 INMET	227
8.3.3 Brazilian aerodromes/DECEA/ICEA	229
8.3.4 Future research	231
REFERENCES.....	234

APPENDICES

- A. Map of Brazil and SWS Details
- B. Isopleth Map of NBR 6123 (ABNT, 1988)
- C. Extreme Distributions of SWS
- D. Event Classification Algorithms and Examples
- E. Comparison of Extreme Value Analyses for Selected SWS
- F. Assorted Tables
- G. Mapped General Wind Trends
- H. Mapped Extreme Wind Trends
- I. Alternative Zone Solutions
- J. Local Polynomial Regression Solution
- K. Determination of Probabilistic Factor S_3
- L. Mapped Residuals of Contour Solutions
- M. Guide to windytips.com

LIST OF FIGURES

Figure 1.1 – Proposed isopleth maps of Brazilian basic wind speeds, V_0 (m/s), left: Almeida (2010), right: Beck and Corrêa (2013)	4
Figure 2.1 – Durst (1960) gust factor curve relating to mean wind speeds of $T = 3600$ s.	8
Figure 2.2 – Normalised von Kármán spectrum of longitudinal component of velocity.	9
Figure 2.3 – Synoptic and thunderstorm profiles vertical wind speeds reference to wind speed at $z = 10$ m (ISO, 2009; AS/NZS 2010; AS/NZS 2011).	12
Figure 2.4 – Development of an extra-tropical cyclone in northern hemisphere (Encyclopedia Britannica, 2010)	14
Figure 2.5 – GOES-13 Satellite imagery of extra-tropical cyclone at 16:30 UTC, 27/10/2016 (CPTEC-INPE, 2018).....	14
Figure 2.6 – Synoptic charts showing the cyclogenesis and growth of an extra-tropical cyclone over southern Brazil and Uruguay, 26-28/10/2016 (Centro da Hidrografia da Marinha, 2018)	15
Figure 2.7 – Annual evolution of jet stream winds (adapted from Gallego et al., 2005).....	17
Figure 2.8 – Cumulative jet path for January, April and July of 1979 (Gallego et al., 2005)..	17
Figure 2.9 – Number of cyclogenesis events detected between 1979 and 2003 (Mendes et al., 2009).....	17
Figure 2.10 – Simplified structure of a tropical cyclone in northern hemisphere	19
Figure 2.11 – Tracks of all tropical cyclones as recorded by the National Hurricane Center and the Joint Typhoon Learning Center from 1945 to 2006.	20
Figure 2.12 – Path and intensity of Hurricane Catarina (McTaggart et al., 2006).....	21
Figure 2.13 – Front page of <i>Diário Catarinense</i> newspaper showing destruction caused by Hurricane Catarina (left); Map of the Santa Catarina regions most affected by Hurricane Catarina (right).	21
Figure 2.14 – Damage caused by subtropical cyclone Eçaí along Santa Catarina coastline, 04/12/2016. Photos taken by Elvis Palma (left) and Rafael Vieira (right).....	22
Figure 2.15 – Three stages of an ordinary, single-cell a) towering cumulus stage, b) mature stage, c) dissipating stage (Markowski and Richardson, 2010).	24
Figure 2.16 – Lifting of gust front in a) isolated cell with no wind shear b) multicellular storm with moderate wind shear (Markowski and Richardson, 2010).....	25

Figure 2.17 – Venn diagram of MCS sub-classifications (Markowski and Richardson, 2010).	26
Figure 2.18 – Cross-section conceptual model of squall line (Markowski and Richardson, 2010).	26
Figure 2.19 – Representation of the main lower troposphere weather systems in South America (adapted from Pes, 2015; Satayamurty et al. 1998; Reboita et al., 2012).	27
Figure 2.20 – Two types of microbursts in relating to cloud height and precipitation intensity (Fujita, 1990).	29
Figure 2.21 – Downburst outflow schematic diagrams: top left – Mason (2017); top right – Goff (1975); bottom – Fujita (1985).	30
Figure 2.22 – Examples of damage from 29/01/2016 downburst event in Porto Alegre, 2016 (Loredo-Souza et al., 2019).	30
Figure 2.23 – Satellite image of water vapour enhancement taken by GOES 13, 23:45 UTC 29/01/2016 (INMET, 2016). Location of Porto Alegre marked by X.	31
Figure 2.24 – Reflective field images from the radar at Santiago, RS, represented by the black dot, on 29/05/2013 (Figueiredo et al., 2019).	32
Figure 2.25 – Terrain and height multiplier, S_2 , per terrain category (for $\tau = 3$ s).	36
Figure 2.26 – F_r of NBR 6123 and corresponding gust factors, G_V	37
Figure 2.27 – Longitudinal turbulence intensity, I , of NBR 6123 (ABNT, 1988).	38
Figure 2.28 – Plots for the determination of drag coefficient, C_a , of NBR 6123 (ABNT, 1988),	40
Figure 2.29 – Dynamic amplification factor, ξ , for CAT II of NBR 6123 (ABNT, 1988).	40
Figure 2.30 – Full-scale measurements of outflow wind speeds (right), ISO 4354 (2009) and AS/NZS 7000 (2010) non-synoptic wind speed profiles compared to full-scale observations, normalised by wind speed at 10 m (right) (Mason, 2017).	46
Figure 2.31 – Downburst (DB) and non-synoptic profiles of wind speed composed of 35% synoptic and 65% downburst (COMP.) as proposed by Miguel et al. (2018).	47
Figure 2.32 – Downburst (DB) and non-synoptic profiles of wind speed composed of 35% synoptic and 65% DB (COMP.) as proposed by Riera (2018).	48
Figure 3.1 – Photo of a completed, hand-written weather observation form at SBHT – Altamira, PA, for 01/11/1988	53
Figure 3.2 – BDC Archives at ICEA in December 2016.	53
Figure 3.3 – Wind speed and direction readings by a) analogue and b) digital processes.	54
Figure 3.4 - Identification of DISMEs and location of ASWS stations (as of May 2018).	59

Figure 3.5 - Growth of INMET ASWS network.....	60
Figure 3.6 – Anemometer admittance function for various distance constants, d	62
Figure 3.7 – Moving average filter in frequency domain for various time intervals, τ	62
Figure 3.8 – The effect of filtering on turbulence spectra, S_{ii}	63
Figure 3.9 – Equivalent frontal area, A (m^2), for varying gust averaging intervals.	65
Figure 3.10 – Comparison of peak factors and gust factors obtained in controlled wind-tunnel tests for three different cup anemometers (adapted from Pirooz and Flay, 2018).	66
Figure 3.11 – Comparison of NBR 6123 gust factors with those calculated by spectral analysis.	68
Figure 3.12 – Birds perching on ultrasonic anemometers (left – NOAA, 2008; right – Schmitt, 2008).....	70
Figure 3.13 – Use of CFD to determine topographic correction factors (Turner et al., 2019). Left: CFD domain around Wellington International Airport. Right: topographic correction factors at The Brothers, NZ.	71
Figure 3.14 – Growth of internal boundary layer due to roughness change (Deaves, 1981)..	73
Figure 3.15 – a) Smooth to rough transition, b) Rough to smooth transition of NBR 6123 (ABNT, 1988).....	74
Figure 3.16 – a) Smooth to rough transition, b) Rough to smooth transition of ESDU 82026 (ESDU, 2002).	76
Figure 3.17 – Satellite image of Porto Alegre, RS (left), land-use GIS map (IBGE, 2014). ...	77
Figure 3.18 – Observed gusts and 10-minute mean velocities for wind-angles $DIR = 220^\circ$ - 240° at SBPA – Porto Alegre, RS, from 06/1996 to 12/2017.	78
Figure 3.19 – Key moments regarding wind observations at Brazilian surface weather stations.	80
Figure 3.20 – The Bendix-Friez aerovane propeller anemometer (Gill, 1973).....	81
Figure 3.21 – Previous installations of anemometers above buildings a) SBCY – Cuiabá, MT, b) SBAU – Araçatuba, SP, c) SBMT – Campo de Marte, SP d) SBKP – Campinas, SP.	83
Figure 3.22 – Anemometer heights at Brazilian aerodromes during 2016-2018.	84
Figure 3.23 – Upwind terrain categories for anemometers at Brazilian aerodrome SWS.	85
Figure 3.24 – Assessment of average terrain category per 45° sector over 500 m centred on location of principal anemometer of SBFI – Foz do Iguaçu, PR (Dated 09/09/2018).	85
Figure 3.25 – Satellite image of SBFI – Foz do Iguaçu, PR, showing razing of vegetation immediately adjacent to the runway (Dated 29/01/2019).	86

Figure 3.26 – Vaisala WAA151 cup anemometer (left), Synchrotac 706 cup anemometer (middle), and RM Young Model 8100 3D ultrasonic anemometer (Gorman, 2004).....	87
Figure 3.27 – Gill WindSonic ultrasonic anemometer	87
Figure 3.28 – Histogram of average upwind terrain categories for anemometers at INMET ASWS.....	88
Figure 3.29 – Assessment of average terrain category per 45° sector over 500 m centred on location of anemometer at A801 – Porto Alegre, RS (left), and A532 – Diamantina, MG (right).....	88
Figure 4.1 – SPECI reports for SBPA (NCEI, WU) and SBPF (REDEMET), 29/08/2005.....	93
Figure 4.2 – SPECI reports for SBPA (NCEI, WU) and SBPA (REDEMET), 30/08/2005. ..	93
Figure 4.3 – Series of V annual maxima at SBGL (Source: ICEA web portal)	94
Figure 4.4 – Periods of operation for anemometers as per runway headings at SBGR.	95
Figure 4.5 – V and DIR daily maxima at SBGR from PSEC-46 (ICEA, 2015).....	95
Figure 4.6 – G daily maxima data at SBGR from PSEC-46 (ICEA, 2015).	96
Figure 4.7 – METAR reports for SBSM, 01/03/2003 (Source: REDEMET)	96
Figure 4.8 – V daily maxima time-series for SBSM from PSEC-46 (ICEA, 2015).....	97
Figure 4.9 – Extreme wind event at SBAE – Arealva, SP, 19/09/2012 at 18:00 UTC. (top: MSS dataset, bottom: PAS-31 dataset).....	98
Figure 4.10 – Number of extreme wind observations for SBPA according to PAS-31 and NCEI datasets, a) $V \geq 30$ kt, b) $G \geq 40$ kt.....	100
Figure 4.11 – Composition of weather observations for SBBE – Belém, PA, as made available by NCEI.....	101
Figure 4.12 – Location of SWS in the Porto Alegre region.	102
Figure 4.13 – Histograms of consecutive hourly differentials for a) V and b) G at A701 – São Paulo, SP.....	104
Figure 4.14 – Tweet issued by ATMET which documents the observation of an extreme wind gust at A880 – Vacaria, RS, on 18/12/2018 (provided by G.J.Z. Núñez).....	106
Figure 4.15 – Web accessed datasets for A880 – Vacaria, RS, for 18/12/2018.....	106
Figure 4.16 – WEB/DISME vs SADMET datasets for a) V and b) G time-series at A845 – Morro da Igreja, SC.....	108
Figure 4.17 – Photographs of damage caused by events listed in Table 4.4.....	110
Figure 4.18 – Number of qualified extreme peak gusts, per range of gust speed, encountered only in INMET’s restricted access database.....	112

Figure 4.19 – Number of qualified extreme peak gusts encountered only in INMET’s restricted access database per station.....	113
Figure 4.20 – Photo of damage caused by strong gusts at SBTA – Taubaté Airforce Base, SP, 27/10/2017 (Source: O Vale).....	114
Figure 5.1 – PDF of 10-minute mean wind speed corrected to $z = 10$ m and $z_0 = 0.07$ m, V_{cor} , normalized by total sampling time, t_{tot} (top); CDF of V_{cor} (bottom) at SBFZ – Fortaleza, CE (left), and SBPA – Porto Alegre, RS (right). Weibull distribution parameters c and w are given in CDF plot.	116
Figure 5.2 – Types I, II and III of GEVD (Holmes, 2015).....	118
Figure 5.3 – Comparison of reduced variate as function of mean recurrence interval (Equation 5.15) to function of return period (Equation 5.9).	121
Figure 5.4 – Example of Gumbel plot (adapted from ESDU, 1990[a]).	125
Figure 5.5 – Resulting distributions from the set of extreme annual maximum gusts (1952-1998) at East Sale, Australia as per Gumbel and Gringorten plotting points (Holmes, 2015).	126
Figure 5.6 – Comparison of GEVD Type I analysis using annual maxima and Method of Independent Storms from 1958 to 1978 at Jersey, UK (Cook, 1982).	128
Figure 5.7 – Normalised Gumbel plot for the mean of 10,000 trials (Cook, 2011).	129
Figure 5.8 – Mean exceedance plot for downburst gusts at Moree, NSW, Australia (Holmes and Moriarty, 1999).	130
Figure 6.1 – Constitution of MSS database for SBBR – Brasília, DF.	138
Figure 6.2 – METAR reports for SBCT – Curitiba, PR, 27-28/08/2009 (Source: Weather Underground).....	139
Figure 6.3 – Temperature time-series extracted from METAR/SPECI reports for SBGR – Guarulhos, SP, 25/08/2014 (Source: REDEMET)	140
Figure 6.4 – Atmospheric pressure time-series extracted from METAR/SPECI reports for SBGR – Guarulhos, SP, 09/09/2011 (Source: REDEMET).....	140
Figure 6.5 – Constitution of the primary (top) and secondary (bottom) anemometers for SBBQ – Barbacena, MG, (PAS-31, 2017).	142
Figure 6.6 – Direction, 10-minute mean wind speed, and maximum hourly gust observation time-series for A218 – Farol Preguiças, MA.....	144
Figure 6.7 – Temperature and atmospheric pressure time-series for A002 – Goiânia, GO, with manually discarded data (grey).....	145
Figure 6.8 – Wind direction time-series for A308 – Parnaíba, PI.	148

Figure 6.9 – Wind direction time-series (top) and predominant monthly wind direction (bottom) for A842 – Nova Fátima, PR.	149
Figure 6.10 – Monthly mean wind speeds for SWS and ECMWF data for SBPV – Porto Velho, RO, MSS dataset (top); monthly means normalised by V_{clim} (bottom).	150
Figure 6.11 – Monthly mean wind speeds for SWS and ECMWF data for SBPA – Cascavel, PR (top); monthly means normalised by V_{clim} (bottom).	151
Figure 6.12 – Monthly mean wind speeds for SWS and ECMWF data for SBPA – Campo Grande, MS (top); monthly means normalised by V_{clim} (middle); percentage of month with valid observations (columns), with percentage of even numbered observations in knots (line) (bottom).	152
Figure 6.13 – V_{obs} for A820 – Marechal Cândido Rondon, PR (top); G_{obs} (middle); monthly mean wind speeds for SWS and ECMWF data (bottom).	153
Figure 6.14 – G_{obs} for SBPA – Parnaíba, PI.	154
Figure 6.15 – G_{obs} for A101 – Manuas, AM.	154
Figure 6.16 – G_{obs} for A237 – Caxias, MA.	154
Figure 6.17 – G_{obs} for SBKG – Campina Grande, PB (top); temporal distribution of Top 100 most extreme events (columns) and trend (line) (bottom).	155
Figure 6.18 – G_{obs} for SBGR – Guarulhos, SP (top); temporal distribution of top 100 most extreme events (columns) and trend (line) (middle); monthly mean wind speeds for SWS and ECMWF data (bottom).	156
Figure 6.19 – Mean values and mean anomalies of the four severity groups of convective storms as reported by Ferreira (2017). Red represents peak G_{obs} of 10-15m/s; green represents peak G_{obs} of 15-20 m/s; purple represents peak G_{obs} of 20-25 m/s; blue represents peak $G_{obs} > 25$ m/s. a) maximum hourly wind gusts, G_{obs} (m/s); b) instantaneous temperature at the hour, T (°C); c) instantaneous atmospheric pressure at the hour, P (hPa); d) instantaneous dew-point temperature at the hour, T_d (°C)	162
Figure 6.20 – Relationships between $T_{med,3}$, $\Delta T_{min,3}$ and $\Delta P_{max,3}$ for 768 convective storms as recorded by INMET ASWS, a) and c); 76 convective storms as recorded by aerodrome SWS b) and d).	165
Figure 6.21 – Plots of $\Delta T_{min,3}$ and $\Delta P_{max,3}$ for all events. Definition of $\Delta Group$ boundaries for $T_{med,3} \geq 30$ °C for a) INMET and b) Aerodrome events, as per Equations 6.13 to 6.15; Definition of $\Delta Group$ boundaries for $T_{med,3} \leq 20$ °C for c) INMET and d) Aerodrome events,	

as per Equations 6.13 to 6.15; $\Delta Group$ assignments for each of the e) INMET and f) Aerodrome events as per Equations 6.13 to 6.15.	167
Figure 6.22 – Normalised mean and mean \pm standard deviation trends of the 632 F&N events classified as non-synoptic by algorithm developed for INMET ASWS (Figure D.1)	175
Figure 6.23 – Normalised mean and mean \pm standard deviation trends of the 133 F&N events classified as synoptic by algorithm developed for INMET ASWS (Figure D.1).....	175
Figure 6.24 – Number of years of valid data, t_{tot} , of all stations analysed.	181
Figure 6.25 – SWS average monthly time in operation presented as a percentage.....	181
Figure 6.26 – MIS and Gumbel plots of simulated extreme winds for simulated distribution (left), and extreme value density for MIS with $r=1$ and Classic Gumbel models (right).....	184
Figure 6.27 – Difference between M_{th} ranked extreme value and U for simulated distribution.	184
Figure 6.28 – Mean (left) and standard deviation (right) of MIS with $r = 4$ model parameters with varying M as a ratio of analytical solution.	186
Figure 6.29 – Mean (left) and standard deviation (right) of Classic Gumbel model parameters with varying M as a ratio of analytical solution.	186
Figure 6.30 – Mean (left) and standard deviation (right) of Classic Gringorten model parameters with varying M as a ratio of analytical solution.....	186
Figure 7.1 – Dominant extreme wind type for $R = 1$ and 50-year mean recurrence intervals, U and G_{50} respectively.....	190
Figure 7.2 – Average development of non-synoptic winds at SBEG – Manaus, AM.....	192
Figure 7.3 – Average development of non-synoptic winds at SBPA – Porto Alegre, RS.	192
Figure 7.4 – Average development of synoptic winds at SBEG – Manaus, AM.....	192
Figure 7.5 – Average development of synoptic winds at SBPA – Porto Alegre, RS.....	192
Figure 7.6 – Histogram of annual rate of extreme events at individual SWS with $t_{tot} \geq 10$ years.....	195
Figure 7.7 – Processed data at SBFL – Florianópolis, SC: Observed gusts, G_{obs} , (top); distribution of top 100 extreme wind events and annual growth rate, pa (middle); homogenised gust time-series, G_{cor} , with event classifications (bottom).....	196
Figure 7.8 – Extreme distribution parameters of governing stations for non-synoptic extreme winds (N): $G_{50,N}$, U_N and a_N	205
Figure 7.9 – Extreme distribution parameters of governing stations for synoptic extreme winds (S): $G_{50,S}$, U_S and a_S	206

Figure 7.10 – Mixed extreme distribution parameters of governing stations (M): $G_{50,M}$, U_M and a_M .	207
Figure 7.11 – Envelope extreme distribution parameters of governing stations (E): $G_{50,E}$ and U_E .	208
Figure 7.12 – Non-synoptic U vs a (N), for all SWS (left) and set of governing SWS (right).	209
Figure 7.13 – Synoptic U vs a (S), for all SWS (left) and set of governing SWS (right).	209
Figure 7.14 – Mixed U vs a (M), for all SWS (left) and set of governing SWS (right).	209
Figure 7.15 – Proposed V_0 isopleth map for NBR 6123.	210
Figure 7.16 – U_N residuals of all stations expressed against sampling period t_{tot} (years).	213
Figure 7.17 – $G_{50,N}$ residuals of all stations expressed against sampling period t_{tot} (years).	213
Figure 7.18 – U_E residuals of governing stations expressed against sampling period t_{tot} (years).	213
Figure 7.19 – $G_{50,E}$ residuals of governing stations expressed against sampling period t_{tot} (years).	213
Figure 7.20 – Percentage of stations per range of e (U): non-synoptic wind speeds for all SWS (left) and envelope wind speeds for governing stations (right).	214
Figure 7.21 – Percentage of stations per range of e (G_{50}): non-synoptic wind speeds for all SWS (left) and envelope wind speeds for governing stations (right).	214
Figure 7.22 – Distribution of e (G_{50}) compared to other studies [e (G_{700}) for Pintar et al., 2015]	214
Figure 7.23 – Difference between most extreme qualified G_{cor} gust speed at individual SWS for study period and V_0 defined in Figure 7.15.	215
Figure 7.24 – Governing stations per range of t_{tot} (left) and $Obs.$ (right).	217
Figure 7.25 – Terrain categories of 45° sectors of governing stations.	217
Figure 8.1 – Wind data chain (Illustration provided by Eric Haddad Parker Guterres).	221
Figure 8.2 – Probabilistic factor, S_3 , of NBR 6123 (ABNT, 1988) and proposed revised S_3 .	223
Figure A.1 – Map of Brazil with ISO 3166-2 state codes. Table A.1 – Brazilian state codes and names.	A-2
Figure B.1 – Isopleth map of Brazilian regional basic wind speeds, V_0 (m/s) (ABNT, 1988).	B-2
Figure B.2 – Draft isopleth map of Brazilian regional basic wind speed, V_0 (m/s) (Padaratz, 1977).	B-3
Figure B.3 – Recreation of Padaratz (1977).	B-4

Figure D.1 – Extreme wind type classifying algorithm for INMET ASWS.	D-2
Figure D.2 – Extreme wind type classifying algorithm for aerodrome SWS with G_{obs} peak gust speed ($\Delta Groups$ 1 & 2 only).	D-3
Figure D.3 – Extreme wind type classifying algorithm for aerodrome SWS with G_{obs} peak gust speed ($\Delta Group$ 3).	D-4
Figure D.4 – Extreme wind type classifying algorithm for aerodrome SWS with G^* (i.e. no G_{obs}) peak gust speed ($\Delta Groups$ 1 & 2 only).	D-5
Figure D.5 – Extreme wind type classifying algorithm for aerodrome SWS with G^* (i.e. no G_{obs}) peak gust speed ($\Delta Group$ 3 only).	D-6
Figure D.6 – Manually classified as non-synoptic. Peak $G_{obs} = 26.4$ m/s at A001 – Brasília, DF, 01/10/2014, 18:00 UTC.	D-7
Figure D.7 – Manually classified as synoptic. Peak $G_{obs} = 22.6$ m/s at A807 – Curitiba, PR, 13/09/2016, 18:00 UTC.	D-7
Figure D.8 – Manually classified as suspect. Peak $G_{obs} = 27.0$ m/s at A301 – Recife, PE, 06/07/2009, 12:00 UTC.	D-7
Figure D.9 – Manually classified as non-synoptic. Peak $G_{obs} = 70$ kt (36.0 m/s) at SULS – Punta del Este, Uruguay, 02/03/2013, 16:00 UTC.	D-8
Figure D.10 – Manually classified as suspect. Peak $G_{obs} = 60$ kt (30.9 m/s) at SAWG – Río Gallegos, Argentina, 19/02/2012, 18:00 UTC.	D-8
Figure D.11 – Manually classified as synoptic. Peak $G_{obs} = 42$ kt (21.6 m/s) at SACO – Córdoba, Argentina, 08/11/2010, 00:28 UTC.	D-8
Figure D.12 – Manually classified as synoptic. Peak $G_{obs} = 38$ kt (19.5 m/s) at SBPA – Porto Alegre, RS, 03/05/2008, 09:00 UTC.	D-9
Figure D.13 – Manually classified as non-synoptic. Peak $G^* = 50$ kt (25.7 m/s) at SBSR – São José do Rio Preto, SP, 22/10/2015, 22:00 UTC.	D-9
Figure D.14 – Manually classified as suspect. Peak $G^* = 103$ kt (53.0 m/s) at SBEG – Manaus, AM, 26/11/2015, 09:00 UTC.	D-9
Figure D.15 – F&N event classified as suspect by INMET algorithm. Peak $G_{obs} = 20.1$ m/s at A830 – São Borja, RS, 03/02/2015, 22:00 UTC.	D-10
Figure D.16 – Infrared channel of GOES 12 satellite enhanced with brightness temperature data, T_B (°C), 03/02/2015, 22:08 UTC.	D-10
Figure D.17 – F&N event classified as synoptic by INMET algorithm. Peak $G_{obs} = 20.1$ m/s at A802 – Rio Grande, RS, 27/08/2011, 15:00 UTC.	D-11

Figure D.18 – Infrared channel of GOES 13 satellite enhanced with brightness temperature data, T_B (°C), 27/08/2011, 14:45 UTC.....	D-11
Figure D.19 – F&N event classified as synoptic by INMET algorithm. Peak $G_{obs} = 26.5$ m/s at A831 – Quaraí, RS, 24/10/2009, 08:00 UTC.	D-12
Figure D.20 – Infrared channel of GOES 12 satellite enhanced with brightness temperature data, T_B (°C), 24/10/2009, 08:09 UTC.....	D-12
Figure D.21 – F&N event classified as non-synoptic by INMET algorithm. Peak $G_{obs} = 26.3$ m/s at A831 – Quaraí, RS, 15/10/2015, 06:00 UTC.....	D-13
Figure D.22 – Infrared channel of GOES 13 satellite enhanced with brightness temperature data, T_B (°C), 15/10/2015, 05:45 UTC.....	D-13
Figure D.23 – F&N event classified as non-synoptic by INMET algorithm. Peak $G_{obs} = 32.0$ m/s at A831 – Quaraí, RS, 16/10/2016, 11:00 UTC.....	D-14
Figure D.24 – Infrared channel of GOES 13 satellite enhanced with brightness temperature data, T_B (°C), 16/10/2016, 11:08 UTC.....	D-14
Figure D.25 – Event classified as non-synoptic by INMET algorithm. Peak $G_{obs} = 41.7$ m/s at A714 – Itapeva, SP, 27/11/2012, 21:00 UTC.....	D-15
Figure D.26 – Event classified as non-synoptic by aerodrome algorithm. Peak $G_{obs} = 72$ kt (37.0 m/s) at SPQT – Iquitos, Peru, 15/05/2009, 19:00 UTC.	D-15
Figure D.27 – Event classified as non-synoptic by aerodrome algorithm. Peak $G_{obs} = 81$ kt (41.7 m/s) at SBLO – Londrina, PR, 20/11/2017, 20:00 UTC.....	D-15
Figure D.28 – Event classified as synoptic by aerodrome algorithm. Peak $G_{obs} = 64$ kt (32.9 m/s) at SBFL – Florianópolis, SC, 04/12/2016, 06:41 UTC.....	D-16
Figure D.29 – Event classified as synoptic by aerodrome algorithm. Peak $G_{obs} = 94$ kt (48.4 m/s) at SUMU – Montevideo, Uruguay, 24/08/2005, 01:35 UTC.....	D-16
Figure D.30 – Event manually re-classified as non-synoptic (automatically classified as suspect by aerodrome algorithm). Peak $G^* = 70$ kt (36.0 m/s) at SBGO – Goiânia, GO, 21/12/1997, 17:50 UTC.....	D-16
Figure D.31 – Frequency of occurrence and peak gust box plots for INMET algorithm exits (Figure D.1).	D-17
Figure D.32 – Frequency of occurrence and peak gust box plots for aerodrome SWS G_{obs} algorithm exits (Figure D.2 and D.3).	D-17
Figure D.33 – Frequency of occurrence and peak gust box plots for aerodrome SWS G^* algorithm exits (Figure D.4 and D.5).	D-17

Figure E.1 – Extreme value distributions for non-synoptic winds at SBUR – Uberaba, MG, $t_{tot} = 27.9$, $M = 28$ years. Annual maximums (top); independent storms (middle); GPD (bottom).	E-2
Figure E.2 – Extreme value distributions for non-synoptic winds at SBPA – Porto Alegre, RG, $t_{tot} = 21.3$, $M = 22$ years. Annual maximums (top); independent storms (middle); GPD (bottom).	E-3
Figure E.3 – Extreme value distributions for non-synoptic winds at SBKP – Campinas, SP, $t_{tot} = 17.0$, $M = 17$ years. Annual maximums (top); independent storms (middle); GPD (bottom).	E-4
Figure E.4 – Extreme value distributions for non-synoptic winds at A502 – Barbacena, MG, $t_{tot} = 13.1$, $M = 13$ years. Annual maximums (top); independent storms (middle); GPD (bottom).	E-5
Figure E.5 – Extreme value distributions for non-synoptic winds at A816 – Novo Horizonte, SC, $t_{tot} = 8.3$, $M = 9$ years. Annual maximums (top); independent storms (middle); GPD (bottom).	E-6
Figure E.6 – Extreme value distributions for non-synoptic winds at A805 – Santo Augusto, RS, $t_{tot} = 6.9$, $M = 7$ years. Annual maximums (top); independent storms (middle); GPD (bottom).	E-7
Figure E.7 – Extreme value distributions for non-synoptic winds at SBCH – Chapecó, SC, $t_{tot} = 4.1$, $M = 5$ years. Annual maximums (top); independent storms (middle); GPD (bottom).	E-8
Figure G.1 – Average V wind speeds (m/s).	G-2
Figure G.2 – Average error, ε , between station monthly means, V_m , at stations and ECMWF ERA-Interim data.	G-2
Figure G.3 – Parameters for Weibull model fitted to V_{cor} (m/s) parent distribution.	G-3
Figure G.4 – Parameters for Weibull model fitted to G_{cor} (m/s) parent distribution.	G-4
Figure H.1 – $T_{med,3}$ (°C) averaged over each set of extreme events (N_N , N_S and N_M).	H-2
Figure H.2 – $-\Delta T_{min,3}$ (°C) averaged over each set of extreme events (N_N , N_S and N_M).	H-3
Figure H.3 – $-\Delta Q_{max,3}$ and $\Delta P_{max,3}$ (hPa) averaged over each set of extreme events (N_N , N_S and N_M).	H-4
Figure H.4 – Peak ratio R_{-3} averaged over each set of extreme events (N_N , N_S and N_M).	H-5
Figure H.5 – Peak ratio R_{+3} averaged over each set of extreme events (N_N , N_S and N_M).	H-6
Figure H.6 – Predominant wind direction for each set of extreme events (N_N , N_S and N_M).	H-7
Figure H.7 – Average gust factor, G_V , for each set of extreme events (N_N and N_S).	H-8
Figure H.8 – Predominant season (months of year) for each set of extreme events (N_N , N_S and N_M).	H-9

Figure H.9 – Predominant hour (UTC) for each set of extreme events (N_N , N_S or N_M).	H-10
Figure H.10 – Percentage of events with thunderstorm observations (TS) for each set of extreme events (N_N , N_S or N_M).	H-11
Figure H.11 – Annual growth rate of extreme wind events, pa (%).	H-12
Figure H.12 – Extreme distribution model parameter a	H-13
Figure H.13 – Extreme distribution model parameter U (m/s).	H-14
Figure H.14 – 50-year return gust speed G_{50} (m/s).	H-15
Figure I.1 – Non-synoptic extreme wind $R = 50$ -year return period homogenised gust speeds for individual stations.	I-6
Figure I.2 – Synoptic extreme wind $R = 50$ -year return period homogenised gust speeds for individual stations.	I-7
Figure I.3 – Definition of zones for Type N extreme winds (non-synoptic).	I-8
Figure I.4 – Type N (non-synoptic) wind speed as function of return period.	I-8
Figure I.5 – Definition of zones for Type S extreme winds (synoptic).	I-9
Figure I.6 – Type S (synoptic) wind speed as function of return period.	I-9
Figure I.7 – Comparison of individual SWS and zone V_R for Type N winds.	I-10
Figure I.8 – Comparison of individual SWS and zone V_R for Type S winds.	I-12
Figure I.9 – Residuals of U for Type N winds against sampling period t_{tot} (years).	I-13
Figure I.10 – Residuals of G_{50} for Type N winds against sampling period t_{tot} (years).	I-13
Figure I.11 – Residuals of U Type S winds against sampling period t_{tot} (years).	I-13
Figure I.12 – Residuals of G_{50} for Type S winds against sampling period t_{tot} (years).	I-14
Figure J.1 – Solutions for governing $G_{50,N}$ using 1 st order polynomial and varying p_L	J-4
Figure J.2 – Solutions for governing $G_{50,N}$ using 2 nd order polynomial and varying p_L	J-5
Figure J.3 – Solutions for governing $G_{50,N}$ using 3 rd order polynomial and varying p_L	J-6
Figure J.4 – Solutions of $G_{50,N}$ for reduced number of governing stations.	J-7
Figure L.1 – Residuals of U_N for all SWS.	L-2
Figure L.2 – Residuals of U_E for governing SWS.	L-3
Figure L.3 – Residuals of $G_{50,N}$ for all SWS.	L-4
Figure L.4 – Residuals of $G_{50,E}$ for governing SWS.	L-5

LIST OF TABLES

Table 2.1 – NBR 6123 roughness lengths and gradient heights per terrain category (adapted from ABNT, 1988)	36
Table 2.2 – β values for NBR 6123 terrain categories (Simiu, 1981; Blessmann, 2013)	37
Table 2.3 – c and $G_{V,3600s}$ for NBR 6123 time-averaging intervals (Blessmann, 2013).....	37
Table 2.4 – Key basic wind speeds details of international wind codes.	41
Table 3.1 – Comparison of wind observation protocols.....	51
Table 3.2 – METAR/SPECI reports with correctly formatted wind observation fields.....	56
Table 3.3 – Bodies and documents responsible for the definition of weather observation protocols at aerodromes within the study region.....	57
Table 3.4 – SYNOP reports with correctly formatted wind observation fields.	58
Table 3.5 – Calculation of expected peak and gust factors for filtered turbulence spectra.....	64
Table 3.6 – Comparison of peak and gust factors for NBR 6123 (ABNT, 1988) with Holmes et al. (2014) and Harris turbulence spectra.....	68
Table 3.7 – Terrain classification of WMO (2014) in terms of roughness length z_0 . Based on Davenport (1960) and Wieringa (1980)	72
Table 4.1 – Common formatting irregularities encountered in METAR/SPECI observations.....	90
Table 4.2 – SYNOP, METAR and ICEA-BDC reports for SBPA – Porto Alegre, RS, at 18:00 UTC 06/12/2003.....	91
Table 4.3 – Extracted data from incorrectly prepared METAR/SPECI reports as presented by third-party databases.....	99
Table 4.4 – Comparison of INMET Web and SADMET observations made during documented extreme wind events.....	109
Table 4.5 – Comparison of INMET DISME and SADMET observations.....	111
Table 4.6 – Number of qualified extreme gusts peak gusts, per DISME, which are encountered only in INMET’s restricted database.	113
Table 4.7 – A comparison of datasets reporting on three different extreme wind events at Taubaté, SP.....	114
Table 6.1 – Extreme distribution parameters for non-synoptic winds, SBGR – Guarulhos, SP.	157
Table 6.2 – Phases in the determination of event classification algorithms.....	160
Table 6.3 – Parametrisation and manual classification of 9 extreme wind events.....	173

Table 6.4 – Parametrisation and automatic classification of 5 F&N extreme wind events at INMET ASWS.	176
Table 6.5 – Parametrisation and final classification of 6 extreme wind events.	178
Table 6.6 – Ratios of MIS model parameters to analytical solution.	183
Table 7.1 – SWS classifications per dataset.	188
Table 7.2 – Station sampling time and non-synoptic extreme distributions in western Santa Catarina and southwestern Paraná.	197
Table 7.3 – Discrimination process for node closest to São Paulo, SP, (-23.5°, -46.5°) for non-synoptic winds.	200
Table 7.4 – Discrimination process for node closest to Rio de Janeiro, RJ, (-23.0°, -43.5°) for non-synoptic winds.	200
Table 7.5 – Proposed probabilistic factors, S_3 , for NBR 6123.	210
Table 7.6 – Details of the most extreme qualified G_{cor} gust speeds at individual SWS which were equal to, or greater than, V_0 as defined in Figure 7.15 ($\varepsilon \geq 0\%$).	216
Table A.1 – Brazilian state codes and names.	A-2
Table A.2 – Selected Brazilian aerodrome surface weather stations.	A-3
Table A.3 – Selected international aerodrome surface weather stations.	A-7
Table A.4 – Selected INMET automatic surface weather stations.	A-9
Table C.1 – Extreme distribution parameters of Class A aerodrome SWS.	C-2
Table C.2 – Extreme distribution parameters of Class A INMET ASWS.	C-7
Table F.1 – Relevant b , p and F_r parameters for the calculation of terrain and height multiplier, S_2 . Table 21 of NBR 6123 (ABNT, 1988).	F-2
Table F.2 – Lieblein’s BLUE Coefficients for $M = 10$ (ESDU, 1990[a]).	F-3
Table F.3 – Lieblein’s BLUE Coefficients for $M = 20$ (ESDU, 1990[a]).	F-3
Table F.4 – Saffir-Simpson Hurricane Wind Scale.	F-4
Table I.1 – Station contributions to Zone N1 wind climate model.	I-2
Table I.2 – Station contributions to Zone S1 wind climate model.	I-2
Table I.3 – Model parameters for Type N winds (non-synoptic) and basic wind speed, $V_{R,N}$	I-10
Table I.4 – Model parameters for Type S winds (synoptic) and basic wind speed, $V_{R,S}$	I-10
Table K.1 – NBR 6123 S_3 factors (ABNT, 1988).	K-3
Table K.2 – Minimum permitted values of probabilistic factor, S_3 (ABNT, 1988).	K-4
Table K.3 – Wind speeds for various mean recurrence intervals, V_R , in m/s ($P_L = 0.63$).	K-5

LIST OF SYMBOLS

Roman Letters:

a	GEVD scale factor
A	equivalent frontal area
b	coefficient in the determination of S_2 as defined by NBR 6123 (ABNT, 1988)
$b_{\Delta T}$	parameters used when calculating $\Delta Group$ limits
c	parameter used in calculation of F_r of NBR 6123 (ABNT, 1988)
c	Weibull scale factor
C	model parameter for GPD analysis
C_a	drag coefficient of NBR 6123 (ABNT, 1988)
C_F	flow distortion correction factor (WMO, 2014)
C_T	correction factor due to topographic effects (WMO, 2014)
d	anemometer distance constant
D	model parameter for GPD analysis
dd	predominant wind direction for SYNOP report
DIR	predominant wind direction
e	residual, or error, between station scalar and model
e_w	weighted sum of residual squares
f	frequency
f	parameter used in the determination of K_x (ESDU, 2002)
F	horizontal distance for internal layer to be in equilibrium with terrain (Deaves,

	1981)
F_G	S_2 factor applied to G_{obs} time-series to correct to $z = 10$ m and $z_0 = 0.07$ m
F_H	modal force of NBR 6123 (ABNT, 1988)
F_r	gust factor as defined by NBR 6123 (ABNT, 1988)
F_V	S_2 factor applied to V_{obs} time-series to correct to $z = 10$ m and $z_0 = 0.07$ m
ff	wind speed in units denoted by i_w of SYNOP report
g	peak factor
G	3-second gust
G^*	equivalent 3-second gust
G_{50}	50-year return wind speed from extreme value analysis at individual SWS
G_{cor}	3-second gust speed corrected to $z = 10$ m, and $z_0 = 0.07$ m
G_{obs}	observed 3-second gust speed
G_V	gust factor
\bar{G}_{50}	weighted average 50-year return wind speed of 8 the closest individual SWS
gg	minutes past the hour of METAR/SPECI or SYNOP report
GG	hour of METAR/SPECI or SYNOP report
h	overall height of structure as per NBR 6123 (ABNT, 1988)
$h_{i,A}$	height of internal boundary layer at point A (ESDU, 2002)
H	overall height of obstacle or structure
$ H_1(f) ^2$	anemometer admittance function (based on distance constant)
$ H_2(f) ^2$	moving average transfer function

$ H_3(f) ^2$	anemometer admittance function (based on time constant)
$ H_A(f) ^2$	aerodynamic admittance function
i_w	indicator of wind speed units for SYNOP reports
I	turbulence intensity
$IIiii$	WMO location identifier for SWS
k	GEVD shape factor
K_s	ratio between reference velocity and velocity at site for thunderstorm design wind speeds (ESDU, 1990[a])
K_x	multiplier for the determination of internal boundary layer wind speed profile (ESDU, 2002)
l_1	width of building as per NBR 6123 (ABNT, 1988)
l_2	depth of building as per NBR 6123 (ABNT, 1988)
L	threshold $R_{\pm 3}$, $R_{\pm 6}$ ratios used to generate \mathcal{H}
L_u	integral length scale
m	rank of value in set of extremes in ascending order
$m_{\Delta T}$	parameter used when calculating $\Delta Group$ limits
M	number of whole years of data
MH	month
N	total cloud cover for SYNOP report
N	number of events
N_{ev}	number of extreme wind events per month
N_{trend}	number of extreme wind events used to determine trends

$Obs.$	percent of month represented by valid wind speed observations
p	exponent in the determination of S_2 as defined by NBR 6123 (ABNT, 1988)
P	probability of non-exceedance
P_{atm}	atmospheric pressure
P_{ins}	P_{atm} at the end of previous hour as observed by INMET ASWS
p_L	power applied to normalised distance used in the determination of datum weighting
P_L	probability of wind speed associated with P will be exceeded at least once over a period of R_L years
P_m	probability of non-exceedance for value of rank m in extreme value analysis
P_{max}	maximum P_{atm} of the previous hour as observed by INMET ASWS
P_{min}	minimum P_{atm} of the previous hour as observed by INMET ASWS
$p(X)$	probability density function
$P(X)$	cumulative distribution function; annual probability of non-exceedance of X
pa	average annual rate of growth of extreme wind events
$PPPP$	atmospheric pressure at mean sea-level for SYNOP report
q	dynamic pressure
QNH	atmospheric pressure at mean sea-level
r	average number of storms per year
R	mean recurrence interval
R_L	lifetime
R_P	return period

R^2	correlation coefficient
$R_{\pm 3}, R_{\pm 6}$	ratio between peak observation and average speeds over ± 3 or 6 hours from peak
\mathcal{R}	reduction of $\{R_{\pm 3}, R_{\pm 6}\}$ to a single value as per L threshold
S_n	indicator of temperature sign for SYNOP report
S_1	topographic multiplier as per NBR 6123 (ABNT, 1988)
S_2	terrain and height multiplier as per NBR 6123 (ABNT, 1988)
S_3	probabilistic multiplier as per NBR 6123 (ABNT, 1988)
$S_u(f)$	turbulence spectra of wind/spectral density function
t	timestep
t_r	response time as per Kwon and Kareem (2014)
t_{tot}	number of years of valid data for SWS
t_{val}	assumed period of validity of a single meteorological observation
T	temperature
T	sampling period
T_B	brightness temperature
T_d	dewpoint temperature
T_{ins}	temperature at the end of previous hour as observed by INMET ASWS
T_{max}	maximum temperature of the previous hour as observed by INMET ASWS
$T_{med,3}$	mean temperature over the three hours prior to a peak gust speed.
T_{min}	minimum temperature of the previous hour as observed by INMET ASWS
TTT	temperature in increments of 0.1 °C for SYNOP report

$T_d T_d T_d$	dewpoint temperature in increments of 0.1 °C for SYNOP report
\bar{u}	mean wind speed of undefined time-averaging interval
u_0	base threshold wind speed of GPD analysis
u_∞	free-stream wind speed
u^*	friction velocity
$u'(t)$	time-series of fluctuations about the mean wind speed
$u(t)$	time-series of wind speed
u_{cor}	corrected wind speed
u_{obs}	observed wind speed
U	GEVD location factor (or mode)
V	10-minute mean wind speed
V_0	basic wind speed as defined in NBR 6123 (ABNT, 1988)
V_{clim}	climatic mean wind speed
V_{cor}	10-minute mean wind speed corrected to $z = 10$ m, and $z_0 = 0.07$ m
V_k	characteristic wind speed as per NBR 6123 (ABNT, 1988)
V_m	monthly mean wind speed
V_{max}	maximum wind speed of downburst outflow as per Savory et al. (2001), Miguel et al. (2018) and Riera (2018).
V_{obs}	observed 10-minute mean wind speed
V_R	predicted wind speed for mean recurrence interval of R years
V_T	mean wind speed over (long) period T
V_τ	mean wind speed over (short) period τ

V_{zx}	internal boundary layer of ESDU 82026 (2002)
x	typical upwind distance
X	variable subjected to statistical analysis
y	reduced variate
y_0	y -intercept of mean exceedance plot in GPD analysis
y_{lim}	lowest reduce variate to be used in model fit
$YEAR$	year
YY	day of the month for METAR/SPECI and SYNOP reports
w	Weibull shape factor
W_i	weighting of each datum
ww	weather indicator for SYNOP report
W_1W_2	present or recent weather indicator for SYNOP report
z	height above ground
z_0	roughness length
$z_{0,obs}$	roughness length of observed data
$z_{0,cor}$	corrected roughness length
z_0^+	the larger of two roughness lengths
z_g	gradient height
z_i	height of internal boundary layer (Deaves, 1981)
z_{max}	height of maximum wind speed of downburst outflow, V_{max} , as per Savory et al. (2001), Miguel et al. (2018) and Riera (2018).
z_t	height of transition layer (Deaves, 1981)

z_x Height of transition layer as per NBR 6123 (ABNT, 1988)

Z denotes time in UTC for METAR/SPECI reports

Greek Letters:

β characteristic wind speed (Padaratz, 1977)

β parameter used in calculation of F_r of NBR 6123 (ABNT, 1988)

γ shape factor (Padaratz, 1977)

γ_f wind load factor

γ_o shape factor of each individual station (Padaratz, 1977)

γ_{mp} weighted average shape factor (Padaratz, 1977)

δ parameter used in the determination of proposed S_3 factors

$\Delta Group$ classification of severity of change in T and P around observation of peak speed

$\Delta DIR_{max,\pm 3}$ maximum change in DIR within a ± 3 -hour window from peak observation

$\Delta P_{max,3}$ largest positive change in atmospheric pressure over 3 hour period

$\Delta Q_{max,3}$ largest positive change in QNH pressure over 3-hour period

ΔT_0 ΔT intercept ($\Delta P = 0$) used when calculating $\Delta Group$ limits

$\Delta T_{min,3}$ largest negative change in temperature over 3 hour period

ε error between two scalars expressed as a percentage

ζ critical damping ratio of NBR 6123 (ABNT, 1988)

η height above ground, z , normalised by z_{max} as per Savory et al. (2001), Miguel et al. (2018) and Riera (2018).

θ parameter used in the determination of proposed S_3 factors

κ	von Kármán constant
λ	average yearly exceedance rate of u_0 in GPD analysis
μ	gradient of mean exceedance plot in GPD analysis
ν	cycling rate
ξ	dynamic amplification factor of NBR 6123 (ABNT, 1988)
σ	standard deviation
σ^2	variance
τ	gust duration/time-averaging interval

LIST OF ABBREVIATIONS AND ACRONYMS

AIP	Aeronautical Information Publication
AIS	Aeronautical Information Service
ABL	Atmospheric Boundary Layer
ABNT	<i>Associação Brasileira de Normas Técnicas</i> (Brazilian Association of Technical Standards)
ASCE	American Society of Civil Engineers (United States)
ASOS	Automatic Surface Observing System (United States)
AS/NZS	Australian/New Zealand Standard
ASWS	Automatic Surface Weather Station
BDC	<i>Banco de Dados Climatológicos</i> (Climatological Database)
BLUE	Best Linear Unbiased Estimators
BoM	Bureau of Meteorology (Australia)
CAPE	Convective Available Potential Energy
CAT	terrain category of NBR 6123 (ABNT, 1988)
CDF	Cumulative Distribution Function
CFD	Computational Fluid Dynamics
CINDACTA	<i>Centro Integrado de Defesa Aérea e Tráfego Aéreo</i> (Integrated Centre of Air Defense and Air Traffic)
CPTEC-INPE	<i>Centro de Previsão de Tempo e Estudos Climáticos – Instituto Nacional de Pesquisas Espaciais</i> (Centre for Weather Forecasting and Climate Studies – National Institute for Space Research)
COMP.	wind speed profile composed of 65% DB and 35% synoptic profiles as per Miguel et al. (2018) and Riera (2018)
COR	identifier for corrected METAR/SPECI report
DB	downburst profile of Miguel et al. (2018) and Riera (2018)
DECEA	<i>Departamento de Controle do Espaço Aéreo</i> (Department of Airspace Control)
DISME	<i>Distrito Meteorológico</i> (Meteorological District)

DS	dust storm
DU	widespread dust
E	envelope (or maximum) of N, S and M distribution
ECMWF	European Centre for Medium-Range Weather Forecasts
EPS	extensive, extra-tropical pressure systems
ESDU	Engineering Science Data Unit
FAB	<i>Força Aérea Brasileira</i> (Brazilian Airforce)
FC	funnel cloud (tornado)
GPD	Generalised Pareto Distribution
GEVD	Generalised Extreme Value Distribution
GIS	Geographic Information System
GOES	Geostationary Operational Environmental Satellite
GTS	Global Telecommunications System
HOMR	Historical Observing Metadata Repository (United States)
IBGE	<i>Instituto Brasileiro de Geografia e Estatística</i> (Brazilian Institute of Geography and Statistics)
ICAO	International Civil Aviation Organization
ICEA	<i>Instituto de Controle do Espaço Aérea</i> (Institute of Airspace Control)
INMET	<i>Instituto Nacional de Meteorologia</i> (National Institute of Meteorology)
INFRAERO	<i>Empresa Brasileira de Infraestrutura Aeroportuária</i> (Brazilian Airport Infrastructure Company)
ISO	International Organization for Standardization
ITCZ	Intertropical Convergence Zone
JAWS	Joint Airport Weather Studies
LAC	<i>Laboratório de Aerodinâmica das Construções</i> (Building Aerodynamics Laboratory)
LIDAR	Light Detection and Ranging
LLJ	Low-Level Jet

M	mixed distribution
MCC	Mesoscale Convective Complex
MCS	Mesoscale Convective System
METAR	Aerodrome Routine Meteorological Report
MIS	Method of Independent Storms
MLE	Maximum Likelihood Estimator
MSS	METAR/SPECI and SYNOP
N	non-synoptic extreme wind
NBR	<i>Norma Brasileira</i> (Brazilian Standard)
NCEI/NCDC	National Centers for Environment Information (formerly National Climatic Data Center; United States)
NIMROD	Northern Illinois Meteorological Research on Downbursts
NIST	National Institute of Standards and Technology (United States)
NM	METAR/SPECI report from NCEI/NCDC
NOAA	National Oceanic and Atmospheric Administration (United States)
NS	SYNOP report from NCEI/NCDC
OPMET	Operational Meteorological Database
PDF	Probability Density Function
PO	dust/sand whirls
POT	Peaks Over Threshold
PSEC	<i>Secretaria da Divisão de Pesquisa</i> (Secretariat of the Research Division)
R-S	rough to smooth
RE	recently occurred weather phenomenon
REDEMET	<i>Rede de Meteorologia do Comando da Aeronáutica</i> (Aeronautical Command Meteorological Network)
RM	METAR/SPECI report from REDEMET
S	synoptic extreme wind
S-R	smooth to rough

SA	widespread sand
SACZ	South Atlantic Convergence Zone
SADMET	<i>Seção de Armazenamento de Dados Meteorológicos</i> (Meteorological Data Storage Section)
SEI	Structural Engineering Institute (United States)
SISCEAB	<i>Sistema de Controle do Espaço Aéreo Brasileiro</i> (Brazilian Airspace Control)
SMN	<i>Servicio Meteorológico Nacional</i> (Argentinian National Meteorological Service)
SQ	squall
SS	sandstorm
SUS	suspect data/observation
SWS	Surface Weather Station
TAF	Terminal Aerodrome Forecast
TC	Tropical Cyclone
TS	thunderstorm
UFRGS	<i>Universidade Federal do Rio Grande do Sul</i> (Federal University of Rio Grande do Sul)
UTC	Coordinated Universal Time
UN	United Nations
VC	within the vicinity of aerodrome (8-16 km)
WM	METAR/SPECI report from Weather Underground
WS	SYNOP report from Weather Underground
WU	Weather Underground
WDS	WEB, DISME and SADMET
WRDS	WEB, Restricted INMET, DISME and SADMET
WEBMET	<i>Sistema Automatizado de Registro e Gerenciamento das Observações Meteorológicas</i> (Automated System for Registration and Management of Meteorological Observations)
WMO	World Meteorological Organization

1. INTRODUCTION

1.1 RELEVANCE OF THE STUDY

The interaction between natural phenomena and manmade structures is the focus of many engineering fields. Wind occupies a unique position in engineering due to spatial and temporal variations which demand static and dynamic approaches for load determination. Techniques that consider incident wind as a stationary process are well-established; however, research continues to highlight the importance of non-stationary winds on the built environment. Adequate modelling techniques of transient non-synoptic winds, specifically those originating from *severe convective storms*, remain inadequately represented in the majority of wind codes. Vertical profiles of horizontal wind speeds for *thunderstorm* events, the term which is commonly used in place of *convective storm* despite its non-dependence on the presence of thunder, are provided by at least two wind codes. However, the divergence between the profiles of each code and lack of thunderstorm specific turbulence, gust factors and aerodynamic coefficients serve to highlight the need for continued research. Various sections of the global wind engineering community are currently engaged in research to develop non-synoptic incident wind models and response determination techniques to be introduced in future wind codes.

The improvement of construction techniques, smarter structural design and advances in material sciences leads to a tendency of building taller and lighter. With this comes greater vulnerability to wind loads due to increased flexibility of structures. Although optimisation of the structure can be achieved from site and geometry specific wind-tunnel investigations, the most important parameter remains the design wind speed from which the vertical profile of incident horizontal wind speeds is derived. The project specific design wind speed is typically determined from a regional basic wind speed defined by the local wind code or from a specially commissioned study. In both instances, and with the exception of regions affected by tropical cyclones for which numerical simulations are commonly utilised, analyses of meteorological data acquired at surface weather stations (SWS) are fundamental to the determination of the local or regional wind climate. Accuracy of design winds speeds is

crucial to any project, as errors are amplified due to the quadratic relationship between wind speed and force.

In Brazil, wind standard NBR 6123 *Forças devidas ao vento em edificações* (ABNT, 1988) details methodology for the evaluation of wind loads. The basic wind speed, V_0 , provided in the form of isopleth map of the country, represents the 3-second gust wind speed which is met, or exceeded, on average, once every 50 years, at a height of 10 m above ground in open and flat terrain. The wind speed varies from 30 m/s in the equatorial regions to 50 m/s in the south and southwest of the country with contours at 5 m/s intervals as shown in Figure B.1 of Appendix B *Isopleth Map of NBR 6123* (ABNT, 1988). Investigations by Vieira Filho (1975) and Padaratz (1977) were responsible for the derivation of the basic wind speed map. The studies used series of annual maximum wind speeds between 1950 and 1974 at 49 aerodrome based SWS, with sampling periods ranging from 4 to 25 years. Extreme value analyses were performed using the Fréchet distribution and a single weighted average shape factor was applied to all stations to generate the isopleth map.

More than 40 years have passed since the Padaratz map was proposed, and despite the continuation of research into Brazilian extreme winds, basic wind speeds of NBR 6123 remain unchanged. In principle, more than 65 years of data are now available for use in an extreme value analysis, in addition to the National Institute of Meteorology (*Instituto Nacional de Meteorologia* – INMET) automatic surface weather station (ASWS) network commissioned in 2000. Riera and Nanni (1989) analysed annual maxima for four cities in Rio Grande do Sul separating stationary synoptic winds from thunderstorm events with the conclusion that stationary synoptic winds were only relevant for return periods less than 10 years. Santos (1989) expanded the investigation to 11 cities in the southern half of Brazil.

More recently, two basic wind speed maps were proposed with large variations between them. Almeida (2010) performed a Gumbel extreme value analysis using annual maxima originating from SYNOP meteorological reports at Brazilian weather stations, with a kriging technique used to interpolate V_0 values between the stations. The contours of the isopleth map, as shown in Figure 1.1, range from 60-90 m/s at 5 m/s intervals – magnitudes typically associated with the most intense tropical cyclones. Unfortunately, it appears the study was free of quality control processes. A review of the source of data used by Almeida (2010) indicates missing wind data fields in SYNOP reports can lead to the erroneous extraction of wind data by automatic extraction routines (refer to Sections 4.1.1 *METAR*, *SPECI* and *SYNOP (MSS)* and

4.1.3.4 *CPTEC-INPE*). Many automatic extraction routines have no way to tell if the wind data field is not present, a common occurrence in SYNOP reports, and subsequently extract incorrect data. For example, a temperature of 29.6 °C is reported as 296, with the extraction routine incorrectly identifying the last two digits, 96, as the mean wind speed in knots (49.4 m/s). The map proposed by Almeida (2010) is effectively a spatial interpolation of extreme value analyses based on erroneous data.

Beck and Corrêa (2013) proposed a map of more plausible basic wind speeds ranging from 28-42 m/s. Gumbel extreme value analysis was performed for sets of annual maxima at stations across Brazil and neighbouring countries, with a fourth order regression model fitted to V_0 scalars at discrete locations. Although the result is an attractive map with smooth contours at 2 m/s intervals, as shown in Figure 1.1, an examination of the methodology reveals some points of concern. No quality controls were cited in the study despite the identification of “weird” wind speeds. Beck and Corrêa (2013) correctly identified their removal from the observation of wind speeds by several processes, and that little could be done to qualify or discard spurious data. The source of meteorological data, Wolfram, obtains its meteorological data from another third-party site (refer to Sections 4.1.3.1 *NCEI* and 4.1.3.2 *Wolfram*) for which known errors are detailed in this study. No consideration was given to the number of hours per day each station operated, frequency of observation, the number of years of operation or exposure of anemometer, including height and roughness of terrain. In addition, incorrect gust factors were applied to generate equivalent gusts from mean wind speeds. The incorrect assumption of a 30-second mean wind speed was taken from Padaratz (1977) and not from official documentation which correctly define a 10-minute mean wind speed. Finally, the simplicity of the map’s contours is deceiving and no explanation is given regarding the large differences between discrete station V_0 and the generated contours. An extreme example is the V_0 of 50 m/s at Petrolina, PE, which is located in north-eastern Brazil and within the 28 m/s contour.

A lack of wind engineering acumen is evident in both Almeida (2010) and Beck and Corrêa (2013). Both studies only produced maps for a 50-year mean recurrence interval and did not offer a model to determine wind speeds for other probabilities of exceedance. Padaratz (1977) was faced with similar issues such as high variability between stations, lack of station metadata and limited data, but applied a rational process to determine the extreme wind climate which safeguarded Brazilian structures for the last four decades.

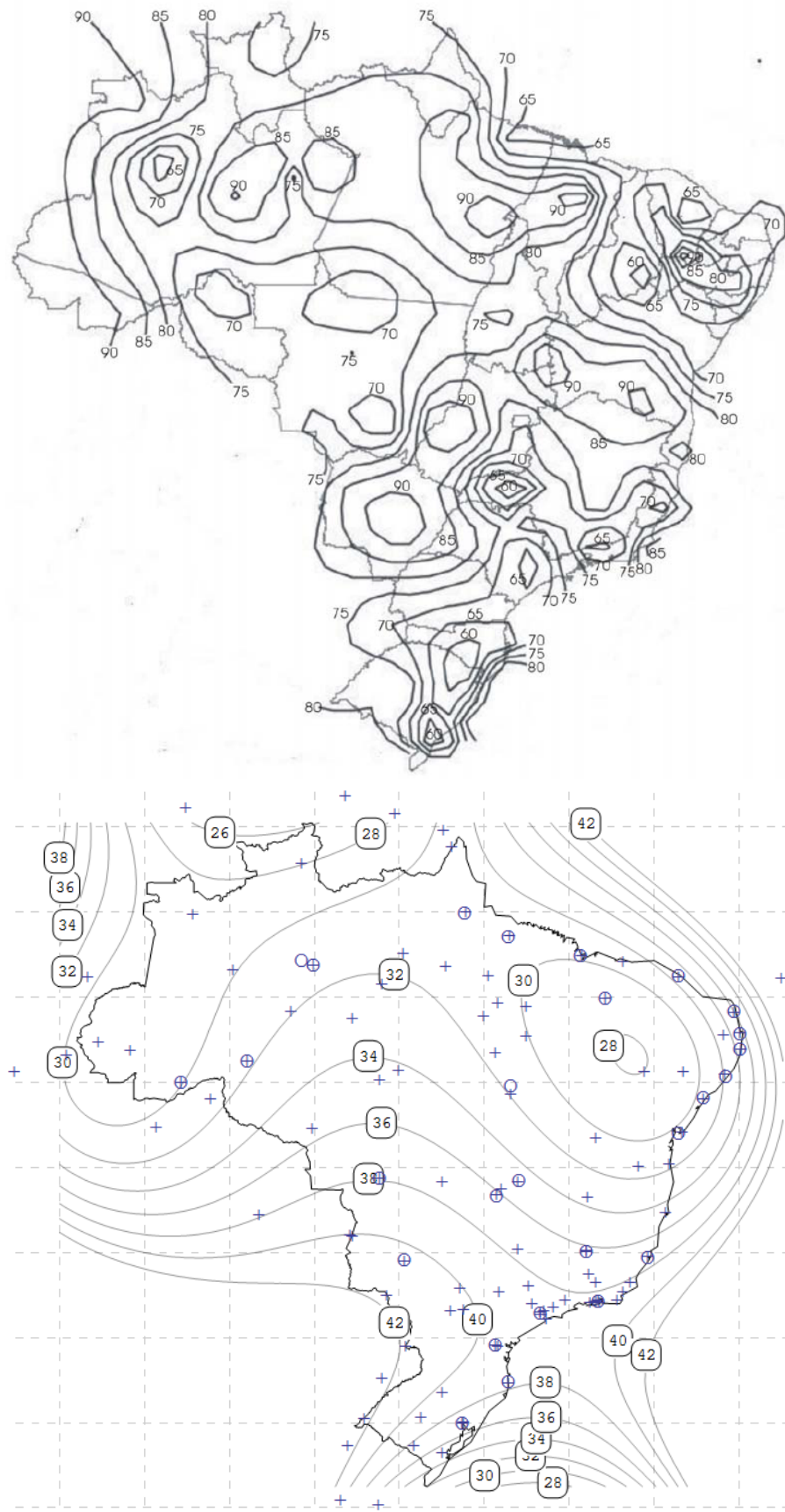


Figure 1.1 – Proposed isopleth maps of Brazilian basic wind speeds, V_0 (m/s), top: Almeida (2010), bottom: Beck and Corrêa (2013)

Holmes et al. (2005) outlined four key criteria which should be met when determining extreme wind speed zoning for a nation:

1. the use of the same instruments, or instruments with the same dynamic characteristics (time or distance constant);
2. in the same type of terrain: open, flat terrain;
3. at the same height above terrain level;
4. during the same period, sufficiently long enough, but preferably longer than 30-40 years.

It was recognised by Holmes et al. (2005) that these requirements are often not met. Anemometers are likely changed several times over the course of decades. Large errors are introduced in time-series, particularly in the observation of gusts, without proper calibration or discontinuation of the same type of instrument. Similarly, exposure conditions relating to anemometer heights and locations are subject to change over the course of time. It is possible to correct to a standard height and terrain roughness, typically 10 m and open field respectively, should sufficient historical metadata be available. It is also recommended by Holmes et al. (2005) to exclude data from anemometers located in city centres. Davenport (1983) identified several errors which could be introduced in any extreme wind climate analysis, including sampling errors for short records, changes in the exposure via height changes and the encroachment of new developments, instrumental errors, archiving errors and climate change. Errors caused by changes in the measurement process from conventional and manual methods to digital and automatic processes are fresher challenges. Additionally, the World Meteorological Organization's (WMO) revised definition of a peak gust as a 3-second moving-average (Beljaars, 1987) motivated at least two countries to investigate the effective gust time-interval of historical observations. In Australia, this led to the redefinition of the peak gust speed as a 0.2-second moving average (Holmes and Ginger, 2012), and a redefinition of a 1-second moving average in the United States (Kwon and Kareem, 2014).

This study was conducted with consideration given to the abovementioned aspects. A detailed investigation into the state-of-the-art methodologies and current understanding of extreme winds and their measurements were conducted, in addition to the revision of the extreme value analysis options and evaluations of meteorological datasets and networks. Given the accumulation of studies which underline the threat of non-synoptic winds to structures in Brazil (Loredo-Souza, 2012; Pes, 2015; Ferreira and Nascimento, 2016[b]; Ferreira, 2017;

Loredo-Souza et al., 2019), the opportunity was also taken to separate extreme wind events by storm type in anticipation of the development of non-synoptic wind models in the near future.

1.2 OBJECTIVES

In order to produce regional wind climate models of Brazil for both synoptic and non-synoptic wind types, a series of objectives must be completed.

- Bibliographic review of current understanding of wind and its characterisation in codes, as well as current best practice in the determination of regional wind climate from extreme value analyses;
- Evaluation of meteorological observation networks operational on a national level in Brazil and associated datasets, whether official or provided by third-parties;
- Development of algorithms and methods for the identification of spurious data and separation of synoptic and non-synoptic peak wind speeds;
- Investigation into historical metadata of all stations, including height, geographic coordinates, equipment, observing processes, in order to homogenise wind speed time-series and determine periods appropriate for extreme value analysis;
- Determination of an appropriate extreme value analysis technique with consideration to quality of data and observing network. Application of technique to extracted sets of extreme non-synoptic and synoptic peak gusts to determine extreme wind climate;
- Mapping of meteorological parameters associated with extreme non-synoptic and synoptic winds, including temperature and pressure changes, wind speed ratios, predominant directions, seasons and times of the day;
- Integration of extreme wind climate models at discrete station locations to generate basic wind speed maps for non-synoptic and synoptic winds. An updated V_0 map is proposed for implementation in a revised NBR 6123.

Along the course of the study, a number of areas relating to the acquisition of meteorological data and management of databanks were identified as requiring improvements on a national scale. Recommendations are also made on the direction of future research, particularly in the area of non-synoptic winds in Brazil. This study aims to be a new beginning and not the final word on extreme winds in the region.

2. EXTREME WINDS

2.1 FUNDAMENTALS

Basic fundamentals of wind characteristics which are referenced throughout the study are briefly explained. Incident models for Atmospheric Boundary Layer winds (ABL) are characterised by the following three components:

1. Vertical mean wind profile, $\bar{u}(z)$;
2. Vertical turbulence intensity profile, $I(z)$;
3. Turbulence spectrum.

The time-series of a wind speed sample, $u(t)$, is split into two components: mean wind speed, \bar{u} , and instantaneous wind speed, $u'(t)$, as per Equation 2.1. The random fluctuations due to turbulence are represented by the series $u'(t)$, and the variation of the wind speed over the sampling time, T , is represented by the standard deviation, σ , as per Equation 2.2. Turbulence intensity, $I(\%)$, is the ratio between the standard deviation of the sample and the mean, as defined in Equation 2.3.

$$u(t) = \bar{u} + u'(t) \quad 2.1$$

$$\sigma = \sqrt{\frac{1}{T} \int_0^T u'(t)^2 dt} \quad 2.2$$

$$I = \frac{\sigma}{\bar{u}} \quad 2.3$$

The time-averaging interval of wind speed, τ , is an important fundamental to be considered when undertaking any wind-related study. When averaged over large time intervals, typically $\tau > 10$ s, wind speeds are referred to as mean wind speeds and the sampling period is best represented by T . Mean wind speeds measured over $T = 10$ min (600 s) and 1 hr (3600 s) are often encountered in climate studies and engineering applications. Averages over large time intervals filter out high-frequency fluctuations and are smaller in magnitude than wind speeds with short τ . For shorter time intervals, $\tau < 5$ -10 s, wind-surges due to turbulence are referred

to as gusts. The analysis and measurement of gusts are much more sensitive to specific definitions than longer interval mean wind speeds, often involving an analysis of the sampling processes and equipment. It is often necessary to convert wind speeds from one time-averaged interval to another, for example, from an hourly mean wind speed, $V_{T=3600s}$ to a peak gust, $V_{\tau=3s}$, which requires a pre-determined peak factor, g , and knowledge of the turbulence intensity, I , relating to the longer of the two time-intervals. The relationship between two wind speeds of different time-averaged intervals is defined in Equation 2.4. For cases in which both peak factor and turbulence intensities are known, a gust factor, G_V , is determined as per Equation 2.5. Many of the peak and gust factors which appear in wind codes used today are based on Durst (1960), which proposed probable values of the peak wind speeds for varying τ and mean hourly wind speeds ranging from 20 to 80 mph at increments of 10 mph. Gust factors from Durst (1960) are shown in Figure 2.1. The Durst curve (1960) is based on data recorded by Giblett (1932) in 1928 using four Dines pressure-tube anemometers at a height of 15.3 m in open farmland punctuated by only a few trees and hedges (Miller, 2011).

$$V_{\tau} = V_T(1 + gI_T) \quad 2.4$$

$$G_V = \frac{V_{\tau}}{V_T} = (1 + gI_T) \quad 2.5$$

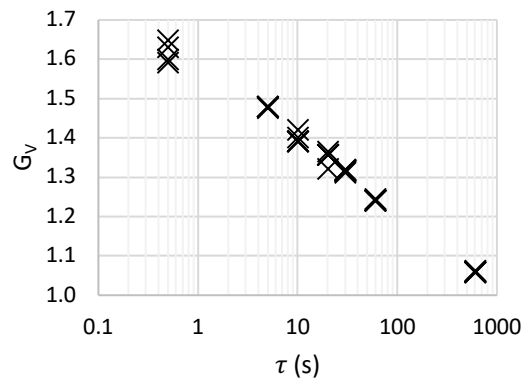


Figure 2.1 – Durst (1960) gust factor curve relating to mean wind speeds of $T = 3600$ s.

Turbulence intensity varies with height above ground, z , and roughness length, z_0 . Rough surfaces and small distances from the earth's surface produce higher turbulence intensities (high z_0 , low $z \rightarrow$ high I); conversely, smooth surfaces and great distances from the earth's surface produce lower turbulence intensities (low z_0 , high $z \rightarrow$ low I). Many publications assign roughness lengths to qualitative terrain categories, such as bodies of water, open fields, suburban and urban areas, and values often vary between publications for similar terrain

types. For example, WMO (2014) adopts $z_0 = 0.03$ m for grassed open flat terrain with few obstacles, and $z_0 = 1.0$ m for terrain with regular, large obstacle coverage, such as suburbs and forests.

The interaction of wind with upstream obstacles is responsible for the generation of turbulence. Eddies are the swirling, or rotating, regimes within the fluid which dislocate with the same mean speed as the overall flow, and are responsible for the fluctuations in instantaneous wind speeds. The size and frequency of eddies are directly related, with high frequency fluctuations occurring over small distances and low frequency fluctuations over large distances. The energy content within fluid flow varies with the frequency of its fluctuations. The distribution of turbulence with frequency, f , is the spectral density function, $S_u(f)$, also referred to as the turbulence spectrum, and the integral of the function is equal to the variance, σ^2 , as shown in Equation 2.6. The von Kármán spectrum, shown in its non-dimensional form in Equation 2.7 and Figure 2.2, is one of the most commonly used spectral density functions in wind engineering. The integral length scale, L_u , is the longitudinal distance for which the spectrum represents. For small L_u , the distribution of energy peaks at high frequencies; conversely, for a large L_u the peak shifts towards the low-frequency end of the spectrum. Similar to wind speed and turbulence intensity, the length scale varies with height and terrain.

$$\sigma^2 = \int S_u(f) df \quad 2.6$$

$$\frac{f S_u(f)}{\sigma^2} = \frac{4 \left(\frac{f L_u}{\bar{u}} \right)}{\left[1 + 70.8 \left(\frac{f L_u}{\bar{u}} \right)^2 \right]^{5/6}} \quad 2.7$$

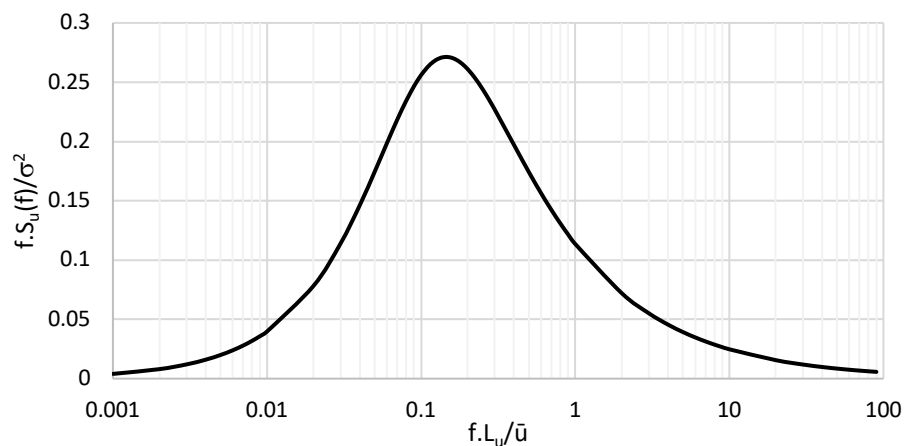


Figure 2.2 – Normalised von Kármán spectrum of longitudinal component of velocity.

2.2 CLASSIFICATION OF EXTREME WINDS

The need to separate wind events by storm type for modelling of extreme wind climates was recognised by Gomes and Vickery (1977), who proposed separation between extensive, extra-tropical pressure systems (EPS), thunderstorms (TS), tropical cyclones (TC) and tornadoes. Despite this, national and international wind load codes have, until now, only prescribed models for the analysis of ABL winds, best represented by EPS in the classification framework of Gomes and Vickery (1977/1978). The need to separate wind events by type is due to their different vertical profiles of mean wind speed and turbulence intensity, turbulence spectrum, gust factors and frequency of occurrence.

Brazil has been adversely affected by all four wind types defined by Gomes and Vickery (1977/1978) over the course of recent history and its extreme wind climate is classified as mixed (Loredo-Souza, 2012). Destruction caused by extreme winds in Brazil between 1961 and 2001 was extensively documented by Blessmann (2013). Although tornadoes are frequently observed in Brazil (Silva Dias, 2011), field measurements detailing valuable information on their structure is scarce. Efforts are presently underway by the American Society of Civil Engineers/Structural Engineering Institute (ASCE/SEI) in the development of a standard for the estimation of tornado design wind speeds (Womble et al., 2016). Hurricane Catarina, which damaged approximately 40,000 homes and caused fatalities in southern Brazil in March, 2004, is the only known TC to have made landfall in Brazil (McTaggart-Cowan et al., 2006; Blessmann, 2013). Due to little information from field measurements of these two wind types in Brazil, their respective extreme wind climates were not considered in this study. As such, the study focusses on the development of extreme wind climates for *synoptic* and *non-synoptic* winds. The basic characteristics of synoptic winds were described in Section 2.1 *Fundamentals*.

Weather occurs over varying distances and time periods, with meteorological scales often split into three groups: planetary scale, synoptic scale and mesoscale. *Planetary scale* systems are the largest and occur for the longest period of time, typically over tens of thousands of kilometers for periods greater than a week. The polar vortex and westerly trade winds of the mid-latitudes (30° to 60°) are two examples of systems on the planetary scale. *Synoptic scale* weather systems act over distances from hundreds to thousands of kilometers, from periods ranging from days to a week or more. Air masses, whether hot/cold or wet/dry, high- and low-pressure systems, jet streams, fronts (major axis), and cyclones are common synoptic scale

phenomena. *Mesoscale* systems range from a few kilometers to hundreds of kilometers in size, typically for a duration of less than a day. Thunderstorms, tornadoes, mesoscale convective systems (MCS), downslope winds and fronts (minor axis) are common mesoscale phenomena.

As suggested by the context of the meteorology scales explained above, synoptic winds are those acting over synoptic scale, but also include wind storms within the planetary scale, whereas non-synoptic winds are considered mesoscale events. The synoptic vs non-synoptic classifying system is used by Holmes (2002) and Durañona (2015). Although the classification nomenclature varies between researchers, their objectives are typically aligned to separate fully-developed ABL winds (synoptic) from outflow winds of severe convective storms (non-synoptic). Some common nomenclature alternatives include EPS vs TS (Riera et al., 1977; Gomes and Vickery, 1977/1978), TS vs non-TS (Choi and Hidayat, 2002; Lombardo et al., 2009); frontal depression vs TS (Kasperski, 2002; De Gaetano et al., 2014). Some have also identified the need to determine models for extreme winds caused by gust fronts (Kasperski, 2002; De Gaetano et al., 2014; Durañona, 2015)

One main difference between synoptic and non-synoptic winds is the vertical profile of horizontal wind speed. Only two current codes, ISO 4354 (2009) and AS/NZS 7000 (2010), specify vertical wind profiles of non-synoptic winds as shown in Figure 2.3. AS/NZS 7000 (2010) is used in the design of overhead power lines in Australia and New Zealand and is based on the Australian and New Zealand wind code, AS/NZS 1170.2 (2011). Figure 2.3 demonstrates the fundamental difference between the non-synoptic and synoptic vertical wind speed profiles, as well as divergence non-synoptic wind models. The flows interact differently with the surface of the earth: whilst the magnitude of the synoptic profile increases with height, the wind speeds of the non-synoptic profile peak at a certain height above ground. This fundamental difference, amongst others, is explained in more detail over the following sections.

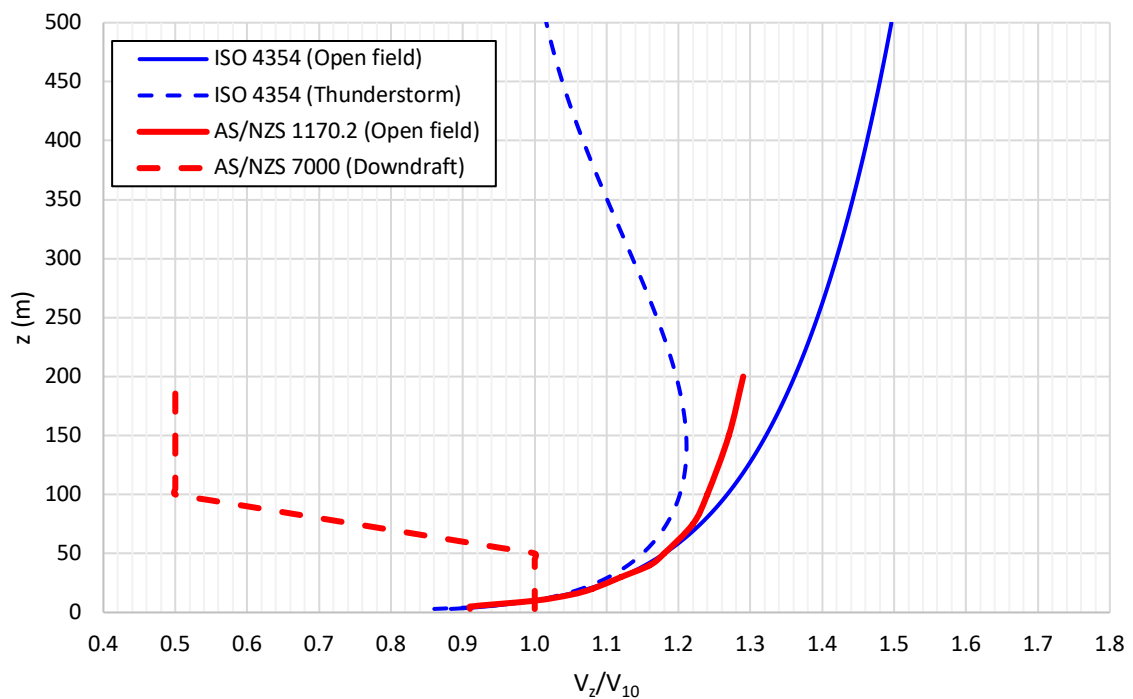


Figure 2.3 – Synoptic and thunderstorm profiles vertical wind speeds reference to wind speed at $z = 10\text{m}$ (ISO, 2009; AS/NZS 2010; AS/NZS 2011).

2.2.1 Synoptic winds

Deaves and Harris (1978) detailed the characteristics of incident wind that, until quite recently, were adopted in most codes and wind engineering applications. Data obtained from synoptic events in northern Europe were synthesised and analysed to produce mean wind speed profiles, turbulence profiles, gust factors and turbulence spectrum which act as the basis of many of current day wind codes. Hence, the synoptic model of Deaves and Harris (1978) is valid for the following set of conditions:

- a strong and steady wind with stationary statistical properties (mean, standard deviation and autocorrelation are constant over a given period);
- neutral atmospheric stability (air parcels do not continue to rise if displaced upwards);
- flat over-land terrain;
- sufficient fetch length, or upwind distance, of uniform roughness to ensure equilibrium flow.

Strong winds which adhere to the conditions above are often referred to as ABL winds and are herein referred to as synoptic winds. The boundary conditions of this model adhere to the

non-slip condition at the earth's surface ($\bar{u} = 0$ at $z = 0$ m), and free-stream speed at the gradient height ($\bar{u} = \bar{u}_\infty$ at $z = z_g$). Models based on logarithmic or power laws are used to express the vertical profile of horizontal wind speed from $z = 0$ to $z = z_g$, and vary depending on the roughness of upstream terrain, z_0 (m), and time-averaging interval, τ . These profiles are often normalised by a reference wind speed, typically at a height of $z = 10$ m in open country terrain, and $\tau = 3$ s, 10 min or 1 hr.

Low-pressure EPS and cyclones are responsible for most destructive synoptic winds. In the southern hemisphere, these low-pressure systems cause winds to blow towards the centre of the system while circulating in a clockwise direction; conversely, high-pressure systems cause winds to blow outward from the centre while rotating in an anti-clockwise direction, also referred to as anti-cyclones. The circulating directions are reversed in the northern hemisphere. Low-pressure systems lift air upwards to higher levels of the atmosphere and are associated with cloud formation and precipitation. High-pressure systems bring air from higher altitudes towards the surface and are associated with clear conditions. Cyclones are split into three main categories: Extra-tropical cyclones, TC and subtropical cyclones.

2.2.1.1 Extra-tropical cyclones

Extra-tropical cyclones are referred to by a number of different names, including mid-latitude cyclones (they are commonly encountered between latitudes of 30° to 60°), depressions, frontal cyclones and frontal depressions. Cyclogenesis of extra-tropical cyclones can occur over both land and ocean and involves interaction between warm and cold fronts, with the energy supplied by the horizontal temperature gradient. The stages of cyclogenesis according to polar front theory are shown in Figure 2.4. Jet streams circulate the globe and operate at heights of 9 to 16 km within the troposphere. They blow from the west to the east and are located along latitudes where warm and cold fronts meet. Two distinct jet streams operate in each hemisphere: the subtropical jet stream and polar jet stream. Typically, a warm front moves poleward while a cold front dislocates towards the equator. If they meet head on, a stationary front is created (A of Figure 2.4). Perturbations in the jet stream, called Rossby waves, initiate a bend or wave in the stationary front (B), which causes a low-pressure region at the surface (C). The denser cold front moves faster than the warm front and circulates behind it to cause an occluded front (D). The warm air is lifted upward over the cold air and generates precipitation and storms. At this point the cyclone is mature and will most likely be

drifting from west to east and poleward. The removal of the cyclone from its warm air source causes an eventual dissipation of the cyclone, referred to as cyclolysis (E).

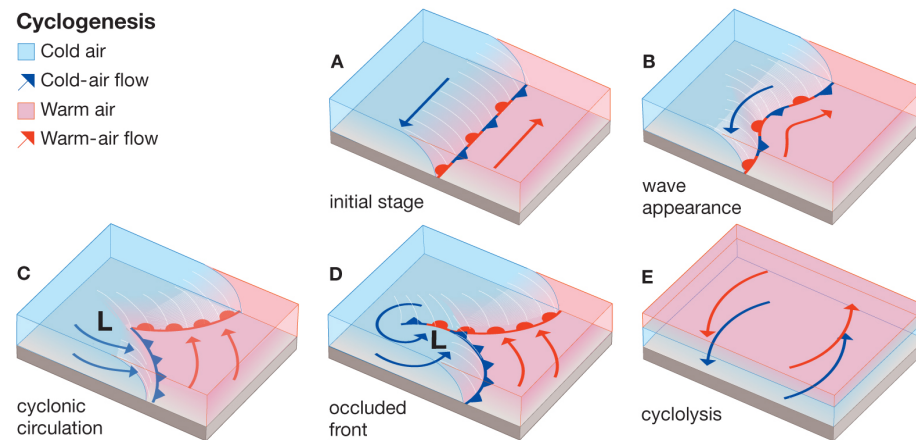


Figure 2.4 – Development of an extra-tropical cyclone in northern hemisphere (Encyclopedia Britannica, 2010)

An example of a severe extra-tropical cyclone which affected Brazilian territory is documented in Figure 2.5 and Figure 2.6. Gusts between 10-30 m/s were observed for almost 48 hours over 27-28/10/2016 by the INMET ASWS at A899 – Chuí, RS, located at Brazil's southern-most point. The satellite image in Figure 2.5 shows the classic comma shape associated with extra-tropical cyclones. The clear region of the cyclone is dry air drawn down from the upper levels of the atmosphere.

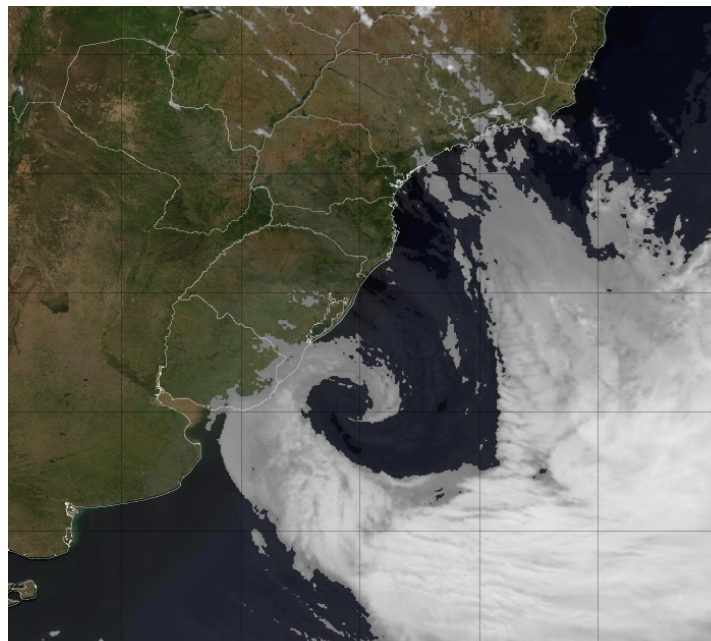


Figure 2.5 – GOES-13 Satellite imagery of extra-tropical cyclone at 16:30 UTC, 27/10/2016 (CPTEC-INPE, 2018)

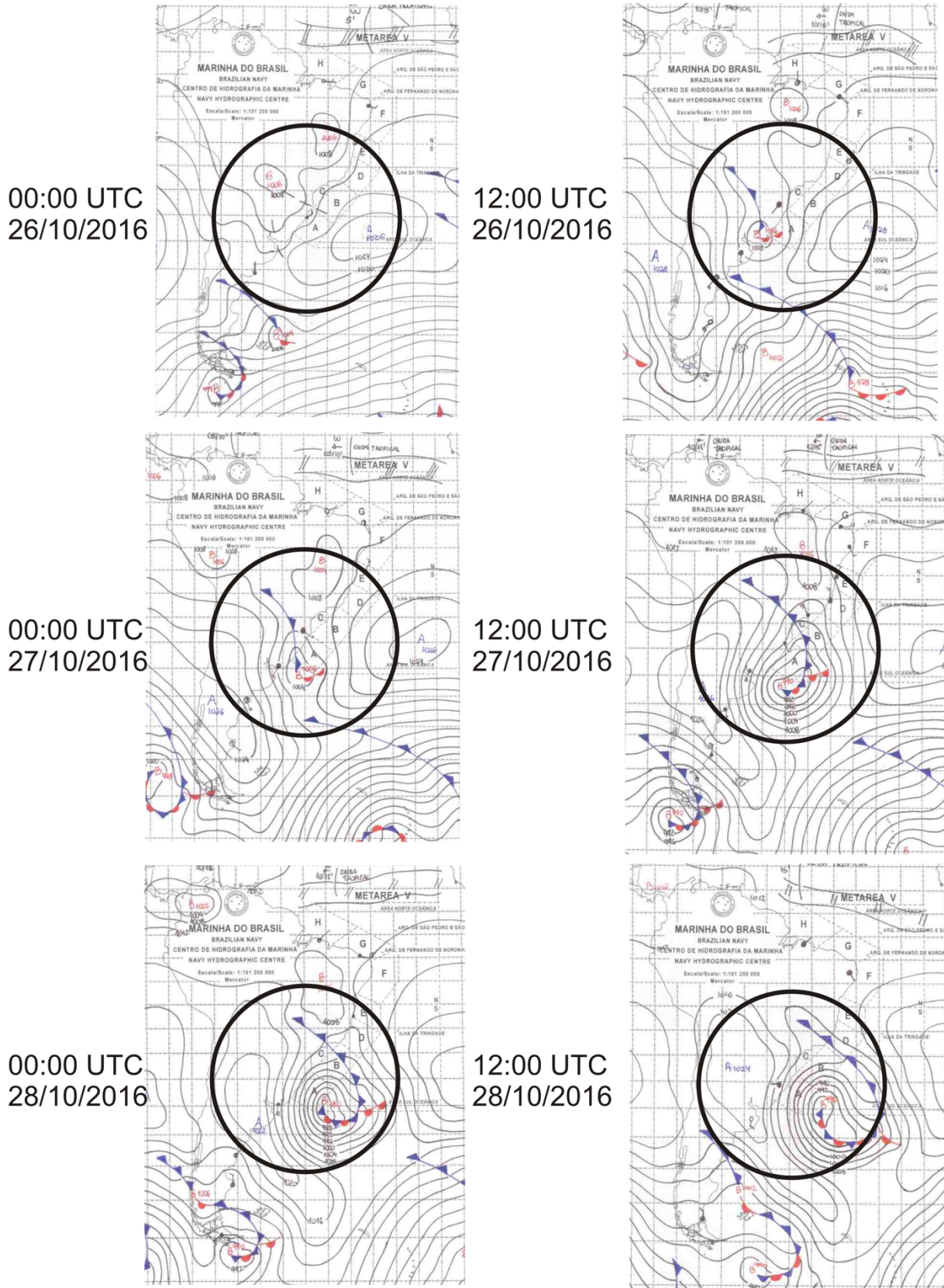


Figure 2.6 – Synoptic charts showing the cyclogenesis and growth of an extra-tropical cyclone over southern Brazil and Uruguay, 26-28/10/2016 (Centro da Hidrografia da Marinha, 2018)

Synoptic charts prepared by the Brazilian Navy of the same event are shown in Figure 2.6. Although no stationary front is observed, these charts show clearly the maturing stages (B) and (C) from Figure 2.5. Despite the low temporal resolution of the charts (12 hr intervals), the large extent and long duration of the cyclone is observed, as well as its progress east and poleward. Within the same set of synoptic charts, two distinct extra-tropical cyclones are also observed moving from west to east over Patagonia and the southern extents of the Atlantic Ocean, which are related to cyclogenesis initiated by the polar jet stream.

Subtropical and polar jet streams are strong influences on the cyclogenesis of extra-tropical cyclones in the southern half of South America, as shown in Figure 2.7 to Figure 2.9. The Southern Hemisphere's jet stream was studied in detail by Gallego et al. (2005) while Mendes et al. (2009) developed a climatology of South American extra-tropical cyclones. Figure 2.7 reveals the winter season as having the strongest subtropical jet stream acting over latitudes from -20° to -40° . The polar jet stream is strongest in spring for latitudes from -50° to -60° . In summer and autumn, a single jet stream is predominant as shown in Figure 2.8, suggesting the subtropical jet stream is almost inexistent during the peak of summer.

The dominant paths of the jet streams in Figure 2.7 and Figure 2.8 correlate to the most frequent extra-tropical cyclogenesis locations shown in Figure 2.9. The highest number of cyclogenesis events is found during winter between latitudes -30° to -45° , in the lee region of the Andes. For all seasons, the majority of cyclogenesis events occur off the east coast of the northern half of Argentina and Uruguay but still several registered cyclogenesis events on the continent and within southern Brazil.

Extra-tropical cyclones formed on the continent typically generate lower wind speeds than when over large bodies of water, such as oceans. This is due to the reduced roughness and lower friction offered by water compared to land surfaces. Cyclones which present rapidly falling pressure at the core tend to be the most destructive and are referred to as "bombs". Such rapid cyclogenesis is encountered in the regions of South America identified in Figure 2.9, as well as other southern hemisphere regions such as southeast of Australia, east of New Zealand and southeast of Africa (Durañona, 2015). These areas are all leeward of mountain ranges, and the lee cyclogenesis is most explosive when over the bodies of water adjacent to land. Although extra-tropical cyclones are synonymous with synoptic winds, convective cells can be found within the warmer regions of a cyclone (Wallace and Hobbs, 2006).

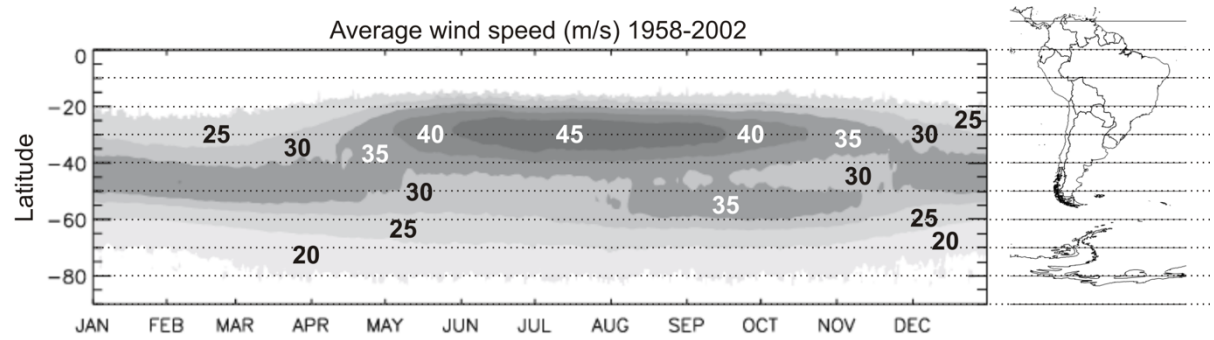


Figure 2.7 – Annual evolution of jet stream winds (adapted from Gallego et al., 2005)

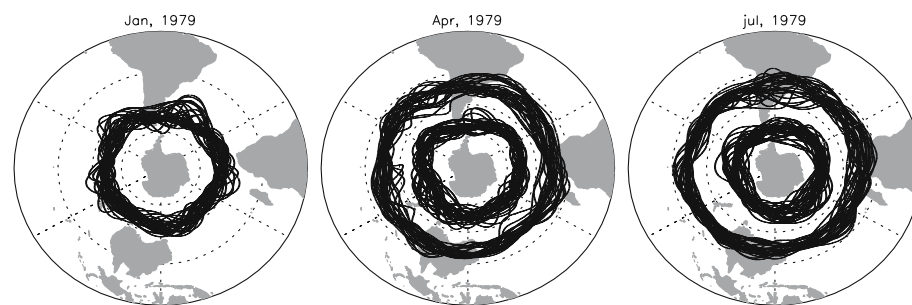


Figure 2.8 – Cumulative jet path for January, April and July of 1979 (Gallego et al., 2005)

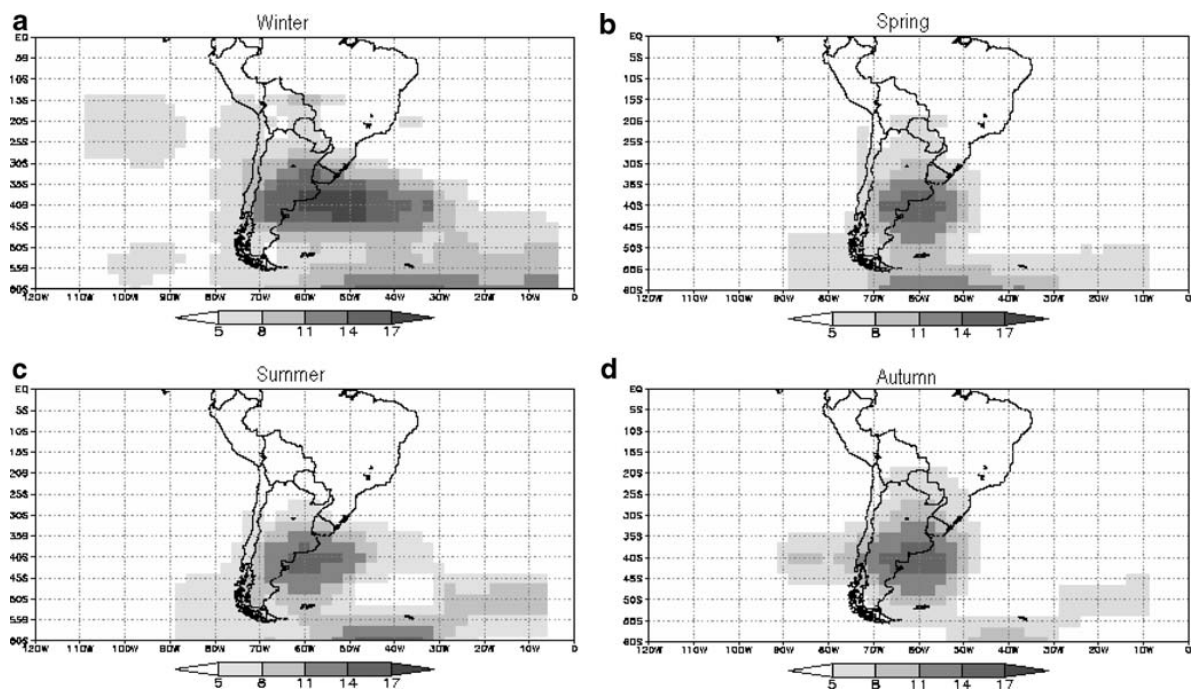


Figure 2.9 – Number of cyclogenesis events detected between 1979 and 2003 (Mendes et al., 2009)

2.2.1.2 Tropical and subtropical cyclones

Although defined as two distinct phenomena, tropical and subtropical cyclones are grouped together in this study due to their close association within Brazil's climatology. The only recorded tropical cyclone to make landfall on the continent, Hurricane Catarina, was initially a subtropical cyclone.

Tropical cyclones are warm-core systems that only form in warm regions of the ocean. They are referred to by different regional names, such as *hurricane* in the Atlantic Ocean and Eastern Pacific Ocean, *typhoons* in the Western Pacific Ocean adjacent to Asia and simply *tropical cyclones* in the rest of the Indian Ocean and Southern Pacific Ocean. Subtropical and TCs are separated from extra-tropical cyclones when developing extreme wind climate models due to the difference in frequency of occurrence and wind speeds. Extra-tropical cyclones are more frequent than subtropical and TCs which produce peak wind speeds of higher magnitudes.

A minimum water temperature of 26°C from the surface to a depth of around 60 m is needed to sustain TCs. Cyclogenesis occurs at latitudes greater than 5° due to the Coriolis effect; for latitudes less than 5° the Coriolis effect is not strong enough to cause the wind to rotate in a vortex manner. In addition to the necessary warm body of water with warm and moist air located above, and a location far enough away from the equator to cause spin, low-levels of wind shear are also required for tropical cyclones to form. The lack of wind shear allows for moist columns of air to rise and form convective cells. While the air is rising the Coriolis Effect causes the column to rotate (when viewed from above, clockwise in the southern hemisphere and anti-clockwise in the northern hemisphere), and pressure at the surface decreases rapidly. TCs typically reach full strength at latitudes of between 20-30°.

TCs tend to degenerate and lose momentum once making landfall or moving to cooling waters. The loss of its energy source, the rising moist air from the warm ocean, and the increased roughness of land combine to cause the weakening of the cyclone and reduction of wind speeds. The horizontal distances of a mature TC are less than those of extra-tropical cyclones but can act over several hundred kilometres at any given time (Holmes, 2015). Although similar in shape to extra-tropical cyclones, TCs are closer in shape to perfect circles due to their closed-system nature and lack the dry current of air which gives extra-tropical cyclones their comma shape.

A simplified structure of TC is shown in Figure 2.10. Air is drawn radially towards the eye at the centre of the system, with the highest winds speeds observed just outside the eyewall located immediately at its boundary. Calm conditions are observed within the eye due to the slowly descending air, with the diameter ranging anywhere between 8 to 80 km. The eyewall is characterised by intense convection, precipitation and rapidly rising warm air. The highest wind speeds are found just outside the eyewall due to convergence of the sinking air within the eye and the air drawn radially towards the eye from beyond. Concentric rings of rainbands are formed further out from the eye and are capable of producing downdrafts as well as tornadic winds once reaching the continent, with updrafts occurring in the zones between the rainbands. The intensity, or maximum sustained wind speeds, of TCs are classified according to the Saffir-Simpson scale as shown in Table F.4 of Appendix F *Assorted Tables*. The Saffir-Simpson scale is based on typical observed wind speeds and destruction, and is used to classify hurricanes in the Atlantic, Caribbean and northern Pacific Ocean east of the International Date Line. Two precursor categories are also defined: tropical depressions with intensity of 17.0 m/s or less, and tropical storms with intensity of between 17.5 m/s and 33.0 m/s.

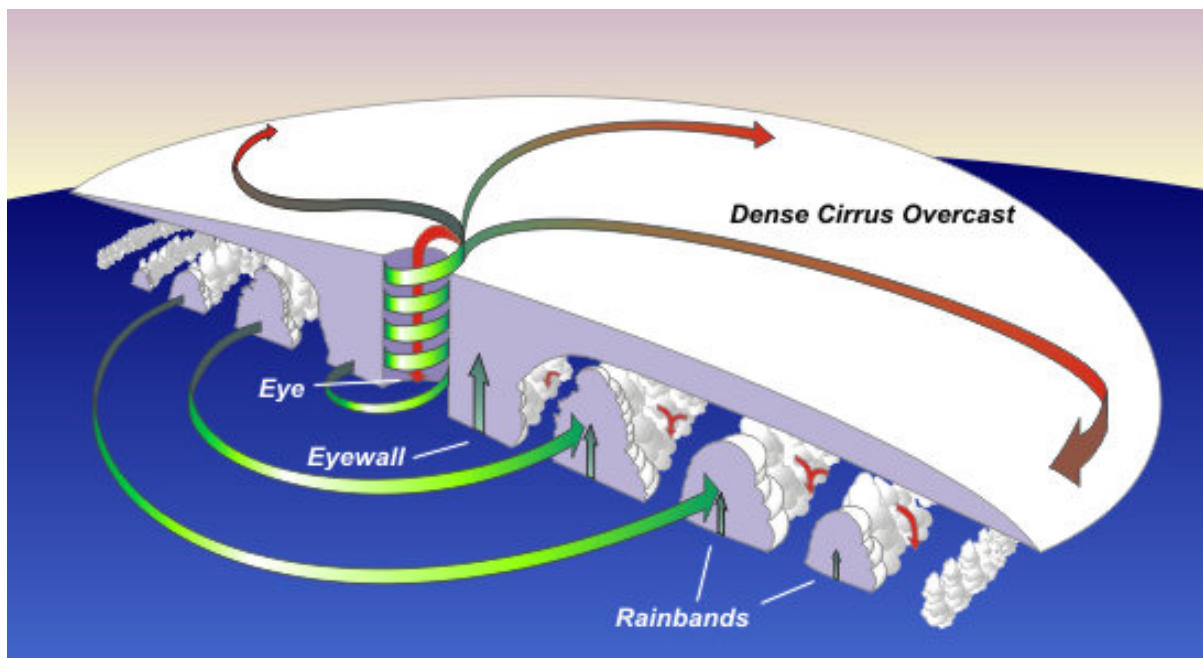


Figure 2.10 – Simplified structure of a tropical cyclone in northern hemisphere¹

¹ https://www.weather.gov/jetstream/tc_structure

The lack of TC activity in the eastern South Pacific and western South Atlantic oceans which surround the majority of South America is demonstrated in Figure 2.11. Strong vertical shear and cool average water temperatures are responsible for the lack of TC activity in the South Atlantic (Pezza et al., 2009). Evans and Braun (2012) identified the cold Malvinas Current, which prevents the poleward drift of the warm Brazilian Current, to be much stronger than its North Atlantic equivalent.

Figure 2.11 shows the lone track of Hurricane Catarina, 2004, whose trajectory is adjacent to the southern Brazil coastline. Catarina began as an extra-tropical cyclone and tropical transition occurred on 23/03/2004 when it reversed direction from its south-eastward track and headed back towards Brazil (Pezza and Simmonds, 2005; McTaggart-Cowan et al., 2006). Catarina became a Category 1 hurricane on March 26 and reached its peak intensity on March 28, with Category 2 maximum winds estimated at 44 m/s (McTaggart-Cowan et al., 2006). The total path and intensity of Hurricane Catarina are shown in Figure 2.12, with evidence of its impact given in Figure 2.13.

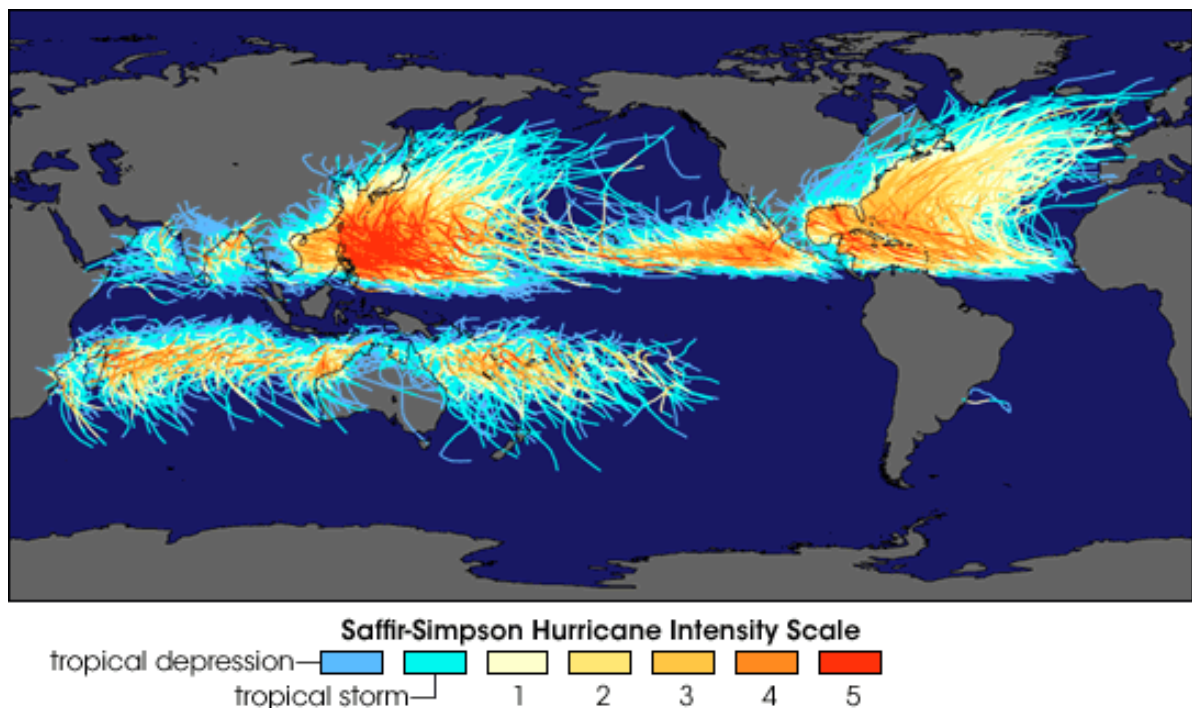


Figure 2.11 – Tracks of all tropical cyclones as recorded by the National Hurricane Center and the Joint Typhoon Learning Center from 1945 to 2006².

² <https://earthobservatory.nasa.gov/images/7079/historic-tropical-cyclone-tracks>

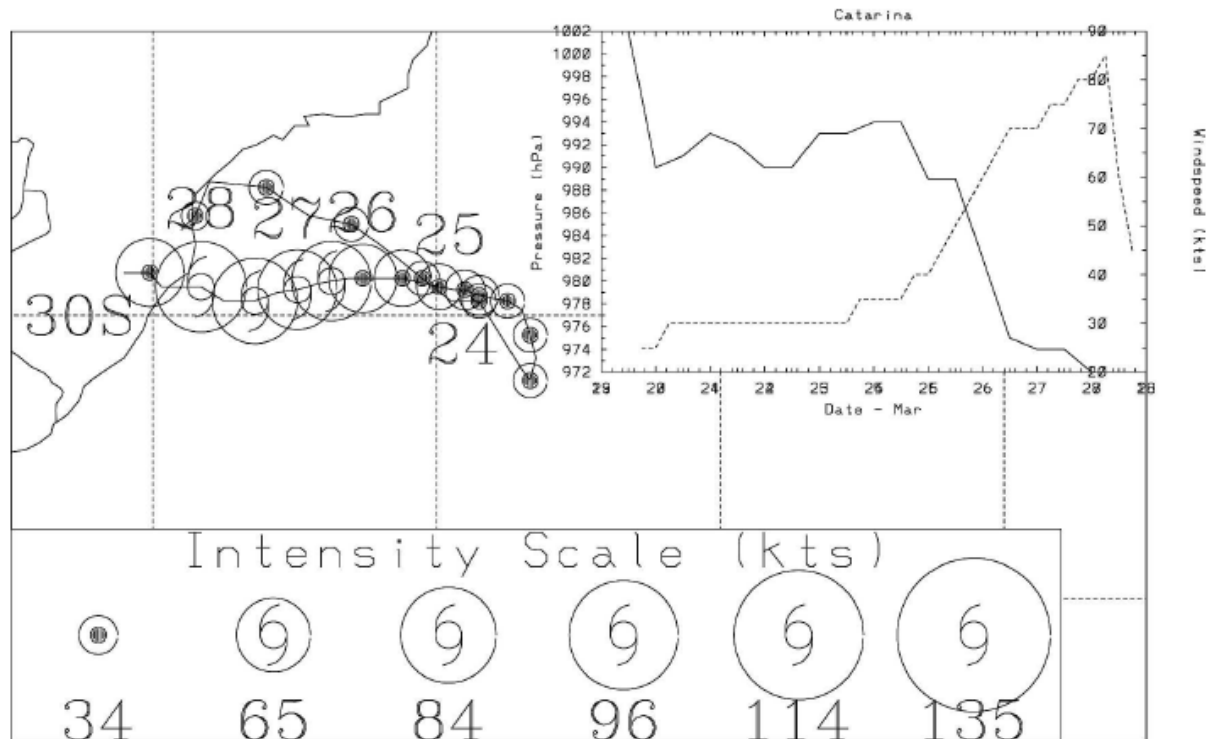


Figure 2.12 – Path and intensity of Hurricane Catarina (McTaggart et al., 2006)

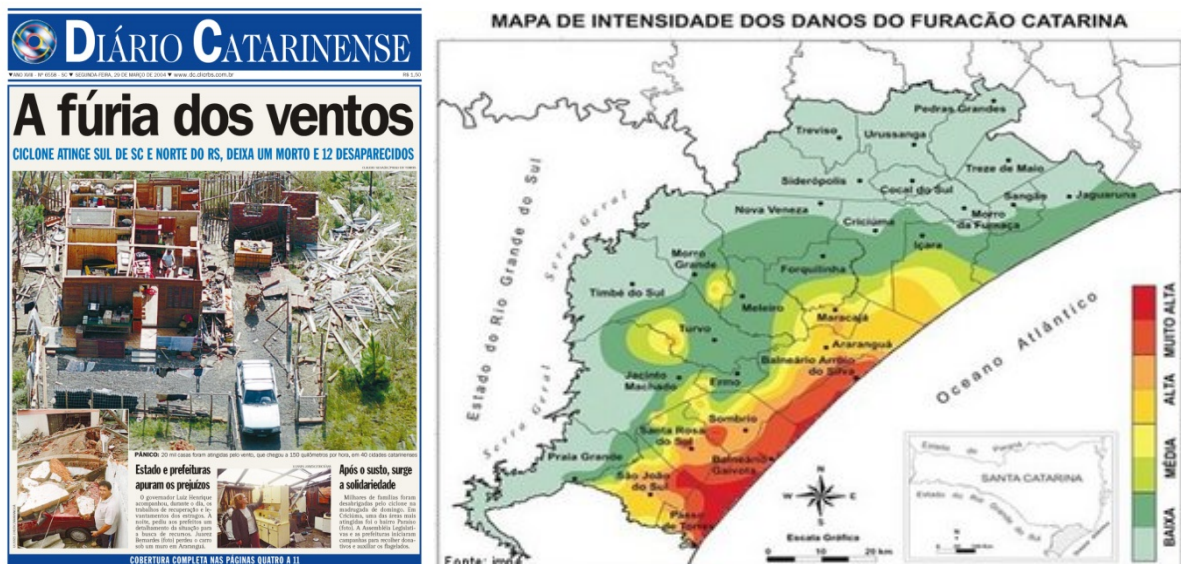


Figure 2.13 – Front page of *Diário Catarinense* newspaper showing destruction caused by Hurricane Catarina (left); Map of the Santa Catarina regions most affected by Hurricane Catarina³ (right).

³ <http://www.geografia.seed.pr.gov.br/modules/galeria/detalhe.php?foto=512&evento=5>

Subtropical cyclones are considered hybrids of extra-tropical and TCs. Like TCs, they are non-frontal, however temperature at the core varies: cold core at the upper-level and warm core at the lower-level. From a study of 63 subtropical cyclones in the South Atlantic Ocean between August 1957 and December 2007, Evans and Braun (2012) determined that the majority were formed in the coastal zone influenced by the warm Brazil Current. It is also suggested that the Andes mountain range is responsible for lee cyclogenesis, and combined with the warm Brazil Current, provide favourable conditions for subtropical cyclogenesis.

Subtropical cyclone Eçaí was responsible for extensive damage to Florianópolis, SC, and surrounding areas on 04/12/2016. Subtropical cyclones in the region do not typically reach maturity (maximum wind speeds) until further off the coast and wind speeds on land are not normally as severe, however in this case the system matured over the island of Florianópolis and extreme winds were experienced in the state capital⁴. A maximum observed gust speed of 64 kt (32.9 m/s) was recorded at aerodrome SBFL – Florianópolis. Time-series of relevant wind speed and meteorological data of the event are plotted in Figure D.28 of Appendix D *Event Classification Algorithms and Examples*.



Figure 2.14 – Damage caused by subtropical cyclone Eçaí along Santa Catarina coastline, 04/12/2016. Photos taken by Elvis Palma (left) and Rafael Vieira (right).

In addition to the two unprecedented landfall events of Hurricane Catarina and subtropical storm Eçaí, other tropical/subtropical anomalies were recently observed. In 1991, a tropical storm formed off the coast of Angola becoming the first tropical system observed by satellites in the South Atlantic, and remains the only such event recorded in the eastern South Atlantic (Loredo-Souza, 2012). Tropical storm Anita formed in March, 2010, off the southern coast of

⁴<http://dc.clicrbs.com.br/sc/noticias/noticia/2016/12/ciclone-subtropical-foi-causa-de-estragos-pelo-estado-8610795.html>

Brazil, but moved eastward. Subtropical cyclone Lexi formed off the coast of Chile in May, 2018, becoming the first subtropical cyclone to ever form in the eastern South Pacific. More recently in March, 2019, tropical storm Iba formed off the coast of Bahia and Espírito Santo before moving southeast.

2.2.2 Non-synoptic winds

If synoptic winds are defined by the four ABL criteria of Deaves and Harris (1978) listed in Section 2.2.1 *Synoptic Winds*, non-synoptic winds may be defined as those which do not meet the four criteria. In reality, there are many types of wind with intermediary characteristics, and the focus of non-synoptic winds in this study is on those which are driven by deep convection with outward flows from downdrafts.

2.2.2.1 Deep, moist convection

Atmospheric stability is when the vertical motion of air *parcels* is restricted; an instability is present when parcels are displaced vertically. Convection refers to the vertical transportation of parcels of air heated near the earth's surface. Doswell (2001) and Markowski and Richardson (2010) use the term *deep, moist convection* to describe convective storms and recognise that, although most are harmless, they have the potential to cause severe weather such as thunder, lightning, hail, rain and extreme winds. This term is preferred to *thunderstorm*, as severe weather can be caused by non-thundering convection. Severe weather is typically the result of the energy released from the phase change of water and damaging straight-line winds within convective storms are associated with the precipitation-cooled outflow which is led by the gust front. According to Markowski and Richardson (2010), there are three different types of non-tornadic extreme winds associated with convective storms:

1. intense meso- γ -scale (2-20 km) downdrafts, better known as *downbursts*;
2. weaker downdrafts that carry large horizontal momentum, such as the descent of a rear-inflow jet to the surface;
3. meso- β -scale (20-200 km) cold pools associated with horizontal pressure gradients large enough to cause damaging winds in the absence of strong downdrafts.

However, both item 1 and 2 of the above are considered downbursts by Wakimoto (2001). Convective available potential energy (CAPE), measured in J/Kg, is the amount of energy a parcel would have if lifted a certain distance. The measurement of CAPE is crucial to the

prediction of severe weather and is considered one of the best indicators of the presence of atmospheric instability. CAPE is determined via thermodynamic diagram, referred to as a sounding, using air temperature and dew point data acquired by weather balloon, satellite, or radiosonde.

Three essential ingredients are needed for the generation of convective storms: moisture, lift and a large decrease in air temperature vertically (high lapse rate). A simplified lifecycle of a single storm cell is shown in Figure 2.15. As a parcel of moist air at the surface is heated, its density decreases, causing the parcel to expand and rise. Widespread lifting may also be achieved by gust fronts, cold fronts and topographical features. The upward motion, the updraft, cools the air parcel, and the moisture within condenses to form water droplets within cumulonimbus clouds. At a critical point, the updraft is no longer able to support the weight of the particles which then start to descend. The particles undergo phase changes, mostly evaporation, which cools the surrounding air to induce negative buoyancy and the cooled air accelerates towards the surface of the earth. The system acts as a heat exchanger, with the warm air eventually being replaced by a downdraft of cold air which alleviates the instability at the earth's surface (Doswell, 2001).

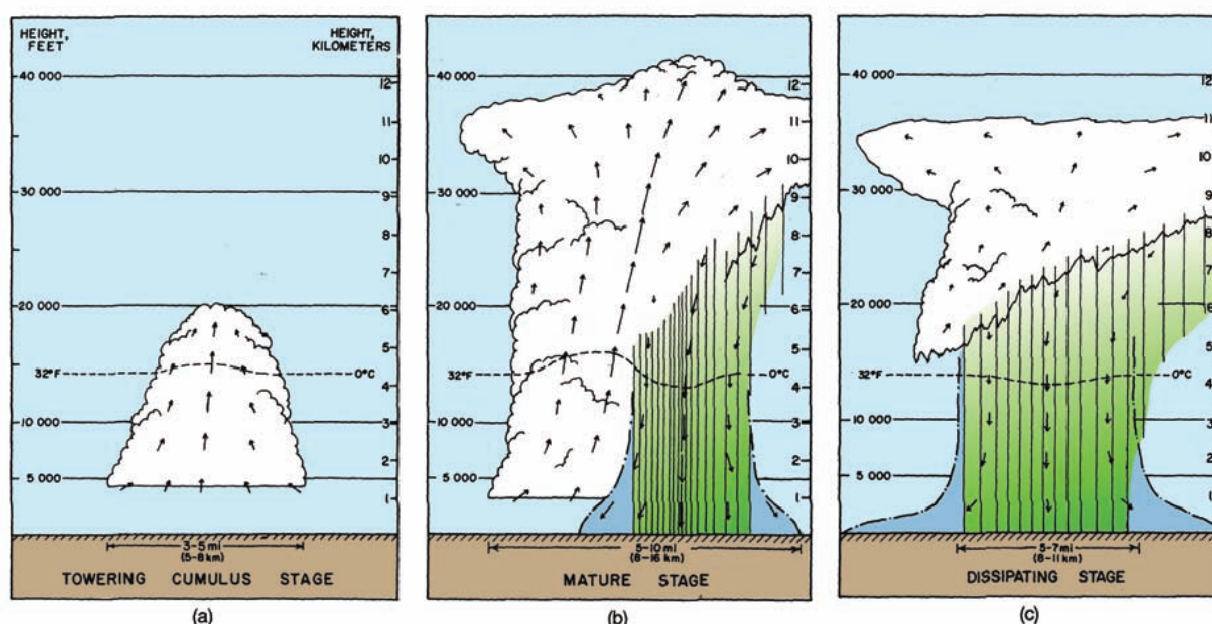


Figure 2.15 – Three stages of an ordinary, single-cell a) towering cumulus stage, b) mature stage, c) dissipating stage (Markowski and Richardson, 2010).

Storms are typically organised in terms of size and structure (Markowski and Richardson, 2010). Some occur in isolation and are discrete, whereas others occur within large complexes

or lines. Isolated convection is typically split into three sub-classifications: single-cell, multicellular and supercell. Single-cell convection consists of only one updraft and severe outflow wind gusts are short lived and rarely pass 25 m/s. Multicellular is the most common form of convection in mid-latitudes, characterised by the replacement of old cells with new cells along the gust front. Each cell has a lifespan of typically 30-60 min with the most severe multicellular storms lasting hours. Supercells are the least common but are the most dangerous. Supercells are characterised by a single dominant updraft, have a long lifespan of between 1-4 hours (some until 8 hours), and have two downdraft regions: rear-flank and forward-flank. Large hail and damaging downbursts are typically associated with heavy precipitation supercells, with most destructive tornadoes generated by supercells.

Vertical wind shear plays a key role in the lifespan of a convective storm. In situations with no, or very low vertical wind shear, the outflow of a storm is unable to lift humid air above the cold pool as represented in Figure 2.16a). The inflow which feeds the updraft is cut-off and the storm's intensity diminishes. However, with vertical shear, the horizontal vorticity is stronger at the leading edge of the outflow boundary, causing warm and humid air to be lifted up and initiate new storm cells, as shown in Figure 2.16b).

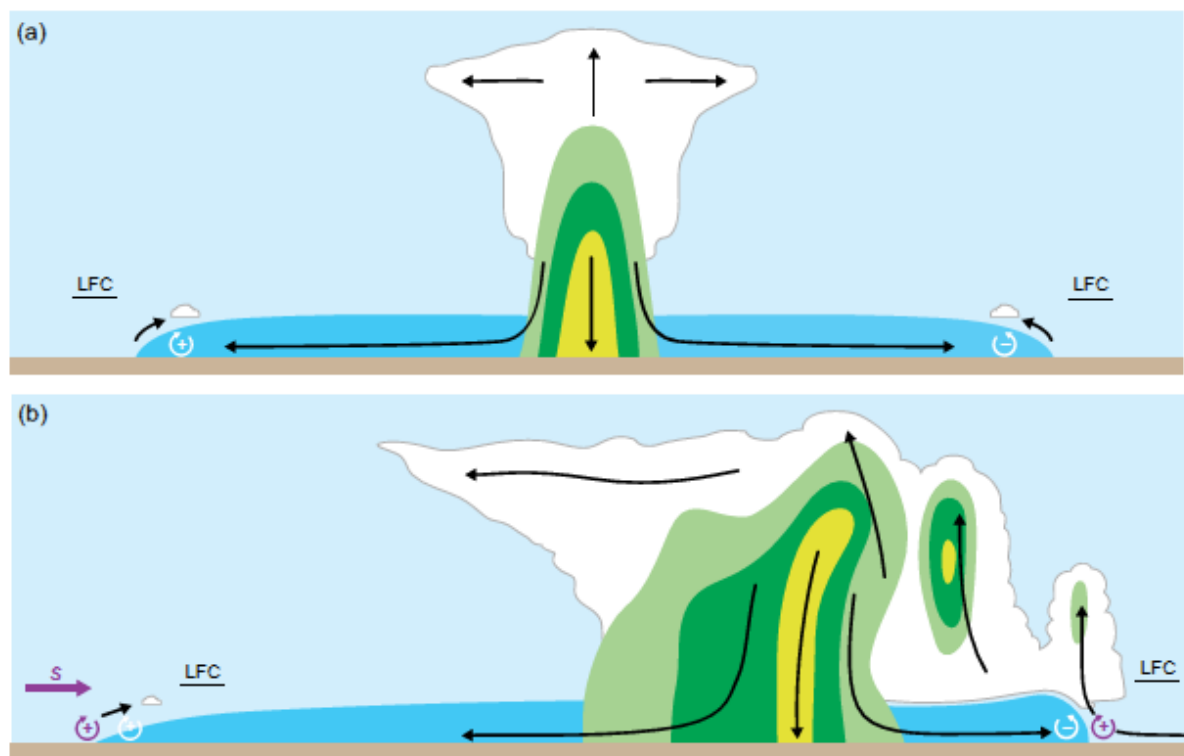


Figure 2.16 – Lifting of gust front in a) isolated cell with no wind shear b) multicellular storm with moderate wind shear (Markowski and Richardson, 2010).

Any grouping of convective systems greater than 100 km in horizontal scale is referred to as a mesoscale convective system (MCS) and most MCSs can be regarded as multicellular convection. A diagram showing the various types and classifications of MCS is given in Figure 2.17. Sizes of sub-classifications in Figure 2.17 are not representative – only the overlapping and positions. Squall lines are organised linearly, while bow echoes are arc-shaped structures within squall lines. Multiple bows embedded within a single line form a line-echo wave pattern, while mesoscale convective complexes (MCCs) have a fairly circular anvil – the upper part of the cloud. Some squall lines and bow echoes are not classified as MCS due to horizontal length scales less than 100 km (Markowski and Richardson, 2010).

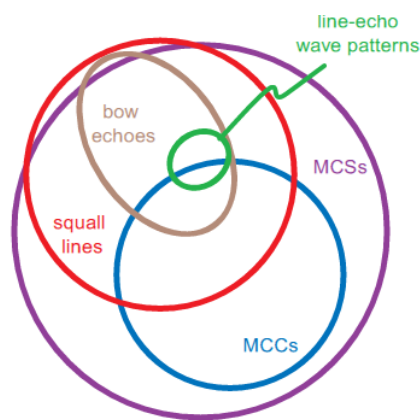


Figure 2.17 – Venn diagram of MCS sub-classifications (Markowski and Richardson, 2010).

The convective towers of squall lines are confined to the leading edge, with inflow lifted up by the gust front as shown in Figure 2.18. The intensity of the descending rear inflow is proportional to the intensity of the squall line.

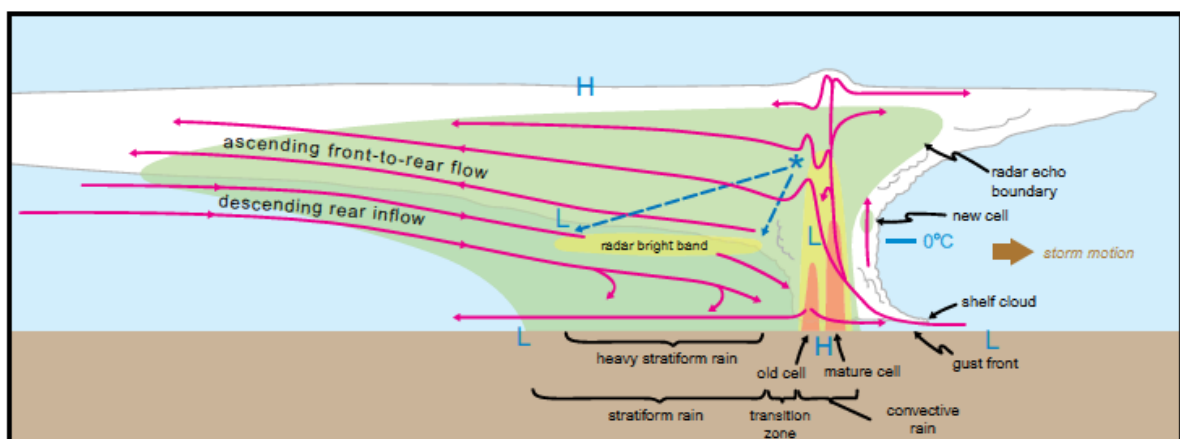


Figure 2.18 – Cross-section conceptual model of squall line (Markowski and Richardson, 2010).

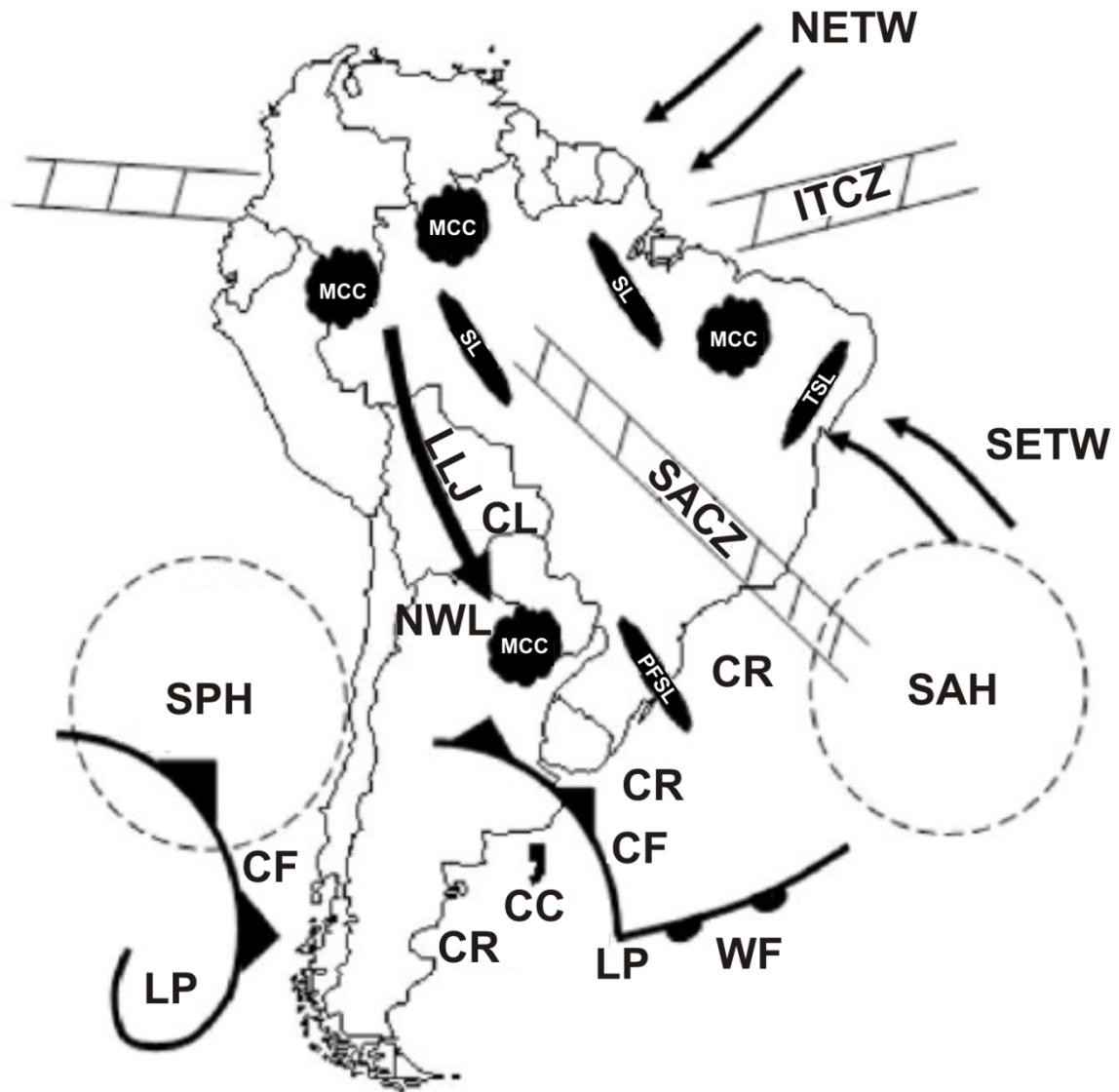


Figure 2.19 – Representation of the main lower troposphere weather systems in South America. CC – comma cloud, CL – Chaco Low, CF – cold front, CR – cyclogenesis region, ITCZ – Intertropical Convergence Zone, LLJ – low-level jet, LP – low-pressure region, MCC – mesoscale convective complex, NETW – Northeastern Trade Winds, NWL – Northwestern Argentina Low, PFSL – pre-frontal squall line, SAH – South Atlantic High, SACZ – South Atlantic Convergence Zone, SL – squall line, SETW – Southeasterly Trade Winds, SPH – South Pacific High, TSL – tropical squall line (adapted from Pes, 2015; Satayamurty et al. 1998; Reboita et al., 2012).

The main weather systems operating across South America are shown in Figure 2.19. The Rio de la Plata Basin, the region including northern Argentina, Paraguay, Uruguay and southern Brazil, is home to some of the world's most intense convective storms (Zipser et al., 2006). Along with the central region of the United States, the region is subject to frequent large MCCs. MCCs in South America are closely related to the subtropical jet stream, which vary little geographically due the jet stream's quasi-stationary nature (Laing and Fritsch, 1997). The low-level jet (LLJ) which brings moisture from the Amazon basin to the area following the eastern edge of the Andes is identified as a main factor to the region's convective activity (Nascimento, 2005). Strong low-level wind shear and disturbances in the subtropical jet stream as it moves over the Andes cause the warm and moist low-level air to be lifted and become unstable due to the region's high lapse rate. The region is one of only two worldwide for which there are intense storms during all seasons of the year (Zipser et al., 2006), the other region is equatorial Africa. Southern Brazil is also affected by advancing cold, dry fronts, originating from polar air masses. These air masses generate pre-frontal squall lines which have the potential to generate damaging gusts from downbursts and other straight-line winds.

The South Atlantic Convergence Zone (SACZ) is a northwest-southeast aligned monsoonal region over mid-Brazil. The region is characterised by clouds, thunderstorms, heavy rain and convergent winds. The Intertropical Convergence Zone (ITCZ) is a similar region in the tropics where the northeast and southeast trade winds converge to create the monsoonal trough. Similar to SACZ, the region appears as a band of clouds which often produces convective storms.

2.2.2.2 *Convective storm straight-line winds*

Downdrafts do not always produce violent winds, but those that do are referred to as downbursts, coined by Fujita (1976) who was the first to differentiate them from tornadoes which were assumed as the responsible phenomenon for much of wind related damage. Fujita (1990) observed starburst patterns in fallen trees during 1970s, which were different from the meandering tracks of tornadoes. This previously undocumented pattern represented a divergent outburst from a jet of descending air, with damage paths either straight-lined or curved. The downburst is defined as a strong downdraft which induces an outburst of destructive winds at the earth's surface. Downbursts have horizontal dimensions less than 10 km (Markowski and Richardson, 2010) and are split into two groups based on size: the *microburst*, a small downburst with severe winds over a distance less than 4 km, and the

macroburst, a larger downburst with severe winds over a distance greater than 4 km (Fujita, 1990). Higher peak wind speeds are associated with the microburst, with typical durations between 5-30 min and wind speeds up to 75 m/s. Two types of microbursts are defined in accordance with the level of precipitation as shown in Figure 2.20, despite the lack of a relationship between rain intensity and ground wind speed. Wet microbursts occur with a low cloud base and accompanied by heavy rain and thunder. Dry microbursts can occur when the cloud base is high and the precipitation evaporates before reaching the earth's surface – a phenomenon called *virga*. A *heat burst* is a microburst-like phenomenon typically associated with decaying convective storms. The heat burst penetrates a shallow stable layer near the earth's surface, and dry and hot wind gusts are experienced at the surface, typically at night.

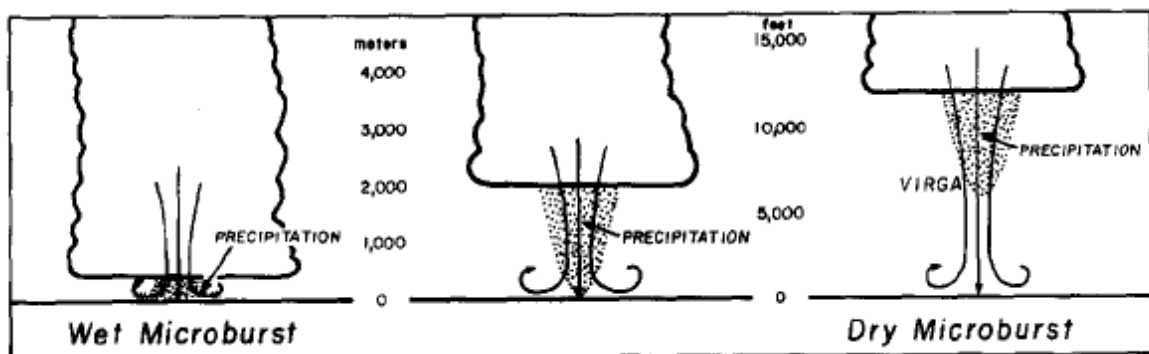


Figure 2.20 – Two types of microbursts in relating to cloud height and precipitation intensity (Fujita, 1990).

Schematic diagrams of downburst outflow are shown in Figure 2.21. A region of high pressure, the meso-high, is located at the base of the descending flow which is pushed outwards to create the outflow front shown in Figure 2.21a). The highest wind speeds occur near the surface and behind the advancing gust front. Figure 2.21b) shows the outflow in greater detail, with higher turbulence at the gust front boundary and cool, dense air lifting the warm air to continue the convective process. Figure 2.21c) shows the 3D nature of the downburst with the outflow boundary taking the form of a ring vortex. According to Fujita (1990), the strongest winds occur directly beneath the vortex axis and at a height of approximately 30-90 m above the earth's surface.

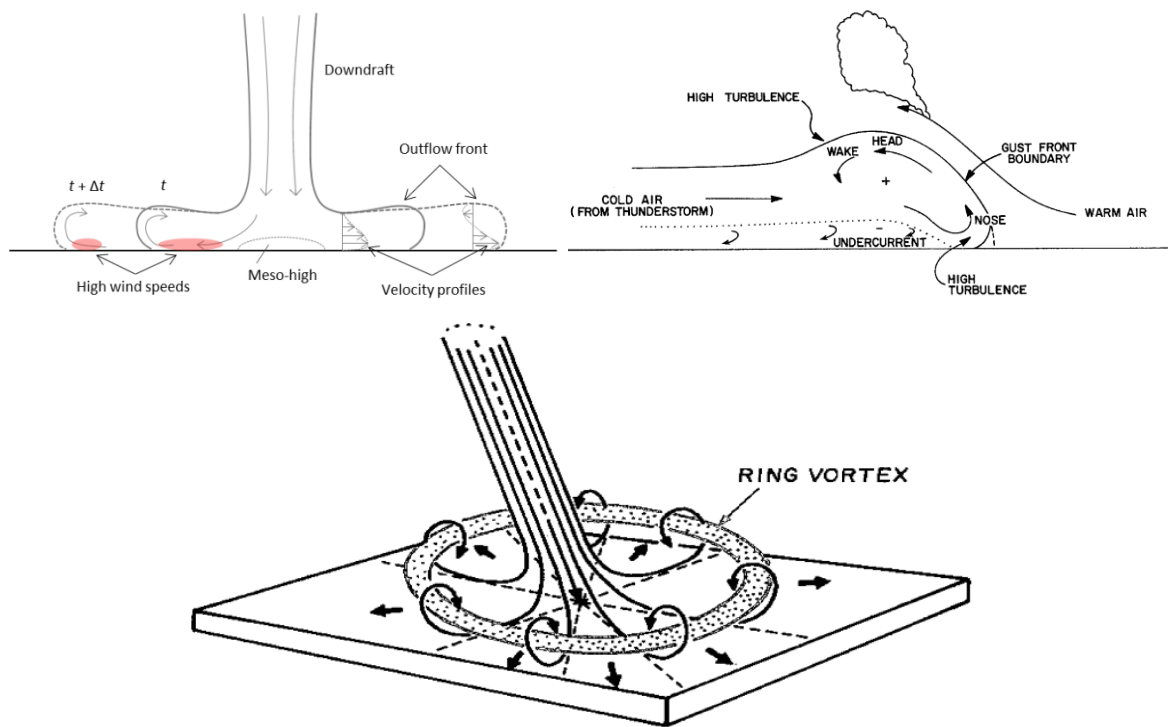


Figure 2.21 – Downburst outflow schematic diagrams: top left – Mason (2017); top right – Goff (1975); bottom – Fujita (1985).

A downburst originating from a supercell was believed to be the cause of damaging winds in Porto Alegre, RS, on the evening of 29/01/2016 (INMET, 2016). Damaging gusts persisted for an hour over the central business district of the city, with the peak gust of 33.2 m/s registered at INMET ASWS A801 – Porto Alegre, RS. Photographic evidence of just some of the damage is shown in Figure 2.22, and enhanced satellite image over the city in Figure 2.23.



Figure 2.22 – Examples of damage from 29/01/2016 downburst event in Porto Alegre (Loredo-Souza et al., 2019).

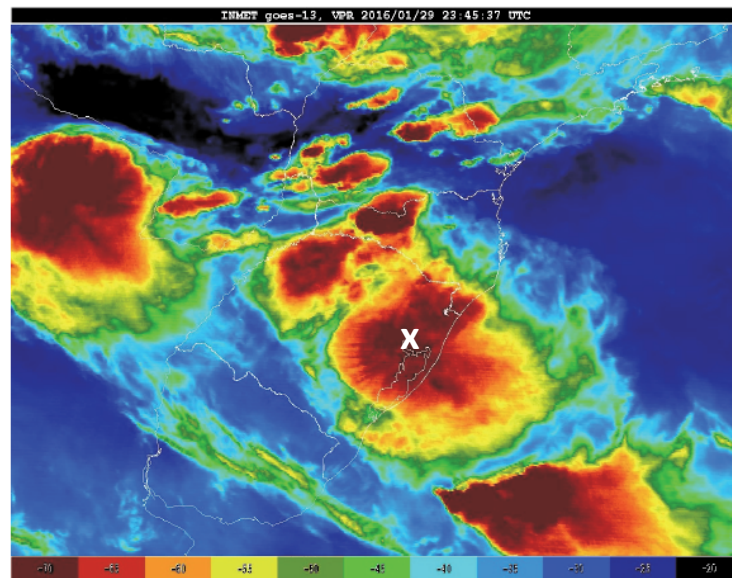


Figure 2.23 – Satellite image of water vapour enhancement taken by GOES 13, 23:45 UTC 29/01/2016 (INMET, 2016). Location of Porto Alegre marked by X.

Damaging winds can be caused by a combination of weak downdraft with strong rear-inflow jets and are typically associated with MCS, with favourable conditions typically found at the apex of bow echoes, but many rear-inflow jets of bow echoes remain elevated and do not bring damaging winds to the surface.

Meso- β -scale cold pools are commonly associated with MCS. In the case of large horizontal pressure gradients, damaging winds can be produced with no contribution from downdrafts. This type of cold pool is formed when the outflows from several storms merge to deepen the outflow, in turn, increasing the surface pressure. Horizontal meso- γ -scale vortices – *mesovortices* – embedded within the lines of squall lines increase the horizontal wind speed at the gust front.

A *derecho* is a type of damaging wind which acts over large distances and is associated with convection with long lifespan. Markowski and Richardson (2010) defined derechos as extreme winds caused by any of the previously mentioned mechanisms, including downbursts. This differs from the Johns and Hirt (1987) definition of derecho as a family of downburst clusters produced by MCS. The passage of a bow echo caused damage in the central region of Rio Grande do Sul on 29/05/2013. A reflective field radar image of the event is shown in Figure 2.24 and could be the first documented derecho in South America (Figueiredo et al., 2019).

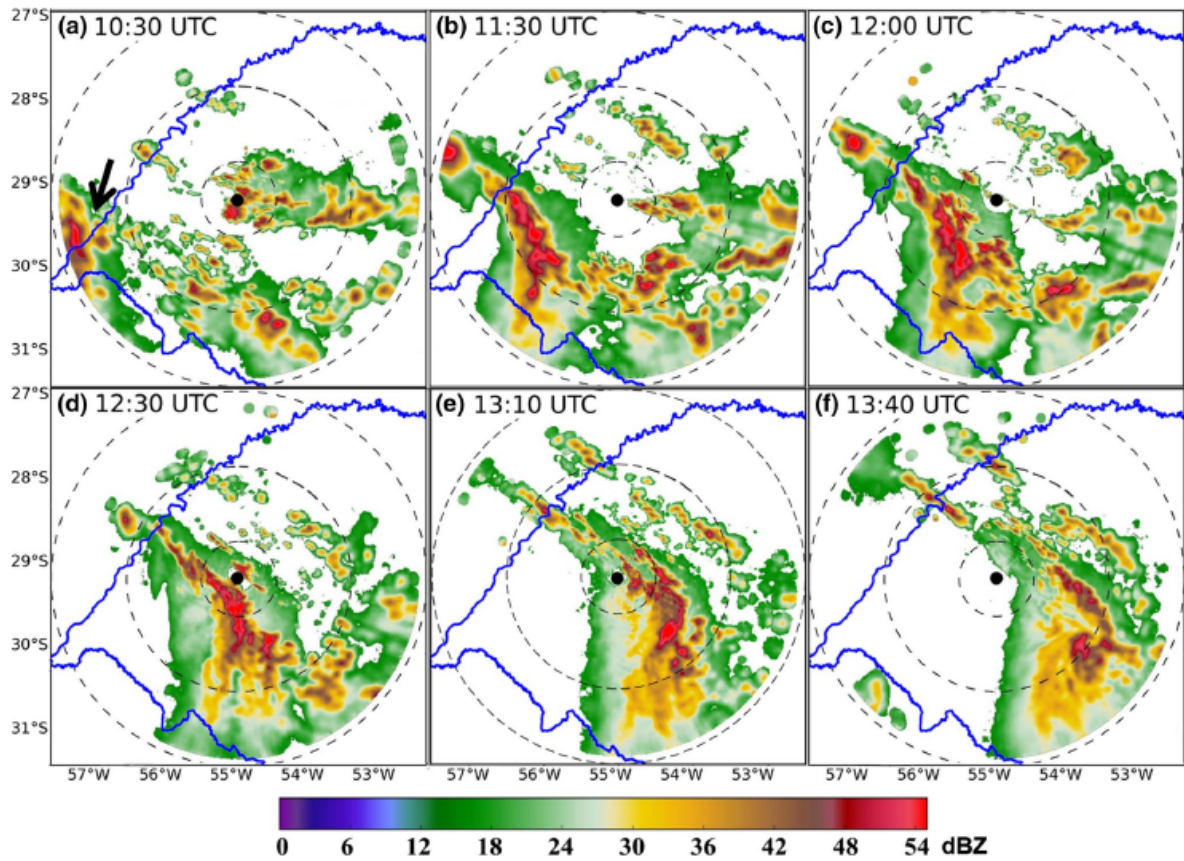


Figure 2.24 – Reflective field images from the radar at Santiago, RS, represented by the black dot, on 29/05/2013 (Figueiredo et al., 2019).

2.3 CODIFICATION OF EXTREME WINDS

The determination of aerodynamic wind loads according to NBR 6123 (ABNT, 1988) applies only to synoptic winds. The characteristic wind speed at height z , V_k , is defined by Equation 2.8.

$$V_k = V_0 S_1 S_2 S_3 \quad 2.8$$

Where,

V_0 : basic wind speed (m/s),

S_1 : topographical factor,

S_2 : terrain and height multiplier,

S_3 : probabilistic factor.

2.3.1 NBR 6123

2.3.1.1 Basic wind speed

Studies undertaken by Vieira Filho (1975) and Padaratz (1977) were responsible for the creation of the isopleth map which defines the regional basic wind speeds, V_0 , of the current Brazilian wind code: *Wind forces on buildings (Forças devidas ao vento em edificações)* - NBR 6123 (ABNT, 1988), as shown in Figure B.1 of Appendix B *Isopleth Map of NBR 6123 (ABNT, 1988)*. The basic velocity, V_0 , is defined as a 3-second gust at a height of $z = 10$ m in open and flat terrain for a mean recurrence interval of 50 years.

Values of V_0 vary from 50 m/s in the extreme south-east and south of Brazil to 30 m/s in the central-north, rising again to 35 m/s in the extreme north-east of the country. Isopleth intervals are defined at 5 m/s increments and interpolation between the intervals is permitted. Isolated regions surrounding Brasília, DF, and Campinas, SP, interrupt the otherwise smooth transition of higher V_0 in the south to lower V_0 in the north.

Annual maxima of hourly 10-minute wind speeds, V_{obs} , and peak gusts, G_{obs} , were obtained by Vieira Filho (1975) from the Brazilian Airforce for 49 aerodrome-based meteorological stations for the period from 1950 to 1974. Due to several stations/years with no recorded annual maxima gust observations, Padaratz (1977) created an artificial series of equivalent gusts, G^* , utilising the V_{obs} maxima with an applied gust factor, G_V , as described in Equation 2.9.

$$G^* = \max (G_{obs}, G_V \cdot V_{obs}) \quad 2.9$$

A gust factor of $G_V = 1.15$ was used, representing an averaging interval conversion from 30 to 3 s according to NBR 6123 (ABNT, 1988). The method of maximum likelihood estimators (MLE) was then applied to the series of G^* annual maxima of each station for the Fréchet distribution given in Equation 2.10, with X representing wind speed. Once the characteristic wind speed, β , and shape factor, γ , of Equation 2.10 were determined for each station, a wind speed could then be determined for a desired mean recurrence interval of R years. The relationship between the annual probability of non-exceedance, P , for a return period of R_P years is defined in Equation 2.11. For periods of 10 years or more, the difference between R and R_P is negligible.

$$P(X) = \exp \left[- \left(\frac{X}{\beta} \right)^{-\gamma} \right] \quad 2.10$$

$$P = 1 - \frac{1}{R_P} \quad 2.11$$

Once β and γ_o were calculated for each of the 49 stations, a weighted mean, γ_{mp} , was calculated for a selected group of 20 stations, with weightings determined by the period of operation of each station. The single shape factor of $\gamma_{mp} = 6.369$ was then combined with β for each station and solved for a probability of non-exceedance of $P = 0.98$, as determined by Equation 2.11 for $R_P = 50$ years, to determine V_0 for each station. The isopleths of Figure B.2 of Appendix B were generated from each station's V_0 , with the exception of those with sampling period less than 5 years, and is similar to the final map of NBR 6123 (ABNT, 1988) shown in Figure B.1. The two 25 m/s zones in the north of the country, and the 40 m/s surrounding Bagé, RS, in the south of Brazil were removed from the Padaratz's (1977) draft version.

An investigation was conducted with the aim of replicating the V_0 NBR 6123 (ABNT, 1988) draft map using the process described in Padaratz (1977). First, a kriging interpolation scheme was used to provide V_0 contours at 5 m/s intervals using β and γ_o of individual stations, as defined in Table 4.2.1 of Padaratz (1977). The resulting map is shown in Figure B.3a) of Appendix B and is radically different from that of NBR 6123 (ABNT, 1988) – with the majority of the south and a large portion of north-western Brazil over 50 m/s. A second map, Figure B3b) of Appendix B, was generated using the single shape factor of $\gamma_{mp} = 6.369$ combined with β for each station, which had the effect of reducing V_0 for the majority of the country. This map is not the same as that of Padaratz (1977), with lower wind speeds present in southern Mato Grosso do Sul and western Paraná, and higher wind speeds in Rio de Janeiro. Trial and error manipulations were made to generate Figure B.3c) of Appendix B which bears a striking resemblance to Padaratz (1977). The manipulations include:

- disregarding of stations at Afonsos, RJ, Bagé, RS, Maceió, AL, Ponta Porã, MS, Santa Cruz, RJ, and Uberlândia, MG, in the generation of interpolation contours by kriging;
- station shape factor γ_o ($V_0 = 49.4$ m/s) used at Foz do Iguaçu, PR, instead of γ_{mp} ($V_0 = 32.3$ m/s);
- the inclusion of station at Rio Branco, AC, with sampling period of 4 years.

Although no description of the above actions is given by Padaratz (1977), it is stated that stations which presented inconsistencies in the series of annual maxima were disregarded.

2.3.1.2 Return periods and risk categories

In the determination of design wind speeds for varying probabilities of exceedance and periods other than 50 years, NBR 6123 uses the probabilistic factor, S_3 , defined in Equation 2.12. The derivation of Equation 2.12 is given in Appendix K *Determination of Probabilistic Factor S_3* which is calculated as a function of P_L and R_L , where P_L is the probability of a certain wind speed being equalled or exceeded over a lifetime of R_L years. Note that P_L and R_L are defined as P_m and m in NBR 6123 (ABNT, 1988) respectively.

$$S_3 = 0.54 \left[-\frac{\ln(1 - P_L)}{R_L} \right]^{-0.157} \quad 2.12$$

Table K.1 of Appendix K contains S_3 for a number of combinations of P_L and R_L as appears in NBR 6123 (ABNT, 1988). Five building groups are determined for which a S_3 must be applied, with descriptions and minimum S_3 values given in Table K.2. The structures with highest civil importance adopt $S_3 = 1.10$, while less important and temporary structures may adopt $S_3 = 0.83$. In most cases $S_3 = 1.00$.

2.3.1.3 Wind characteristics

Horizontal wind speed is a function of height above ground, terrain category and time-averaging interval. NBR 6123 defines five separate terrain categories with their respective roughness lengths, z_0 , and gradient heights, z_g , defined in Table 2.1.

Roughness lengths as and terrain categories of NBR 6123, as defined in Table 2.1, were obtained from Simiu (1981). The basic velocity, V_0 , is defined for open field terrain relating to CAT II with roughness length of $z_0 = 0.07$ m, higher than corresponding open field roughness lengths for other wind codes. Simiu (1981) stated that the choice of $z_0 = 0.07$ m for open field was considered reasonable since aerodromes, where data is acquired to derive basic wind speeds, are not always “clean” enough to warrant the use of $z_0 < 0.07$ m.

The height and terrain multiplier, S_2 , is defined in Equation 2.13. Coefficient b and exponent p are defined for each terrain category, and gust factor, F_r , is a function of the desired time-

averaging interval. The values of b , p and F_r of NBR 6123 (ABNT, 1988) are made available in Table F.1. A visual comparison of the five categories can be made in Figure 2.25 for $\tau = 3$ s.

Table 2.1 – NBR 6123 roughness lengths and gradient heights per terrain category (adapted from ABNT, 1988)

Category	I	II	III	IV	V
z_g (m)	250	300	350	420	500
z_0 (m)	0.005	0.07	0.30	1.0	2.5

$$S_2 = b \cdot F_r \left(\frac{z}{10} \right)^p \quad 2.13$$

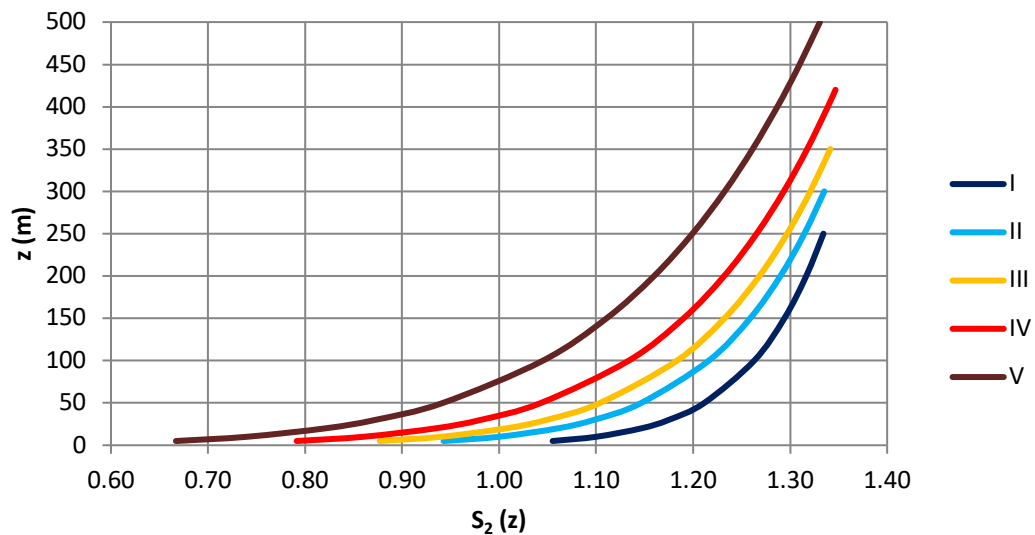


Figure 2.25 – Terrain and height multiplier, S_2 , per terrain category (for $\tau = 3$ s).

Although F_r is referred to as the gust factor, this is actually a misnomer. Typically, a gust factor is applied to a mean wind speed over a long period ($T = 1$ hr or 10 min) to convert mean speed to a gust of shorter time-averaging interval. However, F_r in NBR 6123 converts a $\tau = 3$ s gust to a longer time-averaging interval. To convert to “true” gust factors, G_V , the F_r series must be first divided by the F_r value corresponding to period T . For example, to generate the series of gust factors, $G_{V,T}$, for $T = 3600$ s, the F_r series is divided by 0.65 ($F_r = 0.65$ for $T = 3600$ s). The difference between gust factors, G_V , and F_r is demonstrated in Figure 2.26 for $T = 3600$ s and $T = 600$ s.

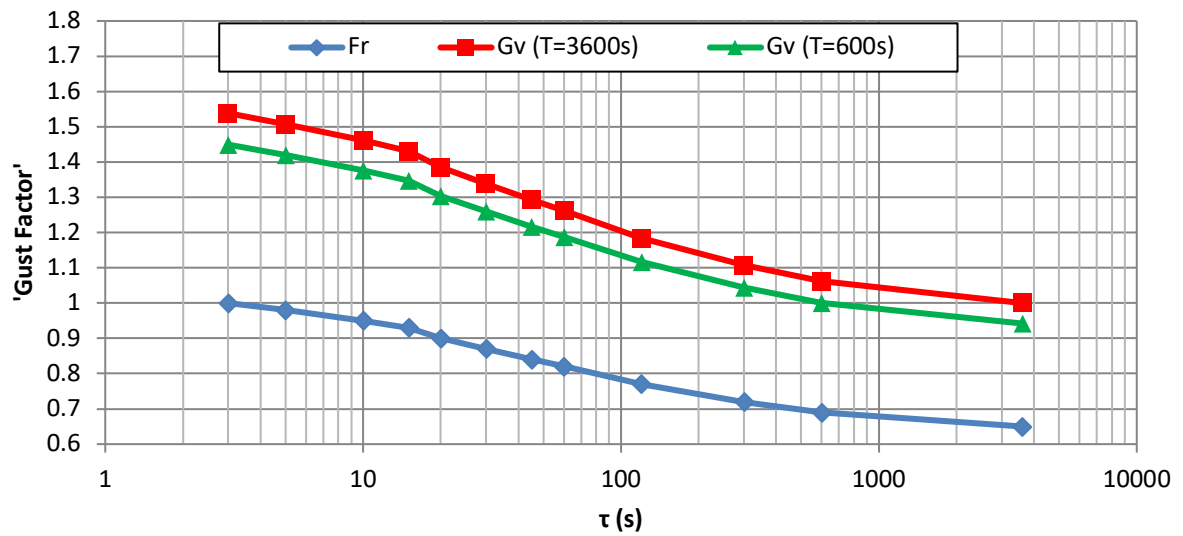


Figure 2.26 – F_r of NBR 6123 and corresponding gust factors, G_V .

The origin of F_r is found in Blessmann (2013) and is calculated using Equation 2.14, with c defined in Table 2.2 per time-averaging interval and β defined in Table 2.3 per terrain category. The definition of β was obtained from Simiu (1981), whilst c of Table 2.2 was adapted from c defined in Simiu (1981) for other time-averaging intervals and based on Durst (1960). For $z_0 = 0.07$ m and $z = 10$ m, the series of $G_{V,3600s}$ is shown in Table 2.3 calculated using Equation 2.14, and is the same as the series calculated and plotted in Figure 2.26.

$$G_{V,3600s} = 1 + \frac{c\sqrt{\beta}}{2.5\ln\left(\frac{z}{z_0}\right)} \quad 2.14$$

Table 2.2 – β values for NBR 6123 terrain categories (Simiu, 1981; Blessmann, 2013)

CAT	I	II	III	IV	V
β	6.00	6.00	5.25	4.85	4.00

Table 2.3 – c and $G_{V,3600s}$ for NBR 6123 time-averaging intervals (Blessmann, 2013)

τ (s)	3	5	10	15	20	30	45	60	120	300	600	3600
c	2.72	2.56	2.32	2.14	2.00	1.73	1.43	1.25	0.92	0.54	0.32	0
$G_{V,3600s}$	1.54	1.51	1.46	1.42	1.39	1.34	1.28	1.25	1.18	1.11	1.06	0

There is an apparent discrepancy between equations used to account for turbulence intensity and peak factors. Equation 2.14 is undoubtedly responsible for the generation of F_r in NBR 6123, but is strikingly similar to Equation 2.5 which defines the gust factor as a function of g and I . Simui (1981) did not define c explicitly as a peak factor, but I was defined by Equation 2.15, suggesting that c is the peak factor. However, according to Blessmann (2013) the vertical profiles of turbulence intensity in NBR 6123, $I(z)$, are defined as per Equation 2.16, where von Kármán's constant is $\kappa = 0.4$.

$$I(z) = \frac{\sqrt{\beta}}{2.5 \ln \left(\frac{z}{z_0} \right)} \quad 2.15$$

$$I(z) = \frac{2.58\kappa}{\ln \left(\frac{z}{z_0} \right)} \quad 2.16$$

Both formulations of turbulence intensity are plotted in Figure 2.27. Differences between the two are constant irrespective of height, but differences are larger for higher terrain categories. Equation 2.16 gives larger I than Equation 2.15 by 5% for CAT I and II, 13% for CAT III, 17% for CAT IV and 29% for CAT V. For this study, Equation 2.15 is assumed to generate the turbulence intensity as used in NBR 6123 (ABNT, 1988). As such, for a roughness length of $z_0 = 0.07$ m for CAT II, the turbulence intensity associated with V_0 is $I = 0.197$ at a height of $z = 10$ m.

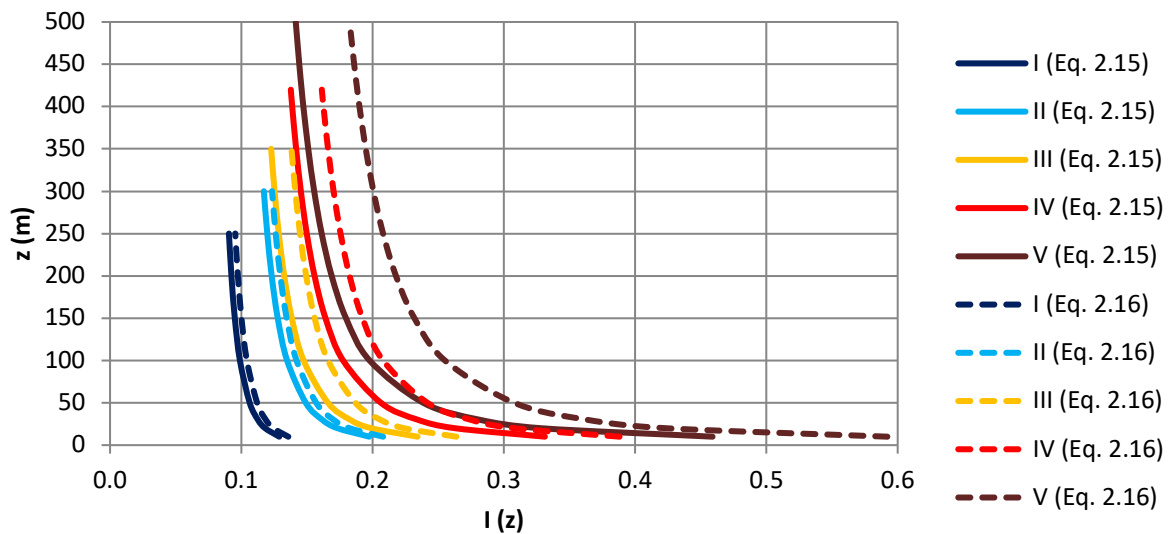


Figure 2.27 – Longitudinal turbulence intensity, I , of NBR 6123 (ABNT, 1988).

The Harris turbulence spectrum, shown in Equation 2.17, is adopted in NBR 6123 (ABNT, 1988) according to Blessmann (2013). The spectral density function assumes a constant integral length scale, L_u , of 1800 m for all heights.

$$\frac{f S_u(f)}{\sigma^2} = \frac{0.6 \left(\frac{f L_u}{\bar{u}} \right)}{\left[2 + \left(\frac{f L_u}{\bar{u}} \right)^2 \right]^{5/6}} \quad 2.17$$

2.3.1.4 Structural wind loads

The drag coefficient, C_a , is an important parameter in the calculation of structural loads for rectangular prismatic buildings. The drag coefficient is a function of the width-to-depth ratio, l_1/l_2 , height-to-width ratio, h/l_1 , and turbulence level as per Figure 2.28. Models for high and low levels of turbulence are defined, but without quantitative definitions of turbulence. According to directives of NBR 6123, a building may be considered in a region of high turbulence when its height does not exceed twice the mean height of neighbouring buildings within a distance of: 500 m for buildings of $h \leq 40$ m; 1,000 m for buildings of $40 < h \leq 55$ m; 2,000 m for buildings of $55 < h \leq 70$ m; and 3,000 m for buildings of $70 < h \leq 80$ m. Significant wind-load reductions are achieved by buildings located in a region of high turbulence. For the example of a building with $h = 180$ m, $l_1 = 30$ m and $l_2 = 45$ m, $C_a = 1.25$ and 0.99 for low and high turbulence regimes respectively. When wind blows perpendicular to the previous configuration, $l_1 = 45$ m and $l_2 = 30$ m, $C_a = 1.46$ and 1.10 for low and high turbulence regimes respectively. For this example, the use of the low turbulence drag coefficient allows for a reduction of 20-25% in the along-wind base overturning moments.

In the determination of dynamic response of structures under wind-loading, NBR 6123 (ABNT, 1988) provides a methodology for the calculation of dynamic amplification factor, ξ . The dynamic amplification factor is plotted against reduced velocity with integral length of turbulence $L_u = 1,800$ m, in two graphs for each terrain category. The two graphs are differentiated by aspect ratios, with six curves given for each graph. The six curves represent each combination of critical damping ratio, $\zeta = 0.01$ and 0.02, with overall building heights $h = 25, 100$ and 300 m. Interpolation between h curves and aspect ratio graphs is required to determine the correct ξ . The dynamic amplification factor is somewhat counter-intuitive as ξ values are inversely proportional to the height of the structure. Two ξ plots for open field

terrain, CAT II, are shown in Figure 2.29. The dynamic amplification factor is used to determine the modal force, F_H , which is then used to determine the fluctuating component wind load for each floor along the height of the structure in combination with the mass distribution and mode shape.

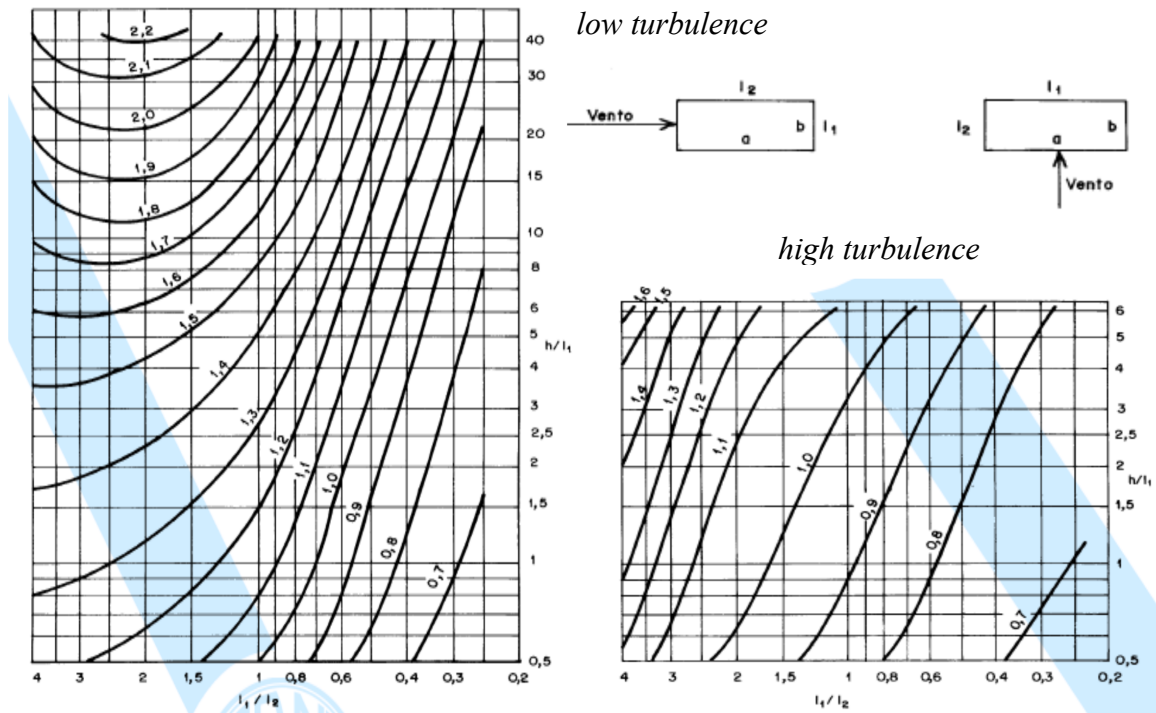


Figure 2.28 – Plots for the determination of drag coefficient, C_d , of NBR 6123 (ABNT, 1988),

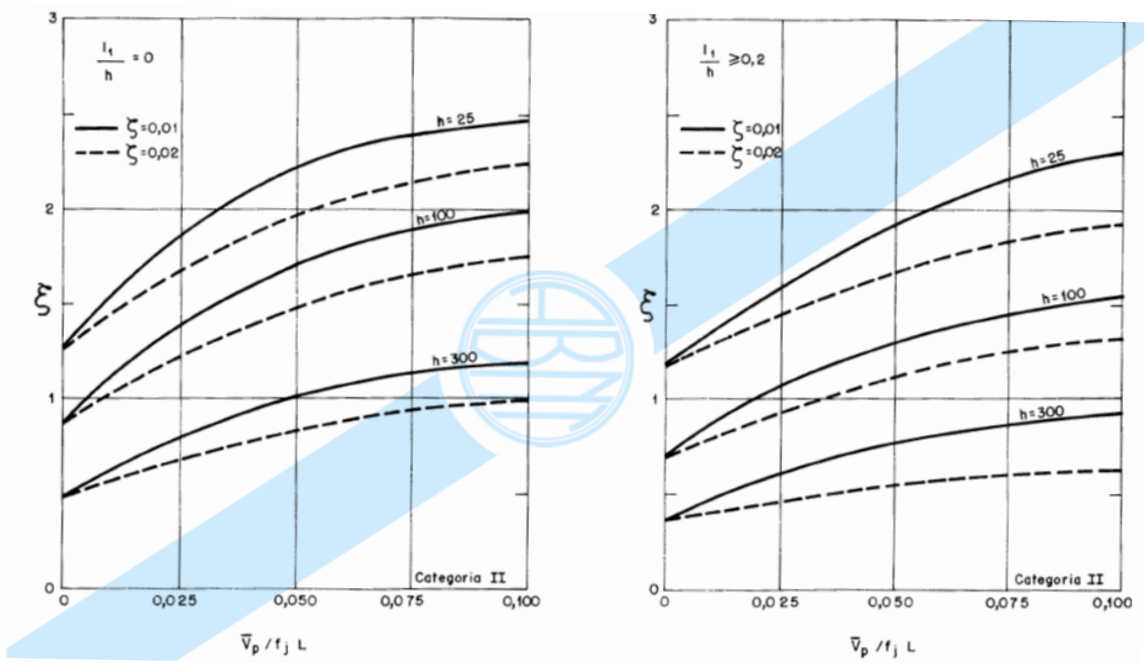


Figure 2.29 – Dynamic amplification factor, ζ , for CAT II of NBR 6123 (ABNT, 1988).

2.3.2 Comparisons with other international wind codes

A number of key parameters relating to basic wind speed for several regionally and internationally important wind codes are compared to those of NBR 6123 (ABNT, 1988) in Table 2.4. Key parameters include the roughness length of the basic wind speed, z_0 , time averaging interval, τ , maximum and minimum wind speeds for the region (for defined mean recurrence intervals in years, R), and range of years for which appropriate conversions are given. The Argentinian and Colombian codes are heavily based on ASCE-7, and the Paraguayan code is based on NBR 6123.

Table 2.4 – Key basic wind speeds details of international wind codes.

Region	Wind Code	Basic Wind Speed Parameters				
		z_0 (m)	τ (s)	GEVD Type	Wind Speed min/max (m/s) (R years)	Range of R (years)
Brazil	NBR 6123 (ABNT, 1988)	0.07	3	II (Fréchet)	30/50 (50)	2-200
Argentina	CIRSOC 102 (2005)	0.02	3	II (Fréchet)	34/67.5 (50)	50
Bolivia	APNB 1225003 (2014)	0.01	3	I (Gumbel)	24/44.3 (50)	5-500
Chile	NCh432.Of71 (1971)	-	-	-	33/41.2 (-)	-
Colombia	NSR-10 (2010)	0.02	3	-	17/36 (50)	50
Ecuador	CPE INEN-NEC-SE-CG 26-1 (2014)	-	inst.	-	21/- (-)	-
Peru	E.020 (2006)	-	-	-	20.8/36.1 (50)	-
Paraguay	NP No. 196 (1991)	0.07	3	II (Fréchet)	40/55 (50)	-
Venezuela	COVENIN 2003 (1989)	-	-	-	19.4/27.8 (50)	-
Uruguay	UNIT 50 (1984)	~ 0.03	3	II (Fréchet)	37.5/43.9 (20)	2-200
Australia/New Zealand ⁵	AS/NZS 1170.2 (2002)	0.02	3	III (GPD)	39/66 (50)	1-10,000; Eq.
	AS/NZS 1170.2 (2011)	0.02	0.2	III (GPD)	39/66 (50)	1-10,000; Eq.
United States	ASCE 7-05 (2005)	0.02	3	I (Gumbel)	38/67 (50)	Eq.
	ASCE 7-10 (2010)	0.02	3	I (Gumbel)	45/76 (300)	300, 700, 1,700; Eq.
	ASCE 7-16 (2016)	0.02	3	III (POT)	31/58 (50)	300, 700, 1,700, 3,000. (10, 25, 100)
Asia-Pacific	HB212 (2002)	0.02	3	III (GPD)	32/60 (50)	Eq.
Singapore	NA to SS EN 1991-1-4 (2009)	0.05	600	-	20 (50)	-
Malaysia	MS 1553 (2002)	0.02	3	-	32.5/33.5 (50)	20, 100

⁵ The peak gust definition for AS/NZS 1170.2 did not change from the 2002 to 2011, but rather the description of its duration was altered from an assumed 3 s period to a 0.2 s moving average definition.

All basic wind speeds are defined at a height of $z = 10$ m for open, flat terrain, however the definition of the roughness length varies. Most codes nominate $z_0 = 0.02$ or 0.03 m for open, flat terrain, including ISO 4354 (2009) and WMO (2014) with $z_0 = 0.03$ not listed in the table. Uruguay's UNIT 50 does not list $z_0 = 0.03$ m as the nominal roughness length, but the corresponding wind profile is nearly identical to that of ISO 4354. Eurocode EN 1991-1-4 with $z_0 = 0.05$ m and Brazil's NBR 6123 (ABNT, 1988) $z_0 = 0.07$ m are two outliers with the roughest definitions of open field terrain.

Most basic wind speeds represent a gust of $\tau = 3$ s. AS/NSZ 1170.2 (2011) was revised from $\tau = 3$ s to 0.2 s based on investigations of historical anemometric equipment used to observe wind data prior to the 1990s (Holmes and Ginger, 2012). A similar investigation was conducted on anemometric equipment used in the United States and a peak gust of $\tau = 1$ s was suggested to be more appropriate than current definition of $\tau = 3$ s used in ASCE-7 (Kwon and Kareem, 2014). The conservative Fréchet extreme value distribution is common in the older wind codes in South America, including Brazil, Paraguay, Uruguay and Argentina; whereas codes that are committed to continual updates and improvements, such as AS/NZS 1170.2 and ASCE-7, have moved from the Gumbel distribution to the Generalised Pareto Distribution (GPD) and Peaks Over Threshold (POT) models, which are essentially Type III Generalised Extreme Value Distributions (GEVD), or reverse Weibull, with speeds limited for large return periods.

Basic wind speeds vary greatly throughout South America despite the fact no country defines a region affected by tropical cyclones. The minimum basic wind speed is found on the Pacific coast of Colombia with 17 m/s, and the highest at Comodoro Rivadavia, located on Argentina's eastern coast of Patagonia, with 67.5 m/s. Chile's wind code defines a basic wind pressure for two zones: cities and open fields/ocean exposures. If converted to a 50-year mean recurrence interval using the defined conversion factor of 1.146 , Uruguay's basic wind speeds range from 43.0 to 50.3 m/s. Region A of Australia and New Zealand, is a non-tropical cyclone region which covers the large majority of the region with a basic wind speed of 39 m/s for $\tau = 0.2$ s and $R = 50$ years. A conversion factor of 0.9 is used to convert this to a wind speed of 35 m/s for $\tau = 3$ s. The non-hurricane zone of contiguous United States ranged from 38 - 40 m/s in ASCE-7 (2002) and ranges from 31 - 41 m/s in the most recent ASCE-7 (2016) for $R = 50$ years, despite evidence showing some regions could have 50-year gust speeds of up to 45 m/s (Lombardo, 2012).

Equatorial regions are known for lack of synoptic extreme winds and are typically only affected by monsoons and thunderstorms. In southeast Asia, the 50-year return wind speed is 32 m/s according to HB-212 (2002), the Malaysian standard defines a 50-year return gust speed of 32.5 m/s for inland regions, and Singapore's 10-minute wind speed converts to a basic gust of 29 m/s. Basic gusts for equatorial South American countries are much lower, with 17 m/s the lowest in Colombia, 21 m/s in Ecuador, 20.8 m/s in Peru and 19.4 m/s in Venezuela. Although the draft isopleth map of Brazil by Padaratz (1977) contained regions of 25 m/s, this was eliminated from the final version as 30 m/s was considered the lowest allowable level for ultimate loads. The disregard of a lower limit of basic wind speed by the northern South American nations could be attributed to their preoccupation with earthquake loads, as these Andean nations are some of the most seismically active regions in the world.

According to NBR 6118 *Projeto de estruturas de concreto – Procedimento* (ABNT, 2014), a wind load factor of $\gamma_f = 1.4$ is applied to wind loads on concrete structures determined for a mean recurrence interval of $R = 50$ years in Brazil. This practice is in line with other regions of the world for which $\gamma_f = 1.4$ -1.6 (Holmes, 2015). Differently, ultimate limit state wind loads are determined for longer mean recurrence intervals (small annual probabilities of exceedance) of between 500 to 1,000 years in Australia (AS/NZS, 2011) and 300 to 3,000 years the United States (ASCE, 2016) without the application of an additional load factor. For both wind codes, the appropriate mean recurrence interval is dependent on the risk category, or importance, of the structure. For the non-hurricane Region A of Australia, this converts to a wind load factor, γ_f , of 1.33 and 1.39 for $R = 500$ and 1,000 years respectively, which would be applied to wind loads calculated using a $R = 50$ -year wind speed. For the state of Nebraska in the United States, a non-hurricane region, equivalent load factors for $R = 50$ year wind speed are γ_f , of 1.38, 1.56, 1.76 and 1.89 for mean recurrence intervals of 300, 700, 1,700 and 3,000 years respectively. A probabilistic factor of NBR 6123 (ABNT, 1988), of $S_3 = 1.18$ is equivalent to $\gamma_f = 1.4$ and represents a mean recurrence interval of $R = 150$ years for the Fréchet distribution of NBR 6123 (ABNT, 1988).

2.3.3 Codification of non-synoptic winds

One of the biggest challenges currently facing the wind engineering community is the accurate characterisation of non-synoptic winds for implementation into wind codes and standards. Much of the focus is on outflow from microbursts, and little attention is given to other convection related extreme winds, such as rear inflow jet + weak downdraft or large horizontal pressure gradient non-synoptic wind types as defined by Markowski and Richardson (2010).

The following summary of Mason (2017) outlines the challenges to codification of non-synoptic winds and pertinent questions which must be addressed. Beginning with a summary of Letchford and Illidge (1999), and using the term *localised windstorms*, Mason (2017) identified four major points of differences between non-synoptic and synoptic winds:

- outflows are highly non-stationary;
- outflows are complex three-dimensional flows;
- wind speed vertical profile does not follow typical log or power law ABL profiles;
- turbulence is lower and correlation higher in outflows than in synoptic winds.

Much of what is known about outflow structures has come from observational studies in the United States, such as Joint Airport Weather Studies (JAWS) and Northern Illinois Meteorological Research on Downbursts (NIMROD), laboratory experiments with impinging jets and Computational Fluid Dynamic (CFD) simulations. Steady jets, initially the focus of laboratory studies, determined some important outflow characteristics including the nose-like shape of the vertical wind profile which peaks at a certain height above ground and then decreases for larger heights. In using a translating jet, Letchford and Chay (2002) identified maximum speeds are encountered in the leading gust front. Impulse jets have more recently been used to better simulate the leading gust front (Mason et al., 2005; Hangan et al., 2017), and further advancements include the use of thermodynamically faithful experiments (Mason et al., 2009).

Laboratory studies also established that wind speed and turbulence profiles near the impingement location of the downdraft varied little for different roughness surfaces (Choi, 2004; Xu and Hangan, 2008). Further from the jet however, peak wind speeds at the outflow boundary decreased and the height of the peak magnitude above ground increased for rougher surfaces. This is expected since the outflow is developing in the same manner as ABL flow,

with ESDU (1990[a]) estimating the maximum wind speed is located approximately 5 km from the storm centre. Tests over topographic features showed a reduction in amplification of wind speeds to be 10-15% less than for ABL winds (Holmes, 1992; Letchford and Illidge, 1999; Wood et al. 2001).

Other important established characteristics include low levels of turbulence in the early stages of the outflow development (Holmes, 2015). A rear-flank downdraft was recorded by several observation towers near Lubbock, Texas, on 04/06/2002, and analysis of wind speed time-series at height of 10 m of one particular tower revealed a turbulence intensity of 10% when a 40-second running average was separated from the time-series, much lower than the typical 17-20% for open, flat terrain. Due to the non-stationary nature of the downdraft, turbulence cannot be characterised in the same manner as for synoptic winds – particularly over longer periods of 10 min or 1 hr. For the same reason gust factors, which are strongly dependent on the positioning and length of the averaging window, can reach values of $G_V > 10$ and lose relevance.

Mason (2017) compared the outflow gust speed profiles of ISO 4354 (2009) and AS/NZS 7000 (2010) to observed profiles of three different full-scale observational studies (Holmes et al., 2008; Lombardo et al., 2014; Gunter and Schroeder, 2015). The height of the peak outflow wind speed ranges considerably, as shown in Figure 2.30. Tower observations of Lombardo et al. (2014) indicate the maximum to be at, or below, a height of 10 m, radar measurements by Gunter and Schroeder (2015) and Hjelmfelt (1988), indicate the maximum wind speeds at heights between 60 m to 200 m, while LIDAR measurements (Light Detection and Ranging) by Repetto et al. (2018) show the peak wind speed to be at a height of 80 m. The profiles of the two wind codes vary greatly with the AS/NZS 7000 profile much less conservative than that of ISO 4354. In addition, these codes do not give consideration to turbulence intensity, aerodynamic shape factors or roughness for these non-synoptic profiles. Not shown in the figures is the recommendation of ESDU (1990[a]) to model thunderstorm outflow by using ABL profile up to a height of 100 m above ground with constant wind speed above.

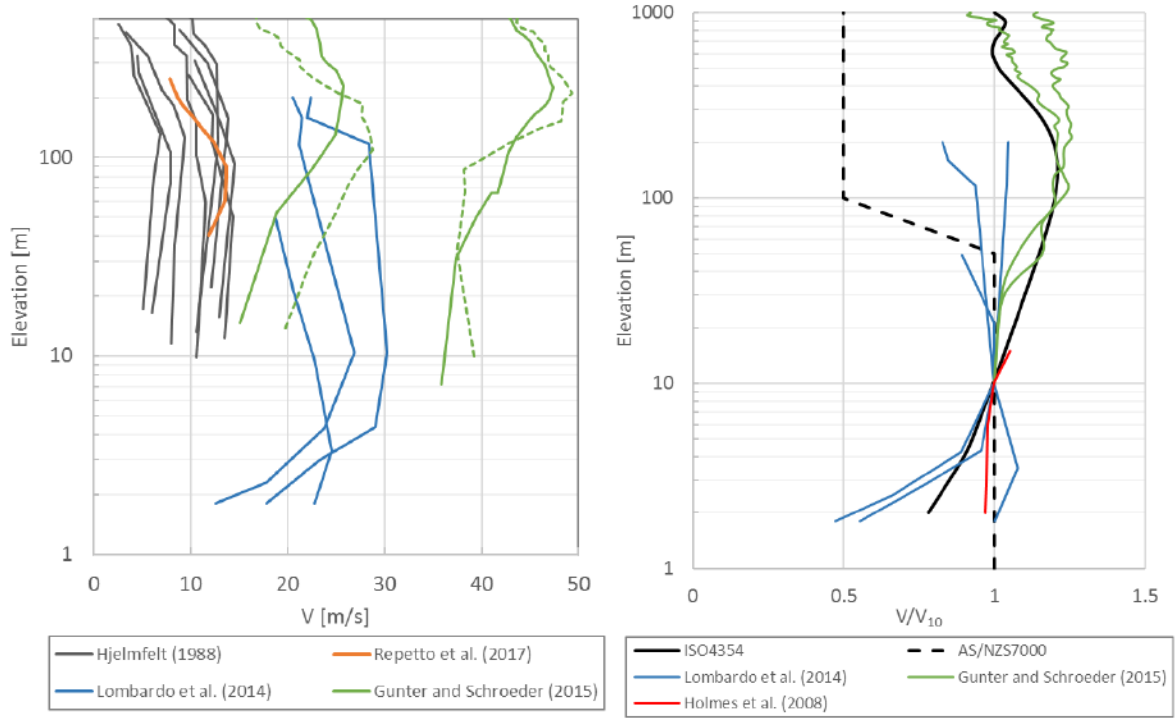


Figure 2.30 – Full-scale measurements of outflow wind speeds (right), ISO 4354 (2009) and AS/NZS 7000 (2010) non-synoptic wind speed profiles compared to full-scale observations, normalised by wind speed at 10 m (right) (Mason, 2017).

Two non-synoptic wind speed profiles were proposed for future implementation in NBR 6123. Miguel et al. (2018) proposed a non-synoptic profile which is composed of 35% standard ABL profile and 65% downburst profile since most severe thunderstorm winds have a synoptic component due to the translation motion of the storm cloud. The vertical profile of horizontal speed from downburst outflow was based on Savory et al. (2001) which is normalised by the maximum gust speed, V_{max} , occurring at height z_{max} . A modified version of the profile defined by Savory et al. (2001) and used by Miguel et al. (2018) is shown in Equations 2.18 and 2.19, with the addition of the factor of 1.22 necessary due to the improper normalisation of the original equation.

$$\frac{V(\eta)}{V_{max}} = 1.22[\exp(-0.15\eta) - \exp(-3.2175\eta)] \quad 2.18$$

$$\eta = \frac{z}{z_{max}} \quad 2.19$$

Five different heights of z_{max} are proposed by Miguel et al. (2018) relating to the magnitude of the gust speed at $z = 10$ m, V_0 , ranging from $z_{max} = 20$ m for $V_0 \leq 30$ m/s to $z_{max} = 160$ m for $V_0 > 60$ m/s. All five downburst outflow profiles (DB) normalised by the wind speed at $z = 10$ m are shown in Figure 2.31, along with the final non-synoptic profiles which are composed of 65% DB and 35% synoptic profile (COMP.). The plot highlights a large divergence from the profiles shown in Figure 2.30 with a maximum factor of 3.53 at $z_{max} = 160$ m for $V_0 > 60$ m/s, meaning that for $V_0 = 70$ m/s the projected horizontal gust speed at $z = 160$ m is almost 250 m/s. By visual comparison with the other profiles of Figure 2.30 and Figure 2.31, the combined profiles for $V_0 < 30$ m/s and $30 \text{ m/s} \leq V_0 < 40$ m/s cases appear to be the most promising. It was for the latter profile that Miguel et al. (2018) calculated building responses for theoretical square-based buildings with heights ranging from 20 to 300 m for both standard ABL model and the proposed non-synoptic profile, with the conclusion that synoptic winds govern the building design for heights exceeding 180 m for the same design wind speed at 10 m.

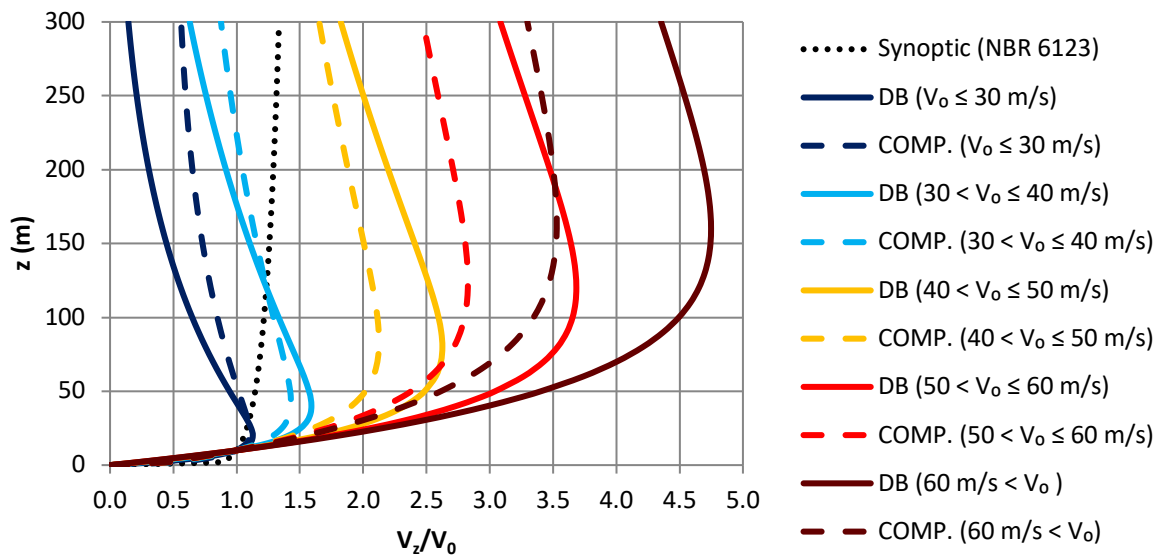


Figure 2.31 – Downburst (DB) and non-synoptic profiles of wind speed composed of 35% synoptic and 65% downburst (COMP.) as proposed by Miguel et al. (2018).

Giving continuation to Miguel et al. (2018), Riera (2018) considered the same 65/35 split between downburst and synoptic profiles and the same five groupings based on winds speed at $z = 10$ m, but changed the proposed DB profile to that of Equation 2.20. The profiles plotted in Figure 2.32 resemble those of AS/NZS 7000 (2010) and the proposed composite non-synoptic profiles are essentially weakened synoptic profiles below height z_{max} , which are further reduced above z_{max} .

$$\frac{V(z)}{V_0} = \frac{\exp\left[-\frac{(z - z_{max})}{2}\right]}{1 + \exp\left[-\frac{(z - z_{max})}{2}\right]} \quad 2.20$$

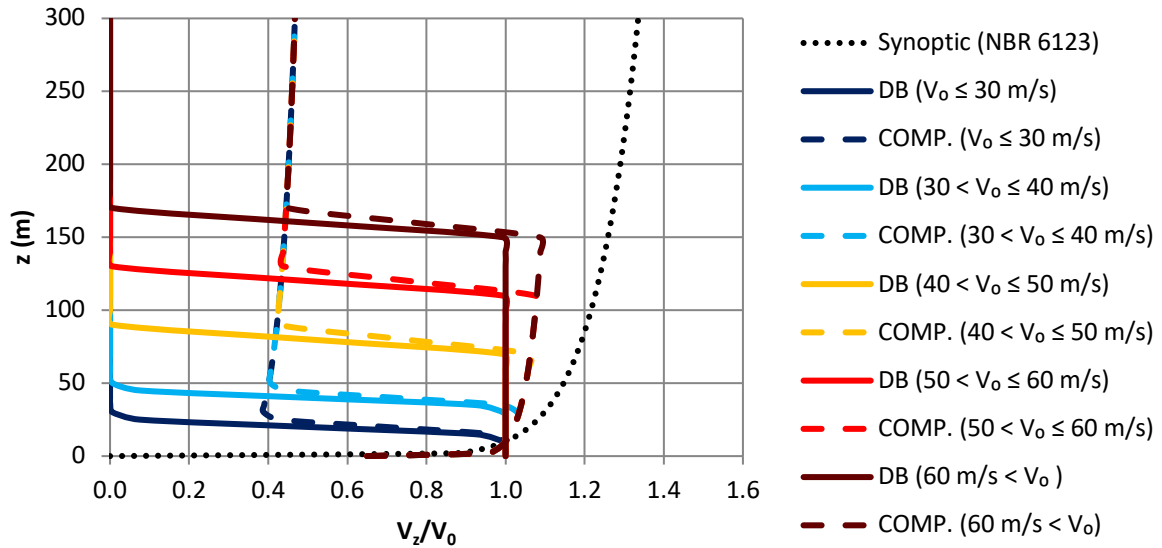


Figure 2.32 – Downburst (DB) and non-synoptic profiles of wind speed composed of 35% synoptic and 65% DB (COMP.) as proposed by Riera (2018).

The use of ABL models to evaluate wind loads in regions dominated by non-synoptic winds was investigated using numerical simulations by Mason et al. (2010). Along-wind loads on a hypothetical building exposed to ABL and downburst-like flows were compared, with results indicating the ABL profile governed loads above 10-20 m while downburst outflow for heights below. For a 200 m tall building, overall along-wind loading from downburst winds is between 5-75% less than ABL winds for the same reference wind speed at a height of 10 m.

3. MEASUREMENT OF WIND

3.1 ORGANISATIONS AND PROTOCOLS

The World Meteorological Organization (WMO), a specialised agency of the United Nations (UN), is responsible for the development of protocols which address installation of equipment and observation procedures at surface weather stations (SWS). Brazil's representative member at WMO is the National Institute of Meteorology (*Instituto Nacional de Meteorologia* – INMET).

According to WMO Publication No. 8 (WMO, 2014), anemometers must be installed at a standard height of $z = 10\text{m}$ above ground in open terrain. The same publication defines open terrain as an area with roughness length $z_0 = 0.03\text{ m}$, where the required distance between any obstacle and the anemometer must be 10 times greater than the height of the obstacle. All obstacles within a given radius of the anemometer should be mapped by the station operator so that observations can be corrected to a standard exposure.

Horizontal wind speeds are reported as averages and/or gusts. 10-minute average wind speeds, V , are reported by SWS and used for forecasting purposes, while 60-minute averages are typically used for climatological statistics. The wind direction is the predominant angle over the averaging time, DIR , measured clockwise from true North. Based on Beljaars' report (1987) which aimed to standardise gust observations, WMO Publications No.'s 8 and 306 (2014; 2015) recommend an averaging interval of 3 seconds to be used when observing gusts. For wind speeds less than 5 m/s, accuracy should be within 0.5 m/s, and 10 % for wind speeds greater than 5 m/s.

Many SWS are located in aerodromes, and as such, the International Civil Aviation Organization (ICAO), another specialised agency of the UN, follows many WMO directives. ICAO's regulatory manual, commonly referred to as Annex 3 (ICAO, 2007), is almost identical to its corresponding WMO Publication No. 49 for international air navigation (2016). Annex 3 asserts that the aeronautical meteorological codes, including METAR/SPECI (aerodrome routine meteorological report) and SYNOP, are developed by WMO as presented in WMO Publication No. 306 – Manual on Codes, Volume I (WMO, 2015).

In Brazil, the Department of Airspace Control (*Departamento de Controle do Espaço Aéreo – DECEA*), a Military Organisation of the Brazilian Airforce (*Força Aérea Brasileira – FAB*) under direction of the Ministry of Defense, is responsible for the regulation and management of Aeronautical Information Service (AIS). DECEA commands SWS at civil and military aerodromes within Brazilian territory, and one of its responsibilities is the observation and prevision of weather conditions; however, management of SWS is left to the aerodrome operator. In the various guides and manuals published by DECEA, including MCA 101-1: Installation of Surface and Altitude Meteorological Stations (*Instalação de Estações Meteorológicas de Superfície e de Altitude*) (DECEA, 2015[a]) and AIP: Aeronautical Information Publication (DECEA, 2018[a]), adherence to WMO and ICAO standards and practices are confirmed, specifically WMO Publication No.'s 8 and 306 (2014; 2015) and ICAO's Annex 3 (2007).

As specified by DECEA (2015[a]; 2018[b]), anemometers are to be installed at a height of $z = 10$ m, measured from the base of supporting mast, with a permitted tolerance of ± 1.0 m. To reduce interference in the observation of wind, any obstacles within a radius of 300 m of the anemometric tower must be located at a distance from the anemometer of at least 10 times their own height (DECEA, 2015[a]). Anemometers are typically installed in proximity of the runway touchdown zone, and depending on the size or the aerodrome, there may be more than one anemometer in operation. The number of anemometers in use, type of anemometer (cup, propeller or ultrasonic), their location and identification of the principal anemometer are detailed in the AIP (DECEA, 2018[b]) for many Brazilian aerodromes – however much of the information is suspected to be outdated. All wind observations are to include V and DIR , while it is recommended that, when observed, peak gusts, G , be measured over an averaging period of 3 seconds (DECEA, 2017). SWS hours of operation depend on the opening hours of the aerodrome: of the 149 Brazilian aerodromes considered for this study, 53 operated at H24 regimes in 2017.

The role of INMET, under the directive of the Brazilian Ministry of Agriculture, Livestock and Supply, is to provide meteorological information through the monitoring, analysis and weather and climate forecasting. In order to fulfil these responsibilities, INMET has its own network of conventional SWS and automatic surface weather stations (ASWS). Although there are some instances of ASWS located within aerodromes, the INMET network is operated independently from those under DECEA's scope. Wind observations V and DIR are

taken at conventional SWS at the hours of 00:00, 12:00 and 18:00 UTC. Although no gust observations are made, conventional stations are fitted with anemographs which could be of interest for future studies. There were 220 conventional SWS in operation in 2016; however, this study does not consider data from the conventional network due to the low temporal resolution of observations. For ASWS, INMET (2011) affirms anemometers are installed at a height of $z = 10$ m above ground, but only requires an area of 14 m x 18 m around the anemometer mast to be free of obstacles. This allows for the possibility of significant obstacles to be located at a distance of 7 m from the anemometer. Wind observations are comprised of wind speed, V (10-minute average), direction, DIR (predominant wind direction over the 10 minutes), and gust, G (peak 3-second average), as confirmed by INMET (2011). As of December, 2017, there was a total of 557 stations in INMET's ASWS network, including 4 located in Uruguay, and 1 in Antarctica.

A comparison of wind observation protocols for the two meteorological networks which operate throughout Brazil is made in Table 3.1, with further details given in the following sections.

Table 3.1 – Comparison of wind observation protocols.

Feature	Meteorological Network	
	Aerodrome SWS	INMET ASWS
Observation	Conventional or hybrid (auto + manual)	Digital
Emission of reports	Manual or automatic	Automatic
Wind speed resolution (units)	1 (kt)	0.1 (m/s)
Time-averaging interval of V (s)	600	600
Time-averaging interval of G (s)	3	3
V observation frequency	Hourly (METAR) or special conditions (SPECI)	Hourly
G observation condition	When $G \geq V + 10$ kt; maximum over 10 minutes	Always; maximum over 60 minutes
DIR resolution (°)	10	1
Height of anemometer (m)	5.5-11	10
Present weather ID	Yes	No

3.1.1 Aerodrome SWS

Meteorological observations at aerodromes are made available over the Global Telecommunications System (GTS) in the form of METAR, SPECI and SYNOP reports, in addition to being stored on local and national databases. In Brazil, the Institute of Airspace Control (*Instituto de Controle do Espaço Aérea* - ICEA) is responsible for the management of data and products related to the Brazilian Airspace Control System (*Sistema de Controle do Espaço Aéreo Brasileiro* - SISCEAB), and conducts research in order to improve SISCEAB. The operation of each SWS is under the responsibility of the aerodrome administrator (INFRAERO, SEIL, DAESP, FAB, etc.). METAR/SPECI and SYNOP meteorological reports are sent from each SWS to the Operational Meteorological database (OPMET) located in Brasília via the Automated System for Registration and Management of Meteorological Observations (*Sistema Automatizado de Registro e Gerenciamento das Observações Meteorológicas* - WEBMET), which are then sent over the GTS. At the aerodrome, several meteorological parameters, including wind, temperature, atmospheric pressure, as well as others including visibility and cloud coverage, are compiled into a single coded string which follows either the METAR/SPECI or SYNOP format. For aerodromes with several anemometers, only wind observations from the principal anemometer are included in METAR/SPECI and SYNOP reports. The same observed meteorological parameters, as well as those observed by additional anemometers, are sent to the Climatological Database (*Banco de Dados Climatológicos* – BDC), under the responsibility of ICEA, located in São José dos Campos. More details regarding WEBMET can be found in MCA 105-16 (DECEA, 2015[b]).

For most Brazilian aerodromes, observations were made by analogue/conventional means and recorded using tabular forms, similar to that shown in Figure 3.1, up until the early 2000s. Forms are archived at ICEA in São José dos Campos as shown in Figure 3.2. The date of change from analogue/conventional to digital readings varies for each aerodrome, and there is no known database which contains such information. The process of digitalising historical surface meteorological records began in October, 1988, and ended in October, 2013 (Rocha, 2016).

The image shows a detailed weather observation form from the Brazilian Meteorological Service (SBHT). The form is titled 'OBSERVAÇÃO METEOROLÓGICA À SUPERFÍCIE' and is dated 01/11/1988. It contains various sections for recording weather data, including time, location, and specific meteorological observations. The form is filled with handwritten data in black ink.

Figure 3.1 – Photo of a completed, hand-written weather observation form at SBHT – Altamira, PA, for 01/11/1988



Figure 3.2 – BDC Archives at ICEA in December 2016.

The implementation of digital processes improved wind observation accuracy. Conventional observations were made using analogue instruments, as shown in Figure 3.3a) and require the observer to mentally calculate means, gusts and predominant wind direction, increasing the

possibility for errors to be introduced into the recorded observation. Analogue processes often also include anemographs in which the amplitude of the wind speed is recorded using a pen/pencil shifting up and down over paper moving in a normal direction at a constant rate; however, no evidence of its historical usage was encountered in Brazilian aerodromes. Digital processes allow for simultaneous calculation of all wind related readings and remove the human error from the observation. The image of a real-time digital reading in Figure 3.3b) also demonstrates the benefits of real-time visualisation of data. A number of data can be understood clearly from a single image. For the example in Figure 3.3b), the black line represents the runway, allowing for identification of wind-shear, and light-green arrow the predominant direction over 2 minutes. The light-green arc represents the range of wind directions over the 2-minute period, and similarly the dark-green arc over a 10-minute period. The number at the centre represents the instantaneous wind speed, and can be toggled by the observer to show real-time means over 10 minutes, or any other pre-programmed averaging period. Similar controls allow for the observer to view the predominant wind direction over 10 minutes, which would be a dark-green arrow in this case.

Digital processes also aid in the compilation and emission of METAR/SPECI reports, and preset limits are utilised to alert the need for a SPECI report to be emitted. The reports are automatically compiled; however, an observer can edit the report before emission. For ASWS, both compilation and emission of the report are done automatically without the need for an observer. The use of ASWS in aerodromes is not yet widespread in Brazil. SBSP – Congonhas, SP, became the first Brazilian aerodrome equipped to emit AUTO METARs on 03/03/2015. This mode is active between the hours of 02:00 and 07:00 UTC and remains the only such aerodrome as of the end of 2017.



Figure 3.3 – Wind speed and direction readings by a) analogue and b) digital processes.

3.1.1.1 METAR/SPECI

Although highly standardised by ICAO and WMO, each country has slight variations in the reporting procedures of METAR/SPECI reports. An inspection of approximately 23 years of reports for 198 stations in the study revealed that the pre-defined structure is often loosely followed. In most cases, the reports are divided into 7 fields: 1. Time and location identifiers; 2. Wind observations; 3. Visibility; 4. Weather descriptors; 5. Cloud information; 6. Air temperature and dewpoint temperature; 7. Atmospheric pressure at sea-level. In some instances, supplementary information can be found after the atmospheric pressure field such as recent weather, wind-shear or weather forecasts. The last character of each report should be “=” to correctly identify its termination for parsing purposes.

The format used to report time and location of the SWS is followed universally, and the space delimiter is used to separate fields. Immediately following the METAR or SPECI identifier at the start of the report is the four-letter location identifier assigned by ICAO. An ICAO ID starting with “S” denotes the South American region, with Brazil’s principal aerodromes starting with “SB”. The following field takes the format *YYGGggZ*, where *YY* is the day of the month, *GG* is the hour, *gg* minutes past the hour and *Z* represents UTC. It is important to note that METAR/SPECI reports contain no information about the month, or year, of the observation, and such information can only be obtained from data external to the report.

For Brazil, reporting procedures are defined by ICA 105-15 (DECEA, 2018[b]) and ICA 105-16 (DECEA, 2017), which subsequently defines 8 acceptable variations of wind observations. The most commonly encountered 7 variations, with accompanying examples, are shown in Table 3.2. Wind speed units utilised in Brazil are knots (kt). *V* and *DIR* are always reported; the peak 3-second gust over the 10-minute period, *G*, is only reported when the criterion in Table 3.1 is met.

The 8th variation is used in the case of an observed *V* or *G* equal to or above 100 kt, represented by *P99KT* (P for “plus”), however its use was not encountered at any Brazilian aerodromes from 1996 to 2017. It is concerning that this protocol does not permit for the accurate recording of wind speeds above 51 m/s. For countries which often experience tropical cyclones, such as USA and Australia, wind speed field is extended to 3 digits when wind speeds above 100 kt are observed.

Table 3.2 – METAR/SPECI reports with correctly formatted wind observation fields.

Type	Date (UTC)	Example	DIR (°)	V (kt)	G (kt)
No wind (calm)	02/07/1996	SBLO 021100Z 00000KT 9000 SCT100 ...	-	0	-
No reading	02/08/2006	SBGO 022100Z ////KT 9999 FEW025 ...	-	-	-
Standard reading	31/12/2015	SBRJ 312300Z 15006KT 9999 FEW035 SCT100 ...	150	6	-
Reading with <i>G</i>	17/12/2013	SBPA 171842Z 11014G24KT CAVOK 29/18 ...	110	14	24
Variation of <i>DIR</i> $\geq 60^\circ$ & $< 180^\circ$, <i>V</i> < 3 kt; or variation of <i>DIR</i> $\geq 180^\circ$	29/12/2008	SBSP 291200Z VRB02KT CAVOK 25/18 ...	-	2	-
Variation of <i>DIR</i> $\geq 60^\circ$ & $< 180^\circ$	05/04/2011	SBSP 051800Z 19007KT 140V240 9999 TS ...	140-240	7	-
Varying <i>DIR</i> , with <i>G</i>	08/12/2003	SBPF 011600Z 27020G30KT 230V290 5000 ...	230-290	20	30

Current practice in Brazil is for METARs to be made on the hour, although this was not always the case with METARs made at 30-minute intervals in the period between 11/1999 and 10/2001. Special METAR reports (SPECI) are made when there is a significant change to meteorological conditions between the hourly METAR observations. A wind-related SPECI report is issued when one or more of the following criteria is met:

- *DIR* shifts by 60° or more since the last observation, and *V* is equal to, or greater than, 10 kt before and/or after the change,
- *V* changes by 10 kt or more since the last observation,
- *G* changes by 10 kt or more since the last observation, and *V* is equal to, or greater than, 15 kt before and/or after the change.

Weather descriptors of interest for extreme wind analysis include thunderstorm (TS), widespread dust (DU), sand (SA), dust/sand whirls (PO), squall (SQ), tornado/funnel cloud/water spout (FC), sandstorm (SS) and dust storm (DS). The weather descriptors are often accompanied by qualifying terms, such as light (-), heavy (+), if the phenomenon is located in the vicinity (8-16 km) of the aerodrome (VC) or if it recently occurred (RE). Should there be no weather phenomenon observed the field remains absent from the report.

The air temperature, T , and dew point temperature, T_d , measured in Celsius, are delimited by “/” between the two 2-digit fields. Negative temperatures are indicated by the use of “M” (for “minus”) before the two digits. For example, a temperature of 10 °C and dewpoint temperature of -2 °C will appear as “10/M02”. If either of the two temperatures is not observed it should be replaced by “//”, and if neither temperature is observed the field should appear as “/////”.

The atmospheric pressure adjusted to sea level, QNH , is the final information to be extracted from the report. The field is prefixed with “Q” which is followed by four digits and is measured in hPa. For example, a QNH of 995 will appear as “Q0995”. If no QNH is observed the field should appear as “Q/////”.

Similar protocols are followed by other South American nations which are included in this study, with the respective bodies and publications listed in Table 3.3, with the exception of Bolivia, French Guiana, Guyana and Suriname, for which corresponding publications were not encountered.

Table 3.3 – Bodies and documents responsible for the definition of weather observation protocols at aerodromes within the study region.

Country	Body Responsible	Corresponding Technical Document Number and Name
Argentina	SMN	Manual de Procedimientos Operativos de Meteorología Aeronáutica Parte V (SMN, 2010)
Brazil	DECEA	ICA 105-16: Códigos Meteorológicos (DECEA, 2017)
Chile	DGAC	DAP 03 07: Observaciones e Informes Meteorológicos (DGAC, 2017)
Paraguay	DINAC	DINAC R 3: Servicio Meteorológicos para la Navegación Aérea Internacional (DINAC, 2017)
Peru	MTC	RAP 303: Servicio Meteorológico para la Navegación Aérea – Apéndice C (MTC, 2015)
UK	CAA	CAP 746: Requirements for meteorological observations at aerodromes (CAA, 2017)
Uruguay	DINACIA	RAU MET: Reglamento sobre el Servicio Meteorológico Aeronáutico (DINACIA, 2010)

3.1.1.2 SYNOP

Reporting procedures for SYNOP observations at Brazilian aerodromes are defined in ICA 105-16 (DECEA, 2017). Unlike METAR/SPECI reports, SYNOP reports from fixed land SWS, as identified by the prefix *AAXX*, are entirely numeric. Fields are delimited by spaces and the total number of fields within each report varies. The first four fields are of most

importance for surface wind observations. SYNOP reports are emitted at 3-hour intervals (00:00, 03:00... 21:00 UTC) and contain *DIR* and *V* but not *G*. Examples of a correctly formatted standard observation and a report with no wind observation are shown in Table 3.4.

Similar to METAR/SPECI reports, information regarding the month and year of the observation is obtained from data to the report. The first field is in the format *YYGGi_w*, where *YY* is the day of the month, *GG* is the hour of the day in 24-hour format, and *i_w* is the units of the wind observation, defined as follows: *i_w* = 0 is estimated speed in m/s, *i_w* = 1 is measured speed in m/s, *i_w* = 3 is estimated speed in kt and *i_w* = 4 is measured speed in kt. The second field *Iiiii* is the location identifier as assigned by WMO, and is commonly referred to as the SYNOP or WMO ID. The third field contains information relating to precipitation, station type, cloud heights and visibility. The fourth field takes the format *Nddff* where *N* is the total cloud cover, *dd* is direction of wind and must be multiplied by 10 to be converted to degrees (*dd* = 36 is North) and *ff* is observed wind speed in the units determined by *i_w*. Calm conditions are represented by *ddff* = 0000. In the case of wind speeds greater than 99, an optional group follows with the format *00fff*, however no such use of this convention has been found while examining South American data for this study.

Table 3.4 – SYNOP reports with correctly formatted wind observation fields.

Type	Date (UTC)	Example	<i>DIR</i> (°)	<i>V</i> (kt)	<i>G</i> (kt)
Standard reading	22/06/2012	AAXX 22184 83612 32470 61906 10196...	190	6	-
No reading	22/06/2012	AAXX 22213 83612 42470 5//// 1////...	-	-	-

The fifth field contains observed temperature data in the format *Is_nTTT*, where 1 is intentionally used to identify the temperature field, *s_n* indicates the sign of the temperature reading, where *s_n* = 0 is positive and *s_n* = 1 is negative, and *TTT* represents the temperature in increments of 0.1 °C. In the standard reading example featured in Table 3.4 the observed temperature is 19.6 °C. The sixth field follows the same format for dewpoint temperature, being *Is_nT_dT_dT_d*. The seventh field relates to atmospheric pressure at sea-level and takes the format *4PPPP*, where 49927 represents *QNH* = 992.7 hPa and 400167 represents *QNH* = 1016.7 hPa. The eighth field contains information regarding precipitation.

The ninth field is optional and relates to present and/or past observed weather. The field is of the format $7_{ww}W_1W_2$, with ww representing the phenomenon observed and W_1W_2 indicating when it occurred. The codes representing ww can be found in Table 4677 of ICA 105-16 (DECEA, 2017).

3.1.2 INMET ASWS

Brazil is divided into 10 Meteorological Districts (*Distrito Meteorológico* - DISME), as shown in Figure 3.4, with each DISME responsible for the management and maintenance of ASWS within its region. The first of INMET's ASWS stations were commissioned in Rio de Janeiro and Brasília in May, 2000. As of May, 2018, there were 583 ASWS in operation, with the large majority commissioned in the period between 2006 and 2008 as demonstrated in Figure 3.5. It is estimated that at least 40 ASWS have been commissioned and subsequently decommissioned over the network's lifetime.

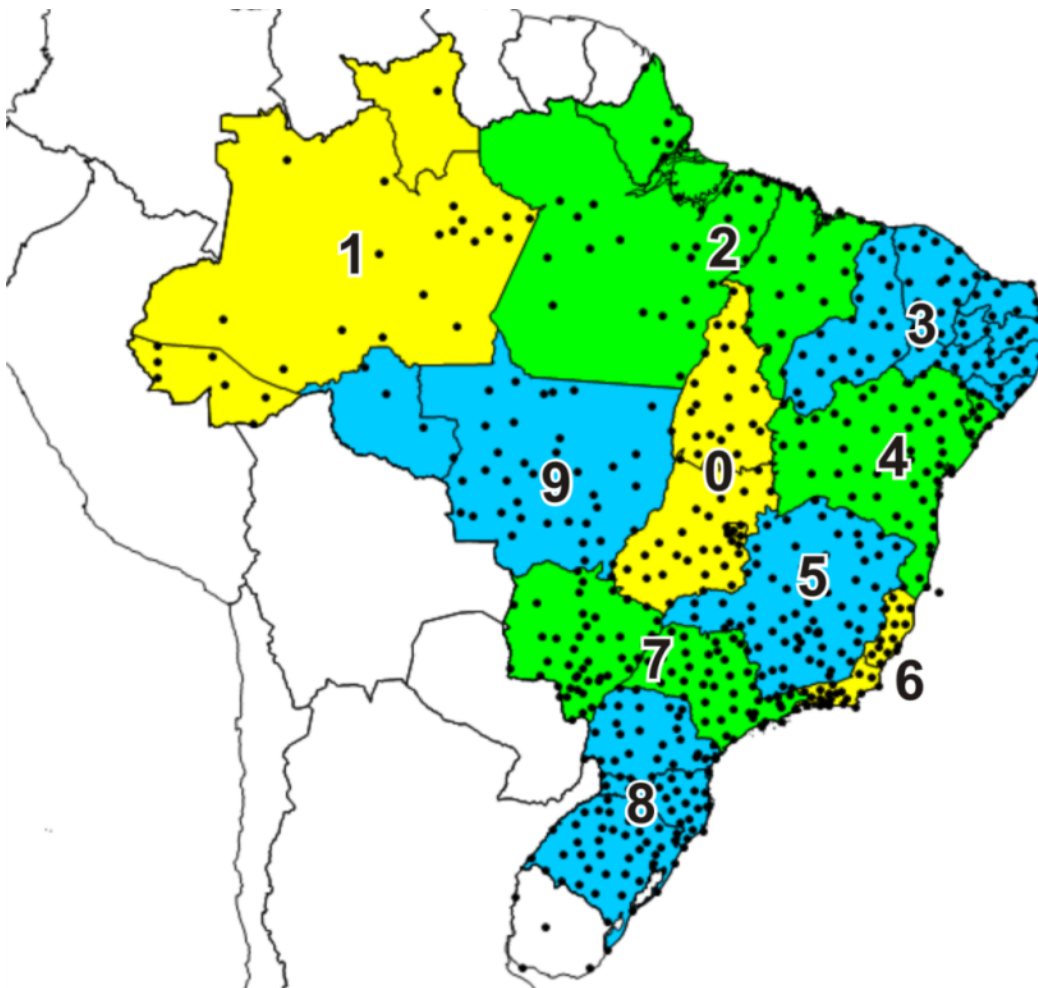


Figure 3.4 - Identification of DISMEs and location of ASWS stations (as of May 2018)

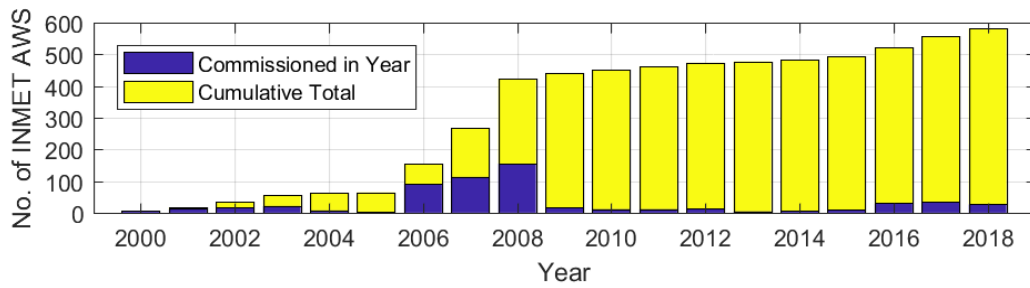


Figure 3.5 - Growth of INMET ASWS network

Meteorological data is transmitted via satellite from each ASWS to INMET headquarters in Brasília. Observations are emitted on an hourly basis, and for each hourly observation, 17 values are reported for 7 different meteorological parameters. Hourly maximum and minimum values, as well as the instantaneous value obtained at the hour mark, are reported for temperature, dewpoint temperature, atmospheric pressure and relative humidity. Instantaneous readings of radiation and the hourly precipitation accumulation are also reported. For wind observations, DIR and V are observed over the last 10 minutes of the preceding hour, while G is the maximum 3-second gust over the previous hour. According to the INMET (2011), wind speeds are sampled at 4 Hz, which are then processed digitally to determine DIR , V and G .

3.2 HOMOGENISATION OF WIND SPEEDS

Without giving consideration to the mean recurrence interval, the basic wind speed, V_0 , of NBR 6123 (ABNT, 1988) is defined as a 3-second gust at a height of 10 m for flat, open field terrain. It follows that all wind speeds which form the set of extreme value analysis to determine climatic models and update V_0 should also represent the same conditions ($z = 10\text{m}$, $z_0 = 0.07\text{ m}$ and $\tau = 3\text{ s}$). However, observed data do not commonly adhere to all three conditions and the wind speed time-series must be homogenised. Anemometer type, observing processes and exposure must be considered when determining appropriate correction factors; however, high-quality historical metadata is needed but difficult to obtain.

3.2.1 Gusts and instrumentation

The 3-second duration was not adopted as an international standard by the WMO to define peak gusts until the early 1990s. Although the “3-second gust” term was used globally prior to

the 1990s, it was considered the best representative estimate of the duration of a peak gust using analogue and conventional means. Differences in observed peak gusts were noticed at many SWS once digital processes were adopted, which led to the commissioning of studies to investigate the effective gust durations of different anemometers and effect of adopting a moving average on wind codes.

The Dines pressure tube anemometer was used in Australia until the early 1990s when it was replaced by cup anemometry. Holmes and Ginger (2012) attributed the origin of the 3-second gust in Australia to Whittingham (1964), who stated that “the Dines anemometer gives a good indication of the speed of strong gusts of 2 to 3 seconds duration”. The transitioning of Australian conventional weather stations to ASWS with cup anemometers caused a noticeable drop in annual maximum peak gusts. Holmes and Ginger (2012) identified three reasons for the change in peak gust amplitudes:

1. The effective gust duration of Dine pressure tube anemometers was determined to be equivalent to a moving average 0.2-second gust;
2. Cup anemometers, as with all rotating anemometers, filter out high frequency content as per the transfer function given in Equation 3.1. The distance constant, d , in metres, is the distance a fluid particle must travel past the sensor to cause it to register a speed of 63% of the actual fluid flow. For heavy cups with high inertia, d is also high. The Synchrotac 706, used in Australia, is one such anemometer with an estimated d of 13 m (Holmes and Ginger, 2012).

$$|H_1(f)|^2 = \frac{1}{1 + \left(\frac{2\pi f d}{\bar{u}}\right)^2} \quad 3.1$$

Where,

$|H_1(f)|^2$: anemometer admittance function

f : frequency, Hz

In two formats, Figure 3.6 illustrates the anemometer admittance function for 4 different distance constants at $\bar{u} = 20$ m/s. The filtering of the signal begins at higher frequencies for low d , and at low frequencies for high d , meaning heavy and slow-responding anemometers are unable to capture higher frequency fluctuations.

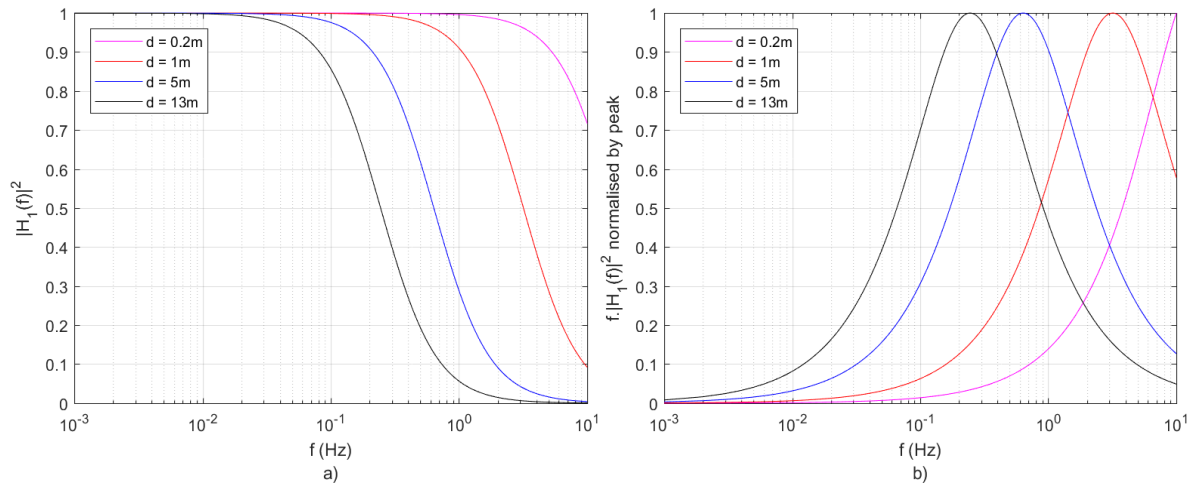


Figure 3.6 – Anemometer admittance function for various distance constants, d .

3. The application of a 3-second moving average filters out frequencies above 0.2 Hz, and completely suppresses frequencies which coincide with multiples 0.33 Hz. The formulation of the filter in the frequency domain is given in Equation 3.2, and an illustration is given in Figure 3.7 for 4 different averaging intervals, τ .

$$|H_2(f)|^2 = \left(\frac{\sin(f\pi\tau)}{f\pi\tau} \right)^2 \quad 3.2$$

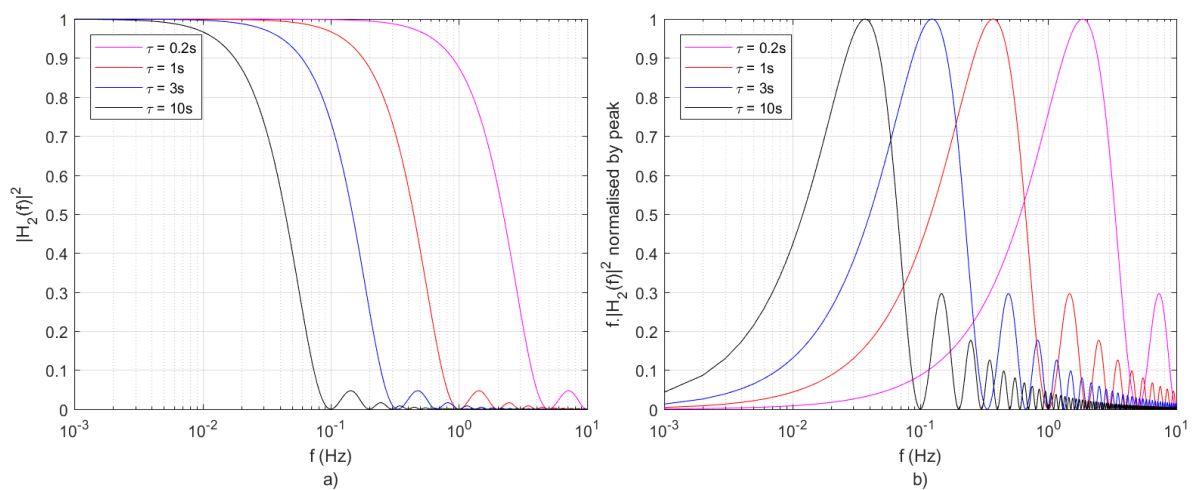


Figure 3.7 – Moving average filter in frequency domain for various time intervals, τ .

Hence, wind data acquired at the Australian ASWS from 1990s onwards was found to be subjected to the double filtering of a moving average and anemometer admittance, expressed in a single form by Equation 3.3. Since the then current regional basic velocities of AS/NZS 1170.2 (2002) were based on data acquired by Dines pressure tube anemometers, the peak gust was redefined to be a moving average 0.2-second gust (Holmes and Ginger, 2012; AS/NZS, 2011).

$$|H(f)|^2 = |H_1(f)|^2 |H_2(f)|^2 \quad 3.3$$

Correction factors were derived by Ginger and Holmes (2012) to convert observed gusts acquired at the newer Australian ASWS with cup anemometry to a 0.2-second gust in order to assist future research. By application of transfer functions to the spectral density of wind turbulence, expected peak and gust factors were then determined by the application of random process theory. The filtering effect of the transfer functions from Equations 3.1, 3.2 and 3.3 to the von Kármán turbulence spectra of Equation 2.7 is shown in Figure 3.8 for $\bar{u} = 20$ m/s, $L_u = 85$ m, $d = 13$ m, $I = 20\%$, $T = 600$ s and $\tau = 3$ s. In order to avoid loss of the standard deviation, a theoretical sampling frequency of $f = 100$ Hz is used.

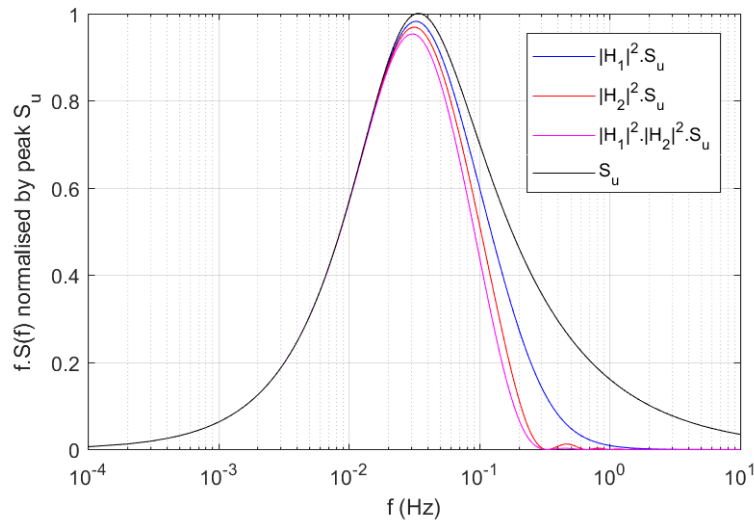


Figure 3.8 – The effect of filtering on turbulence spectra, S_u .


The cycling rate, ν , is calculated from Equation 3.4 and expected peak factor, g , is calculated using Davenport's (1964) closed-form equation for Gaussian processes, as shown in Equation 3.5. For the same set of parameters used to generate Figure 3.8, an example is given in Table

3.5. Note that peak factors are rescaled according to the difference in standard deviations between the filtered and unfiltered processes (Holmes et al., 2014). In the given case, the $\tau = 0.2$ s moving average generates $G_V = 1.682$, while spectra filtered by heavy cup anemometry and a $\tau = 3$ s moving average generates $G_V = 1.483$ – meaning a correction factor of 1.13 must be applied to the second case to adjust to gusts of $\tau = 0.2$ s moving average. The effect of an anemometer with low d (2 m) is minimal in regards to filtering of the $\tau = 0.3$ s moving average as shown in Table 3.5. Factors can be determined via the same process for different combinations of \bar{u} and I .

$$v = \left(\frac{\int_0^\infty f^2 \cdot S_u(f) \cdot |H(f)|^2}{\int_0^\infty S_u(f) \cdot |H(f)|^2} \right)^{1/2} \quad 3.4$$

$$g = \sqrt{2 \ln(vT)} + \frac{0.577}{\sqrt{2 \ln(vT)}} \quad 3.5$$

Table 3.5 – Calculation of expected peak and gust factors for filtered turbulence spectra.

Case	Spectra	Standard deviation, σ (m/s)	Cycling rate, ν (Hz)	Expected peak factor, g	Gust factor, G_V
Turbulence spectra only	S_u	4.0	3.9389	4.1399	1.828
Filters: Cup ($d=13$ m) and moving average ($\tau=3$ s)	$ H_1 ^2 \cdot H_2 ^2 \cdot S_u$	3.3144	0.0531	2.414 	1.483
Filter: Moving average ($\tau=0.2$ s)	$ H_2 ^2 \cdot S_u$	3.8774	0.3653	3.4094	1.682
Filters: Cup ($d=2$ m) and moving average ($\tau=3$ s)	$ H_1 ^2 \cdot H_2 ^2 \cdot S_u$	3.3890	0.0621	2.5144	1.503
Filter: Moving average ($\tau=3$ s)	$ H_2 ^2 \cdot S_u$	3.3916	0.0654	2.5314	1.506

The gust averaging interval is related to the effective frontal area, or equivalent area, A , over which a turbulent eddy is assumed to act. The aerodynamic admittance function proposed by Vickery (1968), shown in Equation 3.6, varies with mean wind speed and equivalent area. By following the same procedure used to determine expected peak factors for the mechanical

admittance and moving averaging filters, peak factors can also be determined for the aerodynamic admittance function. By matching peak factors determined for $|H_A|^2.S_u$ and $|H_2|^2.S_f$, A can be determined for a particular combination of \bar{u} and τ . This was performed by Holmes et al. (2014) and replicated in Figure 3.9 for $\tau = 0.2, 1$ and 3 s and \bar{u} ranging between 10 and 30 m/s ($T = 3600$ s, $I = 0.2$). For $\bar{u} = 30$ m/s and $\tau = 3$ s, $A = 3,200$ m² which equates to a building of height $h = 100$ m and frontal width of 32 m. For the same mean wind speed, the area differs greatly for shorter gust averages, with $A = 16$ m² and 350 m² for $\tau = 0.2$ and 1 s respectively. This implies that pressures determined by design wind speed of $\tau = 3$ s are inadequate for small structures using the quasi-steady principle, and a gust effect factor greater than 1 is necessary in such cases.

$$|H_A(f)|^2 = \frac{1}{\left[1 + \left(\frac{2f\sqrt{A}}{\bar{u}}\right)^{4/3}\right]^2} \quad 3.6$$

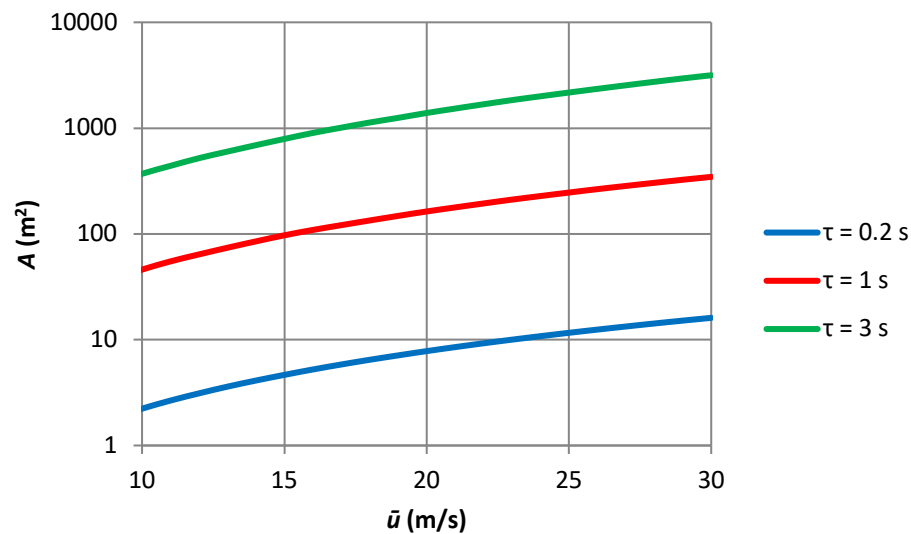


Figure 3.9 – Equivalent frontal area, A (m²), for varying gust averaging intervals.

A similar investigation into the effective gust duration was performed on the observing systems of the United States. Effective peak gust and mean wind speeds in ASCE 7 from 1995 to 2016 are $\tau = 3$ s and $T = 3600$ s respectively. According to Kwon and Kareem (2014), the F420C cup anemometer was used to record wind speeds that were used in the confection of the first peak gust-based wind map of ASCE 7 (1995). The anemograph system was

comprised of the rotating cup, with $d = 9.14$ m, and chart recording mechanism. The recording mechanism introduced a further filter to the recording system, as given in Equation 3.7, which is dependent on the response time of $t_r = 0.2$ s. Using a similar process as Holmes and Ginger (2012), it was determined that peak gusts measured by the system represented a moving averaging interval of $\tau = 1$ s, and proposed revisions to ASCE 7 (2010) were made by Kwon and Kareem (2014).

$$|H_3(f)|^2 = \frac{1}{1 + (2f\pi t_r)^2} \quad 3.7$$

The response characteristics of anemometers in operation in New Zealand were evaluated by Pirooz and Flay (2018). The MK II cups ($d = 14.3$ m) operated as an anemograph with chart recorder until they were replaced by lighter Vector A101, $d = 2.4$ m, and Vaisala WAA151, $d = 1.3$ m (Pirooz and Flay 2018), cup anemometers with digital recorders in the 1990s. The response of all three anemometers were tested in the wind-tunnel over a period of $T = 600$ s for $\bar{u} = 13$ m/s and $I = 0.145$. On average, the Vector A101 and Vaisala WAA151 cups recorded raw gusts that were 7-13% and 9-15% higher than those recorded by the MK II cup, respectively. When considering the $\tau = 3$ s moving average filter, the differences were 2-6% for Vector A101/MK II cups and 1-6% for Vaisala WAA151/MK II cups. The differences in peak factors and gust factors over a range of time-averaging intervals for the three cup anemometers are shown in Figure 3.10. There is generally good agreement between the two lighter cups; however, the heavier MK II cup tends to underestimate gust speeds.

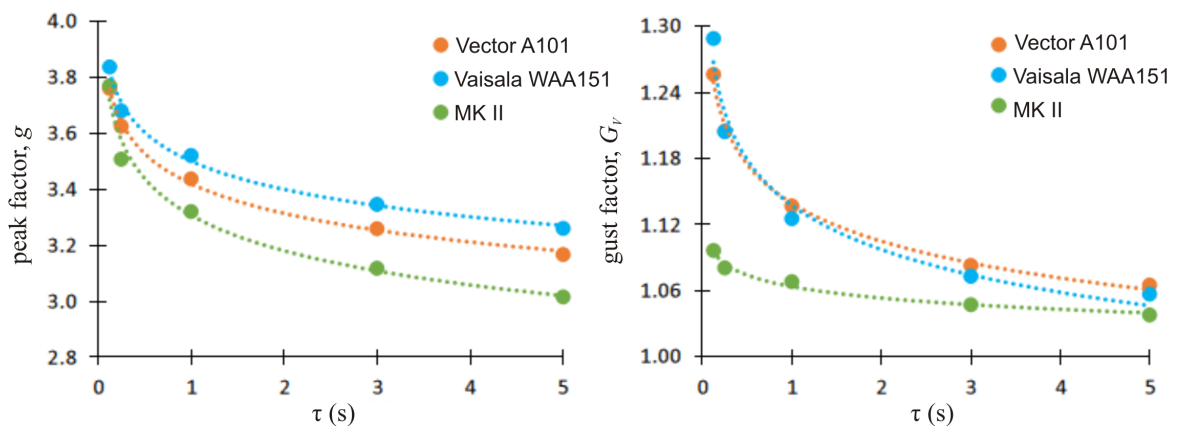


Figure 3.10 – Comparison of peak factors and gust factors obtained in controlled wind-tunnel tests for three different cup anemometers (adapted from Pirooz and Flay, 2018).

The importance of conducting experiments to compare against theoretical models is highlighted by results of Pirooz and Flay (1988). For $\tau = 3$ s, the theoretical expected gust factors for full-scale wind of $L_u = 85$ m are $G_V = 1.347$ ($d = 14.3$ m), 1.370 ($d = 2.4$ m), 1.371 ($d = 1.3$ m) and 1.373 ($d = 0$ m). These vary significantly from those of Figure 3.10 which range from 1.06 ($d = 14.3$ m) to 1.10 ($d = 2.4$ m) due to the smaller integral length scale of $L_u = 0.7$ m of the wind tunnel (Pirooz, 2019), which agree with the theoretical gust factors for $L_u = 0.7$ m of 1.07 ($d = 14.3$ m) to 1.09 ($d = 2.4$ m).

By following the same procedure of Holmes and Ginger (2012) and Holmes et al. (2014) as outlined above, the gust factors of NBR 6123 (ABNT, 1988) were examined. It was established in Section 2.3.1.3 *Wind characteristics* that NBR 6123 gust factors were based on Durst (1960), turbulence intensity is $I = 0.197$ at $z = 10$ m for CAT II ($z_0 = 0.07$ m) and the turbulence spectra is based on Harris (1968; apud Blessman, 2013). An analysis was performed for $\bar{u} = 20$ m/s and $I = 0.197, 0.169, 0.13$ and 0.1 over the range of τ used by NBR 6123. Peak factors, g , gust factors, G_V , and the NBR 6123 version of the gust factor, F_r , for the analysis are shown in Table 3.6. Both versions of the gust factor, G_V and F_r , are plotted in Figure 3.11. Gust factors were also tested at 5 m/s intervals up to $\bar{u} = 40$ m/s with negligible variation.

Ideally, the set of gust factors as determined by the analysis for $I = 0.197$ should be the same as those of NBR 6123 (ABNT, 1988), however this is not the case. Since the basic wind speed in NBR 6123 is defined for $\tau = 3$ s, an adjustment of gust factors for $I = 0.197$ according to this analysis would result in the lowering of design wind speeds at $T = 600$ s and 3600 s by approximately 4.5%. The gust factors from NBR 6123 fit best with gust factors generated by the analysis for $I = 0.169$, which agrees with Holmes et al. (2014) in the conclusion that Durst's (1960) gust factors relate to a turbulence intensity of $I = 0.165$ and should not be used as a universal curve. It is noted that the series of peak factors, g , remained constant for all four turbulence intensities analysed. For low turbulence intensity, $I = 0.1$, the difference between gust factors for $\tau = 3$ s and those of larger averaging periods is reduced as expected. An adjustment of NBR 6123 gust factors to $I = 0.1$ would result in the increase of design wind speeds at $T = 600$ s and 3600 s by approximately 15% and 17% respectively.

Each of the three main types of anemometers, cups, propellers and ultrasonics, has their operational advantages and disadvantages. With moving parts and bearings, propellers and cups need regular maintenance and calibration to avoid wear and the potential reduction of

signal. Propellers are lightweight but tend to underestimate low wind speeds and overestimate high gusts due to high inertia (ESDU, 1990[a]).

Table 3.6 – Comparison of peak and gust factors for NBR 6123 (ABNT, 1988) with Holmes et al. (2014) and Harris turbulence spectra.

τ (s)	3	5	10	15	20	30	45	60	120	300	600	3600
NBR 6123 (ABNT, 1988) – $I = 0.197$, $\bar{u} = 20$ m/s												
F_r	1	0.98	0.95	0.93	0.90	0.87	0.84	0.82	0.77	0.72	0.69	0.65
g ($= c$)	2.72	2.56	2.32	2.14	2.00	1.73	1.43	1.25	0.92	0.54	0.32	0
G_V	1.54	1.51	1.46	1.42	1.39	1.34	1.28	1.25	1.18	1.11	1.06	1
Holmes et al. (2014) method – $I = 0.197$, $\bar{u} = 20$ m/s												
F_r	1	0.97	0.93	0.90	0.87	0.84	0.80	0.78	0.73	0.69	0.66	0.62
g	3.12	2.91	2.54	2.29	2.09	1.80	1.52	1.32	0.92	0.54	0.35	0
G_V	1.62	1.57	1.50	1.45	1.41	1.36	1.30	1.26	1.18	1.11	1.07	1
Holmes et al. (2014) method – $I = 0.169$, $\bar{u} = 20$ m/s												
F_r	1	0.98	0.94	0.91	0.89	0.85	0.82	0.80	0.76	0.71	0.69	0.65
g	3.12	2.91	2.54	2.29	2.09	1.80	1.52	1.32	0.92	0.54	0.35	0
G_V	1.53	1.49	1.43	1.39	1.35	1.30	1.26	1.22	1.16	1.09	1.06	1
Holmes et al. (2014) method – $I = 0.13$, $\bar{u} = 20$ m/s												
F_r	1	0.98	0.95	0.92	0.90	0.88	0.85	0.83	0.80	0.76	0.74	0.71
g	3.12	2.91	2.54	2.29	2.09	1.80	1.52	1.32	0.92	0.54	0.35	0
G_V	1.41	1.38	1.33	1.30	1.27	1.23	1.20	1.17	1.12	1.07	1.05	1
Holmes et al. (2014) method – $I = 0.10$, $\bar{u} = 20$ m/s												
F_r	1	0.98	0.96	0.94	0.92	0.90	0.88	0.86	0.83	0.80	0.79	0.76
g	3.12	2.91	2.54	2.29	2.09	1.80	1.52	1.32	0.92	0.54	0.35	0
G_V	1.31	1.29	1.25	1.23	1.21	1.18	1.15	1.13	1.09	1.05	1.04	1

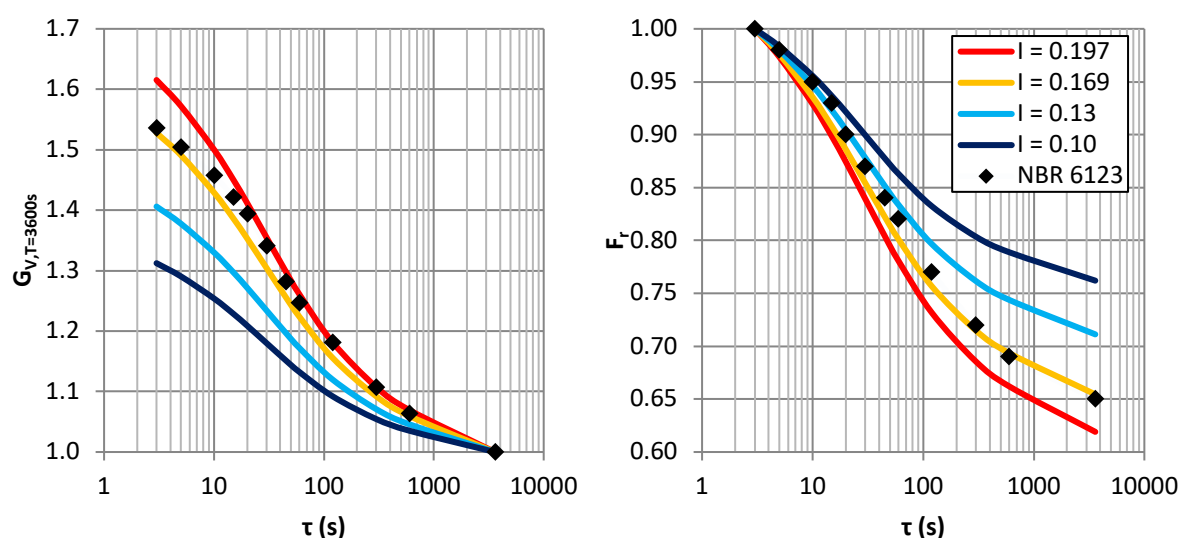


Figure 3.11 – Comparison of NBR 6123 gust factors with those calculated by spectral analysis.

Cup anemometers may also overestimate mean wind speeds due to the delayed deceleration of the rotating mechanism after wind speed decreases. Rotating anemometers also face the prospect of freezing when used in environments which experience temperatures below 0 °C. Ultrasonic anemometers measure the time between emission and reception of an ultrasonic pulse over a fixed distance operate to calculate wind speed, and since there are no moving components, they offer the possibility of increased accuracy and the minimisation of maintenance demands.

Results from studies comparing ultrasonic anemometers to traditional mechanical anemometers indicate higher observed wind speeds by the ultrasonic anemometer, and although the theoretical advantages of the ultrasonic anemometers over cup and propellers are compelling, some outcomes bring the technology's reliability into question. When comparing the Vaisala 425 AH heated ultrasonic anemometer with the Climet aerovane (Wastrack, et al. 2000), the ultrasonic continued functioning as normal during icing conditions while the aerovane did not; however, a suspected random electromagnetic signal caused the ultrasonic's sampling units to change from mph to knots whilst testing in-situ. Gilhousen (2001; apud Bowen, 2008) found the Gill 2D ultrasonic anemometers closely correlated with an aerovane at two coastal and one buoy site for winds under 15 m/s; however, wind speeds measured by the ultrasonic anemometer were 10% higher than the aerovane data during gale winds. The ultrasonic anemometer also gave unrealistic measurement of wind speed during thunderstorms, during and after rainfall or fog. Gorman (2004) noted that the RM Young Model 8100 3D ultrasonic anemometer produced artificially high wind speeds in rainy conditions when testing calibration of the Synchronac 706 cup anemometer, and subsequently discarded rain affected data acquired from the analysis. Short et al. (2006) observed an increase in peak wind speeds by Vaisala WS425 ultrasonic anemometers when compared to mechanical anemometers. Testing in field conditions at the Alcântara Launch Center in Brazil, Fisch (2010) found the Vaisala WS425 ultrasonic anemometer produced higher mean and maximum wind speeds, by 0.5 m/s and 1.0 m/s respectively, when compared to the R.M. Young Model 05305 propeller aerovane.

In 2007, a detailed investigation was conducted by NOAA (National Oceanic and Atmospheric Administration) into the performance of ultrasonic anemometers of the U.S. ASOS (Automatic Surface Observing System) which began to upgrade station anemometry from legacy Belfort model 2000 cups to Vaisala 425NWS Ice Free Wind Sensor in August of

2005 (NOAA, 2008). As of October 2007, only 183 of the 883 sites were yet to be upgraded to the ultrasonic sensor. A marked increase in the number of per-site error messages was noticed in mid-2007, taking the form of missing data or erroneous and extraordinarily high peak gusts. The subsequent investigation found that, along with icing of the anemometer due to failure of the heating element, interference from birds was the main reason for the high number of errors. Schmitt (2008) noted that corrupt samples resulted in bogus peak gusts that can exceed 100 kt on a calm day. Updates to acquisition software to identify errors prior to emission of reports (Schmitt, 2008) and bird ameliorating devices, such as the installation of perches adjacent to the anemometer, were implemented to reduce the number of errors (NOAA, 2008). Bird-related issues were also documented by Wauben (2012), which found that birds temporarily blocked the measurement path of the sensors as well as inflicting permanent damage to Thies 2D ultrasonics in the Netherlands.

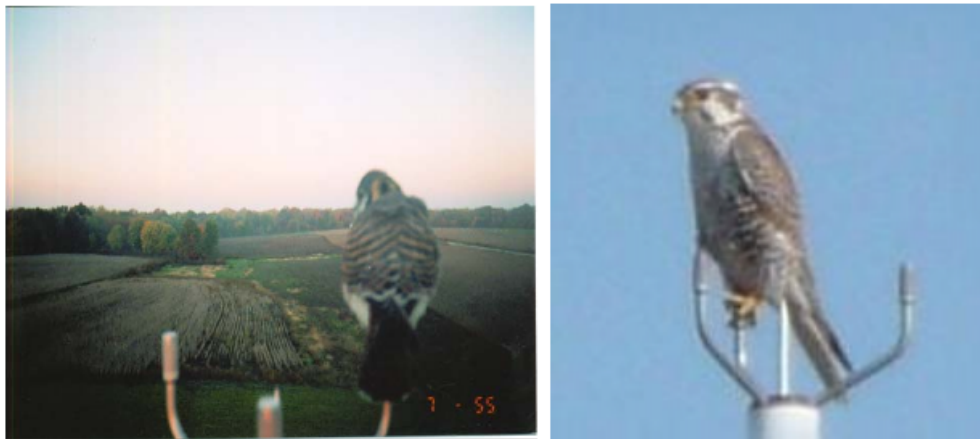


Figure 3.12 – Birds perching on ultrasonic anemometers (left – NOAA, 2008; right – Schmitt, 2008).

3.2.2 EXPOSURE

The height and surrounding environment of the anemometer, its exposure conditions, impact strongly on its observations. WMO (2014) defines three factors for the correction of observed wind speeds, u_{obs} , with roughness exposure, $z_{0,obs}$, at height z m to a standard roughness of $z_{0,cor}$ and height of 10 m for synoptic winds.

$$u_{cor} = u_{obs} \cdot C_F \cdot C_T \cdot \frac{\ln(10/z_{0,obs}) \ln(60/z_{0,obs}) \ln(10/z_{0,cor})}{\ln(z/z_{0,obs}) \ln(10/z_{0,obs}) \ln(60/z_{0,cor})} \quad 3.8$$

The correction factor, C_F , accounts for flow distortion by nearby large obstacles, such as buildings, is a function of wind direction with its best estimation calculated by wind-tunnel modelling. The topographic factor, C_T , is also a function of wind direction and accounts for the changes in topography around the anemometer – wind accelerates over the peaks of hills and mountains and subsequently $C_T < 1$; flat terrain is $C_T = 1$; and in deep valleys $C_T > 1$. Wind-tunnel modelling is the most appropriate form of determining C_T per direction at a particular site, however desktop studies can also be conducted using simplified approaches such 5.2 *Fator topográfica*, S_I of NBR 6123 (ABNT, 1988). Computational Fluid Dynamics (CFD) was used by Turner et al. (2019) to determine topographic correction factors at the anemometer of Wellington International Airport, New Zealand, and another anemometer located atop an island hill, part of The Brothers group of islands in the Cook Strait. The airport is subjected to turbulent eddies from hills located 2 km to the west as shown in Figure 3.13, which also shows the divisional directional factors, ranging from 1.5 to 0.85, which account for wind-speed up due to the steep incline at anemometer location of The Brothers.

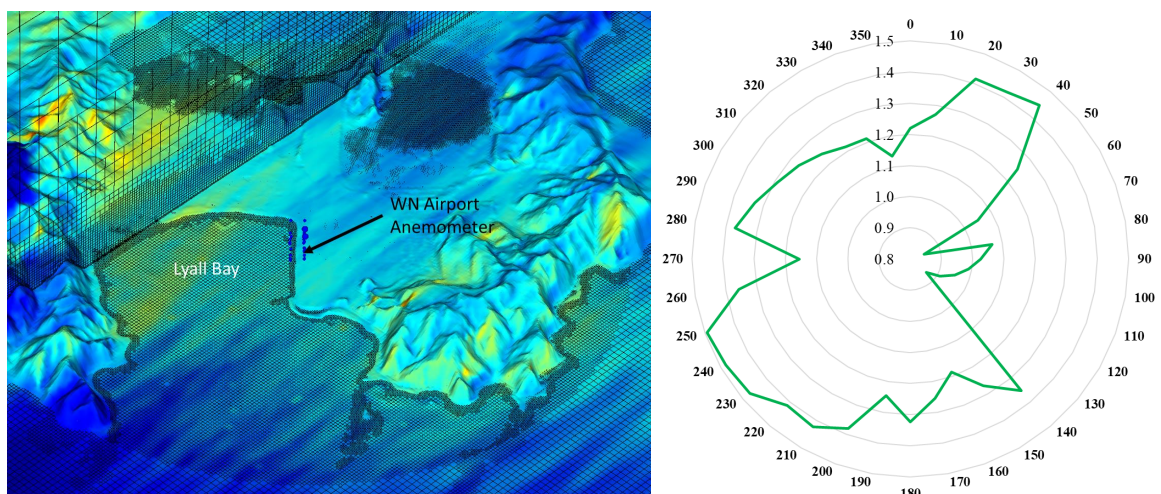


Figure 3.13 – Use of CFD to determine topographic correction factors (Turner et al., 2019). Left: CFD domain around Wellington International Airport. Right: topographic correction factors at The Brothers, NZ.

The majority of analyses which aim to homogenise observed wind speed focus on the estimation of site exposure, $z_{0,obs}$, of Equation 3.8. Methodologies for its determination are many in number and can generate wildly different outcomes, particularly at lower heights such as $z = 10$ m. The most pragmatic and simplest form of assessment is by assigning standardised values of z_0 via visual inspection of the terrain – typically from aerial

photography. A list of terrain categories and their respective roughness lengths according to WMO (2014) is given in Table 3.7.

Table 3.7 – Terrain classification of WMO (2014) in terms of toughness length z_0 . Based on Davenport (1960) and Wieringa (1980)

Class Index	Short terrain description	z_0 (m)
1	Open sea, fetch at least 5 km	0.0002
2	Mud flats, snow; no vegetation, no obstacles	0.005
3	Open flat terrain; grass, few isolated obstacles	0.03
4	Low crops; occasional large obstacles, $x/H > 20$	0.10
5	High crops; scattered obstacles, $15 < x/H < 20$	0.25
6	Parkland, bushes; numerous obstacles, $x/H \sim 10$	0.5
7	Regular large obstacle coverage (suburb, forest)	1.0
8	City centre with high- and low-rise buildings	≥ 2
Note: x is a typical upwind obstacle distance and H is the height of the corresponding major obstacles.		

Should this simple approach be adopted, an appropriate fetch length must be defined. Wieringa (1980), also responsible for Equation 3.8, recommended a fetch length of 2 km for analysis. Criticisms of the WMO backed Wieringa (1980) method of Equation 3.7 include the neglect of the change of friction velocity, u^* , between the two neighbouring terrains, and the assumption that the mean wind speed remains unchanged at a height of $z = 60$ m. These are not good assumptions for ABL winds, and it would be better to assume the wind is invariant at the gradient height, z_g .

Holmes et al. (2018) used a fetch length of 500 m when analysing terrain for application to both synoptic and non-synoptic wind types. AS/NZS 1170.2 (2011) originally recommended an averaging distance upwind of structure of 1 km for structures of $h < 50$ m; an amendment changed this distance to the greater of 40 times the height of the structure under analysis or 500 m (AS/NZS, 2012). For a structure of height 10 m, such as an anemometer tower, the recommended fetch length is 500 m.

Upwind fetches are rarely homogenous and typically the longer the fetch length the more changes in terrain categories. Open fields at airport locations are typically bordered by industrial, suburb, open water and in some cases, tall-building urban environments. Deaves (1981) proposed an internal boundary layer model which was adopted by NBR 6123 (ABNT, 1988). Any combination of x and z , as per Figure 3.14, is located in one of three regions:

1. For $x < 0$ or $z > z_t(x)$, the upstream flow is unchanged and remains in equilibrium with the profile determined by roughness length z_0 ;
2. For $x > 0$ and $z_i(x) < z < z_t(x)$, the flow is in the transition region where there is no equilibrium with z_0 upstream or downstream from $x = 0$, but must be a smooth transition between the two profiles;
3. For $x > F$ or $0 < z < z_i(x)$, equilibrium with profile determined by new roughness length z_0 .

As demonstrated in Figure 3.14, the new, or downstream profile, ‘grows’ from the surface upwards and the layer is thicker the further downwind from the point of transition.

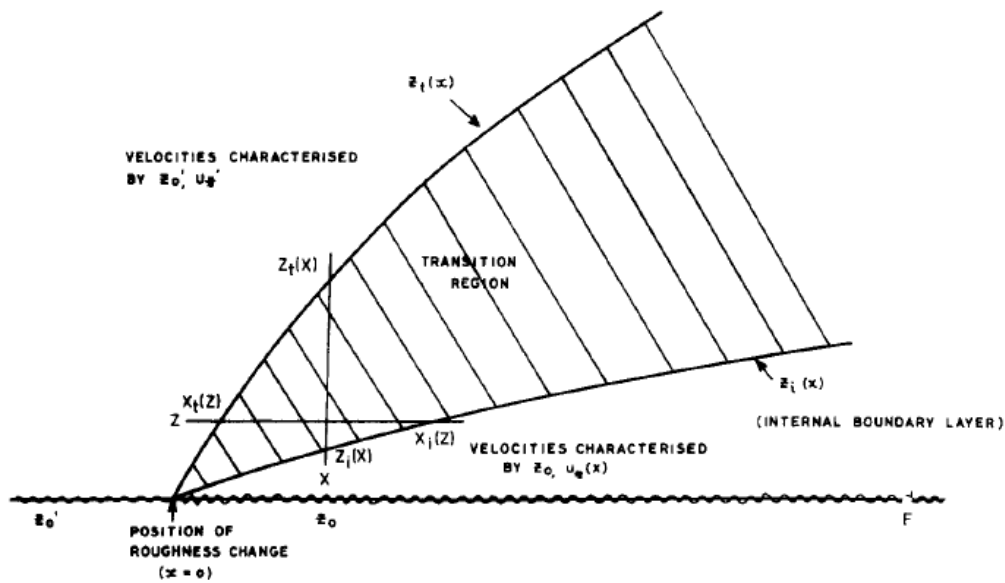


Figure 3.14 – Growth of internal boundary layer due to roughness change (Deaves, 1981).

According to Deaves (1981), Equation 3.9 determines the height of the transition layer, z_t , at distance x from the change in terrain, where z_0^+ is the larger of the two roughness lengths. For S-R transitions, the height of the internal layer is calculated by Equation 3.10, and Equation 3.11 is used for R-S transitions.

$$z_t = 10z_0^+(x/z_0^+)^{0.6} \quad 3.9$$

$$z_i = 0.36z_{02}(x/z_{02})^{0.75} \quad 3.10$$

$$z_i = 0.07x(z_{02}/z_{01})^{0.5} \quad 3.11$$

The method used in NBR 6123 to determine the terrain and height multiplier, S_2 , affected by change in terrain is based heavily on Deaves (1981). Different approaches are required for smooth-to-rough (S-R) transitions and rough-to-smooth (R-S) transitions with illustrative examples given in Figure 3.15. z_x , the equivalent of z_t from Deaves (1981), is calculated using Equation 3.12, with A defined by Equation 3.13 for S-R transitions, and Equation 3.14 for R-S transitions. The maximum height of the internal boundary layer for S-R transitions, z_i , is defined by Equation 3.10. For R-S transition, z_i is the height at which $S_2(z_i) = S_2(z_x)$. Linear interpolation is used for the transition zone between z_x and z_i for both S-R transitions.

$$z_x = Az_{02}(x/z_{02})^{0.8} \quad 3.12$$

$$A = 0.63 - 0.03\ln(z_{02}/z_{01}) \quad 3.13$$

$$A = 0.73 - 0.03\ln(z_{01}/z_{02}) \quad 3.14$$

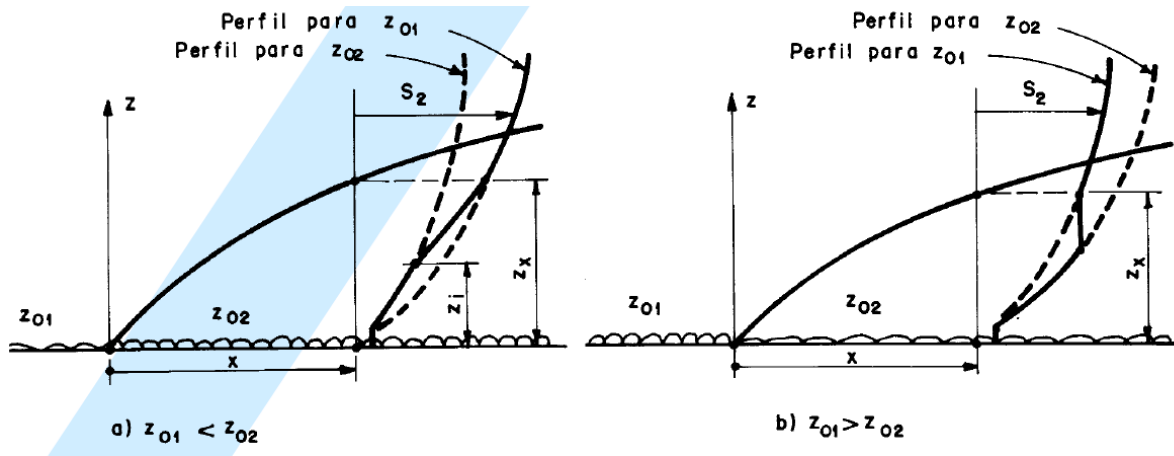


Figure 3.15 – a) Smooth to rough transition, b) Rough to smooth transition of NBR 6123 (ABNT, 1988).

If it is assumed that an anemometer is installed at $z = 10$ m in terrain of $z_0 = 0.07$ m, corresponding to V_0 of NBR 6123 (ABNT, 1988), the most severe R-S transition would be from CAT V of $z_0 = 2.5$ m. A simple analysis is performed to determine the minimum upwind distance, x , that must be of CAT II between the end of CAT V and the anemometer for the internal boundary layer to be fully developed for CAT II, $z_{01} = 2.5$ m, $z_{02} = 0.07$, $z_i = 10$ m and $S_2(z_i) = S_2(z_x) = 1.0$. Equation 2.13 is re-arranged to solve z_x for $S_2 = 1.0$ with corresponding CAT V parameters $b = 0.74$ and $p = 0.15$, giving $z_x = 74$ m. Equation 3.12 is then re-arranged to be a function of z_x and solved for $z_x = 74$, giving $x = 768$ m. However, using Deaves'

(1981) Equation 3.11 for R-S transition with $z_i = 10\text{m}$, gives $x = 84\text{ m}$. As such, the difference between the two methods is in the order of 10.

The ESDU 82026 (2002) method for the determination of vertical wind speed profile accounts for multiple changes in terrain. It was used in the derivation of the Irish regional basic wind speeds (Department of the Environment, Heritage and Local Government, 2009) for fetch length of 40 km. In the case of considering only a single change in terrain, the internal boundary layer, V_{zx} , from the new terrain, z_{02} , has height $h_{i,A}$, at location A as shown in Figure 3.16. For height greater than $h_{i,A}$ the wind speed profile, V_{z1} , follows that defined by the upstream terrain. Until the internal boundary reaches a full-developed profile for z_{02} , V_{z2} , at a certain distance, $h_{i,A}$ continues to grow and the internal boundary layer profile, V_{zx} , is defined by Equation 3.15. K_x is a multiplication factor which is applied to the fully-developed profile V_{z2} , and applies to the entire region from $0 < z < h_{i,A}$, and varies for S-R and R-S, as shown in Equations 3.16 and 3.19 respectively. f is calculated for S-R, Equations 3.17 and 3.18, and R-S, Equations 3.20 and 3.21, while the definition of R can be found in ESDU 82026 (2002) and is a function of other parameters. For V_{zx} to be fully-developed, $K_x = 1$, which only occurs when R, f_{SR} or $f_{RS} = 0$. $R = 0$ only when z_{01} and z_{02} are equal (i.e. no change in terrain), $f_{SR} = 0$ when $x \geq 316\text{ km}$, and $f_{RS} = 0$ when $x \geq 398\text{ km}$. In the case of $x = 10\text{ km}$ of CAT II terrain after an infinite length of CAT V located at Brazil's southern region, $z_{01} = 2.5$, $z_{02} = 0.07$, $R = 0.62$ and $f_{RS} = 0.58$ ($X = 4$), giving $K_x = 0.85$. This means that after 10 km of CAT II terrain, wind speeds in the internal boundary layer are only 85% of a CAT II profile. It can be argued that there is no infinite length of CAT V terrain, and a similar exercise is performed with a CAT I to CAT II change resulting in a 105% CAT II profile calculated at $x = 10\text{ km}$.

$$V_{zx} = K_x V_{z2} \quad 3.15$$

$$K_x = 1 + 0.67R^{0.85}f_{SR} \quad 3.16$$

$$f_{SR} = 0.1143X^2 - 1.372X + 4.087 \text{ for } (X \leq 5.5) \quad 3.17$$

$$f_{SR} = 0 \text{ for } (X > 5.5) \quad 3.18$$

$$K_x = 1 - 0.41Rf_{RS} \quad 3.19$$

$$f_{RS} = 0.0192X^2 - 0.550X + 2.477 \text{ for } (X \leq 5.6) \quad 3.20$$

$$f_{RS} = 0 \text{ for } (X > 5.6) \quad 3.21$$

$$X = \log_{10} x \quad 3.22$$

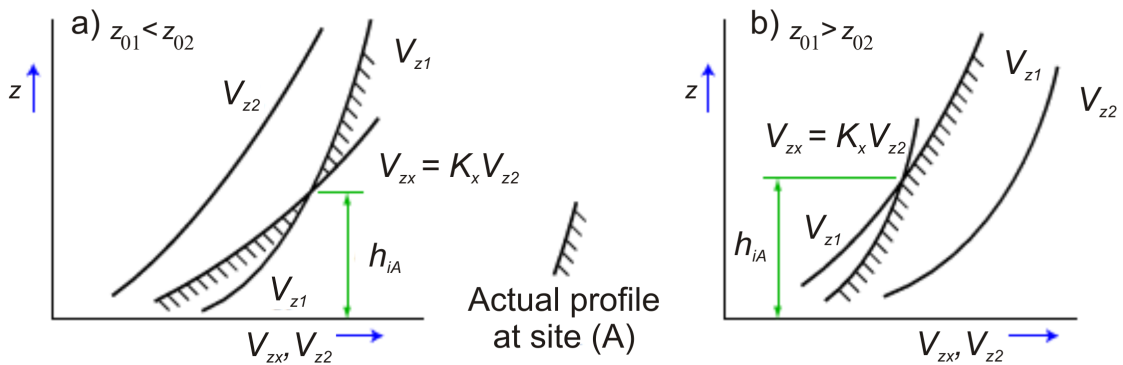


Figure 3.16 – a) Smooth to rough transition, b) Rough to smooth transition of ESDU 82026 (ESDU, 2002).

Other approaches to evaluate upwind terrain roughness and corresponding exposure correction factors include Hydra TL (Verkaik, 2001[b]) and the gustiness model of Masters et al. (2010). The Hydra Two-Layer model was one of three methods implemented by Gatey (2011) in a study of extreme synoptic winds across Europe. Land-use geographic information system (GIS) data were used with pixel resolution of 100 m x 100 m with 44 different classes. Each class was assigned to one of 13 different terrain categories of specific roughness lengths. Terrain was analysed over a total fetch length of 55 km for 12 x 30° sectors at discretised bands ranging from 0.2 km close to the site and 2.5 km at further distances. The Hydra Two-Layer model uses these discretised cells to determine a local and mesoscale footprint. This approach was initially considered for this study but rejected due to the coarseness of land-use GIS information of Brazil. The pixel resolution of *Cobertura e uso da terra* (IBGE, 2014) is 250m x 250m and only 13 land-use categories are defined – with no difference between high-density and low-density urban and suburban areas. The oversimplicity of the land-use GIS map is demonstrated in Figure 3.17 when compared with a satellite image for Porto Alegre, RS, with the location of three SWS shown.

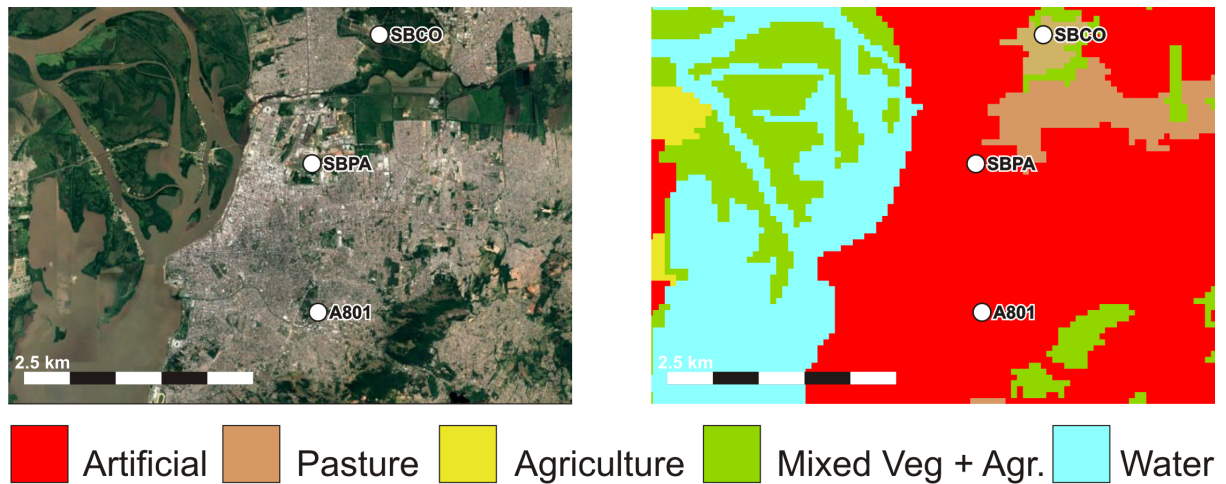


Figure 3.17 – Satellite image of Porto Alegre, RS (left), land-use GIS map (IBGE, 2014).

All previously mentioned methods require the exact location of the anemometer to determine its exposure as a function of wind direction. Such information can be difficult to obtain – particularly when considering the location of the anemometer is not constant over time. The gustiness model of Masters et al. (2010) does not require a known location, but derives gust factors G_V , of observed data per wind-angle or wind-sector, to then calculate z_0 using well-known relationships. The method was implemented at 148 ASWS of the United States using data recorded at high temporal resolution of 1-minute intervals. Data reduction methods were implemented to allow only synoptically driven gusts into the set of G_V analysed, meaning most thunderstorm events were likely removed. This method was initially considered for implementation in this study but rejected for four main reasons:

1. Lack of high-resolution data at both aerodrome SWS and INMET ASWS;
2. No correlation between DIR and G at INMET ASWS;
3. Dominance of non-synoptic events and lack of extreme synoptic events at most Brazilian SWS as determined in preliminary studies (Vallis et al., 2017; Vallis et al., 2018);
4. Filtering of observed gusts at aerodrome SWS as per $G \geq V + 10$ kt rule defined by ICAO (2007). This is demonstrated in Figure 3.18 for SBPA – Porto Alegre, RS, which shows no gust observations below the line defined by $G = V + 10$.

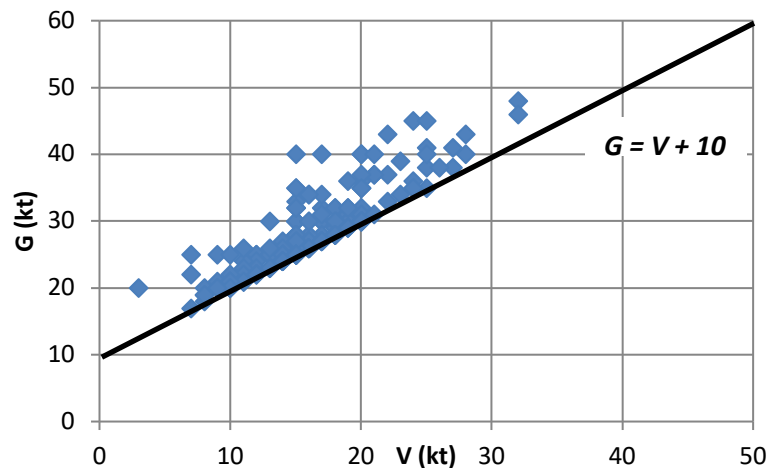


Figure 3.18 – Observed gusts and 10-minute mean velocities for wind-angles $DIR = 220^\circ$ - 240° at SBPA – Porto Alegre, RS, from 06/1996 to 12/2017.

All previously mentioned techniques consider only synoptic wind models with well-known relationships between roughness lengths, vertical wind speed and turbulence intensity profiles and turbulence spectra. Models for non-synoptic wind types are not as well-defined and there is little guidance regarding the homogenisation of non-synoptic wind speeds.

ESDU 87034 (ESDU, 1990[a]) offers a procedure to account for differences in terrain between the reference thunderstorm wind speed and a site wind speed of different terrain. It is proposed that for thunderstorm winds, a typical synoptic wind model for mean wind speed, such as the log-law model, is applicable for up to $z = 100$ m with wind speed remaining constant above $z = 100$ m. It is assumed that the boundary layer is not in equilibrium with terrain conditions of the site with roughness z_{02} of Figure 3.16, and using the method of ESDU 82026 (ESDU, 2002) an arbitrary distance of $x = 5$ km is used to develop an approximate profile. A factor, K_s (thunderstorm), is determined for a combination of reference z_0 and site z_0 which is then applied to the reference wind speed at $z = 10$ m, for example, V_0 , to derive a basic velocity at $z = 10$ m for the site. It is possible to reverse this procedure to correct observed non-synoptic winds to a desired reference roughness length.

Some investigations into thunderstorm and non-synoptic extreme winds do not address the question of homogenisation (Choi and Hidayat, 2002; Ferreira, 2017; Mohr et al., 2017). Holmes (2002) specifically did not apply exposure corrections to downburst events; while Holmes et al. (2018) analysed terrain within a radius of 500 m of known anemometer locations to determine correction factors based on vertical profiles of horizontal wind speed defined in AS/NZS 1170.2 (2011). The same exposure correction factors were applied to both

synoptic and non-synoptic events, however overall correction factors were different due to the assumption of $I = 0.1$ for non-synoptic events.

The height of the anemometer above ground is also of critical concern. Although WMO protocols require the anemometer to be at $z = 10$ m above ground, it is common to encounter stations that do not meet this requirement. Some Belfort cup anemometers were at a height of $z = 6$ m in the United States (Lombardo, 2012), the principal anemometer at Wellington Airport, New Zealand, changed from $z = 11$ m to $z = 7$ m in 1993 (Pirooz et al., 2018) and the anemometer which recorded data responsible for the confection of the Uruguayan basic wind speed map (UNIT, 1984) was located 45 m above ground and 13 m above the roof of a 4-storey building (Durañona, 2014). Data acquired from such a location is severely affected by acceleration over the rooftop which is near impossible to homogenise to a height of $z = 10$ m above ground. Canada's wind code, NBCC 2010 (NRCC, 2010), revised basic wind speeds to exclude data which were recorded from anemometers installed on lighthouses, airport hangars and other structures, which resulted in a decrease of wind speeds at several locations.

3.2.3 METADATA AT STUDY LOCATIONS

Few regions make station metadata available to the public to assist in research, and it is mostly left to research groups to dig for such information. Verkaik (2001[a]) published the locations of anemometers in the Netherlands which Gatey (2011) implemented into a study of European synoptic winds. National Institute of Standards and Technology (NIST) performed an investigation into the exact locations of anemometers at United States aerodromes and made available satellite images via their website⁶. NOAA developed a Historical Observing Metadata Repository (HOMR) web-based product, which lists historical metadata for SWS in the United States⁷. Anemometer type and co-ordinates are given, with photos per 45° to assist in the determination of terrain at some stations. Australia's Bureau of Meteorology (BoM) publishes annual updates of station metadata via their website, however exact locations of many anemometers are not included, particularly for larger aerodromes with multiple anemometers. The following link is an example of the metadata available at YBAS – Alice Springs, NT⁸.

⁶ https://www.itl.nist.gov/div898/winds/NIST_TN/sophie_pictures.htm

⁷ <https://www.ncdc.noaa.gov/homr/>

⁸ http://www.bom.gov.au/clim_data/cdio/metadata/pdf/siteinfo/IDCJMD0040.015590.SiteInfo.pdf

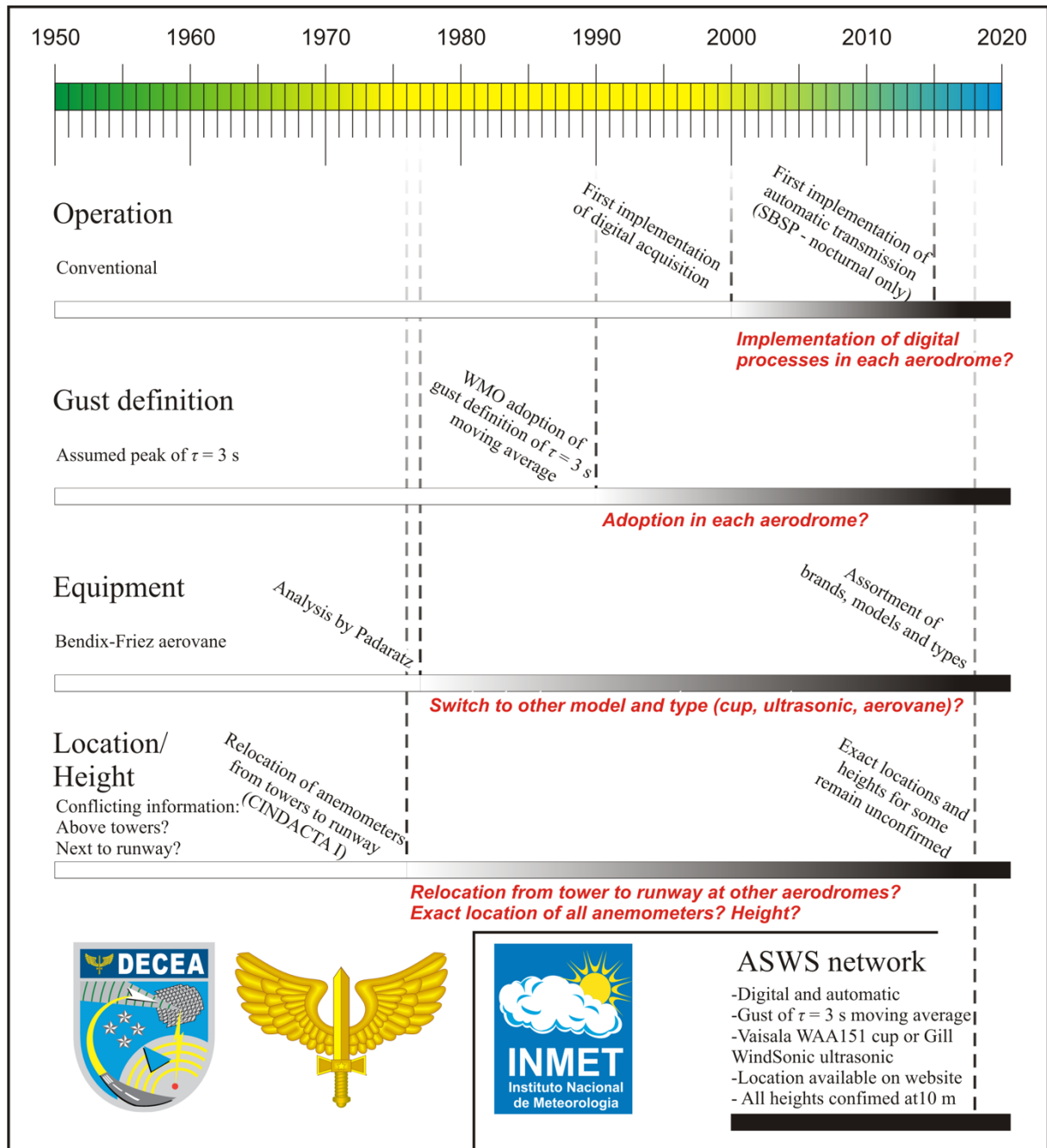


Figure 3.19 – Key moments regarding wind observations at Brazilian surface weather stations.

From 2016 to 2018, efforts were undertaken by volunteers at the Building Aerodynamics Laboratory (*Laboratório Aerodinâmico das Construções – LAC*), UFGRS, to gather historical and current metadata for anemometric equipment at target SWS. With the availability of information such as height, location, terrain exposure, anemometer brand and model, it is theoretically possible to homogenise observed data to a single predetermined height, terrain exposure and time-averaging interval for all stations. A summary of the key historical

moments in the development of wind speed observations at both Brazilian aerodrome SWS and INMET ASWS, as determined by this study, are shown in timeline form in Figure 3.19. The timeline is presented for four categories: station operation, gust definition, anemometric instrumentation and exposure conditions (location and height). Pertinent questions which remain without definitive answers are also listed for each category.

3.2.3.1 Aerodrome SWS

In compiling peak gust and wind speed measurements at 49 Brazilian aerodromes between 1950 and 1974, Vieira Filho (1975) cited FAB protocol (Ministério de Aeronáutica, 1964) which defined the averaging interval of a peak gust as 3-seconds due to the “approximate sensitivity of anemometers”, and as such, the gust duration of 3-seconds was adopted for V_0 in NBR 6123 (ABNT, 1988). Vieira Filho (1975), Padaratz (1977) and Hirata et al. (2010) all stated that Bendix-Friez aerovane anemometers were commonly used at Brazilian airports during this period. The distance constant of the 3-blade Bendix-Friez aerovane Model 120 is $d = 4.6$ m, with $d = 5.8$ m for the 6-blade version (Moses et al., 1968). There is no known record of an investigation into the effective gust response for this recording system, but given similar studies by Holmes and Ginger (2012) and Kwon and Kareem (2014), the effective time-averaging interval is unlikely to be $\tau = 3$ s.



Figure 3.20 – The Bendix-Friez aerovane propeller anemometer (Gill, 1973).

In order to compile metadata at all relevant aerodromes, relevant authorities were contacted, either by telephone or email, including all Brazilian aerodromes of interest, DECEA, ICEA, regional CINDACTA bodies (*Centro Integrado de Defesa Aérea e Tráfego Aéreo* – Integrated Centre of Air Defense and Air Traffic), regional INFRAERO bodies (*Empresa Brasileira de Infraestrutura Aeroportuária* – Brazilian Airport Infrastructure Company), INUMET (Uruguay), SMN (Argentina), Météo – France (French Guiana) and Met Office (UK – Falkland Islands). The Brazilian Aeronautical Information Publication (DECEA, 2018) was also consulted; however it is suspected that details are outdated for many aerodromes.

Vieira Filho (1975) stated that anemometers at Brazilian aerodromes were either at a height of $z = 10$ m above ground, or at such a height that when considering nearby obstacles would give the effect of being at $z = 10$ m, and all stations were considered to be in flat and open terrain. No specific information is given regarding the depth of investigation by Viera Filho (1975), and as such, these statements are more likely to be convenient assumptions more than the result of any investigation. By way of interviews with those working in the installation of meteorological equipment conducted for this current study, it was established that anemometers of CINDACTA I aerodromes were not installed adjacent to runways until 1976, and were located above control towers prior. Such aerodromes include SBSP – Congonhas, SP, SBKP – Campinas, SP, SBSJ – São José dos Campos, SP, SBBR – Brasília, DF, SBAN – Anápolis, GO, SBBH – Pampulha, MG, SBSC – Santa Cruz, RJ and SBYS – Pirassununga, SP. The same was performed the following year for SBGL – Galeão, RJ and SBEG – Manaus, AM. Such information brings serious questions to the validity of the study conducted by Padaratz (1977) to derive the V_0 map of Brazil.

In addition to testimony of meteorological instrumentation professionals, several documents indicate that anemometers continued to be located above buildings for many years after. Four such examples are shown in Figure 3.21. Runway schematics, drawn in 12/2003 and supplied by CINDACTA II, indicate that the principal anemometer at SBCY – Cuiabá, MT, was located above the control tower at that time. Latitude and longitude coordinates from 07/2009 were also given by CINDACTA II for the location of the principal anemometer SBMT – Campo de Marte, SP, which show its installation above a hangar near to the runway. A photo taken at SBAU – Araçatuba, SP, uploaded to the now defunct panoramio.com site by user Leo Benez on 06/12/2007, shows the location of an anemometer atop the aerodrome's control tower. Information for SBKP – Campinas, SP, provided by AIP (DECEA, 2018), suspected to

be now outdated, describes the location of the principal anemometer as 1.47 km from landing point 15 along the runway, and 794 m from its axis. A simple consultation using Google Earth imagery shows this location to be amongst buildings. In addition, the aerodrome operators of SBBU – Bauru, SP, confirmed that until 2002, two anemometers were installed atop the control tower – 18 m above ground level.



a)



b)



c)



d)

Figure 3.21 – Previous installations of anemometers above buildings a) SBCY – Cuiabá, MT, b) SBAU – Araçatuba, SP, c) SBMT – Campo de Marte, SP d) SBKP – Campinas, SP.

The most difficult metadata to obtain from Brazilian aerodrome SWS was type of anemometer, followed by height, with location the easiest to obtain. Very few aerodromes were able to provide any historical information and were mainly restricted to current metadata only. Anemometer type information was taken from AIP (DECEA, 2018) for 75 aerodromes, with only 4 aerodromes providing information and INFRAERO-BELÉM providing information for 2 aerodromes. Cup-type anemometers accounted for 58 aerodromes, aerovane/propeller types for 14 and ultrasonics at 9 aerodromes. AIP information is suspected to be outdated for many aerodromes meaning such counts may not be a true representation. Very few brand and models were confirmed, but those that were include Vaisala WS425 Ultrasonic, Vaisala WMT703A Ultrasonic, Vaisala WAA 151 Cup, $d = 2.0$ m (Vaisala, 2002) and Impulsphysic 43121/43303 (unknown).

As shown in Figure 3.22, the large majority of anemometer heights were unconfirmed. Of those that were confirmed, $z = 10$ m was the most common. Brazilian aerodromes that confirmed low anemometer heights include $z = 6.8$ m at SBIH – Itaituba, PA, $z = 6$ m at SBBU – Bauru, SP, and $z = 5.5$ m at SBPP – Ponta Porã, MS.

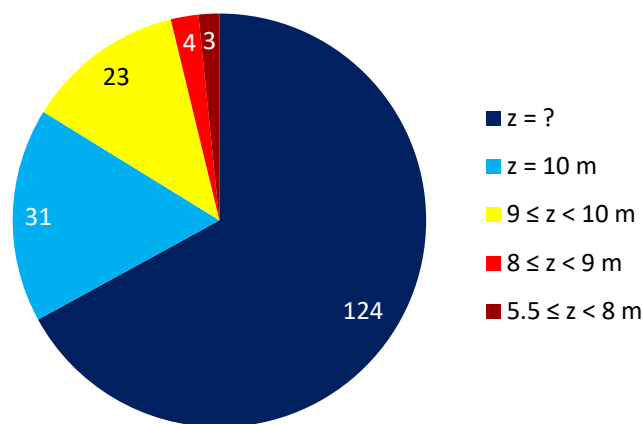


Figure 3.22 – Anemometer heights at Brazilian aerodromes during 2016-2018.

Anemometer locations were either given by relevant authorities, taken from AIP (DECEA, 2018) or estimated using knowledge of the location of the runway heading and a study of satellite photos. An analysis similar to Holmes et al. (2018) was performed at $8 \times 45^\circ$ sectors over a fetch of 500 m for all current anemometer locations. The average terrain category according to NBR 6123 (ABNT, 1988), with the inclusion of intermediate categories, was determined for each sector, with CAT II being the most common as shown in Figure 3.23.

However, there were several instances of CAT III-IV, with the example of SBFI – Foz do Iguaçu, PR, shown in Figure 3.24. Tall and dense vegetation to the west and southwest were determined as CAT IV, while open areas to the east and southeast correspond to CAT II. The other sectors were adjudged to be CAT III and III ½. According to Google Earth, the satellite image of Figure 3.24 was taken on 09/09/2018. A satellite image corresponding to the same location on 29/01/2019 is given in Figure 3.25 which shows vegetation immediately to the west and northwest of the anemometer has been razed, highlighting the changing nature of the terrain surrounding anemometers and the dangers of assuming a constant, or static, surrounding environment.

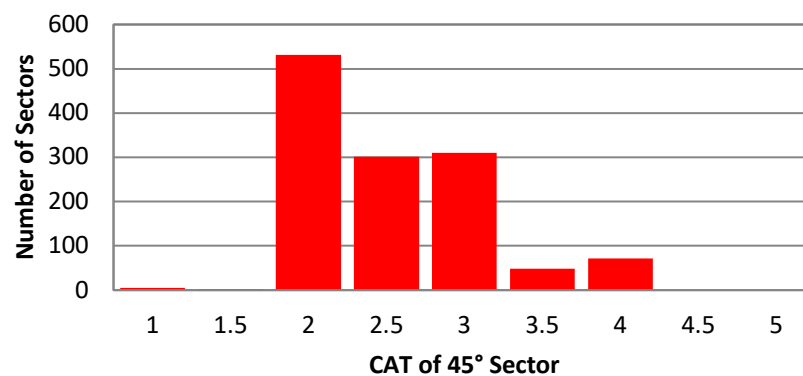


Figure 3.23 – Upwind terrain categories for anemometers at Brazilian aerodrome SWS.

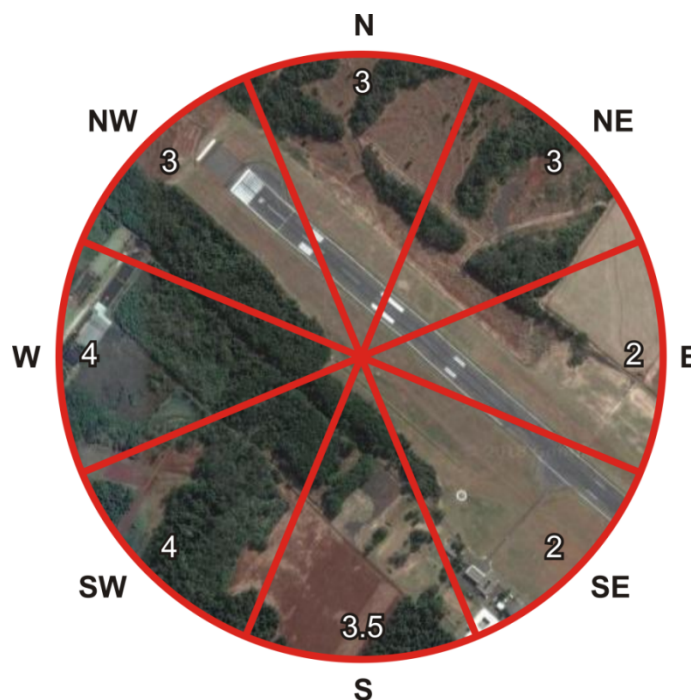


Figure 3.24 – Assessment of average terrain category per 45° sector over 500 m centred on location of principal anemometer of SBFI – Foz do Iguaçu, PR (Dated 09/09/2018).



Figure 3.25 – Satellite image of SBFi – Foz do Iguaçu, PR, showing razing of vegetation immediately adjacent to the runway (Dated 29/01/2019).

3.2.3.2 INMET ASWS

In addition to latitude and longitude coordinates of all ASWS available via INMET's website⁹, information on height, anemometer type/model and changes to any metadata was requested from INMET headquarters in Brasília and from all 10 DISMEs. With the exception of one DISME, all responded with appropriate information, including confirmation that all anemometers are installed at a height of $z = 10$ m.

Information received from INMET confirmed that only two types of anemometers are used in ASWS: Vaisala WAA151 cup or Gill WindSonic ultrasonic. Although there are some small discrepancies between information received from DISMEs and INMET in Brasília, such as the 7th DISME confirming the use of Vaisala WAS 425 ultrasonic anemometers at two stations and the affirmation that the Gill WindSonic ultrasonic has always been used at A001 – Brasília, DF, since the commission of the station on 07/05/2000, despite the anemometer not being released onto the marketplace until 12/2001 (Sims, 2019), metadata is better organized by INMET than for the aerodrome network. A count revealed the Vaisala WAA151 to be the most common, with 340 installations to 161 of the Gill WindSonic in 2018. There were 24 ASWS that changed from Vaisala WAA151 to Gill WindSonic at some point during operation, and 2 ASWS that changed from Gill WindSonic to Vaisala WAA151. The Vaisala WAA151 is a responsive small-cup anemometer and its size can be compared to that of

⁹ <http://www.inmet.gov.br/portal/index.php?r=estacoes/estacoesAutomaticas>

Synchrotac 706, a much heavier cup, in Figure 3.26. The Gill WindSonic, shown in Figure 3.27, uses 4 sensors and has a cap to prevent interference from birds and precipitation.



Figure 3.26 – Vaisala WAA151 cup anemometer (left), Synchrotac 706 cup anemometer (middle), and RM Young Model 8100 3D ultrasonic anemometer (Gorman, 2004).



Figure 3.27 – Gill WindSonic ultrasonic anemometer

Although considered to be permanently fixed locations, records indicate that at least 9 ASWS changed their location during their operational life. Provided coordinates of previous locations were approximations and exact locations are unknown. An analysis of terrain within 500 m of anemometers was also performed with terrain counts shown in Figure 3.28. Overall, exposure conditions for INMET ASWS are much more affected by buildings and vegetation than aerodrome SWS, with CAT III the most frequently encountered terrain category. Exposures of INMET ASWS range from those experienced at coastal locations, urban city centres, mountain peaks, airports and open fields. An example of two contrasting exposure

conditions is shown in Figure 3.29 – with tall vegetation and buildings surrounding all 360° of A801 – Porto Alegre, RS; whilst optimal open field exposure is experienced by A532 – Diamantina, MG, for all angles.

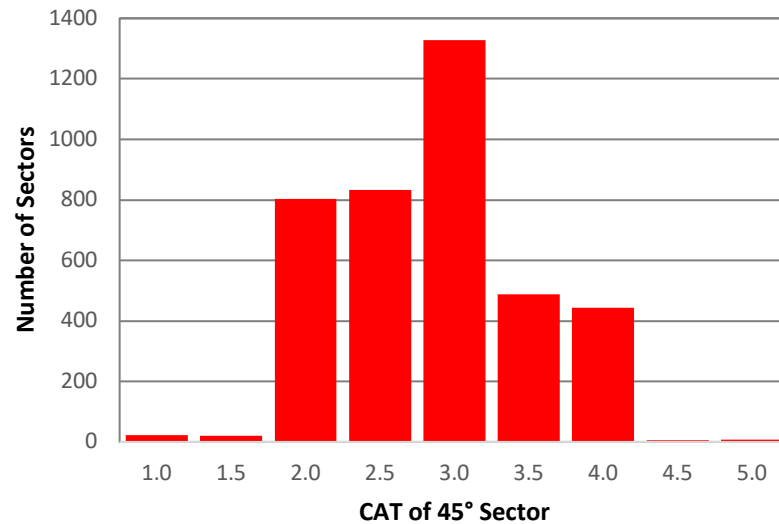


Figure 3.28 – Histogram of average upwind terrain categories for anemometers at INMET ASWS.

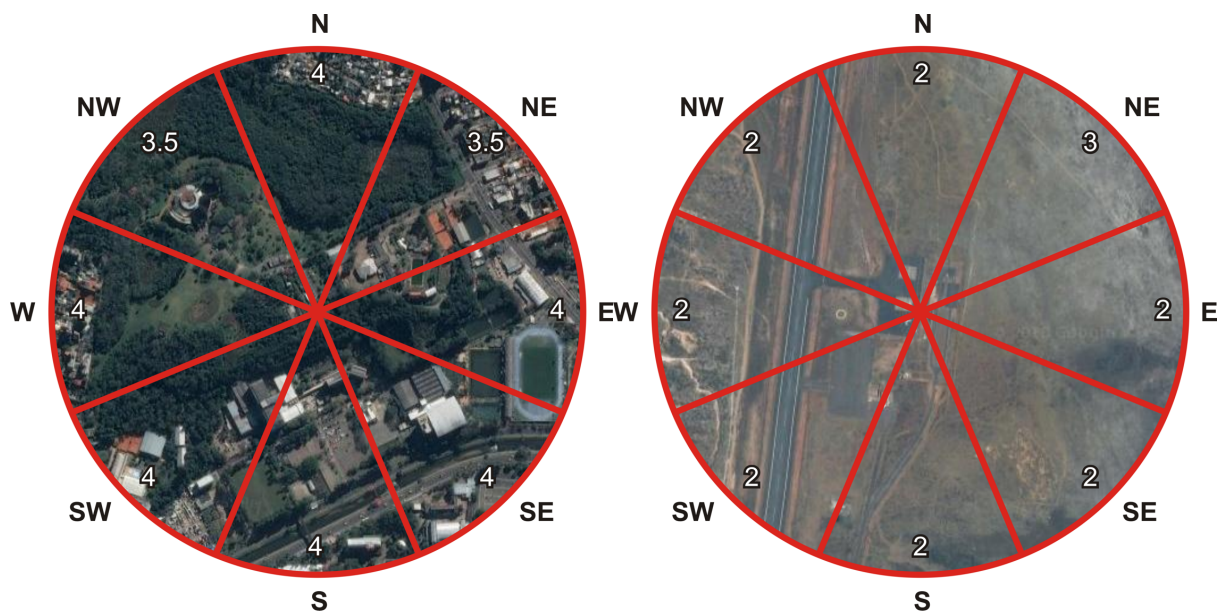


Figure 3.29 – Assessment of average terrain category per 45° sector over 500 m centred on location of anemometer at A801 – Porto Alegre, RS (left), and A532 – Diamantina, MG (right).

4. EVALUATION OF SURFACE WIND DATA SOURCES

Missing and spurious data, as well as changes to station characteristics caused by modifications to equipment or observational processes, are issues which plague almost all meteorological stations. However, there are some problems which relate to only certain datasets or meteorological networks. A description of issues encountered within each dataset and meteorological network are described in this section, and include the manipulation of data, whether intentional or not. Such manipulation may be the result of attempts to remove spurious data, but inadequate scrutinising processes mean real extreme wind events are also discarded with false data.

4.1 AERODROME SWS

4.1.1 METAR, SPECI and SYNOP (MSS)

The dataset extracted from METAR/SPECI or SYNOP meteorological reports, as presented in Section 3.1.1 *Aerodrome SWS*, using methods developed in this study is referred to MSS – distinctly different from data made available by third-party databases which have METAR/SPECI or SYNOP origins. Despite the existence of well-defined reporting protocols, errors in METAR/SPECI reports are common. There are two distinct types of errors: an error in the formatting of the report, and an error in the observation of a correctly formatted report. Both types of error are most often caused by the historically high dependence on manual processes at SWS. Only in the last 10-15 years have many South American airports switched to digital readings and automatic compilation of METAR/SPECI reports, and as such, the chance of encountering errors decreases the more recent the report. These errors can cause problems for automated data extraction routines, and it is pertinent that caution be taken when executing such processes to avoid the use of incorrect data in climate analyses.

A list of the most commonly found formatting errors in METAR/SPECI reports for the study region are reported in Table 4.1. For the large majority of cases, the mistake is a typographic error and its impact is limited to within a single METAR/SPECI report. However, there are other cases in which two or more METAR/SPECI reports are available for the same combination of SWS and timestamp. There are two possible reasons for this: either a second

report is emitted to correct a previously emitted report with an error (from 2012 onwards, *COR*, for “correction”, denotes such a report), or, one or more reports have an incorrect timestamp or month and year metadata.

Table 4.1 – Common formatting irregularities encountered in METAR/SPECI observations.

Irregularity	Date	Example of irregularly formatted METAR/SPECI
No delimiter	06/03/2014	SBSN 060100Z 060100Z15003KT 9999 TS FEW017 FEW020CB SCT100 25/23 Q1012=
Two different METARs joined together	19/06/2003	SBEG 192100Z 11009KT 9999 FEW020 FEW025TCU 32/25 Q1010 SBTT 192100Z 30004KT 9999 SCT020 FEW025TCU BKN300 //// Q1010=
Report is TAF	24/06/2014	SBSP 240211Z 2406/2506 05003KT 8000 NSCTN15/2409Z TX26/2418ZPROB30 2408/2411 3000 BRBECMG 2412/2414 33005KT CAVOKBECMG 2421/2423 05003KT RMK PGF=
Report is SYNOP	15/04/2005	SBJP 151800Z 32570 41414 10312 20234 40109 84200 333 58009=
Report is empty	02/01/2013	SBLO 020047Z =
Too many digits in wind observation	21/04/2003	SBGL 210300Z 090045KT 6000 -RA SCT008 BKN013 24/23 Q1017=
	02/07/2004	SBBE 022100Z 040086KT 9999 SCT013 BKN100 BKN300 26/24 Q1010=
Too few digits in wind observation	30/01/2003	SBBE 300400Z 1102KT 9999 FEW017 SCT300 24/23 Q1011=
	15/09/2003	SBFL 151800Z 3507KT 9999 BKN040 21/12 Q1020=
Units (KT) not clearly stated	03/10/2003	SBFL 030700Z 01006 9999 SCT010 BKN250 18/17 Q1016=
	11/02/2009	SBRJ 110400Z 33002 KR 8000 FEW018 BKN080 26/24 Q1012=
Wind observation field missing	12/02/2003	SBME 121700Z CAVOK 31/27 Q1013 W///S3=
	04/10/2003	SBAF 041200Z 7000 SCT018 BKN090 25/19 Q1021=
Multiple wind observation fields	19/03/2005	SBPA 190040Z 18018KT 17008KT 5000 -RA BKN008 OVC051 24/20 Q1013 WS RWY11=
	12/11/2008	SBSP 122011Z 122002KT 21006KT 3000 TSRA BR BKN013 FEW030CB BKN070 20/18 Q1011=
Wind direction not a multiple of 10°	12/10/2003	SBBE 120800Z 08803KT 9999 FEW017 BKN100 24/24 Q1009=
	04/05/2009	SBSP 041740Z 20927G43KT 9999 BNK025 18/12 Q1017=
Wind direction greater than 360°	07/02/2003	SBSP 070600Z 90005KT CAVOK 24/19 Q1017=
	24/05/2003	SBIH 241700Z 57005KT 9999 FEW025 BKN400 34/24 Q,008=
The letter "O" instead of digit "0"	10/03/2003	SBGL 100900Z OOOOOKT 9999 SCT020 BKN090 25/25 Q1012=
	28/03/2003	SBGR 282200Z 160 O 5KT 9999 BKN020 SCT100 21/18 Q1020=
Digit "9" used instead of digit "0"	24/07/2003	SBJP 242200Z 14997KT 9999 SCT020 24/23 Q1016=
	22/07/2009	SBRP 220400Z 98996KT CAVOK 21/16 Q1014=
Letters used instead of digits	15/01/2003	SBVH 152000Z PEYPPIKT 9999 SCT020 BKN100 29/23 Q1010=
	25/04/2003	SBMO 251400Z APRPQPKT 9999 BKN017 BKN300 28/21 Q1014=
Gust observation reported incorrectly	18/05/2011	SBEG 180024Z 32008G18 3000 RA BKN006 FEW025TCU BKN100 23/21 Q1012=
	25/07/2003	SBCH 251800Z 3301020KT CAVOK 26/16 Q1021=
Variable direction reported incorrectly	04/08/2009	SBMG 041800Z VRB09903KT CAVOK 29/15 Q1018=
	28/04/2008	SBCH 281500Z 330V03020G30KT 9999 FEW045TCU SCT070 25/19 Q1008=
Conflicting reports for same SWS and UTC	18/08/2007	SBPS 181200Z 15007KT 1000 +RA BR SCT009 SCT020 FEW025TCU 20/19 Q1022=
		SBPS 181200Z 11005KT 3000 -RA BR SCT015 SCT020 FEW025TCU 20/19 Q1022 RERA=
Incorrect calm report	12/01/2009	SBSC 120400Z CALMO CAVOK 24/22 Q1016=
Incorrect delimiter	22/03/2004	SBCH 220800Z 140/20KT CAVOK 16/13 Q1016=
Unintelligible information	26/08/2003	SBAF 260600Z 24 063801,-77),4- ?(,010 OVC080 17/17 Q1021=
Use of “RAF” not “G”	19/04/1997	SAWG 191600Z 270/35KT RAF.50KT 30KM 2CU3000FT 04/-04 QNH 10017=

The identification of suspect data for correctly formatted weather reports is a challenge faced in any type of analysis, independent of observing protocols. In the case of MSS and ICEA-BDC data, spurious data is often attributed to typographic errors. It is important that these data be correctly identified and removed as spurious data treated as real extreme values will affect the outcomes of the study. Methods for the identification and treatment of suspect data are covered in Section 6.5 *Identification of synoptic, non-synoptic and suspected false extreme wind events*.

As was the case for METAR/SPECI reports, errors can be found in the formatting of SYNOP reports. Amongst the most commonly encountered types of formatting errors are the incorrect reporting of calm conditions, wind direction greater than 360°, incorrect reporting of date and time, fields joined together due to a missing space delimiter, missing wind observation field and incorrect wind speed unit indicator. The last two error types can have a significant impact on the data extracted from the SYNOP reports.

An example is given in Table 4.2 of three reports of the same observation made at Salgado Filho International Airport, Porto Alegre (SBPA/83871) at 18:00 UTC, 06/12/2003: a SYNOP report, a METAR report and data from ICEA's BDC. This observation is of particular interest due to the $V = 56$ kt reported by two different third-party weather databases. When the SYNOP report is compared to both the METAR report and data from ICEA's BDC, which contain the correct wind speed and direction of $DIR = 290^\circ$ and $V = 10$ kt, the gross error becomes apparent. Additionally, a comparison with METAR reports prior to and after 18:00 UTC show that $V = 10$ kt is more appropriate. An inspection of the SYNOP finds that the fourth grouping, which normally contains the wind observation, actually contains the temperature data, while the wind data is missing from the report altogether. The incorrect reading of $V = 56$ kt is can be explained as the partial reading of a temperature of 25.6 °C.

Table 4.2 – SYNOP, METAR and ICEA-BDC reports for SBPA – Porto Alegre, RS, at 18:00 UTC 06/12/2003.

Type	Report	DIR (°)	V (kt)	G (kt)	T (°C)
SYNOP	AAXX 06184 83971 32970 10256 20084 30129 40134 56012	20	56	-	25.6
METAR	SBPA 061800Z 29010 KT CAVOK 26/08 Q1013	290	10	-	26
ICEA-BDC	PAS-31 (ICEA, 2017)	290	10	-	25.6

An examination of historical SYNOP observations in Brazil revealed that i_w values sometimes indicate wind speeds in m/s and not kt. In nearly all of these cases it was found that wind speeds of SYNOPs with $i_w = 1$ (indicating units of m/s) were double the magnitude of observations made before and after. Since $1 \text{ kt} = 0.5144 \text{ m/s}$, it is likely that infrequent indication of units in m/s in SYNOP reports is due to erroneous i_w indicators, and that units should always be considered as kt unless a regular and frequent use of m/s, $i_w = 1$, is noted.

Historical METAR/SPECI and SYNOP reports can be obtained from a number of sources, including direct access to the Brazilian OPMET via the Aeronautical Command Meteorological Network (*Rede de Meteorologia do Comando da Aeronáutica* – REDEMET) website¹⁰, for which METAR/SPECI reports can be accessed from November, 2002, and SYNOP reports from 2012. Weather Underground¹¹ (WU) and the National Centers for Environmental Information¹² (NCEI) have METAR/SPECI reports available from July 1996 and September 1999 respectively. WU and NCEI/NCDC also make data available which has been extracted from the original weather reports. However, the routines they use to extract data can introduce erroneous data into the datasets. This issue is covered in more detail in Section 4.1.3 *Third-party databases*.

In some cases, observation metadata do not match correctly with dates, times and locations contained within the METAR/SPECI or SYNOP report, particularly for NCEI and WU databases prior to 2006, while data from REDEMET does not present the same issue. An example of erroneous station assignment is encountered in both NCEI and WU's databases for two strong wind observations at SBPA. No such observations are encountered when cross-checked against the REDEMET dataset, however reports containing the same observations are encountered for different stations, SBPF – Passo Fundo, RS, for the case in Figure 4.1 and SBPA – Cascavel, PR, for the case in Figure 4.2. Conversely, neither of the strong wind observations made at SBPF or SBPA according to REDEMET were encountered in the NCEI or WU datasets. It is extremely difficult to identify such errors without a profound cross-checking process between datasets and stations, and such processes may be prohibitively costly in terms of time.

¹⁰ <http://www.redemet.aer.mil.br/>

¹¹ <http://www.wunderground.com/>

¹² <http://www7.ncdc.noaa.gov/CDO/dataproduct>

SBPA 291515Z 34030G50KT 4000 HZ NSC 29/17 Q1003=	(NCEI & WU)
SBPF 291540Z 34030G50KT 4000 HZ NSC 29/17 Q1003=	(REDEMETS)

Figure 4.1 – SPECI reports for SBPA (NCEI, WU) and SBPF (REDEMETS), 29/08/2005.

SBPA 302105Z 29022G32KT 1000 TSRA SCT004 FEW040CB 18/18 Q1009=	(NCEI & WU)
SBCA 302105Z 29022G32KT 1000 TSRA SCT004 FEW040CB 18/18 Q1009=	(REDEMETS)

Figure 4.2 – SPECI reports for SBPA (NCEI, WU) and SBCA (REDEMETS), 30/08/2005.

4.1.2 ICEA-BDC

The BDC managed by ICEA is herein examined through three different frameworks: its website and two different reports requested specifically for this study. Although representative of the same data, each of the three datasets presents different sets of extreme wind speeds and their limitations must be recognised in order to be used correctly. Hourly V data from ICEA-BDC was used by Pes et al. (2017) in a study of wind climate trends in Brazil.

4.1.2.1 ICEA web portal

The System for the Generation and Availability of Climatological Data¹³ (*Sistema de Geração e Disponibilização de Dados Climatológicos*) is the general public's window of access to the BDC. The website makes available historical V monthly maximum for 105 SWS from as early as 1951. The frequency of occurrence per wind direction (increments of 10°) is also available for both V and G . For V , wind speeds are grouped in bands of 5 kt up to 30 kt, with a final group of $V > 30$ kt, for G , wind speeds are grouped in bands of 10 kt up to 60 kt, with a final group of $G > 60$ kt. The data considers all anemometers present at the aerodrome for the period solicited. Without access to the hourly time-series it is difficult to assess the quality of the data being represented, however there are cases in which a lack of quality control can be observed. One example is the series of V annual maxima at SBGL – Galeão, RJ, as shown in Figure 4.3. From 1990 onwards, there is a reported total of 6 annual maxima of $V \geq 90$ kt, wind speeds which are typically generated by tropical cyclones – a phenomenon which does

¹³ <http://clima.icea.gov.br/clima/>

not afflict Rio de Janeiro, and it was subsequently decided that the web portal was not appropriate for a study on extreme wind speed distributions.

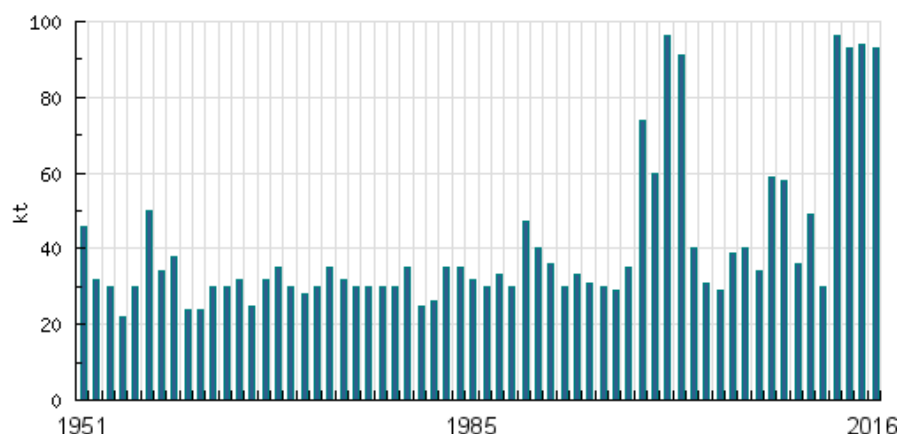


Figure 4.3 – Series of V annual maxima at SBGL (Source: ICEA web portal¹³)

4.1.2.2 PSEC-46

In November of 2015, statistical data was received from ICEA in the form of technical report PSEC-46 (ICEA, 2015). For 70 Brazilian aerodromes the following daily wind data were received: predominant wind direction, mean V , maximum V , and maximum G . Hourly information regarding present weather was also supplied with reference to local time zones (ignoring differences caused by daylight savings). A number of issues were presented while processing data from PSEC-46, including the filtering of real extreme wind events, misplaced data, missing data and spurious data.

For the longest operating aerodromes, the data ranged from January 1st, 1951 until October 26th, 2015, representing a maximum period of almost 65 years. Wind data is given per anemometer which is named after the runway heading. In many cases, an anemometer is referred to as “00” or a combination of the two runway headings, e.g. “18/36”, meaning the anemometer is not located at either end of the runway. “L” (left), “R” (right) and “C” (centre) are used to differentiate parallel runways. It is not uncommon for anemometers to be replaced, relocated or renamed. An example of the history of name/location of anemometers is shown in Figure 4.4 for SBGR – Guarulhos, SP.

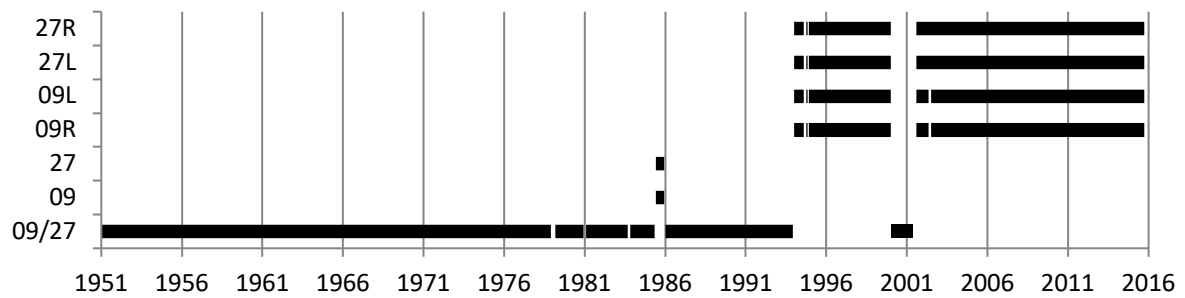


Figure 4.4 – Periods of operation for anemometers as per runway headings at SBGR.

Data from 28 stations presented similar patterns of corrupted V and DIR data for the period between 01/01/1998 and 31/05/2001. For this period, the daily maximum V is higher than the rest of the series and is capped at 36 kt, while DIR is restricted to below 140° . Gust data remains unaffected. The anomaly is easily identified when plotted, and an example is given in Figure 4.5 which shows data for all anemometers at SBGR. Upon inspection of the data and consultation with ICEA, it was determined that the anomaly is due to a swapping of fields in the BDC: DIR data is incorrectly stored in the V field, and vice-versa. Considering that data pertaining to PSEC-46 is in the form of daily maximums and means, the data in this period is unusable.

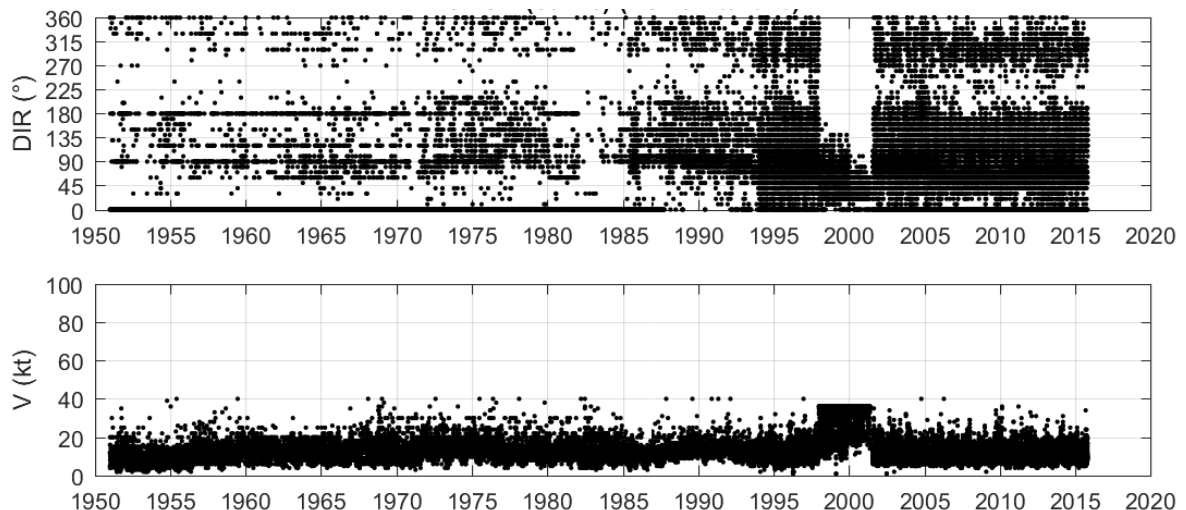


Figure 4.5 – V and DIR daily maxima at SBGR from PSEC-46 (ICEA, 2015).

Gust data for SBGR and SBFI – Foz do Iguaçu, PR, presented similar patterns for the period before 1965. The data for SBGR is shown in Figure 4.6, and appears to represent present weather indicators rather than G data.

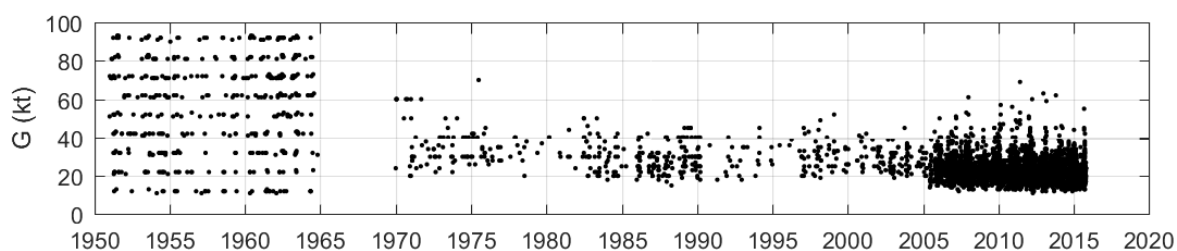


Figure 4.6 – G daily maxima data at SBGR from PSEC-46 (ICEA, 2015).

In theory, wind data within METAR/SPECI reports should be same as data from PSEC-46, with only an adjustment from UTC to local time necessary. However, when a comparison was made between the two for select number of cases, it was found that several extreme V and G values were not present in PSEC-46. An example is given for the event registered at SBSM – Santa Maria, RS, on 01/03/2003. According to the METAR reports, as shown in Figure 4.7, a thunderstorm generated observed wind speeds of $V = 41$ kt and $G = 51$ kt at 16:25 UTC, followed by $V = 20$ kt and $G = 40$ kt at 17:00 UTC. However, according to PSEC-46 the daily maximums for 01/03/2003 were $V = 20$ kt and $G = 40$ kt for the principal anemometer at runway heading 11, and $V = 24$ kt and $G = 55$ kt at the secondary anemometer at runway heading 29. It is observed in Figure 4.8 that the daily maximum V time-series, according to PSEC-46, never passes above 36 kt. It was concluded that a limit of $V = 36$ kt was placed on the data for SBSM, and examinations of data from other stations showed similar outcomes. Upon presenting these findings to ICEA, it was confirmed that a limit for V is set for each station, values above the limit are flagged as suspect, and that PSEC-46 excluded flagged values. Although there were no filters applied to gust data, any G observed in the same report as flagged V values were also flagged. As such, PSEC-46 was deemed unsuitable for this study.

```
SBSM 011600Z 20008KT 9999 BKN030 FEW040CB 31/26 Q1009=
SBSM 011625Z 30041G51KT 0100 R11/0100 R29/0100 +TSRA BKN025 FEW040CB 30/27 Q1010=
SBSM 011700Z 24020G40KT 1500 R11/1000 R29/0800 +TSRA OVC200 29/27 Q1012=
```

Figure 4.7 – METAR reports for SBSM, 01/03/2003 (Source: REDEMETS¹⁰)

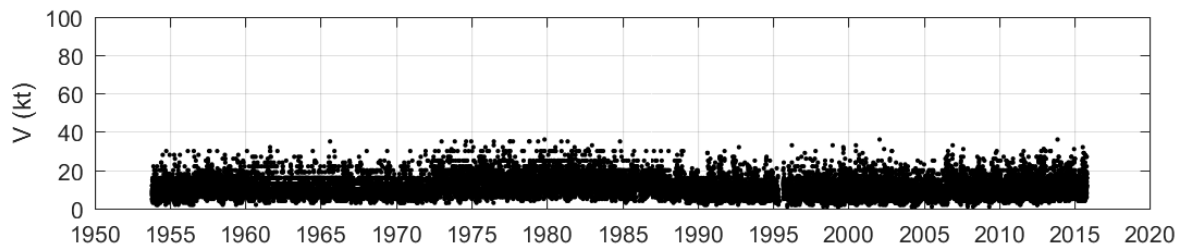


Figure 4.8 – V daily maxima time-series for SBSM from PSEC-46 (ICEA, 2015).

4.1.2.3 PAS-31

The issues outlined in Section 4.1.2.2 *PSEC-46* were presented to ICEA at headquarters in São José dos Campos, SP, in December, 2016. It was decided that a new report be prepared for an expanded selection of aerodromes without the filtering of flagged data. Time-series for DIR , V , G , T , T_d , QNH and present weather identifiers for 151 aerodromes were compiled in PAS-31 (ICEA, 2017). Data was initially requested from the earliest data available (01/01/1951, or from the commissioning of the aerodrome) until 31/12/2016 and was received for 23 stations. Due to the large amount of data requested and the demand placed on ICEA, the data for these 23 stations was received in 5 separate batches spanning a period of approximately 4 months from June 2017. This timeline was deemed unfeasible for the study deadline and so the period of the request was reduced to data from 01/01/1990. The year 1990 was chosen so as to balance the need between maximising the number of years of data and minimising the impact of data acquired using processes which could affect outcomes of the study, such as analogue/conventional readings and anemometers located in different locations or even above control towers. Data for the remaining 128 stations, containing data up until the date of their emission, were subsequently received in two batches on 21/12/2017 (20 stations) and 08/02/2018 (108 stations).

All data received were accompanied by ICEA's qualifying flags to identify gross errors and spurious data, however were not considered in this study. A number of known extreme wind events were confirmed by a comparison between METAR reports and the PAS-31 data, including the event detailed in Figure 4.7. For all stations which presented the issue regarding DIR and V data between 1998 and 2001, as described in Section 4.1.2.2 *PSEC-46*, data were manually switched to the correct fields.

In principle, there should be no divergence between MSS and PAS-31 data due to observations originating from the same source. However, the observations undergo

completely different processes between their original acquisition and appearance in the final dataset. Apart from discontinuities in the time-series of each dataset, some unexpected differences were encountered along the course of the investigation. Present weather indicators are often missing from the PAS-31 data, with the example the most extreme wind event at SBAE – Arealva, SP, shown in Figure 4.1. Both datasets presented a peak gust of 42 kt for the event, with TS reported in the METAR but not in the PAS-31 data. Such information could change the classification of the type of event, in this case, a non-synoptic event could be erroneously classified as synoptic.

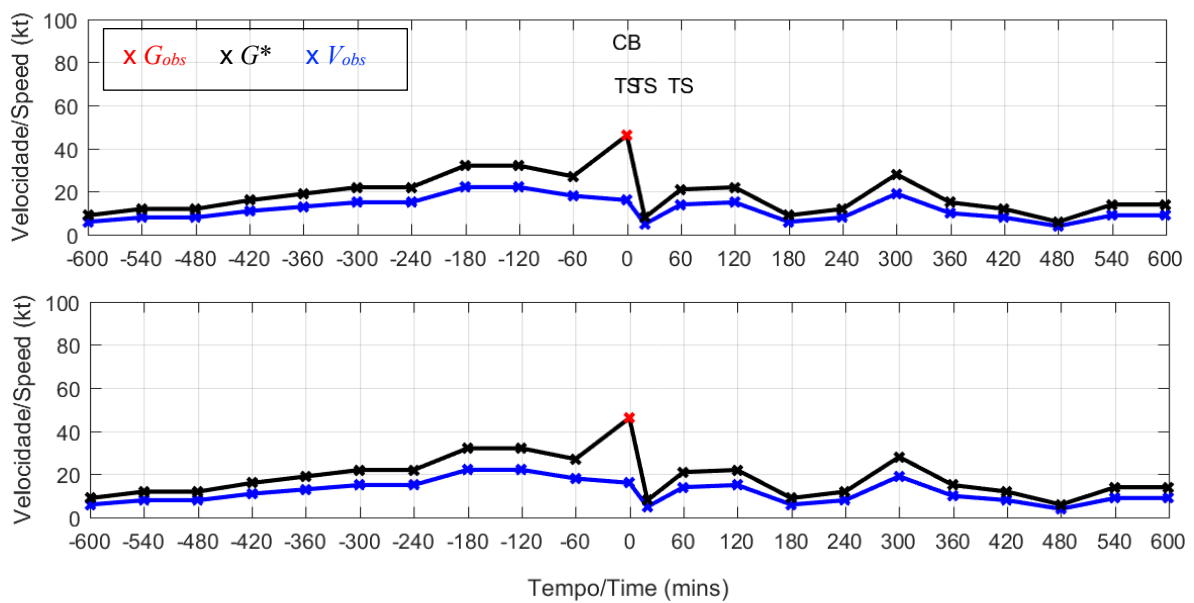


Figure 4.9 – Extreme wind event at SBAE – Arealva, SP, 19/09/2012 at 18:00 UTC. (top: MSS dataset, bottom: PAS-31 dataset).

4.1.3 Third-party databases

There are a number of online databases which house historical weather observations and could be consulted when undertaking climate analyses. These databases have no official role in the generation or management of weather observations at Brazilian SWS, receiving all data via the GTS, and are herein referred to as third-party databases.

Automated data extraction routines used by third-party databases, such as NCEI, WU and CPTEC-INPEC, are developed on error-free reports, and often fail to scrutinise the integrity of the data being processed. In many cases this results in the extraction of incorrect data, causing wind speeds to be higher than actually were observed, or excluded altogether, with

examples shown in Table 4.3. The same problems are present for data extracted from SYNOP reports, with an example given in Table 4.2.

Table 4.3 – Extracted data from incorrectly prepared METAR/SPECI reports as presented by third-party databases

Type of error	Date (UTC)	METAR Report	Extracted Data: <i>DIR</i> (°)/ <i>V</i> (m/s)/ <i>G</i> (m/s)		
			NCEI	CPTEC-INPE	WU
Too many digits	25/03/2008	SBGL 252000Z 160045KT 6000 BKN013 ...	160/23.1/-	0/0/-	160/23.1/-
Too few digits	13/09/2008	SBGL 130500Z 2705KT 9000 FEW015 ...	-/-/-	270/2.6/-	360/-/-
“9” instead of “0”	14/11/1996	SBGR 142000Z 35993KT 6000 SCT25 ...	350/1.5/-	-/-/-	350/47.8/-
Missing units	19/01/2003	SBSP 190500Z 12003 CAVOK 23/19 ...	-/-/-	-/-/-	360/-/-
Missing units	24/11/2015	SAWE 241700Z 29029G36 9999 SCT020 ...	290/29/36	0/0/-	290/14.9/18.5
Use of “RAF” and not “G”	09/10/2002	SAWG 091900Z 27028RAF39KT 9999 ...	-/-/-	-/-/-	360/-/-
Incorrect units	15/03/2009	SBGL 150500Z 33005KTKT 999 SCT010 ...	-/-/-	350/2.6/-	330/2.6/-

A comparison was made between the number of extreme wind observations per year between data presented in PAS-31 and NCEI for Porto Alegre’s Salgado Filho International Airport (SBPA/83971). The period analysed was from 1990 to 2016, with the years 1999, 2000 and 2001 not considered due to missing data in the PAS-31 dataset. The analysis was undertaken for both *V* and *G* time-series, with the following criteria for an extreme wind observation: $V \geq 30$ kt, $G \geq 40$ kt. Results in Figure 4.10 show the NCEI dataset consistently reports more $V \geq 30$ kt observations than the PAS-31 dataset up until 2011, while the number of $G \geq 40$ kt observations are much closer for the two datasets over the entire period. The NCEI contains more $V \geq 30$ kt observations than PAS-31 due to the incorrect extraction of irregularly formatted METAR and SYNOP reports, with the SYNOP reports being more problematic. Examples are given in Table 4.2 and Table 4.3 of how extreme wind speeds can be extracted incorrectly from such reports. The agreeance between the two datasets from 2012 onwards is due to NCEI’s desistance from using SYNOP reports, as illustrated in Figure 4.11.

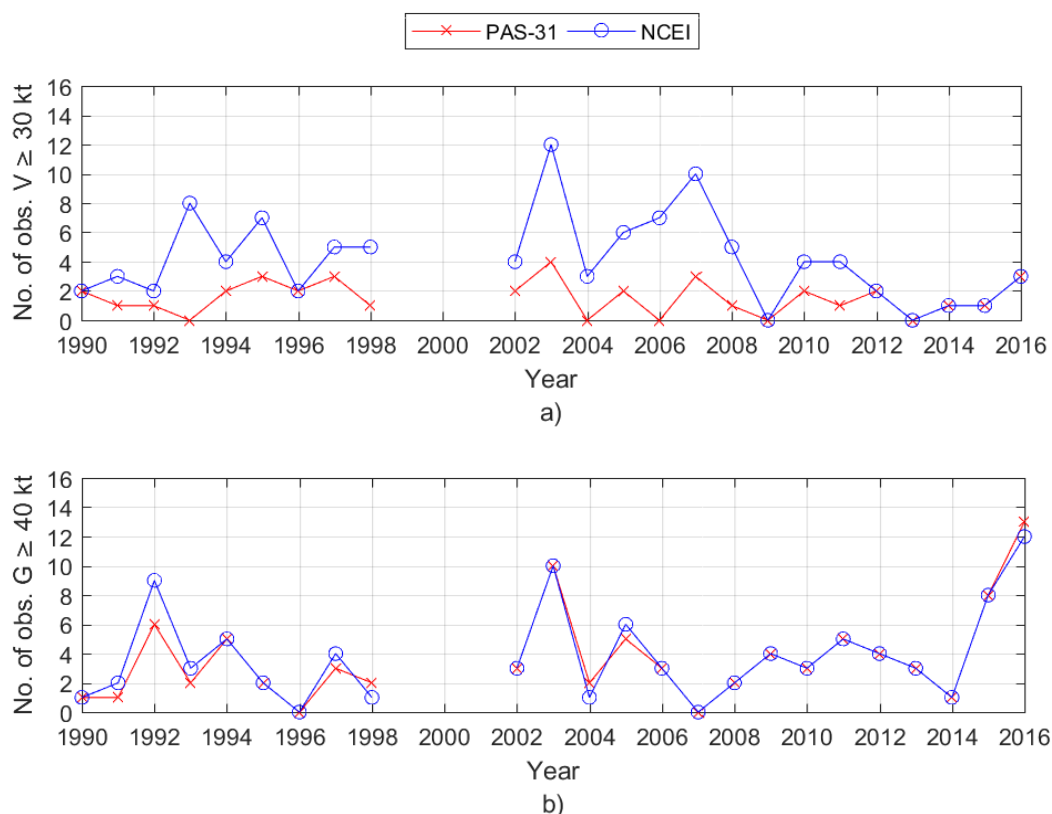


Figure 4.10 – Number of extreme wind observations for SBPA according to PAS-31 and NCEI datasets, a) $V \geq 30$ kt, b) $G \geq 40$ kt.

4.1.3.1 NCEI/NCDC

NCEI, formerly NCDC (National Climatic Data Center), is a branch of NOAA (National Oceanic and Atmospheric Administration), overseen by the US Department of Commerce. The NCEI global surface observation databases are likely the most extensive and comprehensive available to the public. The DS3505 database¹² contains hourly surface observations and is typically the first stop for researchers and wind engineering consultants when undertaking wind climate assessments. Examples of its use around the globe are found in analyses by Burton and Allsop (2009) on Thailand and Australia, Kumar et al. (2012) on India, Gatey (2011) on Europe and Pryor et al. (2009) on the United States. NCEI receives weather reports via the GTS, identifies and extracts parameters from the reports and makes the data available to the public via its website. For many stations, data is available from 1973, however other stations have data for earlier years, including SBBE – Belém, PA, SBBH – Belo Horizonte, MG, and SBKP – Campinas, SP. Data from INMET's conventional network is available for intermittent periods, and data from INMET's ASWS is available from June 2016.

Data is provided in tabulated format and wind observations include *DIR*, *V* and *G* (m/s), which accompanied by qualifiers which indicate whether the data is suspect or not. The origin of each observation is also given (i.e., SYNOP, METAR, SPECI or a combination of SYNOP/METAR, referred to as “MIX”). Data was transferred from ICEA to NCEI for the years before 1973 for some aerodromes and is denoted as “BRA” by NCEI. From September 1999 onwards, the observations are accompanied by the raw observation reports in the remarks section. Wind data is often taken from SYNOP reports when considering the mixed SYNOP/METAR data. A visual demonstration of the number observations and their origins per year is given for SBBE in Figure 4.11, with the period from 1973 onwards representative of 28 other Brazilian aerodromes.

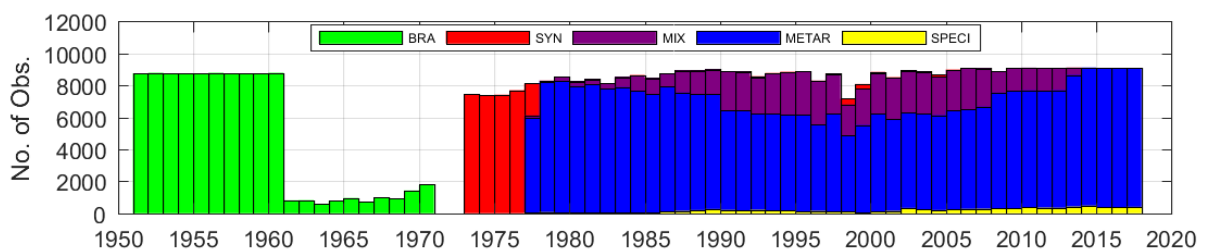


Figure 4.11 – Composition of weather observations for SBBE – Belém, PA, as made available by NCEI.

Within the NCEI framework stations are identified by a combination of name and WMO number. Before downloading data for any station, both identifiers should be checked and verified against an independent or official source of information, such as WMO OSCAR¹⁴. It was found that NCEI merged data from INMET conventional stations with those of aerodrome stations for at least 36 stations. This was the case for SBCO – Canoas Airbase, RS, situated to the north of Porto Alegre, which was incorrectly assigned WMO number 83967 by NCEI. In reality, WMO 83967 is the INMET conventional station located on the docks of Porto Alegre, approximately 10 km to the southwest of SBCO. Data originating from SYNOP reports for stations assigned with incorrect WMO identifiers by NCEI should be omitted from any analysis.

¹⁴ <http://oscar.wmo.int/surface/index.html>



Figure 4.12 – Location of SWS in the Porto Alegre region.

An issue which is specific to NCEI database is the incorrect identification of wind speed units, and hence incorrect magnitude of wind speeds, when the wind observation field within a METAR/SPECI report is not correctly defined. In the case of a missing unit identifier, “KT”, or a blank space between the wind observation and the “KT”, NCEI considers the units to be m/s, effectively doubling the wind observation made in knots. An example of one such observation is shown in Table 4.3.

4.1.3.2 *Wolfram*

Wolfram Mathematica and WolframAlpha¹⁵ offer historical meteorological data as part of their services, which are bundled together with data processing and statistical analysis algorithms. The historical database is essentially a clone of NCEI’s and is subject to the same problems. Wolfram does not make raw METAR/SPECI or SYNOP reports available. Data from Wolfram was used in a study of Brazilian extreme winds by Beck and Corrêa (2013).

4.1.3.3 *Weather Underground*

WU makes available weather forecasts and historical meteorological data via its website¹¹. For many countries outside of the US weather reports are available for SWS from July, 1996. Wind observation parameters *DIR*, *V* and *G* (km/h) are extracted and accompanied by original

¹⁵ <http://www.wolframalpha.com/>

METAR/SPECI or SYNOP report. In some cases, SYNOP and METAR reports are present for the same time. The original source from which WU received raw meteorological reports is unknown, however, due to the presence of Spanish text within some reports, for example “MENSAJE REPARADO” (message repaired) or “MENSAJE RECHAZADO” (message rejected), it can be assumed the source is not from within Brazil. It is noted that no Brazilian meteorological reports with Spanish text were encountered in WU’s database after 2004.

4.1.3.4 CPTEC-INPE

The Centre for Weather Forecasting and Climate Studies of the National Institute of Space Research (*Centro de Previsão de Tempo e Estudos Climáticos do Instituto Nacional de Pesquisas Espaciais – CPTEC-INPE*) manages its own Meteorological Database (*Banco de Dados Meteorológicos - BDM*) which is available to the public via its website¹⁶. Separate databases are available for SYNOP and METAR data, with stations identified by their WMO and ICAO IDs respectively. Historical data is available for many international stations and is not limited to Brazilian territory. METAR data is available from 1999 and SYNOP data is available from 1995, although is very sparse for years prior to 2003. Data is presented in formatted tables and is extracted from the raw observation reports without their inclusion. Wind observation data includes *DIR* and *V* (m/s), but not *G*. Data from SPECI reports are not included in the database. Data from CPTEC-INPE’s SYNOP database was used in a study of Brazilian extreme winds by Almeida (2010).

4.2 INMET ASWS

Meteorological data recorded at INMET’s ASWSs can be accessed via the web portal, regional DISME databases, the national SADMET database and from NCEI. INMET also has a restricted meteorological database from which the public is prohibited from receiving data. With the exception of data available from NCEI, the limitations of each source are herein discussed.

An issue which is present in all datasets is the unexpected frequent repetition of *G* for consecutive observations. The repetition was noted by inspections of time-series and may be due to a programming issue within the data acquisition software. A statistical analysis, which can be considered representative for all ASWS, was performed on data acquired at A701 –

¹⁶ <http://bancodedados.cptec.inpe.br/downloadBDM/>

São Paulo, SP, to demonstrate the anomaly. A total of 90,777 $\times V > 0$ m/s and 96,756 $\times G > 0$ m/s observations were recorded for the period between June, 2006, and December, 2017. $G = 0$ m/s for approximately 2.2 % of this period. Throughout this period, the same V observation was reported for consecutive observations 4,789 times, and 9,755 times for G the time-series, i.e. 5.3% and 10.1% of the time, respectively. This is higher than expected for G when considering that both parameters are reported to the same precision, i.e. 1 decimal place, and the standard deviations are 1.13 m/s for V , and 2.44 m/s for G .

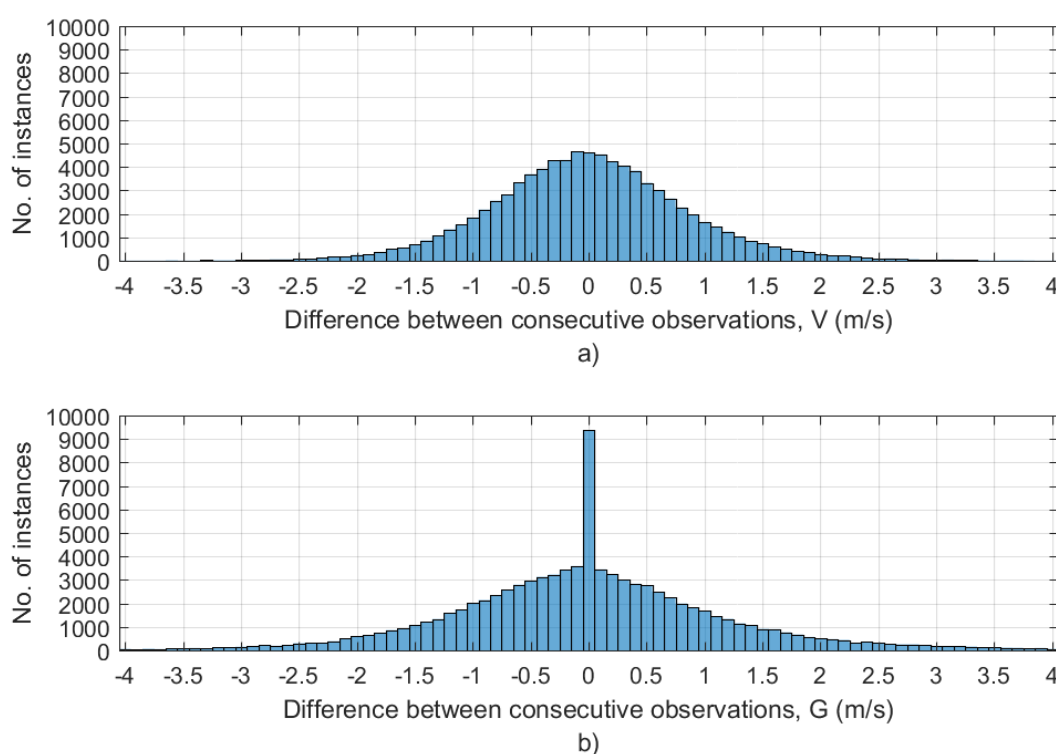


Figure 4.13 – Histograms of consecutive hourly differentials for a) V and b) G at A701 – São Paulo, SP.

Histograms for the differences between consecutive hourly observations, for both V and G , are shown in Figure 4.13 for the range between -4.0 and 4.0 m/s at increments of 0.1 m/s. The frequency of 0 m/s difference between consecutive hourly G observations is approximately 2.5 times greater than what the distribution suggests it should be. This anomaly is not repeated for the V time-series.

4.2.1 INMET web portal

In its initial conception, data was accessed via INMET's website¹⁷ for the life of each ASWS. However, at some point, possibly in 2010 or 2011, access was limited to only the previous 90 days. Since 2017, and as current, data is available via the website for the previous 365 days. The website also details some important metadata, including altitude above sea-level, latitude and longitude coordinates and, in some cases, photos of the ASWS in-situ. Data from the website was continually downloaded over the years for each ASWS analysed in this study, either on a monthly or quarterly basis. Unfortunately, there were periods for which data was corrupted on local servers and supplementary data was needed. The largest period effected was 2010-2011 for all stations.

It is unknown whether filters are applied to data during acquisition at ASWS. Given the fact that SADMET filters extreme values, as explained in the following section, it is possible that similar processes are also applied during the data acquisition. The extent to which INMET removes data from the web after its acquisition is reported in Section 4.2.4 *Restricted INMET Database*. One such case in which data was removed after its observation is documented here. At 17:25 UTC on 18/12/2018, the Twitter account of *Atmosfera Meteorologia Ltda.* (ATMET, handle @atmet) issued a tweet documenting the observation of a 150.1 km/h (41.7 m/s) gust at the INMET ASWS at A880 – Vacaria, RS, as shown in Figure 4.14. The information was accompanied by a satellite image of enhanced water vapour from GOES-16 which shows what appears to be severe convective activity over the section of northern Rio Grande do Sul where Vacaria is located.

Meteorological data was accessed from INMET's website shortly after at 18:12 UTC which confirmed the 41.7 m/s magnitude of the gust registered between 16:00 to 17:00 UTC (14:00 to 15:00 BRST). The data, shown in Figure 4.15, also indicates an approximately 10°C drop in temperature over the hour of the extreme gust, consistent with a downburst event. However, when the same data was accessed again on 02/01/2019, approximately 2 weeks later, the observation of the 41.7 m/s was removed and replaced with a no-reading identifier “////”. A comparison of the two sets of data accessed at different dates is shown in Figure 4.15. This practice casts a doubt on the accuracy and reliability of the INMET network, particularly in regard to the observation of extreme wind.

¹⁷ <http://www.inmet.gov.br/portal/index.php?r=estacoes/estacoesAutomaticas>

For the most part, hourly observed meteorological data is uploaded to the website instantly via satellite. When accessing data via the website, the user is advised that no quality control processes have been applied to the raw data. There are some cases in which the upload of observed data from ASWS to website is delayed, sometimes more than a month after it was observed. There have even been cases in which the observation data is modified over time. This was the case at A335 – Arapiraca, AL, for which data for March, 2018, was accessed on two occasions, 01/04/2018 and 08/6/2018. A comparison of the two datasets showed a divergence for all meteorological parameters from 03/03/2018 21:00 UTC until the end of the month. Both the newer and older data after this timestamp were cross-checked with data from other stations in search of an explanation, but no matches were found. It is unknown which data is the correct representation of meteorological behaviour for this period; however, preference was given to the data accessed at the later date.

4.2.2 SADMET

The Meteorological Data Storage Section (*Seção de Armazenamento de Dados Meteorológicos* – SADMET) is responsible for providing users access to INMET’s national meteorological database. Historical hourly meteorological data for all ASWS was requested for all years of operation in July, 2017. Data for each station was received in CD format from its date of commission until 31/03/2017. The data was received with the following warning translated from Portuguese: “*The data of the automatic stations are raw and have not yet undergone a process of consistency (validation)*”.

A comparison of SADMET data with Web/DISME data revealed the systematic filtering of extreme V and G values within SADMET data. Data from DISMEs are used for the period between 01/01/2010 and 31/12/2011 for which downloaded web data was missing. The full extent for the filtering is unknown, however it is sufficient to assume that the SADMET dataset, used alone, is not appropriate for a study of extreme wind climate. The motivation for the filtering is most likely due to the large amount of spurious data registered by INMET’s ASWS. SADMET’s gross error checking algorithm, most likely a simple threshold filter, is not sophisticated enough to separate real extreme wind events from suspect data.

The most extreme case of filtering is observed for A845 – Morro da Igreja, SC. The station is located at an altitude of 1,790 m, the second highest ASWS since A636 – Parque Nacional

Itatiaia, Rio de Janeiro was commissioned at an altitude of 2,450 m in September of 2017, and often registers extreme winds caused by the low-level jet stream. Time-series of V and G data for A845 from both web/DISME and SADMET datasets are shown in Figure 4.16. In this figure, the application of a low-pass threshold on the SADMET data from 2007 to 2011 is easily identified.

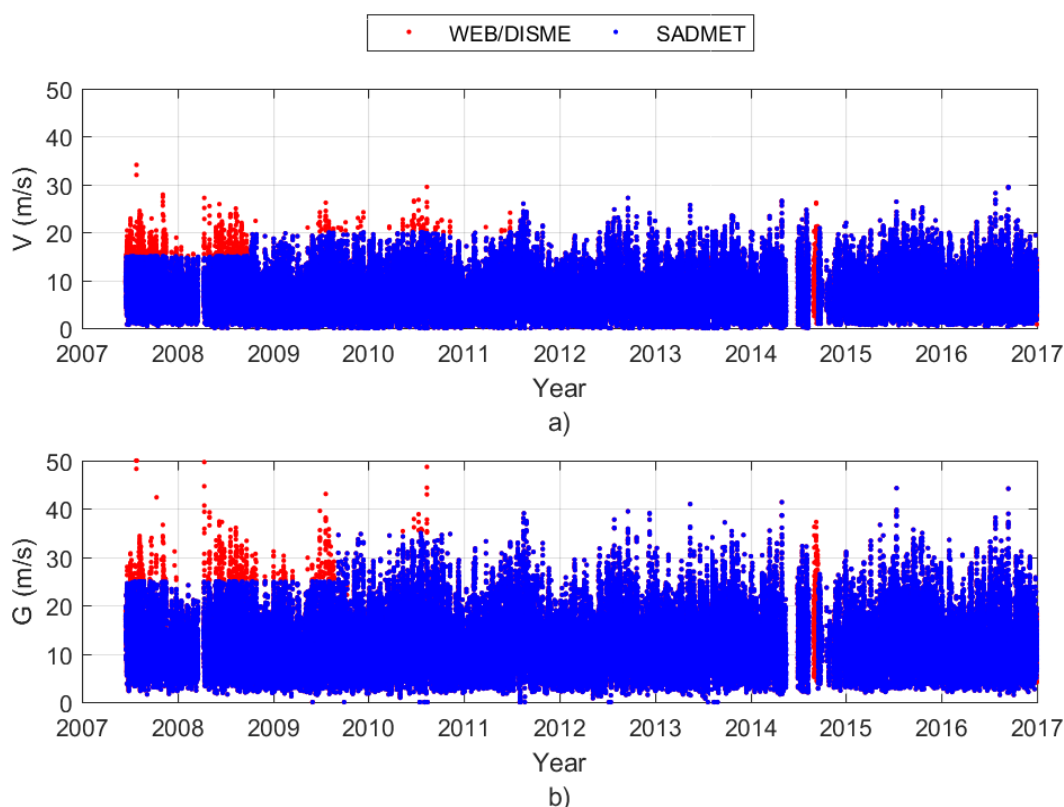


Figure 4.16 – WEB/DISME vs SADMET datasets for a) V and b) G time-series at A845 – Morro da Igreja, SC.

A brief investigation was undertaken to research online news databases to prove the occurrence of extreme wind events which were observed in web dataset but excluded from the SADMET dataset. The results of the investigation are shown in Table 4.4 for 10 examples spread across Brazil. For each of the cases listed, a news article is referenced which describes the event. Photos of some of these cases are also shown in Figure 4.17. Maximum gust values in all of these cases were above 25 m/s, with the highest 41.7 m/s for the event at A714 – Itapeva, SP. The effect of a low-pass threshold of 25 m/s filtering out real wind events on a climatic study of extreme wind is extremely disconcerting. As news websites often remove or archive old reports, extreme wind events of Table 4.4, Table 4.5 and Table 4.7 were exported to PDF format and made available at www.windytips.com.

With a view to rectify the situation, SADMET/INMET were contacted and advised of the missing data accompanied with documented examples. As described earlier, a similar situation regarding filtering of data was encountered for ICEA's PSEC-46 report, and the unfiltered dataset was issued by ICEA once informed of its importance. However, unlike ICEA, INMET were unrelenting to requests to release the unfiltered data, taking the stance that the data failed gross error checks and could not be released to the public. As such, it is concluded that SADMET dataset is unfit for studies involving extreme parameters.

Table 4.4 – Comparison of INMET Web and SADMET observations made during documented extreme wind events.

INMET ID	City	Date, Hour (UTC)	DIR (°)/V (m/s)/G (m/s)		Documented by
			WEB	SADMET	
A001	Brasília, DF	01/10/2014, 18	186/6.1/ 26.4	186/6.1/ NULL	G1 Globo ¹⁹
A104	Rio Branco, AC	13/09/2012, 20	198/2.6/ 27.7	198/2.6/ NULL	A Gazeta do Acre ²⁰
A117	Coari, AM	25/10/2012, 21	147/0.1/ 33.9	147/0.1/ NULL	Amazonas Em Destaque ²¹
F501	BH - Cercadinho, MG	23/11/2015, 23	190/14.8/ 32.7	190/14.8/ NULL	G1 Globo ²²
A510	Viçosa, MG	27/01/2015, 19	141/0.6/ 26.4	141/0.6/ NULL	G1 Globo ²³
A515	Varginha, MG	28/08/2014, 19	74/2.8/ 25.8	74/2.8/ NULL	G1 Globo ²⁴
A527	Teófilo Otoni, MG	14/11/2015, 20	354/2.5/ 27.7	NULL/2.5/ NULL	Aconteceu No Vale ²⁵
A714	Itapeva, SP	27/11/2012, 21	140/5.3/ 41.7	140/5.3/ NULL	G1 Globo ²⁶
A882	Teutônia, RS	05/03/2015, 18	325/10.7/ 27.2	325/10.7/ NULL	Tempo Em Teutônia ²⁷
A906	Guarantã do Norte, MT	19/09/2014, 00	342/0.8/ 25.5	342/0.8/ NULL	Colider News ²⁸ ; Alta Notícias ²⁹

¹⁹<http://g1.globo.com/distrito-federal/noticia/2014/10/mau-tempo-fecha-aeroporto-de-brasilia-e-desvia-voos-para-go-e-mg.html>

²⁰<http://agazetadoacre.com/familia-pede-ajuda-para-reconstruir-casa-destruida-no-ultimo-vendaval/>

²¹<http://amazonasemdestaque.wordpress.com/2012/10/26/forte-tempestade-causa-danos-em-coari/>

²²<http://g1.globo.com/minas-gerais/noticia/2015/11/chuva-forte-atinge-regioes-de-belo-horizonte.html>

²³<http://g1.globo.com/mg/zona-da-mata/noticia/2015/01/corpo-de-bombeiros-atende-ocorrencias-apos-chuva-em-vicosa.html>

²⁴<http://g1.globo.com/mg/sul-de-minas/noticia/2014/08/ventos-chegaram-93-kmhora-durante-chuva-em-varginha-mg.html>

²⁵<http://aconteceunovale.com.br/portal/?p=72959>

²⁶<http://g1.globo.com/sao-paulo/itapetininga-regiao/noticia/2012/11/temporal-provoca-queda-de-arvores-e-estragos-em-itapeva-sp.html>

²⁷<http://www.tempoemteutonia.com.br/noticias/teutonia-registra-vento-de-quase-120-kmh-neste-domingo/>

²⁸<http://www.colidernews.net/site/index.php?criedescr=noticia&id=18296#.WxrDazNKj78>

²⁹<http://www.altanoticias.com/2014/09/vendaval-deixa-um-rastro-de-destruicao.html>



Figure 4.17 – Photographs of damage caused by events listed in Table 4.4.

A comparison between SADMET and web datasets highlighted an inconsistency for stations A726 and A727. All meteorological hourly observations in the SADMET dataset appear to have been swapped from A726 to A727, and vice-versa, from the date of commissioning of each station until 16:00 UTC, 14/03/2007, a period of approximately 6 months. The V monthly means were calculated for both datasets over the entire life of operation of both A726 and A727, and showed the web data for the period up to 14/03/2007 to be consistent with the data acquired in the years after.

4.2.3 DISME

Due to the issues described regarding the SADMET dataset, data for the period 01/01/2010 to 31/12/2011 was solicited from each of the 10 DISMEs. Responses from DISMEs were mixed: complete data for this period was received digitally for the 2nd, 3rd, 7th and 8th DISMEs, 1st and 4th DISMEs advised that no data for the period was available, 5th and 9th DISMEs informed that the data could be accessed via the website and SADMET – avenues already explored, and no response was received from the 6th and 10th DISMEs.

Spot checks were performed on the DISME datasets to evaluate whether filters similar to those used on the SADMET dataset were applied. A number of high G observations were present the DISME datasets that were not in the SADMET dataset, with examples shown in Table 4.5 for each of the four DISMEs which issued datasets. It was concluded that filters

applied to SADMET data are not applied to DISME data, and DISME data are subject to the same processes as data accessed from the website.

Table 4.5 – Comparison of INMET DISME and SADMET observations.

INMET ID	City	Date, Hour (UTC)	<i>DIR</i> (°)/ <i>V</i> (m/s)/ <i>G</i> (m/s)		Documented by
			DISME	SADMET	
A233	Santana do Araguaia, PA	01/02/2011, 22	180/3.9/ 25.4	NULL/3.9/ NULL	-
A335	Piripiri, PI	13/11/2010, 16	236/2.1/ 27.7	NULL/2.1/ NULL	-
A701	São Paulo, SP	21/02/2011, 18	63/3.4/ 26.6	63/3.4/ NULL	UOL Notícias ³⁰
A807	Curitiba, PR	01/04/2011, 21	66/1.6/ 25.2	66/1.6/ NULL	Gazeta do Povo ³¹

4.2.4 Restricted INMET Database

Data from INMET's restricted database were received via extra-official channels as this study was nearing completion. This is the dataset which INMET refused to make available despite the provision of evidence showing the shortcomings of SADMET data. This study was re-initiated to incorporate the new data due to its critical importance in the determination of Brazil's extreme wind climate.

All events identified as missing from the SADMET database in Table 4.4 and Table 4.5 are present in the restricted database. The gust of 41.7 m/s observed in Vacaria and documented in Figure 4.14 and Figure 4.15 is also present. A comparison of datasets revealed hundreds of gust observations, both real and suspicious, missing from WEB and SADMET sources. The missing gusts not present in WEB or SADMET datasets appear to adhere to one of two patterns:

1. Long periods of data (ranging from hours to days) missing from WEB and SADMET sources, or,
2. Targeted removal of gusts above 25 m/s.

It is unknown why long periods of data would be missing from the WEB or SADMET datasets, but the removal of gusts over 25 m/s, which follows the same filtering practice

³⁰<https://noticias.uol.com.br/cotidiano/ultimas-noticias/2011/02/22/sp-ainda-tem-63-semaforos-com-problemas-e-51-arvores-caidas.htm>

³¹<https://www.gazetadopovo.com.br/vida-e-cidadania/chuva-forte-provoca-quedas-de-arvores-e-destelhamentos-em-curitiba-e-rmc-3telsgpn3azovghdww47r351q>

documented in 4.2.2 *SADMET*, is most likely the result of a desire to nullify spurious data. Unfortunately, such a practice discards data from real events along with actual spurious data. Peak gusts only encountered in the restricted database were subjected to the qualification and classification algorithms as defined in Section 6.5 *Identification of synoptic, non-synoptic and suspected false extreme wind events*. Of the 290 qualified events, i.e. peak gusts not classified as suspect, 172 were peak gusts greater than 25 m/s. The histogram of Figure 4.18 shows that approximately 40% of events not present in WEB or *SADMET*, but present in INMET's restricted database, fall in the range of 25-28 m/s.

The location and frequency of peak gusts not available from the WEB or *SADMET* datasets are mapped in Figure 4.19. The station with the most number of events only available via INMET's restricted database is A529 – Passa Quatro, MG, with 7 events over 25 m/s. The following stations each have 4 events with peak gusts over 25 m/s that are only available from the restricted database: A934 – Alto Taquari, MT, A908 – Água Boa, MT, A907 – Rondonópolis, MT, and A747 – Pradópolis, SP. The distribution of the events across the 10 DISMEs is shown in Table 4.6, revealing the 5th, 7th and 9th DISMEs as the most affected. Of the 290 events, 215 were identified as non-synoptic events, and 75 as synoptic events (74%/26%). Of the 172 events with peak gusts greater than 25 m/s, 163 were identified as non-synoptic events, and 9 as synoptic events (95%/5%).

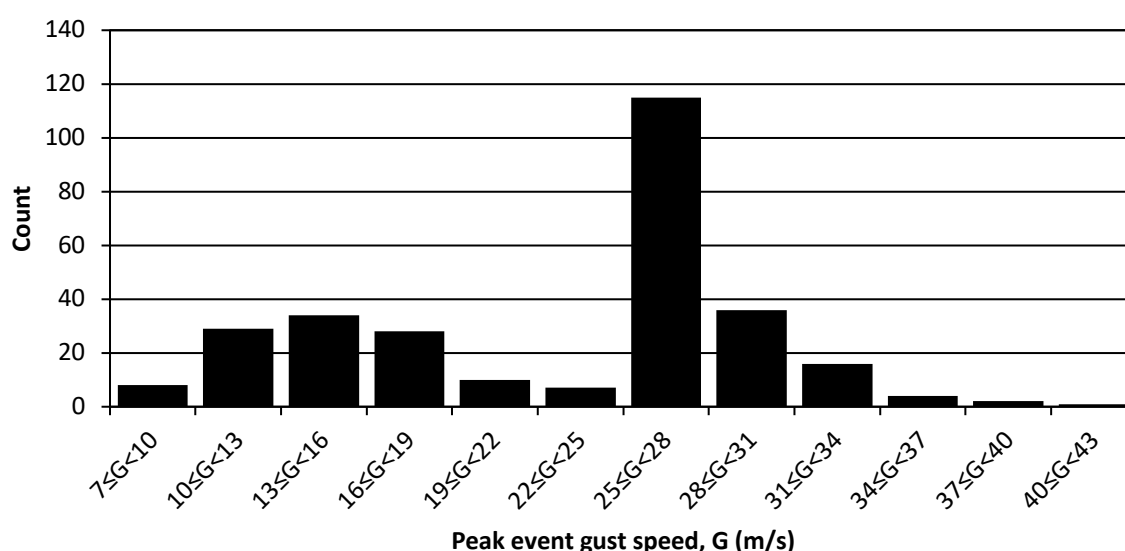


Figure 4.18 – Number of qualified extreme peak gusts, per range of gust speed, encountered only in INMET's restricted access database.

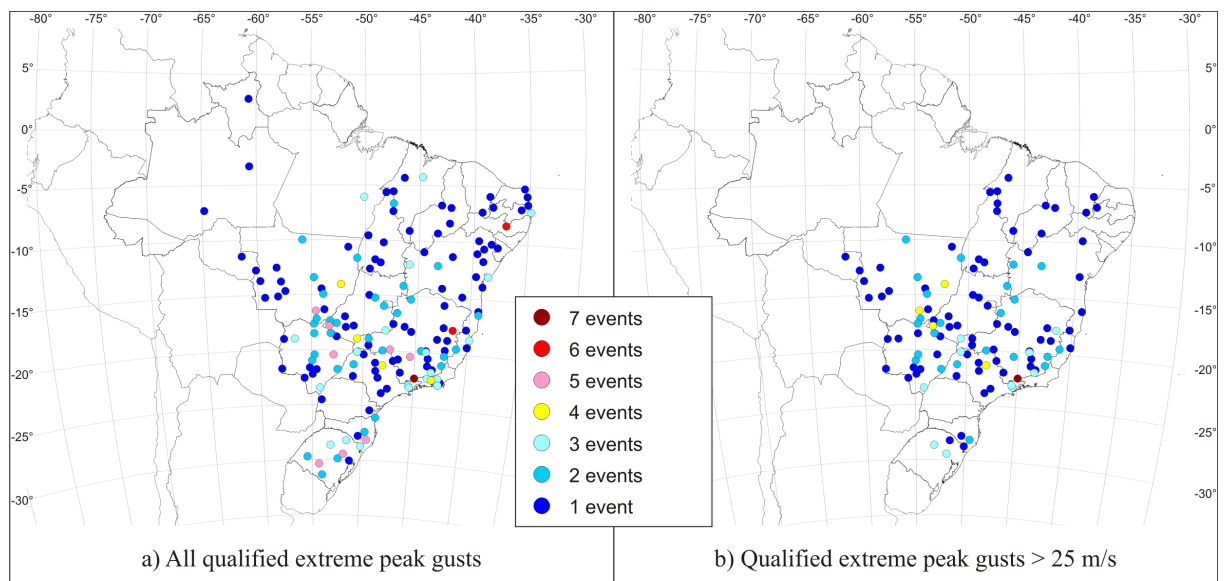


Figure 4.19 – Number of qualified extreme peak gusts encountered only in INMET's restricted access database per station.

Table 4.6 – Number of qualified extreme gusts peak gusts, per DISME, which are encountered only in INMET's restricted database.

DISME	Number of extreme gusts	
	All speeds	> 25 m/s
1 st	3	0
2 nd	12	5
3 rd	20	7
4 th	23	8
5 th	62	46
6 th	18	1
7 th	52	44
8 th	38	11
9 th	37	33
10 th	25	17
Total	290	172

A728 – Taubaté, SP, is one of the stations affected by the redaction of extreme wind events from SADMET and WEB datasets. It is also a particularly unique station due to its location inside SBTA – Taubaté Airforce Base. It is estimated that the primary anemometer of SBTA is located within 500 m of A728. Three extreme wind events with peak gusts over 25 m/s were redacted from the WEB database for A728, as shown in Table 4.7. The peak gusts as reported by SBTA are also shown in Table 4.7, confirming the occurrence of extreme wind events. The event on 27/10/2017 is also documented by news outlets with photos of damages to helicopters and buildings shown in Figure 4.20

Table 4.7 – A comparison of datasets reporting on three different extreme wind events at Taubaté, SP.

Peak gust at A728 <i>DIR (°)/V (m/s)/G (m/s)</i>				Peak gust at SBTA <i>DIR (°)/V (m/s)/G (m/s)</i>		Documented by
Date, Hour (UTC)	WEB	SADMET	RESTR. INMET	Date, Hour (UTC)	REDEMET	
19/12/2016, 18:00	84/1/NULL	84/1/NULL	84/1/25.1	19/12/2016, 17:28	50/11.3/28.3	-
10/10/2017, 20:00	157/13.0/NULL	-	157/13.0/28.1	10/10/2017, 20:02	160/14.4/30.4	-
27/10/2017, 20:00	199/12.6/NULL	-	199/12.6/37.6	27/10/2017, 20:03	40/18.0/30.4	O Vale ³²



Figure 4.20 – Photo of damage caused by strong gusts at SBTA – Taubaté Airforce Base, SP, 27/10/2017 (Source: O Vale)

³²https://www.ovale.com.br/_conteudo/2017/10/nossa_regiao/21939-chuva-de-granizo-em-taubate-causa-prejuizo-no-cavex.html

5. EXTREME VALUE ANALYSIS

5.1 PARENT DISTRIBUTION

The parent distribution represents the population and is not generally useful in the estimation of extreme winds. The Gaussian distribution was proposed for extreme wind prediction in the 1930s (Holmes, 2015), and although ESDU 87034 (ESDU, 1990[a]) proposes a method for extreme wind prediction from the parent distribution, its application is not recommended, particularly in regions where non-synoptic storms participate in the extreme wind climate. Parent distributions are best suited for applications which require inputs on variations around mean wind speeds, such as pedestrian comfort studies, the planning of wind farms and structural fatigue analysis.

The Weibull distribution is widely regarded as the appropriate form for modelling the parent distribution (Holmes, 2015; ESDU, 1990[a]), and the probability density function (PDF), p , takes the form of Equation 5.1 for wind speeds of a fixed averaging interval (e.g. 10 minutes, 1 hour or 3 seconds) X , shape factor w , and scale factor c . The parameters c and w can be easily solved when the distribution is in the cumulative distribution function (CDF) form, $P(X)$, as shown in Equation 5.2. The function $P(X)$ is representative of the probability of non-exceedance of wind speed X , and conversely, $1 - P(X)$ represents the probability of exceedance. Holmes (2015) stated that values of w and c typically fall between 1.3-2.0 and 3-10m/s respectively.

$$p(X) = \frac{wX^{w-1}}{c^w} \exp \left[-\left(\frac{X}{c}\right)^w \right] \quad 5.1$$

$$P(X) = 1 - \exp \left[-\left(\frac{X}{c}\right)^w \right] \quad 5.2$$

An example of parent distributions of two stations at opposite ends of Brazil is given in Figure 5.1. SBFZ – Fortaleza, CE, is located on Brazil's northern coastline in the ITCZ which is known for its constant easterly trade winds, while SBPA – Porto Alegre, RS, is Brazil's

most southern capital city located approximately 100 km from the eastern coastline. The two locations show very different PDF and CDF distributions which is reflected in the Weibull parameters c and w . Fortaleza experiences high mean wind speeds (5.9 m/s) and rarely experiences extreme events with V_{cor} greater than 14 m/s; Porto Alegre, however, regularly experiences extreme events with V_{cor} greater than 14 m/s but has a lower mean wind speed (3.3 m/s). Solving Equation 5.2 for $X = 14$ m/s gives a greater probability of exceedance for Fortaleza than for Porto Alegre by a factor of approximately 10 (1.99×10^{-4} for SBPA; 2.38×10^{-3} for SBFZ). This does not correctly represent the extreme wind climates at both stations and demonstrates the inappropriateness of using the parent distribution for such purposes.

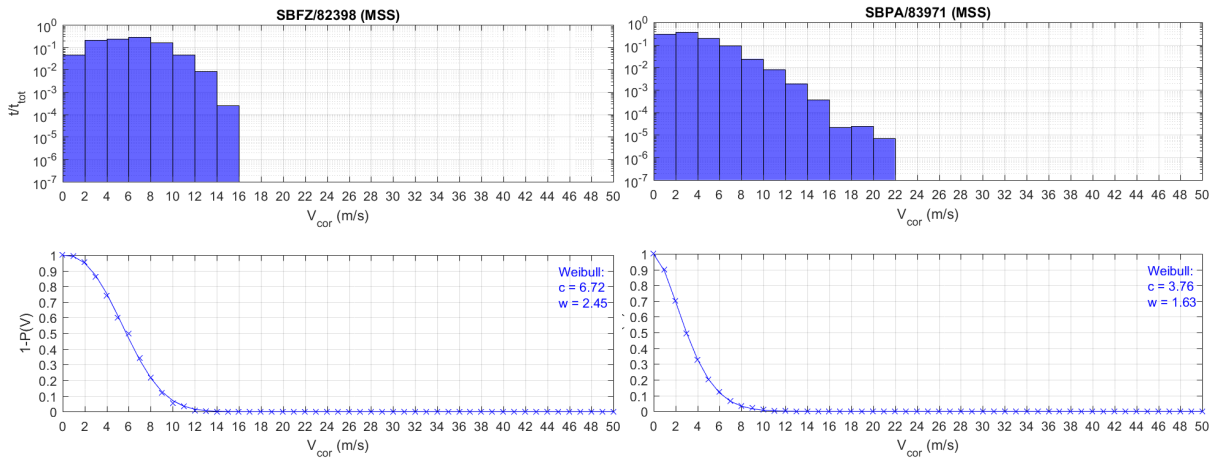


Figure 5.1 – PDF of 10-minute mean wind speed corrected to $z = 10$ m and $z_0 = 0.07$ m, V_{cor} , normalized by total sampling time, t_{tot} (top); CDF of V_{cor} (bottom) at SBFZ – Fortaleza, CE (left), and SBPA – Porto Alegre, RS (right). Weibull distribution parameters c and w are given in CDF plot.

5.2 GENERALISED EXTREME VALUE DISTRIBUTION

Holmes et al. (2005) suggested that while any extreme value analysis method can be used to derive extreme wind climate models, the probability distribution should be part of the Generalised Extreme Value Distribution (GEVD) family. The current GEVD form, as shown in Equation 5.3, is based on three critical parameters: shape factor, k , scale factor, a , and location factor or mode, U . When a is represented as its inverse, $1/a$, it is called dispersion.

$$P(X) = \exp \left[- \left(1 - \frac{k(X - U)}{a} \right)^{\frac{1}{k}} \right] \quad 5.3$$

The GEVD model, as appears in Equation 5.3, was first proposed by von Mises (1936) which built upon Dodd (1923) and Fisher and Tippet (1928), with the latter the first to propose three types of distributions which today are typically referred to as Type I – Gumbel, Type II – Fréchet and Type III – Weibull. Jenkinson (1955) is often credited as being the first to propose the single equation, the three type GEVD model, but failed to cite von Mises (1936). Regardless, in the cases of Fisher and Tippet (1928), von Mises (1936) and Jenkinson (1955), the types are grouped based on the behaviour of the model at the tail, defined below and demonstrated in Figure 5.2.

- Type I – Gumbel: $k = 0$, unbounded, linear;
- Type II – Fréchet: $k < 0$, diverges as $P(X) \rightarrow \infty$;
- Type III – Weibull: $k > 0$, limited as $P(X) \rightarrow \infty$.

Adjustments are often made to Equation 5.3 to simplify models and ease implementation of the extreme value distribution. Firstly, Type I can be reduced to Equation 5.4, which is the limit of Equation 5.3 as $k \rightarrow 0$. Mathematical proof of this reduction can be found in Holmes and Moriarty (1999).

$$P(X) = \exp \left[-\exp \left(-\frac{X - U}{a} \right) \right] \quad 5.4$$

The probability of non-exceedance, $P(X)$, can also be manipulated to assist in the fitting of a linear model when the Type I – Gumbel distribution is assumed. $P(X)$ is then a function of the reduced variate, y , as defined in Equation 5.5.

$$y = \frac{X - U}{a} \quad 5.5$$

With these two simplifications, the key differences between the three GEVD types are demonstrated in Figure 5.2 for $k = 0, +0.2$ and -0.2 . Only the positive side of Figure 5.2 is of interest when performing the analysis for wind speeds, meaning Types I and II can theoretically reach infinite wind speeds, Type II at a much faster rate, while Type III reaches a limit as $y \rightarrow \infty$.

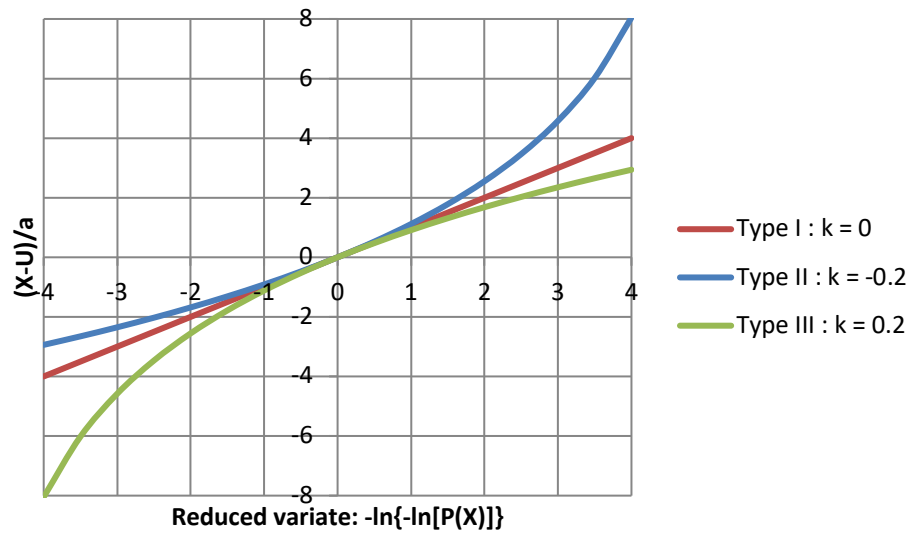


Figure 5.2 – Types I, II and III of GEVD (Holmes, 2015).

The return period, R_P , is related to the annual probability of non-exceedance as shown in Equation 5.6. A re-arrangement of Equation 5.6 is then used to express the reduced variate as a function of return period, as shown in Equation 5.7.

$$R_P = \frac{1}{1 - P} \quad 5.6$$

$$y = -\ln \left[-\ln \left(1 - \frac{1}{R_P} \right) \right] \quad 5.7$$

All three GEVD types are encountered in wind codes around the world. Type I – Gumbel was used for basic wind speeds in the United States (Peterka and Shahid, 1998), Type II – Fréchet was used in Brazil (Padaratz, 1977), Argentina (Riera and Reimundín, 1970) and Paraguay, and Type III – Weibull was used in Australia (Holmes, 2002).

Opinion is divided as to which is the most appropriate GEVD type for wind engineering applications. Thom (1968) observed a better fit of Type II to data acquired at stations across the United States. Viollaz et al. (1975) observed that Type II fit better for some stations across Argentina, whilst Type I was more appropriate for others. Riera et al. (1977) noted that since the outcomes of Viollaz et al. (1975) were to be implemented in the Argentine wind code, the Type II distribution was chosen as it led to “more conservative estimates”. Studies on extreme wind speeds in neighbouring Brazil followed this same reasoning (Padaratz, 1977). Dorman

(1983) opposed the decision to make the decision on “conservative” grounds, and found “administrative” reasons to be more acceptable. Dorman (1982) noted that Type I is the most commonly used probability distribution in wind engineering, and concluded that the optimal model ignores approximately 10% of the highest values. However, the inclusion of such values may lead to Type II as a better fit. In contradiction to Thom (1968), Simiu et al. (1978) demonstrated Type I to be a better fit for United States data and that any deviation away from Type I could be explained by sampling errors. Holmes and Moriarty (1999) stated that Type II is physically unrealistic and should be avoided when modelling extreme winds for high return periods, and reiterated that the traditional method in wind engineering is the Type I distribution. Holmes (2002) argued that there is a physical limit to the wind speed produced in the earth’s atmosphere for a combination of storm type and location, and that since both Types I and II are unbounded for high probabilities of non-exceedance, the limiting Type III is the most appropriate distribution. A summary of 14 studies of extreme winds in Europe published between 1995 and 2009 was presented by Gatey (2011), 12 of which used the Type I distribution and 1 used the Type III – the remaining case used the Generalised Pareto Distribution (GPD) which is closely related to the GEVD.

In regions with mixed extreme wind climates, i.e. any significant combination of tropical cyclones, synoptic winds and non-synoptic winds, it is likely that each storm type have their own different probability distribution. In this case, each storm type must be analysed independently. A combined distribution can be encountered by following Equation 5.8, which takes the envelope of the independent probability distributions. Here, R_c refers to the return period of the combined distribution, and R_1 and R_2 refer to the individual distributions.

$$\left(1 - \frac{1}{R_c}\right) = \left(1 - \frac{1}{R_1}\right) \left(1 - \frac{1}{R_2}\right) \quad 5.8$$

For the Type I – Gumbel distribution, the substitution of $P(X)$ from Equation 5.6 into Equation 5.4 results in the extreme wind speed, V_R , as a function of the return period as per Equation 5.9, which can be expressed in terms of y (as shown in Equation 5.10) when considering Equation 5.7.

$$V_R = U + a \left\{ -\ln \left[-\ln \left(1 - \frac{1}{R_p} \right) \right] \right\} \quad 5.9$$

$$V_R = U + ay \quad 5.10$$

The determination of a wind speed for a return period of $R_P = 1$ year per Equation 5.9 is problematic as $\ln(0)$ is undefined. As shown in Figure 5.3, y approaches $-\infty$ as R_P approaches 1. A common work-around involves the simplification of the reduced variate to be defined by the mean recurrence interval, R . The simplification is achieved with the assumption of a probability of exceedance of $P_L = 1 - 1/e$, as shown in Appendix K *Determination of Probabilistic Factor S_3* , which is independent of R . Substituting this result into Equation K.2 gives Equation 5.11, which then simplifies to Equation 5.12.

$$1 - \exp(-1) \cong 1 - \left(1 - \frac{1}{R}\right)^R \quad 5.11$$

$$\exp\left(-\frac{1}{R}\right) \cong 1 - \frac{1}{R} \quad 5.12$$

The application of the double negative natural logarithm to both sides of Equation 5.12, renders the right-hand side equivalent to the reduced variate when defined as the reciprocal of the annual probability of exceedance, the return period, R_P , as shown in Equation 5.13. The left-hand side simplifies, as shown in Equation 5.14, which is then adopted as the reduced variate in Equation 5.15.

$$-\ln\left[-\ln\left(\exp\left(-\frac{1}{R}\right)\right)\right] \cong -\ln\left[-\ln\left(1 - \frac{1}{R}\right)\right] \quad 5.13$$

$$\ln(R) \cong -\ln\left[-\ln\left(1 - \frac{1}{R}\right)\right] \quad 5.14$$

$$V_R = U + a \cdot \ln(R) \quad 5.15$$

The difference between the two sides of Equation 5.14 are shown in results in Figure 5.3, which a divergence for $R = 1$ to 5 years. For periods greater than 10 years, the difference between the two approaches is negligible and the mean recurrence interval, R , is effectively interchangeable with return period, R_P .

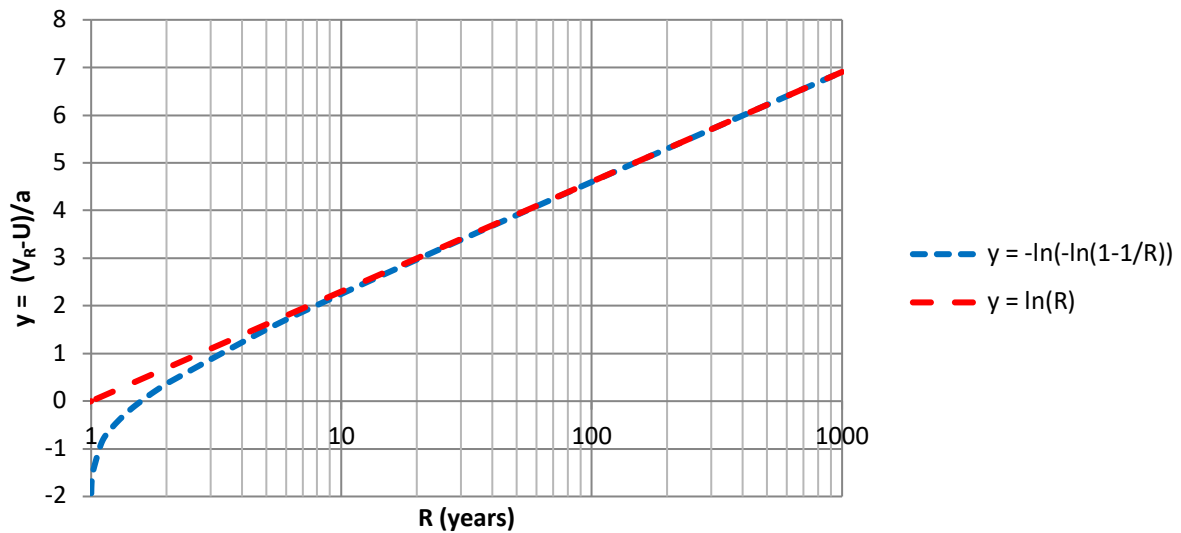


Figure 5.3 – Comparison of reduced variate as function of mean recurrence interval (Equation 5.15) to function of return period (Equation 5.9).

5.2.1 Selection of extreme values

Extreme value analysis requires a set of extreme values from the population. Several different criteria can be used to select the set of extreme values and the chosen selection will have an impact on the resulting model. Traditionally, annual maxima are selected as the set of extreme values due to its simplicity and ease. This is also referred to as “block maxima”, with a block typically defined for each calendar year. This was popular for analysis prior to the computing age, i.e. using graph paper and minimal data analysis. Most current day basic wind speeds defined in wind codes were derived from extreme value analyses of annual maxima, including NBR 6123 of Brazil (ABNT, 1988), CIRSOC 102 of Argentina (INTI, 2005), non-hurricane wind speeds of ASCE 7 (2016) of the United States (Peterka and Shahid, 1998; Vickery et al., 2010). Since an extreme analysis using annual maxima generates only one data point per year, many years of data are required to generate an accurate model. Peterka and Shahid (1998) noted that several hundred years of data are required for the generation of a model with small sampling errors at $R = 50$ years, but observed data of this length does not currently exist. Without giving consideration to changes in station characteristics over its operational

lifetime, typical sample lengths range from 1 year up to 70-80 years. Long observation periods are not typically necessary, as a 20-30 year observation period (20 to 30 data points) is considered acceptable (Cook, 1985; Riera et al., 1977; Gomes and Vickery, 1977). Even so, dependence on a series of annual maxima can be problematic:

- there may be cases in which data is only available for shorter periods (5-10 years);
- instances of discontinuities in data, meaning an annual maxima is not a true representation of that year;
- the lack of representation of storms ranked lower than the annual maximum, but higher than those of other years.

With the advancement of computing processes came the ability to quickly analyse large amounts of data. This allowed for the development of methods more complex and accurate than what can be provided from annual maxima extreme values. Cook (1982) developed a method for extreme analysis based on independent storms, which was a modification of the work of Jensen and Franck (1970) who were required to establish basic wind speeds for Denmark from only 7 years of data. The method, referred to as the Method of Independent Storms (MIS), requires the establishment of a threshold which separates extreme wind speeds from the general population, must define a certain period between peak observations to assure independence between events and allows for discontinuities in time-series. Cook (1982) stated that the method reduces scatter and improves the linearity of data to be fit, which leads to a greater confidence in derived models which is possible from as little as 7 years of data. ESDU Data Item 87034 (ESDU, 1990[a]) set out a modified version of Cook's method and Harris (1999) proposed an improved method of independent storms. The Harris method eliminates bias associated with Cook's method but is "non-trivial" in its implementation.

The selection of extreme values for MIS requires the establishment of a minimum wind speed which separates all events with greater peak wind speeds for the extreme value analysis. Cook (1982) used an average storm rate per year, r , as defined in Equation 5.16 where N is total number of storms and M is number of years of data, of 100 – which was originally suggested by Davenport (1967). Note that $r = 1$ for the extreme values corresponding to the set of annual maxima. Testing the sensitivity of r to the resulting mode and dispersion parameters, Cook (1982) found that results are the same from $r = 4$ to $r = 100$, and when $r < 3$, the corresponding wind speed threshold is high enough to exclude the lowest value of the set of annual maxima. Harris (1999) identified that since Cook (1982) used Lieblein's BLUE

method for the determination of extreme distribution parameters, effectively using only the top 23 of Cook's 1000 observations, meaning Cook was actually using a threshold of $r = 2.3$ for $M = 10$. Harris (1999) recommended the use of $r = 2.5$ when the resulting extreme values are all considered in the calculation of model parameters. Burton and Allsopp (2009) split the difference and used $r = 2.4$.

$$r = \frac{N}{M} \quad 5.16$$

In instances where the threshold takes the form of a wind speed, r becomes a function of this limit due to their inversely proportional relationship. ESDU Data Item 87034 (ESDU, 1990[a]) recommends a threshold of 15 m/s for hourly-mean values and 25 m/s for gust values (at a height of $z = 10\text{m}$), but should be adjusted to generate about 50-100 independent maxima. A threshold of 20.3 m/s for gust speeds was used by Holmes and Moriarty (1999) in a study of downburst winds at Moree, Australia. Studying extreme winds in Australia, Holmes (2002) used a threshold of 22 m/s for a gust-based analysis. In Germany, Kasperski (2002) used a threshold of 14 m/s for an analysis based on hourly-mean wind speeds. In the United States, Lombardo et al. (2009) used a threshold of 18 m/s for a gust-based analysis. Holmes et al. (2018) used a threshold of 25 m/s for a gust-based analysis of six locations in South Australia. As seen in the examples given above, there is no universally agreed wind speed threshold, and individual researchers must make decisions based on their own judgment. Gatey (2011) noted that a selection of a universal storm threshold is difficult and was subsequently required to vary the threshold between stations. Burton and Allsop (2009) asserted that a reasonably high threshold should be established to ensure that only extreme storms are included in the analysis.

The minimum period of time between successive events in order to establish independence is similarly ambiguous. In the example of ESDU Data Item 88037 (ESDU, 1990[b]) the smaller values of event peak speeds separated by two days or less are ignored. Kasperski (2002) required a minimum period of 24 hours between consecutive storms for extreme values to be considered independent. Gatey (2011) required a minimum of 72 hours between maxima to ensure independence. Cook (1982) and Harris (1999) separated storms by lulls – periods where the hourly mean wind speed dropped below 5 m/s.

The grouping of stations located in the same geographical region into a single superstation is common. This is particularly beneficial for regions with several stations with short periods of operation. The technique is essentially an averaging process, and careful consideration must be given to the selection of stations and their relative weightings. If no evaluation process is undertaken regarding the quality of contributing stations the resulting superstation may underestimate wind speeds for long return periods. Holmes (2002) analysed model parameters of individual stations which were judged to have similar statistical properties to define Australia's Region A. On the other hand, Simiu et al. (2003) noted that superstation definitions used to design basic wind speeds in the United States (ASCE, 1995) were unavailable to the wind engineering community.

Cook (1982), ESDU (1990[a]), Harris (1996; 1999) and Burton and Allsopp (2009) are fundamentally different from other extreme wind analyses (Padaratz, 1977; Holmes and Moriarty, 1999; Holmes, 2002; Peterka and Shahid, 1998; Kasperski, 2002) due to the squaring of the wind speed, u , prior to analysis. This is simplistic representation of the dynamic pressure, q , as defined in Equation 5.17, where ρ is the air density.

$$q = \frac{1}{2} \rho u^2 \quad 5.17$$

The motivation for using u^2 is due to the faster convergence to the linear form of GEVD Type 1 than when using v (Cook, 1982). It is also recognised that modelling u^2 typically decreases design wind speeds. Cook (1982) noted a reduction of 10% for design loads and ESDU (1990[a]) indicated a typical reduction of 5% in design wind speeds.

5.2.2 Estimators and determination of model parameters

Once a set of extreme values are chosen, whether block or independent maxima, estimators, or data plotting points, are then assigned. A method to solve model parameters must also be selected.

The most widely used approach in the modelling of extreme winds is referred to as the Classic Gumbel method: a combination of GEVD Type I (Gumbel distribution) for annual maxima with Weibull plotting points (Weibull, 1939) as defined in Equation 5.18. In this case, the number of data points, N , is equal to the number of years, M . The set of extreme values are arranged in ascending order with the lowest value given rank $m = 1$, and the highest given

rank $m = M$. Equation 5.18 assigns each extreme value its associated probability of non-exceedance for any one year.

$$P_m = \frac{m}{M + 1} \quad 5.18$$

The extreme values (y-axis) are then plotted on a Cartesian graph with the corresponding reduced variates (x-axis), y , from the combination of Equations 5.5 and 5.18. A regression line is then fit to the data and the model parameters of Equation 5.10, U and a , are determined. A visual demonstration of this process is given in Figure 5.4.

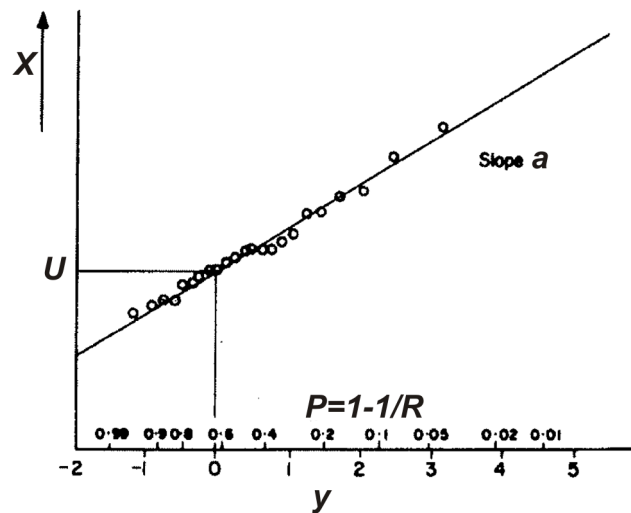


Figure 5.4 – Example of Gumbel plot (adapted from ESDU, 1990[a]).

For GEVD Type I, the plotting positions of Equation 5.18 are considered biased by several researchers (Gatey, 2011; Cook, 2011; Holmes, 2015) particularly for P values near 1. In the evaluation of four methods, Harris (2001) took an unmistakably strong position against the Classic Gumbel method, calling it “obsolete” and commenting:

“Hopefully, no one would seriously consider this method for use now...”

By conducting a Monte Carlo analysis and comparing extreme values predicted by the Classic Gumbel method to an analytical result, Harris (2001) demonstrated large bias and variability inherent to Classic Gumbel method. In case of a population with 20 years of data, this resulted in a bias error of +7.8% for the predicted $R = 50$ years extreme value. The bias inherent in the Classic Gumbel method is due to the equal weighting giving to all data points, even though

confidence in each point is different – the higher the P , the lower the confidence. The use of Gringorten's (1963) plotting points is one several methods which aim to reduce bias error and is one of the easiest to implement. In this method, the same process is followed as the Classic Gumbel method, however Equation 5.18 replaced by Equation 5.19.

$$P_m = \frac{m - 0.44}{M + 0.12} \quad 5.19$$

When compared to Weibull's plotting points, Gringorten's plotting points effectively “stretch out” the distribution meaning extreme value predictions for high P are reduced, while predictions are increased for low P . A practical example is given by Holmes (2015) for a station in East Sale, Australia based on 47 years of annual maxima data.

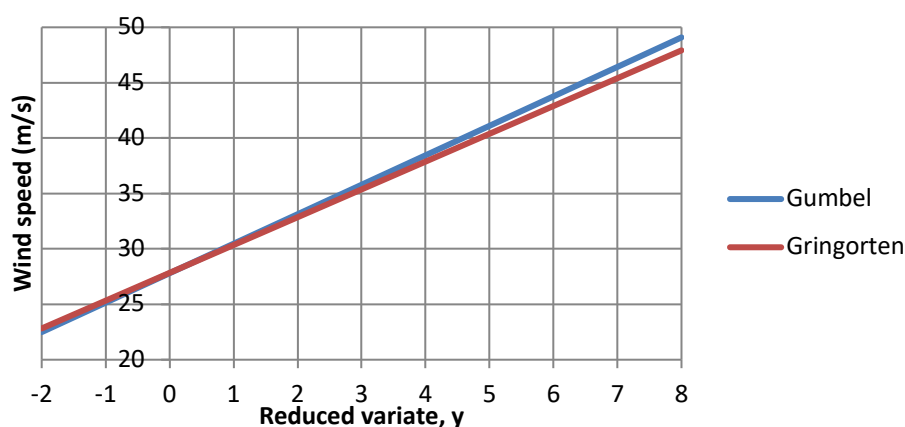


Figure 5.5 – Resulting distributions from the set of extreme annual maximum gusts (1952-1998) at East Sale, Australia as per Gumbel and Gringorten plotting points (Holmes, 2015).

The Gumbel-Lieblein method uses Best Linear Unbiased Estimators (BLUE) developed by Lieblein (1974). The selected extreme data are ranked as normal and y calculated using Weibull's plotting points from Equations 5.5 and 5.18. Tables are then consulted which assign coefficients A_m and B_m to a list of predetermined y . Tables of these coefficients can range in length from $M = 10$ to 20 years (tables are given for $M = 10$ and $M = 20$ years in Appendix F *Assorted Tables*). In the case of $M > 20$ years, coefficients A_m and B_m from Table F.2 of Appendix F are assigned to the 10 points whose y are closest to the y listed in Table F.2, hence the number of points to be used is reduced to 10. The points which are not part of the subset of 10 only indirectly affect the resulting distribution due to their ranks. Once

appropriate coefficients A_m and B_m are selected, model parameters U and a are determined from Equations 5.20 and 5.21 respectively, where X_m is the extreme value for rank m .

$$U = \sum_{m=1}^M A_m X_m \quad 5.20$$

$$a = \sum_{m=1}^M B_m X_m \quad 5.21$$

Cook (1982) stated that the top two ranked events are not critical as the Gumbel-Lieblein method is weighted to favour the middle ranks, meaning predicted values for high P are reduced when compared to the Classic Gumbel method. Harris (2001) calculated the Gumbel-Lieblein method to have a bias error of -0.5% for the predicted $R = 50$ years extreme value using 20 years of data, and subsequently recommends it as the most accurate technique when using small sets of annual maxima.

In the case of the MIS (Cook, 1982) and ESDU (1990[a]), the Weibull estimator is adjusted to that of Equation 5.22 which takes into account the average number of storms per year, r . Reduce variate, y , is subsequently calculated and a regression line fit to the resulting plot. ESDU (1990[a]) recommends ignoring all points for $y < -1$ when fitting the data, as these points are not considered to contribute significantly to the distribution. When Lieblein's BLUE estimators are preferred, Cook (1982) and ESDU (1990[a]) recommend the use of coefficients from the $M = 10$ case, as made available in Table F.2. As shown in Figure 5.6, MIS has the effect of reducing predicted extreme values for high P , while elevating those at low P when comparing against the annual maxima Gumbel-Lieblein technique.

$$P_m = \left(\frac{m}{M+1} \right)^r \quad 5.22$$

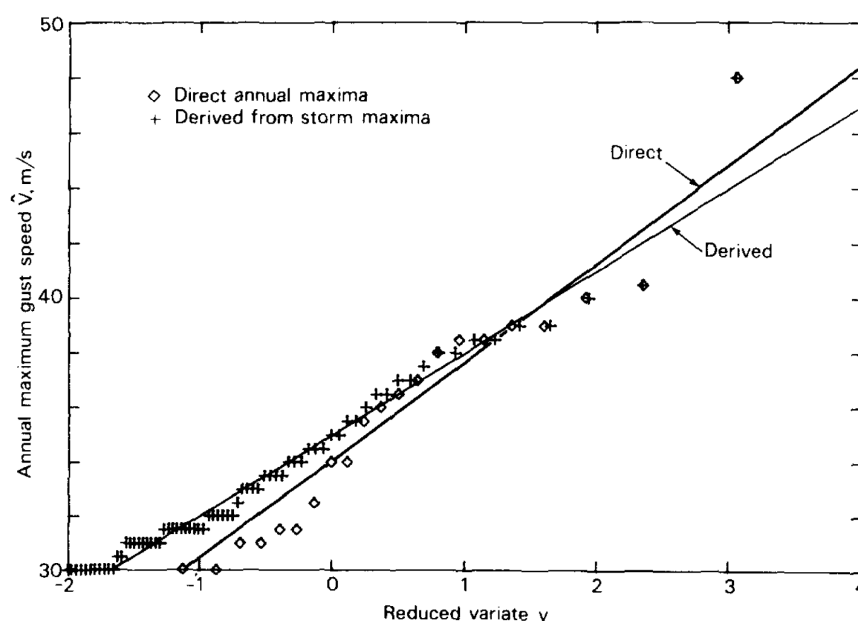


Figure 5.6 – Comparison of GEVD Type I analysis using annual maxima and Method of Independent Storms from 1958 to 1978 at Jersey, UK (Cook, 1982).

Harris (1999) stated that raising P_m to the power of r was a non-linear operation which introduces a systematic bias error, and an improved version of Cook's method (1982) was proposed. The method is rigorous and extensive programming is required for its implementation. A copy of the routine can be found appended to Harris (1999). Harris (1999) maintains the $r \sim 100$ criteria of Cook (1982), but uses only the top $\sim N/40$ events for the analysis in order to restrict the fitting process to the top 2.5% of all storm observations (assuming $r \sim 100$). In combination with assigned weightings, the plotting positions are improved to reduce bias introduced in the Classic Gumbel method. The plotting positions are \bar{y} , as opposed to y , as Harris (1999) argued it is more correct to apply the non-linear transformation first (Equation 5.5) and then use the mean of the transformed variable, \bar{y} , as the plotting position. This differs from classic techniques where the mean of P_m (Equation 5.18) is non-linearly transformed and then plotted. Harris (2001) found the improved MIS (Harris, 1999) showed very small bias of +1.4% for the predicted $R = 50$ years extreme value using 20 years of data. As demonstrated in Figure 5.7, Cook (2011) demonstrated the lack of bias of the methods of Gringorten (1963) and Harris (1996), a preliminary version of Harris (1999), whilst also demonstrating systematic bias error of the Classic Gumbel technique.

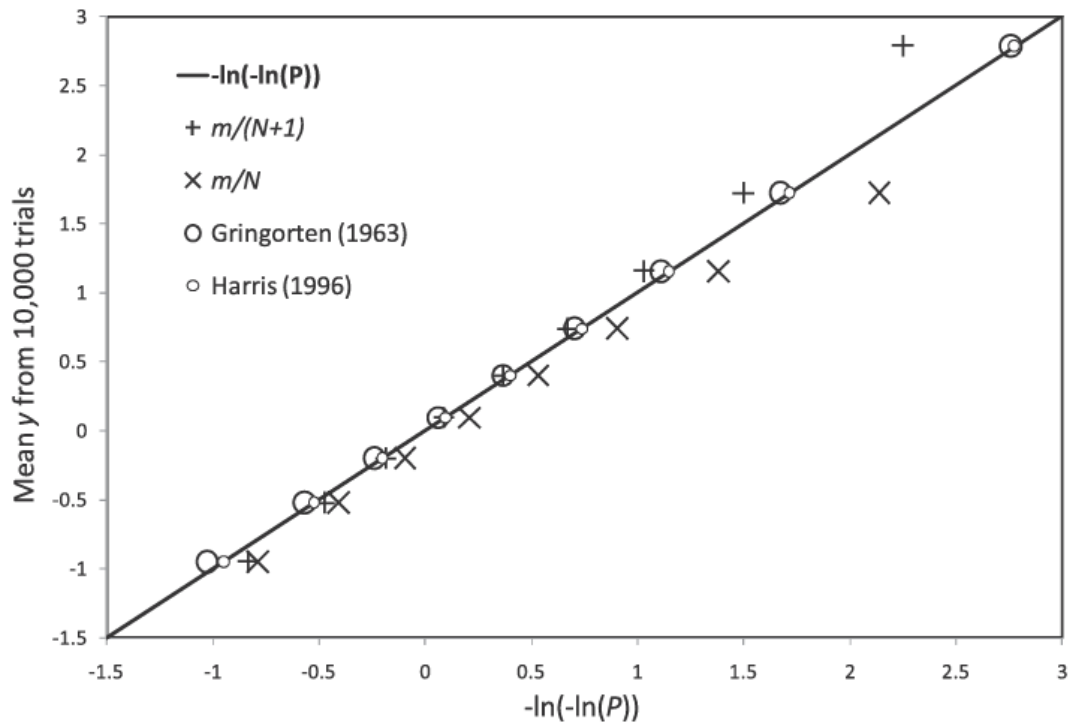


Figure 5.7 – Normalised Gumbel plot for the mean of 10,000 trials (Cook, 2011).

All previously mentioned methods are referred to as *rank-based*, as the ranking of extreme values determines the assigning of individual estimators and probabilities without any influence from the extreme values themselves. There are many parameter-fitting methods which do not require direct estimates of sample probabilities, and include maximum likelihood estimators (MLE), method of moments, probability weighted moments, optimal bias-robust estimators and Bayesian methods. While MLE was used by Padaratz (1977) to define Fréchet model parameters in the formation of the current basic wind speed map of Brazil (ABNT, 1988), this and other methods are not examined here as preference is given to the traditional rank-based methods. More information on these methods can be found in Gatey (2011).

5.3 PEAKS OVER THRESHOLD

The Generalised Pareto Distribution (GPD), also commonly referred to as the Peaks-Over-Threshold (POT) method, is closely related to the GEVD. Examples of its use in wind engineering can be found in Lechner et al. (1992) and Simiu and Heckert (1995) for annual maxima, and Holmes and Moriarty (1999), Holmes (2002) and Holmes et al. (2018) for

independent storms. A brief outline of the method is described below. Holmes and Moriarty (1999) should be consulted for further details.

The general form of the relationship between extreme value, X , and return period, R , is given in Equation 5.23, where u_0 is the base threshold and λ is the average yearly exceedance rate of u_0 . The parameters a and k are the same scale and shape factors, respectively, as for GEVD.

$$V_R = u_0 + \frac{a}{k} [1 - (\lambda R)^{-k}] \quad 5.23$$

Parameters k and a are determined from an analysis of the average excess of the set of thresholds u . Firstly, the base threshold u_0 is selected and u is incremented at even intervals. Holmes and Moriarty (1999) selected $u_0 = 20.3$ m/s and increments of 2 m/s until 34 m/s, making u of 8 thresholds at $\{20.3, 22, 24, \dots, 34\}$ m/s. For each threshold, the average excess of all peak wind speeds above that threshold is calculated and plotted against $(u - u_0)$ as shown in the example given by Holmes and Moriarty (1999) in Figure 5.8. At least ten exceedances of a threshold are necessary for inclusion in the mean exceedance plot (Holmes, 2002). The gradient, μ , and y-intercept, y_0 , are derived from a linear regression model fit to the data. Parameters a and k are then solved using Equations 5.24 and 5.25.

$$k = -\left(\frac{\mu}{\mu + 1}\right) \quad 5.24$$

$$a = y_0(1 + k) \quad 5.25$$

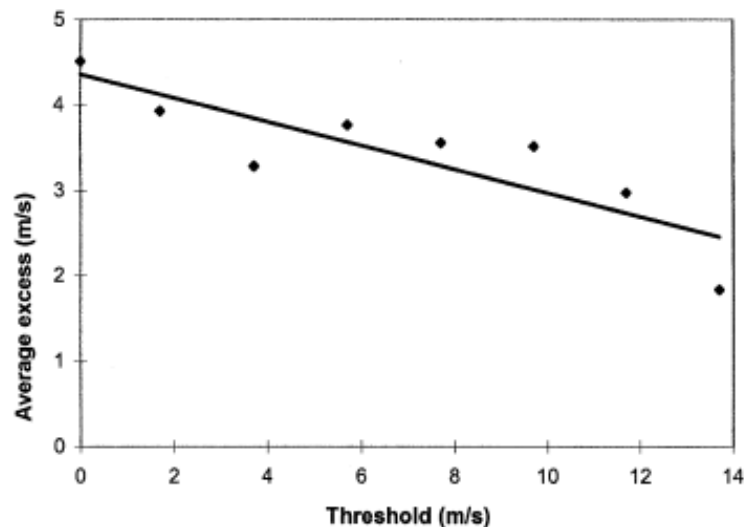


Figure 5.8 – Mean exceedance plot for downburst gusts at Moree, NSW, Australia (Holmes and Moriarty, 1999).

In the case of setting $k = 0$ (GEVD Type I), μ is set to 0 and y_0 becomes an average of the average excess points, Equation 5.23 reduces to Equation 5.15, for U defined by Equation 5.26.

$$U = u_0 + a \ln(\lambda) \quad 5.26$$

When $k > 0$ (GEVD Type III), Equation 5.23 reduces to Equation 5.27 with C and D are defined in Equations 5.28 and 5.29 respectively.

$$V_R = C - \left(\frac{D}{R}\right)^{-k} \quad 5.27$$

$$C = u_0 + \frac{a}{k} \quad 5.28$$

$$D = \frac{a}{k} \lambda^{-k} \quad 5.29$$

Holmes and Moriarty (1999) noted some potential issues with the GPD. Firstly, if a particular storm is significantly higher than other storms, then the mean exceedance plot will not ensure linearity. In such a case, it is possible that derived $k < 0$ (GEVD Type II – Fréchet) which is physically unrealistic. Secondly, the analysis is sensitive to the selection of the u_0 base threshold and the mean exceedance plot may not be linear if u_0 is set too low. Thirdly, true linearity may be difficult to determine in the case of few storms above a certain threshold.

A POT extreme value analysis was conducted by Pintar et al. (2015) on the most recent update to non-hurricane basic wind speeds of the United States in ASCE-7 (ASCE, 2016). For each station, a two-dimensional (time and magnitude of homogenised wind speed) model was fitted using MLE. Stations with a total sampling period of less than 15 years were omitted from the study due to their tendency to underestimate extreme wind speeds.

6. METHODOLOGY FOR THE DETERMINATION OF EXTREME WIND CLIMATE

This section details the development and implementation of the methodology used to determine an extreme wind climate model for each of the analysed SWS. Background information on datasets, extreme wind types and the modelling of extreme value distributions are given in previous chapters and their utilisation is herein described.

6.1 SELECTION OF RAW DATA

A summary of the two national meteorological networks in Brazil is given in Section 3.1 *Organisations and Protocols*, referred to as aerodromes and INMET, and an evaluation of the quality of available datasets relating to each network is made in Section 4 *Evaluation of Surface Wind Data Sources*. A minimum of 3 years of valid data ($t_{tot} \geq 3$) was required from all stations admitted to the study. Although 3 years is unlikely to produce an extreme value distribution of great accuracy and confidence, it is enough to produce a reliable parent distribution. A period of 7 years is considered suitable amount of time for an extreme value analysis to be conducted using MIS (Cook, 1982; ESDU, 1990[a]).

For aerodrome SWS, two sets of data were considered in the analysis:

1. PAS-31 (ICEA, 2017)
 - official ICEA data;
 - Brazilian aerodromes only;
 - multiple anemometers for some aerodromes;
 - analysis interval varies, maximum range from 01/01/1990 until 31/12/2017.
2. MSS
 - generated from decoded METAR/SPECI and SYNOP reports sourced from REDEMETS, NCEI/NCDC and WU;
 - aerodromes from Brazil and neighbouring countries;
 - principal anemometer only;
 - analysis interval varies, maximum range from 01/07/1996 until 31/05/2019.

Although PSEC-46 (ICEA, 2015) contains data from as far back as 1950, it was not utilised in the climate analysis due to the redaction of extreme wind events. Data made available by NCEI/NCDC, typically from 1973 for many international aerodromes, was also not analysed due to issues regarding the extraction of data from raw meteorological reports. Similarly, data already extracted from their original reports and made available by CPTEC-INPE, WU and Wolfram were considered inferior and not utilised in the study. However, METAR/SPECI and SYNOP reports from NCEI/NCDC were utilised in the confection of the MSS database.

All Brazilian land-based aerodromes (offshore helipads were not considered), for which data were available, were admitted to the preliminary study. However, many non-Brazilian aerodromes were discarded prior to analysis for a variety of reasons. Several Argentinian aerodromes were not considered due to large voids in their operational history according to accessible data, and include aerodromes SAAC – Concordia, SAAJ – Junín, SAAV – Santa Fé, SANU – San Juan, SAVT – Trelew, SAVV – Viedma, SAZB – Bahia Blanca and SAZR – Santa Rosa. The most recent meteorological report (i.e. limited to the last hour) for these aerodromes can be obtained from the Argentinian National Meteorological Service (*Servicio Meteorológico Nacional* – SMN) website³³. This suggests that SMN opts not to transmit meteorological reports for many aerodromes to the world via the GTS. The time-series of several aerodromes in Bolivia which operate between 12-16 hours per day were initially considered due to the close proximity to Brazil, but were discarded due to an apparent 35 kt limit of gust observations. These aerodromes also had a tendency to report gusts at increments of 5 kt, reducing confidence in their ability to measure accurately. Five such aerodromes are SLJO – San Joaquín del Beni, SLMG – Magdalena, SLCP – Concepción, SLRB – Roboré and SLSI – San Ignacio de Velasco. Large regions of Peru, Colombia and Paraguay were unaccounted for due to a lack of infrastructure demanding aerodromes with regular meteorological reports.

Four different sources of data for INMET ASWS were detailed in Section 4.2 *INMET ASWS*. A single database composed of these three sources, referred to as WRDS (Web, Restricted INMET, DISME, SADMET), was used in the analysis of INMET data.

WRDS

- The order of allocation is 1) Web data, 2) DISME data 3) SADMET data 4) Restricted INMET data;

³³ <https://www.smn.gob.ar/metar>

- Despite the Restricted INMET dataset being the most complete of the four, it is ranked last due to its obtainment only near the completion of this study;
- single anemometer only;
- analysis interval varies, but with maximum range from 07/05/2000 until 31/05/2019.

ASWS which were taken decommissioned by INMET prior to 2015 were not considered in the study, and such stations include A008 – Faculdade da Terra, DF, A403 – Areembepe, BA, A605 – Niterói, RJ, A654 – Jacarepaguá, RJ and A877 – Guaira, PR. Stations which were commissioned after 1/1/2016 were not considered, but are great in number and may offer quality data to be studied in the years to come. The number of stations commissioned in 2016, 2017 and 2018 (up to October) are 30, 34 and 31, respectively.

6.2 PREPARATION OF TIME-SERIES

A detailed explanation of the processes involved in the preparation of time-series of observed meteorological data pertaining to the three individual databases is given in this section, which is essentially a pre-process to the analyses. The time-series include wind data (DIR , V_{obs} , G_{obs}), temperature (T), atmospheric pressure (QNH or P_{atm}) for all databases, with the addition of present/recent/near weather phenomenon for MSS and PAS-31 data, and CB and TCU clouds for MSS.

The first stage involves the organisation of data in chronological order from oldest to newest. The following naming system is used: $YEAR$, year; MH , month; YY , day; GG , hour; gg , minutes. Two separate parameters are used to represent the date and time of the observation: date, $YEARMHYY$, and timestamp, $GGgg$. The determination of date and timestamps, and subsequent ordering, may seem a relatively straight-forward process; however, complications were encountered within each database. Synthesis of multiple sources into a single time-series was also necessary for the MSS and WRDS databases; while PAS-31 required the identification of primary and secondary anemometers for many aerodromes (tertiary and quaternary anemometers for SBGL – Galeão, RJ, and SBGR – Guarulhos, SP) by runway headings and descriptors which were not fixed over time.

Date and timestamps for all databases also undergo global quality checks. Such checks include making sure YY is not greater than what is permitted by each combination of $YEAR$

and MH , for example, $YY = 29$ is not possible for $MH = 2$ and $YEAR = 2001$, MH must be between 1 and 12, GG must be between 0 and 23 and gg must be between 0 and 59.

Time-series of the observed V and G are assigned the terms V_{obs} and G_{obs} , while parallel time-series, V_{cor} and G_{cor} , defined in Section 6.3 *Homogenisation of wind speed time-series*, represent wind speeds as corrected to the defining parameters of V_0 of NBR 6123 (ABNT, 1988): height of $z = 10$ m, time-averaging interval of $\tau = 3$ seconds and terrain with roughness length of $z_0 = 0.07$ m.

6.2.1 Aerodromes/MSS

The allocation ranking of meteorological reports which constitute MSS is as follows:

1. METAR/SPECI reports from REDEMET (RM),
2. METAR/SPECI reports from WU (WM),
3. METAR/SPECI reports from NCEI/NCDC (NM),
4. SYNOP reports from WU (WS), and
5. SYNOP reports from NCEI/NCDC (NS).

The REDEMET OPMET database is composed of reports that are received prior to being transmitted over the GTS, and is at least one step closer to the point of measurement. For this reason, RM is given the highest priority. Observations from WU are given preference over NCEI/NCDC due to fewer errors in the conversion of time, date and station information in the WU database. METAR/SPECI observations are given preference over SYNOP due to the reporting of gust data, in addition to the problems identified when SYNOP reports are missing the wind observation field. Each of the 5 sources are pre-processed separately for each station and then combined to form the MSS database. Similarly, the three sources which constitute the WRDS database are pre-processed separately prior to merging as one database.

No $YEAR$ or MH data is contained within METAR/SPECI and SYNOP reports, and such information can only be obtained from an external field within each particular database. An automated routine is used to extract YY , GG , gg and station identifier (ICAO code for METAR/SPECI reports; WMO code for SYNOP reports) from each individual report and compare with the external data made available from each source. If all four are the same, the report is cleared; if not, the report is manually compared to previous and following observations. If an understanding of the error can be reached, the relevant date/time data is

changed manually, however if the date and time cannot be determined, or the station identifier is different to that being analysed, the observation does not pass on to the following steps.

Decoding and extractions processes are applied to only MSS data, since PAS-31 and WRDS data are supplied in table format. The process involves three steps:

1. automated decoding and extraction of relevant data from the meteorological reports into their respective tabulated fields;
2. merging of the five source/report types into one coherent file per station;
3. evaluation of data from meteorological reports with irregular formatting, followed by either correction or discarding of the data under scrutiny.

Data is extracted from the METAR/SPECI and SYNOP reports as per formatting protocols given in Section 3.1.1 *Aerodrome SWS*. Each of the fields is also assigned a qualifier which identifies the quality of the data. In addition, a global qualifier is given to the meteorological report. At this point there are only three possible qualifiers:

1. Data is OK;
2. Data is to be discarded from any further analysis;
3. Data is to be reviewed manually.

If there are multiple observations for the same combination of date, timestamp and station, then all observations of that same combination are flagged to be reviewed manually. However, METAR/SPECI reports may contain a correction identifier, *COR*, and if only one of the reports contain this identifier it is automatically selected as the report to be used, and the global qualifiers all other reports of the same combination of date, time and station represent discarded reports. In the case of multiple reports with *COR* identifiers, the observations with no *COR* identifier are excluded and the multiple *COR* observations are flagged to be evaluated manually. Other reasons for marking the meteorological report to be discarded by the global qualifier include the identification of an incorrect meteorological report, i.e. a TAF (terminal aerodrome forecast) or SYNOP report which is identified as METAR/SPECI by the accompanying metadata supplied by the original source, or reports which contain no information other than the timestamp.

The determination of the range of meteorological report which is available for analysis/extraction is of extreme importance for METAR/SPECI reports. Typically, a

METAR/SPECI report will end with “=” to denote the end of the report, however many aerodromes outside of Brazil regularly add extra information onto the end of the report. Such information may include remarks by the observer, short-term or long-term weather forecasts, and will often contain wind, temperature data and weather descriptors in the same format as the observations. Strings such as “BECMG”, “TEMPO”, “FM”, “RMK”, “FCST”, and “INTER”, amongst others, are used to denote the start of the additional reports. All METAR/SPECI reports are scanned for these strings to denote the end of the section which is available for extraction, and any information which follows these strings is not considered for extraction. Similarly, there are cases in which parsing procedures were not undertaken correctly, either by the operators of the source database or at the origin of the meteorological report, which causes two or more reports to be joined together. The reports may be consecutive reports from the same station, or simultaneous reports from different stations. In either case, the joining of reports in one string causes the potential for the wrong data to be extracted. To circumvent such a problem, a list of the 4-letter ICAO identifiers for all South American aerodromes was prepared and each METAR/SPECI report is searched for each one of these ICAO identifiers. Should an ICAO identifier of a different aerodrome be discovered in the METAR/SPECI report of a particular aerodrome, or a second ICAO identifier from the same aerodrome under analysis, all information after and including the denoted identifier is removed from the report.

If the format of each data field does not match the correct format as specified by the protocols in ICA 105-15 (DECEA, 2018[b]) and ICA 105-16 (DECEA, 2017), its qualifier is modified to note that it must be evaluated manually. In some instances, the format is correct but there is an obvious error in the data provided, and may include cases such as $V \geq G$, *DIR* that is not a multiple of 10° and *DIR* greater than 360° . A single *DIR* is extracted for reports with variable wind directions when the maximum and minimum directions are reported. In the case of a variable wind direction without these limits, typically for wind speeds under 10 kt, the wind direction is recorded as null, represented by \emptyset .

All five source/report type combinations undergo the abovementioned processes. At this point, they are merged into one coherent time-series per station according to the ranking specified. The highest ranked source/report is RM, followed by WM and so on. Lower ranked sources are admitted to the MSS time-series only when there is no report available for a higher ranked report of the same date and timestamp. An example of the constitution of

MSS time-series for a particular meteorological station is shown in Figure 6.1. The dominance of RM and WM reports is common for the majority of stations analysed in this study.

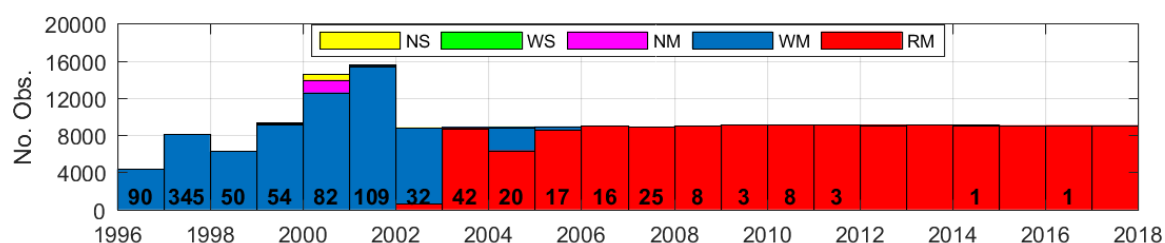


Figure 6.1 – Constitution of MSS database for SBBR – Brasília, DF.

The manual evaluation process is time-costly but necessary for the development of a high-quality MSS database. In the same way that we, humans, are able to process and understand grammatical or pronunciation errors in written and spoken language, it is possible to understand incorrectly formatted weather observations when analysed in a chronological context. Flagged observations are examined one at a time and compared to observations in the hours prior to, and after, the observation being scrutinised. If the observation under examination can be understood, the *DIR*, *V* and *G* data is extracted manually; alternatively, if neither *DIR* nor *V* can be determined, the wind data is marked to be discarded by the wind qualifier and not used in the forthcoming analyses. Similarly, in the case of multiple observations flagged for the same date and time, only the most contextually appropriate observation is cleared to be analysed. A list of the most commonly found errors is shown in Table 4.1. Figure 6.2 gives the example of one such meteorological report which could have an effect on the station’s extreme value analysis depending on how the data is treated. There are 6 digits in the wind field for the 23:30 UTC report, which renders the report irregular (without the “G” symbol to indicate a gust observation, there should only be 5 digits). As such, *V* could be considered as 47 kt, 04 kt or 07 kt, and, in fact, both WU and NCEI/NCDC supply $V = 24.2$ m/s (47 kt) for this observation. However, when viewed in context with the reports before and after, it is obvious that a typing error has occurred and that $V = 4$ kt was most likely the intended observation. Using the manual evaluation process, the wind data from the observation under scrutiny is extracted manually as $DIR = 110^\circ$ and $V = 4$ kt. The number within each column of Figure 6.1 represents the number of wind observations that were “rescued” by the manual evaluation and decoding process. It is noted that the number of corrections needed decreases over time, with only 2 corrections needed over the last 6 years

for SBBR – Brasília, DF. A total of 31,006 wind observations from MSS reports were decoded manually for 149 Brazilian aerodromes.

```
SBCT 272200Z 10006KT 9999 FEW030 15/14 Q1023=
SBCT 272300Z 09004KT 9999 FEW025 14/14 Q1024=
SBCT 272330Z 110047KT 5000 BR SCT002 OVC005 12/11 Q1022=
SBCT 272340Z 11004KT 0800 R15/1800 R33/1800 FG SCT001 BKN002 13/13 Q1024=
SBCT 280000Z 06004KT 0500 R15/0500 R33/0500 FG VV/// 14/14 Q1024=
```

Figure 6.2 – METAR reports for SBCT – Curitiba, PR, 27-28/08/2009 (Source: Weather Underground)

A similar process is used to extract T and QNH data from the meteorological reports. No discernment is used between present/recent/vicinity weather descriptors, and, as such, all are considered as present weather descriptors. A list of weather identifiers of interest is given in Section 3.1.1.1 *METAR/SPECI*, but due to the manual preparation of many years' worth of meteorological reports, spelling mistakes and other codes have the potential to cause an incorrect identification of a descriptor. A list of combination of letters which are not to be ignored is used by the automatic routine to accurately extract weather and cloud descriptors. For example, "MTS", used often by Argentinian aerodromes to represent metres in the reporting of visibility, i.e. 2500MTS, and is to be ignored when searching a report for the string "TS" representing a thunderstorm. Other such strings to be ignored when searching for "TS", include "TSCT" and "SCTS", common misspellings of "SCT" representing scattered cloud, and "KTS", a plural and irregular version of the wind speed units for knots - "KT". Present weather descriptors provided by PAS-31 are in numerical form and following the SYNOP system as defined by Table 4677 of ICA 105-16 (DECEA, 2017).

Once all data are extracted from meteorological reports and flagged reports are treated manually, another automated stage of the pre-process is executed for the T and QNH series of PAS-31 and MSS databases. The purpose is to eliminate sharp peaks of a certain magnitude in the time-series which are most likely caused by a typing error. It is necessary to remove false changes in temperature and pressure as sharp changes in both parameters are used latter to identify cases of non-synoptic extreme wind events.

The algorithm is crude but effective. It works with the assumption that changes to temperature and pressure should be either be slow and gradual or, when a sudden change occurs, the

readings should continue at a similar same level after the change. What should not occur is a sharp change in one direction, followed immediately by a change of similar magnitude in the opposite direction. The most common error found in the time-series of both temperature and pressure is the typing of the wrong digit in the 10's column. Two examples are given in Figure 6.3 and Figure 6.4 of sharp changes to the temperature and atmospheric time-series respectively. The change in T in Figure 6.3 is $-10\text{ }^{\circ}\text{C}$, followed by $+10\text{ }^{\circ}\text{C}$ for consecutive hours; while the change in QNH in Figure 6.4 is $+9\text{ hPa}$, followed by -11 hPa . It is most likely that both observations causing these sudden changes are incorrect by exactly $10\text{ }^{\circ}\text{C}$ and hPa , respectively. As such, an arbitrary threshold of 7 is set, and any observation which has an absolute difference of $7\text{ }^{\circ}\text{C}$, or 7 hPa , or more between itself and the observation immediately prior, and the observation immediately after, is removed from the time-series.

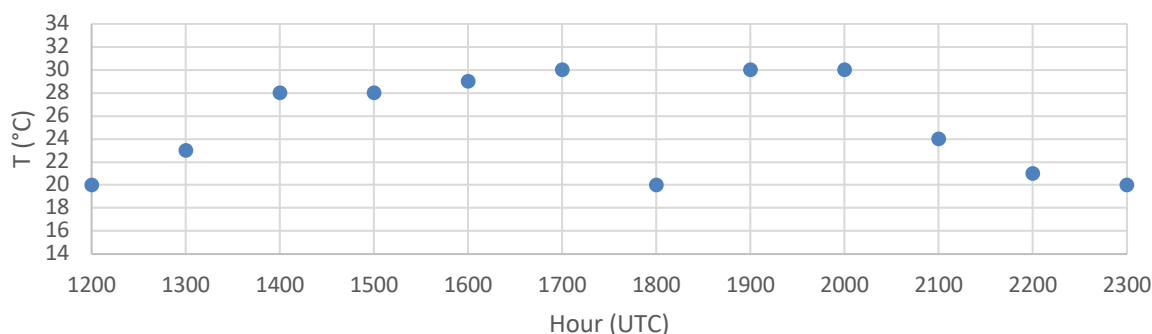


Figure 6.3 – Temperature time-series extracted from METAR/SPECI reports for SBGR – Guarulhos, SP, 25/08/2014 (Source: REDEMET)

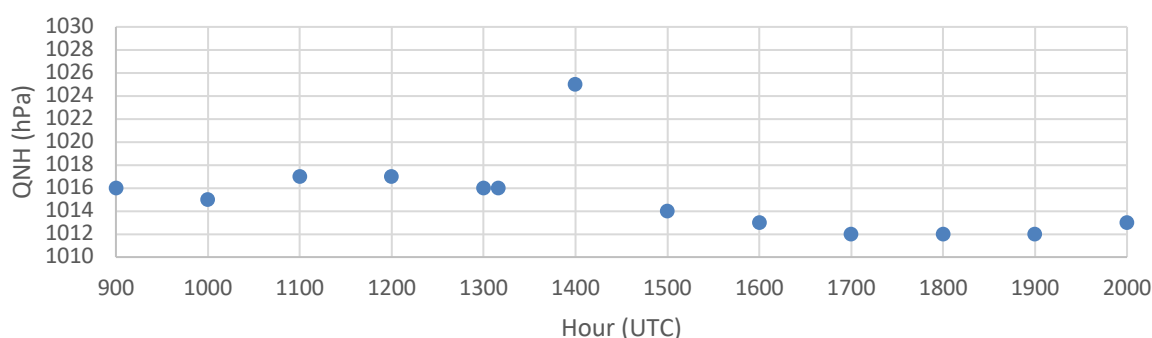


Figure 6.4 – Atmospheric pressure time-series extracted from METAR/SPECI reports for SBGR – Guarulhos, SP, 09/09/2011 (Source: REDEMET)

Global limits, determined by a preliminary manual inspection of the plotted temperature and atmospheric pressure time-series, are also applied to the time-series for both MSS and PAS-31 datasets. Any observation passing above the upper limit, or below the lower limit, is discarded. The limits are customised for each station. For example, permissible temperature and atmospheric pressure ranges for SBFZ – Fortaleza, CE, are 15 to 40 °C, and 1000 to 1025 hPa respectively; while for SBPA – Porto Alegre, RS, the ranges are -5 to 45 °C, and 990 to 1040 hPa respectively.

6.2.2 Aerodromes/PAS-31

Although manual processes are responsible for the preparation of large majority of data supplied in PAS-31, such as the notation of observations on paper, and manual digitisation of records at a later date, no decoding or manual evaluation processes were used in the preparation of time-series in this study. Two main challenges were presented by the PAS-31 database:

1. Identification of stations, and subsequent manual correction of data, affected by the misclassification of both *DIR* and *V* data, as detailed in Sections 4.1.2.2 *PSEC-46* and 4.1.2.3 *PAS-31*,
2. The creation of multiple virtual meteorological stations at aerodromes with multiple anemometers and anemometer names.

Separate files were received from ICEA for each meteorological parameter requested for each aerodrome. Several aerodromes have more than one anemometer, and the name given to each anemometer relates to its location, typically in respect to the headings of the runway(s) of the aerodrome. The creation of continuous wind speed time-series is made challenging due to the alteration of runway names, aerodrome layouts and locations of anemometers. The first step involves the compilation of all names of anemometers for each aerodrome and the period for which data is available. For stations with two simultaneous time-series, primary and secondary anemometers must be assigned via consultation of the AIP (DECEA, 2018[a]) and comparison with data from MSS series with the understanding that wind data in METAR/SPECI reports are recorded by the primary anemometer. Data from tertiary and quaternary anemometers are available at SBGL – Galeão, RJ, and SBGR – Guarulhos, SP. Data is assigned to the primary anemometer for periods in which the anemometer is named “00”, or a combination of the two runway headings, e.g. “18/36”. An example of a station

with a multiple anemometers and names is given in Figure 6.5 for SBBQ – Barbacena, MG. Five different anemometer names were encountered for the station for the period between 1990 and 2017. Time-series in parallel were given from 2010 for anemometers at heading “18”, primary, and “36”, secondary, for the single-runway airport. Data for anemometers named “00”, “PISTA” (Portuguese for “runway”) and “18/36” are considered to be from the primary anemometer, even though it is possible the anemometer was positioned at a different location, or even above a control tower during these periods.

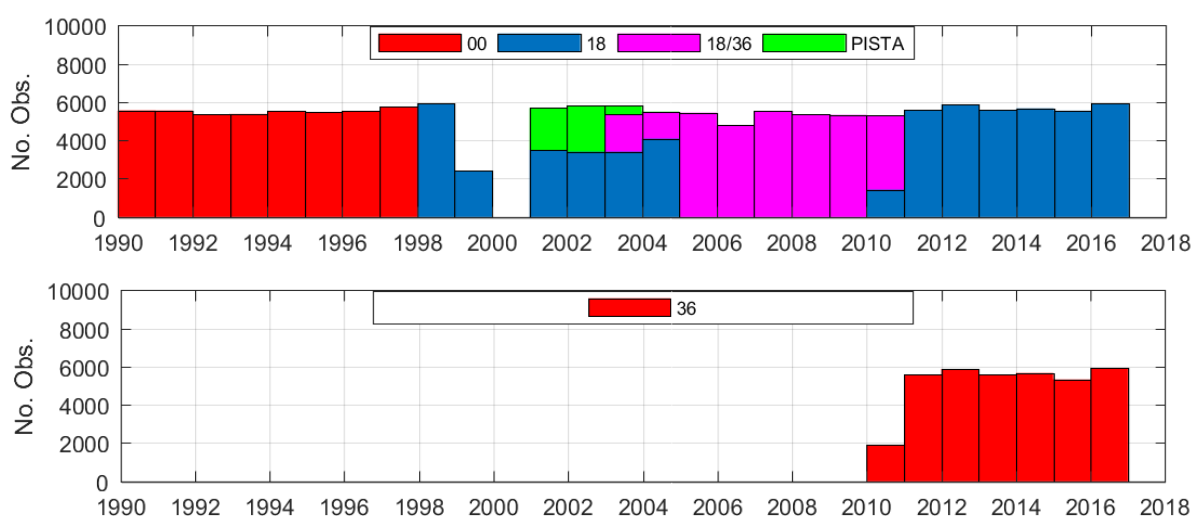


Figure 6.5 – Constitution of the primary (top) and secondary (bottom) anemometers for SBBQ – Barbacena, MG, (PAS-31, 2017).

Once separate wind data is organised into its own file per anemometer ranking, the secondary parameters, such as temperature, atmospheric pressure and present weather descriptors, are loaded for the timestamps which correspond to the already present wind data. This means the same temperature data, for example, is used in conjunction with anemometers operating simultaneously. The algorithm which filters sharp peaks and spurious data as per global limits, as described in Section 6.2.1 *Aerodromes/MSS*, is also applied to the temperature and atmospheric pressure time-series.

Present weather descriptors are converted from the numeric SYNOP system, according to Table 4677 of ICA 105-16 (DECEA, 2017), to string descriptors used by METAR/SPECI reports. Weather descriptors of interest for extreme wind analysis include thunderstorm (13, 17, 18, 29, 90-98 are converted to “TS”), widespread dust, sand, dust/sand whirls, sandstorm, dust storm (7-9 is converted to “PO” and 30-35 is converted to “DU”) and tornado/funnel cloud/water spout (19 is converted to “FC”). Rain showers (25) and hail showers (27) can also

be accompanied by strong winds, but were not considered due to their perceived high frequency of occurrence, particularly for rain.

6.2.3 INMET/WRDS

The INMET network of ASWS operates differently to that of aerodromes and a different approach is required in the preparation of meteorological data time-series. All data is acquired and transmitted automatically without any human interference, meaning typing errors, found frequently in the MSS and PAS-31 data, are not encountered in this dataset. It follows that the processes of manual correction of wind data, the elimination of sharp peaks and application of global limits to temperature and pressure, as performed for the aerodrome data, are not required.

Similar to the MSS dataset, the WRDS dataset is the result of data merged from multiple sources. The allocation ranking of meteorological reports which constitute WRDS is as follows:

1. INMET ASWS reports made available temporarily from INMET's website (WEB),
2. INMET ASWS reports supplied by individual *Meteorological Districts* (DISME),
3. INMET ASWS reports supplied by INMET's *Meteorological Data Storage Unit* (SADMET).
4. INMET ASWS reports obtained from INMET's restricted database.

Each group of meteorological parameters, typically an instantaneous value at the end of the hour with a maximum and minimum of the previous hour, is assigned a single qualifier which determines if the data is valid for analysis or not. For temperature and pressure data, each report is checked for local limits, i.e. for temperature, $T_{min} \leq T_{ins} \leq T_{max}$, and should the data not satisfy this condition the data is not considered in further analyses as indicated by its qualifier. The exception is for wind data, which assigns one qualifier for *DIR* and one for the grouping of *V* and *G*. This is due to several *DIR* time-series being problematic over long periods of time for several stations, however the *V* and *G* data are of good quality and should be retained for analysis. A218 – Farol Preguiças, MA, is an example of such a station, with time-series in Figure 6.6 indicating *DIR* is greater than 180° for all observations over the history of the station.

Valid direction data must be in the range of $0^\circ < DIR \leq 360^\circ$ and be an integer. For wind speed data, unless calm is reported, $V = G = 0$ m/s, both V and G must be positive and $V < G$.

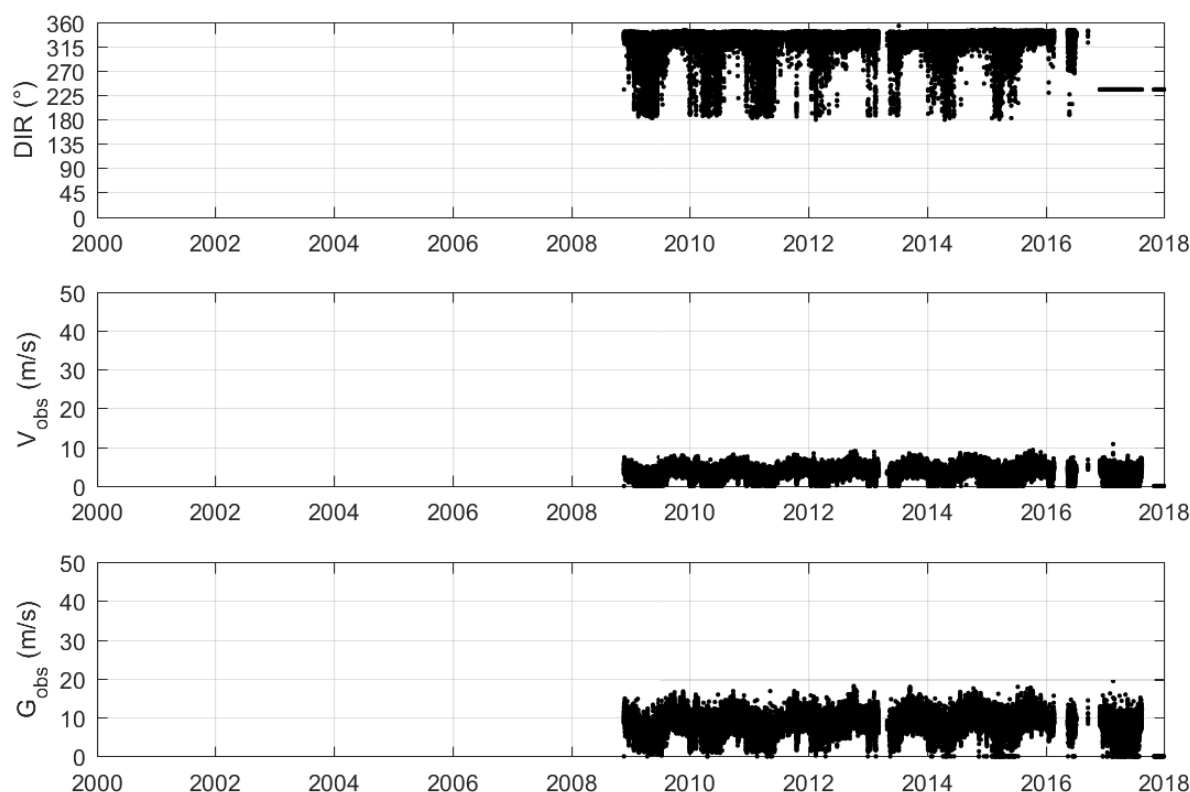


Figure 6.6 – Direction, 10-minute mean wind speed, and maximum hourly gust observation time-series for A218 – Farol Preguiças, MA.

Spurious temperature and atmospheric pressure data are identified and discarded manually. The time-series of the instantaneous parameters, T_{ins} and P_{ins} , are plotted over the course of each station's life, then a visual inspection of the plots is conducted to identify any long-term periods, or individual data, which exhibit large deviations from the pattern established. The qualifiers of the affected data are changed manually for such periods. An example of periods exhibiting spurious data is shown Figure 6.7 for A002 – Goiânia, GO. Due to the unmanned nature of the ASWS, erroneous observations can occur over a period of months, even years, as indicated by the pressure time-series in Figure 6.7. The temperature time-series also exhibits periods of extremely high and low readings, which much be eliminated from any climatic analysis of the station.

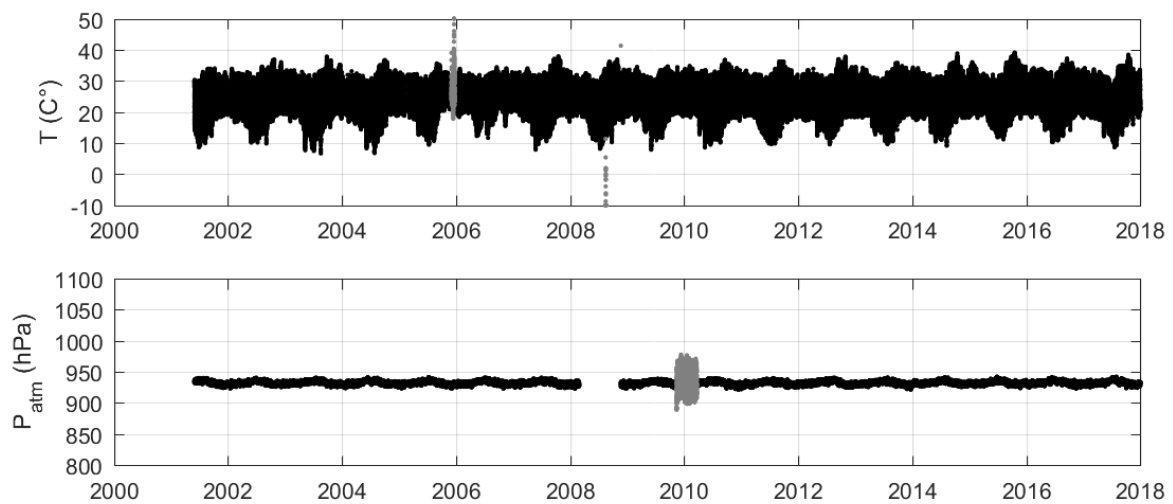


Figure 6.7 – Temperature and atmospheric pressure time-series for A002 – Goiânia, GO, with manually discarded data (grey).

6.3 HOMOGENISATION OF WIND SPEED TIME-SERIES

There are several factors which can influence observed wind speeds as demonstrated in Section 3.2 *Homogenisation of wind speeds*. Amongst them are the surrounding topography and terrain, type of anemometer, height of anemometer and distortion caused by large obstacles in near proximity – all of which can change during the lifetime of a station.

Due to the limited amount of information on anemometer makes and models used in Brazilian aerodromes it was not possible to determine correction factors for anemometer types, which would require extensive testing of several anemometers in both controlled and in-situ conditions. Topographic and distortion factors were also not analysed and are assumed as unity. As such, only height and terrain factors were considered in the homogenisation of wind speeds. The pragmatic and easily implemented method of Holmes et al. (2018) was applied for terrain categories of NBR 6123 (ABNT, 1988).

Terrain correction factors, F_V and F_G , were produced for each anemometer using terrain and height multipliers, S_2 , from the Brazilian wind standard NBR 6123 (ABNT, 1988) which contains five terrain categories (CAT). The analysis was performed for 8 x 45° sectors over a fetch length of 500 m from the anemometer location. To reduce errors, intermediate terrain categories were considered (i.e. CAT II ½ represents terrain between CAT II and III). A value of S_2 is calculated for $\tau = 3$ and 600 seconds (relating to G and V parameter respectively) according to Table F.1 and Equation 2.12. For example, the southern sector within a 500 m

radius from the principal anemometer (height of $z = 6$ m) at SBBU – Bauru, SP, was judged as CAT IV. S_2 values at $z = 10$ m and $z_0 = 0.07$ m for $\tau = 3$ and 600 s are $S_{2,3s} = 1$ and $S_{2,600s} = F_r$ respectively. From Table F.1, $b_{3s}(\text{IV}) = 0.86$; $p_{3s}(\text{IV}) = 0.12$; $p_{600s}(\text{IV}) = 0.23$. F_V and F_G are defined by Equations 6.1 and 6.2 and represent the corrections needed to make this combination of b , p and z in order to give $S_{2,3s}$ and $S_{2,600s}$. Substituting in these variable gives $F_G = 1.24$ and $F_V = 1.31$.

$$F_V = \frac{S_{2,600s}}{b_{3s(\text{CAT})} \cdot F_r \left(\frac{z}{10} \right)^{p_{600s}(\text{CAT})}} \quad 6.1$$

$$F_G = \frac{S_{2,3s}}{b_{3s(\text{CAT})} \left(\frac{z}{10} \right)^{p_{3s}(\text{CAT})}} \quad 6.2$$

In cases of unconfirmed anemometer locations, satellite imagery was analysed to provide an estimated location. In cases of unconfirmed anemometer heights, a conservative $z = 8$ m was adopted. In cases of changes anemometer locations and/or heights, a single location and/or height which best represented all observed data was used.

An equivalent gust, G^* , as defined in Equation 6.5, was a necessary intermediary step for aerodrome SWS observations which do not include an observed gust, G_{obs} . The gust factor, $G_V = 1.45$, is defined in NBR 6123 (ABNT, 1988) for open field exposure at $z = 10$ m. Equation 6.5 makes use of the ICAO rule which states that G should only be reported when the maximum gust over the 10-minute period is 10 kt or more than V . It follows that when G is not observed, the maximum gust over the 10-minute period is assumed to be less than $V + 10$ kt.

$$V_{cor} = F_V \cdot V_{obs} \quad 6.3$$

$$G_{cor} = F_G \cdot G_{obs} \text{ or } G_{cor} = F_G \cdot G^* \quad 6.4$$

$$G^* = \min(1.45V_{obs}, V_{obs} + 10) \text{ kt} \quad 6.5$$

Note that b selected in the calculation of correction factors F_V and F_G corresponds to $\tau = 3$ s and b for $\tau = 600$ s is not utilised as might be expected – meaning the difference between F_V and F_G is dependent only on p values – and is to ensure that $V_{cor} < G_{cor}$. Using the example for

the southern sector of SBBU – Bauru, SP, if b for $\tau = 600$ s ($b_{600s}(IV) = 0.71$ from Table F.1) were used, this would give $F_G = 1.24$ and $F_V = 1.58$. In the case of an observation of $V_{obs} = 40$ kt and $G_{obs} = 50$ kt (even without the observation of a gust, $G^* = 50$ kt according to Equation 6.5), the application of these factors would give the implausible set of corrected observations of $V_{cor} = 63.4$ kt and $G_{cor} = 61.8$ kt.

6.4 SELECTION OF CONTRIBUTING SAMPLING PERIODS

A process of *deactivating* observations, over short or long periods of time, was applied to all three datasets. Deactivated wind observations were those which either exhibited characteristics which deviated significantly from the true, or established baseline, characteristics of a particular station, or observations which were made infrequently. Five key characteristics were analysed for changes: percentage of valid observations per month, predominant wind direction, monthly mean wind speeds and distribution of extreme events.

For an extreme value analysis of MIS, the temporal resolution of observation time-series must be sufficient enough to allow for the correct classification of extreme wind events. While INMET ASWS emit observations at hourly intervals, METAR/SPECI and SYNOP reports can vary from 1-minute intervals up to 3-hourly intervals. To evaluate the frequency of observations, the wind speed time-series were first divided into blocks, with each block ending when a period of 4 hours or more passed between two consecutive observations. An assumed period of validity of each observation, t_{val} , in minutes, was calculated according to Equation 6.6, and was limited to a maximum value of 60 minutes. The total period of validity of each block was calculated by summing the all t_{val} values within the block, and blocks with a total time of less than 6 hours were deactivated and omitted from any further analysis. As such, any stations which observe less than 6 consecutive hours per day were not considered in the analysis, and include aerodromes located in areas of severe convective activity such as SBBG – Bagé, RS, SBNM – Santo Antônio, RS, SBPF – Passo Fundo, RS, and SBTD – Toledo, PR.

$$t_{val,i} = \min(60, timestamp_{i+1} - timestamp_i) \quad 6.6$$

Changes in the wind direction characteristics can be identified by examination of the observed data plots, but these changes can remain hidden if not properly analysed. The majority of

these cases were limited to the INMET ASWS network. An example of a station with a sharp change in wind direction characteristics, identifiable to the naked eye, is shown in Figure 6.8 for A308 – Parnaíba, PI, located on Brazil’s northern coastline within the ITCZ. The ITCZ is well-known for its eastern trade-winds; however, predominant easterly winds were only observed at this station from 2010 onwards, as shown in Figure 6.8. From 2003 to 2010, the station registered predominant winds from the west – implying an incorrect installation of the wind vane by 180° for approximately 6-7 years. Subsequently, wind direction data prior to 2010 was deactivated for this station.

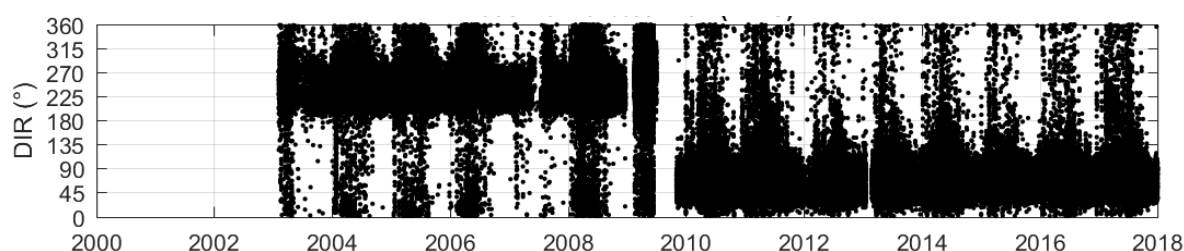


Figure 6.8 – Wind direction time-series for A308 – Parnaíba, PI.

In this study, the predominant monthly wind direction was determined by the 45° sector with the maximum number of observations over the month, independent of wind speeds. A separate plot of the predominant monthly wind direction was analysed for any changes which were not apparent in the observed data plot. An example of the observed *DIR* time-series and predominant monthly wind direction for A842 – Nova Fátima, PR, is shown in Figure 6.9. The predominant monthly wind direction plot reveals a shift in predominant direction from south and southeast to north in 2014, which is difficult to identify in the observed data plot. Due to the difficulties in determining the true predominant wind direction at each location, with the exception of those located in regions where the prevailing wind direction is well documented such as ITCZ, no action was taken to deactivate periods of the *DIR* time-series for many stations. Stations which exhibited traits similar to those in Figure 6.9 include, but are not limited to, A705 – Bauru, SP, A708 – Franca, SP, A713 – Sorocaba, SP, A714 – Itapeva, SP, A715 – São Miguel Arcanjo, SP, A727 – Lins, SP, A730 – Chapadão do Sul, MS, A731 – Maracaju, MS, A737 – Ibitinga, SP, A738, Casa Branca, SP, A740 – São Luis do Paratinga, SP, A746 – Barra do Turvo, SP, A749 – Juti, MS, A821 – Joaquim Távora, PR, A824 – Icaraima, PR, A829 – São José dos Ausentes, RS, A846 – Foz do Iguaçu, PR, A849 – Diamante do Norte, A849, A857 – São Miguel do Oeste, SC, A864 – Major Vieira, SC, A869

– Cidade Gaúcha, PR, A871 – Japira, PR, A874 – São Mateus do Sul, PR, and A876 – Clevelândia, SC.

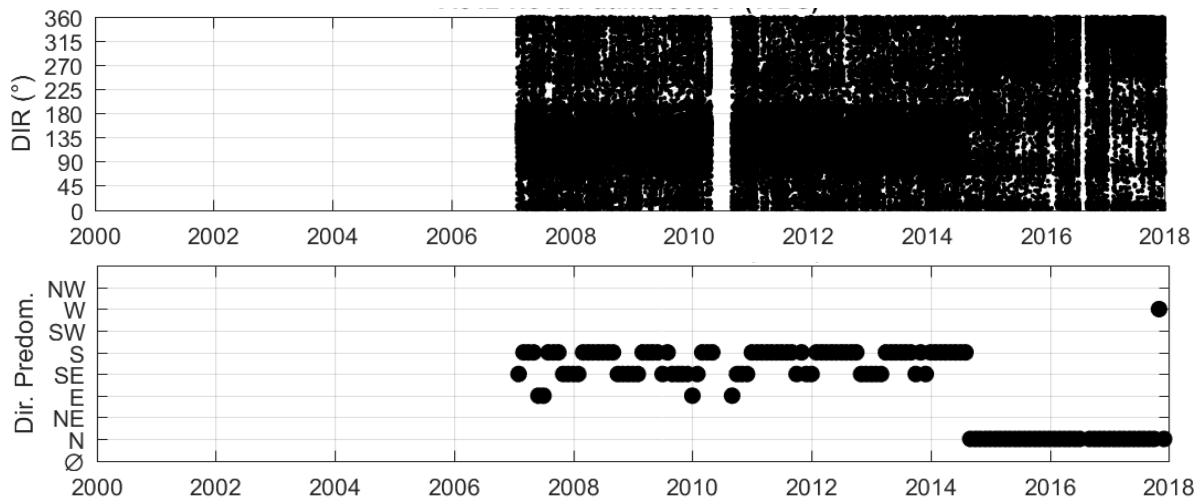


Figure 6.9 – Wind direction time-series (top) and predominant monthly wind direction (bottom) for A842 – Nova Fátima, PR.

A time-series of monthly mean wind speeds, V_m , was calculated from the V_{cor} time-series weighted by the t_{val} assigned to each observation. Each station was also assigned a time-series of synoptic monthly mean wind speeds from the ECMWF (European Centre for Medium-Range Weather Forecasts) ERA-Interim reanalysis data (Dee et al., 2011). Reanalysis data are produced from an assimilation of historical observed data with global weather forecast models. The ERA-Interim data has a horizontal grid spacing of 0.75° (approximately 80 km) for both latitude and longitude, and data was taken from the node closest to each station. For some coastal stations, an ERA-Interim node located further inland was manually assigned, as marine coordinates typically have much higher speeds than those on land. Although ERA-Interim data is available at higher resolutions (up to 0.125°), such grids only oversample the data and do not improve accuracy³⁴. For each station, the ERA-Interim data was plotted alongside V_m derived from observations at the SWS and the two are compared visually. The two series are not expected to be exactly the same, as the ERA-Interim mean is composed of various sources including forecasting models and synoptic readings; while a station's mean is taken from data recorded at a higher resolution. As such, the ERA-Interim data was treated as a guide with the expectation that series should at least be similar to each other.

³⁴ <https://confluence.ecmwf.int/pages/viewpage.action?pageId=56658069>

To assist in the identification of changes in V_m , either gradual or sudden, a climatic mean for each month, January through to December, V_{clim} , was calculated for both SWS and ERA-Interim data. The SWS climatic monthly mean used t_{val} to weight the yearly contributions for each month. V_{clim} was then used to normalise the V_m time-series and the resulting normalised time-series was plotted. An example of the two plots is shown in Figure 6.10 for SBPV – Porto Velho, RO. For this location, both V_m series appear to be almost equal, but when normalised, the SWS data for the period prior to 2001 is between 20 to 100% greater than the SWS data after 2001. As such, the time-series prior to 2001 was deactivated and not considered for further analyses. In the plots, deactivated periods are identified by a fainter line, while active periods are identified by the heavier lines. The deactivation process was done manually by visual estimation and applies to entire months. The deactivated data was not considered when calculating V_{clim} and the process is iterative. The process is very subjective and long periods with $V_m/V_{clim} > 1.25$ or < 0.75 were typically identified for deactivation. ERA-Interim data and most recent station data are used as guides to identify the periods which are established as the “true” representation of local climatic characteristics. The example given in Figure 6.10 is relatively straightforward and clean, however there are stations for which characteristics change frequently, making it difficult to establish a baseline – particularly when metadata is unavailable.

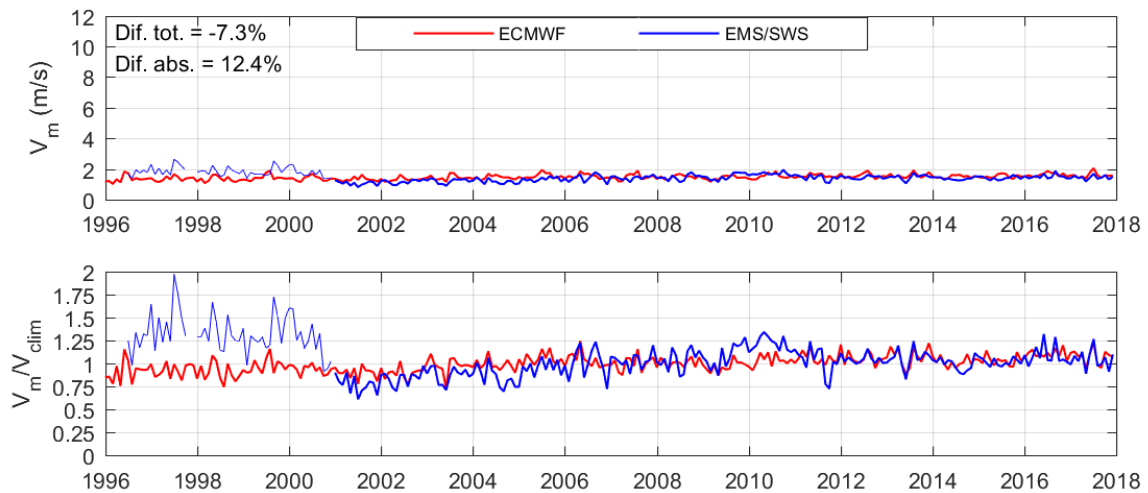


Figure 6.10 – Monthly mean wind speeds for SWS and ECMWF data for SBPV – Porto Velho, RO, MSS dataset (top); monthly means normalised by V_{clim} (bottom).

Two error parameters, *difference-total* and *difference-absolute*, were calculated in an attempt to quantify the relationship between the station and ECMWF monthly means over the active period. Both parameters are means that are calculated using weightings as determined by the

summed t_{val} of each month, but while *difference-total* considers the +/- of the difference between station and ECMWF V_m , *difference-absolute* does not. For SBPV – Porto Velho, RO, in Figure 6.10, the mean absolute difference between the two monthly mean datasets is 12.4%, whereas the net difference over the active period is -7.3%, indicating the data observed at the station is typically less than the mean from the ECWMF ERA-Interim dataset. In this case, these errors are low and give confidence in the quality of the SWS. Differences in the order of up to 20% were considered good, but there are several stations which have differences of up to 80%. It can be difficult to determine which of the reanalysis data or station data is more accurate. One example of a large error between the two is the aerodrome at SBCA – Cascavel, PR, as shown in Figure 6.11. The V_m as measured by the SWS, which operates between 50-80% of the time, is more than double that of the ECMWF monthly mean data. Metadata received from SBCA aerodrome operators confirmed the anemometer was installed at a height of 10 m above ground level in typically open field terrain.

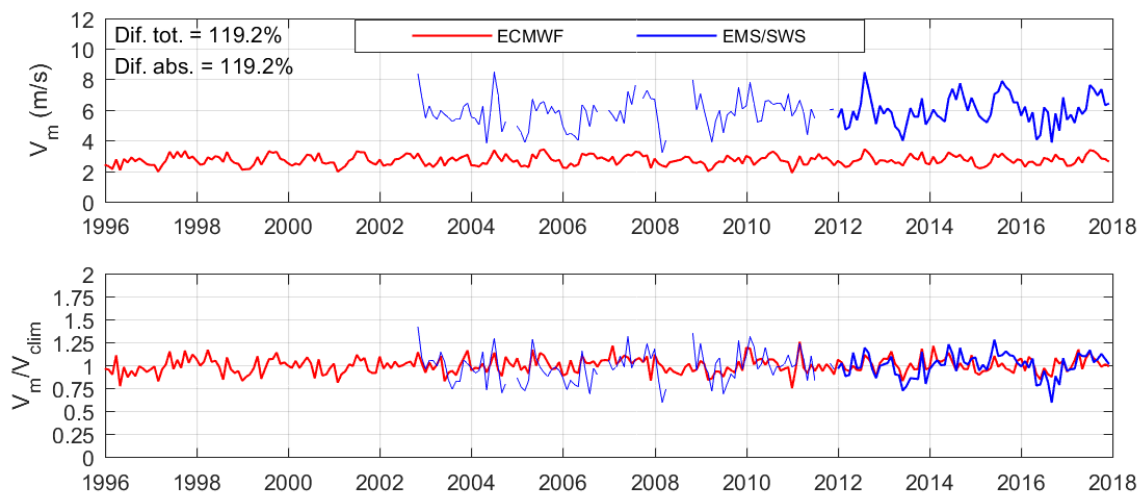


Figure 6.11 – Monthly mean wind speeds for SWS and ECMWF data for SBCA – Cascavel, PR (top); monthly means normalised by V_{clim} (bottom).

There were SWS which exhibited multiple changes in V_m making difficult the identification of periods to be established baselines. The subjective nature of the process, especially without relevant metadata, highlights the potential for errors in the study. However, it is estimated that these errors are much smaller than those of a study in which data is not scrutinised. V_m data for SBCG – Campo Grande, MS, from the MSS and ECMWF ERA-Interim datasets are shown in Figure 6.12. In addition, Figure 6.12 shows the monthly percentage operation with valid observations, $Obs.$ (%), which is defined as a ratio of the sum of t_{val} for all observations

within the month to total time of the month. Also plotted is the percentage of even numbered observations, i.e. $V_{obs} = 2$ kt, 4 kt, 8 kt and so on, per month. Inspecting the plots relating to V_m , a total three change points occurred in 2002, 2007 and 2013, giving four different sets of station characteristics. From the *Obs. (%)* graph it is noted that station operation is near 100% for the majority of months, ruling out a change in operating hours as the cause of the changes in characteristics. The change-point in 2007 occurred at the same time as the percentage of even-numbered observations dropped from near 100% to 50%, possibly indicating a change from a conventional to digital observation system. For all four periods, the station's V_m is shown to be much higher than that of ECMWF, with the highest period being from 2002 to 2007. Considering all of the above, and the fact that no historical metadata was provided, only a current location of the anemometer with installation date unknown, it was decided to deactivate all data prior to the change-point in 2007.



Figure 6.12 – Monthly mean wind speeds for SWS and ECMWF data for SBCG – Campo Grande, MS (top); monthly means normalised by V_{clim} (middle); percentage of month with valid observations (columns), with percentage of even numbered observations in knots (line) (bottom).

The importance of analysing monthly mean wind speeds cannot be underestimated. There are several cases, particularly for INMET ASWS, in which an examination of the month mean time-series was the only way to identify quality issues at SWS. An example is given in Figure

6.13 for A820 – Marechal Cândido Rondon, PR, located in a region of the country with frequent severe non-synoptic events. V_{obs} and G_{obs} time-series appear homogenous and without any significant change over the period of operation, but the V_m time-series indicates a sudden decrease in mean wind speed at the station at the end of 2015, which does not appear to be rectified until some point in 2017. A820 was equipped with a Vaisala WAA151 cup anemometer and it is postulated that a bearing failure caused the reduction of the signal. Since the mean wind speeds were not accurate, the gust wind speeds were also considered inaccurate and extreme wind events recorded during this period must be disregarded.

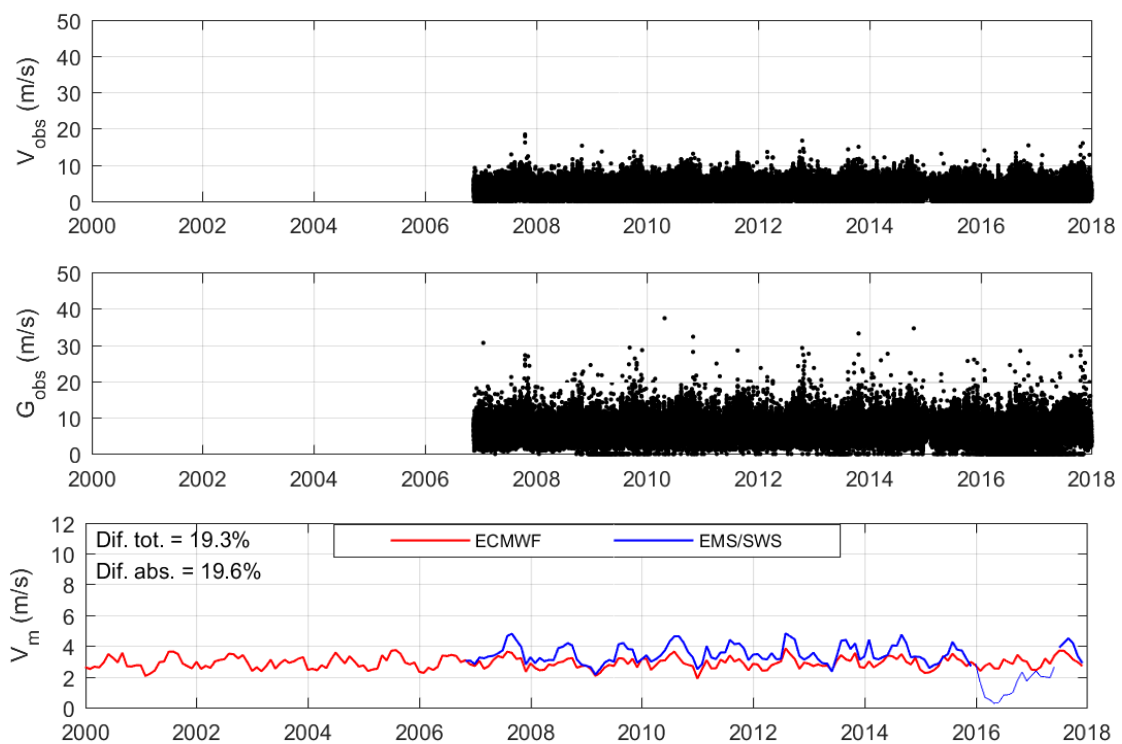


Figure 6.13 – V_{obs} for A820 – Marechal Cândido Rondon, PR (top); G_{obs} (middle); monthly mean wind speeds for SWS and ECMWF data (bottom).

The examination of monthly mean wind speeds does not always reveal changes to the gust time-series. In some cases, a change is obvious from the plot of the G_{obs} . Without any change to the operating hours of SBPB – Parnaíba, PI, a sudden increase in the number of gust observations above 40 kt began in mid-2015 and lasted until near the end of 2016, as shown in Figure 6.14. Infraero-Recife, the body responsible for the management of several of the aerodromes in the region, was contacted to help investigate the motive for this change but was unable to identify any possible cause. As such, the affected period for SBPB was deactivated from further analyses.

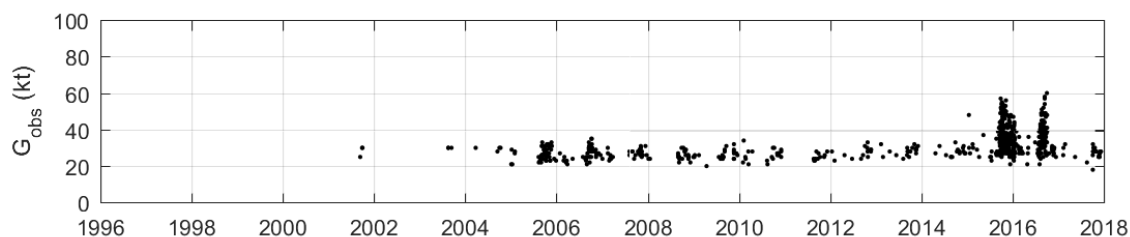


Figure 6.14 – G_{obs} for SBPB – Parnaíba, PI.

High numbers of obvious spurious data were encountered more frequently for INMET ASWS, which consisted of two types. The first involves clusters of high gust speeds over short periods of time, from days to months. An example of this A101 – Manuas, AM, in 2000 as shown in Figure 6.15. A second type, as demonstrated in Figure 6.16 for A237 – Caxias, MA, is the intermittent appearance of spurious data over long periods of time. The quantity of affected data is so much that classifying algorithms, described in Section 6.5 *Identification of synoptic, non-synoptic and suspected false extreme wind events*, were unable to correctly classify some events as suspect, resulting in their supposed validation. If there is a lot of spurious data in the time-series, some will eventually occur at the same time as a sharp decrease in temperature, or increase in pressure, indicators used to identify non-synoptic events. To avoid such misclassification, some long periods with spurious data were deactivated from further analyses.

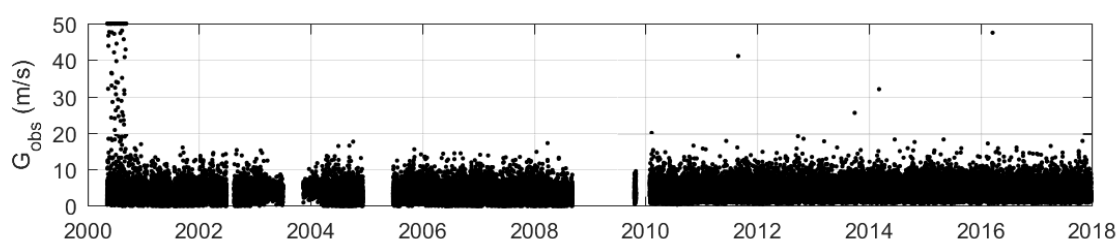


Figure 6.15 – G_{obs} for A101 – Manuas, AM.

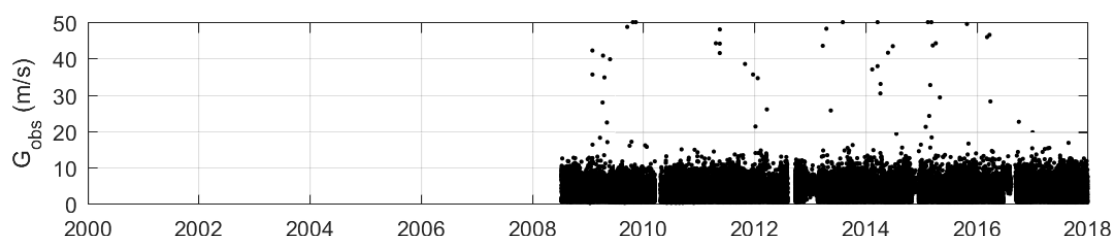


Figure 6.16 – G_{obs} for A237 – Caxias, MA.

Similar phenomena to those encountered at SBPB were encountered at other stations but at a lesser magnitude, including SBKG – Campina Grande, PB, and SBMA – Marabá, PA. A

demonstration of the phenomenon is shown in Figure 6.17. No strange behaviour of the G_{obs} time-series is noticed by the naked eye, however when a temporal distribution of the Top 100 extreme wind events (threshold of $G_{cor} = 13.9$ m/s for SBKG) is plotted on monthly basis, a period of six months, starting just prior to 2014, is revealed to have a high density of events ($N_{ev} > 4$ events per month). This period is very suspicious and would certainly dominate an extreme wind climate modelled using the independent storm method. Again, no information on its cause was obtained from Infraero-Recife, and so this period was deactivated from further analyses.

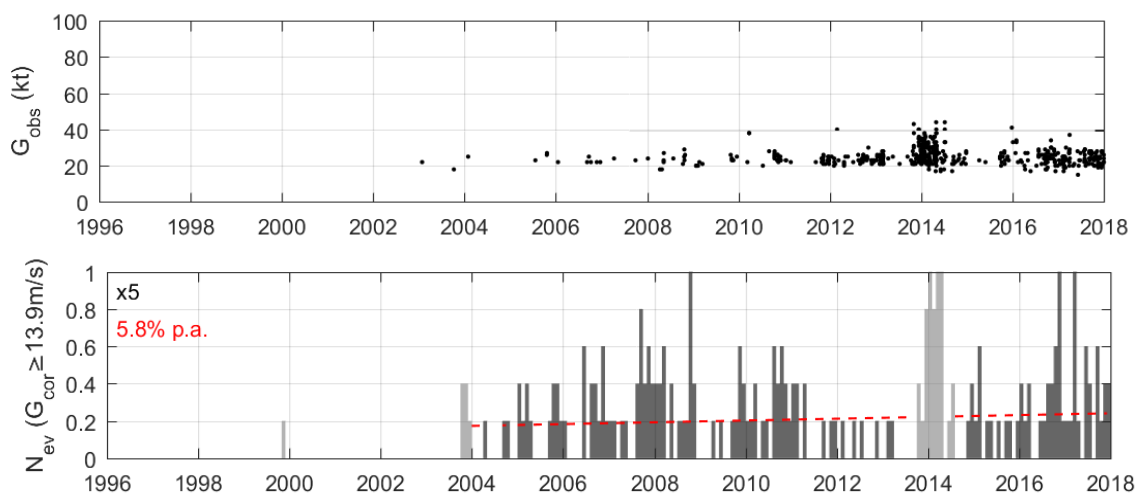


Figure 6.17 – G_{obs} for SBKG – Campina Grande, PB (top); temporal distribution of Top 100 most extreme events (columns) and trend (line) (bottom).

Even with the previous listed analytical tools, there remain cases where it was unclear which periods should be deactivated. Due to the lack of historical metadata a balanced and cautious approach was taken. One particular example is that of SBGR – Guarulhos, SP. An increase in the frequency of gust observations around mid-2005 is seen in the plot of G_{obs} in Figure 6.18. Furthermore, there were 5 events between 2008 and 2017 of peak $G_{obs} \geq 60$ kt. Consulting data from PSEC-46, as shown in Figure 4.6 for SBGR, prior to 2008, the last event to register a peak $G_{obs} \geq 60$ kt was in 1975. An investigation into these 5 events resulted in confirmation of the strength of 3 events by news reports. An event with peak $G_{obs} = 69$ kt was registered at 21:12 UTC on 07/06/2011^{35,36,37}; a peak $G_{obs} = 63$ kt was registered at 20:00 UTC on

³⁵<https://www1.folha.uol.com.br/fsp/cotidian/ff0806201109.htm>

³⁶<https://sao-paulo.estadao.com.br/noticias/geral,vendaval-causa-apagoes-em-pelo-menos-15-bairros-de-sao-paulo,729124>

³⁷<https://sao-paulo.estadao.com.br/noticias/geral,vendaval-provoca-morte-quedas-de-arvores-apagao-e-onda-no-pinheiros-imp-,729364>

24/12/2012; a peak $G_{obs} = 62$ kt was registered at 23:00 UTC on 22/05/2016³⁸; a peak $G_{obs} = 61$ kt was registered at 18:15 UTC on 04/01/2008; a peak $G_{obs} = 60$ kt was registered at 19:27 UTC on 27/03/2012^{39,40}. The temporal distribution of the top 100 events, shown in Figure 6.18, shows an increase in the number of extreme events with peak $G_{cor} \geq 18.4$ m/s from the year 2000 onwards. A higher V_m is also identified in the years prior to 2000. If the threshold of the temporal distribution of extreme events was raised to $G_{cor} \geq 20$ m/s, the distribution would reveal a higher density from 2005 to 2017; and completely concentrated between 2008 and 2016 if increased to $G_{cor} \geq 25$ m/s. This demonstrates the sensitivity of hard thresholds in the determination of extreme events. For SBGR, data prior to 2000 should be ignored for extreme distribution analysis due to the increased V_m ; but it is not clear whether the period between 2000 and 2006 should also be deactivated. The plot of G_{obs} suggests 2006, with higher density of gust observations, should be the start of the analysis, while the temporal distribution of the top 100 extreme events indicates little difference between the 2000-2006 and 2006-2017 periods.

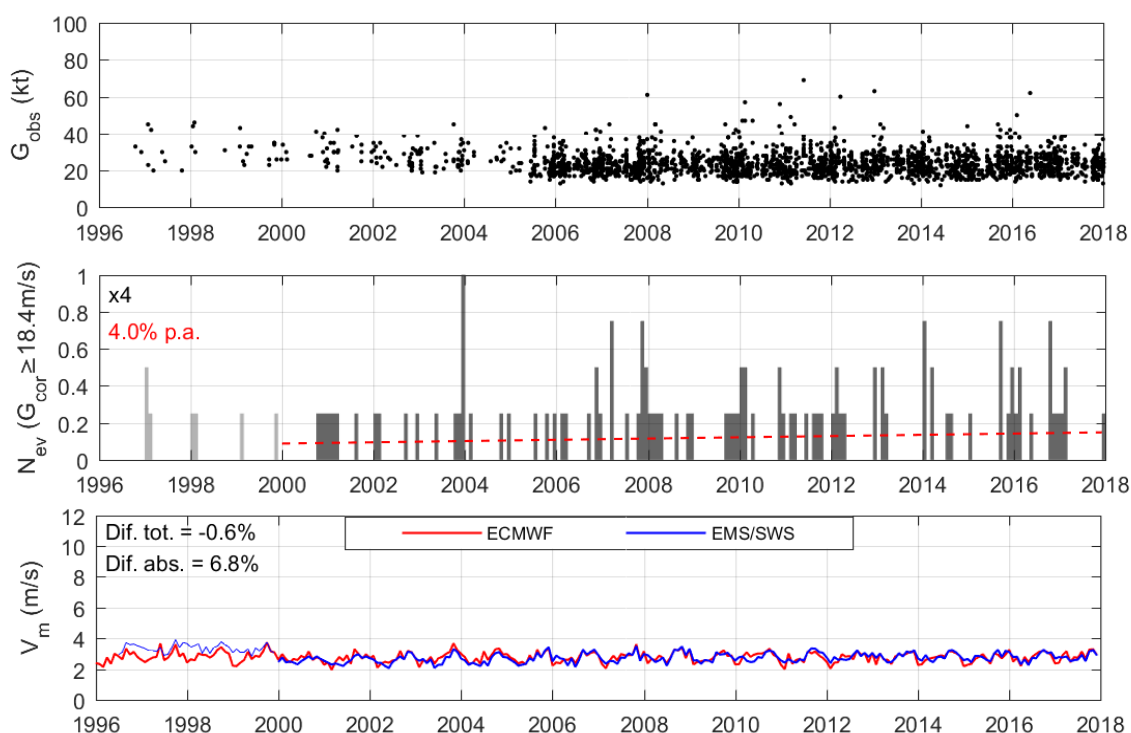


Figure 6.18 – G_{obs} for SBGR – Guarulhos, SP (top); temporal distribution of top 100 most extreme events (columns) and trend (line) (middle); monthly mean wind speeds for SWS and ECMWF data (bottom).

³⁸<http://www.osul.com.br/vendaval-derruba-escada-de-aviao-em-guarulhos/>

³⁹<http://g1.globo.com/sao-paulo/noticia/2013/04/apos-um-ano-fechada-rodoviaria-de-guarulhos-reabre-vazia.html>

⁴⁰<http://www.guarulhosweb.com.br/noticia.php?nr=46576>

To understand the effect of including data from 2000-2006, the extreme value analysis of Section 6.6 *Development of BR-MIS extreme value analysis*, was performed for both periods 2000-2017 and 2006-2017 with results shown in Table 6.1 for the dominant non-synoptic wind type. An increase of 5-6% in a_N and U_N parameters, as well the 50-year return period wind speed for the station, $G_{50,N}$, is reported when the period from 2000 to 2006 is deactivated. This is an acceptable error when discounted a period of 6 years from any station's life of operation. Since the V_m series were in agreeance for the period between 2000 and 2006 and no historical metadata could be attained from relevant authorities, the period remained active for further analyses.

Table 6.1 – Extreme distribution parameters for non-synoptic winds, SBGR – Guarulhos, SP.

Period	a_N	U_N (m/s)	$G_{50,N}$ (m/s)
2000 – 2017	4.0	24.8	40.6
2006 – 2017	4.1	26.4	42.6

The challenges to confidently establish a period of analysis, as demonstrated by the example of SBGR, are faced at many other Brazilian aerodromes. Changes to operational processes (conventional to digital), anemometer exposure (height and location) and anemometer type (cup, propeller or ultrasonic) can be responsible for changes to station characteristics, and for the majority of station no, or very little, historical or current metadata were available from relevant authorities. Without such information, the subjective processes as described above were implemented to best prepare SWS time-series for extreme value analyses.

6.5 IDENTIFICATION OF SYNOPTIC, NON-SYNOPTIC AND SUSPECTED FALSE EXTREME WIND EVENTS

Several studies propose methods of separating non-synoptic events from synoptic events. Gomes and Vickery (1976) associated the daily maximum wind speed on *thunderdays*, days on which thunder is observed, as being directly linked to a thunderstorm. This process was also used by Twisdale and Vickery (1992) and Cook et al. (2003). Riera and Nanni (1989) used a combination of TS observation, cumulonimbus clouds (CB), precipitation and sudden decreases in temperatures after high gusts to identify non-synoptic winds for aerodrome

meteorological observations. Choi and Hidayat (2002) identified TS events by the observation of thunder and rain. Holmes (2002) inspected anemograph traces for days which thunder was recorded to identify the signatures of thunderstorm downdrafts. Lombardo et al. (2009) utilised automated surface observing system data from the U.S., which includes thunderstorm beginning and ending times within the weather observation bulletins made at hourly intervals, as well as special reports during the hour when conditions change. Peak winds occurring within the beginning and ending times were then considered to be part of the thunderstorm extreme wind dataset. Burton and Allsop (2009) considered peak mean wind speed records which were 3 times greater than the observations prior to and after the peak as thunderstorm downbursts. De Gaetano et al. (2014) used high frequency digital anemometer readings (between 2 and 10 Hz), installed at varying heights (10-84 m) in Italian ports to capture extreme wind events. Events were classified as depressions, thunderstorms or gust fronts by application of a semi-automatic process involving quantitative control mechanisms and, when necessary, the author's qualitative judgement based on visual examination of the wind speed time-series and statistical values. Rules relating to the ratio of gust and mean wind speeds were derived which could be used to identify and classify from a larger set of events. Mohr et al. (2017) used a combination of surface observational data and lightning data to identify peak gusts during thunderstorms in a study of the characteristics of convective wind gusts in Germany. Events which occurred during elevated horizontal pressure gradients, associated with cold fronts, were eliminated from the study. Holmes et al. (2018) used a ratio between the peak gust speed and the mean gust speeds for 2 hours before and after the peak to identify non-synoptic events. If both ratios were less than 2, the event was classified as synoptic.

All abovementioned methods have their limitations. Holmes (1999) advised against the use of *thunderdays* to identify non-synoptic extreme winds, as the occurrence of lightning or thunder does not mean that a severe wind gust was caused by convective activity. Doswell (2001) noted that severe weather can also be produced by non-thundering convection. As such, there may be significant events that are incorrectly classified as spurious or synoptic due to the lack of a thunder or lightning observation. Recordings from anemographs are not readily available and, in the case in which they are, manually revision of event is a laborious procedure. The multi-parameter approach of Riera and Nanni (1989) is the only method to consider a sharp decrease in temperature, however no indication of the magnitude of the decrease is given. Wind data recorded at high resolutions are typically only available from specially

commissioned studies, and the majority of wind data are recorded at hourly intervals. Additionally, none of these approaches propose a method of identifying suspected false data.

In this study, non-synoptic winds are those which are most likely best represented by short-duration, thunderstorm outflow models – typically represented by a nose-like vertical profile of horizontal wind speeds – with the maximum wind speed at a certain height above ground which then diminishes at higher altitudes. Synoptic winds are those which are best represented by the well-established ABL models with power or log-law vertical profiles of horizontal wind speed. In this context, the two most important characteristics of Deaves and Harris' (1978) definition of full-developed ABL flow are 1. a strong and steady wind with stationary statistical properties, 2. neutral atmospheric stability. An approach is required to address the grey-zone between classic ABL flow and convective storm outflows. Mason (2017) estimated the overall along-wind downburst loading is between 5-75% less than ABL winds for a 200 m tall structure with same equivalent wind speed at 10 m above ground, and that using an ABL profile as opposed to downburst profile was a conservative approach for buildings greater than 10-20 m. In taking a conservative approach, this study classifies intermediate events as synoptic, which include cold fronts that are typically considered sub-synoptic (or mesoscale) phenomena from a meteorological perspective (Markowski and Richardson, 2010).

The development of an algorithm which could identify non-synoptic and synoptic extreme wind events based on changes in temperature and in pressure around the hour of the recorded peak gust was initially to be only for INMET ASWS. INMET ASWS outnumber aerodrome SWS 3 to 1 in Brazil and operate automatically, however are unmanned and lack equipment to observe thunderstorms. The classifying algorithm of De Gaetano et al. (2014) is unsuitable for this application due to the low temporal resolution of observations. A classifying algorithm in the style of Choi and Hidayat (2002) and Lombardo et al. (2009), which uses the observation of thunder and lightning to determine TS activity, was initially planned for implementation on data acquired at aerodrome SWS, but during the course of the investigation it became apparent that a temperature and pressure based algorithm would also be beneficial for aerodrome SWS since there may be aerodromes without TS observation capabilities, the observer may accidentally omit TS from a meteorological report and there is the possibility of non-thundering convective storms.

Given the differences between each of the meteorological networks, the algorithms must be tailor-made for each observing network. Only observed time-series of wind speed and direction, temperature, atmospheric pressure and where possible, present weather conditions, were utilised in the algorithm. Changes in temperature and atmospheric pressure around the hour of the peak gust are common for convective storms. The development of the algorithms consisted of three phases as summarised in Table 6.2. Phase 1: determination of trends in temperature and pressure changes around the hour of convective storms. Phase 2: the determination of classification algorithms to identify suspect data as well as separate non-synoptic from synoptic extreme events. Phase 3: the verification of the algorithms against the known convective events. The fourth phase was the application of the algorithms to all SWS in the study to determine sets of extreme winds per storm type for extreme value analysis.

Table 6.2 – Phases in the determination of event classification algorithms.

Phase	Description	No. of Events Considered (threshold)	
		INMET ASWS	Aerodrome SWS
1	Analysis of changes in T and P for convective storms	768 (20 m/s)	76 (40 kt)
2	Derivation of sorting algorithms	623 (12-18 m/s)	6,428 (40 kt)
3	Validation of algorithms against convective storms	768 (20 m/s)	76 (40 kt)
4	Application to all study SWS for use in extreme value analysis	73,684 (varies)	37,589 (varies)

6.5.1 Changes in temperature and atmospheric pressure

Meteorologists Ferreira & Nascimento published a series of investigations into the climatology of convective storms in southern Brazil (Ferreira and Nascimento, 2016[a]; 2016[b]; Ferreira, 2017). Two databases fundamental to these investigations are the observed data from INMET's ASWS network and satellite imagery of brightness temperature obtained from GOES (Geostationary Operational Environmental Satellite), for the 11-year period between 01/01/2005 and 31/12/2015. Geographically, the stations were limited to Brazilian territory south of 22°S, a region which partially covers the states of Mato Grosso do Sul and São Paulo, but the entirety of Paraná, Santa Catarina and Rio Grande do Sul. Severe convective storms were identified by the following criteria (Ferreira, 2017):

- Peak wind gust equal to, or greater than, 25 m/s ($G_{obs} \geq 25$ m/s, from INMET data);

- Accumulation of precipitation at the same ASWS for the same hour as observed peak wind gust (from INMET data);
- Brightness temperature of the image pixel nearest to the ASWS equal to, or less than, -55°C ($T_B \leq -55^{\circ}\text{C}$, from GOES data) within ± 1 hour of the peak wind gust.

Events were considered independent when successive peaks of $G_{obs} \geq 25$ m/s were separated by 5 hours or more at the same ASWS. For cases in which the peaks were separated by less than 5 hours, the analysis of the event was based on only first peak. To avoid a contamination of the sample population by strong wind events caused by low-level jet winds and extra-tropical cyclones, special analyses involving the use of synoptic maps were conducted at stations which were located at high elevation, such as A829 – São José dos Ausentes, RS (1,229 m), and A845 – Morro da Igreja, SC (1,790 m), or with a coastal exposure, such as A878 – Mostardas, RS (Ferreira and Nascimento, 2016[a]). Less severe convective storms were identified and grouped together at peak wind gust intervals of 10-15 m/s, 15-20 m/s and 20-25 m/s.

Mean gust speeds, as well as mean anomalies of temperature, dew-point temperature and atmospheric pressure for the four levels of severity as determined by Ferreira (2017) are shown in Figure 6.19. The anomalies are presented over a 21-hour period (± 10 hours from the peak wind gust), which highlight the development of each of the parameters over the event. The plots in Figure 6.19 highlight clear trends for each of the four meteorological parameters over the 10 hours before and after the peak wind gust caused by convective storms: a sharp increase and decrease in gust speed and precipitation around the hour of the peak gust wind speed; slow decrease, followed by sharp increase in atmospheric pressure at the hour of the peak wind gust; slow increase, followed by sharp decrease in temperature and dew-point temperature at the hour of the peak wind gust.

Ferreira and Nascimento generously provided the timestamps and locations of 768 events, herein referred to as F&N events, which matched their criteria for convective storms with peak wind gusts of $G_{obs} \geq 20$ m/s. The parameters of V_{obs} , DIR , G_{obs} , T_{ins} , T_{max} , T_{min} , P_{ins} , P_{max} , P_{min} , were extracted and plotted over a period of ± 10 hours around the hour of the peak G_{obs} . Although Ferreira and Nascimento also mapped the parameters of accumulated precipitation and T_d , these parameters were not considered in this study due to the fact that convective storms can be dry, i.e. no accumulated precipitation. Additionally, T_d follows similar trends to

T , however at a smaller magnitude, and with the aim of producing the simplest wind classifying system possible, it was best to reduce the number of parameters under consideration.

With the aim of capturing changes in T and P , specifically decreases in temperature and increases in pressure over the hours surrounding the peak wind gust, an extra two time-series were derived: $\Delta T_{min,i}$, time-series which determines the largest negative temperature differential over the past two hours (Equation 6.7); and $\Delta P_{max,i}$, time-series which determines the largest positive pressure differential over the past two hours (Equation 6.8). Equations 6.7 and 6.8 are shown for the i^{th} observation in the time-series of any particular INMET ASWS.

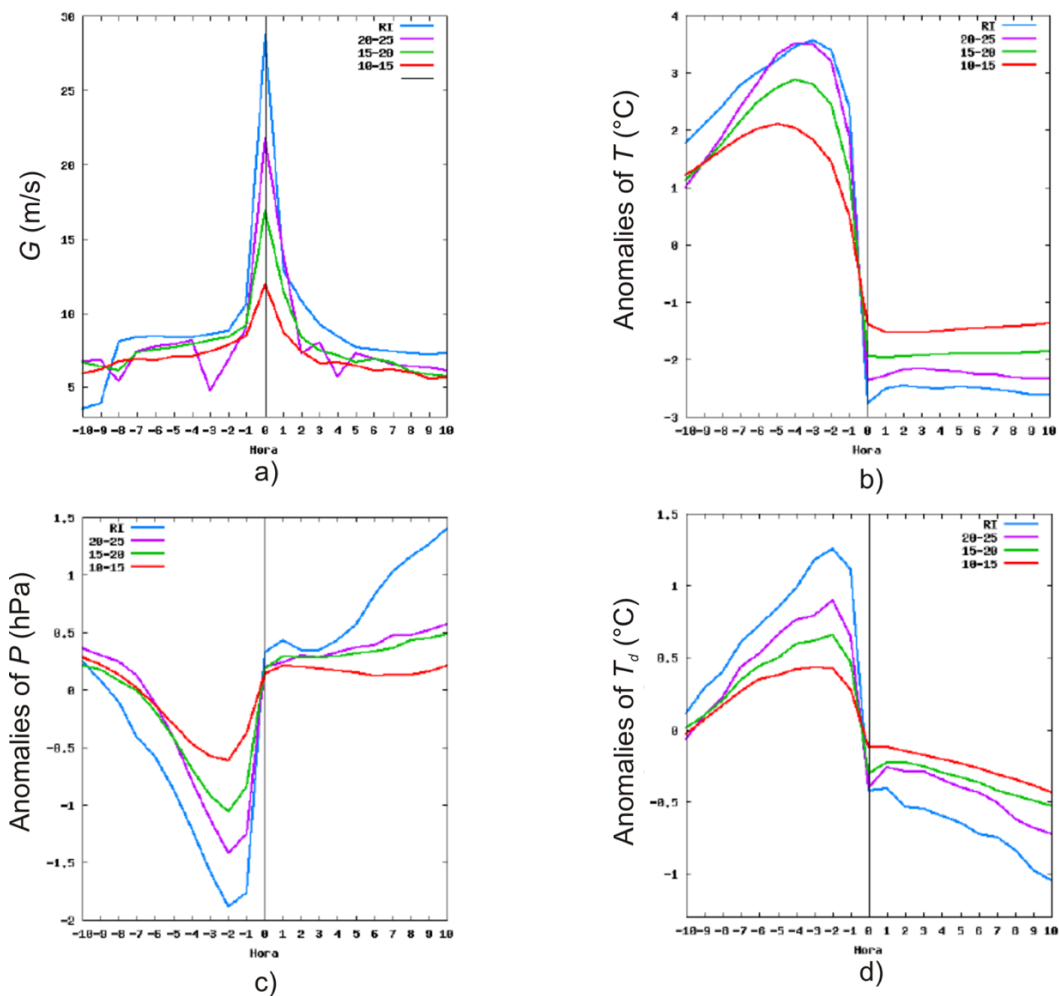


Figure 6.19 – Mean values and mean anomalies of the four severity groups of convective storms as reported by Ferreira (2017). Red represents peak G_{obs} of 10-15m/s; green represents peak G_{obs} of 15-20 m/s; purple represents peak G_{obs} of 20-25 m/s; blue represents peak $G_{obs} > 25$ m/s. a) maximum hourly wind gusts, G_{obs} (m/s); b) instantaneous temperature at the hour, T (°C); c) instantaneous atmospheric pressure at the hour, P (hPa); d) instantaneous dew-point temperature at the hour, T_d (°C)

$$\Delta T_{min,i} = T_{min,i} - T_{max,i-1} \quad 6.7$$

$$\Delta P_{max,i} = P_{max,i} - P_{min,i-1} \quad 6.8$$

The parameters of $T_{med,3}$, $\Delta T_{min,3}$ and $\Delta P_{max,3}$ (Equations 6.9 to 6.11) were then calculated for each of the 768 events under investigation, where j represents the peak wind gust observation. Described qualitatively, $T_{med,3}$ represents the mean temperature of the three hours prior to the peak gust hour; $\Delta T_{min,3}$ represents the largest negative change in temperature from one hour to the next over a potential three-hour window centred around the hour of the peak wind gust; $\Delta P_{max,3}$ represents the largest positive change in atmospheric pressure from one hour to the next over a potential three-hour window centred around the hour of the peak wind gust.

$$T_{med,3} = \text{mean}(T_{ins,j-3}, T_{ins,j-2}, T_{ins,j-1}) \quad 6.9$$

$$\Delta T_{min,3} = \min(\Delta T_{min,j-1}, \Delta T_{min,j}, \Delta T_{min,j+1}) \quad 6.10$$

$$\Delta P_{max,3} = \max(\Delta P_{max,j-1}, \Delta P_{max,j}, \Delta P_{max,j+1}) \quad 6.11$$

A similar process was applied to 13 aerodrome SWS for which MSS data were available, and which were located within 10 km of the INMET ASWS analysed by Ferreira (2017) with peak gusts greater than 10 m/s. The aerodrome SWSs include SBBG – Bagé, RS, SBBI – Bacacheri (Curitiba), PR, SBCO – Canoas, RS, SBCT – Curitiba, PR, SBFI – Foz do Iguaçu, PR, SBFL – Florianópolis, SC, SBMG – Maringá, PR, SBNF – Navegantes, SC, SBPA – Porto Alegre, RS, SBPF – Passo Fundo, PF, SBSM – Santa Maria, RS, SBTR – Torres, RS, and SBUG – Uruguaiana, RS. From the same list of 768 events observed by the INMET ASWS, 76 events were also observed to have peak gusts equal to, or more than, 40 kt (20.6 m/s) at these aerodromes with TS observed. Similar parameters to those in Equations 6.9 to 6.11 were defined for the MSS data with some fundamental differences. With a t_{val} associated with each observation, $T_{med,3}$ is evaluated for the observations made within the period between 3 and 1 hours prior (-180 to -60 mins) to the peak wind speed, with each T observation weighted by its associated t_{val} . To calculate the corresponding value of $\Delta T_{min,3}$, first the minimum temperature is found within the period ranging from 2 hours prior to 1 hour after the peak wind speed (-120 to +60 mins). Once noted, the maximum temperature observed within this 3-hour window, and prior to the minimum temperature, is then identified. $\Delta T_{min,3}$ for the event then becomes the difference between the two. A similar process is applied to

determine $\Delta Q_{max,3}$, however the minimum pressure is subtracted from the maximum pressure. Note that Q is used for atmospheric pressure at aerodrome SWS, and not P , due to the application of a factor to the observation to convert to pressure at mean average sea level, known as QNH .

Figure 6.20 shows plots of the relationships between $T_{med,3}$, $\Delta T_{min,3}$ and $\Delta P_{max,3}$ for the events analysed. A strong correlation between $T_{med,3}$ and $\Delta T_{min,3}$ is observed in Figure 6.20a and b, which indicate that high mean temperatures prior to the convective storm peak wind gust typically result in greater falls in temperature. No relationship is found between $T_{med,3}$ and $\Delta P_{max,3}$, as indicated by the correlation coefficient, R^2 , shown in c) and d) of Figure 6.20. The average value of $\Delta P_{max,3}$ is 4 hPa over the range of $T_{med,3}$ studied. Investigations by Engerer et al. (2008) and Ferreira (2017) also reported mean or median pressure rises around 4 hPa accompanying the passage of gust fronts from convective storms. Agreement is found between the INMET and aerodrome datasets for the fitted regression lines, with the representative equations shown within the plots of Figure 6.20. From these figures it is observed that there are cases of convective storms with little to no change in temperature and pressure, meaning these parameters alone cannot be used to classify extreme wind events. Aerodrome temperature and atmospheric data, as shown in Figure 6.20 and Figure 6.21, appear to be “binned” due to the low-precision of observations which are reported as integers (1 °C and 1 hPa).

With the identification of trends relating to the mean temperature prior to the peak wind gust, $\Delta T_{min,3}$ and $\Delta P_{max,3}$ values were then plotted against each other in Figure 6.21. Due to the definitions of each of the two parameters, the data only ever appear in one quadrant of the Cartesian coordinate system (negative values of $\Delta T_{min,3}$ and positive values of $\Delta P_{max,3}$), and an apparent trade-off between the two parameters for the analysed events is observed. Either there is a large magnitude $\Delta T_{min,3}$ with small magnitude $\Delta P_{max,3}$, a large magnitude $\Delta P_{max,3}$ with small magnitude $\Delta T_{min,3}$, or both $\Delta T_{min,3}$ and $\Delta P_{max,3}$ values are near their respective means. These observations relate to the majority of the data, as there are some cases where both $\Delta T_{min,3}$ and $\Delta P_{max,3}$ are near 0, reinforcing the hypothesis that gust peaks caused by convective storms cannot be identified from changes in temperature and pressure alone. As such, the $\Delta T_{min,3}$ and $\Delta P_{max,3}$ plane was divided into three arbitrarily defined $\Delta Groups$, described below:

- $\Delta Group\ 1$: Severe changes. Magnitudes of $\Delta T_{min,3}$ and/or $\Delta P_{max,3}$ larger than model values as determined by $T_{med,3}$ (by a factor greater than 1.25);
- $\Delta Group\ 2$: Intermediate changes. Magnitudes of $\Delta T_{min,3}$ and/or $\Delta P_{max,3}$ near model values as determined by $T_{med,3}$ (between factors of 1.25 and 0.75);
- $\Delta Group\ 3$: Weak or inverted changes (increase in T or decrease in P)
Magnitudes of $\Delta T_{min,3}$ and/or $\Delta P_{max,3}$ smaller than model values as determined by $T_{med,3}$ (by a factor less than 0.75).

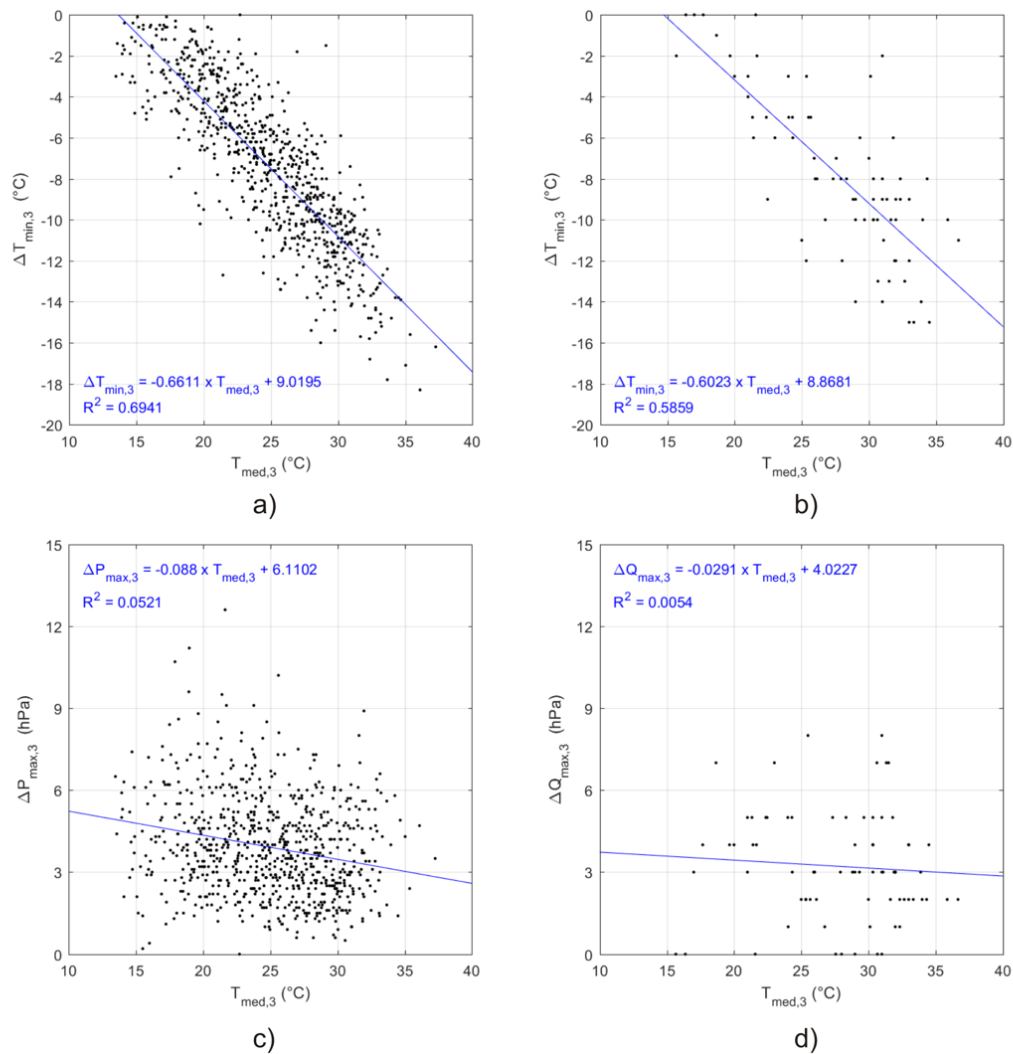


Figure 6.20 – Relationships between $T_{med,3}$, $\Delta T_{min,3}$ and $\Delta P_{max,3}$ for 768 convective storms as recorded by INMET ASWS, a) and c); 76 convective storms as recorded by aerodrome SWS b) and d).

Model values of $\Delta T_{min,3}$ and $\Delta P_{max,3}$ are determined by the regression models fitted to the data presented in Figure 6.20, with values differing slightly between the INMET and aerodrome

datasets, however values determined by INMET ASWS were adopted for both networks due to the larger sample. To determine the limits of each of the three $\Delta Groups$, first the zero intercept of $\Delta T_{min,3}$, ΔT_0 , is determined by Equations 6.12, with Q taking the place of P for data observed at aerodromes, for $m_{\Delta T} = -0.6611$ and $b_{\Delta T} = 9.0195$. The intercept at $\Delta T_{min,3} = 0$ is fixed at $\Delta P_{max,3} = 4$ hPa. Due to $\Delta T_{min,3}$ nearing zero for $T_{med,3} < 20$ °C, the model is truncated at $T_{med,3} = 20$ °C and any values less than 20 °C will adopt $T_{med,3} = 20$ °C when calculating model values of $\Delta T_{min,3}$ and $\Delta P_{max,3}$. To establish a minimum limit of $\Delta T_{min,3}$, a similar decision was taken for values of $T_{med,3} > 30$ °C, and hence any event with $T_{med,3}$ greater than 30 °C adopts $T_{med,3} = 30$ °C when calculating model values of $\Delta T_{min,3}$ and $\Delta P_{max,3}$.

$$\Delta T_0 = \max\left(20, \min(30, T_{med,3})\right) m_{\Delta T} + b_{\Delta T} \quad 6.12$$

Once ΔT_0 is determined for the event under analysis, the event's $\Delta T_{min,3}$ and $\Delta P_{max,3}$ values are then tested to determine the severity of the change in temperature and pressure, as per Equations 6.13 to 6.15. The event adopts a $\Delta Group$ 1, 2 or 3 classification depending on the severity of the change in temperature and pressure around the peak gust hour. The limits of each of the $\Delta Groups$ are dependent on $T_{med,3}$, as demonstrated for $T_{med,3} \geq 30$ °C and $T_{med,3} \leq 20$ °C in a) to d) of Figure 6.21, while e) to f) show the classification of each of the F&N events.

$$\Delta T_{min,3} \leq 1.25\Delta T_0 - \frac{\Delta P_{max,3}\Delta T_0}{4} \quad 6.13$$

$$1.25\Delta T_0 - \frac{\Delta P_{max,3}\Delta T_0}{4} < \Delta T_{min,3} \leq 0.75\Delta T_0 - \frac{\Delta P_{max,3}\Delta T_0}{4} \quad 6.14$$

$$\Delta T_{min,3} > 0.75\Delta T_0 - \frac{\Delta P_{max,3}\Delta T_0}{4} \quad 6.15$$

Of the 768 events analysed from INMET observations, 683 events (89%) were classified as $\Delta Group$ 1, 70 events (9%) were classified as $\Delta Group$ 2 and 15 events (2%) were classified as $\Delta Group$ 3. Of the 76 events analysed from aerodrome observations, 62 events (82%) were

classified as $\Delta Group 1$, 7 events (9%) were classified as $\Delta Group 2$ and 7 events (9%) were classified as $\Delta Group 3$.

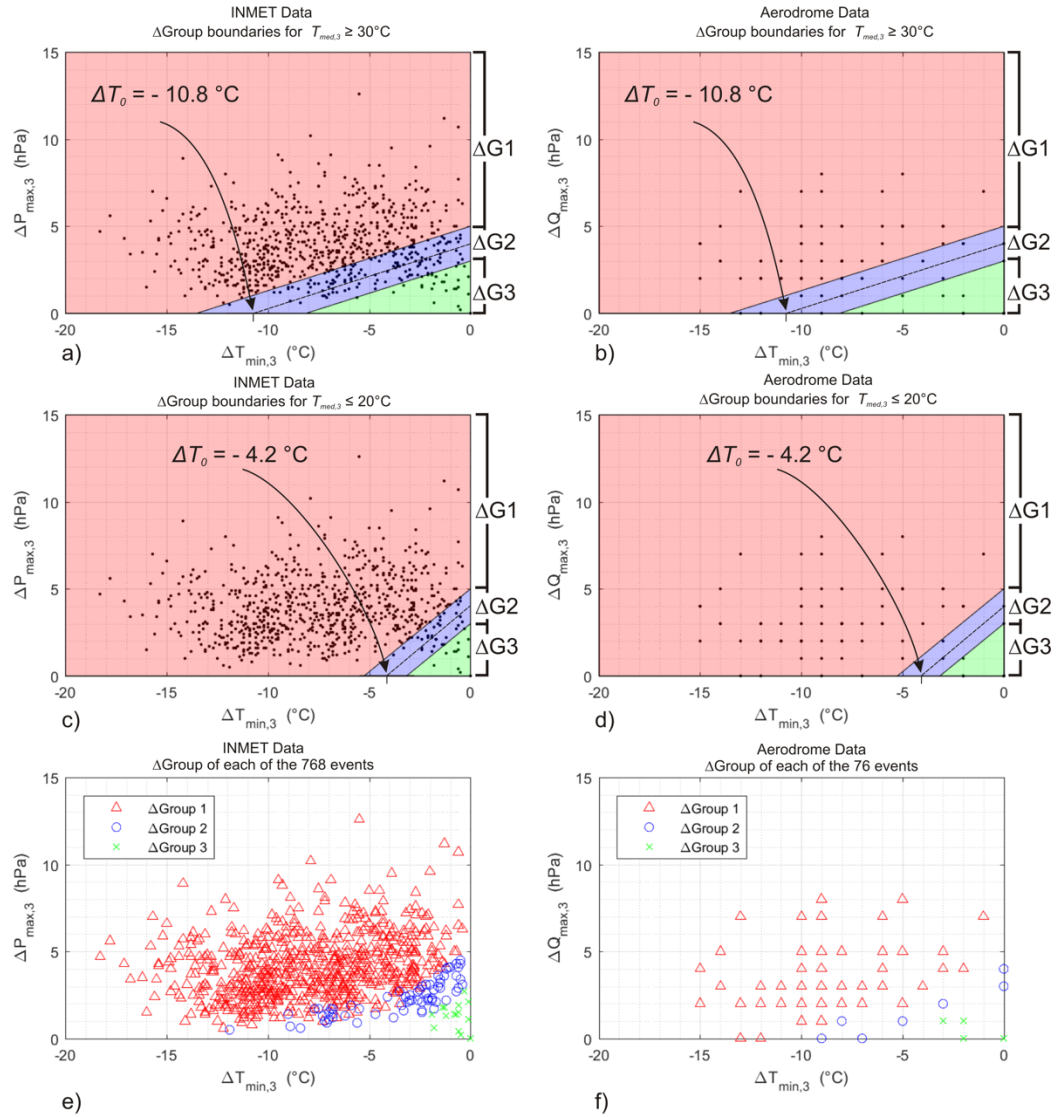


Figure 6.21 – Plots of $\Delta T_{min,3}$ and $\Delta P_{max,3}$ for all events. Definition of $\Delta Group$ boundaries for $T_{med,3} \geq 30^\circ\text{C}$ for a) INMET and b) Aerodrome events, as per Equations 6.13 to 6.15; Definition of $\Delta Group$ boundaries for $T_{med,3} \leq 20^\circ\text{C}$ for c) INMET and d) Aerodrome events, as per Equations 6.13 to 6.15; $\Delta Group$ assignments for each of the e) INMET and f) Aerodrome events as per Equations 6.13 to 6.15.

The good agreement between the classifications of the two datasets, which employ different observational procedures and were analysed for a different sample size, gives confidence to the methods employed to define the $\Delta Groups$. However, the assignment of a $\Delta Group$ alone

does not determine whether an event is non-synoptic, synoptic or suspect, which requires further analyses of time-series of wind parameters (V , G and DIR).

6.5.2 Development of classifying algorithms

The algorithms developed in this study are an advancement on those for temporally low-resolution observations, allowing for the separation of extreme wind events into the categories of synoptic, non-synoptic and suspect, with more parameters and minimal manual input. Up to four types of parameters are used in the algorithms:

1. Peak observation: G_{obs} (G^* when G_{obs} not available), V_{obs} , DIR and G_V ;
2. Relationship between peak observation and observations in the hours before and after (described in detail over the next few paragraphs): R_{-6} , R_{-3} , R_{+3} , R_{+6} , \mathcal{R} , $\Delta DIR_{max,-3}$, $\Delta DIR_{max,+3}$;
3. Change in temperature and atmospheric pressure around the peak observation: $\Delta Group$;
4. Present and recent weather identifiers.

Kasperski (2002) encouraged wind-speeds to be considered in the lead-up to, and after, the peak observation in order to correctly identify wind event types. As the time-intervals between successive observations can be irregular, especially for aerodrome SWS, the use of ratios between the peak observation and mean wind speeds over a certain period of time is a simple and robust approach. This study used ratios, R_G , between the peak gust observation and mean gust speed over the previous six hours, $R_{G,-6}$, the previous three hours, $R_{G,-3}$, the following three hours, $R_{G,+3}$, and the following six hours, $R_{G,+6}$. The assumed duration of validity of each observation, t_{val} , is used in the calculation of the R_G values. The minimum interval of three hours is used due to the interval of three hours between standard SYNOP observations. The ratios relating to the six-hour periods are used to examine the length of time for which high winds are sustained, as well as serving as supplementary parameters to the three-hour ratios for cases in which observations are discontinued due to the closing of a station or missing data. A similar parameter was used by Holmes et al. (2018), but for a period of two hours prior to, and after, the peak wind speed. For the aerodrome SWS, R_G is based solely on the time-series made up of G_{obs} and G^* ; while R_V parameters were also created for INMET data. This extra series of R_V parameters was a necessary extra step in the

verification of real events for INMET ASWS data as G_{obs} and V_{obs} are not always observed at the same time.

The parameter \mathcal{R} acts as a summary of the R series. \mathcal{R} is a single value which varies between 0 and 1 depending on how many R parameters are below a certain threshold. The closer \mathcal{R} is to 1, the more likely the event is synoptic; conversely, the closer \mathcal{R} is to 0, the more likely the event is either suspect or non-synoptic. R parameters are only considered when there is sufficient data available, e.g. if there is no wind data for the period between three and six hours prior to the peak observation there is no valid $R_{G,-6}$ parameter. Threshold values tested, L , vary between values of 2.0, 2.5 and 3.0 depending on dataset and test, and are identified as $\mathcal{R}(L)$. The calculation of \mathcal{R} is as follows:

- For INMET data where peak $V_{obs} \geq 5$ m/s, \mathcal{R} considers both R_G and R_V sets;
- For INMET data where peak $V_{obs} < 5$ m/s, \mathcal{R} considers only the R_G set;
- For aerodrome SWS, \mathcal{R} considers only the R_G set;
- $\mathcal{R}(L)$ is the sum of all valid $R < L$, divided by the number of valid R parameters;
- When $\mathcal{R} = 1$, all valid R parameters are less than L ; when $\mathcal{R} = 0$, all valid R parameters are greater, or equal to, L .

A similar approach was used to determine changes in the wind direction before and after the peak gust observation. The DIR of the peak observation is compared to all DIR observations within a three-hour window before and after, with the largest absolute difference in DIR represented by the parameters $\Delta DIR_{max,-3}$ and $\Delta DIR_{max,+3}$.

Weather descriptors of interest for aerodrome SWS include thunderstorm (TS), widespread dust (DU), sand (SA), dust/sand whirls (PO), squall (SQ), tornado/funnel cloud/water spout (FC), sandstorm (SS) and dust storm (DS). The weather descriptors are often accompanied by qualifying terms, such as light (-), heavy (+), if the phenomenon is located in the vicinity (8-16 km) of the aerodrome (VC) or if it recently occurred (RE). Should there be no weather phenomenon observed the field remains absent from the report. In addition, cloud identifiers relating specifically to cloud formations common during convective storm events were extracted and include the tower cumulus (TCU) and cumulonimbus (CB). Rain, hail and other

cloud formations were considered to be too frequent in occurrence and were not examined. No weather identifiers were used for the INMET dataset.

18 stations located within 10 km of aerodrome SWS which operate between 18-24 hours were selected from the INMET ASWS network. The stations were located all over Brazil, including SBBE – Belém, PA, SBMN – Manaus, AM, SBSM – Santa Maria, RS, SBFI – Foz do Iguaçu, PR, SBCG – Campo Grande, MS, SBBR – Brasília, DF, SBAF – Afonsos Airforce Base, RJ, SBPA – Porto Alegre, RS, SBFL – Florianópolis and SBRF – Recife, PE. A total of 623 independent events with peak G_{obs} greater than a certain threshold were identified from the 18 INMET ASWS. The threshold varied from station to station and was limited to 18 m/s or less. The lowest threshold was for Recife (12 m/s) which generated 27 events for analysis, while a threshold of 18 m/s was used for Foz do Iguaçu which generated 92 events for analysis. A buffer of 48 hours was required between candidate peaks for events to be considered independent. In addition to the calculation of each of the parameters defined earlier, present weather and cloud identifiers were extracted from the paired aerodrome SWS for ± 1 hr around the peak gust observation.

For each of the 623 events, time-series of G_{obs} , V_{obs} , DIR , T_{ins} , T_{max} , T_{min} , P_{ins} , P_{max} , P_{min} and aerodrome weather and cloud identifiers were plotted for a ± 10 -hour period centred on the hour of the peak G_{obs} observation. A process of manual examination of each of the 623 events was undertaken, with each event classified as either synoptic, non-synoptic or suspect based on the follow general concepts:

- Synoptic winds are characterised by sustained high G_{obs} and V_{obs} for long periods while DIR , T and P vary little;
- Non-synoptic winds are characterised by short-duration high G_{obs} , decrease in T , increase in P , change in DIR , observation of TS and TCU or CB clouds; while magnitude of V_{obs} does not necessarily need to be high;
- The arrival of a cold front induces a sharp decrease in T and increase in P . DIR changes to be aligned with the direction of the oncoming front and remains constant for a certain period after the front's crossing. An upward step-change in G_{obs} and V_{obs} is typically observed and wind speeds remain intense for the following hours. The adopted approach classifies cold fronts with strong wind speeds of long-duration as synoptic (greater than 3 hours), while short-duration events as non-synoptic (less than 3 hours);

- Suspect events are characterised by short-duration high G_{obs} with no corresponding decrease in T , increase in P , change in DIR , nor observation of TS, TCU or CB clouds.

Once each of the 623 INMET observed events was assigned manual classifications, the events were sorted into their respective $\Delta Groups$ for the preparation of algorithms for each group. No satellite images were consulted in the manual classification process. In general, the larger the change in T and P (QNH), the more likely the event is to be real and non-synoptic, but this also depends on the ratio of the peak gust observation with those prior and after. The smaller the change in T and P (QNH), and the smaller the R ratios, the more likely the event is synoptic. Rules, using various combinations of the derived parameters, were created and tested for each of the $\Delta Groups$. The events were then classified automatically by these rules and compared against their manual classification. Rules were adapted and refined to minimise the number of events with different manual and automatic classifications. Weather and cloud identifiers are not part of INMET ASWS observations and were not included within the rules created for this dataset.

The final classifying algorithm for each of the $\Delta Groups$ for INMET ASWS is shown in Figure D.1 Appendix D *Event Classification Algorithms and Examples*. In addition to the classification of each event, a code representing the path taken is also assigned to assist in any future optimisation of the algorithm. These codes are also shown in the figures of Appendix D.

A similar approach was used for data acquired at aerodrome SWS. Firstly, all independent events with peak G_{obs} or G^* greater than 40 kt (20.6 m/s) within the study network of 198 aerodrome SWS were identified. This totalled 6,428 events (4,344 with peak gusts from G_{obs} and 2,084 from G^*) whose time-series were then plotted for wind, temperature, pressure and weather and cloud identifiers data for a ± 10 -hour period centred around the time of the peak gust observation. The plots of each of the 6,428 events were reviewed and assigned manual classifications. The aerodrome SWS dataset presented two main differences from the INMET ASWS dataset:

1. Different origins of the peak gust speed under consideration: G_{obs} or V_{obs} (G^*);
2. Observation of TS within ± 1 hr of the peak gust;
3. When G_{obs} is available, V_{obs} is measured for same 10-minute period, making G_V more relevant.

The algorithm used for data observed at aerodrome SWS is shown in Figures D.2 to D.5 of Appendix D. During the manual classification process, it was noted that events whose peaks were calculated from $V_{obs}(G^*)$ were more likely to be suspect, and observations of TS were more likely to be classified as non-synoptic. Given these observations, the aerodrome classifying algorithm was divided into a further four branches for each $\Delta Group$:

1. G_{obs} with TS observed;
2. G_{obs} with no TS observed;
3. G^* with TS observed;
4. G^* with no TS observed.

Time-series of some events which were key to the manual classification process are shown in Figure D.6 to D.8 of Appendix D for INMET ASWS, Figure D.9 to Figure D.12 for aerodrome SWS with peak G_{obs} , and Figure D.13 and Figure D.14 for aerodrome SWS with peak G^* . Note that in all plots, wind direction conventions are North = 360°, East = 90°, South = 180° and West = 270°. Parameters derived for each event are shown in Table 6.3, along with $\Delta Group$ classifications and algorithm exits. Commentary on each of the events follows.

The event in Figure D.6 was considered non-synoptic (N) due to the significant decrease in T and small increase in P observed around the hour of peak gust speed with high, but reasonable, R values for the event. For the event in Figure D.7, despite significant changes in T and P two hours after the peak gust, it was considered synoptic (S) due to low R values and stable DIR . The event of Figure D.8 registered high R values but no significant change in T , P nor DIR , resulting in its classification as suspect (SUS). The heat-burst event in Figure D.9 demonstrates the flexibility which is required of the algorithms. T increased and P decreased, resulting in a $\Delta Group$ 3 classification, however, due to the reasonable R and gust factor ($G_V = 1.4$) values the event was judged as real and non-synoptic. Although the event in Figure D.10 was also classified $\Delta Group$ 3 and of R values similar to Figure D.9, the gust factor is much higher ($G_V = 3.8$) and was considered suspect. Despite a 180° change in DIR at the hour of the peak gust, a decrease in T and increase in P , the event in Figure D.11 was considered synoptic due to the constant direction and long duration of strong wind speeds ($R_{+3} = 1.2$ and $R_{+6} = 1.6$) after the arrival of the cold front. The peak gust of this event does not meet the Deaves and Harris (1978) criteria of fully-developed ABL flow due to its non-stationarity when considering the total period before and after the peak – but is considered stationary

when only considering the period after. Although TS was observed over a period of 8 hours in the Figure D.12 event, DIR remained constant with low R values and was considered synoptic. Although TS was observed two hours after the peak gust speed in Figure D.13, a sudden observation of $V_{obs} = 40$ kt is typically suspicious, but when combined with the large decrease in T and high and reasonable R values, was considered to be a real non-synoptic event. This differs to the event in Figure D.14 which, despite the observation of TS, no decrease in T and only a small increase in P were observed. Since there was no observed gust and a quick scan of the online archives of news outlets in Manaus showed no evidence of an extreme wind event in the city for the corresponding date, the observation was highly suspicious and classified suspect.

Some points of difference between outcomes of this classification system and those of others follow. As reported Table 4.4 of Section 4.2.2 *SADMET*, official data obtained from INMET does not contain the peak gust of 26.4 m/s observed at A001-Brasília, DF, on 01/10/2014, as shown in Figure D.6, despite the documentation of the event by at least one news outlet. According to the classification system of Holmes et al. (2018), the event in Figure D.11 would be classified as non-synoptic due to the peak gust being more than twice the mean of the preceding two hours. According to the systems adopted by Choi and Hidayat (2002) and Lombardo et al. (2009), the events of Figure D.12 and Figure D.14 would be classified as non-synoptic due to the observation on TS.

Table 6.3 – Parametrisation and manual classification of 9 extreme wind events.

Met. Network	Figure	G_V	$R_{G,-6}$ ($R_{V,-6}$)	$R_{G,-3}$ ($R_{V,-3}$)	$R_{G,+3}$ ($R_{V,+3}$)	$R_{G,+6}$ ($R_{V,+6}$)	$T_{med,3}$ (°C)	$\Delta T_{min,3}$ (°C)	$\Delta P_{max,3}$ (hPa)	$\Delta Group$	$\Delta D_{max,-3}$ (°)	$\Delta D_{max,+3}$ (°)	Class	Exit (Fig.)
INMET	D.6	4.3	4.3 (2.2)	4.3 (2.2)	3.8 (3.7)	5.5 (4.0)	31.5	-15.1	2.0	1	66	105	N	10 (D.1)
INMET	D.7	2.9	1.3 (1.1)	1.2 (1.0)	1.4 (1.4)	1.7 (1.5)	28.5	-2.6	0.6	3	24	52	S	22 (D.1)
INMET	D.8	19.3	6.7 (1.3)	6.5 (1.4)	6.2 (1.0)	5.0 (0.8)	22.3	-0.2	0.8	3	49	13	SUS	32 (D.1)
Aero. (G_{obs})	D.9	1.4	2.3	2.8	2.1	3.2	21	0	0	3	70	90	N	117 (D.3)
Aero. (G_{obs})	D.10	3.8	2.8	2.7	2.5	2.7	13.7	0	0	3	20	30	SUS	317 (D.3)
Aero. (G_{obs})	D.11	1.8	2.0	1.8	1.2	1.3	39.6	-13	8	1	160	20	S	212 (D.2)
Aero. (G_{obs})	D.12	1.5	1.6	1.3	1.3	1.6	16.3	0	3	2	20	10	S	210 (D.2)
Aero. (G^*)	D.13	-	4.5	4.7	2.1	2.5	33.7	-12	6	1	90	60	N	123 (D.4)
Aero. (G^*)	D.14	-	15.8	12.4	11.4	14.0	23.7	0	3	2	170	170	SUS	320 (D.5)

6.5.3 Verification of classifying algorithms

The F&N convective storm events were then processed by the respective INMET and aerodrome SWS classification algorithms developed in this study. Of the 768 events observed by INMET ASWS, 632 (82.3%) were classified as non-synoptic, 133 (17.3%) as synoptic and 3 (0.04%) as suspect. All 76 events observed by aerodrome SWS were classified as non-synoptic by the algorithm. An investigation into the apparent “misclassification” of approximately 18% of INMET ASWS events was undertaken.

The three events classified as suspect may actually be extreme non-synoptic events, however problems with the operation of individual ASWS during the event resulted in the events being classified as suspect. An example of the event at A830 – São Borja, RS, is shown in Figure D.15 which depicts a large decrease in temperature at the hour of the peak gust wind speed, and a slight increase in pressure. Satellite imagery, shown in Figure D.16, and radar data were consulted which indicated a discrete-cell storm as the origin of the gust. However, the time-series of wind speed show calm conditions ($G_{obs} = V_{obs} = 0$ m/s) for several hours prior and after the peak speed – suggesting a faulty anemometer. The other two events, at A879 – Canela, RS, and A833 – Santiago, RS, in 2009 and 2010 respectively, occur during suspected faulty periods of operations for each of the stations (reports of many suspected false high wind-gusts).

A visual inspection of the 133 time-series of events classified as synoptic by the algorithm found that wind speeds were either similar in magnitude to the peak gust in the hours before the peak, after the peak, or both before and after the peak gust. Plots of the mean and standard deviations of wind speed (normalised by peak gust), change in direction from hour of peak gust, ΔDIR , and anomalies of T and P are shown for the F&N event classified as non-synoptic and synoptic in Figure 6.22 and Figure 6.23 respectively. Gust peaks are more pronounced for the mean non-synoptic time-series – approximately 2.5 and 1.7 times greater than the maximum gust of the hour before and after the peak respectively, as opposed to 1.5 and 1.3 times greater than the peak gust for the synoptic mean trends. Changes in T , P and DIR are also more severe for the non-synoptic trends than for synoptic.

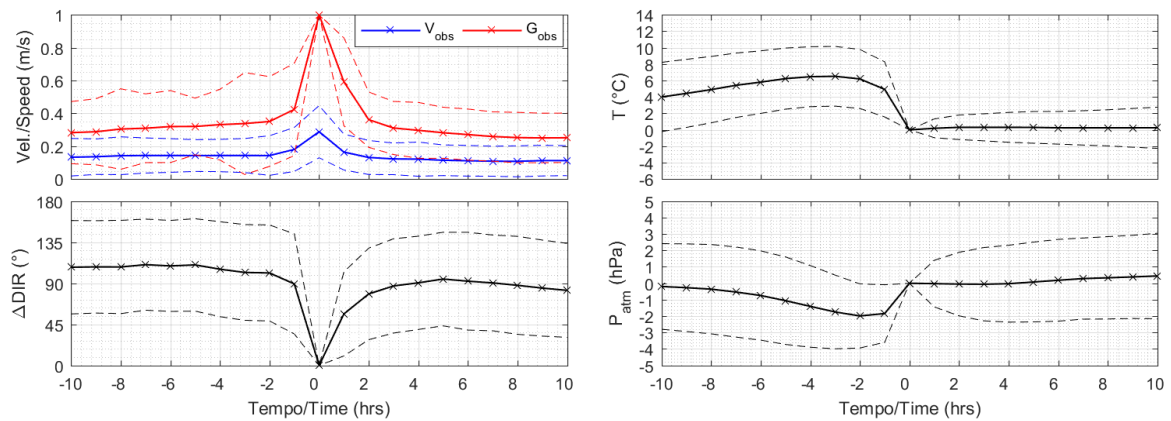


Figure 6.22 – Normalised mean and mean \pm standard deviation trends of the 632 F&N events classified as non-synoptic by algorithm developed for INMET ASWS (Figure D.1)

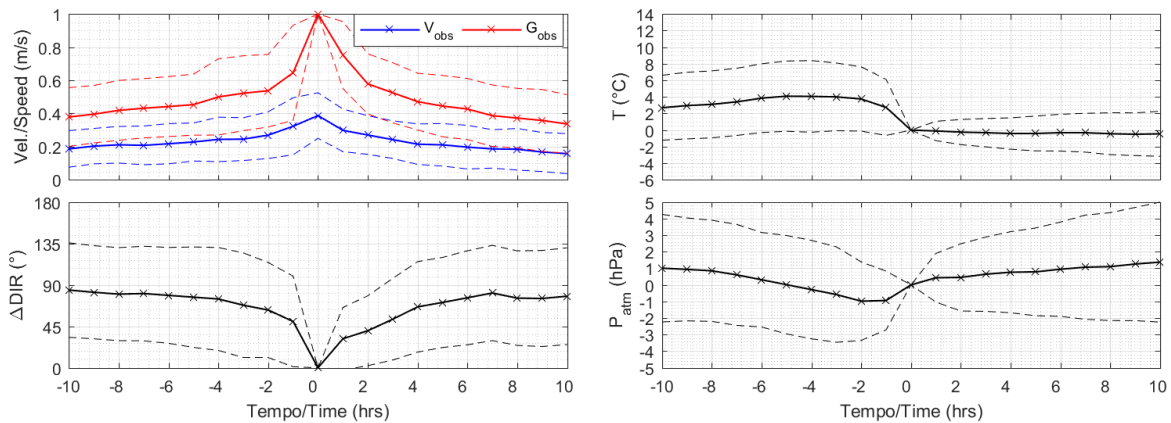


Figure 6.23 – Normalised mean and mean \pm standard deviation trends of the 133 F&N events classified as synoptic by algorithm developed for INMET ASWS (Figure D.1)

Two examples of the 133 F&N events that were classified as synoptic by the automated algorithm are shown in Figure D.17 and Figure D.19. These events highlight the challenges faced in the development of a non-synoptic vs synoptic classifying system. Figure D.17 depicts an event with sustained high wind-speeds, direction and temperature, with pressure varying greatly but tending to decrease over time. The stability of wind and temperature parameters over the 21-hour period suggest a synoptic event, even though a convective system was identified by brightness temperature shown in Figure D.18. Analysis of mean-sea level pressure fields (not shown) indicated ongoing cyclogenesis over southern Uruguay that induced a horizontal pressure gradient over the region that promoted strong east-north-

easterly winds. Despite this, the possibility that the peak gust was caused by a storm embedded in the system cannot be completely ruled out.

The event in Figure D.19 for A831 – Quaraí, RS, was classified as synoptic despite having parameters and time-series very similar to those of Figure D.21, also at Quaraí, which was classified non-synoptic. A consultation of Figure D.19 shows a maximum R_G of 1.9 for the period after the peak gust – combined with a maximum change of direction less than 90° in the three hours after the peak. These two parameters classified the event as synoptic per algorithm exit 20 of Figure D.1. A third event at Quaraí, classified as non-synoptic, is shown in Figure D.23, and enhanced satellite images of all three Quaraí events are shown in Figure D.20, Figure D.22 and Figure D.24. The satellite images appear very similar, with each depicting MCS. Radar data were consulted for the three timestamps confirming that squall lines passing over Quaraí were responsible for the peak gusts observed (Note: the term *squall line* is considered inadequate and outdated by meteorologists for whom the term *quasi-linear convective system* is now preferred). All three events were classified as severe in terms of changes in T and P ($\Delta Group$ 1). There is very little doubt that the Figure D.19 event was non-synoptic in origin and its representative parameters are on the limit non-synoptic classification as defined by this study.

Table 6.4 – Parametrisation and automatic classification of 5 F&N extreme wind events at INMET ASWS.

Met. Network	Figure	G_V	$R_{G,-6}$ ($R_{V,-6}$)	$R_{G,-3}$ ($R_{V,-3}$)	$R_{G,+3}$ ($R_{V,+3}$)	$R_{G,+6}$ ($R_{V,+6}$)	$T_{med,3}$ (°C)	$\Delta T_{min,3}$ (°C)	$\Delta P_{max,3}$ (hPa)	$\Delta Group$	$\Delta D_{max,-3}$ (°)	$\Delta D_{max,+3}$ (°)	Class	Exit (D.1)
INMET	D.15	2.7	18.8 (Inf)	Inf (Inf)	3.0 (Inf)	6.0 (Inf)	28.8	-7.5	1.7	2	180	67	SUS	30
INMET	D.17	2.1	1.7 (1.7)	1.4 (1.7)	1.3 (1.3)	1.2 (1.0)	13.6	-1.4	4.4	1	13	13	S	20
INMET	D.19	2.3	6.8 (6.6)	6.6 (4.9)	1.8 (2.0)	1.9 (1.8)	21.7	-9.5	9.1	1	49	42	S	20
INMET	D.21	2.2	5.6 (7.0)	6.4 (11.0)	1.6 (2.4)	2.3 (3.7)	19.0	-1.3	11.2	1	131	74	N	10
INMET	D.23	2.1	2.8 (5.8)	2.1 (5.5)	6.6 (14.0)	4.5 (5.5)	20.0	-3.9	8.2	1	148	78	N	10

6.5.4 Application of algorithms to study SWS

The developed algorithms were applied to all SWS used in the study and examples of some of the most extreme events are shown in Figure D.25 to Figure D.30 with associated parameters of each event listed in Table 6.5. Likely classic non-synoptic downburst events are captured in Figure D.25 to Figure D.27. The event of Figure D.25 in Itapeva, SP, is another event listed in

Table 4.4 which was wiped from INMET official SADMET records and with damage reported by news outlets. The algorithm designed for INMET ASWS was able to successfully identify this as a non-synoptic event, and not as suspect, due to the changes in T and P around the hour of the peak gust, and without the use of present weather identifiers. An intense non-synoptic event in Iquitos, Peru, is shown in Figure D.26. A G_{obs} of this magnitude (> 35 m/s) is rare in the Amazon basin, however, do indeed occur. For this particular event, there was only one observation of TS, the temperature decreased suddenly but only by 5°C , which then rises again to the same temperature before the peak gust less than 2 hours after. Atmospheric pressure remained stable throughout the event. The most extreme non-synoptic event at a Brazilian aerodrome, as determined by this study, was $G_{obs} = 81$ kt registered at SBLO – Londrina, PR, on 20/11/2017 and shown in Figure D.27. A t_{val} of 10 mins was associated with the peak gust, with a lesser gust of $G_{obs} = 56$ kt observed 7 minutes prior. Temperature dropped by 9°C over the hour of the peak gust, while pressure increased 2 hPa from the peak gust to the following observation. TS was observed for a period between 30 minutes to 1 hour.

Figure D.28 and Figure D.29 show two events classified as synoptic from southern Brazil and Uruguay. Constant temperature and slow increase in pressure are seen in Figure D.28 for the subtropical cyclone which affected the coast of Santa Catarina, Brazil, as described previously in Section 2.2.1.2 *Tropical and subtropical cyclones*. Cyclogenesis of the subtropical cyclone occurred over Florianópolis before moving eastwards, causing sustained high wind speeds along the coast over period of 5 hours. Figure D.29 shows the event which produced the highest gust speeds of the analysis for synoptic winds, occurring in Montevideo, Uruguay. Although the event is an extra-tropical cyclone, the peak gust is noted as a squall by the observer, with a gust factor of $G_V = 2.4$, 65% greater than the value used in typical synoptic models (G_V of 1.45). Durañona (2015) postulated that the additional component caused by a downdraft may have been responsible for the squall, resulting in the super-positioning of an extra burst onto what was already a very strong extra-tropical cyclone. This event highlights the non-binary nature of extreme wind events, which is best represented by a spectrum with synoptic and non-synoptic events at opposing ends. It is debatable whether the event should be classified as synoptic or non-synoptic, but considering the extra-tropical cyclone accounted for approximately 2/3 of the total peak gust a synoptic classification is preferred.

Despite the developed classifying algorithms of this study demonstrating better performance than those which use only TS observations or only wind speed ratios to separate non-synoptic from synoptic, they were used in a semi-automatic manner similar to De Gaetano et al. (2014). The perfect algorithm does not exist. Once the set of extreme synoptic and non-synoptic events were determined by automatic classification algorithms developed in this study, the time-series for the top 30 overall events of each SWS were reviewed manually and re-classified when necessary. An example of an event classified automatically as suspect, but then re-classified manually as non-synoptic is shown in Figure D.30. The peak equivalent gust of $G^* = 70$ kt (36.0 m/s) is 1 kt above the permitted algorithm threshold for aerodrome observations without gust observations and with severe changes in temperature and/or pressure ($\Delta Group$ 1). Even by manual classification it is very difficult to determine whether the event is real or not. On the one hand, the temperature decreased by 8 °C within a period of 70 mins after the peak observation, wind direction changed by 120° and TS was observed; on the other, there was gust observation, no change in atmospheric pressure and $\Delta T_{min,3}$ was only -4 °C. The deciding factor which led to the re-classification of the event as non-synoptic was a desire to ensure safety in design wind speeds.

Table 6.5 – Parametrisation and final classification of 6 extreme wind events.

Met. Network	Figure	G_V	$R_{G,-6}$ ($R_{V,-6}$)	$R_{G,-3}$ ($R_{V,-3}$)	$R_{G,+3}$ ($R_{V,+3}$)	$R_{G,+6}$ ($R_{V,+6}$)	$T_{med,3}$ (°C)	$\Delta T_{min,3}$ (°C)	$\Delta P_{max,3}$ (hPa)	$\Delta Group$	$\Delta D_{max,-3}$ (°)	$\Delta D_{max,+3}$ (°)	Class	Exit
INMET	D.25	7.9	7.2 (2.6)	5.9 (2.0)	7.1 (2.3)	7.7 (2.8)	23.1	-7.6	2.2	1	82	73	N	10 (D.1)
Aero. (G_{obs})	D.26	1.9	4.7	3.6	4.0	6.2	31.0	-8	0	2	70	10	N	110 (D.2)
Aero. (G_{obs})	D.27	2.5	6.3	5.4	5.3	7.2	29.5	-10	2	1	130	100	N	110 (D.2)
Aero. (G_{obs})	D.28	1.4	2.4	1.7	1.5	2.1	20.0	-1	3	2	130	10	S	211 (D.2)
Aero. (G_{obs})	D.29	2.4	2.1	1.8	1.7	1.9	14.0	-2	9	1	40	10	S	212 (D.2)
Aero. (G^*)	D.30	-	5.6	4.7	8.8	10.0	33.0	-4	0	3	60	120	N (SUS)	323 (D.4)

A summary of all event classifications used in the extreme value analysis are shown in Figure D.31 for INMET ASWS (491 stations, 4,169 years, 73,684 events), Figure D.32 for aerodrome SWS with G_{obs} (161 stations, 1,941 years, 18,072 events) and Figure D.33 for aerodrome SWS with G^* (161 stations, 1,941 years, 19,517 events), with peak gusts less than 10 m/s not considered. The total number of suspect events is 866 for INMET ASWS (1.2%), 196 for G_{obs} at aerodrome SWS (1.1%) and 1,744 for G^* at aerodrome SWS (8.9%) – highlighting the reduced confidence in event peak speeds without observed gusts. A total of

51 INMET ASWS events and 76 aerodrome SWS events were manually re-classified, representing 0.01% and 0.05%, respectively, of the top events manually reviewed.

6.6 DEVELOPMENT OF BR-MIS EXTREME VALUE ANALYSIS

Two fundamental assumptions are made regarding the extreme value analysis: 1. Wind climates at all locations are stationary, i.e. are not weakening or strengthening over long periods of time, 2. Gust observations are acquired using a moving time-average of 3 seconds. The assumption regarding a stationary climate would require decades of observations with the same equipment and exposure conditions to definitively prove otherwise, especially in regions where non-synoptic winds are dominant and re-analysis data of synoptic conditions insufficient. Despite this, non-stationary climatic conditions are not guaranteed. Since data used in the study was acquired by third parties, the exact definition of gust may vary from station to station, depending on programming algorithms and mechanical filters of equipment. With no way to control the acquisition routines of each station the definition of gust as $\tau = 3$ s can only be assumed.

Section 5 *Extreme value analysis* outlined the most commonly used methods for extreme value analysis of wind speeds. An examination of the data available revealed few stations with high-quality sample periods greater than 20 years, as demonstrated in Figure 6.24, which also shows 10-12 years of data as the most common period of operation for SWS in the study. Reasons for the limited data include:

- The program to commission INMET ASWS began only in 2000;
- The earliest found METAR/SPECI and SYNOP reports, used in the confection of the MSS database, were available from July of 1996;
- Although ICEA has hourly data from 1950 onwards for several Brazilian aerodromes, PAS-31 data was restricted from 1990 onwards due to:
 - reduction of time required by ICEA to prepare the data request,
 - suspicions that many anemometers were still installed atop control towers in the 1980s due to information indicating the program to relocate anemometers to runways only began in the mid-1970s,
 - uncertainty regarding the exact time-averaging interval of gust observations prior to the early 1990s, when WMO adopted $\tau = 3$ s recommendation by

Beljaars (1987). Exact dates of when the time-averaging interval of $\tau = 3$ s was adopted by each individual aerodrome SWS are also unknown.

The decision regarding selection an appropriate extreme value distribution began with the appropriate shape factor, k . The current V_0 isopleth map of NBR 6123 (ABNT, 1988) is based on the Fréchet distribution, which corresponds to GEVD Type-II with $k > 0$. The exact shape factor, $k = 0.157$, is determined as the inverse of $\gamma_{mp} = 6.369$ (Padaratz, 1977). GEVD Type-II/Fréchet is considered too conservative and projects unrealistically high wind speeds for long return periods. Although a GEVD Type-III/Weibull shape is bounded at high return periods, a feature which agrees with the real-life expectation of a physical limit to extreme wind speeds, it may be too large of a “culture shock” to move from $k > 0$ to $k < 0$ in one swift motion – especially when many SWS analysed were in operation for less than 10 years. Therefore, GEVD-Type I/Gumbel, with $k = 0$, was selected as the most appropriate distribution for V_0 of the revised NBR 6123. The distribution is linear and unbounded at high return periods, but not to the same extent as the Fréchet distribution which diverges upwards.

With such limited data for many stations, all extreme value analyses which operate on a set of annual maxima were deemed inappropriate for the study and a method of independent storms required. The need to use MIS is further established as approximately half of the stations suffer discontinuities regularly as identified in Figure 6.25. Less than 400 stations operate on average in the range of 95-100% per month (this figure does not include periods that were deactivated due to undesired data) with roughly the same number of stations in the 40%-95% range.

The selected approach must favour safety but should not be overbearingly conservative. The focus on safety is compounded by the multiple examples of INMET censoring real cases of extreme winds in Section 4.2 *INMET ASWS* and uncertainty regarding anemometer types and lack of historical metadata records at Brazilian aerodrome SWS. As such, the extreme value analysis of q (u^2) as opposed to u , used by Cook (1982), ESDU (1990[a]) and Harris (1999), was rejected due to its propensity to derive lower wind speeds. Also rejected was the use of Lieblein’s BLUE method, which heavily favours mid-range values and reduces the influence of tail values on the determined model, also resulting in typically lower wind speeds.

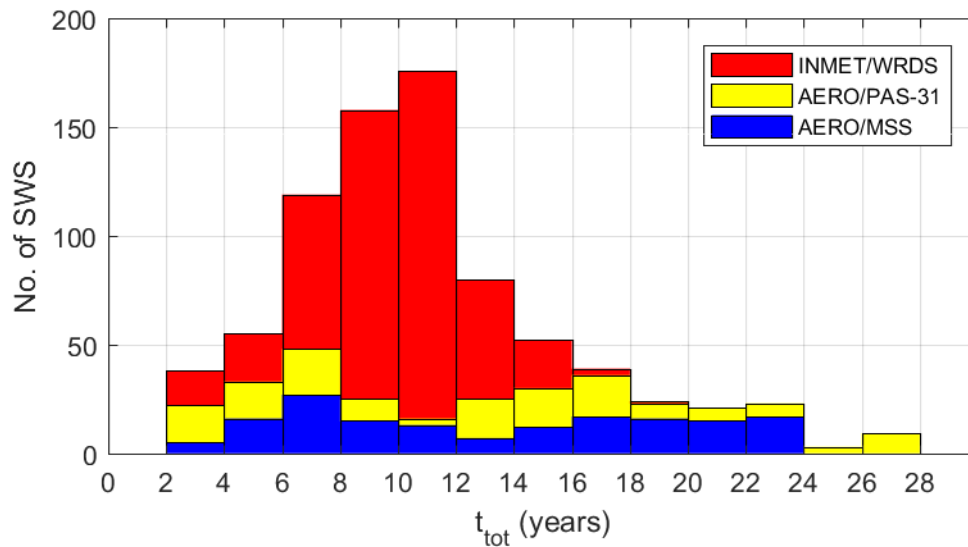


Figure 6.24 – Number of years of valid data, t_{tot} , of all stations analysed.

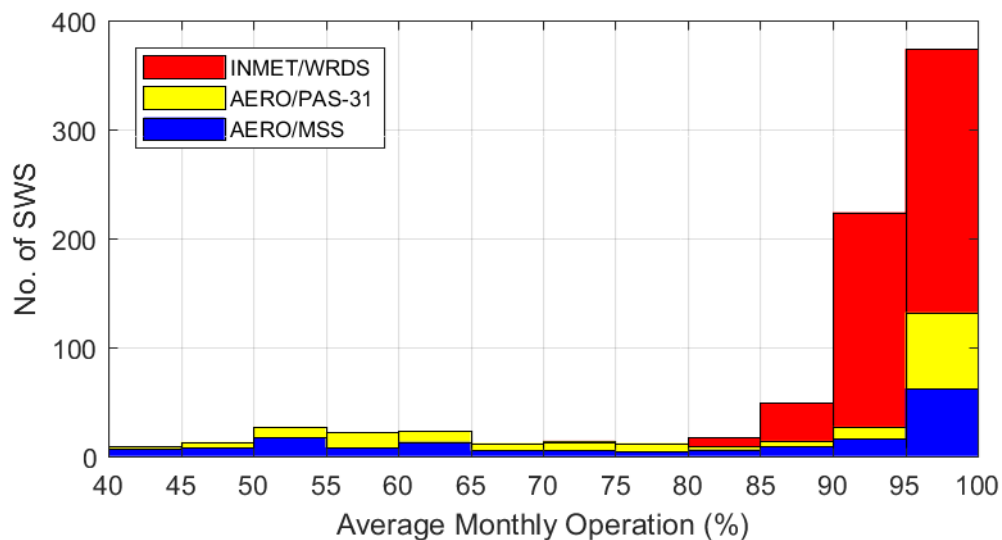


Figure 6.25 – SWS average monthly time in operation presented as a percentage.

Extreme value analysis methods based on independent storms were considered for implementation and include those of Cook (1982), ESDU (1990a), Holmes and Moriarty (1999) and Harris (1999). Cook (1982) and Harris (1999) require the identification of approximately 100 events per year ($r \sim 100$) regardless of the magnitude of the storms. This is near impossible when also considering the aim of separating by storm type, as it is very difficult to distinguish non-synoptic events from synoptic events for peak gusts up to 10-15 m/s. The GPD method of Holmes and Moriarty (1999) was not used due to its emphasis on $k < 0$, even though it can be modified to accommodate $k = 0$.

The Method of Independent Storms of Cook (1982) and ESDU (1990a) was chosen as the basis of the extreme value analysis. Given the large variation in extreme wind speeds across the continent, preference was given to threshold defined by the average number of storms, r , as opposed to a wind speed threshold. The minimum number of events for analysis per station was selected as 20, with the total number of events determined by Equation 6.16. A minimum of 48 hours between successive events was required to establish independence.

$$N = \max(20, t_{tot} \cdot r) \quad 6.16$$

A preliminary study (Vallis et al., 2018) used a threshold of $r = 1$ to limit the effect of lower wind speeds on the distribution in an attempt to generate conservative results. This approach essentially becomes a modified Classic Gumbel approach with the series of annual maxima swapped for the most extreme M peak speeds. However, the mean recurrence interval is distorted due to the loss of correlation between extreme wind speeds and time. In the case of the Classic Gumbel approach, each extreme value represents one year, or one trial – this is not the case for a MIS approach with $r = 1$.

In order to better understand MIS in comparison with traditional approaches, a Monte Carlo simulation was performed using randomly generated gust speeds, G , as outlined in Harris (2001). A random number generator was used to generate a probability, p , between 0 and $1 - 1 \times 10^{-15}$, which was then used in Equation 6.17 to generate G for $n = 100$ events per year over $M = 10,000$ years. The analytic result for $R = 50$ years is set at $G_{50} = 40$ m/s. Scale factor, a , is determined in Equation 6.18 where y_{50} represents the reduced variate for $R = 50$ years. Analytical solutions are therefore: $G_{50} = 40$ m/s, $a = 4.70$ and $U = 21.65$ m/s.

$$X = -a \cdot \ln(1 - p) \quad 6.17$$

$$a = \frac{G_{50}}{y_{50} + \ln(n)} \quad 6.18$$

$$U = a \cdot \ln(n) \quad 6.19$$

Plotting positions were determined using Equation 6.20 for $r = 1, 2, 4$ and 8 , in addition to the Classic Gumbel. Extreme value sets and their estimators are plotted for each of the five approaches in Figure 6.26.

$$P_m = \left(\frac{m}{N+1} \right)^r \quad 6.20$$

Values for MIS models are given in Table 6.6 as ratios of the analytical results. A set of results is given for the linear model fitted to all y points, and a second set for models fit to only $y \geq -1$. Good agreement is found between all models for the right tail (high y) but vary at the left tail (low y). MIS with $r = 1$ begins to diverge from the Classic Gumbel plot at approximately $y = 3$ and plateaus at a constant wind speed around $y = -1$. A probability density plot of both MIS with $r = 1$ and Classic Gumbel extreme values is given in Figure 6.26, with PDF as determined from the fitting of a linear model to the corresponding extreme value distribution. The heavy left tail of MIS has the effect of reducing a and increasing U when compared to the Classic Gumbel approach, however differences in U are smaller for larger r . With larger r , the plateauing begins at lower y and lower wind speeds. For $r = 8$, the divergence from the Classic Gumbel data begins between $-1 < y < 0$, however the left tail extends until approximately $y = -4.5$.

To reduce the effect of the plateauing left tails of MIS models, the set of extremes with corresponding $y < -1$ is ignored when linear regression is performed. This approach is recommended by ESDU (1990[a]) which claims that such values will not contribute significantly to the analysis. Results in Table 6.6 show model parameters are closer to unity for the four values of r examined, giving confidence to its implementation. Such results indicate the inclusion of extremely low y values, $y < -1$ in this case, have a negative impact on the accuracy of the MIS models; slightly different to the view held by ESDU (1990[a]). MIS with $r = 4$ and $y \geq -1$ was selected as the optimal model to be adopted in principal, since $r = 8$ would increase the demand on classification algorithms to identify much weaker storms that are typically out of their scope.

Table 6.6 – Ratios of MIS model parameters to analytical solution.

r	All y			only $y \geq -1$		
	U	a	G_{50}	U	a	G_{50}
1	1.12	0.76	0.95	1.11	0.80	0.97
2	1.08	0.76	0.94	1.06	0.86	0.97
4	1.05	0.76	0.92	1.03	0.92	0.98
8	1.01	0.76	0.90	1.02	0.95	0.99

Further Monte Carlo simulations were undertaken to determine the relationship between mode, U , and extreme value for a mean recurrence interval of $R = 1$ year. The mean recurrence interval, or return period, R , is the average period for which a certain velocity is equalled or surpassed once. Following this definition, the corresponding wind speed for $R = 1$ should be the M^{th} ranked individual storm peak speed over M years, since the speed is equalled or surpassed M times over M years – an average of once a year. However, this does not hold true for short sampling periods and M must be sufficiently long enough to suppress sampling errors. The M^{th} ranked speed, X_M was compared to the analytical mode, $U = 21.65$ m/s, for $M = 10, 20, 50, 1 \times 10^2, 2 \times 10^2, 5 \times 10^2 \dots 1 \times 10^6$ years for three trials. Results are plotted in Figure 6.27 which indicates the difference converges to 0 at $M > 1000$ years. As such, it is acceptable to assume U equivalent to a wind speed with mean recurrence interval of 1 year.

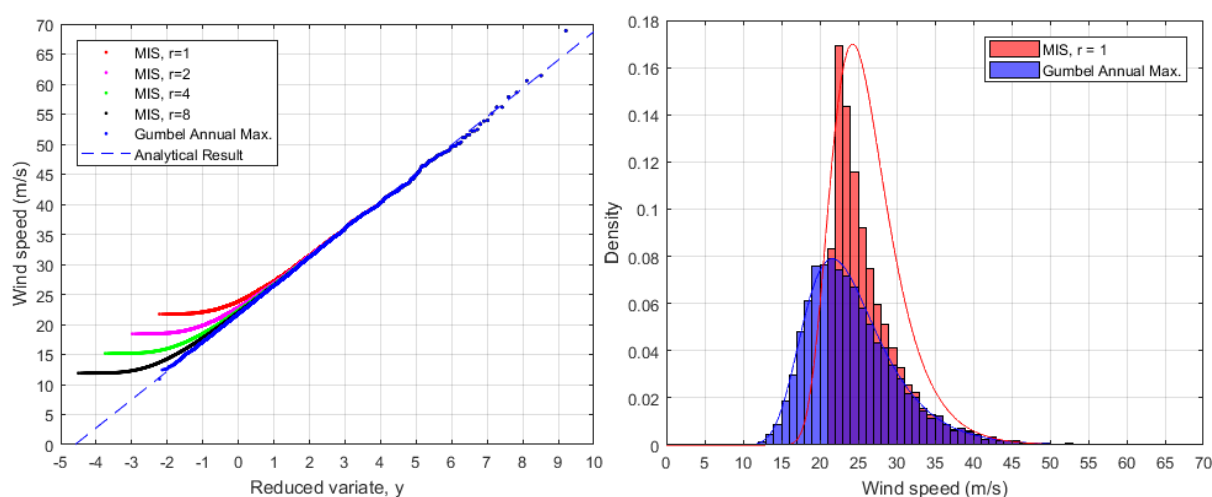


Figure 6.26 – MIS and Gumbel plots of simulated extreme winds for simulated distribution (left), and extreme value density for MIS with $r = 1$ and Classic Gumbel models (right).

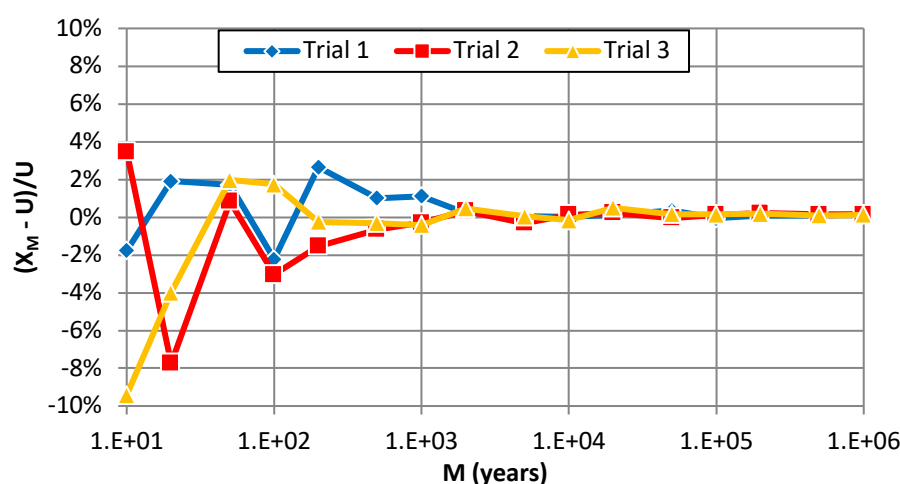


Figure 6.27 – Difference between M_{th} ranked extreme value and U for simulated distribution.

An investigation into the effect of sample period, M , on results was conducted since operation of SWS varies from 2 to 28 years in this study, and not an ideal case of 10,000 years. The same simulated population of Figure 6.26 for $M = 10,000$ years, was divided eight different ways: 5,000 trials of $M = 2$ year periods, 2,500 trials of $M = 4$ year periods, 2,000 trials of $M = 5$ year periods, 1,250 trials of $M = 8$ year periods, 1,000 trials of $M = 10$ year periods, 625 trials of $M = 16$ year periods, 500 trials of $M = 20$ year periods and 400 trials of $M = 25$ year periods. MIS with $r = 4$ and $y \geq -1$, Classic Gumbel and Classic Gringorten approaches were applied to each trial. The least-squares method of linear regression was used to derive models for each trial, with mean and standard deviation of U , a and G_{50} of all trials then determined as ratios of the analytical results which are plotted in Figure 6.28 to Figure 6.30. It should be noted that the differences between U , a and G_{50} for Classic Gumbel and Gringorten approaches for $M = 10,000$ years were negligible.

A comparison of the three approaches shows the Classic Gumbel to be the worst performing for the tested sample periods. The Gringorten model was the best performing of the means, but standard deviations remained high for low M – especially for a . Standard deviations of the MIS approach were comparable to those of Gringorten, but means were not as close to unity. To improve the performance of the proposed MIS method for sample periods of less than 10 years, a relaxed y threshold, y_{lim} , was tested. The threshold adjusts linearly to the sampling period as per Equation 6.21, t_{tot} in the case of operation time which is not an integer, to be $y_{lim} = -1$ for $t_{tot} = 10$, and $y_{lim} = -3$ for $t_{tot} = 2$. Results of the relaxation of y for shorter sampling periods, shown in Figure 6.28, indicate improved performance due to the reduction in standard deviation. The cost for this implementation is the reduction of means of a for $M < 8$ to approximately 0.90 of the analytical solution, however G_{50} is much closer to unity than without the relaxation of y .

$$y_{lim} = \frac{t_{tot} - 14}{4} \quad 6.21$$

The Method of Independent Storms used in this study to determine extreme wind distributions at individual stations across Brazil and South America, herein referred to as BR-MIS, takes the following form:

- identification of most extreme N (Equation 6.16) peak gust speeds per wind type: non-synoptic and synoptic;

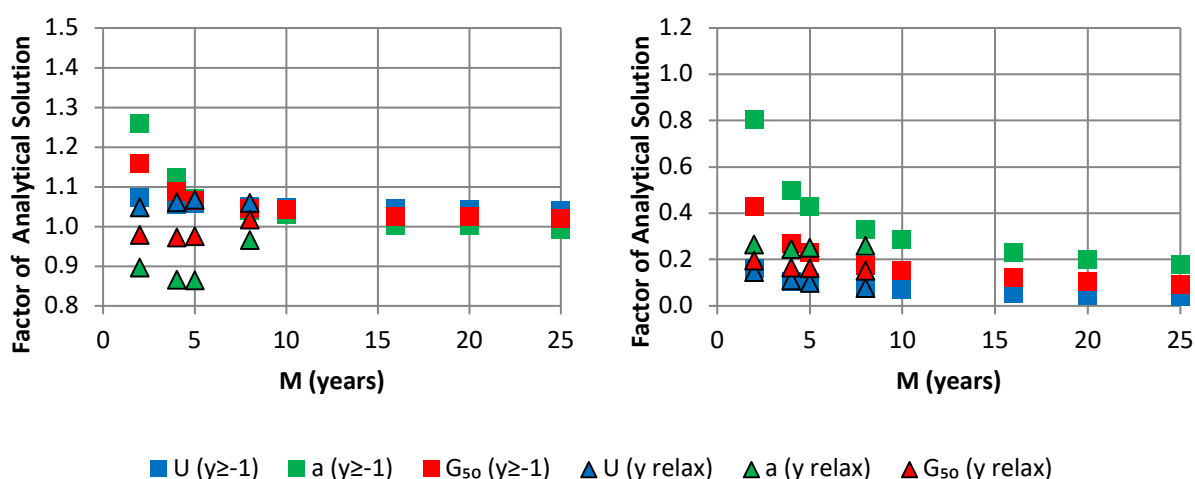


Figure 6.28 – Mean (left) and standard deviation (right) of MIS with $r = 4$ model parameters with varying M as a ratio of analytical solution.

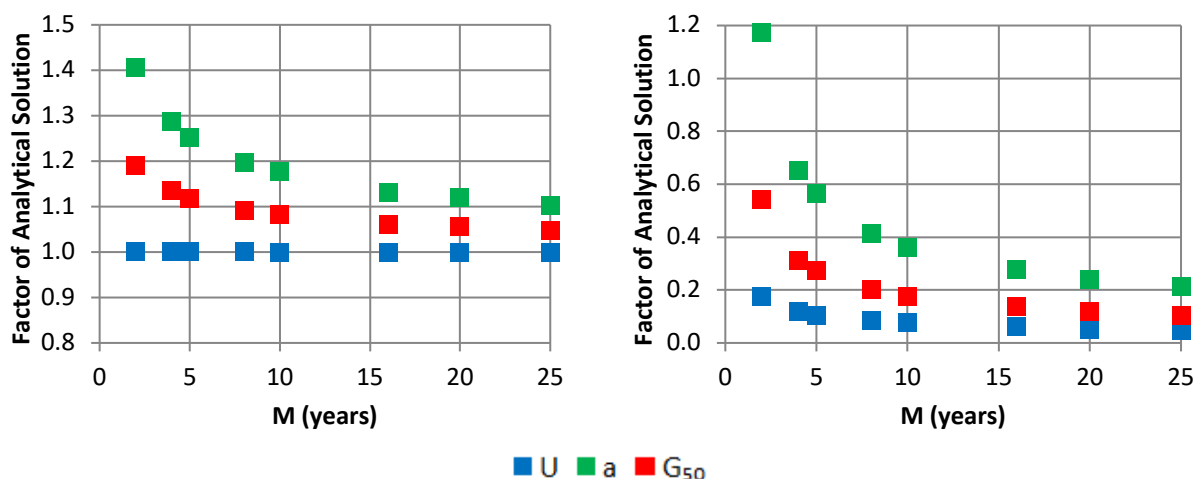


Figure 6.29 – Mean (left) and standard deviation (right) of Classic Gumbel model parameters with varying M as a ratio of analytical solution.

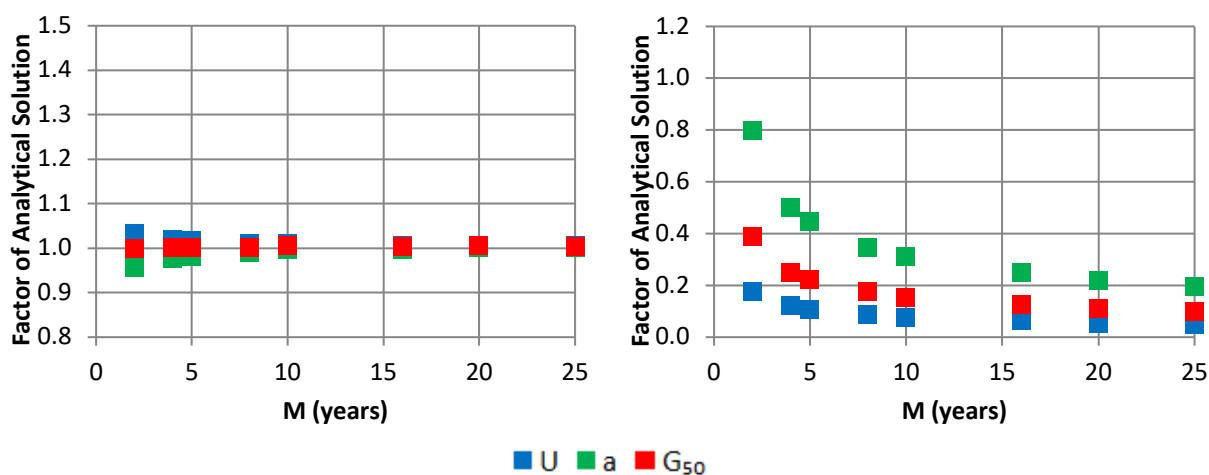


Figure 6.30 – Mean (left) and standard deviation (right) of Classic Gringorten model parameters with varying M as a ratio of analytical solution.

- minimum period of 48 hours between event peaks in order to establish independence;
- minimum average number of storms per year $r=4$ for each wind type;
- probability of ranked events are determined from Equation 6.20;
- model parameters U and a of Equation 6.22 determined from linear regression using least-squares method;
- for sampling period of $t_{tot} \geq 10$ years, linear regression model is only fitted to $y \geq -1$;
- for sampling period of $2 \leq t_{tot} < 10$ years, linear regression model is only fitted to $y \geq y_{lim}$ as determined by Equation 6.21;
- for the determination of mean recurrence wind speeds for R years, Equation 6.22 is simplified to take the form in Equation 6.23 (e.g., G_{50} represents peak gust speeds for $R = 50$).

$$V_R = U + ay \tag{6.22}$$

$$V_R = U + a \ln(R) \tag{6.23}$$

The performance of BR-MIS was tested for 7 different stations with sampling periods ranging from 4 to 28 years, for the dominant non-synoptic wind type, and compared against 9 different methods (Classic Gumbel, Classic Gringorten, BLUE annual maxima, MIS $r=1$ least-squares, BLUE $r=4$, Harris for q , Harris for u , GPD with $k \neq 0$ and $k = 0$). Resulting distributions are shown in Figures E.1 to E.7 in Appendix E *Comparison of Extreme Value Analyses for Selected SWS*. Only the top N events as defined by Equation 6.16 were considered and $r = 100$ was manually set for the testing of the Harris method. In general, GPD, Harris for q and BLUE approaches result in lower wind speeds at high return periods, BR-MIS gives mid-range wind speeds when compared to annual maxima methods and is more conservative wind speeds when compared to other MIS approaches. Limitations to the GPD approach are highlighted in Figures E.2 and E.7 where manual manipulation was required to fit the linear model to the average excess vs threshold plots. This was due to limitations identified by Holmes and Moriarty (1999) regarding the lack of linearity when one, or too few, events are represented at higher thresholds. Many of the thresholds tested also did not adhere to Holmes' (2002) recommended minimum of 10 events per threshold.

7. RESULTS AND DISCUSSION

Due to the high volume of data used and generated by this study, plots of observed data and processed results for all SWS can be found at the purpose-built website⁴¹. An explanatory manual of results is found in Appendix M *Guide to windytips.com*.

Stations selected for the study are listed in Appendix A *Map of Brazil and SWS Details* with altitude above sea level, latitude and longitude. Station identifiers such as ICAO ID, INMET ID and WMO ID are given where applicable. Table A.2 contains details on Brazilian aerodrome SWS, Table A.3 for international aerodrome SWS and Table A.4 for INMET ASWS. Although observed at the same aerodromes, MSS and PAS31 datasets are treated as separate SWS. Quality classifications A, B or C in are assigned to each SWS and are listed in Tables A.2 to A.4. In the case of multiple anemometers for PAS-31 data, classifications are assigned to each anemometer in order.

- Class A – valid sample operating period, $t_{tot} \geq 3$ years, average monthly percentage operation with valid observations, $Obs. (\%) \geq 50\%$;
- Class B – same specifications as Class A, however low confidence in observed data or known location of anemometer to be above a building;
- Class C – infrequent or low-quality data, $t_{tot} < 3$ years or $Obs. (\%) < 50\%$.

Discretion was used to advance some classifications from C to A, including the MSS dataset of SBCC – Cachimbo, PA, with $Obs.$ of 47 %. For Class A SWS, result plots are given for all analyses. For SWS of B classification, only Observed Data and Processed Data are shown. For SWS of C classification, only Observed Data are shown.

Table 7.1 – SWS classifications per dataset.

Classification	INMET ASWS	Aerodrome SWS	
		MSS	PAS-31
A	483	160	155
B	6	14	9
C	5	24	26
Total	494	198	190

⁴¹ www.windytips.com

7.1 GENERAL WIND TRENDS

Average wind speeds at analysed SWS are shown in Figure G.1 of Appendix G *Mapped General Wind Trends*. The north-eastern and southern regions of Brazil have the highest average wind speeds, and although coastal locations are typically higher with 4-6 m/s at $z = 10\text{m}$, mean wind speeds of 3-4m/s are found at locations 100s of kilometres inland from the coast. Differences between ERA-Interim data and observed mean wind speeds, ε , are shown in Figure G.2. Positive ε indicates observed V_m is greater than the ERA-Interim model V_m . Mean observed speeds at aerodromes are typically higher than those observed by INMET ASWS and provided by the ERA-Interim model. Geographical mapping of c and w Weibull parameters for parent distributions are also provided for V_{cor} and G_{cor} in Figures G.3 and G.4 respectively.

7.2 EXTREME WIND TRENDS

The trends of parameters associated with extreme wind events are mapped across the study region in Figures H.1 to H.14 of Appendix H *Mapped Extreme Wind Trends*. Results shown represent the average trends over the set of N_{trend} extreme wind speeds used in the extreme value analysis for non-synoptic (N), synoptic (S) and mixed distributions (M), and are separated by meteorological network with the MSS dataset representing aerodrome SWS. N_{trend} is defined in the same manner as N from Equation 6.16, but with $r = 1.5$ to include only the most extreme events. Mapped parameters include average $T_{med,3}$, $\Delta T_{min,3}$, $\Delta P_{max,3}$ ($\Delta Q_{max,3}$), R_{-3} , R_{+3} and G_V , predominant DIR , season and time of the day, percentage of extreme events with TS present (aerodrome SWS only), annual growth rate of extreme events, pa , and BR-MIS extreme value distribution model parameters a and U for individual SWS.

One of the clearest outcomes of the study is the dominance of non-synoptic extreme wind events over synoptic events at both low and high return periods for the majority of Brazil. Figure 7.1 indicates the dominant storm type for $R = 1$ year (U) and $R = 50$ years (G_{50}) for each of the SWS of Class A. There is generally good agreement between results from aerodrome SWS and INMET ASWS, and both networks indicate dominance of non-synoptic over synoptic with the exception of the coastal region stretching from Espírito Santo to Maranhão. Synoptic winds are dominant over non-synoptic for $R = 1$ for many stations in Brazil's northeast, however many of these same stations are dominated by non-synoptic winds for $R = 50$. As indicated by Figure 7.1b) for INMET ASWS, there are some stations in Brazil's south which indicate a dominance of synoptic winds over non-synoptic winds for

$R = 1$, only Uruguay's southern coastline remains dominated by synoptic winds at $R = 50$. As such, parameter trends for the mixed distribution plots of Appendix H are dominated by non-synoptic winds for the majority of Brazilian locations.

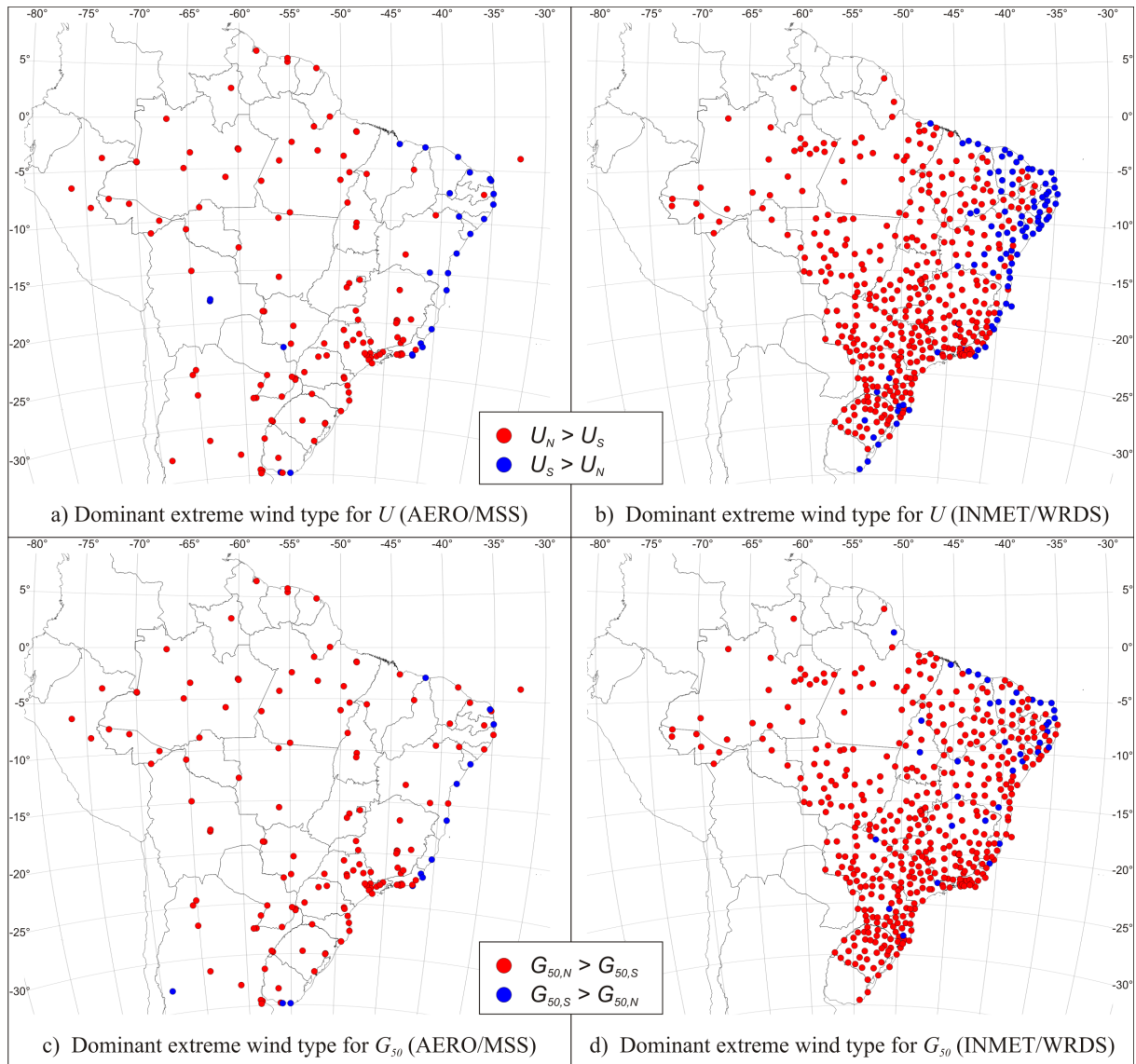


Figure 7.1 – Dominant extreme wind type for $R = 1$ and 50-year mean recurrence intervals, U and G_{50} respectively.

From Figure H.1, mean temperatures prior to the peak gust speed, $T_{med,3}$, are highest in the north, mid-west and inland locations in the northeast and southeast in the range of 29-34°C. Data from INMET ASWS indicate lower $T_{med,3}$ (20-26°C) across the southern states of Paraná, Santa Catarina and Rio Grande do Sul, although this trend is not reflected strongly by aerodrome SWS and could be due to the higher spatial resolution of INMET ASWS. $T_{med,3}$ is typically less for synoptic extreme winds and significantly less for the most southern third of

Brazil. The largest mean temperature decrease around the hour of the peak gust, $\Delta T_{min,3}$, is found in the mid-west states as shown in Figure H.2, with average changes in temperature around -10 to -12 °C for non-synoptic winds. The magnitude of temperature decreases is less at coastal locations and almost negligible along the north-eastern coastline. Synoptic extreme winds also indicate very little change in temperature, with the exception of synoptic winds at inland locations of São Paulo and Mato Grosso do Sul according to INMET ASWS, which reach an average of -8 °C. Increases in atmospheric pressure are much higher for non-synoptic events than for synoptic events across the country. The largest increases in atmospheric pressures were registered in Rio Grande do Sul, Brazil's most southern state, with an average increase of 4 hPa. The mean pressure increase around the hour of peak wind speed decreases from south to north. In Figure H.3, some INMET ASWS in the southern states show mean maximum increases of more than 1.6-2.4 hPa for synoptic events.

The ratio of peak gusts to the average gusts over a period of 3 hours prior to and after the peak, R_{-3} and R_{+3} respectively, are shown in Figures H.4 and H.5. The highest ratios for non-synoptic winds are found at inland SWS in the north, averaging over 5 for R_{-3} and R_{+3} at several stations. In the southern states, R_{+3} ratios (2.0-3.0) are typically lower than R_{-3} ratios (3.0-4.0) at INMET ASWS for non-synoptic winds, which suggests a stronger synoptic component than in regions further north. This difference may also be a consequence of the repeated observation issue detailed in Section 4.2 *INMET ASWS*. Ratios are much lower at north-eastern stations for non-synoptic winds than any other region in the country. By design of the classification algorithms, ratios for synoptic winds are typically low (< 2.5) and are lowest at coastal locations.

The differences in the development of extreme winds at opposite ends of Brazil are shown in Figure 7.2 to Figure 7.5. The figures show the normalised mean and standard deviations of gust and 10-minute mean wind speeds, G_{cor} and V_{cor} respectively, at SBEG – Manaus, AM, in the north and SBPA – Porto Alegre, RS, in the south, for the extreme non-synoptic and synoptic wind speeds. In this context, the term “extreme” is used relatively for each location. For example, the most extreme synoptic wind event at SBEG has a peak G_{obs} of only 30 kt, unlikely to cause significant damage, and is the 169th ranked event in order of peak gust speed. In comparing non-synoptic winds, with gust speeds are typically at 28% of the peak in the hour prior to the peak and 40% in the hour after at SBPA – as opposed to the 20% and 23% at SBEG. This could indicate a stronger background synoptic component to non-synoptic

winds or, that convective storms act over longer periods in the south. Standard deviation for the hour after the peak is much higher at SBPA – totalling 60% of the peak gust when combined with the mean. The sharp peaks of the non-synoptic winds are contrasted with the development of synoptic winds which show gradual growth and decay. A pronounced peak remains for synoptic winds at SBEG, which may indicate the presence of some low-speed non-synoptic events in the set of extreme synoptic values. Synoptic trends are much smoother at SBPA, which indicates the presence of much stronger and developed synoptic wind storms when compared to SBEG.

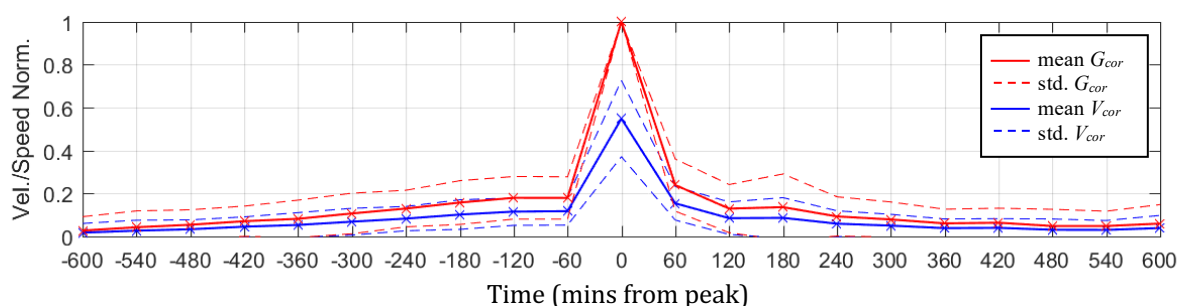


Figure 7.2 – Average development of non-synoptic winds at SBEG – Manaus, AM.

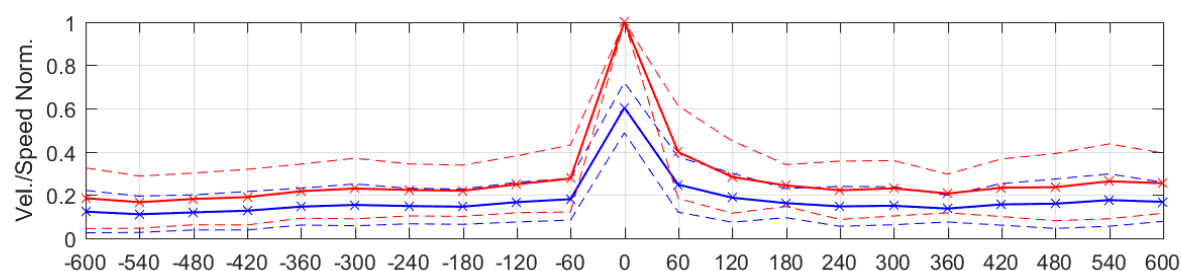


Figure 7.3 – Average development of non-synoptic winds at SBPA – Porto Alegre, RS.

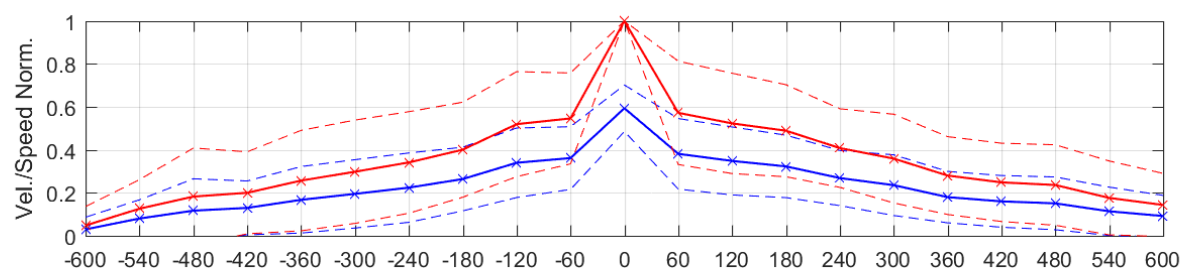


Figure 7.4 – Average development of synoptic winds at SBEG – Manaus, AM.

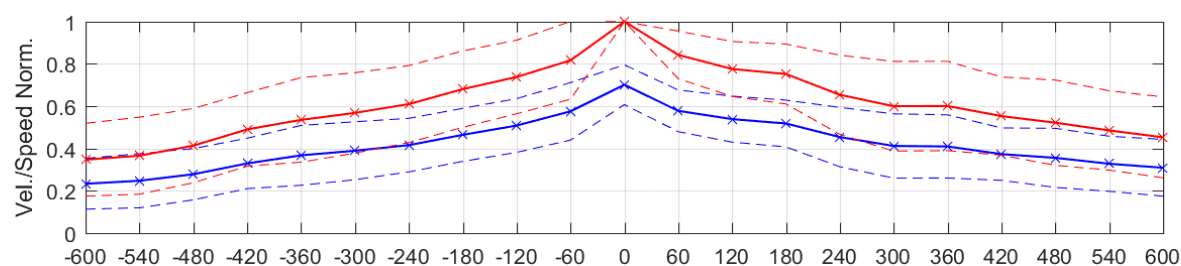


Figure 7.5 – Average development of synoptic winds at SBPA – Porto Alegre, RS.

Predominant wind directions for extreme winds are mapped in Figure H.6. Non-synoptic winds are associated with winds from the south to west quadrant in the southern states of RS, SC, PR, SP and MS. Southern and southwestern non-synoptic winds are also predominant in Uruguay, Paraguay and northern Argentina. In the mid-west and north of Brazil the direction of non-synoptic winds varies, however several stations indicate predominant non-synoptic winds from the east and northeast. In the northeast, synoptic and non-synoptic winds are predominantly from the east. Synoptic winds are predominantly from the north or south at western parts of RS, SC, PR and majority of MS and MT. Coastal locations of RS and SC, as well as Uruguay, show that extreme synoptic winds typically are from the west. It may be expected that strongest winds on the southern Brazilian coast arrive from the ocean (easterlies), and so the dominance of westerlies are unexpected. This can be explained by the frequency of strong extra-tropical cyclones which form over the Rio Plata bordering Argentina and Uruguay and dislocate to the east. With the centre of these clockwise-rotating extra-tropical cyclones to the south of Brazil, the southern Brazilian coastal region is affected by the northern most part of the cyclone which blows from the west.

Average gust factors, G_V , at aerodrome SWS are mapped in Figure H.7. Gust factors at INMET ASWS were considered irrelevant due to the lack of temporal correlation between V and G observations. Mean G_V for extreme synoptic winds are generally lower than G_V for non-synoptic winds, with the highest G_V encountered in Brazil's north for non-synoptic winds. On average, gust factors around $G_V \sim 2$ for non-synoptic winds and $G_V \sim 1.8$ for synoptic winds. These gust factors differ greatly from the $G_V = 1.45$ for synoptic winds of NBR 6123 (ABNT, 1988). Holmes (2014) proposed a turbulence intensity of $I = 0.1$ for non-synoptic storms, which, from Table 3.6, derives $G_V = 1.27$ for $T = 600$ s and $\tau = 3$ s. Theoretical G_V for non-synoptic storms less than that of synoptic winds defined by NBR 6123, but the average G_V as measured by SWS for non-synoptic storms is greater than measured G_V for synoptic winds. This highlights a divergence between the theoretical approach of low turbulence intensity for non-synoptic winds and gust factors determined from field observations in this study.

The times of year and hours most affected by extreme winds for each SWS are mapped in Figure H.8 and Figure H.9 respectively. The year is broken into 4 x 3 month groups which represent the austral seasons: December to February (summer), March to May (autumn), June to August (winter) and September to November (spring). Non-synoptic winds are

predominant in the autumn for the coastal region of the north and northeast; summer for the state of Rio Grande do Sul, Uruguay, Argentina, coastal regions of Santa Catarina and Paraná, and inland regions of the northeast and northern Minas Gerais. The remaining majority of Brazil is affected by non-synoptic extreme winds in the spring. Spring is also the predominant season for synoptic winds across the majority of the country, although several localised regions indicate winter and summer predominance. The spring and summer months are the most frequent times for extreme winds when considering the set of extremes from the mixed distribution. Non-synoptic winds typically occur in the afternoon to evening (17-22 UTC). At some locations in the west of Rio Grande do Sul and northern Argentina, early hours of the morning (23-4 UTC) are the most predominant. Synoptic events typically occur in the late afternoon (14-16 UTC) or early evening (17-19 UTC).

The percentage of extreme winds which occurred in conjunction with TS observations at aerodrome SWS are mapped in Figure H.10. TS observations are strongly linked to non-synoptic winds, but not exclusively. At several stations throughout the continent TS were observed for 70-90% of extreme non-synoptic winds, with the northeastern coastline reporting the lowest percentages ($< 30\%$). For synoptic winds, the large majority of stations recorded all of extreme synoptic wind events without TS observations, however several stations in the south, bounded by northeastern Argentina, Uruguay, western Rio Grande do Sul and Santa Catarina, reported up to 10% of synoptic extreme winds with observed TS. It is likely that the combination of TS and synoptic winds occur when extra-tropical cyclones act over the region over long periods.

One of the main foundations of the study is the assumption of a stationary extreme wind climate. There is currently much interest on the effects of climate change on a global scale, with concerns that higher mean temperatures could increase the frequency of extreme wind events – rendering the stationary climate assumption obsolete. A simple exercise was performed to determine the rate of growth per annum, pa (%), of extreme wind events at individual SWS. For each station, the temporal distribution of the most extreme 100 wind events, without separation of storm type, was determined for month blocks, and a line of best fit applied to the distribution. Months with valid observations ($Obs.$) $< 50\%$ and stations with $t_{tot} < 10$ years were not considered. A histogram of the overall results is shown in Figure 7.6 for pa of 5% bandwidths, and mapped results in Figure H.11. It is difficult to determine an overall trend for Brazil and South America from Figure H.11, with a decrease in pa at INMET

ASWS in Minas Gerais the only noticeable regional trend. Figure 7.6 identifies a greater number of SWS with a positive pa , with the range $0 \leq pa < 5\%$ being the most frequent.

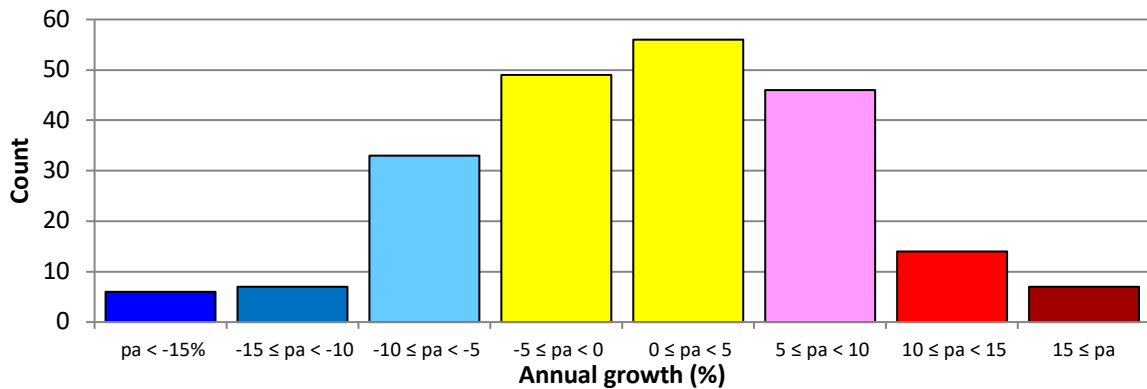


Figure 7.6 – Histogram of annual rate of extreme events at individual SWS with $t_{tot} \geq 10$ years.

Although the results indicate a tendency for an increase in the frequency extreme winds, it is possible that station operation between 10 and 28 years is not sufficient to clearly establish such trends. Changes in monitoring equipment and processes also reduce prevent strong conclusions from being drawn. Results from SBFL – Florianópolis, SC, show the challenges faced when trying to establish the growth or decay in frequency of extreme wind events. Figure 7.7 shows processed data at SBFL from the MSS dataset, and plots indicate a growth in both frequency and magnitude of extreme wind events, resulting in an apparent 12.4% annual growth of extreme wind events. The two most extreme synoptic events occurred in recent years, with the 2016 event the first subtropical cyclone to directly hit the city and cause highest ever verified gust speed observed at SBFL ($G_{obs} = 64$ kt). The frequency of non-synoptic events with $G_{cor} > 25$ m/s also increased over the last 10 years. A change in the frequency and magnitude of gust observations is seen in 2008. However, these increases may be the result of the introduction of digital and/or automated processes in data acquisition and/or a possible change in anemometer type from mechanical to ultrasonic as opposed to climatic changes. Without critical historical metadata it is impossible to declare that such increases are directly linked to climate changes, although does not mean that such changes are not occurring. This inconclusive finding regarding extreme wind trends differs from that of Pes et al. (2017) which indicated that 45% of all Brazilian aerodrome SWS reported a significant positive trend for extreme 10-minute mean wind speeds between 1947 and 2014.

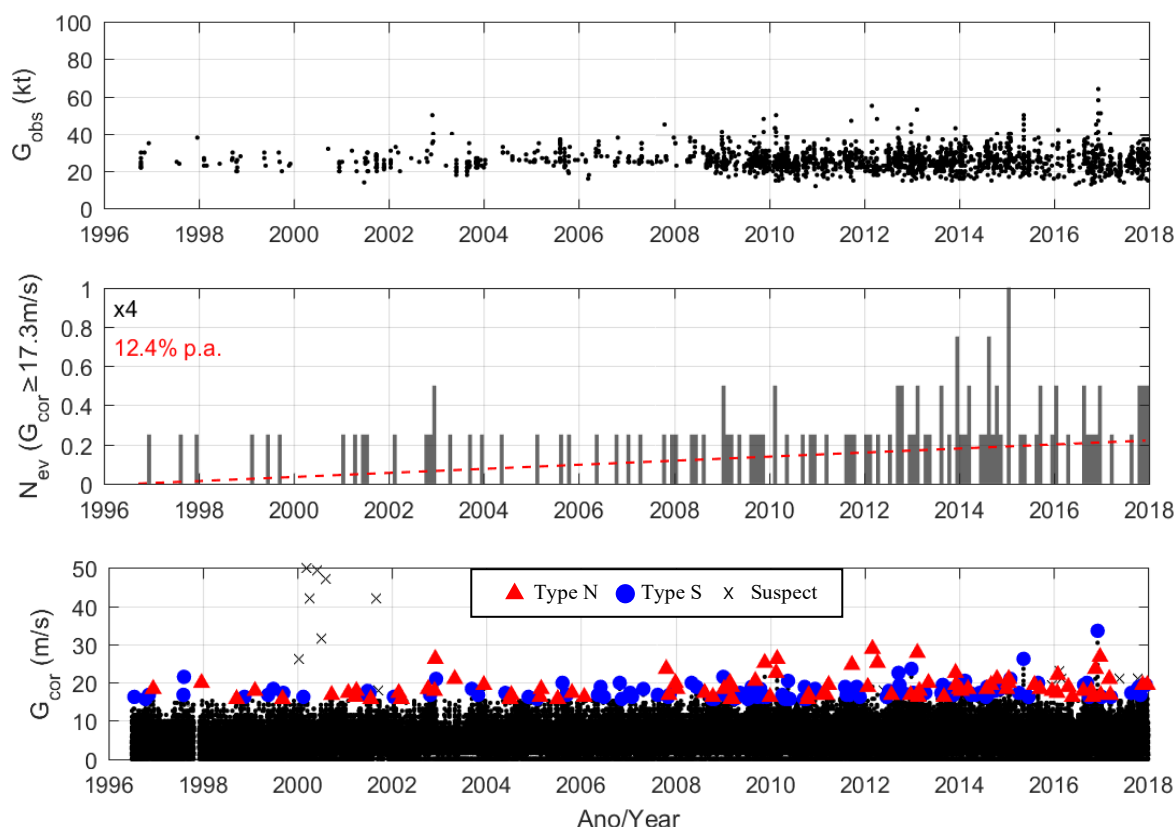


Figure 7.7 – Processed data at SBFL – Florianópolis, SC: Observed gusts, G_{obs} , (top); distribution of top 100 extreme wind events and annual growth rate, pa (middle); homogenised gust time-series, G_{cor} , with event classifications (bottom).

7.3 DETERMINATION OF REGIONAL BASIC WIND SPEEDS

Model parameters a and U for each SWS of Class A are mapped in Figures H.12 and H.13 of Appendix H for non-synoptic (Type N), synoptic (Type S) and mixed distributions. Corresponding peak gust speeds for $R = 50$ years, G_{50} , are mapped in Figure H.14. In Figure H.12 large variations in a are observed at stations in close proximity, particularly for Type N winds. This was to be expected as indicated by the simulated results of Figure 6.28. In Figure H.13 for U , the variations are smaller, and U tends to be higher at southern stations and weakens in magnitude when moving north for both Type N and S winds. Despite this, a high degree of variability is noted between neighbouring SWS for 50-year return wind speeds. A difference of almost 18 m/s in $G_{50,N}$ wind speeds at A816 – Novo Horizonte, PR, and A876 – Clevelândia, SC, in the southwest of the country is one of the most striking examples of the high degree variability. A distance of approximately 50 km separates the two INMET stations, which both use Vaisala WAA151 cup anemometers. Total sampling time and extreme value results of both stations, in addition to 6 other stations in the region, are shown in Table 7.2.

For these 8 stations, an average $G_{50,N} = 41.4$ m/s is determined, which is weighted by t_{tot} of each station. Theoretically, these SWS should be reporting G_{50} of similar magnitudes. It is difficult to explain the motivation for such large variations without detailed investigations into the each and every station. Such an investigation may uncover differences in the processing of data (i.e. programming of gust averaging $\tau \neq 3$ s), effects of topography, terrain or anemometer equipment.

Table 7.2 – Station sampling time and non-synoptic extreme distributions in western Santa Catarina and southwestern Paraná.

SWS (Dataset)	t_{tot} (years)	a_N	U_N (m/s)	$G_{50,N}$ (m/s)
SBCH (MSS)	5.2	4.4	33.8	50.8
A843 (WRDS)	8.1	4.7	30.1	48.3
A816 (WRDS)	9.5	4.5	29.7	47.4
A857 (WRDS)	10.8	3.6	26.1	40.3
A858 (WRDS)	8.5	3.6	26.3	40.2
A855 (WRDS)	9.5	3.5	26.4	40.1
A848 (WRDS)	9.9	3.1	24.5	36.6
A876 (WRDS)	6.7	1.6	23.5	29.9

The present challenge involves the generation of regional wind climate models with consideration to the parameters a , U , G_{50} and t_{tot} as determined at individual SWS. The basic wind speeds of NBR 6123 must prioritise safety over load optimisation, but must not be overbearingly conservative. As outlined in previous chapters, there are a number of issues regarding datasets, unknown metadata and observation processes which could impact the accuracy of the extreme value analyses at individual SWS. None of the 4 key criteria defined by Holmes et al. (2005) as listed in Section 1.1 *Relevance of the study* was met by stations of the study, despite attempts to correct gust speeds to $z = 10$ m and CAT II.

Basic regional wind speeds defined by national codes and standards typically take the form of zone or contour maps. Example of zone maps include AS/NZS 1170.2 for Australia and New Zealand (2011), ASCE-7 for non-hurricane wind speeds within continental United States (2010), HB 212-2002 for the Asia-Pacific Region (Standards Australia, 2002), DIN EN 1991-1-4/NA:2010-2012 Germany's National Annex of the Eurocode (Deutsche Norm, 2010), and NSR-10 of Colombia (AIS, 2010). Codes with contour maps include the NBR 6123 of Brazil (ABNT, 1988), CIRSOC 102 of Argentina (INTI, 2005), NP No. 196 of Paraguay (INTN, 1991), coastal hurricane regions of ASCE-7 in the United States (2010). The most recent

version of ASCE-7 (2016) permits interpolation between isolines for both non-hurricane and hurricane wind speeds. Although the Uruguayan code, UNIT 50-84 (1984), contains a contour map, the accompanying text states that the country is divided into two zones by a boundary 25 km inland from the margins of the Uruguay River, La Plata River and the Atlantic coast.

Zone maps allow for easy administration and for a reduction in user misinterpretation or multiple interpretations, while contour maps are better suited to areas affected by tropical cyclones (Holmes et al., 2005). It is recommended that zones follow limits easily identifiable on maps, such as state, city or province borders. Holmes et al. (2005) recommend a 3 m/s minimum contour spacing for gust speeds for a 50-year return period. Based on these recommendations, initial proposals of zonal V_0 for non-synoptic and synoptic wind types are found in Appendix I *Alternative Zone Solutions*. Figures I.1 and I.2 show the G_{50} values for individual and manually selected governing SWS, for a sampling period ending 31/12/2017 for MSS, PAS-31 and WDS data. Data for the INMET ASWS were from the now redundant WDS database, which did not contain observations of events only kept in the restricted database only accessible to INMET employees. The selection of governing SWS and definition of zones, Figure I.3 for non-synoptic and Figure I.4 for synoptic winds, were performed manually and with a bias toward generating conservative wind speeds due to the unknown impact of redacted extreme wind speeds by INMET. Weighted averages were used to determine a , U and V_R values of each zone, as listed in Table I.3 and Table I.4 of non-synoptic and synoptic winds, and plotted in Figure I.4 and I.6 respectively. Further details of the process are given in Appendix I.

The three events described in Table 4.7 of Section 4.2.4 *Restricted INMET Database* at A728 – Taubaté, SP, serve as an example of the influence the withholding of key data by INMET had on the initial outcomes of this study. For the WDS database (until 31/12/2017), the non-synoptic 50-year wind speed at A728 was $G_{50,N} = 33.9$ m/s, but $G_{50,N} = 39.2$ m/s for the more complete WRDS database (until 31/05/2019). With the inclusion of data from INMET's restricted database, a higher level of confidence can be attributed to the outcomes of extreme value analyses of INMET ASWS. This allowed for the development of a contour, or isopleth, solution based on interpolation between neighbouring SWS. Such a solution is desirable as the current map of V_0 (Figure B.1 of Appendix B) is of the same format meaning an easier transition for users of NBR 6123.

Despite the inclusion of previously redacted data, the proposed V_0 map must be conservative due to failure of Brazilian meteorological networks to fulfil the four key criteria for the determination of basic wind speeds as outlined by Holmes et al. (2005). The range of 20.9 m/s between maximum and minimum 50-year return period wind speeds for non-synoptic winds for stations in the same region, as shown in Table 7.2, supports the notion contoured map which permits interpolation must favour caution and safety. As such, stations were selected to form the basis of interpolation by local polynomial regression. These stations, herein referred to as *governing stations*, were identified via an objective filtering process described below. Separate lists of governing stations were created for non-synoptic (N), synoptic (S) and mixed distributions (M), in addition to the *envelope* (E) result, which are the maximum G_{50} and U wind speeds of N, S and M distributions.

A grid with intervals of $0.5^\circ \times 0.5^\circ$ (approximately 50 km x 50 km) was generated for latitudes between -35° and 5° , and longitudes between -75° and -35° . For each node of the grid, the following test was performed:

1. Identification of the closest 8 SWS. If the closest SWS was located more than 100 km from the node, steps 2 and 3 were not performed and the process advanced to the next node.
2. For the selected 8 SWS, an average G_{50} was determined, \bar{G}_{50} , at the node using each SWS's t_{tot} as weighting. For Brazilian aerodromes with multiple datasets and anemometers (MSS and PAS-31), the dataset/anemometer with the longest sampling period was chosen to represent the aerodrome. For example, dataset PAS31-1 (1st anemometer) was selected to represent SBPA – Porto Alegre, RS, as it had the longest sampling period, $t_{tot} = 25.5$ years, compared to MSS with $t_{tot} = 22.7$ years and PAS31-2 (2nd anemometer) with $t_{tot} = 24.4$ years. Due to reporting suspiciously low extreme distributions, the 3rd and 4th anemometers of SBGL – Galeão, RJ, and SBGR – Guarulhos, SP, were not permitted to represent their respective aerodromes.
3. Of the selected 8 SWS, those with $G_{50} < \bar{G}_{50} - 3$ (m/s) were identified as underperformers.
4. Once the test was applied at all nodes, all stations identified as underperformers were removed from the list, and those remaining became governing stations for the particular wind type/distribution (N, S, M or E).

Examples of the application of the abovementioned process are given at the node nearest to São Paulo, SP, in Table 7.3 and at the node nearest Rio de Janeiro, RJ, in Table 7.4. The values of $\bar{G}_{50,N}$ are 35.7 and 32.1 m/s were determined at the respective locations, resulting in the identification of three underperforming stations for each. It should be noted that the removal of the underperforming stations would result in $\bar{G}_{50,N} = 37.7$ m/s and $\bar{G}_{50,N} = 36.3$ m/s for the nodes nearest São Paulo and Rio de Janeiro respectively.

Table 7.3 – Discrimination process for node closest to São Paulo, SP, (-23.5°, -46.5°) for non-synoptic winds.

SWS (Dataset)	t_{tot} (years)	$G_{50,N}$ (m/s)	$G_{50,N} < \bar{G}_{50,N} - 3$
SBGR (MSS)	19.4	40.0	NO
A701 (WRDS)	12.8	36.5	NO
SBSP (MSS)	22.0	35.9	NO
A755 (WRDS)	6.0	31.1	YES
SBST (MSS)	5.8	31.5	YES
SBJD (MSS)	5.9	37.8	NO
SBBP (MSS)	3.0	41.0	NO
SBSJ (PAS31-1)	18.0	31.7	YES
Total	92.8	$\bar{G}_{50,N} = 35.7$ m/s	

Table 7.4 – Discrimination process for node closest to Rio de Janeiro, RJ, (-23.0°, -43.5°) for non-synoptic winds.

SWS (Dataset)	t_{tot} (years)	$G_{50,N}$ (m/s)	$G_{50,N} < \bar{G}_{50,N} - 3$
A602 (WRDS)	14.3	36.1	NO
SBJR (PAS31-1)	15.5	23.1	YES
A621 (WRDS)	11.7	37.6	NO
SBAF (PAS31-1)	14.6	28.1	YES
SBSC (PAS31-1)	23.0	27.8	YES
A652 (WRDS)	11.9	41.2	NO
A601 (WRDS)	13.8	34.1	NO
SBGL (PAS31-1)	18.5	34.3	NO
Total	123.2	$\bar{G}_{50,N} = 32.1$ m/s	

The governing stations for each wind type/distribution are identified in Tables C.1 and C.2 of Appendix C *Extreme Distributions of SWS*. The locations of the governing stations, along with corresponding values of G_{50} and U , are mapped in Figure 7.8 for non-synoptic winds, Figure 7.9 for synoptic winds, Figure 7.10 for mixed distribution and Figure 7.11 for the

envelope case. These figures also contain the isopleth solutions for Brazilian territory only. Refer to Appendix J *Local Polynomial Regression Solution* for detailed information on the interpolation scheme responsible for the generation of contours. Local regression was used by Pintar et al. (2015) in the determination of non-hurricane basic wind speed maps in the most recent ASCE-7 (2016). Stations influenced by extreme topography were not considered in the determination of the contour solutions, and include A845 – Morro da Igreja, SC, A610 – Pico do Couto, RJ, and F501 – Cercadinha, MG. In order to guarantee a maximum contour of 46 m/s (nearly 10% less than 50.8 m/s at SBCH – Chapecó, SC, the highest $G_{50,N}$ in the region), a number of governing stations were removed from interpolation of N, M and E maps in the southwestern region of Brazil. These stations were A858 – Xanxerê, SC, A857 – São Miguel do Oeste, SC, A855 – Planalto, PR, A853 – Cruz Alta, RS, SBCA – Cascavel, PR, SARI – Puerto Iguazu, Argentina, and SARP – Pousadas, Argentina. Of all Class A Brazilian SWS, 57% were selected as governing stations for the non-synoptic case and 70% for the synoptic case.

To ensure a robust solution of V_0 , a sensitivity test involving the removal of governing stations prior to the implementation of local polynomial regression was performed. In the same way that a structure with some load bearing elements removed must still be able to remain standing without any serious deformation or risk to occupants, a robust model must remain coherent in the case of missing input data. Tests were performed for the set of governing stations of $G_{50,N}$, dominant over $G_{50,S}$ for the majority of the country, with results shown in Figure J.4 of Appendix J. Three modified solutions were tested with 10%, 20% and 40% of governing stations removed prior to implementation of the local polynomial regression. In order to ensure a random selection of stations to be removed, the 381 stations were first ordered alphabetically in terms of their ICAO/INMET code. Every 10th station was removed for the 90% case, shown in Figures J.4a) and b), every 9th and 10th station were removed for the 80% case, shown in Figures J.4c) and d), and every 7th, 8th, 9th and 10th station were removed for the 60% case, shown in Figures J.4e) and f). The resulting contour solutions of Figure J.4 are almost identical to Figure 7.8b) for all governing SWS. The expansion of the $39 \leq G_{50,N} < 42$ m/s band across the central region of southern Mato Grosso is the only notable difference between the contours of Figure J.4 and Figure 7.8b). In reality, this difference is in the order of only 1 m/s, but appears greater due to the coarse contour intervals of 3 m/s. The similarities between the contour solution with 40% of governing stations removed, shown in Figure J.4f), and the solution with all governing stations of Figure

7.8b) indicate the robustness of the approach used to determine a contoured solution from data at discrete locations.

From Figure 7.8b), $G_{50,N}$ ranges from 24 m/s in the northeast to 46 m/s in the southwest region with a nucleus in western Santa Catarina. From Figure 7.9b), $G_{50,S}$ ranges from 40 m/s in the southern most extreme of Brazil, to less than 21 m/s in the Amazon region in the northwest. $G_{50,N}$ wind speeds are dominant over $G_{50,S}$ for all Brazil, but this is not the case for U wind speeds, with $U_S > U_N$ for the coastal region of the north, northeast and Espírito Santo, which is in agreeance with with Figure 7.1. From Figure 7.8d), U_N ranges from 15 m/s in the northeast to 30 m/s in western Santa Catarina. From Figure 7.9d), U_S ranges from less 13 m/s in the Amazon, to a regional maximum of 19 m/s on the northern coasts of Ceará and Rio Grande do Norte. U_S dips below 19 m/s for long extents of the northeastern and eastern coastlines, before rising over 21 m/s on the coasts of southern Espírito Santo and northern Rio de Janeiro. The most extreme U_S of 26 m/s is encountered at Chuí, RS, the most southern point of the country.

The dominance of non-synoptic winds over synoptic winds is confirmed by the mirroring of the $G_{50,N}$ contours of Figure 7.8b) by $G_{50,M}$ and $G_{50,E}$ maps in Figure 7.10b) and Figure 7.11b) respectively. Despite this, there are some regions of the country where U_M and U_E , shown in Figure 7.10d) and Figure 7.11d), are higher than U_N , shown in Figure 7.8d), due to the contribution of extreme synoptic events to the mixed distribution. Such regions include:

- The northern coastline extending from Belém, PA, to Natal, RN, which increases from a minimum of $U_N = 15$ m/s to $U_M = U_E = 19$ m/s.
- The northeastern coast and inland regions extending from Natal, RN, to Porto Seguro, BA, which increases by approximately 2 m/s from U_N to U_M .
- The southern half of Rio Grande do Sul, which increases by approximately 2 m/s from U_N to U_M and U_E .

Basic wind speeds for Brazil were determined with consideration given to the above results. Separate maps of V_0 for non-synoptic and synoptic winds can be generated from Figure 7.8b) and Figure 7.9b) in the future when an appropriate convective storm outflow model is developed, tested and accepted. Until then, ABL models for synoptic winds remain the default option for simulating incident extreme winds. A single V_0 map proposed for use in NBR 6123, as shown in Figure 7.15, was developed with the understanding that non-synoptic winds govern for a return period of $R = 50$ years, but that synoptic winds are significant in some

regions for lower R . A minimum basic gust speed of 30 m/s for $R = 50$ years as proposed by Padaratz (1977) is to be maintained despite some regions, particularly regions in the north and northeast, exhibiting basic wind speeds which could be as low as 24 m/s. The use of a minimum basic wind speed of 30 m/s for non-synoptic winds is in agreement with other international codes:

- 50-year return period basic gust speed of 32 m/s for equatorial Asian countries including Indonesia, Papua New Guinea, Singapore and Malaysia as defined by HB 212-2002 (Standards Australia, 2002);
- basic 10-minute wind speed of 20 m/s for Singapore as defined by NA to SS EN 199-1-1-4: 2009 (SSC, 2009). Application of a 3-second gust factor of $G_V = 1.45$ converts 20 m/s to a basic gust speed of 29 m/s;
- basic 3-second gust speed of 32.5 m/s at inland locations for Malaysia as defined by MS 1553:2002 (DSM, 2002);
- Site wind speed of AS/NZS 1170.2 (2011) must not be less than 30 m/s for permanent structures.

The proposed map of V_0 of Figure 7.15 is based on the non-synoptic extreme wind speeds of Figure 7.8b) for a 50-year return period, with adjustments made in some regions. A model is also provided to determine wind speeds of other return periods. As described in Section 2.3.1.2 *Return periods and risk categories*, the probabilistic factor of the current NBR 6123 (ABNT, 1988), S_3 , is responsible for the conversion of V_0 to other return periods, but was derived for the Fréchet distribution as per Equation 2.12. A new definition of S_3 is required which reflects the GEVD Type I – Gumbel distribution. If a relationship is established between U and a in the form of Equation 7.1 with $\delta = 0$, S_3 can be derived as a function of lifetime, R_L , and probability of exceedance over R_L years, P_L . If $\delta \neq 0$, S_3 will be defined as a function of R_L , P_L , U and a , and separate maps of U and a will need to be provided.

$$U = \theta a + \delta \quad 7.1$$

The relationship between U and a for individual SWS is shown in Figure 7.12 for non-synoptic winds, Figure 7.13 for synoptic winds and Figure 7.14 for mixed distribution. Separate U vs a plots are given for two different sets of stations: 1) all SWS and, 2) governing SWS. Trends between U and a are notably different for each distribution (N, S, or M). Three

different linear relationships between U and a , with $\delta = 0$, are plotted for non-synoptic governing stations in Figure 7.12. $\theta = 7.309$ was determined from the weighted average of U/a for the set of governing stations, with weightings provided by t_{tot} , while $\theta = 6.752$ was determined from a least squares linear regression. For $\delta = 0$, θ is a rounded average of these two models, as presented in Equation 7.2.

$$U = 7a \quad 7.2$$

The proposed set of S_3 , given in Table 7.5, is generated from Equation 7.3. The derivation of Equation 7.3 is given in Appendix K *Determination of Probabilistic Factor S_3* , in addition to Table K.3 containing wind speeds for various mean recurrence intervals, V_R , for probability of exceedance $P_L = 0.63$.

Residuals are the difference between the input data and resulting model. In this study, the input data are the scalars of individual SWS and the resulting models are the proposed isopleth map and probabilistic factors. Mapped residuals are available in Appendix L *Mapped Residuals of Contour Solutions* for the initial solution of Figure 7.8b) and the final solution of Figure 7.15. Four different sets of residuals, e , were analysed to assess the appropriateness of the initial and final solutions: U_N and $G_{50,N}$ values for all SWS, in Figure L.1 and Figure L.3 respectively, and $G_{50,E}$ and U_E for governing SWS, in Figure L.2 and Figure L.4 respectively. Residuals for the non-synoptic distributions at all SWS portray the proposed solution as conservative due to the inclusion of stations with less extreme wind speeds which were not used in the confection of V_0 and S_3 . Residuals for envelope 50-year return period wind speeds of the governing set of SWS, and their associated U_E wind speeds, reveal any regions of the country for which the proposed solution is unconservative.

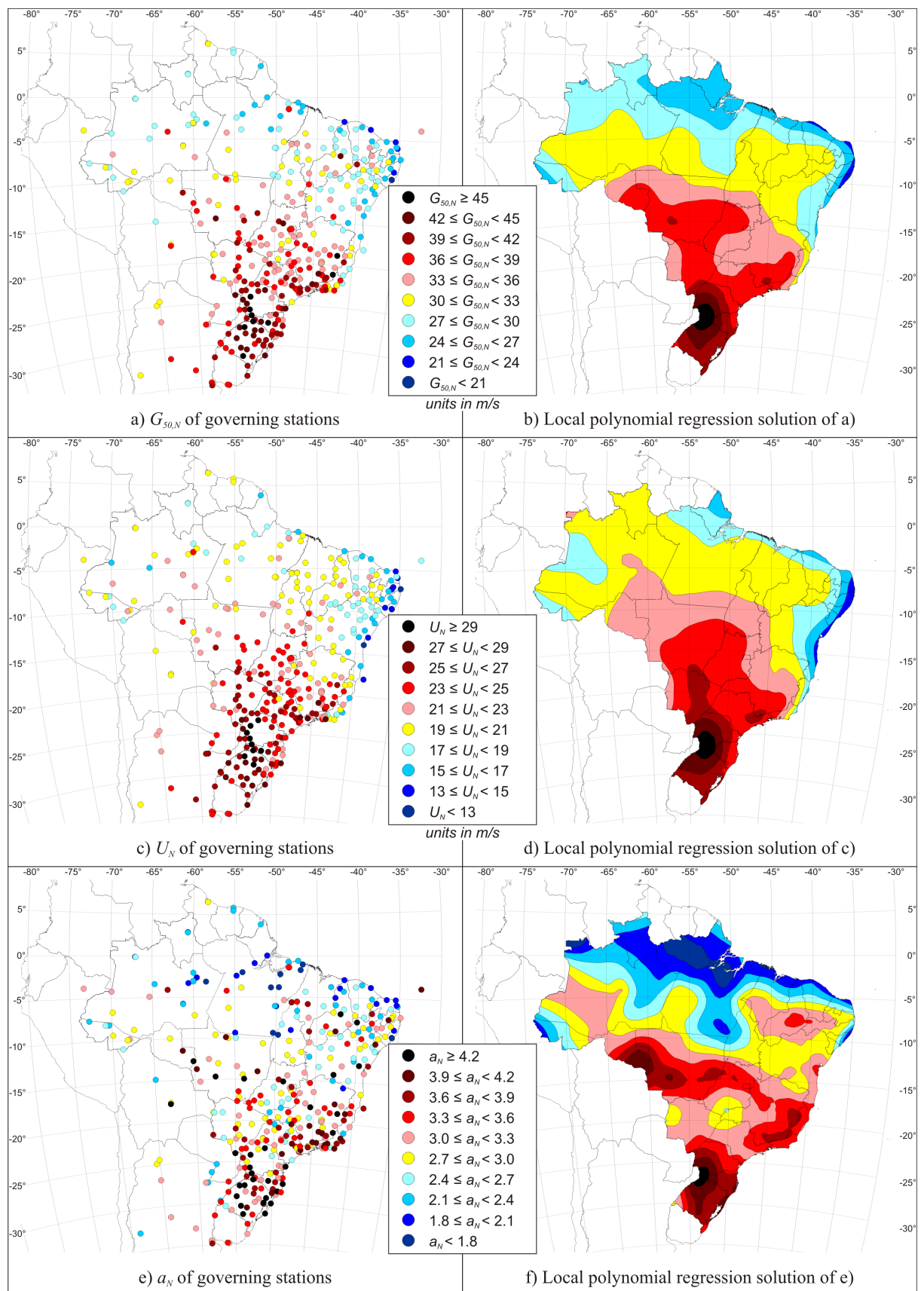


Figure 7.8 – Extreme distribution parameters of governing stations for non-synoptic extreme winds (N): $G_{50,N}$, U_N and a_N .

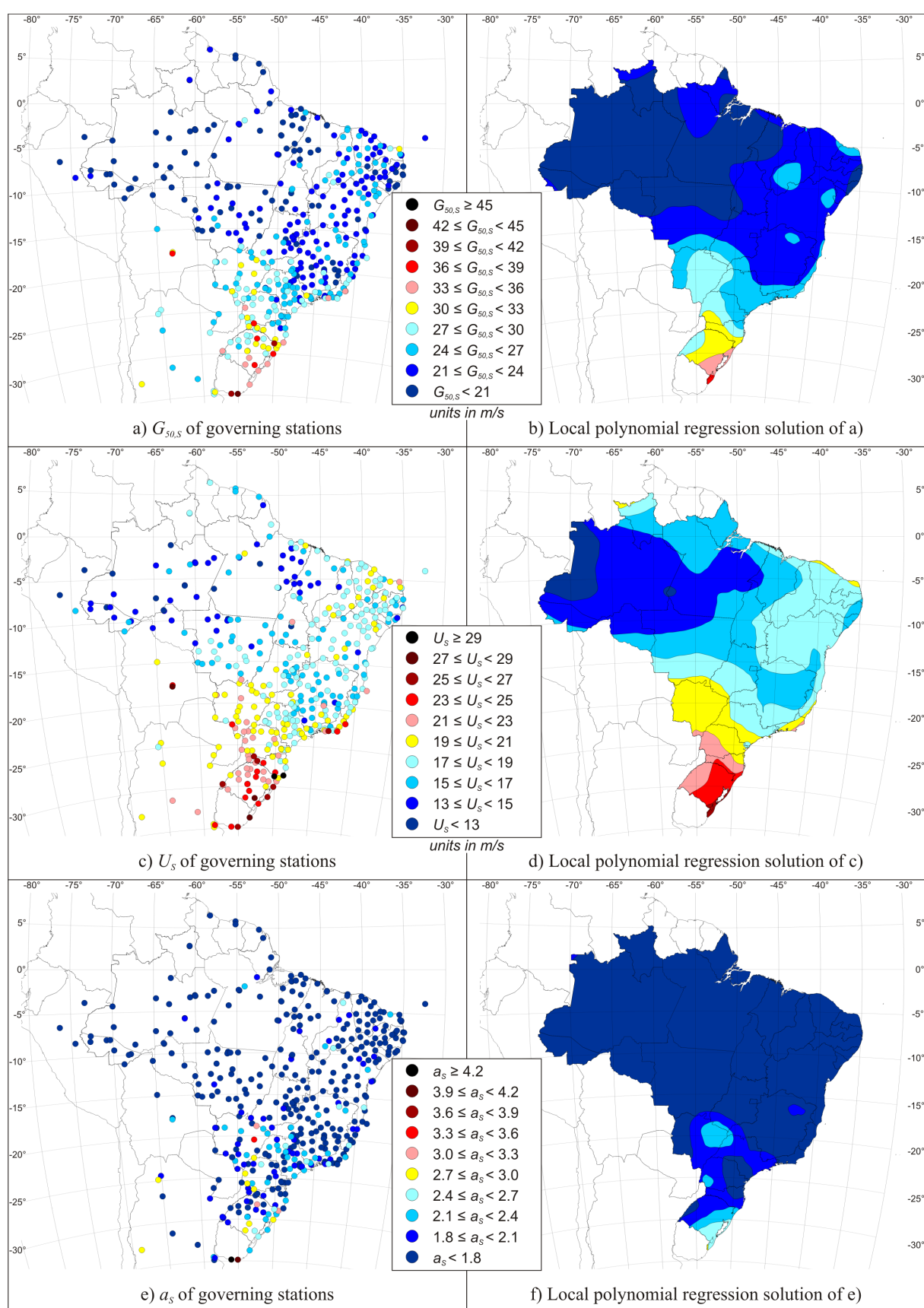


Figure 7.9 – Extreme distribution parameters of governing stations for synoptic extreme winds (S): $G_{50,S}$, U_s and a_s .

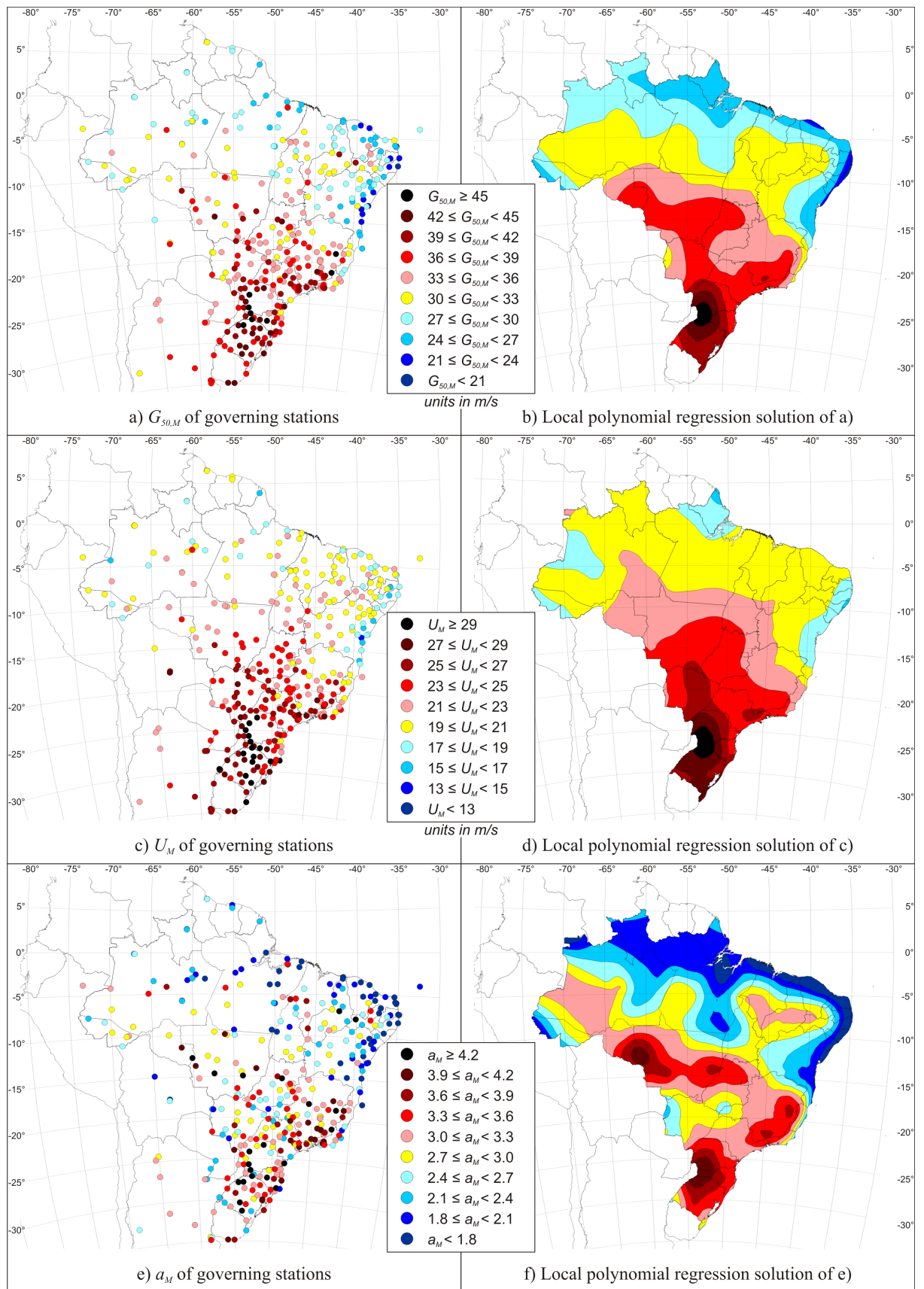


Figure 7.10 – Mixed extreme distribution parameters of governing stations (M): $G_{50,M}$, U_M and a_M .

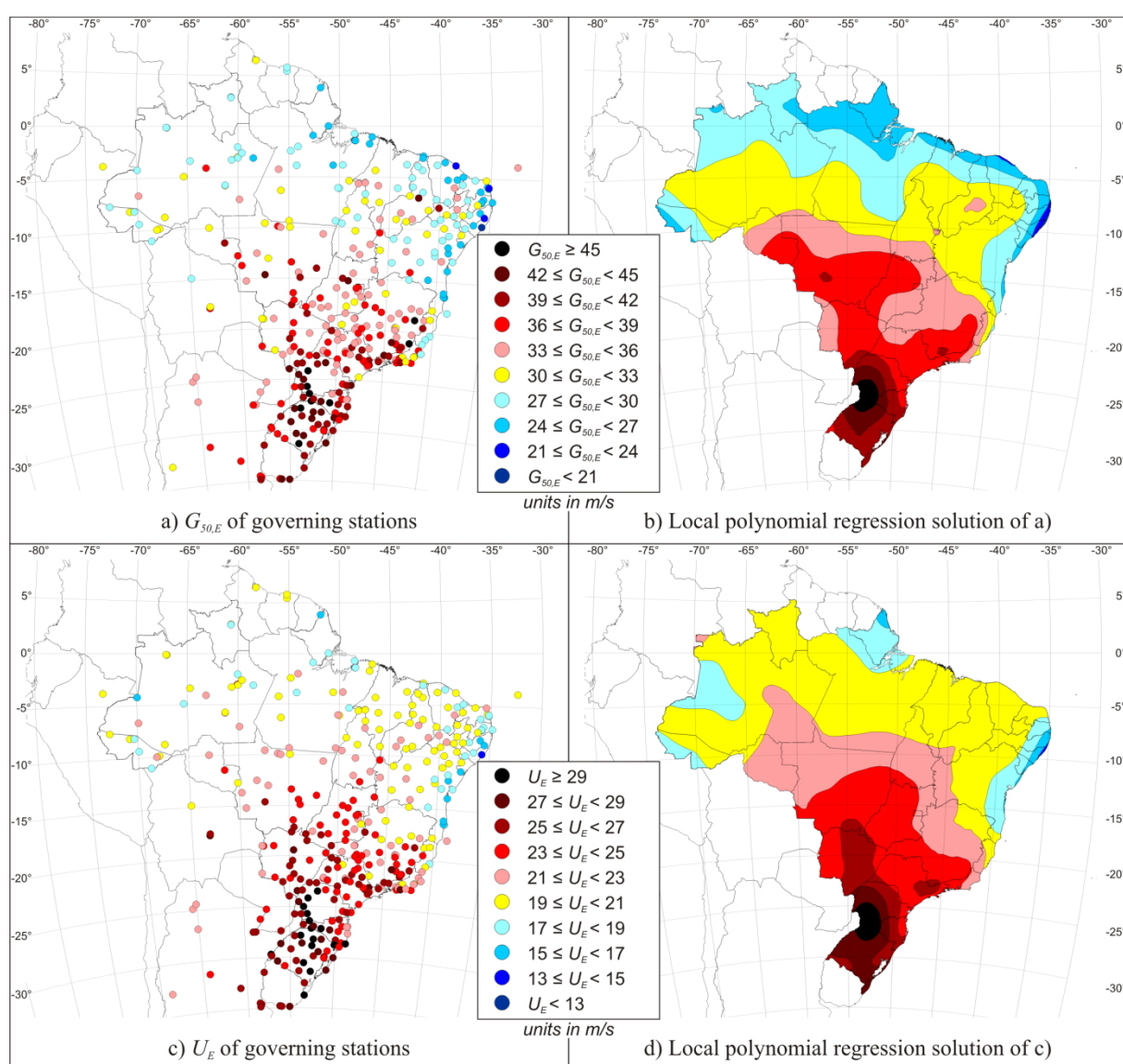


Figure 7.11 – Envelope extreme distribution parameters of governing stations (E): $G_{50,E}$ and U_E .

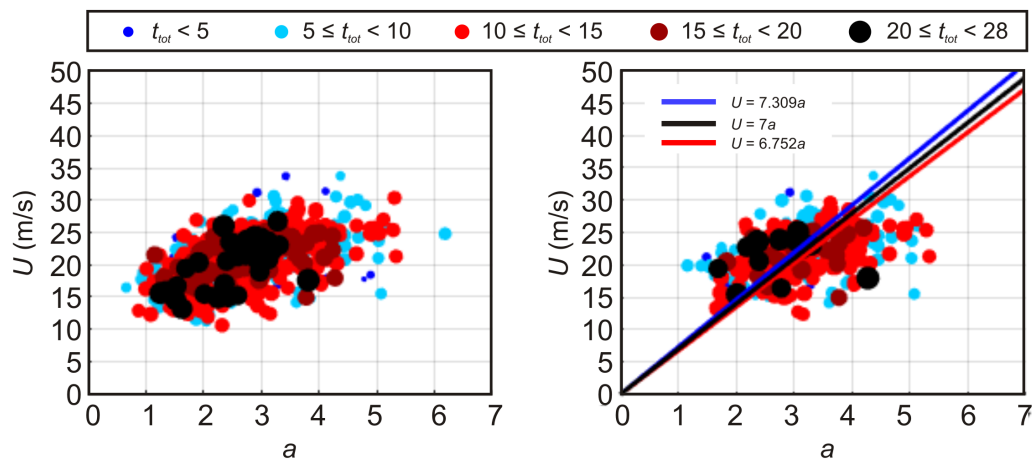


Figure 7.12 – Non-synoptic U vs a (N), for all SWS (left) and set of governing SWS (right).

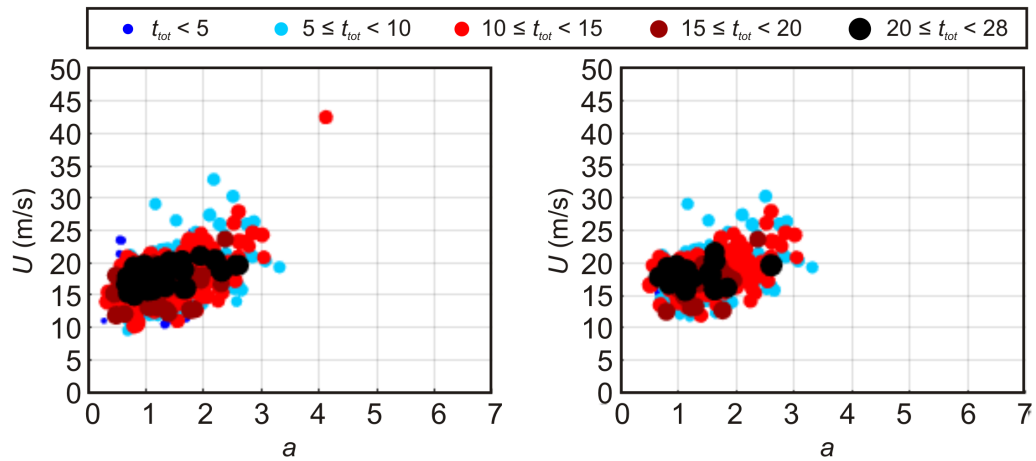


Figure 7.13 – Synoptic U vs a (S), for all SWS (left) and set of governing SWS (right).

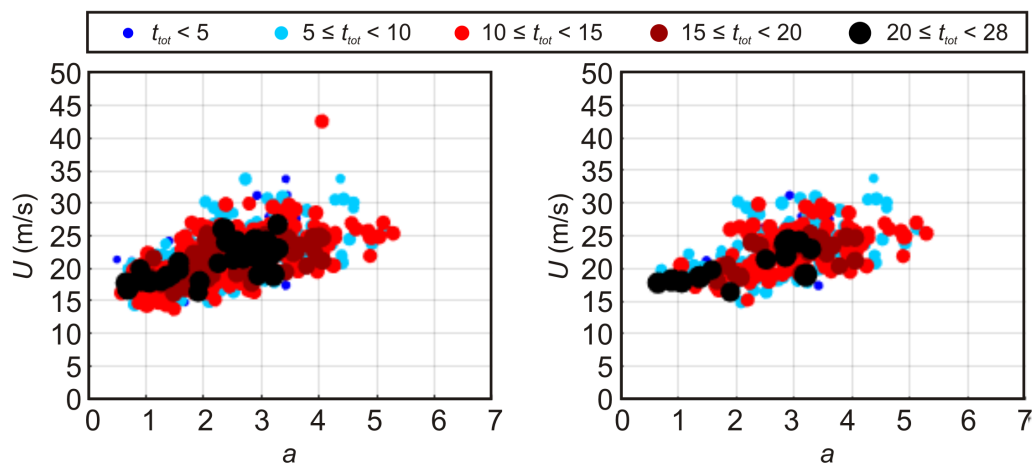


Figure 7.14 – Mixed U vs a (M), for all SWS (left) and set of governing SWS (right).

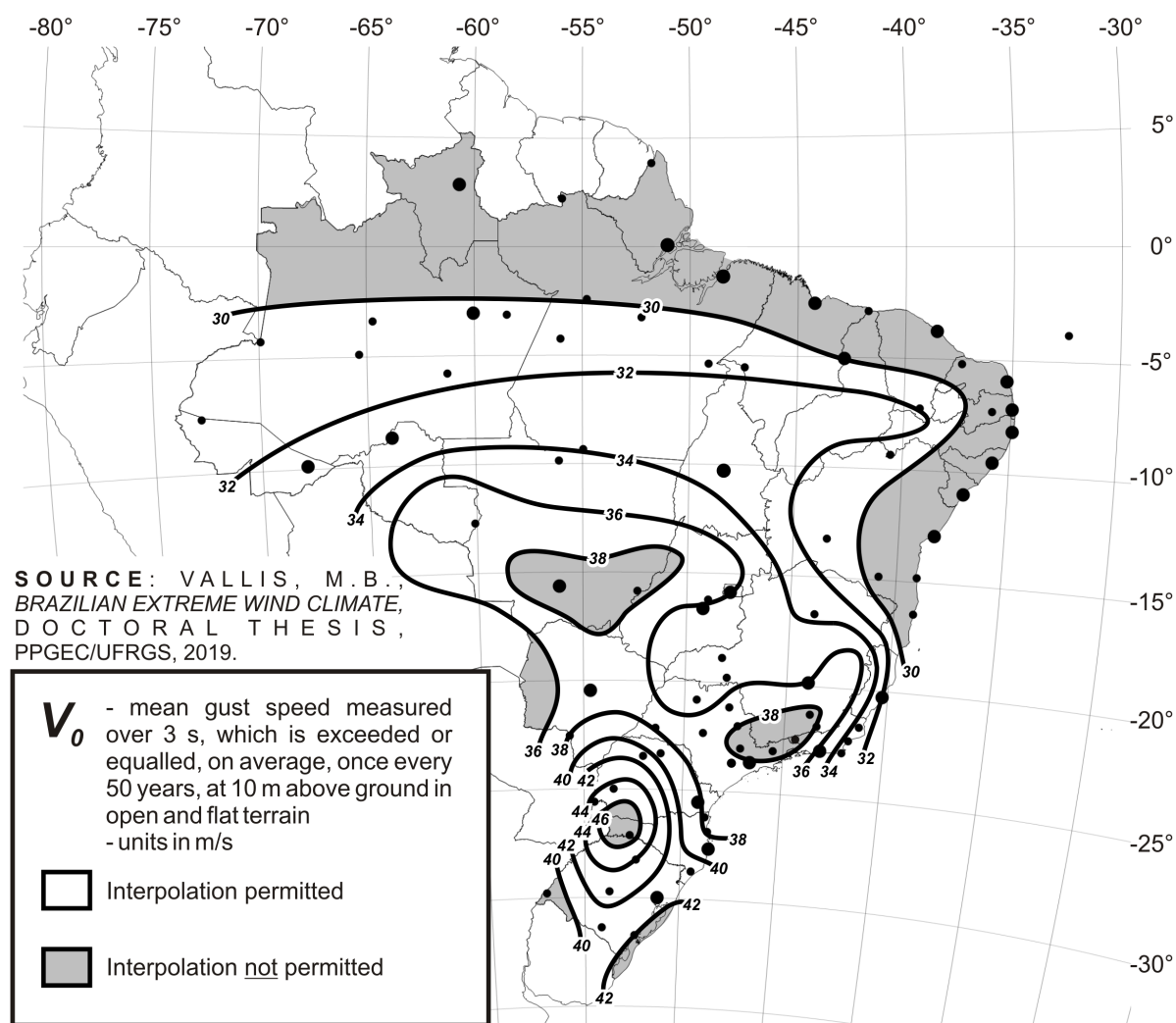


Figure 7.15 – Proposed V_0 isopleth map for NBR 6123.

$$S_3 = \frac{1}{10.9} \left\{ 7 - \ln \left[- \frac{\ln(1 - P_L)}{R_L} \right] \right\} \quad 7.3$$

Table 7.5 – Proposed probabilistic factors, S_3 , for NBR 6123.

R_L (years)	Values of S_3 for P_L					
	0.10	0.20	0.50	0.63	0.75	0.90
1	0.85	0.78	0.68	0.64	0.61	0.57
5	1.00	0.93	0.82	0.79	0.76	0.71
10	1.06	0.99	0.89	0.85	0.82	0.78
50	1.21	1.14	1.03	1.00	0.97	0.92
100	1.27	1.20	1.10	1.07	1.03	0.99
500	1.42	1.35	1.25	1.21	1.18	1.14
1,000	1.48	1.41	1.31	1.28	1.25	1.20

Despite both sets of G_{50} residuals indicating a fit which ranges from safe to optimal for the initial solution of Figure 7.8b), as shown in Figure L.3b) for $G_{50,N}$ and Figure L.4b) for $G_{50,E}$, the map of U_E residuals with respect to the initial solution, shown in a) and b) of Figure L.2, reveals two regions of the country with $U_E > 10\%$ higher than $V_{R=1}$ provided by the initial solution. The regions are Chuí at the southern extreme of Rio Grande do Sul, and a region with a radius of approximately 200 km centred at the intersection of the Pará-Mato Grosso border with Tocantins. In order to keep the same S_3 factors which are optimised for the majority of the country, adjustments were made to the V_0 map. In the south, the $V_0 = 42$ m/s contour which follows the coast of Rio Grande do Sul was extended to incorporate Chuí, initially assigned $V_0 = 40$ m/s. This raises the $V_{R=1}$ from 26 m/s to 27 m/s, which is still approximately 8% less than $U_E = U_M = 29.3$ m/s as determined for A899 – Chuí, RS. In the north, contours of $V_0 = 30$ to 34 m/s were smoothed and translated further north, resulting in an increase from $V_0 = 30$ m/s to 33 m/s for the region around which intersects Pará, Mato Gross and Tocantins. These changes resulted in elimination of both $e > 10\%$ for U_E as shown in Figure L.2d). Although e remains between 5-10% in some regions of the country for U_E , the residuals of these regions are negligible when considering e of $G_{50,E}$.

The same four cases of residuals mapped in Appendix L are plotted against the sampling period of each station, t_{tot} , in Figure 7.16 to Figure 7.19. Means (solid lines) and mean ± 1 standard deviations (broken lines) are also plotted in each of the figures. Individual stations which are significantly higher than the proposed model are identified in each plot. A845 – Moro da Igreja, SC, A610 – Pico do Couto, RJ, and A652 – Forte de Copacabana, RJ, are undoubtedly affected by significant topographic effects, while the other anomalous stations deserve further investigations to determine the motivating factors responsible for their spurious extreme value distributions. The aerodromes SBBE – Belém, PA, and SBEG – Manaus, AM, are two stations with the longest sampling times, $t_{tot} = 17.1$ and 19.0 years respectively, which are identified as having significantly high residuals: SBEG with U_N and U_E approximately 25% higher than the proposed solution, and SBBE with $G_{50,N}$ and $G_{50,E}$ approximately 20% higher than the proposed solution.

Figure 7.20 and Figure 7.21 serve as summaries of Figure 7.16 to Figure 7.19, indicating the percentage of stations within each e range for t_{tot} brackets of 5-year intervals, with exception for the $20 \leq t_{tot} < 28$ -year bracket. In all figures from Figure 7.16 to Figure 7.21, the use of t_{tot} weightings to select the set of governing stations is responsible for the decrease of mean

residuals, i.e. greater conservatism, for longer serving stations. Considering $t_{tot} = 10$ years as the median sampling period, mean and standard deviation residuals are -5% and 13% for U_N of all stations, and 0% and 8% for U_E of governing stations. For G_{50} , the corresponding values are -10% and 10%, and -1% and 9% respectively. These residuals indicate the good fit of the proposed model to the governing set of stations for the envelope distribution, and conservativeness when considering all stations.

Comparisons between the residuals of Padaratz (1977), the current V_0 map of NBR 6123 (ABNT, 1988), Holmes (2002) in the determination of Region A of AS/NZS 1170.2 (2011), and Pintar et al. (2015) in the determination of $R = 700$ -year non-hurricane basic wind speeds of ASCE-7 (2016) are made in Figure 7.22. Padaratz (1977) derived Fréchet distribution parameters β_i and γ_i for each of the 49 stations analysed, with sampling periods ranging from 2 to 25 years. A single weighted-average, γ_{mp} , was then determined from 20 stations and applied to extreme value models of all stations to determine wind speeds for G_{50} , which was then plotted and smoothed to form the contour map. Figure 7.22 shows approximately 45% of stations generated G_{50} greater than $1.05 \times V_0$ as defined in the isopleth map of NBR 6123 (ABNT, 1988). This percentage is reduced to approximately 15% when G_{50} is determined using the same γ_{mp} at all stations. Holmes (2002) analysed 43 stations in Australia's non-TC region, an area comparable to approximately 80% of Brazil's territory, with an average of $t_{tot} = 37.5$ years per station, to derive a single regional wind climate. Differences between station models and Region A wind climate were minimal, with 50% of stations generating G_{50} within $\pm 5\%$ that of the zone, as indicated in Figure 7.22. Similarly, 55% of stations generated non-hurricane G_{700} within $\pm 5\%$ of the mapped solution in Pintar et al. (2015), which used data from 575 stations with a minimum sampling period of 15 years to wind speeds for varying R across the contiguous United States (ASCE-7, 2016). For $R = 700$ years, the basic wind speed ranges from 40 to 51 m/s; for $R = 50$ years, the range is from 33 to 41 m/s.

Considering total column of the e (G_{50}) plot in Figure 7.21, 87% of all stations have $G_{50,N}$ values which are less than $1.05 \times V_0$, curiously the same proportion as Padaratz (1977) for γ_{mp} and Holmes (2002). This proportion drops to 80% when considering the governing set of stations for $G_{50,E}$, for which 40% of stations fall in the optimal $-5\% \leq e < 5\%$ range. Despite this, approximately 10% of governing stations are greater than $1.10 \times V_0$ for $G_{50,E}$, which halves to 5% when considering $G_{50,N}$ of all stations, indicating a small element of risk with the proposed V_0 of Figure 7.15.

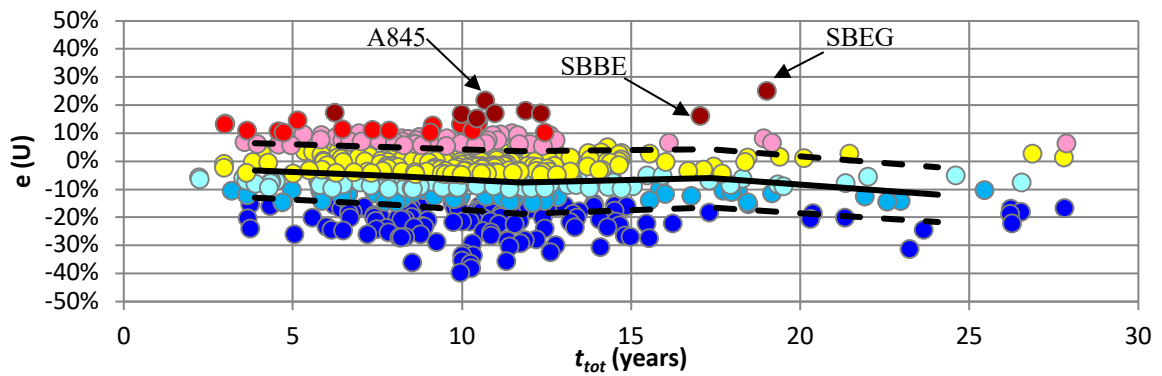


Figure 7.16 – U_N residuals of all stations expressed against sampling period t_{tot} (years).

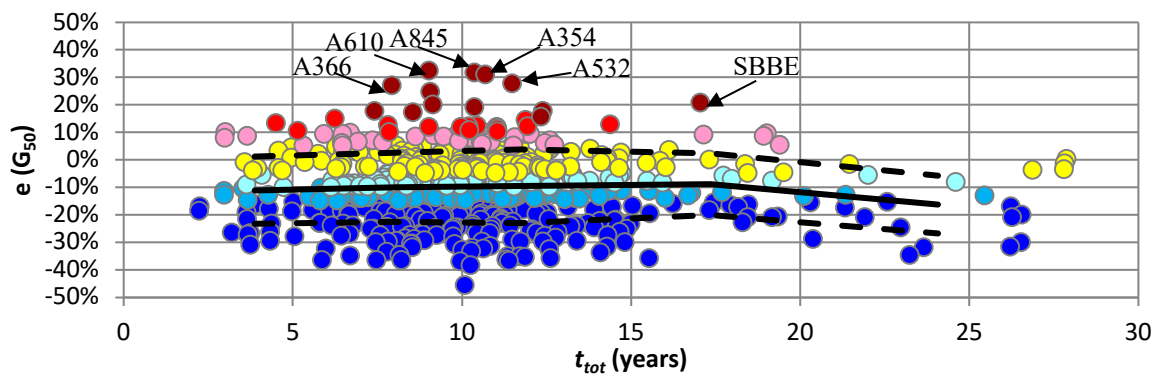


Figure 7.17 – $G_{50,N}$ residuals of all stations expressed against sampling period t_{tot} (years).

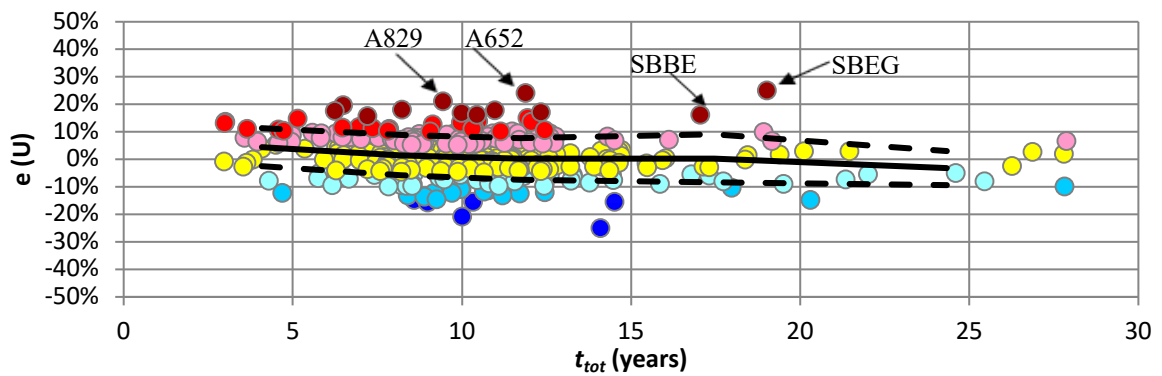


Figure 7.18 – U_E residuals of governing stations expressed against sampling period t_{tot} (years).

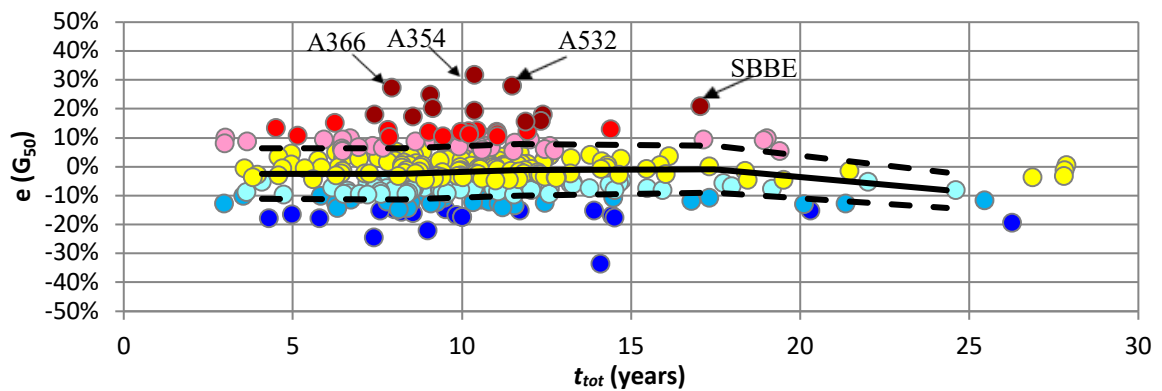


Figure 7.19 – $G_{50,E}$ residuals of governing stations expressed against sampling period t_{tot} (years).

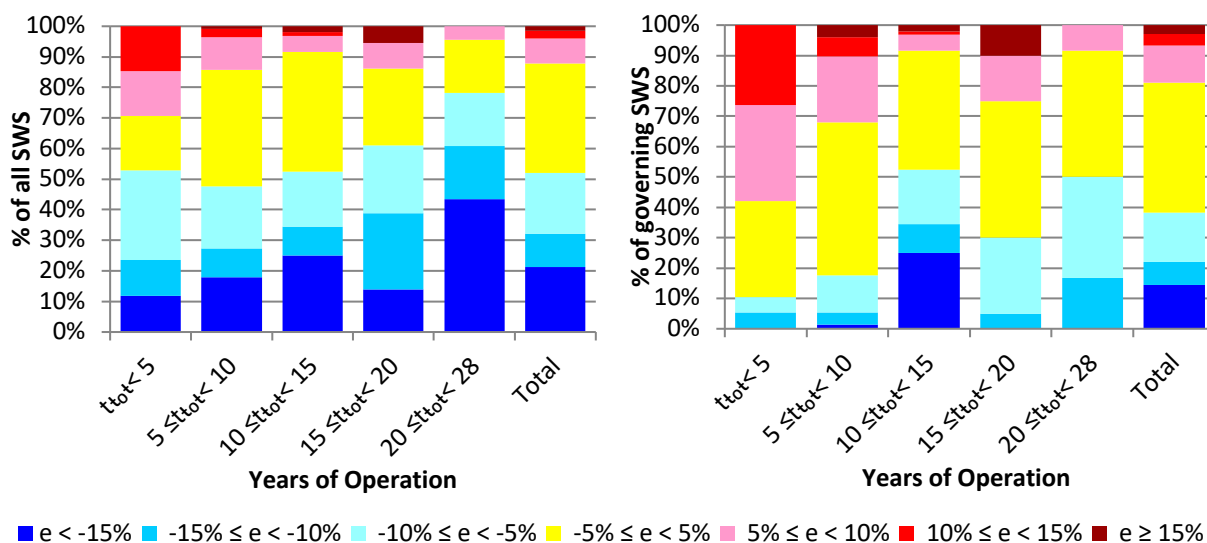


Figure 7.20 – Percentage of stations per range of e (U): non-synoptic wind speeds for all SWS (left) and envelope wind speeds for governing stations (right).

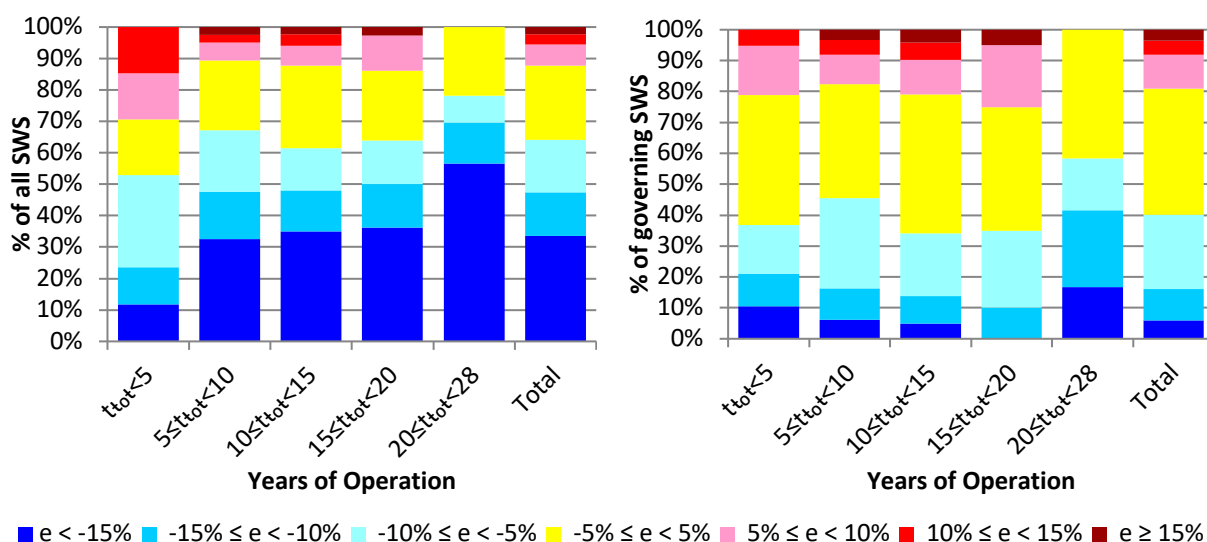


Figure 7.21 – Percentage of stations per range of e (G_{50}): non-synoptic wind speeds for all SWS (left) and envelope wind speeds for governing stations (right).

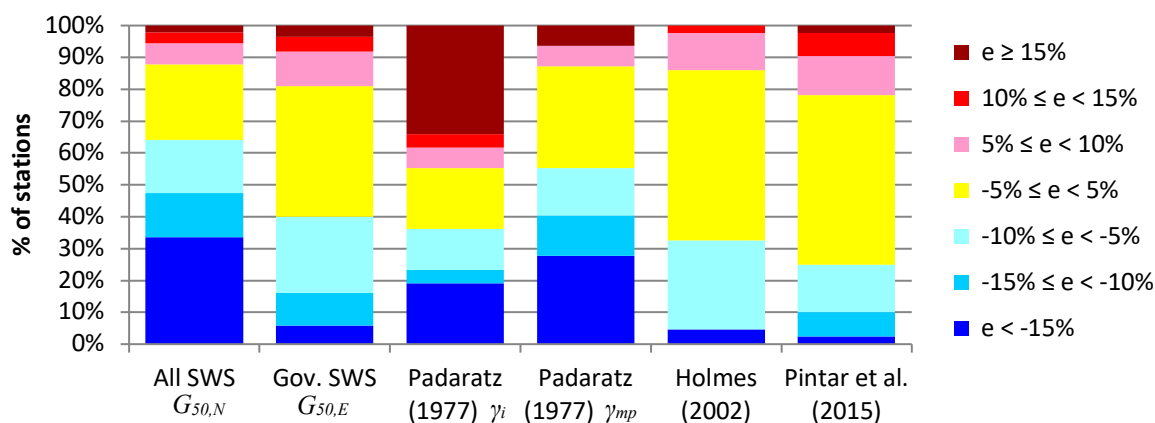


Figure 7.22 – Distribution of e (G_{50}) compared to other studies [e (G_{700}) for Pintar et al., 2015]

The maximum homogenised gust, G_{cor} , recorded at each SWS was compared to the proposed V_0 of Figure 7.15. The error between the two, ε , is expressed as a percentage with respect to V_0 and mapped in Figure 7.23. The map can be interpreted as a warning to users who may wish to further reduce V_0 from that proposed in Figure 7.15. For the majority of locations across the country, a gust of at least $0.85 \times V_0$ was registered at meteorological station within 100 km for the sampling period analysed in this study (which ranges from 3 to 28 years). Approximately 50% of all stations registered a maximum gust which was 80% or more than the proposed V_0 , and 7% of all stations registered maximum gusts which were equal to, or greater than, V_0 . The station, location, date, hour, wind speeds and directions of maximum gusts which equaled or exceeded proposed V_0 are given in Table 7.6. With the exception of the event at A845 – Morro da Igreja, SC, all events were classified as non-synoptic in origin.

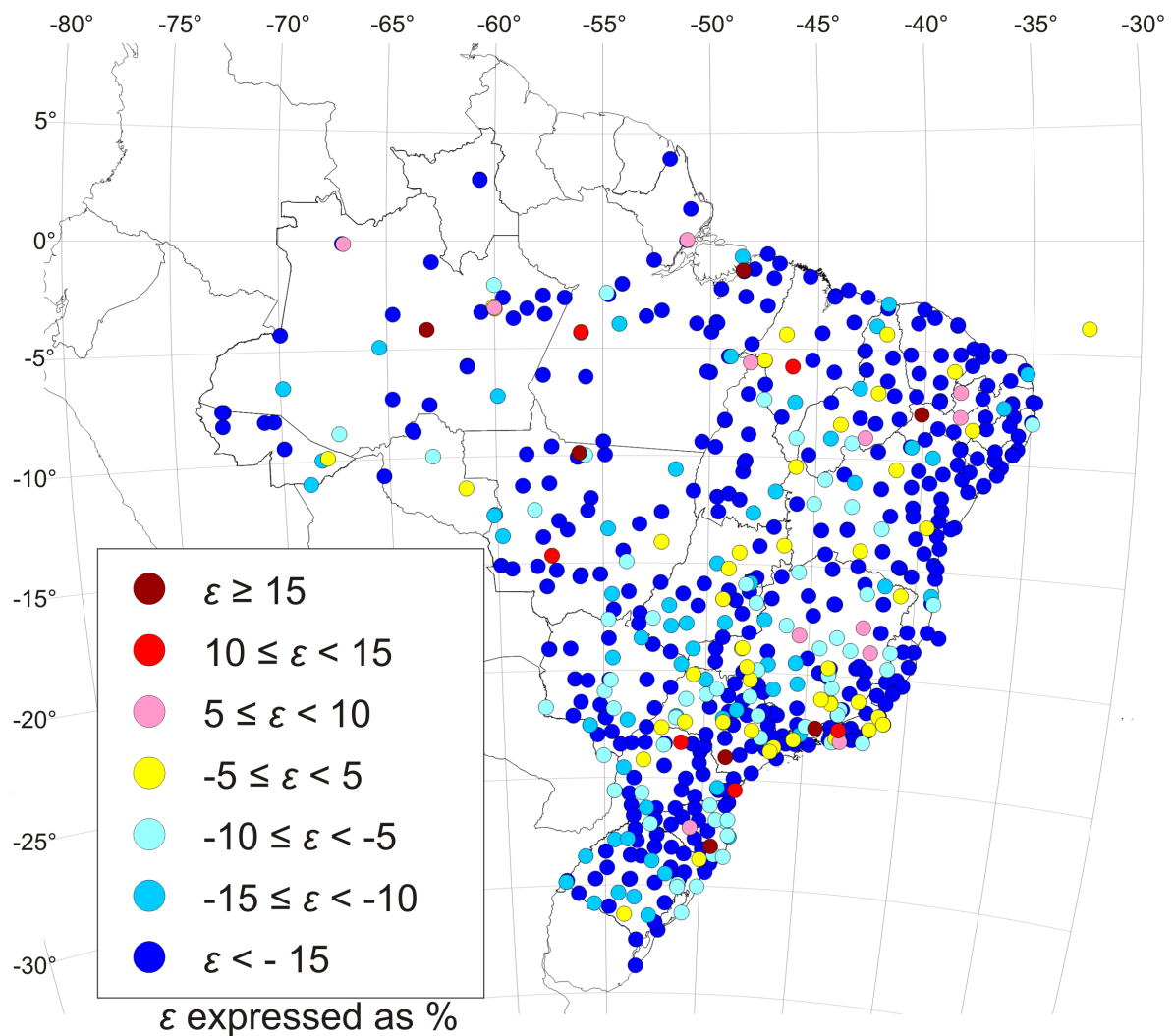


Figure 7.23 – Difference between most extreme qualified G_{cor} gust speed at individual SWS for study period and V_0 defined in Figure 7.15.

Table 7.6 – Details of the most extreme qualified G_{cor} gust speeds at individual SWS which were equal to, or greater than, V_0 as defined in Figure 7.15 ($\varepsilon \geq 0\%$).

Station ID	WMO ID	City, State	Date	Hour (UTC)	DIR (°)	V_{obs} (m/s)	G_{obs} (m/s)	G_{cor} (m/s)
A044	81821	Araguatins, TO	13/11/2010	04:00	220	3.3	32.6	34.7
A101	81730	Manaus, AM	30/09/2013	16:00	117	5.8	25.5	31.9
A117	81770	Coari, AM	25/10/2012	21:00	147	2.2	33.9	36.1
A207	81823	Grajaú, MA	06/02/2013	21:00	53	2.6	32.1	35.7
A238	81788	Buritcupu, MA	21/10/2016	21:00	69	4.2	29.1	30.0
A333	81774	São Gonçalo, PB	08/02/2018	03:00	29	1.8	31.4	33.4
A345	81989	São Raimundo Nonato, PI	27/11/2015	00:00	291	4.2	31.2	33.2
A349	81954	Ibimirim, PE	12/04/2011	19:00	142	5.1	29.5	30.4
A350	81912	Serra Talhada, PE	21/01/2012	23:00	216	4.8	31.5	33.5
A354	81869	Oeiras, PI	01/01/2013	22:00	62	2.9	32.5	32.5
A366	81910	Ouricuri, PE	30/12/2014	21:00	45	11.5	39.1	39.1
A426	86694	Guanambi, BA	17/10/2013	22:00	104	9.2	30.8	30.8
A434	86675	Amargosa, BA	25/02/2010	16:00	278	5.1	29.4	31.3
A514	86849	São João Del Rei, MG	16/11/2008	23:00	198	5.6	38.7	39.9
A517	86852	Muriaé, MG	05/12/2007	20:00	143	5.6	33.2	38.6
A528	86779	Três Marias, MG	04/01/2015	01:00	263	2.8	37.2	38.4
A532	86783	Governador Valadares, MG	04/02/2010	23:00	59	13.7	37.4	38.6
A541	86761	Capelinha, MG	20/11/2010	18:00	142	11.7	34.7	35.8
A609	86874	Resende, RJ	03/11/2008	21:00	93	11.5	43.0	45.7
A610	86876	Pico do Couto, RJ	17/12/2012	19:00	303	10.8	35.5	41.3
A652	86887	Forte de Copacabana, RJ	06/01/2017	00:00	302	13.4	28.2	38.1
A714	86905	Itapeva, SP	27/11/2012	21:00	140	5.3	41.7	44.4
A726	86868	Piracicaba, SP	21/07/2013	19:00	214	11.0	35.7	38.0
A728	86911	Taubaté, SP	27/10/2017	20:00	199	12.6	37.6	37.6
A829	86967	São José dos Ausentes, RS	29/10/2007	00:00	353	7.9	38.4	40.9
A845	86968	Morro da Igreja, SC	13/04/2008	18:00	294	27.2	49.7	52.9
A847	86935	Ilha do Mel, PR	24/12/2008	20:00	114	3.3	38.9	43.2
A860	86956	Curitibanos, SC	21/07/2011	06:00	176	6.9	43.3	44.6
A902	86682	Tangará da Serra, MT	15/10/2014	21:00	222	3.6	39.9	42.4
SBAT	82965	Alta Floresta, MT	23/10/2015	20:30	140	23.7	38.6	40.2
SBBE	82193	Belém, PA	17/09/2004	19:20	360	7.7	31.9	34.7
SBBQ	83118	Barbacena, MG	02/10/2015	20:14	240	23.1	37.6	39.5
SBBU	83722	Bauru, SP	12/01/2019	19:38	50	15.4	33.4	37.5
SBCF	83566	Confins, MG	27/07/2015	20:00	240	22.6	35.5	37.3
SBEG	82333	Manaus, AM	02/10/2003	19:40	140	15.4	30.9	30.9
SBGO	83424	Goiânia, GO	21/12/1997	14:50	360	30.9	36.0	36.3
SBIH	82444	Itaituba, PA	20/09/2011	22:00	270	25.7	30.9	34.1
SBLO	83768	Londrina, PR	20/11/2017	20:00	200	16.5	41.7	43.2
SBMQ	82099	Macapá, AP	19/04/2013	18:48	100	27.3	32.4	32.4
SBUA	82107	São Gabriel da Cachoeira, AM	08/08/2005	20:05	80	7.2	27.8	31.6

The sampling periods, t_{tot} , of all governing stations for N and S distributions are shown in Figure 7.24, which indicates a strong reliance on stations with lifespans in the range of $5 \leq t_{tot} < 15$ years and monthly observation rates greater than 90%. Type N contours of Figure 7.8 were determined from a 81/19 split between INMET ASWS and aerodrome SWS, with a similar 84/16 split for Type S contours of Figure 7.9. With the dominance of INMET ASWS over aerodrome SWS, there is a negligible effect of anemometer equipment on overall results due to the use of only two types of anemometers by INMET ASWS, both highly sensitive and with low distance constants. Additionally, digital processes have always been in use at INMET ASWS while the same is not true at aerodrome SWS. Figure 7.25 shows the majority of 45° sectors of contributing stations are exposed to roughness of CAT II to III.

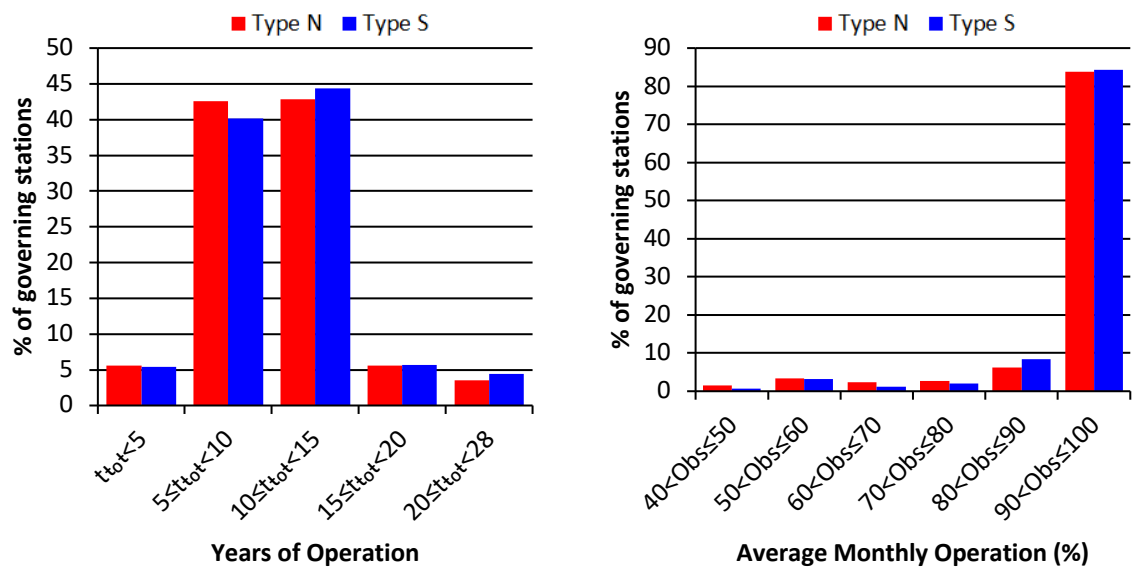


Figure 7.24 – Governing stations per range of t_{tot} (left) and $Obs.$ (right).

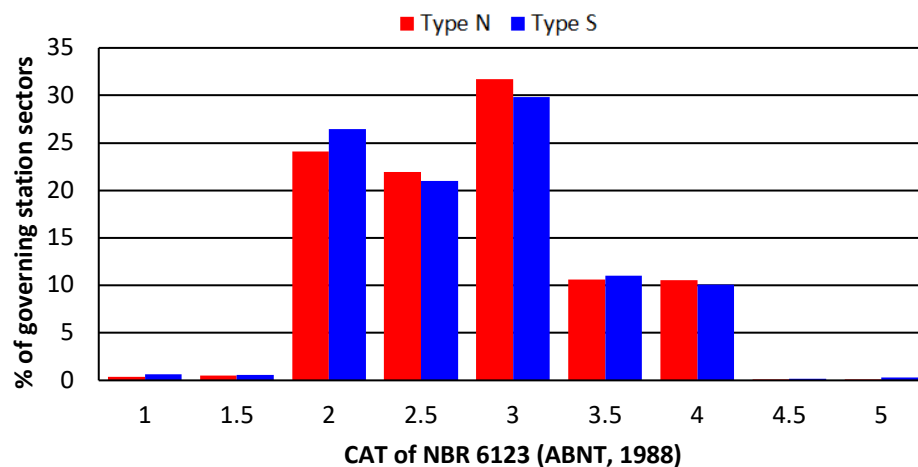


Figure 7.25 – Terrain categories of 45° sectors of governing stations.

8. CONCLUSIONS AND RECOMMENDATIONS

8.1 SUMMARY

A study was performed to determine the extreme wind climate of Brazil. Fundamental concepts of wind engineering were reviewed, including ABL wind characteristics, progress in the understanding of non-synoptic winds for civil engineering applications, measurement of wind and gusts, and extreme value analysis techniques. Attempts to obtain historical metadata, fundamental to the establishment of baseline parameters, at all stations achieved limited success. Several meteorological datasets were examined from both aerodrome and INMET surface weather stations. Wind speed time-series, on which the extreme value analysis was based, were first subjected to rigorous quality assessment processes to identify periods of operation not consistent with baseline characteristics of each station. Such periods were then deactivated or discarded from further analyses. Gust speeds were corrected to a height of $z = 10$ m in open, flat field conditions as defined by CAT II of NBR 6123 (ABNT, 1988). Algorithms were developed to identify and discard suspected false peaks, in addition to separating peak gusts by storm type. A modified version of the ESDU (1990[a]) Method of Independent Storms extreme value analysis, referred to as BR-MIS, was developed for short sampling periods and time-series with discontinuities. The BR-MIS technique was applied to extreme value sets of synoptic and non-synoptic speeds at all appropriate locations, with model parameters determined using least-squares linear regression. A set of governing stations were selected by the objective removal of stations which underreported extreme value parameters. The proposed V_0 map and accompanying S_3 values were based on the dominant non-synoptic extreme wind climate. Contours were derived using local polynomial regression and adjusted in two regions to reduce significant errors for low mean recurrence intervals. Alternative zone solutions were also provided based on preliminary versions of meteorological data for which a number of extreme wind events at INMET stations were not present. A website was set-up to facilitate access to results on a station by station basis.

8.2 EXTENDED CONCLUSIONS

The notion that wind data provided by third-parties, official government organisations or not, are “ready-to-use” was discredited in this study. Not all data are alike, with several factors influential in the processes preceding climatological studies. A *wind data chain*, shown in Figure 8.1, shows these factors in approximately the same order as they occur.

1. Gust factors, turbulence intensities and vertical profiles of horizontal wind speeds vary between synoptic and non-synoptic winds and storm-specific corrections may be necessary to homogenise wind speeds. In assuming different turbulence intensities, Holmes et al. (2018) used different correction factors for synoptic and non-synoptic wind speeds when converting to a gust time-averaging interval of $\tau = 0.2$ s. No such action was taken in this study.
2. Surrounding topography may accelerate wind speeds at the measurement site, or reduce wind-speeds if located in a valley. Topographic effects were not analysed in this study, but may affect even anemometers at aerodromes such as SBCF – Confins, MG, which is located above escarpment with inclination of 15% to the southwest.
3. Upwind terrain surface roughness determines the vertical profiles of horizontal wind speeds. Sectors with a fetch length of 500 m were analysed by visual inspection with correction factors determined from S_2 of NBR 6123 (ABNT, 1988).
4. Location of anemometers on top of buildings and near large obstacles distorts the wind flow. No analysis was conducted to identify and correct data from anemometers affected by near-field distortion, but periods of operation for which anemometers were located above buildings were deactivated from analysis.
5. The anemometer height above ground directly affects the observation of wind speeds, with higher masts resulting in observations of greater magnitudes. INMET ASWS are all installed at 10 m, but heights of those at aerodrome SWS vary between 5.5 m and 11 m with many remaining unknown.
6. Interference from rain, hail, fog, birds and thunderstorms can alter wind speed readings – typically causing error messages or spurious readings. The extent to which data used in this study were affected is unknown.
7. Dynamic characteristics of mechanical anemometers filter high-frequency fluctuations. Due to lack of historical and current information on anemometer types at

-
- aerodrome SWS, the overall impact remains unknown. Of metadata received for a fraction of all aerodromes no heavy cup anemometers ($d > 5$ m) were encountered.
8. Observing processes, whether conventional or digital, impact heavily on the accuracy of observed wind speeds. Attempts were made to reduce the impact of conventional observations and limit gusts to only those acquired for a moving average of $\tau = 3$ s.
 9. Interference by humans occurs on several levels and is not always a negative factor in the chain. Even for digital observation processes at aerodrome SWS, operators are still able to edit meteorological reports before issuance. Cases of manual censoring of extreme wind speeds were documented in the study.
 10. Coding of observation and transmission. Errors in the preparation of the report, parsing errors, updated *COR* reports (aerodromes), transferral from paper tables to digital databases, and transmission lag of weeks (INMET) can be influential on the make-up of datasets.
 11. Data can be corrupted or lost by data servers when in storage. INMET Web data of 2010 to 2011 stored on local servers were wiped, data at two INMET stations were somehow swapped in the SADMET dataset, and wind direction data was swapped with wind speed data for several aerodromes in ICEA's BDC.
 12. Decoding of observations and use. Examples of failures of automated data extraction routines by third-party databases were documented and a semi-automated approach was taken in this study. The final application of the data and processes used to identify spurious data varies between users.

Efforts should be made to simplify the algorithms developed in this study, particularly for aerodrome SWS. One possibility is restricting the algorithm to only the most frequently taken paths, with manual classification used for the rest, however such an approach would increase processing time and require more work from the operator. The neglecting of all events without an observed gust is also another option, however many years of data would be omitted due to the late adoption of digital processes at many South American aerodromes. The algorithm developed for SWS aerodrome stations has the potential to be used at any location in the world but is only applicable to wind speed observations made in knots.

Limitations of the synoptic vs non-synoptic classifying system are apparent, particularly regarding the separation of frontal systems from long-duration convective storms. The approach of this study is biased to the classification of long-duration extreme winds with

constant wind direction as synoptic. However, long-lived (active) outflows can be maintained by a sequence of transient surges of strong convective winds that could sustain a non-ABL profile for long periods.

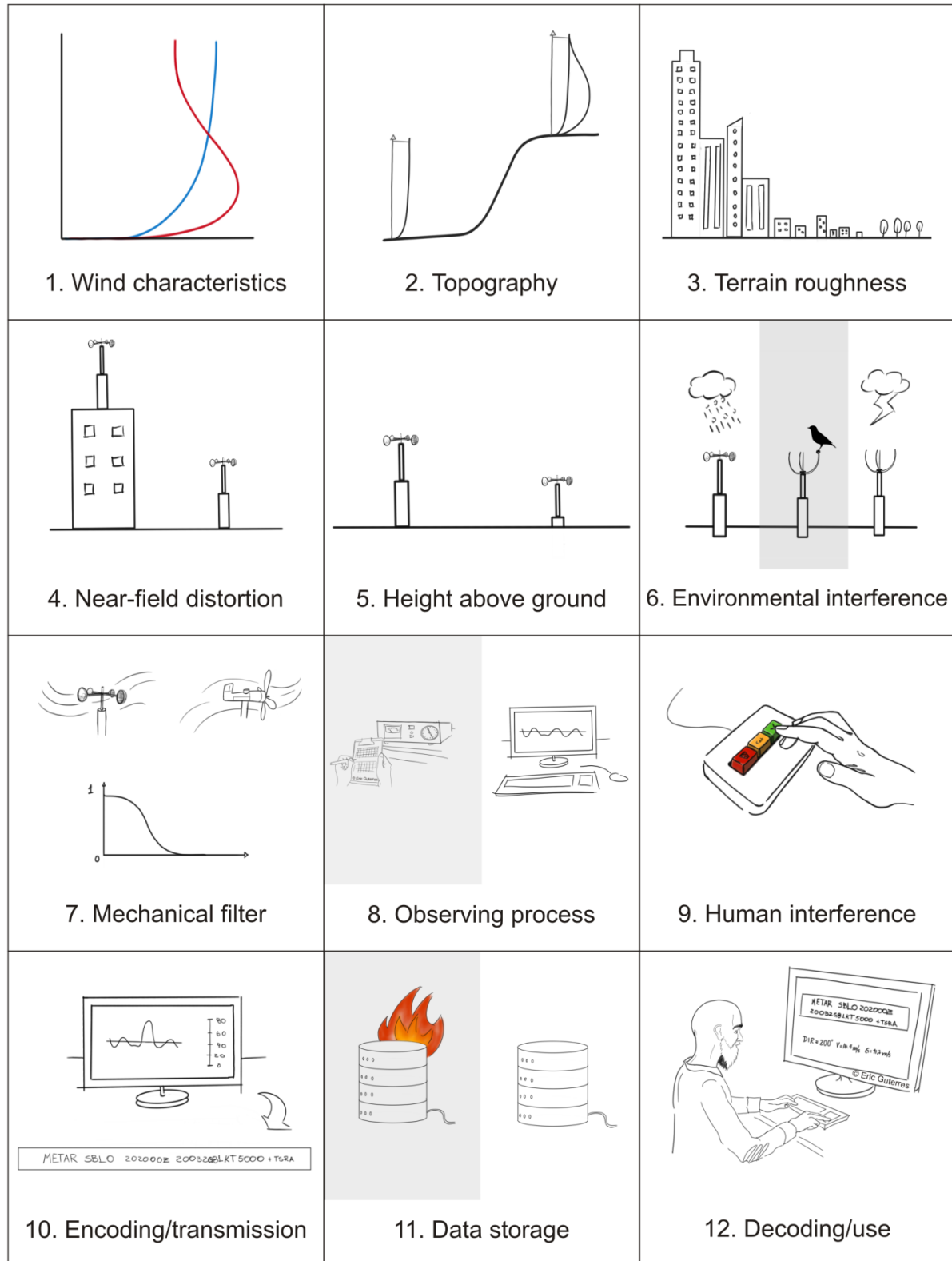


Figure 8.1 – Wind data chain (Illustration provided by Eric Haddad Parker Guterres).

As such, it is important to understand the possible impacts of the misclassification of storm type on an extreme values analysis. For A831 – Quaraí, RS, the “misclassified” event of Figure D.19 ($G_{obs} = 26.5$ m/s) is the top ranked synoptic and 11th ranked overall independent storm for the site in terms of gust speed, with the most extreme non-synoptic and overall event that of Figure D.23 ($G_{obs} = 32.0$ m/s). This example is representative for the study region which exhibits dominance of short-duration non-synoptic events. The bias towards the classification of intermediate events as synoptic is considered a case of “stealing from the rich to give to the poor” and is considered a conservative approach for structures above 20 m in height. However, this may not necessarily be true for other regions of the world. In terms of extreme value distributions, taking mid- to low-extreme values from one set to become high values in a second parallel set has the effect of increasing model wind speeds for long periods (> 20 years) for both sets, but reduces the wind speeds for low periods (1-5 years) of the first set.

Regardless of the above justification, efforts should be made to develop and establish clear criteria for the definition of non-synoptic and synoptic (ABL) winds for temporally low-resolution meteorological data acquired at surface weather stations. In addition to the approach taken by this study, three other possible avenues are suggested. 1. More rigorous analysis of individual events with the use of additional tools such as weather satellite and radar imagery and lightning mapping, 2. The classification of long-duration frontal events as non-synoptic classification, as per Holmes et al. (2018), 3. The introduction of a third extreme wind category for gust fronts, as per Kasperski (2002) and De Gaetano et al. (2014).

The establishment of western Paraná, Santa Catarina and Rio Grande do Sul as the region with the most extreme non-synoptic wind climate by this study is consistent with Ferreira and Nascimento (2016[b]), which determined the region to experience the highest frequency of convectively induced gusts above 25 m/s. Data from INMET ASWS indicate lower mean R_{+3} ratio of peak events in the region in comparison to the rest of the country, suggesting squall lines and long duration MCS are responsible for regional destructive winds, also in good agreement with studies by Laing and Fritsch (1997), Zipser et al. (2006) and Ferreira and Nascimento (2016[b]). Trends in mean temperature and changes in temperature and pressure are no different in this region of $V_0 = 44-46$ m/s to those of neighbouring regions of $V_0 = 40-44$ m/s.

The main difference between the severity of non-synoptic winds in the tropics (north Brazil) and midlatitudes (south Brazil) is due to the lack of strong vertical wind shear in the tropics. Additionally, convection in the tropics stabilises the environment much quicker than large-scale processes can act to destabilise the atmosphere, meaning the instability caused by heat at low-levels in the atmosphere is released shortly after its creation. In midlatitudes, the instability is not always released immediately and can be stored in the environment for up to several days. Severe convection is the result of a long build-up which ends with an explosive release of the instability (Emanuel, 1994; apud Doswell, 2001).

8.3 RECOMMENDATIONS

8.3.1 NBR 6123

The final results of this study are the basic wind speed map for Brazil of Figure 7.15 and associated wind climate model as proposed by Equation 7.3 and Table 7.5. The proposed V_0 map is defined by contours increments of 2 m/s for time-averaging interval of $\tau = 3$ s, return period of $R = 50$ years at a height of $z = 10$ m in open, flat terrain. V_0 speeds range from 46 m/s to 30 m/s and are strongly linked to the non-synoptic extreme wind climate of the country. In Figure 8.2, a comparison is made between the set of probabilistic factors, S_3 , which determines the wind speeds of return periods other than 50 years, of NBR 6123 (ABNT, 1988) and those proposed by this study. Proposed wind speeds for low return periods ($R < 50$ years) are higher; while wind speeds for high return periods ($R > 50$ years) are lower. This is quantified as an increase of approximately 19% in wind speeds for a mean recurrence interval of $R = 1$ year, and a decrease of 9% for a mean recurrence interval of $R = 200$ years.

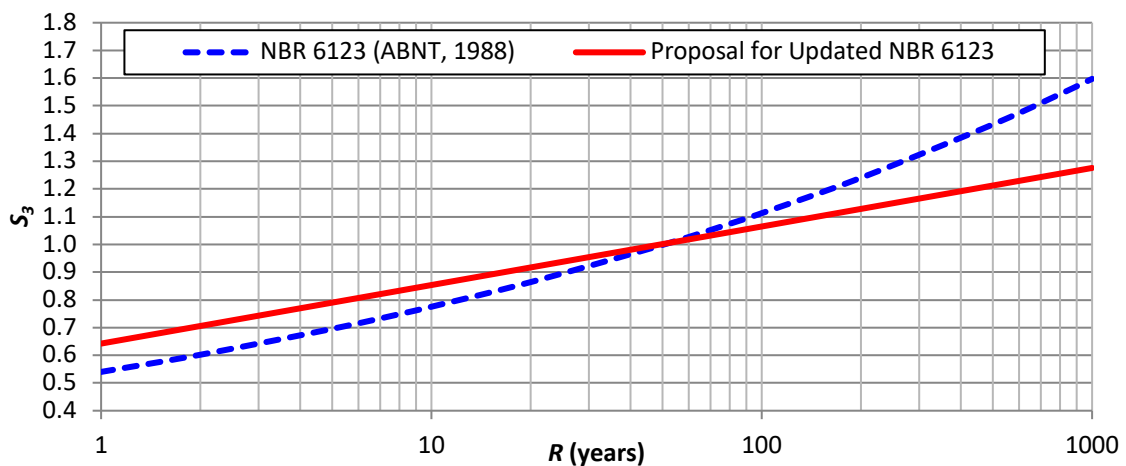


Figure 8.2 – Probabilistic factor, S_3 , of NBR 6123 (ABNT, 1988) and proposed revised S_3 .

The loading factor of $\gamma_f = 1.4$ of NBR 6118 (ABNT, 2014) is equivalent to $S_3 = 1.18$ due to the squared relationship between force and speed. This represents $R = 150$ years for the set of S_3 of NBR 6123 (ABNT, 1988), but $R = 300$ years for S_3 proposed in this study. The combination of importance factor of $S_3 = 1.1$ (ABNT, 1988), which is assigned to Group 1 buildings of critical strategic importance during a disaster, and $S_3 = 1.18$, gives $S_3 = 1.30$ which represents $R = 270$ years for NBR 6123 (ABNT, 1988), but $R = 1,300$ years for S_3 proposed in this study.

Since there is currently no widely accepted desktop methodology for the determination of non-synoptic wind loads, it may be necessary to use standard ABL approaches in conjunction with the proposed V_0 solution of Figure 7.15. However, it is estimated that for a 200 m tall building, the overall along-wind loading from downburst winds is between 5-75% less than ABL winds for the same basic wind speed (Mason, 2017). ESDU (1990[a]) suggests the use of ABL profiles up to a height of 100 m, with wind speed constant above 100 m, for the determination of non-synoptic wind loads. This may be a conservative approach for structural loads of tall-buildings, but may not adequately provide loads for low structures or pressures for façade and building envelope design.

The risks and shortcomings of the proposed V_0 map of Figure 7.15 must be considered prior to its adoption into an updated version of NBR 6123. The proposed solution does not consider the potential for a tropical cyclone. At least one tropical cyclone has made landfall in Brazil, Hurricane Catarina which hit southern Santa Catarina in 2004, but was not intercepted by any of the meteorological stations used in this study. As such, the determination of a tropical cyclone zone along the south coast may be considered necessary. The wind climate model of a tropical cyclone zone would be based on speculative assumptions rather than meteorological observations. Australia's Region B (AS/NZS, 2011) could serve as a template, as it is considered a weak tropical cyclone zone, or an intermediate zone between a moderate to severe TC zone (Regions C and D) and synoptic/thunderstorm zone (Region A). The corresponding basic wind speed of Region B is $V_{50} = 40$ m/s for $\tau = 3$ s ($V_{50} = 44$ m/s for $\tau = 0.2$ s). Furthermore, it is unknown how the exact location and extents of such a zone would be proposed or on what assumptions it would be based.

Errors between datum points (stations) and an integrated solution (V_0 map) are expected, but despite the adoption of a conservative approaches in the determination of the proposed V_0 map, some SWS extreme distributions give significantly greater wind speeds than those of the

proposed solution. The northern aerodromes of SBBE – Belém, PA, and SBEG – Manaus, AM, are two such stations. Should the errors (U_N of SBEG approximately 25% greater, and $G_{50,N}$ of SBBE approximately 20% greater than proposed solution) be considered too unconservative for these two stations with long sampling periods (19.0 years for SBEG and 17.1 years for SBBE), V_0 values for these regions will need to be increased, despite other stations in the region indicating less extreme non-synoptic wind climatologies.

The proposed V_0 map may also suffer changes due to administrative reasons. Such reasons could include the need to reduce large difference between the current and proposed solutions. Some of the largest differences proposed include a decrease in V_0 from 45 m/s to 38 m/s (-16%) at Campinas, SP, a decrease from 50 m/s to 42 m/s (-16%) at Chuí, RS, and an increase from 30 m/s to 38 m/s (+27%) in central Mato Grosso. There may be a tendency to consider the basic wind speeds determined by Padaratz (1977) as canon due to its enduring presence in the national psyche (approximately 40 years). In order to establish the proposed wind climate model of this study as an advancement of Padaratz (1977), several features of methodology used by Padaratz are here critiqued and judged inappropriate for a modern basic wind speed map. It must be remembered that data, access to information and technology were limited in 1977, and approaches adopted by Padaratz were to favour the security of Brazilian construction projects. For the same reasons, conservative approaches were made in this study in light of uncertainty regarding station metadata and filtering of real extreme events by a public agency.

In addition to the obvious advances in technology (digital and automatic acquisition and processing of data), a higher spatial resolution of stations were available for use in this study. In Brazil alone, more than 8,000 station-years were analysed for the 752 Class A stations; a maximum of 910 station-years were analysed for 49 stations by Padaratz (1977). The mid-west state of Mato Grosso covers an area of approximately 900,000 km². Only one station from Mato Grosso was available for statistical analysis in 1977, significantly less than the 39 stations used in this study.

A lack of historic wind-induced failures of structures designed using procedures defined in NBR 6123 (ABNT, 1988) could be used as an argument against the increasing of V_0 in particular regions of the country. Despite the practical validity of the argument, it does not consider that the incident wind model of NBR 6123 (ABNT, 1988) is an ABL model and may vary greatly from a non-synoptic model which would be more appropriate for Brazil. There is

also the possibility that processes in the wind-loading chain of NBR 6123 (ABNT, 1988) are conservative by nature, deliberate or not. Two keys elements in this chain were identified in this study and are the errors in the definition of gust factors and turbulence intensities. Additionally, the use of prescribed loading factors, such as $\gamma_f = 1.4$ of NBR 6118 (ABNT, 2014), could also be responsible for the prevention of failures in regions whose current V_0 is significantly less than what is proposed in this study.

Whether intentional or not, the Fréchet distribution utilised by Padaratz (1977) served as a conservative measure, which had the effect of compensating for several issues for which there were no other solutions at the time. Such issues include anemometers located above control towers, the assumption that all were installed at $z = 10$ m above ground, lack of an analysis of surrounding terrain and conventional and manual observation processes which were very unlikely to record peak gusts for moving average of $\tau = 3$ s. Questionable practices include the use of a gust factor to convert V_{obs} from $T = 30$ s to $\tau = 3$ s, even though the averaging was done mentally by the observer, the application of a single weighted average shape factor, γ_{mp} , to all station distributions to generate the basis of the isopleth map, only for certain stations to be discarded and γ_{mp} to be ignored in favour of station specific γ_o at Foz do Iguaçu, PR. In addition, the map is difficult to interpret with some poorly positioned contours leading to uncertainty and the possibility of the selection of an incorrect basic wind speed, or more commonly, various interpretations for the same location.

A review of the incident ABL wind model used in NBR 6123 (ABNT, 1988) revealed some inconsistencies which must be addressed. The turbulence intensity is poorly defined – with one definition (Simiu, 1981) used to generate the series of gust factors while a different definition is used elsewhere (Blessmann, 2013). It is unknown which version of turbulence intensity was used in the determination of drag coefficients, C_a , and dynamic amplification factors, ξ . Differences between the gust factors derived from Durst (1960) and the technique developed by Holmes and Ginger (2012) were also documented. In moving forward, vertical profiles of turbulence intensity must first be defined for each terrain category. This could provide the opportunity to re-define the roughness length of flat, open terrain, CAT II ($z_0 = 0.07$ m), to be closer to the nominated values of most wind codes and publications ($z_0 = 0.02$ or 0.03 m). Once turbulence intensities are defined, gust factors can be determined using the methodology of Holmes and Ginger (2012) and should also be verified by wind-tunnel tests. Numerical and physical testing should also be performed to determine new C_a and ξ based on

corrected I and F_r . As this study has shown non-synoptic winds to be dominant over both short and long return periods for the majority of Brazil, the need for NBR 6123 to have a separate C_a graph for buildings in high-turbulence conditions should be reviewed in light of studies indicating that thunderstorm outflows have low turbulence intensities ($I = 0.1$) and terrain roughness has little effect on maximum speeds.

8.3.2 INMET

In principle, INMET's network of ASWS has the potential to be the biggest technological advancement in understanding extreme winds in Brazil over the last 20 years. Since the early 2000s the network has grown to over 600 automatic stations across the country. The automatic processes involved in the observation and transmission of meteorological data effectively reduces human error to zero. All anemometers are installed at a height of $z = 10$ m since the commissioning of each ASWS, digital processes are used in the determination of hourly peak gusts of $\tau = 3$ s moving average and anemometers restricted to either Vaisala WAA151 cup (small distance constant, high responsiveness) or Gill WindSonic ultrasonic (almost negligible distance constant, very high responsiveness).

Despite these technological advances, a number of issues must be addressed by the organisation which reduce confidence its ability to accurately observe extreme winds in open field conditions. The minimum clearance perimeter around the mast is only 14 m x 18 m, much less than the 300 m minimum radius as specified by DECEA. An evaluation of terrain conditions within 500 m of all INMET ASWS determined that 57% of 45° wind sectors to be of suburban, high density urban or forest terrain, with roughness lengths higher than CAT II of NBR 6123 (ABNT, 1988). Although corrections were made in an attempt to homogenise wind speeds, their impact is limited when wind flow is distorted by obstacles in the immediate surroundings of the anemometer. Holmes et al. (2005) recommended stations in dense urban surrounds should not be used in the analysis of extreme winds. As such, it is recommended that all new stations should be located in open, flat fields 5 km from terrain with high roughness lengths such as forest, suburban and urban areas.

The most alarming outcome of the study was the discovery that INMET redacts real cases of extreme wind speeds observed at ASWS. Several examples of deleted peak gusts above 25 m/s in the official SADMET dataset are documented in this study and should shock researchers and meteorologists who depend on INMET ASWS for extreme climate analyses.

One case of a retroactive exclusion of a peak gust above 40 m/s from the INMET web portal was also encountered and documented. The full extent of the practice is unknown by the scientific community and public at large, and must be revealed and rectified, not only for future observations, but historically redacted observations such as those documented by the study. An extreme value analysis is only as good as the data it uses, and if an official government agency is actively and indiscriminately discarding good data with bad, confidence in such analysis is diminished.

Another concerning aspect is the amount of time taken to rectify technical issues at ASWS. Predominant wind direction time-series at several stations change by up to 180° at some point during operation, such as A308 – Parnaíba, MA, which registered predominant westerly winds for a period of over six years in a region where easterlies are known to dominant, leading to the understanding that wind direction measuring equipment was installed incorrectly. In some cases, the erroneous period can easily be identified, but in most cases it is difficult to identify without the assistance of INMET to inspect the equipment and inform the public on the issue. These issues are not limited to just wind direction, with several instances of poor performing anemometers and barometers identified. In one of the worst examples, the anemometer at A823 – Inácio Martins, PR, exhibited reduced performance progressively over a period of four years before reparative action was taken. Similarly, unreliable observations were made by the barometer over the first five years of operation of A203 – São Luís, MA.

It is understood that the INMET ASWS reporting frequency protocol (maximum gust over previous hour, G_{obs} , and mean wind speed and predominant direction, V_{obs} and DIR , relating to last 10 minutes of the hour) was based on recommendations of the Finnish Meteorological Institute. Whether true or not, current day observations of G_{obs} , V_{obs} and DIR made by Finnish SWS are made at 10-minute intervals. Higher temporal resolution of observations would be most recommended in Brazil, particularly due to the frequency of downburst and transient events of duration periods less than 10 minutes. In the case of V_{obs} , G_{obs} and DIR made at 10-minute intervals, correlation between G_{obs} and DIR and V_{obs} could be achieved at INMET ASWS which is not possible under current hourly intervals. A further recommendation is to follow meteorological institutions of the United States and Australia in the adoption of observations at 1-minute intervals. High-resolution data would allow for the implementation of advanced techniques, such as Masters et al. (2010), in the determination of upwind roughness length per wind sector, in addition to the availability of richer information for

researches investigating non-synoptic winds in Brazil. As a minimum, the peculiar finding of statistically high occurrence of consecutive hourly maximum gusts of equal magnitudes, as documented in Section 4.2 *INMET ASWS*, must result in an investigation of software installed at all INMET ASWS.

Although not considered to be a serious issue, some contradictions were noted regarding metadata received from DISMEs and INMET headquarters. INMET confirmed the use of only Gill WindSonic ultrasonic or Vaisala WAA151 cup anemometers at ASWS, but 7th DISME reported two stations using Vaisala WAS 425. Additionally, the Gill WindSonic was confirmed to at A001 – Brasília, DF, from its commissioning on 07/05/2000. This information is likely incorrect since the Gill WindSonic was not released on the market until 12/2001. These small discrepancies demonstrate a need for INMET ASWS metadata to be better organised and open to the public.

8.3.3 Brazilian aerodromes/DECEA/ICEA

Due the lack of a single, centralised authority responsible for operation SWS installations at Brazilian aerodromes, the process of homogenisation of wind speeds undertaken in this study could be described as a token theoretical exercise, rather than a fundamental task. Although ICEA receives data from all aerodromes, the body has no control over SWS installations nor the documentation of their metadata. DECEA is the governing authority which determines protocols to be following by the SWS of each aerodrome and is best-positioned to conduct detailed investigations. Such investigations should aim to answer the following questions for each aerodrome SWS:

- When did digital acquisition of data replace conventional processes?
- When was the WMO definition of gust as a 3-second moving average implemented?
- When were anemometers changed and what was the anemometer type/model?
- What are the exact locations of anemometers, and where were they previous installed (and when)? Similarly, for the anemometer heights.
- When were anemometers re-located from atop control towers to adjacent to runways?

It is likely that the implementation of digital processes and the adoption of the 3-second moving average gust occurred at the same time for each aerodrome. In this case, all gust data prior should not be considered in any future extreme wind investigations, unless the purpose of the investigation is to determine correction factors of past data recorded by conventional

processes. Additionally, the AIP should be updated regarding current anemometer types and locations frequently. It is recommended that historical metadata be documented and managed online with access given to the public, similar to BoM, NIST and NOAA.

As per recommendations made for INMET ASWS, observations made at higher resolutions of 10-minute or 1-minute intervals would generate richer data for scientific studies and give greater confidence in the accuracy of observed peak gusts. Such higher resolution data do not need to be reported via the GTS and could be kept on DECEA/ICEA data servers for specific climatic studies, similar to practices adopted by BoM and NOAA. In order to reduce sampling errors and improve homogenisation between aerodromes, the adoption of a single anemometer type/model at all aerodromes is recommended.

Efforts to upgrade SWS to operate unmanned are already underway but only for a very select group of aerodromes. Although a hybrid operating system (automated acquisition and human control) is optimal, the upgrading of all aerodrome to automatic emission of METAR/SPECI reports for after-hours should be national goal. Priority should be given to aerodromes located in regions of intense non-synoptic winds operating for only a fraction of the day. Automated systems could be used to observe weather during after-hours periods at aerodromes such as SBBG – Bagé RS, SBCA – Cascavel, SC, SBCH – Chapecó, RS, SBNM – Santo Antônio, RS, SBPF – Passo Fundo, RS, SBPK – Pelotas, RS, SBTD – Toledo, PR, and SBUG – Uruguaiana. Meteorological data garnered from these locations would be invaluable to the meteorological and engineering communities researching extreme winds.

Investigations into the operation of four specific aerodrome SWS should be conducted. The quality of the wind speed time-series at SBBW – Barra dos Garças, MT, has degenerated since 2013 and may have reverted to conventional operation. Metadata information received from the aerodrome indicates the same anemometer has been in operation since 1986. There is a significant difference (over 100%), between monthly mean wind speeds at SBCA – Cascavel, PR, and re-analysis data from ECMWF, reducing confidence in the aerodrome to accurately observe wind speeds. Approximately 80% of 10-minute mean wind speed observations are even-numbered which suggests conventional operation until the end of 2017. This is also the case at SBCH – Chapecó, and both stations should be upgraded to digital processes if not already. Two years' of unusually high gust observations (double the magnitude of other periods) were reported at SBPB – Parnaíba, PI between 2015 and 2016.

The cause of this must be identified in order to avoid a repeat of the anomaly at other aerodrome SWS.

8.3.4 Future research

The dominance of non-synoptic winds in Brazil over synoptic winds were established in this study, yet much remains unknown about the characteristics of non-synoptic winds due to the number of convective modes and sub-classifications. The climatology of southern Brazil offers a fantastic opportunity for the wind engineering and meteorological communities to understand more about extreme winds from convective storms. Outcomes from such studies are guaranteed to have global repercussions. The key recommendations of Mason (2017) regarding wind characterisation, which involve the acquisition of field observations to generate enough data to build a statistically sound model of non-synoptic events (vertical and horizontal wind profiles, turbulence spectra, turbulence intensities and aerodynamic coefficients), should be undertaken in Brazil. Greater emphasis should be placed on understanding that convective storms are most accurately represented as range of models as opposed to a single downburst model. Field observations may take the form of fixed vertical arrays of anemometers located in areas of known severe convective activity or moveable remote sensor systems such as Doppler radar and LIDAR systems. It is the recommendation of this study, that such field campaigns should always be “tethered” by measurements at the surface ($z = 10$ m) in order to develop relationships with SWS data and basic wind speeds defined in wind codes. Such measurements will help validate proposed non-synoptic wind-loading models, such as those of Miguel et al. (2018) and Riera (2018).

There is great potential to build on advances made by this study. Several state-of-the-art methodologies cited in this study could not be adopted due to limitations in observing processes and lack of metadata at Brazilian SWS, meaning pragmatic and conservative approaches were necessary to ensure safety in Brazilian construction projects. Many approaches were subjective, including the evaluation of upstream roughness and initial manual classification process involved in the development of wind classification algorithms. Such approaches should be replaced by more advanced methods in the future.

There may be regions in Brazil whose extreme wind climatologies are less severe than determined by this study. The magnitudes of potential reductions are demonstrated in Figure L.3 of Appendix L, which considers the error between the proposed V_0 and a solution which

considers all stations, with the -5 to -10% residual dominating the majority of the country. However, for this level of reduction to be introduced in a future revision of V_0 , as a minimum, greater confidence is needed in the operation of Brazilian SWS. The adoption of recommendations made in this study by INMET and DECEA will go a long way to increasing confidence in their respective meteorological networks.

Despite the lack of a register containing the types/models of all anemometers in operation at Brazilian aerodromes, an investigation should be conducted into the operational performance and characteristics of anemometers most frequently encountered in this study (Gill WindSonic ultrasonic, Vaisala WAA151 cup, Bendix-Friez aerovane, Vaisala WS425 ultrasonic and Vaisala WMT705 ultrasonic). For each anemometer, peak and gust factors can be generated from spectral analyses of samples acquired via wind-tunnel tests for a range of wind speeds and turbulence intensities and compared with theoretical values. Such tests would determine if, and what, correction factors are necessary for each anemometer. In-situ tests should also be conducted to determine their comparative performance in the field and how vulnerable each is to natural elements, such as birds, rain, hail, fog and thunderstorms.

The effect of topography on wind speed measurements was not considered in this study but may be responsible for large variations between SWS of the same region. CFD approaches, such as that of Turner et al. (2019), could be undertaken in parallel with wind-tunnel tests to check for validity. Similarly, a variety of terrain analysis methods could be explored, particularly for fetch lengths greater than 500 m. However, caution should be taken when applying directional correctional factors at INMET ASWS, and when interpreting directional results, due to the manner in which observations are currently reported and the large number of erroneous or suspect direction observations which are documented in this study.

There are regions of the country which may have real extreme wind climatologies less severe than those proposed by this study. Results from several stations across Brazil indicate 50-year return wind speeds less than 30 m/s. Such regions include the northeast which could potentially have non-synoptic V_0 of as low as 22-25 m/s. Research should be conducted to establish an internationally recognised minimum basic wind speed. A quick look at observed wind speed data across Singapore, Malaysia and Indonesia, where codes also specify basic wind speeds of similar magnitude, also indicate the potential for basic wind speeds to be lowered. According to NCEI/NCDC data, the highest gust observed at WSSS – Changi, Singapore, between 1997 and 2017 was 38 kt (19.6 m/s) in July, 2014. Basic wind speeds less

than 30 m/s are present in some Andean nations of South America, however governing loads in these nations are typically seismic. At present, the minimum limit of 30 m/s is essentially an unwritten law within the wind engineering community without any known studies to enforce it.

The adoption of meteorological terminology in place of commonly used wind engineering jargon is key to the development of our understanding of the nuances and complexities involved in extreme winds of both synoptic and non-synoptic winds. Over the course of this study, several terms were encountered which attempt to describe a certain type of extreme wind model. *Synoptic* winds, were used to cover a variety of wind types which adhere to the ABL set of characteristics, including those referred to as EPS, various types of cyclones, stationary winds, non-TS winds and frontal depressions. Similarly, *non-synoptic* was used as an umbrella for extreme winds originating from convective storms, which are often referred to as localised wind storms, downbursts, TS winds and non-stationary winds. Instead of a classification system based on meteorological phenomenon, it is recommended that a *wind model* nomenclature be used. As such, the classification of extreme wind events would best be described as *ABL* winds vs *outflow* winds.

It is recommended that the basic wind maps of NBR 6123 be updated on 10-yearly basis. Hopefully, many of the issues raised in this study will be resolved over the next 10 years and in such a case, future Brazilian basic wind speeds should adopt a GPD or POT type analysis which establishes limits for long return periods. Such approaches were not possible in this study due to low confidence in data and short sampling periods of many SWS. Independent of the extreme value analysis method, another 10 more years of wind data acquired by uniform digital processes will prove invaluable for the continued development of Brazilian regional basic wind speed models.

REFERENCES

- ALMEIDA, L.D. DE. **Estudo para atualização do mapa de ventos da NBR 6123**. 2010. Tese de Doutorado. Engenharia de Infraestrutura Aeronáutica, Instituto Tecnológico de Aeronáutica, São José dos Campos, São Paulo.
- AMERICAN SOCIETY OF CIVIL ENGINEERS. **ASCE Standard 7-95**, 1995.
- AMERICAN SOCIETY OF CIVIL ENGINEERS. **ASCE Standard 7-10**, 2010.
- AMERICAN SOCIETY OF CIVIL ENGINEERS. **ASCE Standard 7-16**, 2016.
- ASSOCIAÇÃO BRASILEIRA DE NORMAS TÉCNICAS. **NBR 6123: Forças devidas ao vento em edificações**. Rio de Janeiro, 1988.
- ASSOCIAÇÃO BRASILEIRA DE NORMAS TÉCNICAS. **NBR 6118: Projeto de estruturas de concreto - Procedimento**. Rio de Janeiro, 2014.
- ASOCIACIÓN COLOMBIANA DE INGENIERÍA SÍSMICA. **NSR-10 Reglamento Colombiano de Construcción Sismo Resistente**. 2010
- AUSTRALIAN/NEW ZEALAND STANDARD. **AS/NZS 1170.2 Structural design actions Part 2: Wind Actions**, 2002.
- AUSTRALIAN/NEW ZEALAND STANDARD. **AS/NZS 7000 Overhead line design – Detailed procedures**, 2010.
- AUSTRALIAN/NEW ZEALAND STANDARD. **AS/NZS 1170.2 Structural design actions Part 2: Wind Actions**, 2011.
- AUSTRALIAN/NEW ZEALAND STANDARD. **Amendment No. 2 to AS/NZS 1170.2 Structural design actions Part 2: Wind Actions**, 2012.
- BECK, A.T.; CORRÊA, M.R.S. **New Design Chart for Basic Wind Speeds in Brazil**. Latin American Journal of Solids and Structures, vol. 10, pp.707-723, 2013.
- BELJAARS, A.C.M. **The Measurement of Gustiness at Routine Wind Stations – A Review**. Royal Netherlands Meteorological Institute, 1987.
- BLESSMANN, J. **O Vento na Engenharia Estrutural**. 2ª Edição, Editora da UFRGS, Porto Alegre, 2013.

BOWEN, B.M. **Improved Wind and Turbulence Measurements Using a Low-Cost 3-D Sonic Anemometer at a Low-Wind Site.** The Open Atmospheric Science Journal, vol. 2, (1), 2008.

BURTON, M.D.; ALLSOP, A.C. Predicting Design Wind Speeds from Anemometer Records: Some Interesting Findings. **Proceedings of the 11th Americas Conference on Wind Engineering**, 2009, San Juan, Puerto Rico.

CENTRO DE HIDROGRAFIA DA MARINHA. Cartas Sinóticas <https://www.marinha.mil.br/chm/dados-do-smm-cartas-sinoticas/cartas-sinoticas>. Accessed 12/11/2018.

CENTRO DE PREVISÃO DE TEMPO E ESTUDOS CLIMÁTICOS/INSTITUTO NACIONAL DE PESQUISAS ESPACIAS. Acervo de Imagens <http://satelite.cptec.inpe.br/home/index.jsp>. Accessed 13/11/2018.

CHOI, E.C.C.; HIDAYAT, F.A. **Gust factors for thunderstorm and non-thunderstorm winds.** Journal of Wind Engineering and Industrial Aerodynamics, vol. 90, pp. 1683-1696, 2002.

CHOI, E.C.C. **Field measurement and experimental study of wind speed profile during thunderstorms.** Journal of Wind Engineering and Industrial Aerodynamics, vol. 92, pp. 275-290, 2004

CIVIL AVIATION AUTHORITY. **CAP 746: Requirements for meteorological observations at aerodromes.** Issue 4, March, 2017.

COOK, N.J. **Towards better estimation of extreme winds.** Journal of Wind Engineering and Industrial Aerodynamics, vol. 9, pp. 295-323, 1982.

COOK, N.J. **The Designer's Guide to Wind Loading of Building Structures: Background, Damage Survey, Wind Data, and Structural Classification.** Building Research Establishment, Dept. of the Environment, London, 1985.

COOK, N.J.; HARRIS, R.I.; WHITING, R. **Extreme wind speeds in mixed climates revisited.** Journal of Wind Engineering and Industrial Aerodynamics, vol. 91, pp. 403-422, 2003.

COOK, N.J. **Comments on "Plotting Positions in Extreme Value Analysis", Correspondence.** Journal of Applied Meteorology and Climatology, vol. 50, pp. 255-266, 2011.

DAVENPORT, A.G. **Rationale for determining design wind velocities.** ASCE Journal of the Structural Division, vol. 86, pp. 39-68, 1960.

DAVENPORT, A.G. Note on the distribution of the largest value of a random function with application to gust loading. **Proceedings of the Institution of Civil Engineers**, vol. 28, No. 2, pp. 187-196, 1964.

DAVENPORT, A.G. The dependence of wind loads on meteorological parameters. **Proceedings 2nd International Conference on Wind Effects on Buildings and Structures**, Ottawa, University of Toronto Press, 1967.

DAVENPORT, A.G. The relationship of reliability to wind loading. **Journal of Wind Engineering and Industrial Aerodynamics**, vol. 13, pp.3-27, 1983.

DE GAETANO, P.; REPETTO, M.P.; REPETTO, T.; SOLARI, G. **Separation and classification of extreme wind events from anemometric records**. *Journal of Wind Engineering and Industrial Applications*, vol. 126, pp. 132-143, 2014.

DEAVES, D.M. **Computations of wind flow over changes in surface roughness**. *Journal of Wind Engineering and Industrial Aerodynamics*, vol. 7, pp. 65-94, 1981.

DEAVES, D.M.; HARRIS, R.I. **A mathematical model of the structure of strong winds**. CIRIA Report No. 76, May, 1978.

DEE, D.P.; UPPALA, S.M.; SIMMONS A.J.; BERRISFORD, P.; POLI, P.; KOBAYASHI, S.; ANDRAE, U.; BALMASEDA, M.A.; BALSAMO, G.; BAUER, P.; BECHTOLD, P.; BELJAARS, A.C.M.; VAN DE BERG, L.; BIDLOT, J.; BORMANN, N.; DELSOL, C.; DRAGANI, R.; FUENTES, M.; GEER, A.J.; HAIMBERGER, L.; HEALY, S.B.; HERSBACH, H.; HÓLM, E.V.; ISAKSEN L.; KÅLLBERG, P.; KÖHLER, M.; MATRICARDI, M.; MCNALLY, A.P.; MONG-SANZ, B.M.; MORCRETTE, J.-J.; PARK, B.-K.; PEUBEY, C.; DE ROSNAY, P.; TAVOLATO, C.; THÉPAUT, J.-N.; VITART, F. **The ERA-Interim reanalysis: configuration and performance of the data assimilation system**. *Quarterly Journal of the Royal Meteorological Society*, vol. 137, pp. 553-597, 2011.

DEPARTMENT OF STANDARDS MALAYSIA. **MS 1553:2002 Code of Practice on Wind Loading for Building Structure**, Malaysian Standard. 2002.

DEPARTMENT OF THE ENVIRONMENT, HERITAGE AND LOCAL GOVERNMENT. **Irish National Annex to the Wind Eurocode (EN1991-1-4). Derivation of the Wind Map**. October, 2009.

[a] DEPARTAMENTO DE CONTROLE DO ESPAÇO AÉREO. **MCA 101-1: Instalação de estações meteorológicas de superfície e de altitude**. Rio de Janeiro, January, 2015.

[b] DEPARTAMENTO DE CONTROLE DO ESPAÇO AÉREO. **MCA 105-16: Manual de Operação do WEBMET**. Rio de Janeiro, December, 2015.

DEPARTAMENTO DE CONTROLE DO ESPAÇO AÉREO. **ICA 105-16: Códigos Meteorológicos**. Rio de Janeiro, February, 2017.

[a] DEPARTAMENTO DE CONTROLE DO ESPAÇO AÉREO. **AIP: Publicação de Informação Aeronáutica**. Rio de Janeiro, March, 2018.

[b] DEPARTAMENTO DE CONTROLE DO ESPAÇO AÉREO. **ICA 105-15: Manual de estações meteorológicas de superfície**. Rio de Janeiro, March, 2018.

DEUTSCHE NORM. **DIN EN 1991-1-4:2010-12 National Annex to Wind Eurocode**. 2010

DIRECCION GENERAL DE AERONAUTICA CIVIL. **DAP 03 07: Observaciones e Informes Meteorológicos**. November, 2017.

DIRECCIÓN NACIONAL DE AERONÁUTICA CIVIL. **DINAC R 3: Servicio Meteorológico para la Navegación Aérea Internacional**. 4th Edition (R00), August, 2017.

DIRECCION NACIONAL DE AVIACION CIVIL E INFRAESTRUCTURA AERONAUTICA. **RAU MET: Reglamento sobre el Servicio Meteorológico Aeronáutico**. August, 2010.

DODD, E. **The Greatest and the Least Variate Under General Laws of Error**. Transactions of the American Mathematical Society, vol. 25, No. 4, 1923.

DORMAN, C.M.L. **Extreme Values – An Improved Method of Fitting**. Journal of Wind Engineering and Industrial Aerodynamics, vol. 10, pp. 177-190, 1982.

DORMAN, C.M.L. **Extreme Wind Gust Speeds in Australia, Excluding Tropical Cyclones**. Transactions of The Institution of Engineers, Australia, Civil Engineering, vol. CE 25, No. 2, pp. 96-106, 1983.

DOSWELL III, C.A. **Severe Convective Storms**. Monograph, The American Meteorological Society, 2001.

DURAÑONA, V. Revisión de la estadística y mapa de vientos extremes establecidos por la norma uruguaya UNIT 50-84. **Proceedings of XXXVI Jornadas Sudamericanas de Ingeniería Estructural**, Montevideo, Uruguay, November 19- 21, 2014.

DURAÑONA, V. **Extreme Wind Climate of Uruguay**. 2015. Doctorate Thesis, Facultad de Ingeniería, Universidad de la República, Montevideo.

DURST, C.S. **Wind speeds over short periods of time**. The Meteorological Magazine, vol. 89, No. 1056, July, 1960.

EMANUEL, K.A. **Atmospheric Convection**. Oxford University Press, 1994.

ENCYCLOPEDIA BRITANNICA. Copyright 2010. **Evolution of a waves (frontal) cyclone**. <https://www.britannica.com/science/cyclogenesis/media/148022/1036>. Last accessed 30/3/2019.

ENGERER, N.A.; STENSRUD, D.J.; CONIGLIO, M.C. **Surface Characteristics of Observed Cold Pools**. American Meteorological Society Monthly Weather Review, vol. 136, No. 12, pp. 4839-4849, 2008

[a] ENGINEERING SCIENCES DATA UNIT. **Data Unit 87034 – World-wide extreme wind speeds. Part 1: Origins and Methods of Analysis**, 1990.

[b] ENGINEERING SCIENCES DATA UNIT. **Data Unit 88037 – World-wide extreme wind speeds. Part 2: Examples using various methods of analysis**, 1990.

ENGINEERING SCIENCES DATA UNIT. **Data Unit 82026 – Strong winds in the atmospheric boundary layer. Part 1: hourly-mean wind speeds**, 2002.

EVANS, J.L.; BRAUN, A. **A Climatology of Subtropical Cyclones in the South Atlantic**. Journal of Climate, vol. 25, pp. 7328-7340, 2012.

FERREIRA, V. **Comportamento das variáveis meteorológicas em situações de rajadas de vento geradas por tempestades severas com base nas estações automáticas do INMET**. 2014. Trabalho de Conclusão de Curso. Curso de Graduação em Meteorologia, Centro de Ciências Naturais e Exatas, Universidade Federal de Santa Maria (UFSM), Santa Maria, RS, Brasil.

[a] FERREIRA, V.; NASCIMENTO, E.L. **Discriminação entre rajadas de vento convectivas e não-convectivas**. Ciência e Natura, Especial IX Workshop Brasileiro de Micrometeorologia, vol. 38, pp. 225-231, 2016.

[b] FERREIRA, V.; NASCIMENTO, E.L. Convectively-induced severe wind gusts in southern Brazil: surface observations, atmospheric environment, and association with distinct convective modes. **Proceedings of the American Meteorological Society's 19th Conference on Severe Local Storms**, Portland, Oregon, November 2016.

FERREIRA, V. **Um estudo observacional de rajadas de vento geradas por tempestades severas no sul do Brasil**. 2017. Dissertação de Mestrado. Programa de Pós-Graduação em Meteorologia, Centro de Ciências Naturais e Exatas, Universidade Federal de Santa Maria (UFSM), Santa Maria, RS, Brasil.

FIGUEIREDO, E.L. DE.; NASCIMENTO, E.L.; OLIVEIRA, M.I. DE. **Analysis of two derecho events in Southern Brazil**. Meteorology and Atmospheric Physics, pp. 1-20, 2019.

FISCH, G. **Comparisons between aerovane and sonic anemometer wind measurements at Alcântara Launch Center**. Journal of Aerospace Technology and Management, vo. 2, No.1, pp. 105-110, 2010.

FISHER, R.A.; TIPPETT, L.H.C. Limiting forms of the frequency distribution of the largest or smaller member of a sample. **Proceedings of the Cambridge Philosophical Society**, vol. 24, pp. 180-190, 1928.

FUJITA, T.T. **Spearhead echo and downburst near the approach end of a John F. Kennedy Airport runway, New York City.** Satellite and Mesometeorology Research Project Research Paper 137, University of Chicago, 1976.

FUJITA, T.T. **The downburst: microburst and macroburst.** Satellite and Mesometeorology Research Project Research Paper 210, University of Chicago, 1985.

FUJITA, T.T. **Downbursts: Meteorological Features and Wind Field Characteristics.** Journal of Wind Engineering and Industrial Aerodynamics, vol. 36, pp. 75-86, 1990.

GALLEGO, D.; RIBERA, P.; GARCIA-HERRERA, R.; HERNANDEZ, E.; GIMENO, L. **A new look for the Southern Hemisphere jet stream.** Climate Dynamics, vol. 24, pp. 607-621, 2005.

GATEY, D.A. **The analysis of extreme synoptic winds.** 2011. Doctorate Thesis. Faculty of Engineering Science, The University of Western Ontario, London, Ontario.

GIBLETT, M.A. **The structure of wind over level country.** Geophysical Memoirs No. 54, Meteorological Office, London, 1932.

GILHOUSEN, D.B. An evaluation of Gill sonic anemometers in the marine environment. **American Meteorological Society's 11th Symposium on Meteorological Observations and Measurements.** Albuquerque, NM, 2001.

GILL, G.C. **The helicoid anemometer: A long neglected but valuable anemometer.** Atmosphere, vol. 11, No. 4, pp. 145-155, 1973.

GOFF, R.C. **Thunderstorm-Outflow Kinematics and Dynamics.** NOAA Technical Memorandum ERL NSSL-5, National Severe Storms Laboratory, December, 1975.

GOMES, L.; VICKERY, B.J. **On thunderstorm wind gusts in Australia: with particular reference to Observatory Hill, Sydney.** Research report, No. R277, University of Sydney, School of Engineering, 1976.

GOMES, L.; VICKERY, B.J. **On the prediction of extreme wind speeds from the parent distribution.** Journal of Industrial Aerodynamics, vol. 2, pp. 21-36, 1977.

GOMES, L.; VICKERY, B.J. **Extreme wind speeds in mixed wind climates.** Journal of Industrial Aerodynamics, vol. 2, pp. 231-344, 1977-1978.

GORMAN, J. **Instrument Test Report 677, The Conversion Equation of the Synchrotac 706 Anemometer.** Bureau of Meteorology, Regional Instrument Centre, 2004.

GRINGORTEN, I.I. **A Plotting Rule for Extreme Probability Paper.** Journal of Geophysical Research, vol. 68, No. 3, pp. 813-814, 1963.

GUNTER, W.S.; SCHROEDER, J.L. **High-resolution full-scale measurements of thunderstorm outflow winds**. Journal of Wind Engineering and Industrial Aerodynamics, vol. 138, pp. 13-26, 2015.

HANGAN, H.; REFAN, M.; JUBAYER, C.; ROMANIC, D.; PARVU, D.; LOTUFO, J.; COSTACHE, A. **Novel techniques in wind engineering**. Journal of Wind Engineering and Industrial Aerodynamics, vol. 171, pp. 12-33, 2017.

HARRIS, R.I. Measurements of wind structures at heights up to 598ft above ground level. **Symposium on Wind Effects on Buildings and Structures**, Loughborough, Loughborough University of Technology, vol. 1, No. 1, 1968.

HARRIS, R.I. **Gumbel re-visited – a new look at extreme value statistics applied to wind speeds**. Journal of Wind Engineering and Industrial Aerodynamics, vol. 59, pp. 1-22, 1996.

HARRIS, R.I. **Improvements to the ‘Method of Independent Storms’**. Journal of Wind Engineering and Industrial Aerodynamics, vol. 80, pp. 1-30, 1999.

HARRIS, R.I. **The accuracy of design values predicted from extreme value analysis**. Journal of Wind Engineering and Industrial Aerodynamics, vol. 89, pp. 153-164, 2001.

HIRATA, M.H.; ARAÚJO, R.; ARAÚJO, C.; MACHADO, R. **Coleta de Dados de Vento Estrategicamente Distribuídos pelo Território Nacional, 2º Relatório – Contatos com Possíveis Fontes**. Program Energia Brasileiro-Alemão. Nº do Programa 2007:21894-001.00. December, 2010.

HJELMFELT, M.R. **Structure and Life Cycle of Microburst Outflows Observed in Colorado**. Journal of Applied Meteorology, vol. 27, pp. 900-927, 1988

HOLMES, J.D. Physical modelling of thunderstorm downdrafts by wind tunnel jet. **Proceedings of 2nd Australian Wind Engineering Society Workshop**, Melbourne, 1992.

HOLMES, J.D. MORIARTY, W.W. **Application of the generalized Pareto distribution to extreme value analysis in wind engineering**. Journal of Wind Engineering and Industrial Aerodynamics, vol. 83, pp. 1-10, 1999.

HOLMES, J.D. Modelling of extreme thunderstorm winds for wind loading of structures and risk assessment. **Proceedings of 10th International Conference on Wind Engineering**, Copenhagen, Denmark, 21-24 June, 1999.

HOLMES, J.D. **A Re-analysis of Recorded Extreme Wind Speeds in Region A**. Australian Journal of Structural Engineering, vol. 4, No. 1, pp. 29-40, 2002.

HOLMES, J.D.; KASPERSKI, M.; MILLER, C.A.; ŻURAŃSKI J.A.; CHOI E.C.C. **Extreme wind prediction and zoning**. Wind and Structures, vol. 8, No. 4, pp. 269-281, 2005.

HOLMES, J.D. HANGAN, H.; SCHROEDER, J.L.; LETCHFORD, C.W.; ORWIG, K.D. **A forensic study of the Lubbock-Reese downdraft of 2002**. Wind and Structures, vol. 11, No. 2, pp. 137-152, 2008.

HOLMES, J.D.; GINGER, J.D. **The gust wind speed duration in AS/NZS 1170.2**. Australian Journal of Structural Engineering, vol. 13, No. 3, pp. 207-218, 2012.

HOLMES, J.D.; ALLSOP, A.C.; GINGER, J.D. **Gust durations, gust factors and gust response factors in wind codes and standards**. Wind and Structures, vol. 19, No. 3, pp. 339-352, 2014.

HOLMES, J.D. **Wind Loading of Structures**. CRC Press, 3rd Edition, 2015.

HOLMES, J.D.; WANG, C.H.; OLIVER, S. Extreme winds for six South Australian locations. **Proceedings of the 19th Australasian Wind Engineering Society Workshop**, April 4-6, 2018, Torquay, Australia, 2018.

INSTITUTO BRASILEIRO DE GEOGRAFIA E ESTATÍSTICA. **Cobertura e uso da terra, 2014**. <https://ww2.ibge.gov.br/home/geociencias/recursosnaturais/usodaterra/default.shtm>
Last accessed 20/3/2019.

INSTITUTO DE CONTROLE DO ESPAÇO AÉREO. **Dados Climatológicos de Estações Meteorológicas de Superfície**. Technical Report PSEC-46. São José dos Campos, November, 2015.

INSTITUTO DE CONTROLE DO ESPAÇO AÉREO. **Dados Climatológicos de Estações Meteorológicas de Superfície**. Technical Report PAS-31. São José dos Campos, June, 2017.

INSTITUTO NACIONAL DE METEOROLOGIA. **Rede de Estações Meteorológicas Automáticas do INMET**. Nota Técnica No. 001/2011/SEGER/LAIME/CSC/INMET, 2011.

INSTITUTO NACIONAL DE METEOROLOGIA. **Tempestade ocorrida em Porto Alegre no final do dia 29/01/2016**. Nota Técnica, publicada 19/02/2016, acessado 02/04/2019. http://www.inmet.gov.br/portal/notas_tecnicas/nota_impressa_1_poa.pdf.

INSTITUTO NACIONAL DE TECNOLOGÍA INDUSTRIAL. **CIRSOC 102 Reglamento Argentino del Acción del Viento sobre Las Construcciones**, 2005.

INSTITUTO NACIONAL DE TECNOLOGÍA Y NORMALIZACION. **NP No. 196 Acción del Viento en Las Construcciones**. Norma Paraguaya, 1991.

INSTITUTO URUGUAYO DE NORMAS TECNICAS. **UNIT 50-84, Norma uruguaya para Acción del Viento sobre Construcciones**, 1984.

INTERNATIONAL CIVIL AVIATION ORGANIZATION. **Annex 3 to the Convention on International Civil Aviation – Meteorological Service for International Air Navigation.** 16th Edition, Montreal, 2007.

INTERNATIONAL ORGANIZATION FOR STANDARDIZATION. **ISO 4354:2009(E) Wind actions on structures.** 2009.

JENKINSON, A.F. **The frequency distribution of the annual maximum (or minimum) values of meteorological elements.** Quarterly Journal of the Royal Meteorological Society, 81, pp. 158-171, 1955.

JENSEN, M.; FRANCK, N. **The Climate of Strong Winds in Denmark.** Danish Technical Press, Copenhagen, 1970.

JOHNS, R.H.; HIRT, W.D. **Derechos: Widespread Convectively Induced Windstorms.** Weather and Forecasting, vol. 2, pp. 32-49, 1987.

KASPERSKI, M. **A new wind zone map of Germany.** Journal of Wind Engineering and Industrial Aerodynamics, vol. 90, pp. 1271-1287, 2002.

KUMAR, K.S.; CINI, C.; SIFTON, V. Assessment of design wind speeds for metro cities of India. **Proceedings of the 7th International Colloquium on Bluff Body Aerodynamics and Applications**, 2012, Shanghai, China.

KWON, D.K.; KAREEM, A. **Revisiting Gust Averaging Time and Gust Effect Factor in ASCE 7.** Technical Note, ASCE Journal of Structural Engineering, vol. 140 (11), 2014.

LAING, A.G.; FRITSCH, J.M. **The global population of mesoscale convective complexes.** Quarterly Journal of the Royal Meteorological Society, vol. 123, pp. 389-405, 1997.

LECHNER, J.A.; LEIGH S.D.; SIMIU E. **Recent Approaches to Extreme Value Estimation with Application to Wind Speeds. Part I: the Pickands Method.** Journal of Wind Engineering and Industrial Aerodynamics, vol. 41, pp. 509-519, 1992.

LETCHFORD, C.W.; ILLIDGE, G. Turbulence and topographic effects in simulated thunderstorm downdrafts by wind tunnel jet. **Proceedings of the 10th International Conference on Wind Engineering**, Copenhagen, Denmark, 1999.

LETCHFORD, C.W.; CHEN, L. **Numerical simulation of extreme winds from thunderstorm outbursts.** Journal of Wind Engineering and Industrial Aerodynamics, vol. 95, pp. 977-990, 2007.

LIEBLEIN, J. **Efficient Methods of Extreme-Value Methodology.** Technical Report NBSIR 74-602, National Bureau of Standards, Washington, D.C., October 1974.

LOMBARDO, F.T.; MAIN, J.A.; SIMIU E. **Automated extraction and classification of thunderstorm and non-thunderstorm wind data for extreme-value analysis.** Journal of Wind Engineering and Industrial Aerodynamics, vol. 97, pp. 120-131, 2009.

LOMBARDO, F.T. **Improved extreme wind speed estimation for wind engineering applications.** Journal of Wind Engineering and Industrial Aerodynamics, vol. 104-106, pp. 278-284, 2012.

LOMBARDO, F.T.; SMITH, D.A.; SCHROEDER, J.L. MEHTA, K.C. **Thunderstorm characteristics of importance to wind engineering.** Journal of Wind Engineering and Industrial Aerodynamics, vol. 125, pp. 121-132, 2014.

LOREDO-SOUZA, A.M. Meteorological events causing extreme winds in Brazil. **Wind and Structures: An International Journal**, vol. 15, no. 2, 2012.

LOREDO-SOUZA, A.M.; LIMA, E.G.; VALLIS, M.B.; ROCHA, M.M.; WITTEWER, A.R.; OLIVEIRA, M.G.K. Downburst related damages in Brazilian buildings: are they avoidable? **Journal of Wind Engineering and Industrial Aerodynamics**, vol. 185, pp. 33-40, 2019.

MARKOWSKI, P.; RICHARDSON, Y. **Mesoscale Meteorology in Midlatitudes.** John Wiley and Sons, Ltd. 2010.

MASON, M.S.; LETCHFORD, C.W.; JAMES, D.L. **Pulsed wall jet simulation of a stationary thunderstorm downburst, Part A: Physical structure and flow field characterization.** Journal of Wind Engineering and Industrial Aerodynamics, vol. 93, No. 7, pp. 557-580, 2005.

MASON, M.S.; WOOD, G.S; FLETCHER, D.F. **Numerical simulation of downburst winds.** Journal of Wind Engineering and Industrial Aerodynamics, vol. 97, pp. 523-539, 2009.

MASON, M.S.; FLETCHER, D.F.; WOOD, G.S. **Numerical simulation of idealised three-dimensional downburst wind fields.** Engineering Structures, vol. 32, No. 11, pp. 3558-3570, 2010.

MASON, M.S. Towards Codification of Localised Windstorms: Progress and Challenges. **Proceedings of 9th Asia-Pacific Conference on Wind Engineering.** Auckland, New Zealand, 3-7 December, 2017.

MASTERS, F.J.; VICKERY, P.J.; BACON, P.; RAPPAPORT, E.N. **Toward objective, standardized intensity estimates from surface wind speed observations.** Bulletin of the American Meteorological Society, vol. 91, No. 12, pp. 1665- 1682, 2010.

MCTAGGART-COWAN, R.; BOSART, L.F; DAVIS, C.A.; ATALLAH, E.H.; GYAKUM, J.R.; EMANUEL, K.A. **Analysis of Hurricane Catarina (2004).** American Meteorological Society Monthly Weather Review, vol. 134, pp. 3029-3053 2006.

MENDES, D.; MARENGO, J.A.; SOUZA E.P.; MENDES, M. **Climatology of extratropical cyclones over the South American-southern oceans sector**. Theoretical and Applied Climatology, vol. 100, No. 3, pp. 239-250, 2009.

MIGUEL, L.F.F.; RIERA, J.D.; FADEL MIGUEL, L.F. **Assessment of downburst wind loading on tall structures**. Journal of Wind Engineering and Industrial Aerodynamics, vol. 174, pp.252-259, 2018.

MILLER, C.A. **Revisiting the Durst gust factor curve**. Canadian Journal of Civil Engineering, vol. 38, pp. 998-1001, 2011.

MINISTÉRIO DA AERONÁUTICA. **MMA-105-2A, CAP VIII**. Rio de Janeiro, 1964.

MINISTERIO DE TRANSPORTE Y COMUNICACIONES. **RAP 303: Servicio Meteorológico para la Navegación Aérea, Apéndice C**. December, 2015.

MOHR, S.; KUNZ, M; RICHTER, A.; RUCK, B. **Statistical characteristics of convective wind gusts in Germany**. Natural Hazards and Earth System Sciences, vol. 17, pp. 957-969, 2017.

MOSES, H.; ROBINSON, E.; SMITH, M.E.; GILL, G.C.; WILKINS, E.M.; DICKSON, C.R. **Chapter 6: Meteorological Instruments for Use in the Atomic Energy Industry, Meteorology and Atomic Energy**. U.S. Atomic Energy Commission and SLADE, D. pp. 257-300, 1968.

NASCIMENTO, E.L. **Previsão de tempestades severas utilizando-se parâmetros convectivos e modelos de mesoescala: Uma estratégia operacional adotável no Brasil?** Revista Brasileira de Meteorologia, vol. 20, No. 1, pp. 121-140, 2005.

NATIONAL OCEANOGRAPHIC AND ATMOSPHERIC ADMINISTATION. **ASOS Ice Free Wind Problem Resolution Project Plan (IPRPP)**. Memorandum. Maryland, January 28, 2008

NATIONAL RESEARCH COUNCIL OF CANADA. **National Building Code of Canada 2010, Volume 2**.

PADARATZ, I.J. **Velocidade básica do vento do Brasil**. 1977. Tese de mestrado, Escola de Engenharia, UFRGS, Porto Alegre.

PES, M.P. **Impactos das variações e mudanças climáticas sobre os ventos extremos e seus efeitos no setor elétrico brasileiro**. 2015. Tese de doutorado, Curso de Pós-Graduação em Ciência do Sistema Terrestre, INPE.

PES, M.P.; PEREIRA, E.B; MARENGO, J.A.; MARTINS, F.R. **Climate trends on the extreme winds in Brazil**. Renewable Energy, vol. 109, pp. 110-120, 2017.

PETERKA, J.A.; SHAHID, S. **Design Gust Wind Speeds in the United States**. Journal of Structural Engineering, vol. 124, 2, pp. 207-214, 1998.

PEZZA, A.B.; SIMMONDS, I. **The first South Atlantic hurricane: Unprecedented blocking, low shear and climate change**. Geophysical Research Letters, vol. 32, L15715, 2005.

PEZZA, A.B.; SIMMONDS, I.; PEREIRA FILHO, A.J. **Climate perspective on the large-scale circulation associated with the transition of the first South Atlantic hurricane**. Royal Meteorological Society's International Journal of Climatology, vol. 29, pp. 1116-1130, 2009.

PINTAR, A.L., SIMIU, E., LOMBARDO, F.T., LEVITAN, M. **Maps of Non-hurricane Non-tornadic Wind Speeds With Specified Mean Recurrence Intervals for the Contiguous United States Using a Two-dimensional Poisson Process Extreme Value Model and Local Regression**. NIST Special Publication 500-301, U.S. Department of Commerce, 2015.

PIROOZ, A.A.S; FLAY, R.G.J. Response Characteristics of Anemometers Used in New Zealand. **Proceedings of the 19th Australasian Wind Engineering Society Workshop**, April 4-6, 2018, Torquay, Australia, 2018.

PIROOZ, A.A.S; FLAY, R.G.J.; TURNER, R. Effects of site relocation and instrument type on recorded wind data characteristics at Wellington Airport. **Proceedings of the 19th Australasian Wind Engineering Society Workshop**, April 4-6, 2018, Torquay, Australia, 2018.

PIROOZ, A.A.S. Private communication, received 16/04/2019.

PRYOR, S.C.; BARTHELMIE, R.J.; YOUNG, D.T.; TAKLE, E.S.; ARRITT, R.W.; FLORY, D.; GUTOWSKI JR., W.J.; NUNES, A.; ROADS, J. **Wind speed trends over the contiguous United States**. Journal of Geophysical Research, vol. 114, 2009.

REBOITA, M.S.; KRUSCHE, N.; AMBRIZZI, T.; ROCHA, R.P. DA. **Entendendo o Tempo e o Clima na América do Sul**. Terræ Didática, vol 8. No. 1, pp. 34-50, 2012.

REPETTO, M.P.; BURLANDO M.; SOLARI, G.; DE GAETANO, P. **A web-based GIS platform for the safe management and risk assessment of complex structural and infrastructural systems exposed to wind**. Advances in Engineering Software, vol. 117, pp. 29-45, 2018.

RIERA, J.D.; REIMUNDIN, J.C. **Sobre la distribución de velocidades máximas de viento en la República Argentina**. INFORME I-70-3, Laboratorio de Ensayo de Estructuras, Universidad Nacional de Tucumán, 1970.

RIERA, J.D.; VIOLLAZ, A.J.; REIMUNDIN, J.C. **Some recent results on probabilistic models of extreme wind speeds**. Journal of Industrial Aerodynamics, vol. 2, pp. 271-287, 1977.

RIERA, J.D.; NANNI, L.F. **Pilot study of extreme wind velocities in a mixed climate**. Journal of Wind Engineering and Industrial Aerodynamics, vol. 32, pp. 11-20, 1989.

RIERA, J.D. **On the Vertical Profile of the Wind Velocity Induced by Downbursts**. **Proceedings of XXXVIII Jornadas Sudamericanas de Ingeniería Estructural**, Lima, Peru, October 24-26, 2018.

ROCHA, A.M.M. DA. **Histórico e importância do Banco de Dados Climatológicos da Aeronáutica**. Parte No. 745/PBCP, Protocolo COMAER No. 67610.003380/2013-01. São José dos Campos, 24 de outubro de 2016.

SANTOS, M.L.W. DOS. **Regionalização das velocidades extremas e temperaturas do vento no centro-sul do Brasil**. 1989. Dissertação de mestrado, Escola de Engenharia, UFRGS, Porto Alegre.

SATYAMURTY, P.; NOBRE, C.A; SILVA DIAS, P.L. South America. In: KAROLY, D.J.; VINCENT D.G. **Meteorology of the Southern Hemisphere**, American Meteorological Society, pp. 119-139, 1998

SAVORY, E.; PARKE, G.A.R.; ZEINODDINI, M.; TOY, N.; DISNEY, P. **Modelling of tornado and microburst-induced wind loading and failure of a lattice transmission tower**. Engineering Structures, vol. 23, pp. 365-375, 2001.

SCHMITT, C. **Primer for the ASOS Software Version 3.10 Ice Free Wind Sensor Quality Control Algorithm, 2008**. https://www.weather.gov/media/asos/ASOS%20Implementation/IFWS%20QC%20Algorithm_primer.pdf Last accessed 13/3/2019.

SERVICIO METEOROLOGICO NACIONAL. **Manual de Procedimientos Operativos de Meteorologia Aeronautica (MAPROMA) Parte V**. May, 2010.

SHORT, D.A.; WHEELER.; M.M. **RSA/Legacy Wind Sensor Comparison. Part II: Eastern Range**. NASA Contractor Report CR-2006-214205. May, 2006.

SILVA DIAS, M.A.F. **An Increase in the Number of Tornado Reports in Brazil**. American Meteorological Society, vol. 3, pp. 209-217, 2011.

SIMIUI, E.; BIETRY, J.; FILLIBEN, J.J. **Sampling Errors in the Estimation of Extreme Winds**. Journal of the Structural Division, vol. 104 (3), pp.491-501, 1978.

SIMIUI, E. **Modern developments in wind engineering: part 1**. Engineering Structures, vol. 3, pp. 233-241, 1981.

SIMIU, E.; WILCOX R.; SADEK, F.; FILLIBEN, J. **Wind Speeds in ASCE 7 Standard Peak-Gust Map: Assessment**. Journal of Structural Engineering, vol. 129, pp. 427-439, 2003.

SIMIU, E.; HECKERT, N.A. **Extreme Wind Distribution Tails: A ‘Peaks Over Threshold’ Approach**. NIST Building Science Series 174, 1995.

SIMS, M. **Gill Instruments**, Private communication, received 04/12/2019.

SINGAPORE STANDARDS COUNCIL. **National Annex to Singapore Standard EN 199-1-4:2009, General actions – Wind actions**. 2009

STANDARDS AUSTRALIA. **HB 212-2002 Design Wind Speeds for the Asia-Pacific Region**. Sydney, Australia. December, 2002.

THOM, H.C.S. **New distributions of extreme winds in the United States**. Journal of the Structural Division, New York, ASCE, vol. 94, pp.1787-1802, 1968.

TURNER, R.; PIROOZ, A.A.S.; FLAY, R.G.J.; MOORE, S.; REVELL, M. **Use of High-Resolution Numerical Models and Statistical Approaches to Understand New Zealand Historical Wind Speed and Gust Climatologies**. Journal of Applied Meteorology and Climatology, vol. 58, No. 6, pp. 1195-1218, 2019.

TWISDALE, L.A.; VICKERY, P.J. **Research on Thunderstorm Wind Design Parameters**. Journal of Wind Engineering and Industrial Aerodynamics, vol. 41, pp. 545-556, 1992.

VAISALA. **User’s Guide, Anemometer WAA151 - M210293en-A**. Helsinki, 2002.

VALLIS, M.B.; LOREDO-SOUZA, A.M.; WATRIN, L.C. A review of Brazilian wind data. **Proceedings of The 13th Americas Conference on Wind Engineering**, Gainesville, Florida, May 21- 24, 2017.

VALLIS, M.B.; LOREDO-SOUZA, A.M.; WATRIN, L.C.; BÊNIA, M.C.D. Ventos extremos do leste da cordilheira dos Andes. **Proceedings of XXXVIII Jornadas Sudamericanas de Ingeniería Estructural**, Lima, Peru, October 24-26, 2018.

[a] VERKAIK, J.W. **Documentation on wind speed measurements in the Netherlands. KNMI-HYDRA project, Phase report 1**. Technical Report KNMI – Koninklijk Nederlands Meteorologisch Instituut, 2001.

[b] VERKAIK, J.W. **A method for the geographical interpolation of wind speed over heterogeneous terrain, Phase report 11 and 12**. Technical Report KNMI Koninklijk Nederlands Meteorologisch Instituut, 2001.

VIEIRA FILHO, J.M.S. **Velocidades máximas do vento no Brasil**. 1975. Tese de mestrado, Escola de Engenharia, UFRGS, Porto Alegre.

VICKERY, B.J. **Load fluctuations in turbulent flow.** ASCE Journal of the Engineering Mechanics Division, vol. 94, No. 1, pp. 31-46, 1968.

VICKERY, P.J.; WADHERA, D.; GALSWORTHY, J.; PETERKA, J.A.; IRWIN P.A.; GRIFFIS, L.A. **Ultimate Wind Load Design Gust Wind Speeds in the United States for Use in ASCE-7.** Journal of Structural Engineering, vol. 136, pp. 613-625, 2010.

VIOLLAZ, A.; RIERA J.D.; REIMUNDIN J.C. **Estudio de la de la distribución de velocidades máximas de viento en la República Argentina.** INFORME I-75-1, Laboratorio de Ensayo de Estructuras, Universidad Nacional de Tucumán, 1975.

VON MISES, R. **La distribution de la plus grande de n valeurs.** Reprinted in Selected Papers of Richard von Mises, American Mathematical Society, 2, pp. 271-294, 1936.

WALLACE, J.M.; HOBBS, P.V. **Atmospheric Science: An Introductory Survey,** Elsevier Academic Press, 2nd Edition, 2006.

WAKIMOTO, R.M. **Convectively driven high wind events. In: Severe Convective Storms,** C. A. DOSWELL III (Editor), American Meteorological Society Monograph, vol. 28, No. 50, pp. 255-298, 2001.

WASTRACK, K.K; PITTMAN, D.E.; HATMAKER, J.E.; HAMBERGER, L.W. **Comparison of Wind Sensors – Ultrasonic versus Wind Vane/Anemometer,** NUMUG Meeting, Las Vegas, NV. October, 2000.

WAUBEN, W.M.F. Experiences with sonic wind sensors in operational conditions. **Proceedings of World Meteorological Organization, Technical Conference on Meteorological and Environmental Instruments and Methods of Observation,** Brussels, 2012.

WEIBULL, W. **A statistical theory of the strength of materials.** Generalstabens Litografiska Anstalts Förlag, Stockholm, 1939.

WHITTINGHAM, H.E. **Extreme wind gusts in Australia.** Bureau of Meteorology, Bulletin No. 46, 1964.

WIERINGA, J. **Representativeness of wind observations at airports.** Bulletin of the American Meteorological Society, vol. 61, pp. 962-971, 1980.

WOMBLE, J.A.; LADUE, J.G.; LEVITAN, M.L.; BROWN-GIAMMANCO, T.; COULBOURNE, B.; LOMBARDO, F.T; KOPP, G.A; **Development of the ASCE/SEI Standard for the Estimation of Tornado Wind Speeds. Proceedings of Canadian Society for Civil Engineering Annual Conference.** London, Canada, June 1-4, 2016.

WOOD, G.S.; KWOK, K.C.S.; MOTTERAM, N.A.; FLETCHER, D.F. **Physical and numerical modelling of thunderstorm downbursts.** Journal of Wind Engineering and Industrial Aerodynamics, vol. 89, pp 535-552, 2001.

WORLD METEOROLOGICAL ORGANIZATION. **Guide to Meteorological Instruments and Methods of Observation (WMO-8)**. Geneva, 2014.

WORLD METEOROLOGICAL ORGANIZATION. **Manual on Codes, International Codes, Volume I.1, Annex II to the WMO Technical Regulations, Part A – Alphanumeric Codes (WMO-306)**. Geneva, 2011 Edition (updated in 2015).

WORLD METEOROLOGICAL ORGANIZATION. **Technical Regulations, Basic Documents No. 2, Volume II – Meteorological Service for International Air Navigation (WMO-49)**. Geneva, 2016.

XU, Z; HANGAN, H. **Scale, boundary and inlet condition effects on impinging jets**. Journal of Wind Engineering and Industrial Aerodynamics, vol. 96, pp. 2383-2402, 2008.

ZIPSER, E.J.; CECIL, D.J.; LIU, C.; NESBITT, S.W.; YORTY, D.P. **Where are the most intense thunderstorms on Earth?** Bulletin of the American Meteorological Society, vol. 87, No. 8, pp. 1057-1071, 2006.

APPENDIX A

MAP OF BRAZIL AND SWS DETAILS

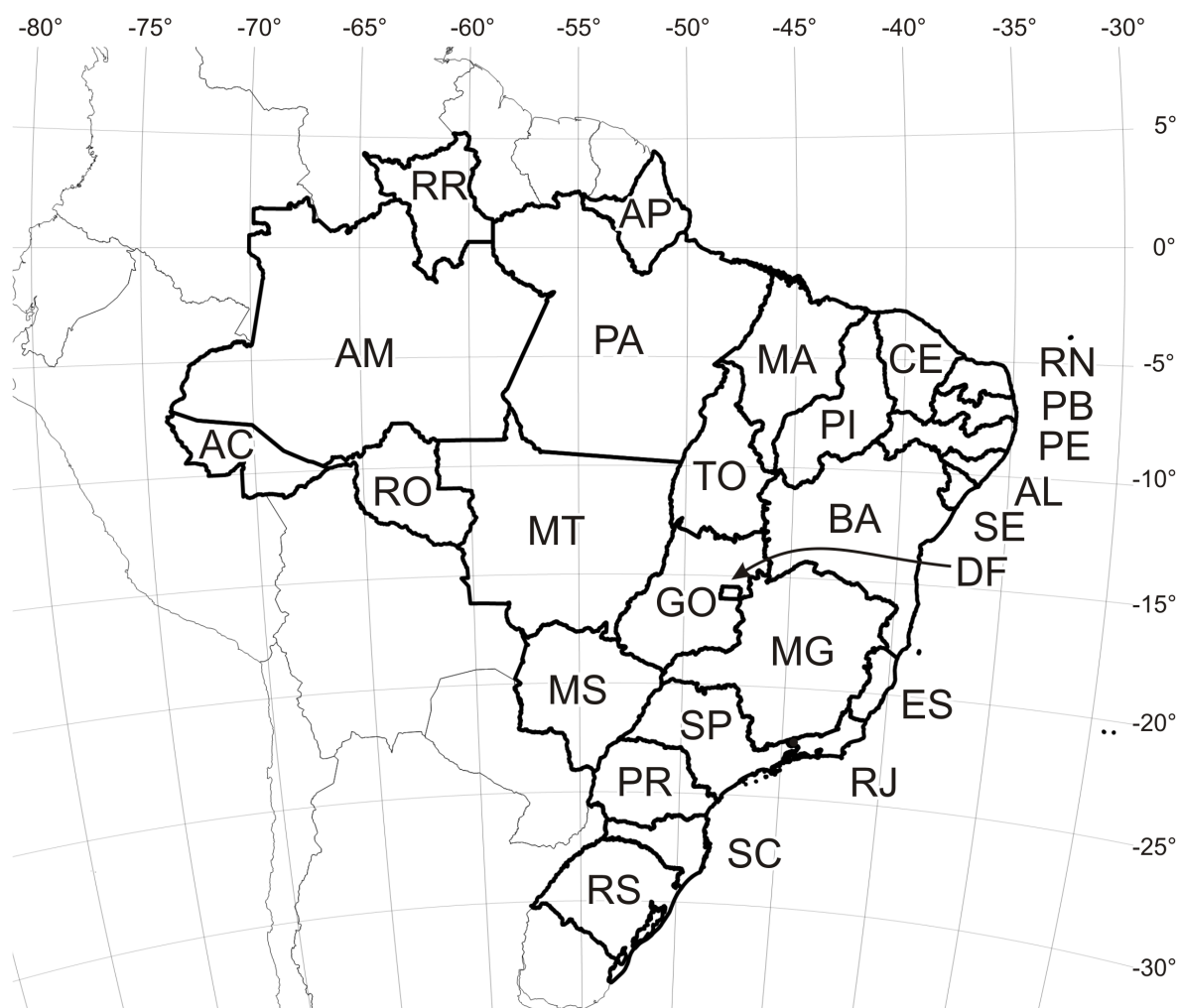


Figure A.1 – Map of Brazil with ISO 3166-2 state codes.

Table A.1 – Brazilian state codes and names.

ISO 3166-2	State
AC	Acre
AL	Alagoas
AP	Amapá
AM	Amazonas
BA	Bahia
CE	Ceará
DF	Distrito Federal
ES	Espírito Santo
GO	Goiás
MA	Maranhão
MT	Mato Grosso
MS	Mato Grosso do Sul
MG	Minas Gerais
PA	Pará

ISO 3166-2	State
PB	Paraíba
PR	Paraná
PE	Pernambuco
PI	Piauí
RJ	Rio de Janeiro
RN	Rio Grande do Norte
RS	Rio Grande do Sul
RO	Rondônia
RR	Roraima
SC	Santa Catarina
SP	São Paulo
SE	Sergipe
TO	Tocantins

Table A.2 – Selected Brazilian aerodrome surface weather stations

ICAO ID	WMO ID	Name	State	Alt. (m)	Lat. (°)	Lon. (°)	MSS	PAS31
SBAA	82862	BENDITO ROQUE	PA	199	-8.35	-49.30	A	A
SBAE	-	AREALVA	SP	594	-22.16	-49.07	A	A
SBAF	83748	BASE AÉREA DOS AFONSOS	RJ	34	-22.87	-43.38	A	A
SBAM	82030	AMAPÁ	AP	14	2.07	-50.87	C	C
SBAN	83419	BASE AÉREA DE ANÁPOLIS	GO	1137	-16.23	-48.97	A	AA
SBAQ	-	BARTOLOMEU DE GUSMÃO	SP	711	-21.80	-48.14	B	C
SBAR	83095	SANTA MARIA	SE	7	-10.98	-37.07	A	A
SBAT	82965	PILOTO OSWALDO MARQUES DIAS	MT	289	-9.87	-56.11	A	A
SBAU	-	DARIO GUARITA	SP	415	-21.14	-50.42	C	C
SBAX	-	ROMEU ZEMA	MG	999	-19.56	-46.97	B	C
SBBE	82193	VAL DE CANS	PA	17	-1.38	-48.48	A	AA
SBBG	83981	COMANDANTE GUSTAVO KRAEMER	RS	183	-31.38	-54.12	C	C
SBBH	83583	PAMPULHA	MG	789	-19.85	-43.95	A	A
SBBI	83011	BACACHERI	PR	932	-25.40	-49.23	A	AA
SBBP	-	ARTHUR SIQUEIRA	SP	880	-22.98	-46.54	A	A
SBBQ	83118	MAJOR BRIGADEIRO DOORGAL BORGES	MG	1115	-21.27	-43.76	A	AA
SBBR	83378	PRESIDENTE JUSCELINO KUBITSCHKE	DF	1066	-15.87	-47.92	A	AA
SBBU	83722	COMANDANTE JOÃO RIBEIRO DE BARROS	SP	617	-22.35	-49.05	A	A
SBBV	82022	ATLAS BRASIL CANTANHEDE	RR	84	2.85	-60.69	A	AA
SBBW	83359	BARRA DO GARÇAS	MT	350	-15.86	-52.39	B	B
SBBZ	-	UMBERTO MODIANO	RJ	3	-22.77	-41.97	C	C
SBCA	-	CORONEL ADALBERTO MEDES DA SILVA	PR	754	-25.00	-53.50	A	A
SBCB	-	CABO FRIO	RJ	7	-22.92	-42.07	A	A
SBCC	82930	CACHIMBO	PA	537	-9.33	-54.97	A	AB
SBCD	-	CAÇADOR	SC	1029	-26.79	-50.94	C	C
SBCF	83566	CONFINS	MG	827	-19.64	-43.97	A	AA
SBCG	83612	ANTÔNIO JOÃO	MS	559	-20.47	-54.67	A	AA
SBCH	-	SERAFIN ENOSS BERTASO	SC	654	-27.13	-52.65	A	A
SBCI	82764	BRIGADEIRO LYSIAS AUGUSTO RODRIGUES	MA	172	-7.32	-47.47	B	A
SBCJ	82567	CARAJÁS	PA	629	-6.12	-50.00	A	AA
SBCM	-	DIOMÍCIO FREITAS	SC	28	-28.73	-49.43	A	A
SBCN	-	NELSON RIBEIRO GUIMARÃES	GO	685	-17.73	-48.61	C	C
SBCO	83952	BASE AÉREA DE CANOAS	RS	8	-29.95	-51.15	A	AA
SBCP	83103	BARTOLOMEU LISANDRO	RJ	17	-21.70	-41.30	A	A
SBCR	83554	CORUMBÁ	MS	141	-19.01	-57.67	A	AA
SBCT	83840	AFONSO PENA	PR	911	-25.53	-49.18	A	AA
SBCV	83497	CARAVELAS	BA	11	-17.65	-39.25	C	C
SBCX	83942	CAMPO DOS BUGRES	RS	754	-29.20	-51.19	C	C
SBCY	83362	MARECHAL RONDON	MT	188	-15.65	-56.12	A	A

Table A.2 (cont...) - Selected Brazilian aerodrome surface weather stations

ICAO ID	WMO ID	Name	State	Alt. (m)	Lat. (°)	Lon. (°)	MSS	PAS31
SBCZ	82705	CRUZEIRO DO SUL	AC	194	-7.60	-72.77	A	A
SBDN	83616	PRESIDENTE PRUDENTE	SP	450	-22.18	-51.43	A	A
SBDO	-	FRANCISCO DE MATOS PEREIRA	MS	458	-22.20	-54.93	A	A
SBEG	82333	EDUARDO GOMES	AM	80	-3.04	-60.05	A	AA
SBEK	82640	JACAREACANGA	PA	99	-6.23	-57.78	A	A
SBES	83759	SÃO PEDRO DA ALDEIA	RJ	19	-22.81	-42.09	A	AA
SBFI	83827	CATARATAS	PR	239	-25.60	-54.48	A	AA
SBFL	83899	HERCÍLIO LUZ	SC	5	-27.67	-48.55	A	AA
SBFN	82400	GOVERNADOR CARLOS WILSON	PE	58	-3.85	-32.42	A	A
SBFS	-	HELIPORTO SÃO TOMÉ	RJ	3	-22.03	-41.07	A	A
SBFZ	82398	PINTO MARTINS	CE	25	-3.78	-38.53	A	AA
SBGL	83746	GALEÃO	RJ	9	-22.80	-43.25	A	AAAA
SBGM	83016	GUAJARÁ-MIRIM	RO	146	-10.78	-65.28	A	A
SBGO	83424	SANTA GENOVEVA	GO	747	-16.63	-49.22	A	A
SBGP	-	EMBRAER UNIDADE GAVIÃO PEIXOTO	SP	609	-21.76	-48.40	A	A
SBGR	83778	GUARULHOS	SP	750	-23.43	-46.47	A	AAAA
SBGU	-	TANCREDO THOMAS DE FARIA	PR	1065	-25.39	-51.52	C	C
SBGV	-	CORONEL ALTINO MACHADO DE OLIVEIRA	MG	171	-18.90	-41.98	C	C
SBGW	83708	EDU CHAVES	SP	537	-22.79	-45.20	A	A
SBHT	82354	ALTAMIRA	PA	112	-3.25	-52.25	A	A
SBIC	82335	ITACOATIARA	AM	43	-3.13	-58.48	B	B
SBIH	82444	ITAITUBA	PA	33	-4.24	-56.00	A	A
SBIL	83349	JORGE AMADO	BA	4	-14.82	-39.03	A	A
SBIP	-	USIMINAS	MG	239	-19.47	-42.49	A	A
SBIT	-	HIDROELÉTRICA	GO	497	-18.44	-49.21	B	B
SBIZ	82565	PREFEITO RENATO MOREIRA	MA	131	-5.53	-47.46	A	A
SBJA	-	HUMBERTO GHIZZO BORTOLUZZI	SC	34	-28.68	-49.06	C	C
SBJC	-	BRIGADEIRO PROTÁSIO DE OLIVEIRA	PA	16	-1.42	-48.46	A	A
SBJD	-	COMANDANTE ROLIM ADOLFO AMARO	SP	757	-23.18	-46.94	A	A
SBJF	83112	FRANCISCO ÁLVARES DE ASSIS	MG	911	-21.79	-43.39	A	A
SBJI	-	JOSÉ COLETO	RO	178	-10.87	-61.85	C	-
SBJP	82800	PRESIDENTE CASTRO PINTO	PB	66	-7.15	-34.95	A	A
SBJR	83054	JACAREPAGUÁ	RJ	3	-22.99	-43.37	A	A
SBJU	-	ORLANDO BEZERRA DE MENEZES	CE	424	-7.22	-39.27	A	A
SBJV	83905	LAURO CARNEIRO DE LOYOLA	SC	4	-26.22	-48.80	A	A
SBKG	82796	PRESIDENTE JOÃO SUASSUNA	PB	502	-7.27	-35.90	A	AC
SBKP	83721	VIRACOPOS	SP	657	-23.01	-47.14	A	AA
SBLE	83242	CHAPADA DIAMANTINA	BA	511	-12.48	-41.28	C	C
SBLJ	-	ANTÔNIO CORREIA PINTO DE MACEDO	SC	934	-27.78	-50.28	C	C

Table A.2 (cont...) - Selected Brazilian aerodrome surface weather stations

ICAO ID	WMO ID	Name	State	Alt. (m)	Lat. (°)	Lon. (°)	MSS	PAS31
SBLO	83768	GOVERNADOR JOSÉ RICHÁ	PR	569	-23.33	-51.13	A	A
SBLP	83289	BOM JESUS DA LAPA	BA	443	-13.26	-43.41	A	-
SBLS	83588	BASE AÉREA DE LAGOA SANTA	MG	852	-19.66	-43.90	A	AA
SBMA	82563	JOÃO CORREA DA ROCHA	PA	109	-5.37	-49.13	A	A
SBMD	82091	MONTE DOURADO	PA	206	-0.89	-52.60	A	A
SBME	83749	MACAÉ	RJ	2	-22.34	-41.77	A	A
SBMG	83628	SÍLVIO NAME JUNIOR	PR	545	-23.48	-52.01	A	A
SBMK	83436	MÁRIO RIBEIRO	MG	668	-16.71	-43.82	A	A
SBML	-	FRANK MILOYE MILENKOVICH	SP	650	-22.20	-49.93	C	C
SBMN	82332	PONTA PELADA	AM	81	-3.15	-59.99	A	AA
SBMO	82993	ZUMBI DOS PALMARES	AL	118	-9.51	-35.79	A	A
SBMQ	82099	ALBERTO ALCOLUMBRE	AP	17	0.05	-51.07	A	A
SBMS	82592	GOVERNADOR DIX-SEPT ROSADO	RN	23	-5.20	-37.36	A	A
SBMT	83779	CAMPO DE MARTE	SP	722	-23.51	-46.64	B	B
SBMY	82532	MANICORÉ	AM	53	-5.82	-61.28	A	A
SBNF	83926	MINISTRO VICTOR KONDER	SC	5	-26.88	-48.65	A	A
SBNM	-	SEPÉ TIARAJU	RS	322	-28.28	-54.17	C	C
SBNT	82599	AUGUSTO SEVERO	RN	52	-5.91	-35.24	A	AC
SBOI	82017	OIAPOQUE	AP	19	3.85	-51.80	B	BB
SBPA	83971	SALGADO FILHO	RS	3	-29.99	-51.17	A	AA
SBPB	82288	PREFEITO DOUTRO JOÃO SILVA FILHO	PI	7	-2.89	-41.73	A	A
SBPC	83644	EMBAIXADOR WALTHER MOREIRA SALLES	MG	1260	-21.84	-46.57	A	A
SBPF	-	LAURO KURTZ	RS	724	-28.24	-52.33	C	C
SBPJ	83065	BRIGADEIRO LYSIAS	TO	236	-10.29	-48.36	A	A
SBPK	83984	PELOTAS	RS	18	-31.72	-52.33	A	A
SBPL	82984	SENADOR NILO COELHO	PE	384	-9.36	-40.57	A	A
SBPN	83063	PORTO NACIONAL	TO	265	-10.72	-48.40	A	A
SBPP	83703	PONTA PORÃ	MS	657	-22.55	-55.70	A	A
SBPR	83571	CARLOS PRATES	MG	928	-19.91	-43.99	A	A
SBPS	83460	PORTO SEGURO	BA	51	-16.44	-39.08	A	AA
SBPV	82824	GOVERNADOR JORGE TEIXEIRA DE OLIVEIRA	RO	88	-8.70	-63.90	A	A
SBQV	83345	PEDRO OTACÍLIO FIGUEIREDO	BA	915	-14.86	-40.86	A	A
SBRB	82917	PLÁCIDO DE CASTRO	AC	193	-9.87	-67.89	A	AA
SBRF	82899	GILBERTO FREYRE	PE	10	-8.13	-34.92	A	AA
SBRJ	83755	SANTOS DUMONT	RJ	3	-22.91	-43.16	A	A
SBRP	83652	DOUTOR LEITE LOPES	SP	550	-21.13	-47.77	A	A
SBSC	83115	BASE AÉREA DE SANTA CRUZ	RJ	3	-22.94	-43.72	A	AA
SBSG	-	SÃO GONÇALO DO AMARANTE	RN	83	-5.77	-35.37	A	A
SBSJ	83829	PROFESSOR URBANO ERNESTO STUMPF	SP	646	-23.23	-45.86	A	AA

Table A.2 (cont...) - Selected Brazilian aerodrome surface weather stations

ICAO ID	WMO ID	Name	State	Alt. (m)	Lat. (°)	Lon. (°)	MSS	PAS31
SBSL	82281	MARECHAL HUGO DA CUNHA MACHADO	MA	54	-2.58	-44.23	A	AA
SBSM	83937	SANTA MARIA	RS	88	-29.71	-53.69	A	AA
SBSN	82244	MAESTRO WILSON FONSECA	PA	60	-2.42	-54.79	A	AA
SBSP	83780	CONGONHAS	SP	802	-23.63	-46.66	A	AA
SBSR	-	SÃO JOSÉ DO RIO PRETO	SP	543	-20.82	-49.41	A	A
SBST	83818	BASE AÉREA DE SANTOS	SP	3	-23.93	-46.30	A	A
SBSV	83248	DEPUTADO LUÍS EDUARDO MAGALHÃES	BA	20	-12.91	-38.32	A	AA
SBTA	83784	BASE DE AVIAÇÃO DE TAUBATÉ	SP	581	-23.04	-45.52	A	A
SBTB	-	TROMBETAS	PA	87	-1.49	-56.40	C	C
SBTC	-	HOTEL TRANSAMÉRICA	BA	6	-15.35	-39.00	B	B
SBTD	-	LUÍZ DAL CANALLE FILHO	PR	562	-24.69	-53.70	C	C
SBTE	82579	SENADOR PETRÔNIO PORTELLA	PI	67	-5.06	-42.82	A	A
SBTF	82318	TEFÊ	AM	57	-3.38	-64.72	A	A
SBTG	-	PLÍNIO ALARCOM	MS	326	-10.87	-51.68	C	-
SBTK	82808	JOSÉ GALERA DOS SANTOS	AM	197	-8.16	-70.78	B	A
SBTR	-	TORRES	RS	8	-29.41	-49.81	C	C
SBTS	82026	TIRIOS	PA	344	2.22	-55.95	B	B
SBTT	82411	TABATINGA	AM	85	-4.26	-69.94	A	A
SBTU	82360	TUCURUÍ	PA	253	-3.78	-49.72	A	A
SBTV	-	TERRA VISTA	BA	50	-16.54	-39.11	C	C
SBUA	82107	SÃO GABRIEL DA CACHOEIRA	AM	76	-0.15	-66.98	A	A
SBUF	82894	PAULO AFONSO	BA	269	-9.40	-38.25	A	A
SBUG	83928	RUBEM BERTA	RS	78	-29.78	-57.03	A	A
SBUL	83525	TEM.-CEL. AVIADOR CÉSAR BOMBONATO	MG	943	-18.88	-48.22	A	AA
SBUR	83576	MÁRIO DE ALMEIDA FRANCO	MG	809	-19.77	-47.96	A	A
SBUY	-	URUCU	AM	64	-4.88	-65.36	A	A
SBVG	-	MAJOR BRIGADEIRO TROMPOWSKY	MG	922	-21.59	-45.47	C	C
SBVH	83208	BRIGADEIRO CAMARÃO	RO	615	-12.70	-60.10	A	A
SBVT	83649	EURICO DE AGUIAR SALLES	ES	3	-20.25	-40.28	A	AA
SBYA	82068	IAURETÊ	AM	105	0.61	-69.18	C	C
SBYS	83671	CAMPO DE FONTENELLE	SP	600	-21.98	-47.33	A	AA
SBZM	-	ZONA DA MATA	MG	411	-21.51	-43.17	A	A

Table A.3 - Selected international aerodrome surface weather stations

ICAO ID	WMO ID	Name	Country	Alt. (m)	Lat. (°)	Lon. (°)	MSS
EGYP	88889	RAF MOUNT PLEASANT	UK	74	-51.82	-58.47	A
SAAR	87480	ROSÁRIO ISLAS MALVINAS	AR	25	-32.90	-60.78	A
SABE	87582	AEROPARQUE JORGE NEWBERRY	AR	6	-34.56	-58.42	A
SACO	87344	PAJAS BLANCAS	AR	474	-31.32	-64.21	A
SADF	87553	SAN FERNANDO	AR	3	-34.45	-58.59	A
SAEZ	87576	MINISTRO PISTARINI	AR	20	-34.83	-58.54	A
SAME	87418	EL PLUMERILLO	AR	704	-32.83	-68.79	A
SANT	87121	TENIENTE GENERAL BENJAMÍN MATIENZO	AR	450	-26.84	-65.10	A
SAOC	87453	RÍO CUARTO	AR	421	-33.09	-64.26	B
SARC	87166	DOCTOR FERNANDO PIRAGINE NIVEYRO	AR	62	-27.45	-58.75	A
SARE	87155	RESISTENCIA	AR	52	-27.45	-59.06	A
SARF	87162	FORMOSA	AR	60	-26.21	-58.23	A
SARI	87097	CATARATAS DEL IGUAZÚ	AR	270	-25.74	-54.47	A
SARL	87289	PASO DE LOS LIBRES	AR	70	-29.69	-57.15	A
SARP	87178	LIBERTADOR GEN. JOSÉ DE SAN MARTIN	AR	131	-27.39	-55.97	A
SASA	87047	MARTÍN MIGUEL DE GÜEMES	AR	1221	-24.85	-65.48	A
SASJ	87046	GOBERNADOR HORACIO GUZMÁN	AR	920	-24.39	-65.10	A
SAVC	87860	GENERAL ENRIQUE MOSCONI	AR	58	-45.79	-67.47	A
SAWE	87934	GOBERNADOR RAMÓN TREJO NOEL	AR	22	-53.78	-67.75	A
SAWG	87925	PILOTO CIVIL NORBERTO FERNÁNDEZ	AR	19	-51.61	-69.31	A
SAWH	87938	USHUAIA MALVINAS ARGENTINAS	AR	22	-54.84	-68.30	A
SAZM	87692	ASTOR PIAZZOLLA	AR	21	-37.93	-57.57	A
SAZN	87715	PRESIDENTE PERÓN	AR	271	-38.95	-68.16	A
SAZS	87765	TENIENTE LUIS CANDELARIA	AR	840	-41.15	-71.15	A
SCBA	85874	BALMACEDA	CL	524	-45.92	-71.69	A
SCCI	85934	CARLOS IBÁÑEZ DEL CAMPO	CL	37	-53.00	-70.85	A
SCRM	89056	TENIENTE RODOLFO MARSH MARTIN	CL	45	-62.19	-58.99	B
SGAS	86218	SILVIO PETTIROSSI	PY	89	-25.24	-57.52	A
SGEN	86294	TENIENTE AMIN AYUB GONZALEZ	PY	91	-27.23	-55.84	B
SGES	86246	GUARANÍ	PY	247	-25.46	-54.84	A
SKLT	80398	ALFREDO VÁSQUEZ COBO	CO	84	-4.19	-69.94	A
SLCO	85041	CAPITÁN ANÍBAL ARAB	BO	272	-11.04	-68.78	A
SLET	85245	EL TROMPILLO	BO	418	-17.81	-63.17	A
SLPS	85289	CAPITÁN SALVADOR OGAYA GUTIERREZ	BO	134	-18.98	-57.82	A
SLTR	85154	TENIENTE JORGE HENRICH ARAUZ	BO	155	-14.82	-64.92	A
SLVR	85244	VIRU VIRU	BO	373	-17.64	-63.14	A
SMJP	81225	JOHAN ADOLF PENGEL	SR	15	5.45	-55.19	A
SMZO	81200	ZORG EN HOOP	SR	7	5.81	-55.19	A
SOCA	81405	FÉLIX EBOUÉ	GF	9	4.82	-52.36	A
SPCL	84515	CAPITÁN FAP DAVID ABENSUR RENGIFO	PE	149	-8.38	-74.57	A

Table A.3 (cont...) - Selected international aerodrome surface weather stations

ICAO ID	WMO ID	Name	Country	Alt. (m)	Lat. (°)	Lon. (°)	MSS
SPQT	84377	CNEL. FAP FRANCISCO SECADA VIGNETTA	PE	126	-3.78	-73.31	A
SPST	84455	FAP GUILLERMO DEL CASTILLO PAREDES	PE	282	-6.51	-76.37	A
SUAA	86575	ÁNGEL S. ADAMI	UY	53	-34.79	-56.26	A
SUCA	86560	LAGUNA DE LOS PATOS	UY	20	-34.46	-57.77	B
SUDU	86530	SANTA BERNARDINA	UY	93	-33.36	-56.50	A
SULS	86586	LAGUNA DEL SAUCE	UY	35	-34.86	-55.09	A
SUMU	86580	CARRASCO	UY	32	-34.84	-56.03	A
SUSO	86360	NUEVA HESPÉRIDES	UY	42	-31.44	-57.99	A
SYCJ	81002	CHEDDI JAGAN	GY	30	6.50	-58.25	A

Table A.4 – Selected INMET automatic surface weather stations

INMET ID	WMO ID	Name	State	Alt. (m)	Lat. (°)	Lon. (°)	WRDS
A001	86715	BRASÍLIA	DF	1161	-15.7893	-47.9258	A
A002	86734	GOIÂNIA	GO	727	-16.6428	-49.2202	A
A003	86755	MORRINHOS	GO	751	-17.7451	-49.1017	A
A004	86690	NIQUELÂNDIA	GO	664	-14.4694	-48.4858	A
A009	86607	PALMAS	TO	292	-10.1907	-48.3018	A
A010	86650	PARANÃ	TO	285	-12.6149	-47.8719	A
A011	86773	SÃO SIMÃO	GO	492	-18.9691	-50.6334	A
A012	86736	LUZIÂNIA	GO	1001	-16.2605	-47.9670	A
A013	86709	ARAGARÇAS	GO	327	-15.9027	-52.2452	A
A014	86712	GOIÁS	GO	513	-15.9397	-50.1414	A
A015	86689	ITAPACI	GO	551	-14.9798	-49.5400	A
A016	86752	JATAÍ	GO	670	-17.9236	-51.7175	A
A017	86692	POSSE	GO	830	-14.0892	-46.3665	A
A018	86649	PEIXE	TO	251	-12.0154	-48.5445	A
A019	86630	GURUPI	TO	279	-11.7458	-49.0497	A
A020	81941	PEDRO AFONSO	TO	190	-8.9687	-48.1773	A
A021	81900	ARAGUAÍNA	TO	231	-7.1040	-48.2012	A
A022	86713	GOIANÉSIA	GO	667	-15.2202	-48.9901	A
A023	86730	CAIAPÔNIA	GO	740	-16.9668	-51.8176	A
A024	86691	ALTO PARAÍSO DE GOIÁS	GO	1265	-14.1331	-47.5233	A
A025	86753	RIO VERDE	GO	780	-17.7853	-50.9649	A
A026	86751	MINEIROS	GO	713	-17.5693	-52.5965	A
A027	86732	PARAÚNA	GO	679	-16.9625	-50.4255	A
A028	86731	IPORÁ	GO	610	-16.4231	-51.1488	A
A032	86670	MONTE ALEGRE DE GOIÁS	GO	551	-13.2535	-46.8903	A
A033	86756	PIRES DO RIO	GO	757	-17.3042	-48.2841	A
A034	86777	CATALÃO	GO	901	-18.1548	-47.9276	A
A035	86774	ITUMBIARA	GO	491	-18.4098	-49.1921	A
A036	86737	CRISTALINA	GO	1211	-16.7849	-47.6130	A
A037	86735	SILVÂNIA	GO	952	-16.6798	-48.6182	A
A038	86632	DIANÓPOLIS	TO	728	-11.5944	-46.8472	A
A039	86629	FORMOSO DO ARAGUAIA	TO	215	-11.8874	-49.6082	A
A040	86608	MATEIROS	TO	791	-10.4344	-45.9219	A
A041	81983	MARIANÓPOLIS DO TOCANTINS	TO	187	-9.5764	-49.7233	A
A043	81902	CAMPOS LINDOS	TO	427	-8.1547	-46.6393	A
A044	81821	ARAGUATINS	TO	131	-5.6437	-48.1118	A
A045	86716	ÁGUAS EMENDADAS	DF	1030	-15.5965	-47.6258	A
A046	86711	GAMA (PONTE ALTA)	DF	990	-15.9351	-48.1374	A
A052	86631	SANTA ROSA DO TOCANTINS	TO	306	-11.4290	-48.1849	B

Table A.4 (cont...) - Selected INMET automatic surface weather stations

INMET ID	WMO ID	Name	State	Alt. (m)	Lat. (°)	Lon. (°)	WRDS
A054	86648	ARAGUAÇU	TO	231	-12.5922	-49.5287	A
A101	81730	MANAUS	AM	49	-3.1037	-60.0155	A
A102	81963	PARQUE ESTADUAL CHANDLESS	AC	185	-9.3584	-69.9263	A
A104	81965	RIO BRANCO	AC	224	-9.9578	-68.1652	A
A108	81881	CRUZEIRO DO SUL	AC	220	-7.6106	-72.6811	A
A109	81843	EIRUNEPÉ	AM	122	-6.6503	-69.8686	A
A110	81927	BOCA DO ACRE	AM	112	-8.7768	-67.3326	A
A111	81888	LÁBREA	AM	62	-7.2607	-64.7885	A
A112	81890	HUMAITÁ	AM	54	-7.5525	-63.0713	A
A113	81893	APUI	AM	157	-7.2055	-59.8886	A
A117	81770	COARI	AM	34	-4.0975	-63.1453	A
A119	81729	MANACAPURU	AM	37	-3.2946	-60.6284	A
A120	81732	AUTAZES	AM	20	-3.5833	-59.1294	A
A121	81733	ITACOATIARA	AM	42	-3.1333	-58.4828	A
A122	81734	MAUÉS	AM	25	-3.3990	-57.6738	A
A123	81703	PARINTINS	AM	19	-2.6392	-56.7562	A
A124	81702	URUCARÁ	AM	18	-2.5347	-57.7581	A
A125	81700	RIO URUBU	AM	113	-2.6337	-59.6006	A
A126	81699	PRESIDENTE FIGUEIREDO	AM	61	-2.0566	-60.0258	A
A128	81648	BARCELOS	AM	30	-0.9873	-62.9243	A
A133	81810	MANICORÉ	AM	41	-5.7885	-61.2883	A
A134	81643	SÃO GABRIEL DA CACHOEIRA	AM	80	-0.1252	-67.0612	A
A135	81615	BOA VISTA	RR	82	2.8169	-60.6908	A
A136	81921	PORTO WALTER	AC	205	-8.2672	-72.7478	A
A137	81922	MARECHAL THAUMATURGO	AC	221	-8.9500	-72.7868	C
A138	81924	FEIJÓ	AC	157	-8.1427	-70.3436	A
A140	86620	EPITACIOLÂNDIA	AC	225	-11.0238	-68.7352	A
A201	81680	BELÉM	PA	21	-1.4112	-48.4395	A
A202	81682	CASTANHAL	PA	47	-1.3009	-47.9480	A
A203	81715	SÃO LUÍS	MA	55	-2.5268	-44.2136	A
A204	81903	BALSAS	MA	271	-7.4556	-46.0275	A
A205	81901	CAROLINA	MA	183	-7.3373	-47.4598	A
A206	81749	CHAPADINHA	MA	104	-3.7427	-43.3521	A
A207	81823	GRAJAÚ	MA	232	-5.8161	-46.1622	A
A209	81739	MEDICILÂNDIA	PA	252	-3.5109	-52.9635	A
A210	81742	PACAJÁ	PA	89	-3.8437	-50.6381	A
A211	81737	PLACAS	PA	100	-3.8640	-54.2164	A
A212	81745	PARAGOMINAS	PA	85	-3.0099	-47.3431	A
A213	81711	TOMÉ AÇU	PA	43	-2.5926	-48.3606	A

Table A.4 (cont...) - Selected INMET automatic surface weather stations

INMET ID	WMO ID	Name	State	Alt. (m)	Lat. (°)	Lon. (°)	WRDS
A214	81786	RONDON DO PARÁ	PA	229	-4.7845	-48.0711	A
A215	81660	SALINÓPOLIS	PA	23	-0.6189	-47.3566	A
A217	81716	FAROL SANTANA	MA	10	-2.2708	-43.6240	A
A218	81717	FAROL PREGUIÇAS	MA	5	-2.5924	-42.7075	A
A219	81687	TURIAÇU	MA	36	-1.6612	-45.3726	A
A220	81790	BACABAL	MA	22	-4.2431	-44.7950	A
A221	81825	BARRA DO CORDA	MA	154	-5.5068	-45.2371	A
A222	81866	COLINAS	MA	175	-6.0332	-44.2334	A
A223	81985	ALTO PARNAÍBA	MA	284	-9.1082	-45.9320	A
A224	81863	ESTREITO	MA	183	-6.6533	-47.4182	A
A225	81822	IMPERATRIZ	MA	118	-5.5557	-47.4598	A
A226	81685	BRAGANÇA	PA	41	-1.0473	-46.7858	A
A227	81658	SOURE	PA	13	-0.7278	-48.5158	A
A229	81743	TUCURUÍ	PA	138	-3.8228	-49.6750	A
A230	81860	SERRA DOS CARAJÁS	PA	707	-6.0774	-50.1423	A
A231	81778	ITAITUBA	PA	24	-4.2770	-55.9931	A
A232	81675	ÓBIDOS	PA	90	-1.8808	-55.5199	C
A233	81982	SANTANA DO ARAGUAIA	PA	177	-9.3386	-50.3503	A
A234	81859	TUCUMÃ	PA	321	-6.7432	-51.1419	B
A235	81784	NOVO REPARTIMENTO	PA	101	-4.2440	-49.9393	A
A236	81710	CAMETÁ	PA	10	-2.2397	-49.4998	A
A237	81792	CAXIAS	MA	85	-4.8214	-43.3437	C
A238	81788	BURITICUPU	MA	175	-4.3206	-46.4495	A
A239	81706	MONTE ALEGRE	PA	101	-2.0000	-54.0758	A
A240	81820	MARABÁ	PA	117	-5.3664	-49.0512	A
A241	81940	CONCEIÇÃO DO ARAGUAIA	PA	176	-8.3036	-49.2828	A
A242	81609	OIAPOQUE	AP	15	3.8136	-51.8625	A
A243	81628	TARTARUGALZINHO	AP	21	1.4967	-50.9167	A
A244	81637	PORTO GRANDE	AP	74	0.7028	-51.4278	C
A246	81855	MINA PALITO	PA	260	-6.3198	-55.7873	A
A248	81684	CAPITÃO POÇO	PA	79	-1.7347	-47.0575	A
A249	81638	MACAPÁ	AP	17	0.0353	-51.0886	A
A250	81707	SANTARÉM	PA	137	-2.5027	-54.7204	A
A301	81958	RECIFE	PE	11	-8.0593	-34.9592	A
A302	81639	SÃO PEDRO E SÃO PAULO	PE	2	0.9169	-29.3459	C
A303	81998	MACEIÓ	AL	84	-9.5512	-35.7702	A
A304	81839	NATAL	RN	47	-5.8372	-35.2079	A
A305	81758	FORTALEZA	CE	30	-3.8157	-38.5378	A
A306	81754	SOBRAL	CE	92	-3.7482	-40.3457	A

Table A.4 (cont...) - Selected INMET automatic surface weather stations

INMET ID	WMO ID	Name	State	Alt. (m)	Lat. (°)	Lon. (°)	WRDS
A307	81991	PETROLINA	PE	373	-9.3883	-40.5233	A
A308	81752	PARNAÍBA	PI	52	-3.0867	-41.7831	A
A309	81953	ARCO VERDE	PE	684	-8.4335	-37.0555	A
A310	81877	AREIA	PB	573	-6.9755	-35.7181	A
A311	81868	FLORIANO	PI	126	-6.7614	-43.0034	A
A312	81827	TERESINA	PI	75	-5.0348	-42.8013	A
A313	81916	CAMPINA GRANDE	PB	546	-7.2256	-35.9048	A
A314	81797	GUARAMIRANGA	CE	866	-4.2614	-38.9311	A
A315	81911	BARBALHA	CE	409	-7.3009	-39.2711	A
A316	81875	CAICÓ	RN	171	-6.4675	-37.0849	A
A317	81836	MACAU	RN	17	-5.1510	-36.5731	A
A318	81834	MOSSORÓ	RN	29	-4.9041	-37.3669	A
A319	81873	IGUATU	CE	222	-6.3964	-39.2690	A
A320	81918	JOÃO PESSOA	PB	34	-7.1654	-34.8156	A
A321	81913	PATOS	PB	264	-7.0798	-37.2729	A
A322	81955	GARANHUNS	PE	828	-8.9110	-36.4934	A
A323	81994	PÃO DE AÇUCAR	AL	21	-9.7492	-37.4308	A
A324	81872	TAUÁ	CE	411	-6.0175	-40.2813	A
A325	81831	QUIXERAMOBIM	CE	221	-5.1746	-39.2894	A
A326	81987	BOM JESUS DO PIAUÍ	PI	296	-9.0833	-44.3264	A
A327	81995	PALMEIRA DOS ÍNDIOS	AL	278	-9.4203	-36.6204	A
A328	81917	SURUBIM	PE	421	-7.8396	-35.8011	A
A329	81951	CABROBÓ	PE	343	-8.5040	-39.3153	A
A330	81950	PAULISTANA	PI	376	-8.1323	-41.1429	A
A331	81848	SÃO JOÃO DO PIAUÍ	PI	237	-8.3650	-42.2504	A
A332	81832	MORADA NOVA	CE	45	-5.1367	-38.3566	A
A333	81774	SÃO GONÇALO	PB	237	-6.8358	-38.3116	A
A334	81914	MONTEIRO	PB	606	-7.8945	-37.1247	A
A335	81794	PIRIPIRI	PI	158	-4.2760	-41.7946	A
A336	81846	ALVORADA DO GURGUÉIA	PI	261	-8.4416	-43.8654	A
A337	81988	CARACOL	PI	515	-9.2859	-43.3244	A
A338	81751	ESPERANTINA	PI	88	-3.8994	-42.2595	A
A339	81798	JAGUARUANA	CE	17	-4.8535	-37.7772	A
A340	81835	APODI	RN	131	-5.6266	-37.8150	A
A341	81956	CARUARU	PE	570	-8.2361	-35.9856	A
A342	81830	CRATEÚS	CE	298	-5.1866	-40.6721	A
A343	81908	PICOS	PI	233	-7.0710	-41.4040	A
A344	81838	CALCANHAR	RN	10	-5.1599	-35.4876	A
A345	81989	SÃO RAIMUNDO NONATO	PI	383	-9.0332	-42.7011	A

Table A.4 (cont...) - Selected INMET automatic surface weather stations

INMET ID	WMO ID	Name	State	Alt. (m)	Lat. (°)	Lon. (°)	WRDS
A346	81905	URUÇUI	PI	399	-7.4414	-44.3451	A
A347	81909	CAMPOS SALES	CE	578	-7.0777	-40.3627	A
A348	81915	CABACEIRAS	PB	392	-7.4832	-36.2865	A
A349	81954	IBIMIRIM	PE	434	-8.5096	-37.7116	A
A350	81912	SERRA TALHADA	PE	499	-7.9543	-38.2951	A
A351	81952	FLORESTA	PE	327	-8.6103	-38.5922	A
A352	81878	CAMARATUBA	PB	136	-6.5618	-35.1353	A
A353	81996	ARAPIRACA	AL	237	-9.8046	-36.6192	A
A354	81869	OEIRAS	PI	154	-6.9741	-42.1468	A
A355	86619	CORURIBE	AL	82	-10.1285	-36.2863	A
A356	81997	SÃO LUIS DO QUITUNDE	AL	14	-9.2875	-35.5659	A
A357	81957	PALMARES	PE	164	-8.6667	-35.5679	A
A358	81833	JAGUARIBE	CE	149	-5.9056	-38.6278	A
A359	81756	ITAPIOCA	CE	104	-3.4843	-39.5887	A
A360	81755	ACARAÚ	CE	67	-3.1211	-40.0873	A
A361	81829	CASTELO DO PIAUÍ	PI	269	-5.3492	-41.5123	A
A362	81828	SÃO PEDRO DO PIAUÍ	PI	296	-5.9110	-42.7187	A
A363	81870	VALENÇA DO PIAUÍ	PI	313	-6.3993	-41.7400	A
A364	81986	GILBUÉS	PI	425	-9.8752	-45.3458	A
A365	81847	CANTO DO BURITI	PI	312	-8.1179	-42.9757	A
A366	81910	OURICURI	PE	458	-7.8847	-40.1011	A
A367	81876	SANTA CRUZ	RN	227	-6.2279	-36.0266	A
A401	86678	SALVADOR	BA	48	-13.0055	-38.5058	A
A402	86652	BARREIRAS	BA	474	-12.1247	-45.0270	A
A404	86651	LUIS EDUARDO MAGALHÃES	BA	761	-12.1524	-45.8297	A
A405	86764	CARAVELAS	BA	6	-17.7394	-39.2586	A
A406	86657	CRUZ DAS ALMAS	BA	220	-12.6754	-39.0896	A
A407	86674	ITIRUÇU	BA	757	-13.5278	-40.1198	A
A408	86656	ITABERABA	BA	250	-12.5241	-40.2997	A
A409	86616	ARACAJU	SE	4	-10.9524	-37.0543	A
A410	86699	ILHÉUS	BA	80	-14.6588	-39.1814	A
A411	81993	PAULO AFONSO	BA	255	-9.3781	-38.2268	A
A412	86655	MACAJUBA	BA	339	-12.1317	-40.3542	A
A413	86658	FEIRA DE SANTANA	BA	230	-12.1962	-38.9674	A
A414	86697	VITÓRIA DA CONQUISTA	BA	879	-14.8864	-40.8013	A
A415	86633	SANTA RITA DE CÁSSIA	BA	450	-11.0028	-44.5250	A
A416	86671	CORRENTINA	BA	552	-13.3324	-44.6174	A
A417	86638	ITABAIANINHA	SE	205	-11.2725	-37.7950	A
A418	86672	BOM JESUS DA LAPA	BA	448	-13.2511	-43.4054	A

Table A.4 (cont...) - Selected INMET automatic surface weather stations

INMET ID	WMO ID	Name	State	Alt. (m)	Lat. (°)	Lon. (°)	WRDS
A419	86614	POÇO VERDE	SE	367	-10.7380	-38.1084	A
A420	86615	CARIRA	SE	290	-10.3997	-37.7475	A
A421	86618	BREJO GRANDE	SE	6	-10.4740	-36.4821	A
A422	86765	ABROLHOS	BA	21	-17.9630	-38.7033	A
A423	81990	REMANSO	BA	397	-9.6257	-42.0772	A
A424	86635	IRECÊ	BA	768	-11.3290	-41.8645	A
A425	86654	LENÇOIS	BA	438	-12.5579	-41.3888	A
A426	86694	GUANAMBI	BA	552	-14.2081	-42.7483	A
A427	86745	PORTO SEGURO	BA	86	-16.3890	-39.1824	A
A428	86611	SENHOR DO BONFIM	BA	532	-10.4431	-40.1482	A
A429	86634	BARRA	BA	408	-11.0849	-43.1390	A
A430	86673	PIATÃ	BA	1284	-13.1557	-41.7741	A
A431	86639	CONDE	BA	32	-11.8119	-37.6162	B
A432	86609	BURITIRAMA	BA	506	-10.7229	-43.6512	A
A433	86696	BRUMADO	BA	473	-14.1819	-41.6723	A
A434	86675	AMARGOSA	BA	398	-13.0095	-39.6169	A
A435	81992	UAUÁ	BA	451	-9.8336	-39.4956	A
A436	86612	QUEIMADAS	BA	310	-10.9846	-39.6170	A
A437	86724	UNA	BA	74	-15.2802	-39.0913	A
A438	86677	MARAÚ	BA	6	-13.9069	-38.9722	A
A439	86653	IBOTIRAMA	BA	425	-12.1931	-43.2134	A
A440	86636	JACOBINA	BA	441	-11.2051	-40.4650	A
A441	86637	SERRINHA	BA	338	-11.6646	-39.0229	A
A442	86613	EUCLIDES DA CUNHA	BA	432	-10.5372	-38.9966	A
A443	86610	DELFINO	BA	646	-10.4549	-41.2070	A
A444	86676	VALENÇA	BA	93	-13.3436	-39.1267	A
A445	86698	IPIAÚ	BA	132	-14.1713	-39.6925	A
A446	86723	ITAPETINGA	BA	271	-15.2446	-40.2296	A
A447	86744	BELMONTE	BA	90	-16.0880	-39.2154	A
A448	81984	CURACÁ	BA	370	-9.0013	-39.9124	A
A450	86605	JEREMOABO	BA	261	-10.0807	-38.3460	A
A502	86850	BARBACENA	MG	1169	-21.2284	-43.7677	A
A505	86796	ARAXÁ	MG	1018	-19.6057	-46.9496	A
A506	86740	MONTES CLAROS	MG	646	-16.6863	-43.8438	A
A507	86776	UBERLÂNDIA	MG	875	-18.9171	-48.2557	A
A508	86743	ALMENARA	MG	189	-16.1668	-40.6878	A
A509	86870	MONTE VERDE	MG	1545	-22.8616	-46.0434	A
A510	86824	VIÇOSA	MG	698	-20.7626	-42.8640	A
A511	86801	TIMÓTEO	MG	493	-19.5738	-42.6224	A

Table A.4 (cont...) - Selected INMET automatic surface weather stations

INMET ID	WMO ID	Name	State	Alt. (m)	Lat. (°)	Lon. (°)	WRDS
A512	86775	ITUITABA	MG	540	-18.9529	-49.5251	A
A513	86823	OURO BRANCO	MG	1048	-20.5566	-43.7562	A
A514	86849	SÃO JOÃO DEL REI	MG	930	-21.1065	-44.2509	A
A515	86848	VARGINHA	MG	950	-21.5665	-45.4043	A
A516	86819	PASSOS	MG	782	-20.7452	-46.6339	A
A517	86852	MURIAÉ	MG	283	-21.1049	-42.3759	A
A518	86851	JUIZ DE FORA	MG	937	-21.7700	-43.3643	A
A519	86793	CAMPINA VERDE	MG	559	-19.5392	-49.5181	A
A520	86794	CONCEIÇÃO DAS ALAGOAS	MG	573	-19.9859	-48.1516	A
A521	86800	BELO HORIZONTE - PAMPULHA	MG	854	-19.8839	-43.9694	A
A522	86763	SERRA DOS AIMORÉS	MG	212	-17.7988	-40.2499	A
A523	86778	PATROCÍNIO	MG	978	-18.9967	-46.9859	A
A524	86820	FORMIGA	MG	878	-20.4549	-45.4538	A
A525	86795	SACRAMENTO	MG	913	-19.8753	-47.4341	A
A526	86693	MONTALVÂNIA	MG	520	-14.4082	-44.4041	A
A527	86762	TEÓFILO OTONI	MG	467	-17.8928	-41.5154	A
A528	86779	TRÊS MARIAS	MG	931	-18.2009	-45.4598	A
A529	86873	PASSA QUATRO	MG	1017	-22.3958	-44.9619	A
A530	86846	CALDAS	MG	1077	-21.9181	-46.3830	A
A531	86871	MARIA DA FÉ	MG	1281	-22.3146	-45.3730	A
A532	86783	GOVERNADOR VALADARES	MG	198	-18.8304	-41.9770	A
A533	86782	GUANHÃES	MG	853	-18.7868	-42.9429	A
A534	86803	AIMORÉS	MG	288	-19.5328	-41.0908	A
A535	86798	FLORESTAL	MG	754	-19.8854	-44.4169	A
A536	86797	DORES DO INDAIÁ	MG	721	-19.4819	-45.5939	A
A537	86781	DIAMANTINA	MG	1359	-18.2311	-43.6483	A
A538	86780	CURVELO	MG	669	-18.7477	-44.4538	A
A539	86720	MOCAMBINHO	MG	454	-15.0860	-44.0160	A
A540	86784	MANTENA	MG	255	-18.7806	-40.9865	A
A541	86761	CAPELINHA	MG	932	-17.7055	-42.3893	A
A542	86738	UNAÍ	MG	641	-16.5541	-46.8819	A
A543	86695	ESPINOSA	MG	565	-14.9123	-42.8085	A
A544	86718	BURITIS	MG	894	-15.5243	-46.4355	A
A545	86759	PIRAPORA	MG	505	-17.2581	-44.8356	A
A546	86757	GUARDA-MOR	MG	997	-17.5613	-47.1993	A
A547	86739	SÃO ROMÃO	MG	490	-16.3627	-45.1238	A
A548	86719	CHAPADA GAÚCHA	MG	873	-15.3002	-45.6174	A
A549	86722	ÁGUAS VERMELHAS	MG	754	-15.7515	-41.4578	A
A550	86742	ITAOBIM	MG	272	-16.5757	-41.4856	A

Table A.4 (cont...) - Selected INMET automatic surface weather stations

INMET ID	WMO ID	Name	State	Alt. (m)	Lat. (°)	Lon. (°)	WRDS
A551	86721	RIO PARDO DE MINAS	MG	850	-15.7231	-42.4358	A
A552	86741	SALINAS	MG	487	-16.1603	-42.3103	A
A553	86758	JOÃO PINHEIRO	MG	877	-17.7848	-46.1194	A
A554	86802	CARATINGA	MG	609	-19.7358	-42.1371	A
A555	86821	IBIRITÉ (ROLA MOÇA)	MG	1199	-20.0315	-44.0112	A
A556	86825	MANHUAÇU	MG	819	-20.2634	-42.1828	A
A557	86822	CORONEL PACHECO	MG	411	-21.5467	-43.2610	A
A560	86788	POMPÉU	MG	705	-19.2396	-45.0082	A
A561	86811	SÃO SEBASTIÃO DO PARAÍSO	MG	845	-20.9099	-47.1143	A
A601	86878	SEROPÉDICA	RJ	35	-22.7579	-43.6848	A
A602	86914	RIO DE JANEIRO - MARAMBAIA	RJ	9	-23.0503	-43.5957	A
A603	86877	DUQUE DE CAXIAS - XERÉM	RJ	24	-22.5898	-43.2822	A
A604	86854	CAMBUCI	RJ	60	-21.5877	-41.9583	A
A606	86892	ARRAIAL DO CABO	RJ	3	-22.9755	-42.0215	A
A607	86855	CAMPOS	RJ	17	-21.7148	-41.3440	A
A608	86891	MACAÉ	RJ	25	-22.3763	-41.8121	A
A609	86874	RESENDE	RJ	439	-22.4509	-44.4448	A
A610	86876	PETRÓPOLIS - PICO DO COUTO	RJ	1758	-22.4649	-43.2915	A
A611	86875	VALENÇA	RJ	367	-22.3581	-43.6957	A
A612	86830	VITÓRIA	ES	9	-20.2711	-40.3061	A
A613	86804	SANTA TERESA	ES	976	-19.9884	-40.5796	A
A614	86805	LINHARES	ES	38	-19.3569	-40.0687	A
A615	86829	ALFREDO CHAVES	ES	14	-20.6365	-40.7418	A
A616	86786	SÃO MATEUS	ES	29	-18.6762	-39.8641	A
A617	86828	ALEGRE	ES	129	-20.7504	-41.4889	A
A618	86888	TERESÓPOLIS - PARQUE NACIONAL	RJ	991	-22.4489	-42.9871	A
A619	86913	PARATY	RJ	3	-23.2235	-44.7269	A
A620	86890	CAMPOS - SÃO TOMÉ	RJ	7	-22.0416	-41.0519	A
A621	86879	RIO DE JANEIRO - VILA MILITAR	RJ	30	-22.8613	-43.4114	A
A622	86853	PRESIDENTE KENNEDY	ES	69	-21.1008	-41.0394	A
A623	86785	NOVA VENÉCIA	ES	156	-18.6953	-40.3906	A
A624	86889	NOVA FRIBURGO-SALINAS	RJ	1065	-22.3348	-42.6769	A
A652	86887	RIO DE JANEIRO - FORTE DE COPACABANA	RJ	26	-22.9883	-43.1904	A
A657	86827	AFONSO CLÁUDIO	ES	507	-20.1042	-41.1069	A
A659	86893	SILVA JARDIM	RJ	19	-22.6458	-42.4156	A
A667	86885	SAQUAREMA	RJ	26	-22.8712	-42.6091	A
A701	86910	SÃO PAULO (MIRANTE DE SANTANA)	SP	786	-23.4963	-46.6201	A
A702	86810	CAMPO GRANDE	MS	528	-20.4472	-54.7226	A
A703	86857	PONTA PORÃ	MS	668	-22.5524	-55.7163	A

Table A.4 (cont...) - Selected INMET automatic surface weather stations

INMET ID	WMO ID	Name	State	Alt. (m)	Lat. (°)	Lon. (°)	WRDS
A704	86813	TRÊS LAGOAS	MS	329	-20.7900	-51.7122	A
A705	86865	BAURU	SP	636	-22.3581	-49.0289	A
A706	86872	CAMPOS DO JORDÃO	SP	1663	-22.7502	-45.6038	B
A707	86863	PRESIDENTE PRUDENTE	SP	432	-22.1199	-51.4086	A
A708	86818	FRANCA	SP	1003	-20.5845	-47.3825	A
A709	86860	IVINHEMA	MS	377	-22.3004	-53.8229	A
A710	86792	PARANAÍBA	MS	408	-19.6955	-51.1818	A
A711	86845	SÃO CARLOS	SP	859	-21.9804	-47.8839	A
A712	86923	IGUAPE	SP	3	-24.6717	-47.5459	A
A713	86907	SOROCABA	SP	609	-23.4260	-47.5856	A
A714	86905	ITAPEVA	SP	743	-23.9819	-48.8858	A
A715	86906	SÃO MIGUEL ARCANJO	SP	676	-23.8520	-48.1648	A
A716	86866	OURINHOS	SP	443	-22.9490	-49.8945	A
A717	86768	NHUMIRIM	MS	102	-18.9887	-56.6229	A
A718	86864	RANCHARIA	SP	399	-22.3728	-50.9747	A
A719	86808	AQUIDAUANA	MS	151	-20.4754	-55.7840	A
A720	86770	COXIM	MS	251	-18.5121	-54.7361	A
A721	86858	DOURADOS	MS	463	-22.1939	-54.9114	A
A722	86807	MIRANDA	MS	132	-20.3955	-56.4317	A
A723	86833	PORTO MURTINHO	MS	79	-21.7059	-57.8865	A
A724	86767	CORUMBÁ	MS	112	-18.9967	-57.6375	A
A725	86904	AVARÉ	SP	776	-23.1017	-48.9410	A
A726	86868	PIRACICABA	SP	566	-22.7031	-47.6233	A
A727	86840	LINS	SP	461	-21.6660	-49.7349	A
A728	86911	TAUBATÉ	SP	582	-23.0417	-45.5208	A
A729	86815	VOTUPORANGA	SP	510	-20.4032	-49.9660	A
A730	86772	CHAPADÃO DO SUL	MS	821	-18.8022	-52.6026	A
A731	86834	MARACAJU	MS	389	-21.6090	-55.1775	A
A732	86789	SÃO GABRIEL DO OESTE	MS	646	-19.4203	-54.5531	A
A733	86814	JALES	SP	460	-20.1650	-50.5951	A
A734	86838	VALPARAÍSO	SP	382	-21.3191	-50.9302	A
A735	86839	JOSÉ BONIFÁCIO	SP	408	-21.0857	-49.9204	A
A736	86841	ARIRANHA	SP	525	-21.1329	-48.8404	A
A737	86843	IBITINGA	SP	497	-21.8556	-48.7997	A
A738	86844	CASA BRANCA	SP	734	-21.7806	-47.0753	A
A739	86869	ITAPIRA	SP	635	-22.4151	-46.8053	A
A740	86912	SÃO LUIS DO PARAÍTINGA	SP	862	-23.2284	-45.4171	A
A741	86867	BARRA BONITA	SP	534	-22.4712	-48.5576	A
A742	86791	CASSILÂNDIA	MS	495	-19.1225	-51.7207	A

Table A.4 (cont...) - Selected INMET automatic surface weather stations

INMET ID	WMO ID	Name	State	Alt. (m)	Lat. (°)	Lon. (°)	WRDS
A743	86836	RIO BRILHANTE	MS	324	-21.7749	-54.5281	A
A745	86924	MOELA	SP	32	-24.0478	-46.2633	B
A746	86922	BARRA DO TURVO	SP	660	-24.9628	-48.4164	A
A747	86842	PRADÓPOLIS	SP	540	-21.3384	-48.1140	A
A748	86816	BARRETOS	SP	534	-20.5592	-48.5450	A
A749	86859	JUTI	MS	375	-22.8572	-54.6056	A
A750	86894	AMAMBAÍ	MS	434	-23.0025	-55.3294	A
A751	86895	SETE QUEDAS	MS	398	-23.9669	-55.0242	A
A752	86896	ITAQUIRAÍ	MS	338	-23.4495	-54.1819	A
A753	86817	ITUVERAVA	SP	611	-20.3598	-47.7752	A
A754	86809	SIDROLÂNDIA	MS	471	-20.9816	-54.9719	A
A755	86908	BARUERÍ	SP	777	-23.5239	-46.8695	A
A756	86812	ÁGUA CLARA	MS	324	-20.4444	-52.8758	A
A757	86856	BELA VISTA	MS	206	-22.1015	-56.5408	A
A758	86835	JARDIM	MS	252	-21.4785	-56.1377	A
A759	86837	BATAGUASSU	MS	392	-21.7501	-52.4713	A
A760	86771	COSTA RICA	MS	727	-18.4927	-53.1713	A
A761	86769	SONORA	MS	495	-17.6353	-54.7605	A
A801	86988	PORTO ALEGRE	RS	41	-30.0535	-51.1748	A
A802	86995	RIO GRANDE	RS	5	-32.0788	-52.1677	A
A803	86977	SANTA MARIA	RS	103	-29.7250	-53.7205	A
A804	86983	SANTANA DO LIVRAMENTO	RS	328	-30.8424	-55.6131	A
A805	86952	SANTO AUGUSTO	RS	490	-27.8543	-53.7912	A
A806	86958	FLORIANÓPOLIS-SÃO JOSÉ	SC	5	-27.6025	-48.6201	A
A807	86933	CURITIBA	PR	923	-25.4487	-49.2306	A
A808	86981	TORRES	RS	8	-29.3504	-49.7333	A
A809	86973	URUGUAIANA	RS	74	-29.8399	-57.0819	A
A810	86950	SANTA ROSA	RS	273	-27.8905	-54.4800	A
A811	86993	CANGUÇU	RS	447	-31.4033	-52.7007	A
A812	86986	CAÇAPAVA DO SUL	RS	421	-30.5453	-53.4671	A
A813	86978	RIO PARDO	RS	107	-29.8721	-52.3820	A
A814	86970	URUSSANGA	SC	41	-28.5326	-49.3152	A
A815	86969	SÃO JOAQUIM	SC	1400	-28.2756	-49.9346	A
A816	86938	NOVO HORIZONTE	SC	944	-26.4065	-52.8504	A
A817	86946	INDAIAL	SC	72	-26.9137	-49.2680	A
A818	86930	IVAÍ	PR	804	-25.0108	-50.8539	A
A819	86921	CASTRO	PR	994	-24.7870	-49.9993	A
A820	86916	MARECHAL CÂNDIDO RONDON	PR	392	-24.5333	-54.0192	A
A821	86903	JOAQUIM TÁVORA	PR	513	-23.5053	-49.9464	A

Table A.4 (cont...) - Selected INMET automatic surface weather stations

INMET ID	WMO ID	Name	State	Alt. (m)	Lat. (°)	Lon. (°)	WRDS
A822	86919	NOVA TEBAS	PR	656	-24.4373	-51.9630	A
A823	86929	INÁCIO MARTINS	PR	1209	-25.5679	-51.0779	A
A824	86897	ICARAIMA	PR	381	-23.3904	-53.6359	A
A825	86917	GOIOERÊ	PR	452	-24.1585	-53.0306	A
A826	86975	ALEGRETE	RS	121	-29.7091	-55.5255	A
A827	86992	BAGÉ	RS	226	-31.3478	-54.0133	A
A828	86954	ERECHIM	RS	777	-27.6577	-52.3058	A
A829	86967	SÃO JOSÉ DOS AUSENTES	RS	1229	-28.7486	-50.0579	A
A830	86960	SÃO BORJA	RS	81	-28.6501	-56.0163	A
A831	86982	QUARAÍ	RS	113	-30.3686	-56.4371	A
A832	86984	SÃO GABRIEL	RS	115	-30.3415	-54.3109	A
A833	86976	SANTIAGO	RS	390	-29.1916	-54.8857	A
A834	86990	TRAMANDAÍ	RS	5	-30.0103	-50.1359	A
A835	86899	MARINGÁ	PR	549	-23.4054	-51.9328	A
A836	86996	JAGUARÃO	RS	31	-32.5348	-53.3759	A
A837	86964	SOLEDADE	RS	660	-28.8592	-52.5424	A
A838	86989	CAMAQUÃ	RS	92	-30.8080	-51.8342	A
A839	86963	PASSO FUNDO	RS	681	-28.2268	-52.4036	A
A840	86979	BENTO GONÇALVES	RS	623	-29.1646	-51.5342	A
A841	86955	JOAÇABA	SC	768	-27.1693	-51.5590	A
A842	86901	NOVA FÁTIMA	PR	664	-23.4153	-50.5777	A
A843	86927	DOIS VIZINHOS	PR	546	-25.6991	-53.0953	A
A844	86965	LAGOA VERMELHA	RS	834	-28.2224	-51.5128	A
A845	86968	MORRO DA IGREJA (BOM JARDIM DA SERRA)	SC	1790	-28.1270	-49.4796	A
A846	86925	FOZ DO IGUAÇU	PR	235	-25.6018	-54.4831	A
A847	86935	ILHA DO MEL	PR	4	-25.4945	-48.3260	A
A848	86936	DIONÍSIO CERQUEIRA	SC	808	-26.2866	-53.6331	A
A849	86861	DIAMANTE DO NORTE	PR	368	-22.6394	-52.8902	A
A850	86862	PARANAPOEMA	PR	309	-22.6583	-52.1345	A
A851	86947	ITAPOÁ	SC	6	-26.0813	-48.6418	A
A852	86961	SÃO LUIZ GONZAGA	RS	246	-28.4171	-54.9624	A
A853	86962	CRUZ ALTA	RS	427	-28.6034	-53.6736	A
A854	86951	FREDERICO WESTPHALEN	RS	489	-27.3957	-53.4294	A
A855	86926	PLANALTO	PR	399	-25.7219	-53.7479	A
A856	86953	PALMEIRA DAS MISSÕES	RS	614	-27.9204	-53.3180	A
A857	86937	SÃO MIGUEL DO OESTE	SC	655	-26.7767	-53.5045	A
A858	86940	XANXERÊ	SC	879	-26.9387	-52.3981	A
A859	86943	CAÇADOR	SC	944	-26.8192	-50.9855	A
A860	86956	CURITIBANOS	SC	978	-27.2886	-50.6043	A

Table A.4 (cont...) - Selected INMET automatic surface weather stations

INMET ID	WMO ID	Name	State	Alt. (m)	Lat. (°)	Lon. (°)	WRDS
A861	86944	RIO DO CAMPO	SC	592	-26.9375	-50.1454	A
A862	86945	RIO NEGRINHO	SC	857	-26.2484	-49.5806	A
A863	86957	ITUPORANGA	SC	480	-27.4184	-49.6469	A
A864	86942	MAJOR VIEIRA	SC	800	-26.3937	-50.3632	A
A865	86931	LAGES	SC	953	-27.8022	-50.3355	A
A866	86972	SANTA MARTA (FAROL)	SC	34	-28.6044	-48.8133	A
A867	86971	ARARANGUÁ	SC	2	-28.9314	-49.4979	A
A868	86948	ITAJAÍ	SC	10	-26.9509	-48.7620	A
A869	86898	CIDADE GAÚCHA	PR	366	-23.3592	-52.9319	A
A871	86902	JAPIRA	PR	693	-23.7733	-50.1806	A
A872	86920	VENTANIA	PR	1093	-24.2804	-50.2102	A
A873	86934	MORRETES	PR	50	-25.5089	-48.8087	A
A874	86931	SÃO MATEUS DO SUL	PR	780	-25.8356	-50.3690	A
A875	86941	GENERAL CARNEIRO	PR	1009	-26.3985	-51.3537	A
A876	86939	CLEVELÂNDIA	PR	966	-26.4172	-52.3487	A
A878	86994	MOSTARDAS	RS	4	-31.2483	-50.9063	A
A879	86980	CANELA	RS	831	-29.3688	-50.8272	A
A880	86966	VACARIA	RS	970	-28.5136	-50.8827	A
A881	86985	DOM PEDRITO	RS	157	-30.9925	-54.8153	A
A882	86987	TEUTÔNIA	RS	80	-29.4503	-51.8243	A
A883	86974	IBIRUBÁ	RS	455	-28.6535	-53.1119	A
A884	86991	CAMPO BOM	RS	23	-29.6743	-51.0640	A
A899	86998	CHUIÍ	RS	7	-33.7423	-53.3722	A
A901	86705	CUIABÁ	MT	242	-15.5593	-56.0630	A
A902	86682	TANGARÁ DA SERRA	MT	440	-14.6501	-57.4316	A
A903	86664	SÃO JOSÉ DO RIO CLARO	MT	340	-13.4540	-56.6773	A
A904	86645	SORRISO	MT	379	-12.5551	-55.7229	A
A905	86662	CAMPO NOVO DOS PARECIS	MT	525	-13.7859	-57.8385	A
A906	81979	GUARANTÃ DO NORTE	MT	284	-9.9526	-54.8978	A
A907	86728	RONDONÓPOLIS	MT	290	-16.4624	-54.5802	A
A908	86686	ÁGUA BOA	MT	440	-14.0165	-52.2117	A
A909	86749	ALTO ARAGUAIA	MT	753	-17.3394	-53.2241	A
A910	81976	APIACÁS	MT	218	-9.5634	-57.3936	A
A912	86707	CAMPO VERDE	MT	748	-15.5314	-55.1356	A
A913	86661	COMODORO	MT	577	-13.7080	-59.7624	A
A914	86625	JUARA	MT	263	-11.2802	-57.5266	A
A915	86684	PARANATINGA	MT	477	-14.4213	-54.0355	A
A916	86647	QUERÊNCIA	MT	361	-12.6273	-52.2209	A
A917	86626	SINOP	MT	367	-11.9822	-55.5660	A

Table A.4 (cont...) - Selected INMET automatic surface weather stations

INMET ID	WMO ID	Name	State	Alt. (m)	Lat. (°)	Lon. (°)	WRDS
A918	86606	CONFRESA	MT	233	-10.6395	-51.5715	A
A919	81975	COTRIGUAÇU	MT	265	-9.9063	-58.5722	A
A920	86624	JUÍNA	MT	365	-11.3751	-58.7748	A
A921	86628	SÃO FÉLIX DO ARAGUAIA	MT	201	-11.6190	-50.7279	A
A922	86701	VILA BELA DA SANTÍSSIMA TRINDADE	MT	213	-15.0627	-59.8729	A
A924	81977	ALTA FLORESTA	MT	292	-10.0773	-56.1792	A
A925	81932	PORTO VELHO	RO	87	-8.7937	-63.8459	A
A926	81978	CARLINDA	MT	294	-9.9706	-55.8275	A
A927	86643	NOVO MUNDO	MT	426	-12.5219	-58.2314	A
A928	86663	NOVA MARINGÁ	MT	334	-13.0386	-57.0922	A
A929	86665	NOVA UBIRATÃ	MT	466	-13.4111	-54.7521	A
A930	86666	GAÚCHA DO NORTE	MT	376	-13.1849	-53.2574	A
A931	86685	SANTO ANTÔNIO DO LESTE	MT	664	-14.9279	-53.8836	A
A932	86729	GUIRATINGA	MT	525	-16.3416	-53.7661	A
A933	86748	ITIQUEIRA	MT	593	-17.1751	-54.5017	A
A934	86750	ALTO TAQUARI	MT	862	-17.8410	-53.2895	A
A935	86704	PORTO ESTRELA	MT	148	-15.3247	-57.2258	A
A936	86703	SALTO DO CÉU	MT	301	-15.1248	-58.1271	A
A937	86702	PONTES DE LACERDA	MT	273	-15.2346	-59.3462	A
A938	86642	VILHENA	RO	583	-12.7349	-60.1578	A
A939	86622	CACOAL	RO	184	-11.4458	-61.4341	A
A940	81970	ARIQUEMES	RO	128	-9.9490	-62.9619	A
A941	86726	CÁCERES	MT	124	-16.0744	-57.6928	A
F501	86799	BELO HORIZONTE - CERCADINHO	MG	1200	-19.9800	-43.9587	A
U560	86560	COLONIA/URUGUAY	-	22	-34.4510	-57.7675	B
U565	86565	ROCHA/URUGUAY	-	18	-34.4936	-54.3124	A

APPENDIX B

ISOPLETH MAP OF NBR 6123 (ABNT, 1988)

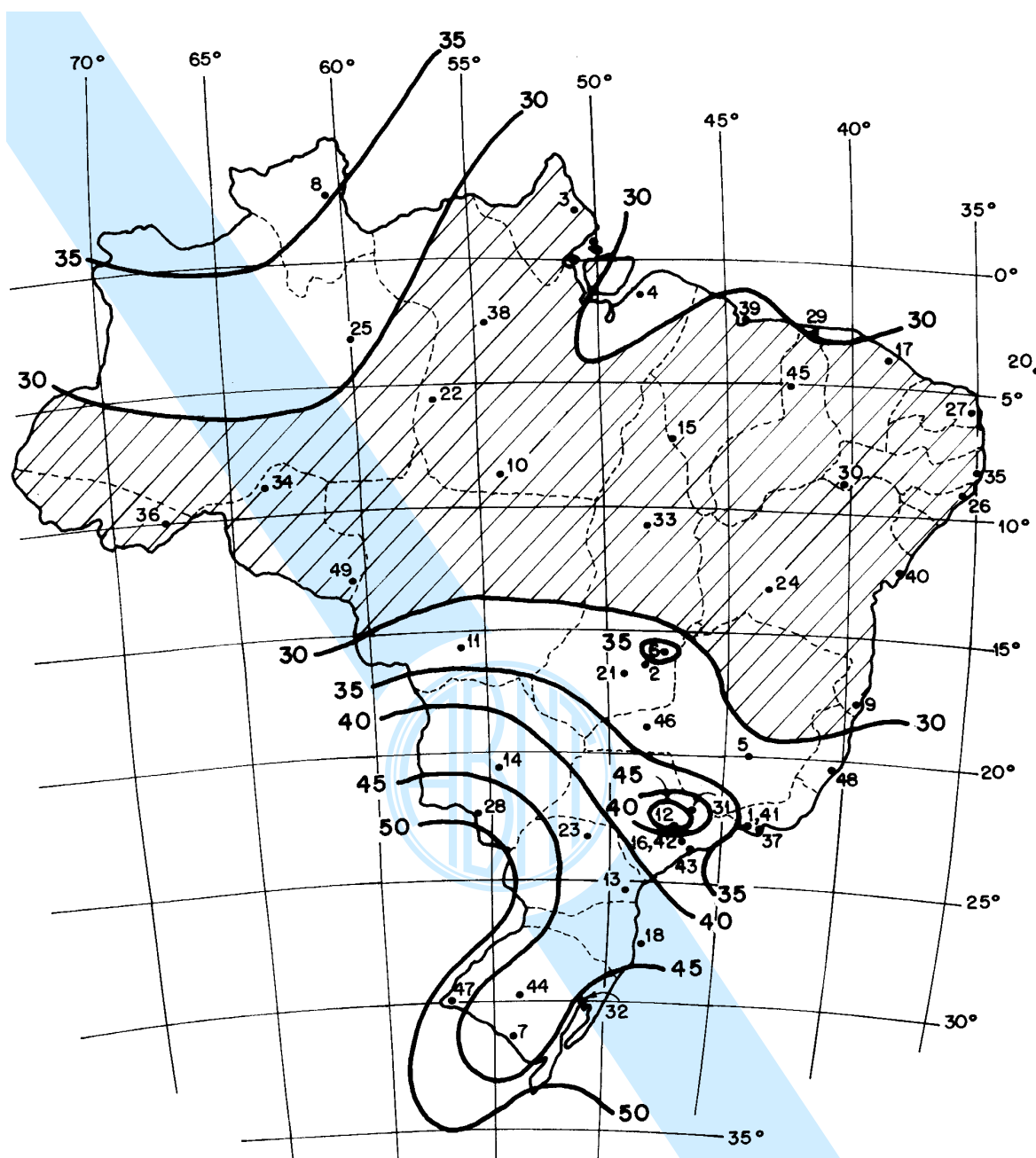


Figure B.1 – Isopleth map of Brazilian regional basic wind speeds, V_0 (m/s) (ABNT, 1988).

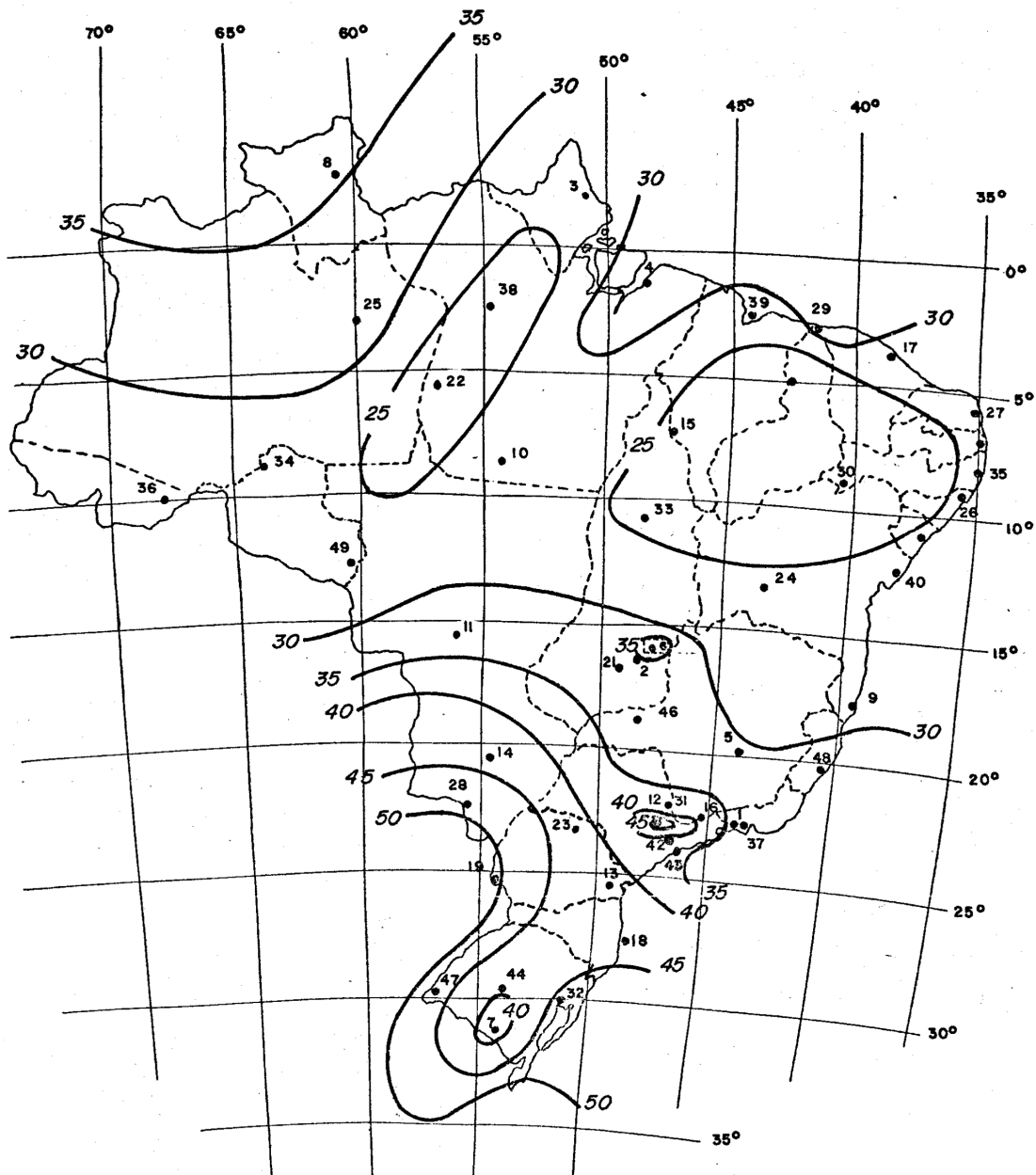


Figure B.2 – Draft isopleth map of Brazilian regional basic wind speed, V_0 (m/s) (Padaratz, 1977).

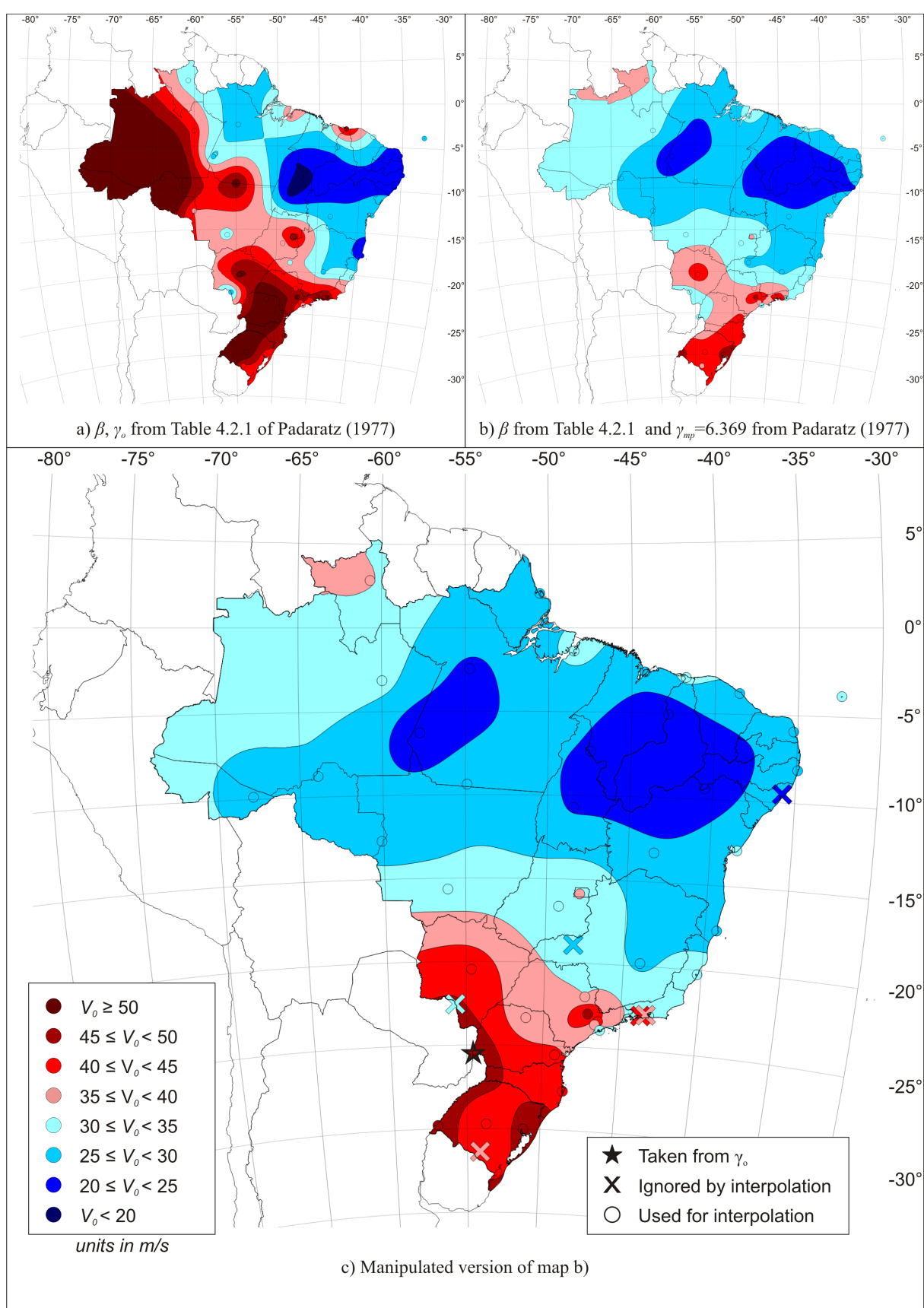


Figure B.3 – Recreation of Padaratz (1977).

APPENDIX C

EXTREME DISTRIBUTIONS OF SWS

Table C.1 – Extreme distribution parameters of Class A aerodrome SWS

ICAO ID	DATA-SET	t_{tot} (yrs)	Obs. (%)	Non-Synoptic				Synoptic				Mixed Distribution				Envelope	
				a_N	U_N (m/s)	R_N^2	$G_{50,N}$ (m/s)	a_S	U_S (m/s)	R_S^2	$G_{50,S}$ (m/s)	a_M	U_M (m/s)	R_M^2	$G_{50,M}$ (m/s)	U_E (m/s)	$G_{50,E}$ (m/s)
SBAA	MSS	6.5	42	1.93	17.5	0.93	25.0	0.67	13.6	0.88	16.2	1.93	17.5	0.93	25.0	17.5	25.0
	PAS31-1	6.8	45	1.99	17.3	0.93	25.1	0.76	13.7	0.90	16.7	1.93	17.3	0.91	24.9	17.3	25.1
SBAE	MSS	8.4	95	3.14	21.2	0.89	33.4*	0.86	18.2	0.94	21.5	2.89	21.4	0.86	32.7*	21.4	33.4*
	PAS31-1	6.2	99	1.82	20.6	0.96	27.6	1.35	18.8	0.79	24.1	1.74	21.1	0.94	27.9	21.1	27.9
SBAF	MSS	14.5	95	2.50	18.3	0.81	28.0	1.30	16.1	0.94	21.1	2.30	18.7	0.78	27.6	18.7	28.0
	PAS31-1	14.6	96	2.56	18.1	0.83	28.1	1.24	15.8	0.86	20.6	2.40	18.5	0.80	27.8	18.5	28.1
SBAN	MSS	16.0	98	2.70	20.4	0.98	30.9	0.91	16.7	0.93	20.2*	2.65	20.5	0.98	30.8	20.5	30.9
	PAS31-1	13.9	100	2.97	19.9	0.95	31.5	1.22	16.8	0.94	21.5	2.85	20.1	0.95	31.2	20.1	31.5
	PAS31-2	1.9	95	2.18	18.6	0.96	27.1	1.09	15.7	0.94	20.0	1.70	18.6	0.92	25.2	18.6	27.1
SBAR	MSS	11.4	100	1.42	13.4	0.96	18.9	0.89	15.9	0.90	19.4	0.89	16.0	0.91	19.5	16.0	19.5
	PAS31-1	9.0	100	1.22	13.5	0.97	18.2	0.88	15.9	0.81	19.3	0.87	15.9	0.81	19.3	15.9	19.3
SBAT	MSS	9.0	63	3.72	21.5	0.58	36.0	0.80	12.5	0.95	15.6	3.72	21.5	0.58	36.0	21.5	36.0
	PAS31-1	17.2	64	4.09	21.1	0.85	37.1*	1.39	12.3	0.80	17.7*	4.05	21.2	0.84	37.0*	21.2	37.1*
SBBE	MSS	17.1	97	3.56	22.3	0.97	36.2*	1.11	14.8	0.96	19.2*	3.56	22.3	0.97	36.2*	22.3	36.2*
	PAS31-1	15.1	100	3.61	22.6	0.96	36.7	1.05	14.8	0.96	18.9	3.61	22.6	0.96	36.7	22.6	36.7
	PAS31-2	7.0	93	1.95	20.9	0.93	28.5	0.60	14.5	0.88	16.9	1.95	20.9	0.93	28.5	20.9	28.5
SBBH	MSS	9.4	100	3.20	22.1	0.95	34.6*	1.35	13.8	0.92	19.0	3.20	22.1	0.95	34.6*	22.1	34.6*
	PAS31-1	7.0	100	2.43	22.1	0.94	31.6	0.80	13.4	0.94	16.5	2.43	22.1	0.94	31.6	22.1	31.6
SBBI	MSS	10.7	66	2.89	25.1	0.94	36.3	0.78	19.1	0.97	22.1	2.89	25.1	0.94	36.3	25.1	36.3
	PAS31-1	13.2	78	3.17	24.7	0.98	37.0*	1.58	19.5	0.83	25.7*	3.04	24.9	0.98	36.7*	24.9	37.0*
	PAS31-2	2.9	69	1.18	21.6	0.84	26.2	0.89	18.0	0.93	21.5	1.12	21.6	0.84	25.9	21.6	26.2
SBBP	MSS	3.0	46	3.45	27.6	0.96	41.0*	0.57	17.3	0.88	19.5	3.45	27.6	0.96	41.0*	27.6	41.0*
	PAS31-1	2.3	48	3.92	27.8	0.95	43.1	0.65	17.3	0.93	19.9	3.90	27.8	0.95	43.1	27.8	43.1
SBBQ	MSS	5.8	62	4.15	22.6	0.72	38.8*	1.27	14.5	0.92	19.5	4.08	22.6	0.71	38.6*	22.6	38.8*
	PAS31-1	4.3	63	4.05	22.9	0.65	38.7	1.31	14.8	0.89	19.9	3.96	22.9	0.63	38.4	22.9	38.7
	PAS31-2	3.9	62	2.99	21.0	0.88	32.7	1.41	15.1	0.95	20.6	2.90	21.1	0.87	32.4	21.1	32.7
SBBR	MSS	12.4	100	2.81	23.1	0.96	34.1	1.40	16.4	0.93	21.8	2.76	23.2	0.96	34.0	23.2	34.1
	PAS31-1	13.8	99	3.63	23.2	0.96	37.4*	1.41	16.3	0.94	21.8*	3.59	23.2	0.96	37.3*	23.2	37.4*
	PAS31-2	6.1	99	2.26	21.7	0.97	30.6	1.15	15.6	0.85	20.1	2.22	21.7	0.97	30.4	21.7	30.6
SBBU	MSS	16.1	98	3.33	25.3	0.93	38.3*	1.43	19.9	0.96	25.4*	3.28	25.4	0.92	38.2*	25.4	38.3*
	PAS31-1	14.0	100	2.48	24.8	0.96	34.4	1.85	20.5	0.96	27.8	2.30	25.0	0.96	34.0	25.0	34.4
SBBV	MSS	20.1	99	1.69	19.5	0.97	26.0*	0.90	18.2	0.87	21.7*	1.58	19.8	0.97	25.9*	19.8	26.0*
	PAS31-1	16.7	95	1.56	19.6	0.96	25.7	0.48	18.1	0.88	19.9	1.50	19.7	0.95	25.5	19.7	25.7
	PAS31-2	5.2	92	1.59	18.4	0.92	24.6	0.66	17.2	0.94	19.8	1.16	18.7	0.85	23.3	18.7	24.6
SBCA	MSS	4.6	62	2.92	31.2	0.92	42.6*	0.55	23.5	0.91	25.7	2.92	31.2	0.92	42.6*	31.2	42.6*
	PAS31-1	3.6	59	4.11	31.4	0.93	47.5	0.59	23.4	0.86	25.7	3.45	31.3	0.96	44.7	31.4	47.5
SBCB	MSS	8.5	52	1.68	17.4	0.93	23.9	1.29	22.1	0.90	27.1*	1.29	22.1	0.90	27.1	22.1	27.1
	PAS31-1	3.5	56	2.44	19.2	0.90	28.7	0.54	21.4	0.83	23.5	0.50	21.4	0.80	23.3	21.4	28.7
SBCC	MSS	6.7	47	1.97	22.4	0.90	30.0*	0.38	14.9	0.79	16.4	1.97	22.4	0.90	30.0*	22.4	30.0*
	PAS31-1	5.6	46	1.88	22.8	0.90	30.1	0.38	14.9	0.83	16.4	1.88	22.8	0.90	30.1	22.8	30.1
SBCF	MSS	22.1	97	3.14	22.6	0.96	34.9	1.13	15.8	0.93	20.2	3.14	22.6	0.96	34.9	22.6	34.9
	PAS31-1	24.6	99	2.85	21.9	0.98	33.0*	1.02	15.7	0.94	19.7*	2.85	21.9	0.98	33.0*	21.9	33.0*
	PAS31-2	23.1	95	3.19	22.3	0.91	34.7	1.11	16.1	0.96	20.5	3.19	22.3	0.91	34.7	22.3	34.7
SBCG	MSS	11.7	100	2.86	25.9	0.94	37.1*	0.79	18.6	0.95	21.6	2.86	25.9	0.94	37.1*	25.9	37.1*
	PAS31-1	9.8	98	2.82	26.5	0.93	37.5	0.71	18.7	0.93	21.4	2.82	26.5	0.93	37.5	26.5	37.5
	PAS31-2	10.0	98	3.29	25.4	0.92	38.2	1.29	18.9	0.90	23.9	3.26	25.4	0.92	38.1	25.4	38.2
SBCH	MSS	5.2	80	4.37	33.8	0.93	50.8*	1.54	23.0	0.94	29.0*	4.37	33.8	0.93	50.8*	33.8	50.8*
	PAS31-1	3.9	77	3.42	33.7	0.81	47.1	1.72	22.6	0.94	29.3	3.42	33.7	0.81	47.1	33.7	47.1
SBCI	PAS31-1	6.2	44	1.97	17.6	0.92	25.3	1.10	11.9	0.97	16.2	1.97	17.6	0.92	25.3	17.6	25.3
SBCJ	MSS	7.1	53	2.22	19.5	0.98	28.1	1.32	12.2	0.82	17.4	2.16	19.5	0.98	27.9	19.5	28.1
	PAS31-1	8.2	67	2.07	19.1	0.96	27.2*	1.85	12.6	0.89	19.9*	1.97	19.2	0.96	26.9*	19.2	27.2*
	PAS31-2	7.7	67	2.31	19.0	0.97	28.0	1.16	12.2	0.90	16.7	2.31	19.0	0.97	28.0	19.0	28.0
SBCM	MSS	6.1	64	2.82	21.2	0.97	32.2	1.03	17.0	0.96	21.0	2.50	21.3	0.97	31.1	21.3	32.2
	PAS31-1	6.7	62	2.84	20.9	0.97	32.0	1.05	16.9	0.97	21.0	2.53	21.1	0.97	31.0	21.1	32.0
SBCO	MSS	12.7	78	4.20	25.7	0.99	42.1	1.38	20.3	0.98	25.7	4.05	25.9	0.99	41.7	25.9	42.1
	PAS31-1	17.3	76	4.23	24.5	0.98	41.0*	1.35	20.0	0.98	25.3	4.05	24.7	0.98	40.5*	24.7	41.0*
	PAS31-2	15.5	75	4.23	22.3	0.88	38.8	1.08	19.2	0.97	23.4	3.92	22.6	0.84	37.9	22.6	38.8
SBCP	MSS	11.8	72	1.64	18.2	0.95	24.6	1.04	20.7	0.97	24.7	1.01	20.9	0.97	24.8	20.9	24.8
	PAS31-1	12.8	74	1.46	17.9	0.94	23.6	1.02	20.6	0.97	24.6*	0.97	20.7	0.97	24.5	20.7	24.6
SBCR	MSS	7.8	63	2.63	22.7	0.94	32.9	1.24	21.7	0.97	26.6	2.04	23.6	0.91	31.6	23.6	32.9
	PAS31-1	8.0	72	2.65	22.6	0.95	33.0*	1.11	21.7	0.97	26.1*	2.03	23.5	0.90	31.4*	23.5	33.0*
	PAS31-2	4.1	64	2.21	23.5	0.97	32.1	1.47	19.5	0.97	25.3	1.95	23.6	0.94	31.2	23.6	32.1
SBCT	MSS	19.4	100	2.00	22.3	0.97	30.1	0.89	19.4	0.92	22.9*	1.97	22.4	0.98	30.1	22.4	30.1
	PAS31-1	18.8	100	2.02	22.1	0.97	30.0	0.77	19.3	0.92	22.3	1.97	22.2	0.97	29.8	22.2	30.0
	PAS31-2	16.0	100	1.15	21.5	0.97	26.0	1.02	18.4	0.92	22.3	1.13	21.6	0.97	26.0	21.6	26.0
SBCY	MSS	16.7	99	2.42	23.5	0.98	33.0	1.16	16.0	0.91	20.6	2.42	23.5	0.98	33.0*	23.5	33.0
	PAS31-1	15.3	99	2.55	23.7	0.97	33.7	2.30	16.7	0.89	25.7	2.45	23.9	0.96	33.4	23.9	33.7

* indicates the station is a member of the governing set of stations for a particular distribution (N, S, M or E)

Table C.1 (cont...) - Extreme distribution parameters of Class A aerodrome SWS

ICAO ID	DATA-SET	t_{tot} (yrs)	Obs. (%)	Non-Synoptic				Synoptic				Mixed Distribution				Envelope	
				a_N	U_N (m/s)	R_N^2	$G_{50,N}$ (m/s)	a_S	U_S (m/s)	R_S^2	$G_{50,S}$ (m/s)	a_M	U_M (m/s)	R_M^2	$G_{50,M}$ (m/s)	U_E (m/s)	$G_{50,E}$ (m/s)
SBCZ	MSS	12.6	62	2.26	19.1	0.95	28.0*	0.86	10.9	0.94	14.3	2.26	19.1	0.95	28.0*	18.6	28.0*
	PAS31-1	12.2	67	2.49	18.6	0.96	28.3	0.86	10.6	0.97	13.9	2.49	18.6	0.96	28.3	24.0	28.3
SBDN	MSS	19.7	90	3.03	23.9	0.96	35.7	1.55	18.4	0.97	24.5	2.97	24.0	0.96	35.6	24.1	35.7
	PAS31-1	27.8	100	2.99	24.0	0.97	35.7*	1.63	18.9	0.97	25.3*	2.93	24.1	0.97	35.6*	20.7	35.7*
SBDO	MSS	3.7	54	1.44	20.6	0.93	26.2	0.52	18.8	0.91	20.8	1.17	20.7	0.93	25.3	20.8	26.2
	PAS31-1	3.4	60	1.60	20.7	0.94	27.0	0.58	18.8	0.93	21.0	1.26	20.8	0.94	25.8	24.1	27.0
SBEG	MSS	17.3	99	2.29	24.1	0.97	33.1	1.23	13.5	0.96	18.3	2.29	24.1	0.97	33.1	24.0	33.1
	PAS31-1	19.0	98	2.27	24.0	0.97	32.9*	1.05	13.2	0.96	17.2*	2.27	24.0	0.97	32.9*	22.4	32.9*
	PAS31-2	9.0	94	1.52	22.4	0.81	28.3	1.59	12.9	0.95	19.1	1.52	22.4	0.81	28.3	17.9	28.3
SBEK	MSS	7.0	43	2.69	17.9	0.93	28.4	1.39	11.9	0.96	17.4	2.66	17.9	0.92	28.3	16.7	28.4
	PAS31-1	11.5	51	2.78	16.7	0.94	27.5	1.55	11.0	0.96	17.1*	2.78	16.7	0.94	27.5	20.9	27.5
SBES	MSS	6.2	59	2.33	16.0	0.92	25.1	0.78	20.9	0.97	23.9*	0.76	20.9	0.97	23.8	21.1	25.1
	PAS31-1	4.7	59	3.04	16.1	0.96	27.9	0.77	21.1	0.96	24.1	0.75	21.1	0.97	24.0	21.6	27.9
	PAS31-2	4.7	58	3.07	18.9	0.94	30.9	1.52	20.5	0.91	26.4	2.03	21.6	0.92	29.6	26.7	30.9
SBFI	MSS	22.5	98	3.28	26.7	0.92	39.5	1.32	18.8	0.97	23.9	3.28	26.7	0.92	39.5	26.0	39.5
	PAS31-1	26.6	98	2.34	26.0	0.97	35.2	1.38	19.0	0.97	24.4	2.34	26.0	0.97	35.2	23.3	35.2
	PAS31-2	15.7	96	3.50	23.3	0.91	37.0	1.08	17.4	0.94	21.6	3.50	23.3	0.91	37.0	22.1	37.0
SBFL	MSS	22.2	97	2.92	20.9	0.98	32.3	2.60	19.6	0.84	29.8	3.07	22.1	0.97	34.0	21.7	34.0
	PAS31-1	26.2	98	2.95	20.8	0.97	32.3	2.31	18.8	0.78	27.8*	3.05	21.7	0.98	33.6	22.2	33.6
	PAS31-2	22.9	95	3.12	20.9	0.97	33.0	2.55	19.6	0.85	29.6	3.14	22.2	0.98	34.4	20.2	34.4
SBFN	MSS	4.5	62	4.12	17.9	0.87	34.0*	0.65	18.5	0.91	21.1*	1.89	20.2	0.56	27.6*	20.4	34.0*
	PAS31-1	3.8	62	4.89	18.4	0.84	37.5	0.62	18.5	0.90	20.9	1.87	20.4	0.54	27.7	24.5	37.5
SBFS	MSS	6.5	51	2.33	15.4	0.92	24.5	2.36	24.5	0.80	33.7*	2.36	24.5	0.80	33.7*	25.0	33.7*
	PAS31-1	1.8	52	4.78	17.8	0.82	36.4	1.78	24.9	0.83	31.8	1.75	25.0	0.84	31.8	19.8	36.4
SBFZ	MSS	7.4	100	1.81	15.4	0.87	22.5*	0.71	19.8	0.89	22.6*	0.71	19.8	0.89	22.6*	19.9	22.6*
	PAS31-1	6.1	100	2.47	14.0	0.88	23.7	0.70	19.9	0.89	22.7	0.70	19.9	0.89	22.7	20.0	23.7
	PAS31-2	6.2	100	2.27	15.1	0.86	24.0	0.68	20.0	0.89	22.6	0.68	20.0	0.89	22.6	22.7	24.0
SBGL	MSS	16.4	100	2.18	22.7	0.79	31.2	1.11	18.3	0.95	22.6	2.18	22.7	0.79	31.2	23.4	31.2
	PAS31-1	18.5	99	2.79	23.4	0.93	34.3*	0.98	18.4	0.96	22.2*	2.79	23.4	0.93	34.3*	20.4	34.3*
	PAS31-2	14.8	99	1.65	20.2	0.94	26.7	1.15	17.6	0.94	22.0	1.56	20.4	0.94	26.5	19.5	26.7
	PAS31-3	18.7	100	1.85	19.5	0.97	26.7	0.85	15.9	0.89	19.2	1.82	19.5	0.98	26.6	20.3	26.7
	PAS31-4	14.0	95	1.78	20.1	0.97	27.1	1.34	17.5	0.96	22.7	1.67	20.3	0.96	26.8	18.2	27.1
SBGM	MSS	7.4	45	2.15	18.2	0.97	26.6	0.71	13.4	0.91	16.2	2.15	18.2	0.97	26.6	17.2	26.6
	PAS31-1	7.5	47	1.69	17.2	0.94	23.8	1.09	13.3	0.90	17.5*	1.69	17.2	0.94	23.8	22.8	23.8
SBGO	MSS	14.7	99	2.18	22.8	0.99	31.3	1.85	16.2	0.96	23.4	2.14	22.8	0.98	31.2	23.1	31.3
	PAS31-1	21.5	99	2.91	23.0	0.92	34.4*	1.35	16.8	0.93	22.0*	2.88	23.1	0.92	34.3*	25.6	34.4*
SBGP	MSS	6.7	42	3.89	25.4	0.96	40.6*	1.84	18.4	0.91	25.6*	3.47	25.6	0.96	39.1*	25.1	40.6*
	PAS31-1	2.5	39	3.47	24.5	0.81	38.0	1.88	19.1	0.80	26.4	3.49	25.1	0.85	38.7	24.8	38.7
SBGR	MSS	19.4	100	3.90	24.8	0.98	40.0*	1.17	16.9	0.96	21.5	3.90	24.8	0.98	40.0*	24.9	40.0*
	PAS31-1	17.6	99	4.00	24.9	0.97	40.5	1.16	17.0	0.95	21.5	4.00	24.9	0.97	40.5	22.1	40.5
	PAS31-2	15.3	99	3.07	22.1	0.95	34.1	1.11	16.6	0.92	21.0	3.07	22.1	0.95	34.1	21.5	34.1
	PAS31-3	20.5	99	2.72	21.4	0.96	32.0	1.34	16.2	0.95	21.5	2.69	21.5	0.95	32.0	22.7	32.0
	PAS31-4	16.1	99	2.90	22.7	0.99	34.0	0.89	15.8	0.90	19.2	2.90	22.7	0.99	34.0	21.8	34.0
SBGW	MSS	9.2	56	2.56	21.8	0.95	31.8	0.84	13.9	0.92	17.2	2.56	21.8	0.95	31.8	22.5	31.8
	PAS31-1	14.5	55	2.89	22.5	0.90	33.8*	0.74	15.0	0.86	17.8	2.89	22.5	0.90	33.8*	14.9	33.8*
SBHT	MSS	7.8	76	1.71	14.3	0.94	21.0	1.65	12.4	0.86	18.8*	1.45	14.9	0.94	20.5	16.5	21.0
	PAS31-1	6.7	84	2.56	15.2	0.95	25.2	2.57	14.0	0.92	24.1	2.29	16.5	0.95	25.4	19.8	25.4
SBIH	MSS	5.9	68	3.60	19.8	0.65	33.9*	0.81	11.7	0.90	14.8	3.60	19.8	0.65	33.9*	20.0	33.9*
	PAS31-1	5.7	72	3.73	20.0	0.67	34.6	0.69	11.0	0.87	13.6	3.73	20.0	0.67	34.6	17.8	34.6
SBIL	MSS	18.7	95	1.51	16.0	0.96	21.9	1.10	17.2	0.94	21.5	0.92	17.8	0.95	21.4	18.2	21.9
	PAS31-1	26.5	95	1.34	15.8	0.98	21.0	1.11	17.9	0.90	22.2*	0.89	18.2	0.94	21.7*	17.5	22.2
SBIP	MSS	5.1	52	2.34	17.5	0.82	26.7	0.87	13.3	0.90	16.7	2.22	17.5	0.78	26.2	16.3	26.7
	PAS31-1	3.7	56	1.56	16.3	0.81	22.4	0.79	13.4	0.85	16.4	1.43	16.3	0.76	21.9	19.3	22.4
SBIZ	MSS	7.9	82	2.50	19.2	0.96	29.0	1.29	13.1	0.76	18.1	2.44	19.3	0.97	28.8	19.8	29.0
	PAS31-1	12.4	75	3.25	19.7	0.93	32.4*	1.65	14.1	0.82	20.5*	3.20	19.8	0.92	32.3*	18.3	32.4*
SBJC	MSS	5.8	52	1.62	18.3	0.90	24.6*	0.46	12.6	0.53	14.4	1.62	18.3	0.90	24.6*	18.5	24.6*
	PAS31-1	5.2	53	1.68	18.5	0.91	25.0	0.72	13.1	0.85	15.9	1.68	18.5	0.91	25.0	26.6	25.0
SBJD	MSS	5.9	53	2.86	26.6	0.98	37.8*	0.96	19.8	0.96	23.5*	2.86	26.6	0.98	37.8*	26.8	37.8*
	PAS31-1	4.5	52	3.11	26.8	0.96	39.0	0.76	19.7	0.94	22.7	3.10	26.8	0.95	38.9	18.8	39.0
SBJF	MSS	9.3	57	2.26	18.7	0.97	27.5	0.63	16.3	0.88	18.7	2.15	18.8	0.96	27.2	19.3	27.5
	PAS31-1	14.1	62	2.63	19.3	0.95	29.5	0.63	16.4	0.85	18.9	2.60	19.3	0.95	29.4	17.0	29.5
SBJP	MSS	14.1	98	1.48	13.1	0.96	18.9	1.05	17.0	0.90	21.1	1.04	17.0	0.89	21.1	16.8	21.1
	PAS31-1	23.3	99	1.62	13.2	0.96	19.5	0.66	16.7	0.90	19.3*	0.68	16.8	0.92	19.5	17.7	19.5
SBJR	MSS	9.9	65	1.98	17.1	0.96	24.8	1.33	15.9	0.96	21.1	1.73	17.7	0.95	24.4	17.3	24.8
	PAS31-1	15.5	70	1.62	16.7	0.95	23.1	1.35	15.8	0.97	21.0	1.46	17.3	0.95	23.0	16.3	23.1
SBJU	MSS	14.3	87	1.93	15.7	0.97	23.2	0.37	15.4	0.75	16.9	1.45	16.3	0.88	22.0	16.3	23.2
	PAS31-1	12.9	86	1.93	15.6	0.96	23.1	0.35	15.5	0.74	16.8	1.40	16.3	0.83	21.8	21.1	23.1

* indicates the station is a member of the governing set of stations for a particular distribution (N, S, M or E)

Table C.1 (cont...) - Extreme distribution parameters of Class A aerodrome SWS

ICAO ID	DATA-SET	t_{tot} (yrs)	Obs. (%)	Non-Synoptic				Synoptic				Mixed Distribution				Envelope	
				a_N	U_N (m/s)	R_N^2	$G_{50,N}$ (m/s)	a_S	U_S (m/s)	R_S^2	$G_{50,S}$ (m/s)	a_M	U_M (m/s)	R_M^2	$G_{50,M}$ (m/s)	U_E (m/s)	$G_{50,E}$ (m/s)
SBJV	MSS	12.3	75	3.13	20.9	0.90	33.1	2.06	14.8	0.80	22.8	3.07	21.1	0.91	33.1	21.1	33.1
	PAS31-1	13.1	76	3.07	20.5	0.88	32.5	1.96	14.7	0.78	22.4	3.08	20.7	0.90	32.7*	20.7	32.7
SBKG	MSS	11.9	82	2.78	16.4	0.94	27.2	0.79	15.7	0.93	18.7	1.99	17.4	0.94	25.2	17.4	27.2
	PAS31-1	20.3	75	2.59	15.3	0.96	25.3*	0.69	15.3	0.89	18.0	1.90	16.4	0.96	23.8*	16.4	25.3*
SBKP	MSS	18.4	100	3.36	24.3	0.98	37.4*	1.02	18.6	0.82	22.6	3.31	24.3	0.98	37.2*	24.3	37.4*
	PAS31-1	16.6	99	3.40	24.6	0.99	37.9	1.09	18.8	0.85	23.0	3.35	24.7	0.98	37.8	24.7	37.9
	PAS31-2	14.1	97	2.50	23.4	0.98	33.2	1.11	18.4	0.96	22.8	2.45	23.5	0.98	33.0	23.5	33.2
SBLO	MSS	14.4	100	4.90	24.9	0.91	44.0*	1.18	15.8	0.95	20.4	4.90	24.9	0.91	44.0*	24.9	44.0*
	PAS31-1	12.9	100	5.03	24.9	0.89	44.5	1.27	15.7	0.95	20.7	5.03	24.9	0.89	44.5	24.9	44.5
SBLP	MSS	7.7	43	2.07	17.0	0.67	25.1	1.31	14.4	0.93	19.5	2.05	17.2	0.68	25.2	17.2	25.2
SBLs	MSS	6.7	71	2.87	21.4	0.94	32.6*	0.61	14.8	0.68	17.2	2.84	21.4	0.94	32.5*	21.4	32.6*
	PAS31-1	5.6	70	2.12	20.8	0.90	29.1	0.63	14.9	0.69	17.4	2.08	20.8	0.90	28.9	20.8	29.1
	PAS31-2	4.7	66	2.27	20.7	0.92	29.6	1.14	15.7	0.96	20.1	2.20	20.7	0.91	29.3	20.7	29.6
SBMA	MSS	14.3	100	1.40	16.3	0.95	21.8	0.80	10.3	0.82	13.4	1.40	16.3	0.95	21.8	16.3	21.8
	PAS31-1	13.0	100	1.39	16.5	0.94	21.9	0.83	10.4	0.84	13.6	1.39	16.5	0.94	21.9	16.5	21.9
SBMD	MSS	7.9	68	1.97	17.6	0.97	25.3	1.93	14.0	0.87	21.5	1.94	17.9	0.98	25.5	17.9	25.5
	PAS31-1	8.6	71	1.93	17.1	0.96	24.6*	1.98	13.7	0.86	21.4*	1.97	17.4	0.98	25.1*	17.4	25.1*
SBME	MSS	16.1	98	4.27	18.0	0.95	34.6	1.25	17.4	0.89	22.3	3.42	19.5	0.90	32.8	19.5	34.6
	PAS31-1	27.8	99	3.81	17.6	0.92	32.5*	1.29	17.2	0.95	22.2	3.20	19.0	0.89	31.5*	19.0	32.5*
SBMG	MSS	10.0	88	2.79	30.0	0.95	40.8*	1.23	19.1	0.85	23.9	2.79	30.0	0.95	40.8*	30.0	40.8*
	PAS31-1	8.5	86	3.25	29.8	0.96	42.5	1.23	19.6	0.94	24.4	3.25	29.8	0.96	42.5	29.8	42.5
SBMK	MSS	6.5	88	2.89	20.5	0.97	31.8	1.10	14.4	0.91	18.7	2.75	20.6	0.96	31.3	20.6	31.8
	PAS31-1	15.1	75	2.10	19.2	0.97	27.4	1.10	14.5	0.94	18.8	2.06	19.3	0.97	27.3	19.3	27.4
SBMN	MSS	10.7	100	2.89	19.3	0.88	30.6	1.30	13.3	0.98	18.3*	2.89	19.3	0.88	30.6	19.3	30.6
	PAS31-1	17.7	97	2.05	18.4	0.97	26.4	1.35	12.7	0.97	18.0	2.05	18.4	0.97	26.4	18.4	26.4
	PAS31-2	4.6	88	1.41	18.6	0.91	24.1	1.69	11.5	0.92	18.1	1.41	18.6	0.91	24.1	18.6	24.1
SBMO	MSS	14.8	100	1.76	14.1	0.94	21.0*	0.52	16.6	0.72	18.6*	0.69	16.8	0.83	19.5	16.8	21.0
	PAS31-1	13.2	98	1.85	13.6	0.92	20.9	0.62	16.6	0.78	19.0	0.78	16.8	0.84	19.9	16.8	20.9
SBMQ	MSS	19.2	99	1.70	17.0	0.98	23.7	0.46	15.3	0.82	17.0	1.64	17.1	0.97	23.5	17.1	23.7
	PAS31-1	17.8	99	2.96	17.6	0.82	29.2	0.82	15.5	0.90	18.8	2.83	17.8	0.80	28.9	17.8	29.2
SBMS	MSS	9.8	52	1.20	16.0	0.93	20.7	0.61	17.8	0.90	20.2	0.71	17.9	0.90	20.7	17.9	20.7
	PAS31-1	9.4	55	1.26	16.1	0.94	21.0	0.61	17.8	0.90	20.2	0.72	17.9	0.91	20.7	17.9	21.0
SBMY	MSS	4.1	44	2.35	21.1	0.92	30.2*	1.80	12.7	0.57	19.7*	2.30	21.3	0.92	30.2*	21.3	30.2*
	PAS31-1	3.7	46	2.35	21.3	0.92	30.4	1.80	12.8	0.57	19.9	2.30	21.5	0.92	30.4	21.5	30.4
SBNF	MSS	12.7	78	2.61	21.4	0.95	31.6	1.70	19.6	0.98	26.3	2.14	22.2	0.93	30.5	22.2	31.6
	PAS31-1	17.7	78	3.59	21.8	0.94	35.8*	1.59	19.3	0.99	25.5*	3.26	22.4	0.92	35.1*	22.4	35.8*
SBNT	MSS	21.1	95	2.01	15.5	0.78	23.3	1.13	18.9	0.90	23.3	1.45	19.0	0.85	24.7	19.0	24.7
	PAS31-1	26.3	99	2.25	14.9	0.85	23.7*	1.04	18.5	0.88	22.6*	1.37	18.7	0.84	24.1*	18.7	24.1*
SBPA	MSS	22.7	99	2.75	23.9	0.92	34.7	1.63	20.3	0.96	26.7	2.56	24.2	0.91	34.2	24.2	34.7
	PAS31-1	25.5	99	3.11	23.5	0.96	35.7*	2.20	20.4	0.90	29.0*	3.08	24.1	0.97	36.1*	24.1	36.1*
	PAS31-2	24.4	95	2.77	22.7	0.82	33.5	1.41	20.2	0.98	25.7	2.59	23.0	0.79	33.1	23.0	33.5
SBPB	MSS	11.2	65	1.73	15.7	0.82	22.5	1.16	20.5	0.69	25.0	1.16	20.6	0.71	25.1	20.6	25.1
	PAS31-1	14.5	58	1.93	15.9	0.93	23.4*	1.06	20.5	0.74	24.6*	1.05	20.5	0.75	24.6*	20.5	24.6*
SBPC	MSS	7.7	50	3.03	18.7	0.90	30.5	0.80	13.7	0.96	16.8	3.00	18.7	0.89	30.4	18.7	30.5
	PAS31-1	14.5	54	3.67	20.5	0.92	34.8*	1.23	14.9	0.97	19.7	3.62	20.6	0.93	34.7*	20.6	34.8*
SBPJ	MSS	15.5	98	2.74	20.7	0.95	31.4*	1.87	17.9	0.97	25.2*	2.55	21.1	0.96	31.1*	21.1	31.4*
	PAS31-1	15.5	98	2.87	21.4	0.97	32.6	1.97	18.1	0.96	25.8	2.56	21.9	0.97	31.9	21.9	32.6
SBPK	MSS	11.3	55	2.95	22.3	0.92	33.8	1.79	20.0	0.96	27.0	2.56	23.0	0.90	33.0	23.0	33.8
	PAS31-1	16.3	59	3.66	20.9	0.97	35.2	1.49	20.0	0.98	25.8	3.00	22.2	0.94	33.9	22.2	35.2
SBPL	MSS	16.3	86	1.47	16.9	0.92	22.6	0.84	16.7	0.86	20.0	1.26	17.6	0.90	22.5	17.6	22.6
	PAS31-1	22.6	81	2.36	17.0	0.89	26.2	0.88	16.9	0.86	20.3*	1.93	18.0	0.83	25.5	18.0	26.2
SBPN	MSS	6.6	43	2.22	16.6	0.97	25.3	1.66	13.6	0.85	20.1	1.81	17.0	0.95	24.1	17.0	25.3
	PAS31-1	10.9	50	3.06	16.0	0.87	28.0	1.88	12.7	0.94	20.0*	2.87	16.4	0.86	27.6	16.4	28.0
SBPP	MSS	8.6	49	2.35	23.4	0.96	32.6	1.74	23.9	0.84	30.7	1.69	25.2	0.88	31.7	25.2	32.6
	PAS31-1	12.3	51	2.86	24.7	0.90	35.8*	1.75	23.6	0.87	30.5*	1.90	26.0	0.76	33.4*	26.0	35.8*
SBPR	MSS	8.6	53	2.25	22.2	0.93	30.9	0.88	17.0	0.93	20.4*	2.25	22.2	0.93	30.9	22.2	30.9
	PAS31-1	8.3	59	2.23	22.0	0.95	30.7	0.87	17.0	0.93	20.4	2.23	22.0	0.95	30.7	22.0	30.7
SBPS	MSS	17.3	94	2.25	15.7	0.94	24.5	1.79	18.3	0.76	25.3*	2.08	18.6	0.84	26.7*	18.6	26.7*
	PAS31-1	15.9	98	2.05	15.3	0.97	23.3	1.07	18.1	0.94	22.3	1.04	18.4	0.92	22.5	18.4	23.3
	PAS31-2	5.9	95	1.70	14.2	0.98	20.9	1.27	17.8	0.93	22.7	1.21	17.8	0.92	22.6	17.8	22.7
SBPV	MSS	18.2	99	2.13	18.9	0.91	27.3	1.77	12.7	0.88	19.6*	2.13	19.0	0.92	27.3	19.0	27.3
	PAS31-1	16.8	99	1.81	18.6	0.88	25.7	1.84	12.8	0.89	20.0	1.83	18.7	0.90	25.8	18.7	25.8
SBQV	MSS	10.4	63	2.54	16.7	0.87	26.6	0.77	17.0	0.66	20.0	2.08	17.8	0.82	25.9	17.8	26.6
	PAS31-1	16.8	60	2.44	16.8	0.97	26.4*	0.62	17.2	0.91	19.7	1.67	18.1	0.90	24.7*	18.1	26.4*
SBRB	MSS	19.5	99	3.13	19.2	0.90	31.4*	1.22	13.2	0.95	18.0*	3.13	19.2	0.90	31.4*	19.2	31.4*
	PAS31-1	17.1	99	2.57	19.2	0.93	29.2	1.20	13.1	0.96	17.8	2.57	19.2	0.93	29.2	19.2	29.2
	PAS31-2	9.4	97	2.41	19.1	0.94	28.4	1.58	12.0	0.89	18.2	2.38	19.1	0.94	28.4	19.1	28.4

* indicates the station is a member of the governing set of stations for a particular distribution (N, S, M or E)

Table C.1 (cont...) - Extreme distribution parameters of Class A aerodrome SWS

ICAO ID	DATA-SET	t_{tot} (yrs)	Obs. (%)	Non-Synoptic				Synoptic				Mixed Distribution				Envelope	
				a_N	U_N (m/s)	R_N^2	$G_{50,N}$ (m/s)	a_S	U_S (m/s)	R_S^2	$G_{50,S}$ (m/s)	a_M	U_M (m/s)	R_M^2	$G_{50,M}$ (m/s)	U_E (m/s)	$G_{50,E}$ (m/s)
SBRF	MSS	22.2	97	2.42	15.0	0.87	24.4	0.67	17.8	0.88	20.5	1.26	18.1	0.64	23.0	18.1	24.4
	PAS31-1	23.7	99	1.52	14.5	0.95	20.4	0.68	17.6	0.94	20.3*	0.65	17.8	0.92	20.3*	17.8	20.4
	PAS31-2	7.4	90	1.74	13.4	0.90	20.2	1.37	16.8	0.89	22.2	1.35	17.0	0.91	22.2	17.0	22.2
SBRJ	MSS	20.7	90	2.39	20.6	0.98	29.9	1.18	17.7	0.98	22.3	2.25	20.8	0.96	29.6	20.8	29.9
	PAS31-1	21.3	97	2.58	21.3	0.95	31.3*	0.98	17.7	0.95	21.5	2.51	21.4	0.94	31.1*	21.4	31.3*
	MSS	17.5	93	3.07	25.1	0.98	37.1	1.63	16.0	0.94	22.3	3.07	25.1	0.98	37.1	25.1	37.1
SBRP	PAS31-1	26.9	99	2.89	24.3	0.98	35.6*	1.68	16.1	0.94	22.6*	2.89	24.3	0.98	35.6*	24.3	35.6*
	MSS	16.1	98	2.39	21.0	0.96	30.3	0.82	19.3	0.96	22.5	2.08	21.4	0.96	29.5	21.4	30.3
	PAS31-1	23.0	100	1.91	20.4	0.96	27.8	0.79	19.4	0.93	22.5*	1.56	20.9	0.96	27.0	20.9	27.8
SBSC	PAS31-2	14.4	99	1.87	18.3	0.97	25.6	0.63	18.7	0.93	21.2	1.31	19.4	0.96	24.5	19.4	25.6
	MSS	5.0	98	1.82	17.2	0.97	24.3*	1.06	20.8	0.91	24.9*	1.04	20.9	0.91	24.9*	20.9	24.9*
	PAS31-1	3.6	97	1.46	17.0	0.88	22.7	1.04	21.2	0.91	25.3	1.04	21.2	0.91	25.3	21.2	25.3
SBSG	MSS	16.2	99	2.62	22.5	0.95	32.7	0.78	17.0	0.95	20.0	2.62	22.5	0.95	32.7	22.5	32.7
	PAS31-1	18.0	99	2.40	22.3	0.96	31.7	0.71	17.4	0.95	20.1	2.40	22.3	0.96	31.7	22.3	31.7
	PAS31-2	14.9	90	3.23	22.4	0.97	35.0	1.09	16.6	0.91	20.9	3.23	22.4	0.97	35.0	22.4	35.0
SBSJ	MSS	18.3	99	1.31	18.0	0.95	23.1	0.68	17.9	0.92	20.6*	1.09	18.6	0.96	22.9	18.6	23.1
	PAS31-1	16.7	99	1.31	17.8	0.94	22.9	0.67	17.9	0.91	20.5	1.01	18.5	0.93	22.5	18.5	22.9
	PAS31-2	5.6	95	1.55	16.6	0.90	22.6	0.80	16.3	0.86	19.5	1.25	17.3	0.88	22.2	17.3	22.6
SBSL	MSS	10.7	81	3.10	25.0	0.94	37.1	1.63	21.7	0.93	28.0	2.89	25.3	0.93	36.6	25.3	37.1
	PAS31-1	21.9	82	2.46	23.5	0.94	33.1	1.94	21.1	0.96	28.7*	2.39	24.1	0.95	33.4	24.1	33.4
	PAS31-2	17.0	76	3.48	22.6	0.96	36.2	1.46	19.2	0.92	24.9	3.13	23.0	0.93	35.2	23.0	36.2
SBSM	MSS	19.2	99	1.84	20.5	0.91	27.7*	1.23	16.7	0.86	21.5*	1.84	20.5	0.91	27.7*	20.5	27.7*
	PAS31-1	17.2	97	1.91	20.6	0.90	28.1	1.28	16.9	0.87	21.9	1.91	20.6	0.90	28.1	20.6	28.1
	PAS31-2	6.2	98	1.70	19.4	0.84	26.1	0.66	14.9	0.90	17.4	1.70	19.4	0.84	26.1	19.4	26.1
SBSN	MSS	22.0	96	3.30	23.0	0.95	35.9*	1.25	17.6	0.95	22.5*	3.29	23.0	0.95	35.9*	23.0	35.9*
	PAS31-1	19.1	96	3.25	23.0	0.98	35.7	1.25	17.9	0.95	22.8	3.23	23.0	0.98	35.6	23.0	35.7
	PAS31-2	13.8	88	2.85	21.5	0.93	32.6	1.27	18.6	0.99	23.5	2.76	21.7	0.92	32.4	21.7	32.6
SBSP	MSS	15.9	97	3.74	20.2	0.85	34.8*	1.61	15.7	0.80	22.0	3.78	20.4	0.87	35.1*	20.4	35.1*
	PAS31-1	6.1	98	3.32	21.6	0.77	34.6	1.31	16.3	0.81	21.4	3.32	21.8	0.79	34.7	21.8	34.7
	MSS	5.8	62	2.50	21.7	0.89	31.5	2.18	19.5	0.98	28.0*	2.27	22.4	0.89	31.3	22.4	31.5
SBSR	PAS31-1	5.0	62	1.70	20.3	0.97	26.9	1.96	19.9	0.97	27.6	1.45	21.4	0.97	27.0	21.4	27.6
	MSS	22.2	97	1.30	15.8	0.97	20.9	1.13	17.7	0.96	22.1	1.05	17.9	0.95	22.0	17.9	22.1
	PAS31-1	26.2	99	1.25	15.6	0.98	20.5	1.13	17.8	0.98	22.2*	1.06	18.0	0.97	22.1*	18.0	22.2
SBST	PAS31-2	12.3	97	1.36	15.7	0.83	21.0	1.22	17.4	0.89	22.2	1.21	17.6	0.91	22.3	17.6	22.3
	MSS	3.0	74	3.62	27.6	0.91	41.8*	0.99	14.6	0.98	18.4	3.62	27.6	0.91	41.8*	27.6	41.8*
	PAS31-1	2.1	68	3.71	28.8	0.90	43.3	0.85	14.5	0.98	17.8	3.71	28.8	0.90	43.3	28.8	43.3
SBTA	MSS	18.5	94	1.87	16.4	0.96	23.7	0.48	11.9	0.92	13.8	1.87	16.4	0.96	23.7	16.4	23.7
	PAS31-1	16.8	99	1.48	16.2	0.86	22.0	0.63	12.1	0.90	14.6	1.48	16.2	0.86	22.0	16.2	22.0
	MSS	4.0	53	2.22	20.4	0.91	29.1*	1.56	14.0	0.92	20.1*	2.13	20.4	0.89	28.7*	20.4	29.1*
SBTE	PAS31-1	3.3	54	2.06	20.8	0.87	28.8	1.39	13.4	0.82	18.8	2.06	20.8	0.87	28.8	20.8	28.8
	MSS	4.6	47	2.55	21.0	0.93	31.0	1.03	12.0	0.91	16.0	2.55	21.0	0.93	31.0	21.0	31.0
SBTK	PAS31-1	5.4	59	2.59	20.6	0.93	30.7*	1.06	11.7	0.92	15.9*	2.59	20.6	0.93	30.7*	20.6	30.7*
	MSS	5.9	54	1.42	19.3	0.97	24.8	1.20	11.7	0.92	16.4*	1.42	19.3	0.97	24.8	19.3	24.8
SBTT	PAS31-1	5.2	54	1.51	19.3	0.96	25.2	1.23	12.0	0.92	16.7	1.51	19.3	0.96	25.2	19.3	25.2
	MSS	6.5	41	2.37	16.6	0.86	25.9	0.69	13.5	0.89	16.2	2.15	16.8	0.80	25.1	16.8	25.9
SBTU	PAS31-1	12.6	55	1.00	16.3	0.92	20.2	0.79	14.0	0.88	17.1*	0.92	16.4	0.89	20.0	16.4	20.2
	MSS	7.0	48	2.75	20.0	0.70	30.7	0.73	9.8	0.91	12.7	2.75	20.0	0.70	30.7	20.0	30.7
SBUA	PAS31-1	7.1	56	2.57	19.2	0.62	29.2*	0.68	9.6	0.86	12.2	2.57	19.2	0.62	29.2*	19.2	29.2*
	MSS	9.5	51	2.38	18.4	0.98	27.6*	0.84	18.0	0.92	21.2	1.69	19.3	0.90	25.8	19.3	27.6*
SBUF	PAS31-1	9.3	55	2.09	17.9	0.90	26.0	0.91	17.5	0.92	21.0	1.56	18.7	0.83	24.7	18.7	26.0
	MSS	6.7	59	2.51	28.5	0.94	38.3	1.17	20.7	0.95	25.2	2.51	28.5	0.94	38.3	28.5	38.3
SBUG	PAS31-1	13.7	62	2.37	26.4	0.97	35.6	2.07	21.4	0.96	29.5*	2.29	26.6	0.96	35.5*	26.6	35.6
	MSS	17.9	95	3.39	24.2	0.96	37.5	1.53	18.6	0.91	24.5	3.32	24.4	0.96	37.3	24.4	37.5
SBUL	PAS31-1	18.9	96	3.52	24.3	0.98	38.0*	2.21	19.2	0.87	27.9*	3.45	24.6	0.98	38.1*	24.6	38.1
	PAS31-2	6.2	99	3.25	23.9	0.88	36.6	1.18	17.7	0.96	22.3	3.23	23.9	0.87	36.5	23.9	36.6
SBUR	MSS	19.6	93	2.37	23.6	0.97	32.9	1.55	18.0	0.98	24.1	2.35	23.6	0.97	32.8	23.6	32.9
	PAS31-1	27.9	100	2.88	23.8	0.97	35.1*	1.23	19.3	0.97	24.1*	2.85	23.9	0.97	35.0*	23.9	35.1*
	MSS	4.7	53	3.28	17.0	0.79	29.8*	1.33	10.5	0.45	15.7	3.42	17.4	0.85	30.8*	17.4	30.8*
SBUY	PAS31-1	3.8	52	1.34	14.1	0.93	19.3	1.36	10.8	0.47	16.1	1.67	14.8	0.93	21.3	14.8	21.3
	MSS	14.0	64	2.14	19.6	0.94	28.0	1.10	14.9	0.94	19.2	2.14	19.6	0.94	28.0	19.6	28.0
SBVH	PAS31-1	21.3	77	2.97	18.9	0.90	30.5	0.80	14.9	0.92	18.0	2.94	19.0	0.90	30.4	19.0	30.5
	MSS	20.4	93	1.54	16.7	0.97	22.7	0.97	19.7	0.88	23.5*	0.90	19.9	0.87	23.4	19.9	23.5
SBVT	PAS31-1	19.3	98	1.78	16.8	0.94	23.8	0.96	19.9	0.91	23.7	0.89	20.1	0.88	23.5	20.1	23.8
	PAS31-2	6.1	98	3.85	14.8	0.90	29.8	1.12	19.5	0.67	23.9	1.27	19.8	0.77	24.7	19.8	29.8
SBYS	MSS	6.5	75	3.24	26.7	0.96	39.3	2.21	18.8	0.82	27.4	3.18	26.9	0.96	39.2	26.9	39.3
	PAS31-1	7.4	95	3.39	26.3	0.97	39.6*	1.86	18.0	0.93	25.2*	3.35	26.3	0.97	39.4*	26.3	39.6*
	PAS31-2	7.1	92	3.45	24.5	0.89	38.0	2.23	18.2	0.95	26.9	3.36	24.7	0.89	37.8	24.7	38.0
SBZM	MSS	3.8	49	3.14	24.3	0.98	36.5*	1.38	12.9	0.94	18.3	3.14	24.3	0.98	36.5*	24.3	36.5*
	PAS31-1	3.2	50	3.48	24.6	0.98	38.2	1.55	13.7	0.96	19.7	3.48	24.6	0.98	38.2	24.6	38.2

Table C.1 (cont...) - Extreme distribution parameters of Class A aerodrome SWS

ICAO ID	DATA-SET	t_{tot} (yrs)	Obs. (%)	Non-Synoptic				Synoptic				Mixed Distribution				Envelope	
				a_N	U_N (m/s)	R_N^2	$G_{50,N}$ (m/s)	a_S	U_S (m/s)	R_S^2	$G_{50,S}$ (m/s)	a_M	U_M (m/s)	R_M^2	$G_{50,M}$ (m/s)	U_E (m/s)	$G_{50,E}$ (m/s)
EGYP	MSS	19.4	98	2.10	20.4	0.94	28.6	1.49	30.8	0.98	36.6	1.49	30.8	0.98	36.6	30.8	36.6
SAAR	MSS	21.4	94	3.17	26.1	0.98	38.4*	1.40	21.5	0.94	27.0*	3.04	26.2	0.98	38.1*	26.2	38.4*
SABE	MSS	20.9	96	2.54	26.0	0.97	35.9*	2.09	23.5	0.92	31.7*	2.50	26.6	0.97	36.4*	26.6	36.4*
SACO	MSS	22.4	98	3.28	23.7	0.90	36.5*	1.35	21.3	0.98	26.6*	3.08	24.1	0.88	36.1*	24.1	36.5*
SADF	MSS	12.9	84	3.07	24.9	0.98	36.9*	2.22	20.1	0.97	28.8*	2.85	25.2	0.97	36.4*	25.2	36.9*
SAEZ	MSS	22.5	98	3.64	25.0	0.98	39.2*	1.73	20.7	0.97	27.4*	3.34	25.4	0.97	38.4*	25.4	39.2*
SAME	MSS	22.4	98	2.36	20.9	0.89	30.1*	2.86	19.4	0.97	30.6*	2.48	22.1	0.92	31.8*	22.1	31.8*
SANT	MSS	21.8	95	3.29	22.7	0.94	35.5*	1.74	19.2	0.94	26.0*	3.22	22.9	0.95	35.5*	22.9	35.5*
SARC	MSS	17.8	92	2.22	25.3	0.92	33.9*	1.95	20.3	0.94	27.9*	2.18	25.4	0.92	33.9*	25.4	33.9*
SARE	MSS	22.2	97	3.03	26.2	0.96	38.0*	1.58	19.0	0.85	25.2	3.01	26.3	0.97	38.0*	26.3	38.0*
SARF	MSS	21.9	95	2.36	24.0	0.90	33.2*	1.18	20.3	0.96	24.9*	2.28	24.2	0.89	33.1*	24.2	33.2*
SARI	MSS	9.3	99	3.20	25.9	0.94	38.4*	0.97	17.8	0.85	21.6	3.20	25.9	0.94	38.4*	25.9	38.4*
SARL	MSS	16.7	87	2.34	28.8	0.93	37.9*	1.99	25.2	0.92	33.0*	2.15	29.2	0.92	37.6*	29.2	37.9*
SARP	MSS	22.2	97	3.33	25.5	0.90	38.5*	1.32	16.9	0.96	22.1	3.33	25.5	0.90	38.5*	25.5	38.5*
SASA	MSS	21.7	95	2.89	21.5	0.92	32.8*	2.89	17.4	0.91	28.7*	3.10	22.1	0.96	34.2*	22.1	34.2*
SASJ	MSS	21.5	94	2.86	21.7	0.87	32.9*	1.98	20.3	0.83	28.0	2.84	22.5	0.87	33.6*	22.5	33.6*
SAVC	MSS	22.3	97	2.46	21.3	0.95	30.9	1.76	33.6	0.98	40.5	1.76	33.6	0.98	40.5	33.6	40.5
SAWE	MSS	16.5	72	2.22	17.4	0.96	26.0	1.63	31.5	0.96	37.8	1.63	31.5	0.96	37.8	31.5	37.8
SAWG	MSS	22.2	97	2.68	21.0	0.93	31.5	1.83	33.5	0.98	40.6	1.83	33.5	0.98	40.6	33.5	40.6
SAWH	MSS	17.6	88	2.20	25.4	0.97	34.0	1.72	33.9	0.95	40.6	1.72	33.9	0.95	40.6	33.9	40.6
SAZM	MSS	21.5	94	2.68	20.6	0.98	31.0	1.24	21.4	0.92	26.2	1.97	22.3	0.97	30.1	22.3	31.0
SAZN	MSS	18.2	86	2.55	20.6	0.98	30.6	2.89	26.0	0.78	37.2	2.89	26.2	0.79	37.4	26.2	37.4
SAZS	MSS	20.2	88	2.45	17.0	0.81	26.5	1.94	28.3	0.97	35.8	1.94	28.3	0.97	35.8	28.3	35.8
SCBA	MSS	14.5	93	2.43	14.0	0.84	23.5	1.34	30.4	0.93	35.6	1.34	30.4	0.93	35.6	30.4	35.6
SCCI	MSS	22.5	98	3.27	19.4	0.95	32.2	1.12	33.0	0.89	37.3	1.12	33.0	0.89	37.3	33.0	37.3
SGAS	MSS	22.2	97	2.23	24.7	0.93	33.4*	1.40	19.5	0.93	25.0*	2.21	24.8	0.93	33.4*	24.8	33.4*
SGES	MSS	15.3	88	2.40	24.8	0.90	34.1	0.81	18.6	0.92	21.8	2.40	24.8	0.90	34.1	24.8	34.1
SKLT	MSS	6.5	62	3.19	16.8	0.91	29.2*	0.76	8.9	0.86	11.8	3.19	16.8	0.91	29.2*	16.8	29.2*
SLCO	MSS	9.9	54	4.90	20.1	0.88	39.2	0.62	15.1	0.58	17.5	4.90	20.1	0.88	39.2	20.1	39.2
SLET	MSS	13.3	58	4.61	20.7	0.95	38.7*	2.19	28.1	0.95	36.7*	2.44	28.6	0.94	38.1*	28.6	38.7*
SLPS	MSS	10.1	56	2.91	20.3	0.93	31.7*	1.98	19.4	0.93	27.1*	2.27	21.6	0.91	30.5*	21.6	31.7*
SLTR	MSS	10.2	58	2.30	19.7	0.92	28.7*	1.50	19.2	0.92	25.1*	2.01	20.7	0.93	28.5*	20.7	28.7*
SLVR	MSS	21.4	99	2.74	21.0	0.97	31.6*	1.63	24.6	0.92	31.0*	1.64	25.0	0.95	31.4*	25.0	31.6*
SMJP	MSS	7.4	96	2.22	20.6	0.86	29.3*	1.29	15.9	0.97	21.0*	2.20	20.6	0.85	29.2*	20.6	29.3*
SMZO	MSS	3.5	64	2.20	19.3	0.92	27.9*	1.31	15.3	0.90	20.4*	2.04	19.4	0.91	27.4*	19.4	27.9*
SOCA	MSS	21.7	97	1.49	15.7	0.95	21.5	0.92	15.1	0.93	18.7*	1.37	16.2	0.95	21.6	16.2	21.6
SPCL	MSS	6.9	95	1.27	17.7	0.94	22.7	1.62	15.4	0.97	21.8*	1.14	17.9	0.94	22.4	17.9	22.7
SPQT	MSS	18.2	98	3.23	19.0	0.72	31.6*	1.78	12.0	0.95	18.9*	3.23	19.0	0.72	31.6*	19.0	31.6*
SPST	MSS	6.1	68	1.54	15.6	0.96	21.6	0.75	12.6	0.88	15.5*	1.47	15.6	0.95	21.4	15.6	21.6
SUAA	MSS	8.6	51	3.43	23.9	0.96	37.2*	1.57	25.2	0.93	31.3	1.93	26.5	0.87	34.0	26.5	37.2*
SUDU	MSS	9.5	51	3.05	22.9	0.98	34.8	1.75	21.1	0.97	27.9	2.46	23.8	0.94	33.3	23.8	34.8
SULS	MSS	18.9	83	2.82	23.3	0.79	34.3	4.01	26.6	0.97	42.3*	3.89	27.6	0.98	42.8*	27.6	42.8*
SUMU	MSS	22.5	98	3.00	24.5	0.96	36.2*	4.26	24.0	0.80	40.6*	4.16	26.4	0.85	42.6*	26.4	42.6*
SUSO	MSS	5.5	51	3.38	26.2	0.97	39.4*	0.89	20.8	0.92	24.3	3.18	26.3	0.96	38.7*	26.3	39.4*
SYCJ	MSS	20.2	92	2.88	19.8	0.92	31.1*	1.09	18.5	0.92	22.7*	2.51	20.5	0.87	30.3*	20.5	31.1*

* indicates the station is a member of the governing set of stations for a particular distribution (N, S, M or E)

Table C.2 – Extreme distribution parameters of Class A INMET ASWS

INMET ID	DATA-SET	t_{tot} (yrs)	Obs. (%)	Non-Synoptic				Synoptic				Mixed Distribution				Envelope	
				a_N	U_N (m/s)	R_N^2	$G_{50,N}$ (m/s)	a_S	U_S (m/s)	R_S^2	$G_{50,S}$ (m/s)	a_M	U_M (m/s)	R_M^2	$G_{50,M}$ (m/s)	U_E (m/s)	$G_{50,E}$ (m/s)
A001	WRDS	18.5	97	2.7	19.5	0.97	30.1	1.0	15.9	0.96	19.9*	2.6	19.6	0.96	30.0	19.6	30.1
A002	WRDS	17.5	97	1.9	22.0	0.94	29.5	1.9	17.4	0.91	25.0*	1.8	22.3	0.92	29.4	22.3	29.5
A003	WRDS	14.7	95	2.6	23.0	0.95	33.0*	1.2	18.2	0.92	23.1	2.5	23.0	0.94	32.8*	23.0	33.0*
A004	WRDS	14.7	95	3.2	23.4	0.92	35.9*	1.1	17.2	0.97	21.3*	3.2	23.4	0.92	35.9*	23.4	35.9*
A009	WRDS	13.7	95	1.2	21.4	0.98	26.2	1.3	21.2	0.97	26.4*	1.0	22.2	0.96	26.3	22.2	26.4
A010	WRDS	8.0	94	2.9	23.3	0.97	34.6*	1.4	17.0	0.96	22.6*	2.9	23.3	0.96	34.5*	23.3	34.6*
A011	WRDS	11.0	96	2.2	26.3	0.94	34.7*	1.9	19.1	0.91	26.7*	2.1	26.4	0.95	34.4*	26.4	34.7*
A012	WRDS	12.3	98	3.0	21.4	0.96	33.0*	1.3	16.7	0.95	21.8*	2.9	21.4	0.96	32.9*	21.4	33.0*
A013	WRDS	11.0	94	2.1	22.2	0.96	30.2	1.1	16.2	0.90	20.4*	2.1	22.2	0.96	30.2	22.2	30.2
A014	WRDS	10.4	98	2.6	23.2	0.94	33.3*	1.4	19.0	0.98	24.4*	2.5	23.3	0.94	33.0*	23.3	33.3*
A015	WRDS	9.9	95	3.8	24.8	0.93	39.8*	0.9	15.8	0.96	19.4	3.8	24.8	0.93	39.8*	24.8	39.8*
A016	WRDS	11.2	98	2.7	25.3	0.95	36.0*	2.0	19.5	0.99	27.4*	2.6	25.4	0.95	35.7*	25.4	36.0*
A017	WRDS	11.7	97	3.2	23.1	0.87	35.6*	1.4	19.3	0.96	24.8*	3.1	23.3	0.87	35.4*	23.3	35.6*
A018	WRDS	11.0	92	2.9	22.7	0.98	33.9*	0.6	14.4	0.97	16.8	2.9	22.7	0.98	33.9*	22.7	33.9*
A019	WRDS	12.2	98	1.6	21.0	0.92	27.3	0.9	15.9	0.98	19.2*	1.6	21.0	0.92	27.3	21.0	27.3
A020	WRDS	7.8	95	2.1	20.8	0.85	29.0*	0.6	13.6	0.95	15.9	2.1	20.8	0.85	29.0*	20.8	29.0*
A021	WRDS	7.6	87	1.1	19.0	0.95	23.2	1.6	17.5	0.96	23.6*	0.9	19.4	0.93	22.8	19.4	23.6
A022	WRDS	8.6	93	5.0	23.7	0.93	43.4*	1.7	16.4	0.94	23.3*	4.9	23.8	0.92	43.0*	23.8	43.4*
A023	WRDS	10.5	95	3.4	23.9	0.98	37.3*	1.1	17.0	0.94	21.5	3.4	23.9	0.98	37.3*	23.9	37.3*
A024	WRDS	11.7	98	2.7	20.0	0.96	30.4	1.7	17.0	0.97	23.6*	2.4	20.5	0.95	29.7	20.5	30.4
A025	WRDS	10.4	95	2.7	23.7	0.99	34.1*	1.4	18.6	0.94	23.9*	2.6	23.7	0.98	34.0*	23.7	34.1*
A026	WRDS	8.6	93	3.6	22.0	0.87	35.9*	1.1	16.8	0.97	21.0	3.5	22.0	0.87	35.8*	22.0	35.9*
A027	WRDS	5.9	95	1.8	21.8	0.99	28.7	0.7	16.4	0.94	19.2	1.8	21.8	0.99	28.7	21.8	28.7
A028	WRDS	5.0	94	2.2	22.7	0.97	31.3	1.2	15.6	0.97	20.3	2.2	22.7	0.97	31.3	22.7	31.3
A032	WRDS	10.1	94	2.4	21.0	0.97	30.4	1.6	17.5	0.95	23.6*	2.2	21.3	0.98	29.7	21.3	30.4
A033	WRDS	10.0	98	2.5	22.8	0.95	32.6*	1.3	16.4	0.92	21.5	2.5	22.8	0.95	32.6*	22.8	32.6*
A034	WRDS	11.0	97	2.0	21.5	0.97	29.5	0.8	16.4	0.98	19.6	2.0	21.5	0.97	29.5	21.5	29.5
A035	WRDS	8.6	97	2.4	23.8	0.95	33.1*	1.0	16.4	0.98	20.3	2.4	23.8	0.95	33.1*	23.8	33.1*
A036	WRDS	10.0	99	3.6	19.8	0.83	33.8*	0.9	17.0	0.96	20.5*	3.4	20.0	0.80	33.4*	20.0	33.8*
A037	WRDS	8.5	98	1.4	18.7	0.97	24.2	1.4	15.6	0.97	21.1*	1.3	18.8	0.96	23.9	18.8	24.2
A038	WRDS	10.3	96	2.8	22.1	0.96	33.0*	0.7	16.4	0.90	19.3	2.8	22.1	0.96	33.0*	22.1	33.0*
A039	WRDS	9.7	91	2.3	20.8	0.97	29.8	0.5	15.9	0.93	17.7	2.3	20.8	0.97	29.8	20.8	29.8
A040	WRDS	6.2	94	3.3	24.1	0.90	36.8*	1.1	18.1	0.92	22.4*	3.1	24.1	0.88	36.2*	24.1	36.8*
A041	WRDS	5.8	89	1.7	22.8	0.98	29.6*	1.2	16.6	0.99	21.2*	1.7	22.8	0.98	29.6*	22.8	29.6*
A043	WRDS	3.9	87	2.1	19.4	0.77	27.6	0.6	14.3	0.98	16.5	2.1	19.4	0.77	27.6	19.4	27.6
A044	WRDS	9.2	95	3.8	19.9	0.79	34.8*	1.7	13.9	0.92	20.6*	3.7	20.0	0.78	34.6*	20.0	34.8*
A045	WRDS	10.5	99	2.0	19.1	0.93	26.9	1.6	16.7	0.92	23.1*	1.9	19.5	0.94	26.7	19.5	26.9
A046	WRDS	4.6	97	3.3	24.4	0.88	37.2*	1.1	18.2	0.93	22.5*	3.1	24.4	0.84	36.4*	24.4	37.2*
A054	WRDS	3.0	94	2.3	21.9	0.94	31.0	1.1	15.5	0.88	19.9*	2.3	21.9	0.93	30.7	21.9	31.0
A101	WRDS	14.1	87	2.5	19.8	0.78	29.7*	1.3	14.9	0.99	20.0*	2.5	19.8	0.78	29.7*	19.8	29.7*
A102	WRDS	6.2	89	2.8	18.5	0.91	29.6*	1.1	13.1	0.96	17.5*	2.8	18.5	0.91	29.5*	18.5	29.6*
A104	WRDS	6.4	88	2.8	22.0	0.95	32.8*	1.1	16.0	0.92	20.4*	2.8	22.0	0.95	32.7*	22.0	32.8*
A108	WRDS	3.6	93	1.7	18.5	0.91	25.1	1.2	14.6	0.96	19.4*	1.6	18.5	0.89	24.6	18.5	25.1
A109	WRDS	3.7	90	3.0	22.0	0.94	33.7*	0.9	13.1	0.97	16.8*	3.0	22.0	0.94	33.7*	22.0	33.7*
A110	WRDS	9.3	89	2.9	19.4	0.88	30.9*	0.9	13.9	0.91	17.6*	2.9	19.4	0.88	30.9*	19.4	30.9*
A111	WRDS	8.7	82	2.0	19.2	0.92	27.2	1.0	12.9	0.91	16.6*	2.0	19.2	0.92	27.2	19.2	27.2
A112	WRDS	6.5	92	1.8	20.8	0.97	27.7	1.2	14.0	0.91	18.7*	1.8	20.8	0.97	27.7	20.8	27.7
A113	WRDS	5.0	90	2.8	22.5	0.96	33.4*	1.0	13.3	0.96	17.3*	2.8	22.5	0.96	33.4*	22.5	33.4*
A117	WRDS	9.2	94	3.8	22.4	0.76	37.2*	1.4	15.1	0.97	20.4*	3.8	22.4	0.76	37.2*	22.4	37.2*
A119	WRDS	8.4	97	1.8	20.7	0.95	27.8*	0.8	16.0	0.96	19.0*	1.8	20.7	0.95	27.8*	20.7	27.8*
A120	WRDS	5.9	89	0.7	16.5	0.95	19.0	0.6	12.2	0.98	14.5	0.7	16.5	0.95	19.0	16.5	19.0
A121	WRDS	9.5	96	1.8	18.6	0.95	25.5*	1.2	14.1	0.83	18.9*	1.7	18.6	0.95	25.4*	18.6	25.5*
A122	WRDS	9.7	95	2.1	18.0	0.95	26.3	0.6	12.2	0.97	14.6	2.1	18.0	0.95	26.3	18.0	26.3
A123	WRDS	5.8	87	1.3	17.8	0.92	23.1	0.5	13.7	0.99	15.6	1.3	17.8	0.92	23.1	17.8	23.1
A124	WRDS	10.4	95	1.1	17.5	0.97	21.9	1.2	13.6	0.96	18.2*	1.1	17.5	0.97	21.9	17.5	21.9
A125	WRDS	10.2	94	2.1	19.8	0.96	27.8*	0.5	13.5	0.98	15.6	2.1	19.8	0.96	27.8*	19.8	27.8*
A126	WRDS	10.4	93	2.2	18.9	0.80	27.7*	0.9	12.9	0.99	16.5	2.2	18.9	0.80	27.7*	18.9	27.7*
A128	WRDS	8.6	92	0.9	17.7	0.96	21.3	1.1	12.9	0.96	17.3*	0.9	17.7	0.96	21.3	17.7	21.3
A133	WRDS	3.0	94	1.9	20.3	0.93	27.9*	1.2	14.1	0.92	18.6*	1.9	20.3	0.92	27.8*	20.3	27.9*
A134	WRDS	6.5	95	2.0	19.5	0.96	27.1*	0.6	11.6	0.99	14.1	2.0	19.5	0.96	27.1*	19.5	27.1*
A135	WRDS	8.0	95	2.4	18.9	0.96	28.2*	0.8	15.4	0.96	18.6*	2.3	19.0	0.96	28.0*	19.0	28.2*
A136	WRDS	7.8	88	1.3	18.2	0.98	23.4	1.7	14.5	0.85	21.0*	1.4	18.4	0.98	23.9	18.4	23.9
A138	WRDS	8.2	92	2.3	18.8	0.91	27.6*	1.5	14.1	0.94	19.9*	2.2	18.9	0.90	27.5	18.9	27.6*
A140	WRDS	9.2	96	2.6	18.8	0.97	29.0*	1.1	15.2	0.95	19.4*	2.5	18.9	0.96	28.7*	18.9	29.0*
A201	WRDS	14.5	90	1.7	18.1	0.98	24.8*	1.0	14.0	0.97	17.9*	1.7	18.1	0.98	24.8*	18.1	24.8*
A202	WRDS	11.3	89	1.0	19.4	0.94	23.3	1.0	17.0	0.94	20.8*	1.0	19.4	0.94	23.1	19.4	23.3
A203	WRDS	13.2	89	2.0	15.0	0.96	22.8	0.9	16.7	0.97	20.0*	1.2	17.0	0.92	21.8	17.0	22.8

* indicates the station is a member of the governing set of stations for a particular distribution (N, S, M or E)

Table C.2 (cont...) - Extreme distribution parameters of Class A INMET ASWS

INMET ID	DATA-SET	t_{tot} (yrs)	Obs. (%)	Non-Synoptic				Synoptic				Mixed Distribution				Envelope	
				a_N	U_N (m/s)	R_N^2	$G_{50,N}$ (m/s)	a_S	U_S (m/s)	R_S^2	$G_{50,S}$ (m/s)	a_M	U_M (m/s)	R_M^2	$G_{50,M}$ (m/s)	U_E (m/s)	$G_{50,E}$ (m/s)
A204	WRDS	10.5	94	3.2	19.2	0.94	31.6*	0.9	15.6	0.97	19.3	3.1	19.3	0.94	31.5*	19.3	31.6*
A205	WRDS	9.4	92	2.7	21.0	0.95	31.3*	2.0	16.5	0.96	24.3*	2.5	21.2	0.94	31.1*	21.2	31.3*
A206	WRDS	9.6	92	2.2	19.3	0.97	27.9*	1.5	16.8	0.96	22.6*	2.0	19.6	0.98	27.5*	19.6	27.9*
A207	WRDS	7.7	95	3.7	19.8	0.65	34.0*	0.8	14.7	0.97	17.7*	3.7	19.8	0.65	34.0*	19.8	34.0*
A209	WRDS	4.3	97	1.3	16.1	0.96	21.2	0.5	12.0	0.96	14.0	1.3	16.1	0.96	21.2	16.1	21.2
A210	WRDS	6.3	86	1.5	20.0	0.92	26.1*	0.7	13.3	0.91	16.0	1.5	20.0	0.92	26.1*	20.0	26.1*
A211	WRDS	9.9	93	2.7	18.3	0.95	29.0*	0.5	13.3	0.84	15.1	2.7	18.3	0.95	29.0*	18.3	29.0*
A212	WRDS	9.2	95	1.0	18.8	0.97	22.5	1.3	14.7	0.93	19.9*	0.9	18.8	0.97	22.4	18.8	22.5
A213	WRDS	10.0	90	1.5	19.9	0.97	25.6	1.2	13.8	0.92	18.6*	1.5	19.9	0.97	25.6	19.9	25.6
A214	WRDS	8.2	95	1.7	19.9	0.95	26.5	0.9	15.0	0.96	18.3*	1.7	19.9	0.95	26.5	19.9	26.5
A215	WRDS	5.6	96	2.3	15.4	0.96	24.5*	0.7	17.9	0.93	20.8*	0.8	18.2	0.97	21.2	18.2	24.5
A217	WRDS	8.2	92	1.4	14.0	0.93	19.6	0.8	16.9	0.97	20.1	0.8	16.9	0.97	20.0	16.9	20.1
A218	WRDS	7.5	89	1.1	14.6	0.99	19.0	0.7	17.4	0.96	20.4	0.7	17.5	0.95	20.3	17.5	20.4
A219	WRDS	8.2	98	1.2	18.0	0.93	22.7	1.3	17.8	0.98	22.9*	0.9	18.8	0.96	22.2	18.8	22.9
A220	WRDS	9.2	92	1.7	19.2	0.97	25.9	0.7	14.6	0.90	17.3	1.7	19.2	0.97	25.9	19.2	25.9
A221	WRDS	10.5	94	1.9	18.3	0.81	25.8	1.4	15.0	0.97	20.3*	1.8	18.4	0.77	25.5	18.4	25.8
A222	WRDS	10.0	93	2.5	19.9	0.96	29.8*	1.0	14.6	0.95	18.4	2.5	19.9	0.96	29.8*	19.9	29.8*
A223	WRDS	10.4	95	3.7	19.5	0.94	33.8*	1.0	14.4	0.92	18.3	3.6	19.5	0.93	33.7*	19.5	33.8*
A224	WRDS	10.0	93	2.3	20.4	0.94	29.4*	1.1	14.1	0.94	18.2*	2.3	20.4	0.94	29.4*	20.4	29.4*
A225	WRDS	10.9	97	3.6	20.1	0.95	34.1*	1.1	14.6	0.95	18.9*	3.6	20.1	0.95	34.1*	20.1	34.1*
A226	WRDS	8.0	92	1.4	19.9	0.98	25.3*	1.5	19.1	0.98	24.8*	1.3	20.5	0.98	25.5*	20.5	25.5*
A227	WRDS	8.4	95	2.3	18.1	0.86	27.2*	1.0	17.2	0.95	21.2*	1.9	18.8	0.80	26.4*	18.8	27.2*
A229	WRDS	4.7	98	1.5	21.2	0.95	27.0*	1.1	15.0	0.97	19.3*	1.5	21.2	0.95	27.0*	21.2	27.0*
A230	WRDS	8.0	91	2.3	20.9	0.92	29.7*	1.0	17.9	0.99	21.6*	2.1	21.0	0.91	29.2*	21.0	29.7*
A231	WRDS	9.0	94	2.0	21.3	0.96	29.1	1.4	15.9	0.95	21.5*	1.9	21.3	0.96	28.9	21.3	29.1
A233	WRDS	9.1	94	1.8	21.9	0.95	28.7*	0.7	15.0	0.92	17.7	1.8	21.9	0.95	28.7*	21.9	28.7*
A235	WRDS	2.2	96	1.6	18.1	0.90	24.4	0.3	11.1	0.96	12.1	1.6	18.1	0.90	24.4	18.1	24.4
A236	WRDS	8.5	90	1.2	19.9	0.97	24.4*	0.7	14.4	0.91	17.1*	1.2	19.9	0.97	24.4*	19.9	24.4
A238	WRDS	8.7	99	2.5	20.7	0.78	30.3*	0.9	15.9	0.89	19.4*	2.4	20.7	0.76	30.1*	20.7	30.3*
A239	WRDS	5.6	93	1.6	19.9	0.78	26.0*	2.3	19.3	0.92	28.1*	2.0	21.0	0.87	28.7*	21.0	28.7*
A240	WRDS	9.2	93	3.3	17.9	0.93	30.6*	1.1	13.5	0.98	17.6*	3.2	18.0	0.93	30.5*	18.0	30.6*
A241	WRDS	9.8	92	2.5	20.6	0.97	30.5*	0.8	14.7	0.92	17.9	2.5	20.6	0.97	30.5*	20.6	30.5*
A242	WRDS	8.4	90	2.4	16.0	0.95	25.2*	1.6	14.6	0.89	20.7*	2.3	16.7	0.98	25.6*	16.7	25.6*
A243	WRDS	4.4	75	1.3	17.9	0.94	23.0	1.4	17.0	0.86	22.6*	1.3	18.5	0.89	23.5	18.5	23.5
A246	WRDS	6.3	91	2.9	19.7	0.94	30.9*	1.0	12.5	0.86	16.2	2.9	19.7	0.94	30.9*	19.7	30.9*
A248	WRDS	6.3	94	1.5	19.5	0.90	25.5*	1.1	16.2	0.84	20.4*	1.5	19.6	0.93	25.7*	19.6	25.7*
A249	WRDS	4.3	91	1.8	17.4	0.81	24.6*	0.7	15.4	0.82	18.0*	1.8	17.7	0.83	24.6*	17.7	24.6*
A250	WRDS	3.7	98	1.7	16.9	0.91	23.5	1.2	14.9	0.85	19.4*	1.6	17.2	0.90	23.3	17.2	23.5
A301	WRDS	11.3	95	1.7	12.4	0.98	19.1	1.0	14.5	0.96	18.3*	1.0	14.7	0.96	18.7	14.7	19.1
A303	WRDS	14.1	97	1.7	13.3	0.91	19.8*	0.3	14.0	0.97	15.3	1.0	14.4	0.73	18.4	14.4	19.8*
A304	WRDS	12.6	92	1.1	12.3	0.86	16.5	1.2	18.3	0.86	22.9*	1.2	18.3	0.86	22.9*	18.3	22.9*
A305	WRDS	12.6	90	1.6	13.0	0.97	19.3	0.6	16.2	0.87	18.4	0.6	16.3	0.91	18.5	16.3	19.3
A306	WRDS	12.6	85	2.6	17.6	0.96	27.7*	1.6	18.7	0.98	25.0*	1.8	19.8	0.98	26.9*	19.8	27.7*
A307	WRDS	10.2	96	2.7	18.2	0.89	28.7*	1.2	17.7	0.95	22.6*	2.3	19.2	0.88	28.1*	19.2	28.7*
A308	WRDS	13.9	88	1.6	16.3	0.98	22.6	1.7	18.4	0.88	25.0*	1.7	18.7	0.93	25.4*	18.7	25.4*
A309	WRDS	13.3	96	3.2	15.6	0.90	28.0*	1.7	17.2	0.83	23.7*	2.6	18.1	0.88	28.1*	18.1	28.1*
A310	WRDS	13.0	96	2.9	13.7	0.91	25.1*	0.8	17.8	0.99	21.0*	1.0	18.1	0.99	21.9	18.1	25.1*
A311	WRDS	13.3	96	2.8	19.1	0.96	30.2*	1.0	15.8	0.96	19.8	2.8	19.2	0.96	30.1*	19.2	30.2*
A312	WRDS	11.6	92	2.0	19.2	0.98	27.0*	1.1	13.7	0.86	18.1	2.0	19.2	0.98	27.0*	19.2	27.0*
A313	WRDS	11.1	97	2.9	14.9	0.93	26.1*	0.9	16.7	0.96	20.4*	1.6	17.3	0.95	23.8*	17.3	26.1*
A314	WRDS	11.3	95	2.3	10.6	0.94	19.7	0.8	19.7	0.86	22.7*	0.8	19.7	0.86	22.7	19.7	22.7
A315	WRDS	10.8	92	2.7	18.0	0.92	28.3*	1.1	15.4	0.89	19.6*	2.6	18.2	0.93	28.2*	18.2	28.3*
A316	WRDS	10.2	92	2.0	19.0	0.97	26.7	1.5	17.4	0.95	23.3*	1.8	19.6	0.98	26.4*	19.6	26.7
A317	WRDS	11.1	92	2.0	16.9	0.98	24.9*	2.2	19.5	0.98	27.9*	1.9	20.0	0.98	27.5*	20.0	27.9*
A318	WRDS	11.4	94	1.5	13.8	0.98	19.5	1.7	16.8	0.88	23.4*	1.6	16.9	0.88	23.4	16.9	23.4
A319	WRDS	3.2	82	1.3	17.8	0.96	22.7	1.1	17.2	0.98	21.4*	0.9	18.2	0.93	21.9	18.2	22.7
A320	WRDS	10.0	91	3.1	12.7	0.94	24.7*	0.8	16.9	0.96	20.1	1.3	17.1	0.88	22.2*	17.1	24.7*
A321	WRDS	11.0	92	2.3	19.4	0.96	28.5*	1.7	19.0	0.97	25.5*	1.7	20.6	0.94	27.5*	20.6	28.5*
A322	WRDS	7.5	98	1.9	12.0	0.87	19.3	0.9	15.9	0.99	19.6*	0.9	15.9	0.98	19.5	15.9	19.6
A323	WRDS	9.9	96	3.0	17.9	0.98	29.5*	1.0	16.4	0.98	20.2	2.4	18.6	0.97	27.9*	18.6	29.5*
A324	WRDS	10.4	97	2.6	18.7	0.99	28.6*	1.5	18.4	0.98	24.4*	1.9	19.9	0.98	27.5	19.9	28.6
A325	WRDS	6.5	92	2.0	16.8	0.96	24.4	1.8	19.9	0.90	26.8*	1.7	20.2	0.90	26.7*	20.2	26.8*
A326	WRDS	8.8	95	2.7	21.6	0.99	32.1*	2.1	18.0	0.92	26.4*	2.6	22.1	0.98	32.1*	22.1	32.1*
A327	WRDS	11.6	97	2.8	14.9	0.95	25.9*	1.1	17.1	0.95	21.4*	1.7	17.7	0.93	24.3*	17.7	25.9*
A328	WRDS	8.3	96	1.9	14.0	0.95	21.4	0.8	17.0	0.95	20.2*	0.7	17.1	0.94	19.9	17.1	21.4
A329	WRDS	8.5	99	2.9	20.7	0.95	31.9*	0.8	18.5	0.94	21.8*	2.3	21.3	0.94	30.1*	21.3	31.9*
A330	WRDS	11.3	95	3.1	20.2	0.96	32.1*	1.4	19.6	0.97	25.0*	2.4	21.3	0.96	30.6*	21.3	32.1*

* indicates the station is a member of the governing set of stations for a particular distribution (N, S, M or E)

Table C.2 (cont...) - Extreme distribution parameters of Class A INMET ASWS

INMET ID	DATA-SET	t_{tot} (yrs)	Obs. (%)	Non-Synoptic				Synoptic				Mixed Distribution				Envelope	
				a_N	U_N (m/s)	R_N^2	$G_{50,N}$ (m/s)	a_S	U_S (m/s)	R_S^2	$G_{50,S}$ (m/s)	a_M	U_M (m/s)	R_M^2	$G_{50,M}$ (m/s)	U_E (m/s)	$G_{50,E}$ (m/s)
A331	WRDS	11.3	95	1.8	18.4	0.96	25.5	1.1	17.9	0.97	22.2*	1.4	19.1	0.91	24.6	19.1	25.5
A332	WRDS	10.8	92	2.1	18.4	0.92	26.6*	1.3	17.3	0.98	22.5*	1.9	18.9	0.95	26.5*	18.9	26.6*
A333	WRDS	10.3	91	3.7	19.5	0.82	34.0*	2.0	17.3	0.96	25.2*	3.5	20.2	0.82	33.9*	20.2	34.0*
A334	WRDS	11.1	95	1.8	17.0	0.97	24.0	1.2	18.2	0.86	22.8*	1.3	18.8	0.91	24.0	18.8	24.0
A335	WRDS	10.0	92	2.3	20.4	0.82	29.6*	0.9	16.9	0.96	20.3	2.3	20.4	0.82	29.6*	20.4	29.6*
A336	WRDS	8.8	96	3.4	20.5	0.93	33.6*	2.1	19.0	0.98	27.2*	2.9	21.6	0.92	32.9*	21.6	33.6*
A337	WRDS	10.4	91	2.9	18.7	0.84	30.0*	2.5	19.5	0.90	29.1*	3.0	20.7	0.90	32.5*	20.7	32.5*
A338	WRDS	8.5	96	1.9	19.4	0.89	26.8*	2.5	16.0	0.94	25.9*	2.0	19.9	0.92	27.6*	19.9	27.6*
A339	WRDS	7.6	93	2.3	15.4	0.91	24.3	1.7	17.7	0.82	24.3*	1.8	18.4	0.90	25.4*	18.4	25.4*
A340	WRDS	8.5	95	2.0	19.6	0.99	27.5*	1.5	18.2	0.96	23.9*	1.4	20.2	0.99	25.8*	20.2	27.5*
A341	WRDS	10.7	93	2.9	15.3	0.94	26.8*	0.9	15.8	0.98	19.1	1.7	16.9	0.98	23.7*	16.9	26.8*
A342	WRDS	10.0	95	1.5	18.3	0.85	24.3	1.0	17.8	0.98	21.9*	0.9	19.1	0.83	22.8	19.1	24.3
A343	WRDS	7.3	86	1.3	18.7	0.96	23.9	0.8	16.7	0.97	19.8	1.2	18.8	0.97	23.4	18.8	23.9
A344	WRDS	6.3	89	1.9	14.4	0.82	21.8*	0.9	20.5	0.94	23.9*	0.9	20.5	0.94	23.9*	20.5	23.9*
A345	WRDS	10.7	95	4.0	17.4	0.79	33.1*	1.1	19.0	0.96	23.2*	2.9	20.0	0.68	31.4*	20.0	33.1*
A346	WRDS	10.3	98	1.7	13.0	0.85	19.7	0.8	13.1	0.97	16.1	1.5	13.8	0.88	19.6	13.8	19.7
A347	WRDS	7.5	96	2.9	18.2	0.97	29.6*	1.3	19.0	0.92	24.0*	1.8	20.2	0.96	27.3	20.2	29.6*
A348	WRDS	10.9	97	4.0	16.9	0.99	32.7*	1.2	17.6	0.96	22.5*	2.7	19.1	0.95	29.6*	19.1	32.7*
A349	WRDS	10.6	97	3.3	19.2	0.89	32.0*	1.2	17.1	0.96	21.9*	2.9	19.7	0.84	31.0*	19.7	32.0*
A350	WRDS	10.2	95	3.6	20.9	0.85	34.8*	0.9	17.0	0.95	20.5*	3.5	20.9	0.84	34.6*	20.9	34.8*
A351	WRDS	7.0	95	2.3	18.8	0.99	28.0*	1.2	18.1	0.95	22.8*	1.5	19.8	0.96	25.5	19.8	28.0*
A352	WRDS	6.5	93	2.0	11.3	0.94	19.2	0.7	16.2	0.96	18.8	0.7	16.2	0.96	18.8	16.2	19.2
A353	WRDS	8.5	99	2.1	12.3	0.97	20.4	1.2	15.8	0.92	20.6*	1.2	15.9	0.92	20.5	15.9	20.6
A354	WRDS	10.4	96	5.3	21.3	0.92	42.1*	1.6	17.6	0.95	24.0*	4.9	21.9	0.90	41.0*	21.9	42.1*
A355	WRDS	10.3	96	2.1	11.9	0.96	20.0	0.7	14.4	0.93	17.1	0.9	14.7	0.97	18.1	14.7	20.0
A356	WRDS	10.1	94	0.9	12.9	0.77	16.3	1.3	14.2	0.95	19.1*	1.3	14.3	0.97	19.6	14.3	19.6
A357	WRDS	9.0	91	2.1	15.2	0.95	23.3*	0.7	15.0	0.98	17.8	1.2	16.2	0.96	20.9	16.2	23.3*
A358	WRDS	10.4	97	3.0	22.1	0.99	33.7*	1.0	19.0	0.97	22.8*	2.8	22.3	0.98	33.2*	22.3	33.7*
A359	WRDS	9.8	95	2.1	16.7	0.98	24.9*	0.7	18.5	0.99	21.3*	0.9	18.9	0.95	22.6*	18.9	24.9*
A360	WRDS	8.8	96	1.8	14.8	0.93	21.8	1.1	17.7	0.99	22.1*	1.2	17.9	0.98	22.7	17.9	22.7
A361	WRDS	7.4	96	1.6	17.2	0.94	23.5	1.8	17.4	0.93	24.5*	1.6	18.5	0.97	24.7	18.5	24.7
A362	WRDS	9.4	94	2.4	19.3	0.96	28.4*	1.8	15.0	0.96	22.1*	2.3	19.4	0.97	28.3*	19.4	28.4*
A363	WRDS	9.6	96	2.4	19.4	0.98	29.0*	1.5	17.4	0.97	23.1*	2.1	19.9	0.97	28.2*	19.9	29.0*
A364	WRDS	8.8	94	1.2	18.7	0.93	23.3	1.2	17.9	0.97	22.5*	0.9	19.2	0.92	22.9	19.2	23.3
A365	WRDS	8.2	94	2.4	19.1	0.96	28.4	1.7	18.3	0.94	25.0*	2.0	20.1	0.96	27.9	20.1	28.4
A366	WRDS	7.9	91	5.0	21.0	0.82	40.6*	1.5	18.2	0.95	24.2*	4.4	22.0	0.76	39.1*	22.0	40.6*
A367	WRDS	8.2	94	2.6	15.2	0.95	25.2*	0.9	16.6	0.98	20.0	1.3	17.4	0.98	22.6	17.4	25.2*
A401	WRDS	15.5	91	3.8	15.0	0.95	29.7*	1.8	18.0	0.97	25.1*	2.1	18.9	0.98	27.0*	18.9	29.7*
A402	WRDS	14.7	95	2.5	18.5	0.85	28.4	1.1	16.1	0.98	20.6*	2.5	18.7	0.85	28.3	18.7	28.4
A404	WRDS	14.7	95	2.4	21.1	0.96	30.4*	0.9	17.1	0.94	20.8*	2.3	21.2	0.96	30.3*	21.2	30.4*
A405	WRDS	13.4	89	2.8	14.7	0.97	25.8	0.9	18.3	0.98	21.9*	1.3	18.7	0.98	23.7	18.7	25.8
A406	WRDS	14.7	92	1.9	14.8	0.98	22.1	0.8	15.7	0.95	18.8	1.1	16.3	0.95	20.7	16.3	22.1
A407	WRDS	15.0	95	2.3	14.0	0.97	23.0	1.2	14.7	0.98	19.3*	1.4	15.7	0.93	21.2	15.7	23.0
A408	WRDS	15.9	98	2.4	18.2	0.98	27.5*	1.5	17.3	0.98	23.2*	2.0	19.1	0.98	26.9*	19.1	27.5*
A409	WRDS	12.8	95	2.1	13.5	0.99	21.5	0.8	15.9	0.87	19.2	1.1	16.2	0.92	20.3	16.2	21.5
A410	WRDS	8.5	95	1.4	15.4	0.87	20.8	0.8	16.4	0.97	19.6*	1.1	16.8	0.94	21.2	16.8	21.2
A411	WRDS	13.1	94	1.9	17.6	0.95	24.8	1.7	17.7	0.97	24.2*	1.5	18.9	0.96	24.9	18.9	24.9
A412	WRDS	12.8	92	2.7	18.3	0.94	28.8*	0.6	17.1	0.97	19.6	2.3	18.8	0.89	27.8*	18.8	28.8*
A413	WRDS	11.2	95	2.6	15.4	0.96	25.7*	0.9	15.3	0.97	18.9	1.7	16.7	0.97	23.3*	16.7	25.7*
A414	WRDS	10.3	93	2.3	13.6	0.97	22.7	0.9	15.3	0.98	18.8	1.2	15.8	0.98	20.4	15.8	22.7
A415	WRDS	11.3	94	2.5	19.6	0.87	29.4*	1.3	16.8	0.99	21.8*	2.4	19.8	0.84	29.0*	19.8	29.4*
A416	WRDS	9.4	92	2.5	19.2	0.96	29.1*	1.4	14.7	0.90	20.0	2.4	19.4	0.95	28.8*	19.4	29.1*
A417	WRDS	11.7	97	2.5	15.8	0.96	25.4*	0.8	15.8	0.96	19.1	1.8	16.8	0.91	23.9*	16.8	25.4*
A418	WRDS	10.6	94	1.8	19.0	0.99	25.9	1.8	17.2	0.94	24.1*	1.6	19.6	0.98	25.7	19.6	25.9
A419	WRDS	10.2	96	2.7	15.1	0.95	25.5*	1.6	19.0	0.97	25.3*	1.5	19.4	0.97	25.3*	19.4	25.5
A420	WRDS	9.9	93	3.9	17.4	0.94	32.8*	1.6	18.6	0.96	24.7*	2.1	20.2	0.97	28.4*	20.2	32.8*
A421	WRDS	10.0	94	1.9	11.6	0.98	18.9	0.7	14.3	0.85	17.3	0.8	14.5	0.93	17.6	14.5	18.9
A422	WRDS	7.2	86	3.6	14.2	0.95	28.3*	1.3	22.1	0.94	27.1*	1.2	22.2	0.94	26.8*	22.2	28.3*
A423	WRDS	10.7	96	2.6	18.6	0.95	28.7*	1.3	16.8	0.98	22.0*	2.2	19.2	0.93	27.6	19.2	28.7
A424	WRDS	10.0	98	2.4	17.8	0.96	27.2	1.5	17.6	0.97	23.2*	1.9	19.0	0.99	26.4	19.0	27.2
A425	WRDS	10.6	96	1.3	18.4	0.95	23.5	1.5	15.4	0.97	21.3*	1.1	18.6	0.96	23.0	18.6	23.5
A426	WRDS	10.4	94	4.3	20.2	0.95	36.9*	0.8	20.6	0.97	23.5*	2.9	22.1	0.83	33.6*	22.1	36.9*
A427	WRDS	10.3	95	2.8	15.3	0.88	26.2*	1.0	13.9	0.90	17.9	2.0	16.2	0.94	24.1	16.2	26.2*
A428	WRDS	9.5	94	1.6	17.4	0.95	23.8	1.9	17.3	0.77	24.5*	1.8	18.5	0.89	25.6	18.5	25.6
A429	WRDS	10.6	96	2.6	19.3	0.93	29.7*	1.1	16.5	0.94	20.6	2.6	19.5	0.93	29.5*	19.5	29.7*
A430	WRDS	11.1	100	3.0	17.8	0.91	29.6*	0.6	19.6	0.91	21.8*	1.7	20.2	0.65	26.7*	20.2	29.6*
A432	WRDS	7.0	90	2.2	18.4	0.97	26.9	0.9	16.9	0.96	20.6	1.7	18.9	0.94	25.4	18.9	26.9

* indicates the station is a member of the governing set of stations for a particular distribution (N, S, M or E)

Table C.2 (cont...) - Extreme distribution parameters of Class A INMET ASWS

INMET ID	DATA-SET	t_{tot} (yrs)	Obs. (%)	Non-Synoptic				Synoptic				Mixed Distribution				Envelope	
				a_N	U_N (m/s)	R_N^2	$G_{50,N}$ (m/s)	a_S	U_S (m/s)	R_S^2	$G_{50,S}$ (m/s)	a_M	U_M (m/s)	R_M^2	$G_{50,M}$ (m/s)	U_E (m/s)	$G_{50,E}$ (m/s)
A433	WRDS	10.9	98	1.7	18.5	0.94	25.2	1.8	15.8	0.93	22.8*	1.5	18.9	0.90	24.8	18.9	25.2
A434	WRDS	7.4	99	5.1	15.5	0.86	35.3*	0.8	15.9	0.95	19.0	3.1	18.1	0.66	30.0*	18.1	35.3*
A435	WRDS	10.6	96	3.3	18.7	0.96	31.7*	1.4	17.9	0.83	23.2*	2.9	19.7	0.97	30.9*	19.7	31.7*
A436	WRDS	10.6	96	2.8	18.8	0.98	29.9*	1.9	19.0	0.98	26.4*	2.2	20.5	0.98	29.1*	20.5	29.9*
A437	WRDS	10.3	94	1.9	12.8	0.93	20.4	0.8	14.2	0.81	17.4	1.2	14.7	0.91	19.4	14.7	20.4
A438	WRDS	10.0	93	3.2	12.4	0.76	24.7*	1.0	14.6	0.87	18.6	2.2	15.2	0.66	23.8*	15.2	24.7*
A439	WRDS	10.3	93	2.9	22.0	0.93	33.5*	1.0	17.6	0.97	21.4*	2.9	22.0	0.93	33.4*	22.0	33.5*
A440	WRDS	10.6	96	1.3	16.0	0.96	21.1	1.0	16.0	0.97	19.8	0.9	16.8	0.98	20.2	16.8	21.1
A441	WRDS	10.6	98	2.1	15.8	0.97	24.1	2.2	17.0	0.87	25.6*	2.2	17.8	0.91	26.5*	17.8	26.5*
A442	WRDS	8.6	86	2.8	18.4	0.97	29.2*	1.7	17.4	0.98	23.8*	1.9	19.5	0.95	27.0*	19.5	29.2*
A443	WRDS	10.6	97	3.3	17.9	0.91	30.9*	1.3	17.7	0.96	22.6*	2.6	19.2	0.85	29.5*	19.2	30.9*
A444	WRDS	8.8	90	2.4	14.2	0.87	23.4	0.8	13.5	0.93	16.8	2.1	14.9	0.87	23.0*	14.9	23.4
A445	WRDS	9.7	98	1.7	15.1	0.96	21.6	0.6	13.5	0.95	16.0	1.6	15.2	0.96	21.4	15.2	21.6
A446	WRDS	9.4	96	1.6	17.4	0.98	23.7	1.6	16.2	0.81	22.3*	1.7	18.0	0.97	24.5	18.0	24.5
A447	WRDS	9.3	95	2.1	13.7	0.97	21.7	2.7	15.8	0.78	26.2*	2.5	16.4	0.80	26.2*	16.4	26.2*
A448	WRDS	3.6	93	2.3	18.7	0.98	27.8*	1.0	18.0	0.95	22.0*	1.2	19.3	0.97	24.1	19.3	27.8*
A450	WRDS	3.8	98	1.9	14.6	0.97	22.0	1.8	19.3	0.87	26.5*	1.7	19.3	0.84	26.2*	19.3	26.5
A502	WRDS	14.1	97	3.9	23.6	0.96	38.6*	1.3	18.4	0.98	23.4*	3.8	23.7	0.95	38.4*	23.7	38.6*
A505	WRDS	16.0	99	3.0	22.4	0.96	34.0*	1.4	16.7	0.75	22.0*	2.9	22.5	0.96	34.0*	22.5	34.0*
A506	WRDS	13.4	98	2.6	20.1	0.97	30.4	1.4	16.1	0.97	21.6*	2.5	20.2	0.97	30.2	20.2	30.4
A507	WRDS	14.7	94	3.4	22.6	0.97	35.9*	1.3	17.3	0.85	22.5*	3.3	22.7	0.96	35.6*	22.7	35.9*
A508	WRDS	14.7	95	2.8	19.2	0.89	30.1	1.0	15.5	0.96	19.4	2.7	19.3	0.88	29.9	19.3	30.1
A509	WRDS	11.7	98	1.4	19.2	0.91	24.6	2.6	20.9	0.89	31.1*	2.3	21.4	0.85	30.4	21.4	31.1
A510	WRDS	13.5	98	3.1	19.5	0.94	31.8	0.6	13.5	0.97	16.0	3.1	19.5	0.94	31.8	19.5	31.8
A511	WRDS	11.9	93	1.8	17.0	0.99	23.9	1.1	13.2	0.91	17.7*	1.7	17.1	0.99	23.8	17.1	23.9
A512	WRDS	12.7	97	2.2	22.1	0.98	30.6	1.4	17.0	0.91	22.4	2.2	22.1	0.98	30.6	22.1	30.6
A513	WRDS	12.8	99	2.9	24.1	0.93	35.5*	1.0	18.2	0.96	22.0*	2.9	24.1	0.93	35.5*	24.1	35.5*
A514	WRDS	12.3	96	3.9	28.5	0.97	43.9*	1.6	19.6	0.98	26.0*	3.9	28.5	0.97	43.9*	28.5	43.9*
A515	WRDS	12.5	97	1.7	20.9	0.93	27.5	1.5	16.0	0.99	21.7*	1.7	20.9	0.93	27.4	20.9	27.5
A516	WRDS	11.5	94	3.2	23.9	0.96	36.4*	1.7	15.7	0.98	22.2*	3.2	23.9	0.96	36.4*	23.9	36.4*
A517	WRDS	9.1	96	5.1	26.1	0.96	46.1*	0.9	17.2	0.98	20.6*	5.1	26.1	0.96	46.1*	26.1	46.1*
A518	WRDS	10.9	98	3.3	25.4	0.92	38.1*	2.2	19.7	0.97	28.4*	3.1	25.6	0.91	37.7*	25.6	38.1*
A519	WRDS	12.5	97	2.7	21.9	0.98	32.5*	1.2	16.7	0.86	21.2	2.7	21.9	0.98	32.4*	21.9	32.5*
A520	WRDS	12.5	98	2.3	24.7	0.96	33.7*	2.2	17.9	0.94	26.4*	2.2	24.8	0.96	33.5*	24.8	33.7*
A521	WRDS	12.6	99	2.8	23.2	0.98	33.9*	1.4	16.5	0.96	21.8*	2.8	23.2	0.98	33.9*	23.2	33.9*
A522	WRDS	10.7	98	3.3	19.1	0.98	32.0*	1.5	16.3	0.72	22.1*	3.2	19.5	0.97	32.0*	19.5	32.0*
A523	WRDS	10.8	95	1.4	20.2	0.96	25.6	1.5	16.3	0.96	22.2*	1.4	20.2	0.96	25.5	20.2	25.6
A524	WRDS	12.6	98	4.1	22.3	0.96	38.4*	1.5	17.0	0.97	22.9*	4.1	22.3	0.96	38.2*	22.3	38.4*
A525	WRDS	12.6	98	3.3	24.5	0.96	37.4*	0.9	18.1	0.95	21.6*	3.3	24.5	0.96	37.4*	24.5	37.4*
A526	WRDS	5.8	93	1.6	18.4	0.74	24.6	1.3	17.3	0.98	22.3*	1.5	19.0	0.77	24.9	19.0	24.9
A527	WRDS	11.8	98	3.1	22.2	0.97	34.3*	1.2	14.3	0.95	18.9	3.1	22.2	0.97	34.3*	22.2	34.3*
A528	WRDS	12.5	98	4.3	20.3	0.76	37.1*	1.3	16.4	0.92	21.6*	4.2	20.4	0.76	37.0*	20.4	37.1*
A529	WRDS	11.1	97	4.1	26.2	0.98	42.2*	2.2	20.4	0.93	29.0*	3.9	26.5	0.99	41.8*	26.5	42.2*
A530	WRDS	10.9	98	2.3	19.9	0.94	28.8	2.2	14.2	0.85	22.9*	2.3	20.1	0.95	29.1	20.1	29.1
A531	WRDS	12.2	98	2.7	17.6	0.93	27.9	1.5	13.6	0.84	19.6	2.6	17.7	0.94	28.1	17.7	28.1
A532	WRDS	11.5	97	5.3	25.4	0.95	46.0*	1.8	15.9	0.86	22.8*	5.3	25.4	0.95	46.0*	25.4	46.0*
A533	WRDS	11.9	100	3.4	23.1	0.93	36.3*	1.0	15.1	0.97	18.9*	3.4	23.1	0.93	36.3*	23.1	36.3*
A534	WRDS	7.8	95	3.8	24.6	0.99	39.4*	1.5	17.5	0.82	23.4*	3.7	24.7	0.99	39.0*	24.7	39.4*
A535	WRDS	10.9	99	2.5	17.2	0.96	26.9	1.1	12.4	0.97	16.9	2.5	17.2	0.96	26.8	17.2	26.9
A536	WRDS	10.9	96	2.7	24.5	0.99	34.9*	1.1	16.5	0.95	20.9*	2.7	24.5	0.99	34.9*	24.5	34.9*
A537	WRDS	11.8	99	3.4	19.7	0.90	33.1*	1.8	17.7	0.95	24.5*	3.1	20.4	0.87	32.4*	20.4	33.1*
A538	WRDS	12.3	98	3.1	21.3	0.91	33.3*	1.5	15.2	0.99	21.2*	3.1	21.3	0.91	33.3*	21.3	33.3*
A539	WRDS	11.2	96	1.8	18.0	0.95	25.1	1.6	14.8	0.95	20.9	1.7	18.2	0.95	24.9	18.2	25.1
A540	WRDS	11.5	97	4.0	19.5	0.97	35.0*	0.7	13.2	0.97	15.8	4.0	19.5	0.97	35.0*	19.5	35.0*
A541	WRDS	11.5	99	4.0	20.3	0.83	35.8*	1.1	15.5	0.98	19.6	4.0	20.3	0.83	35.7*	20.3	35.8*
A542	WRDS	11.7	98	3.2	21.7	0.96	34.3*	1.4	15.5	0.95	21.2*	3.2	21.8	0.96	34.3*	21.8	34.3*
A543	WRDS	11.1	96	2.4	19.0	0.98	28.3*	1.7	18.5	0.99	25.1*	1.8	20.2	0.97	27.3*	20.2	28.3*
A544	WRDS	10.7	92	2.2	20.8	0.93	29.4	1.5	17.4	0.81	23.1*	2.2	21.0	0.94	29.4	21.0	29.4
A545	WRDS	11.5	97	1.4	18.7	0.94	24.1	2.3	16.1	0.92	25.0*	1.6	19.1	0.96	25.4	19.1	25.4
A546	WRDS	6.5	100	3.4	25.0	0.93	38.2*	1.5	17.9	0.94	23.7*	3.3	25.0	0.92	38.1*	25.0	38.2*
A547	WRDS	11.7	97	3.1	20.6	0.94	32.5*	1.8	16.8	0.99	23.7*	2.8	20.9	0.92	31.9*	20.9	32.5*
A548	WRDS	10.7	95	3.4	22.3	0.96	35.5*	1.6	17.2	0.96	23.3*	3.3	22.4	0.95	35.2*	22.4	35.5*
A549	WRDS	10.7	97	2.1	20.4	0.99	28.5*	1.3	17.2	0.93	22.2*	1.9	20.5	0.99	28.1	20.5	28.5
A550	WRDS	10.3	99	1.3	18.6	0.96	23.7	2.2	17.1	0.90	25.5*	1.7	19.2	0.94	25.7	19.2	25.7
A551	WRDS	11.3	98	2.1	18.8	0.96	27.1	1.9	18.0	0.93	25.2*	2.0	19.7	0.94	27.5	19.7	27.5
A552	WRDS	10.0	99	2.8	20.3	0.90	31.2	2.6	16.5	0.95	26.6*	2.7	20.8	0.92	31.4	20.8	31.4
A553	WRDS	7.0	98	3.2	24.0	0.98	36.5*	1.3	17.6	0.98	22.5*	3.1	24.0	0.98	36.3*	24.0	36.5*

* indicates the station is a member of the governing set of stations for a particular distribution (N, S, M or E)

Table C.2 (cont...) - Extreme distribution parameters of Class A INMET ASWS

INMET ID	DATA-SET	t_{tot} (yrs)	Obs. (%)	Non-Synoptic				Synoptic				Mixed Distribution				Envelope	
				a_N	U_N (m/s)	R_N^2	$G_{50,N}$ (m/s)	a_S	U_S (m/s)	R_S^2	$G_{50,S}$ (m/s)	a_M	U_M (m/s)	R_M^2	$G_{50,M}$ (m/s)	U_E (m/s)	$G_{50,E}$ (m/s)
A554	WRDS	11.8	98	2.6	20.1	0.96	30.3	1.5	15.1	0.96	20.9*	2.5	20.2	0.96	30.1	20.2	30.3
A555	WRDS	10.0	100	2.4	21.2	0.98	30.4	1.7	21.7	0.95	28.3*	1.6	22.9	0.93	29.2	22.9	30.4
A556	WRDS	7.8	95	3.1	23.1	0.96	35.0*	1.1	15.6	0.97	20.0*	3.1	23.1	0.96	35.0*	23.1	35.0*
A557	WRDS	6.5	97	3.8	24.3	0.92	39.1*	1.2	13.6	0.87	18.2	3.8	24.3	0.92	39.1*	24.3	39.1*
A560	WRDS	2.3	85	2.1	21.0	0.96	29.0	1.2	17.3	0.96	22.0*	1.8	21.0	0.95	28.1	21.0	29.0
A561	WRDS	3.7	96	2.4	22.2	0.94	31.6	1.0	15.2	0.93	19.2	2.4	22.2	0.94	31.4	22.2	31.6
A601	WRDS	13.8	96	3.3	21.4	0.99	34.1*	1.3	17.1	0.95	22.2*	3.1	21.6	0.99	33.7*	21.6	34.1*
A602	WRDS	14.3	93	3.1	24.2	0.98	36.1*	1.9	21.7	0.96	29.1*	2.6	25.0	0.97	35.2*	25.0	36.1*
A603	WRDS	13.2	93	4.0	21.2	0.95	37.0*	1.0	15.5	0.98	19.2	4.0	21.2	0.95	36.9*	21.2	37.0*
A604	WRDS	8.2	98	2.3	19.4	0.90	28.4	0.6	12.6	0.95	15.1	2.3	19.4	0.90	28.4	19.4	28.4
A606	WRDS	12.0	95	4.1	20.8	0.97	36.9*	1.7	23.1	0.99	29.8*	2.4	24.3	0.96	33.7*	24.3	36.9*
A607	WRDS	11.1	95	4.0	20.8	0.97	36.4*	1.7	20.0	0.86	26.5*	3.4	22.0	0.95	35.4*	22.0	36.4*
A608	WRDS	12.1	95	2.9	19.1	0.96	30.3*	1.3	19.8	0.96	24.8*	1.7	21.1	0.90	27.6	21.1	30.3*
A609	WRDS	11.9	95	4.1	25.4	0.68	41.5*	2.0	17.5	0.93	25.3*	4.1	25.4	0.67	41.4*	25.4	41.5*
A610	WRDS	9.0	84	6.2	24.8	0.95	48.9	2.2	32.9	0.98	41.4	2.7	33.7	0.95	44.3	33.7	48.9
A611	WRDS	11.7	98	3.0	21.1	0.96	32.9	0.9	14.0	0.89	17.6	3.0	21.1	0.96	32.9	21.1	32.9
A612	WRDS	12.5	98	3.2	15.6	0.99	27.9*	1.2	17.0	0.96	21.8	1.9	18.0	0.98	25.4	18.0	27.9*
A613	WRDS	11.2	94	3.5	16.4	0.96	29.9	1.7	18.6	0.97	25.3*	1.9	19.5	0.97	27.0	19.5	29.9
A614	WRDS	11.5	96	2.7	17.4	0.92	28.0	1.4	17.6	0.97	23.2*	2.0	18.9	0.84	26.7	18.9	28.0
A615	WRDS	12.2	98	2.2	19.1	0.94	27.6	2.5	17.3	0.84	27.2*	2.5	19.9	0.93	29.8*	19.9	29.8*
A616	WRDS	11.7	96	2.0	14.0	0.88	21.7	2.0	16.3	0.91	24.1*	2.1	16.8	0.96	25.1	16.8	25.1
A617	WRDS	12.4	98	2.3	19.0	0.95	28.1	1.4	14.0	0.96	19.4	2.3	19.0	0.94	28.0	19.0	28.1
A618	WRDS	8.6	99	3.9	17.1	0.97	32.4*	1.8	16.9	0.89	24.1*	2.8	19.1	0.95	29.8	19.1	32.4*
A619	WRDS	12.1	97	1.9	20.7	0.97	28.3	1.1	15.4	0.94	19.5	1.9	20.7	0.97	28.3	20.7	28.3
A620	WRDS	8.9	99	3.7	15.7	0.89	30.0*	1.1	21.7	0.97	26.1*	1.1	21.8	0.96	26.0	21.8	30.0*
A621	WRDS	11.7	96	4.0	22.2	0.93	37.6*	1.0	17.7	0.95	21.6*	3.9	22.2	0.92	37.5*	22.2	37.6*
A622	WRDS	10.1	92	2.2	21.0	0.93	29.7*	1.7	20.6	0.78	27.0*	1.9	22.1	0.96	29.7*	22.1	29.7*
A623	WRDS	10.5	96	3.4	19.4	0.95	32.8*	1.8	15.4	0.87	22.4*	3.2	19.8	0.96	32.4*	19.8	32.8*
A624	WRDS	8.3	95	2.2	17.8	0.99	26.5	1.1	18.7	0.93	22.8	1.2	19.5	0.94	24.0	19.5	26.5
A652	WRDS	11.9	98	3.6	27.2	0.96	41.2*	2.5	26.1	0.89	36.0*	3.3	28.6	0.98	41.6*	28.6	41.6*
A657	WRDS	7.3	96	2.4	21.5	0.96	30.8	1.0	15.2	0.96	19.3	2.4	21.5	0.96	30.8	21.5	30.8
A659	WRDS	3.7	96	1.9	17.3	0.90	24.8	0.7	14.9	0.92	17.7	1.7	17.5	0.89	24.1	17.5	24.8
A667	WRDS	3.6	97	2.6	20.9	0.94	30.9*	1.6	18.8	0.96	25.0*	2.0	21.5	0.95	29.1	21.5	30.9*
A701	WRDS	12.8	99	2.7	26.2	0.99	36.5*	2.0	20.7	0.89	28.5*	2.6	26.4	0.99	36.4*	26.4	36.5*
A702	WRDS	15.6	97	2.2	24.3	0.96	32.8	1.4	19.7	0.94	25.3*	2.0	24.5	0.97	32.4	24.5	32.8
A703	WRDS	14.3	97	2.9	21.5	0.98	32.8	1.3	19.9	0.95	25.0*	2.3	22.3	0.94	31.4	22.3	32.8
A704	WRDS	14.1	93	2.3	22.3	0.92	31.2	1.3	16.2	0.96	21.1	2.3	22.3	0.92	31.2	22.3	31.2
A705	WRDS	13.4	92	1.7	21.7	0.95	28.2	1.6	17.4	0.96	23.7*	1.6	21.7	0.94	28.1	21.7	28.2
A707	WRDS	14.4	98	3.1	22.5	0.93	34.6*	1.5	18.2	0.97	24.0*	2.9	22.7	0.91	34.2	22.7	34.6*
A708	WRDS	14.9	98	1.9	19.3	0.98	26.9	1.2	16.1	0.98	20.6*	1.8	19.5	0.99	26.7	19.5	26.9
A709	WRDS	12.7	92	3.9	26.1	0.96	41.1*	2.1	21.1	0.98	29.3*	3.6	26.5	0.97	40.4*	26.5	41.1*
A710	WRDS	8.3	88	2.7	23.5	0.90	34.2*	2.2	19.6	0.98	28.2*	2.6	23.8	0.90	34.0*	23.8	34.2*
A711	WRDS	9.9	97	1.8	20.9	0.93	27.9	2.0	18.9	0.89	26.6*	1.9	21.4	0.93	28.8	21.4	28.8
A712	WRDS	10.6	91	2.5	23.3	0.97	32.9*	2.2	18.7	0.91	27.1*	2.3	23.6	0.96	32.7*	23.6	32.9*
A713	WRDS	12.1	98	2.1	23.9	0.99	32.0	2.1	18.3	0.95	26.4*	2.0	24.0	0.99	31.8	24.0	32.0
A714	WRDS	11.6	96	3.9	24.7	0.64	40.0*	1.7	20.3	0.98	26.8*	3.8	24.8	0.62	39.7*	24.8	40.0*
A715	WRDS	11.3	93	1.8	23.5	0.98	30.7	2.1	18.7	0.89	26.9*	1.7	23.7	0.97	30.5	23.7	30.7
A716	WRDS	8.3	91	3.2	25.1	0.94	37.5*	0.9	18.6	0.99	22.3	3.2	25.1	0.94	37.5*	25.1	37.5*
A717	WRDS	8.5	92	2.6	23.4	0.98	33.4*	2.1	19.3	0.93	27.6*	2.4	23.8	0.98	33.2	23.8	33.4*
A718	WRDS	9.6	93	3.4	24.7	0.87	37.9*	1.6	18.6	0.98	25.0*	3.4	24.7	0.87	37.8*	24.7	37.9*
A719	WRDS	11.0	91	2.4	20.8	0.94	30.0	1.0	17.5	0.94	21.3	2.3	20.8	0.94	29.9	20.8	30.0
A720	WRDS	7.0	93	2.6	22.7	0.95	32.7	1.6	17.5	0.93	23.7	2.5	22.8	0.95	32.4	22.8	32.7
A721	WRDS	11.1	94	3.3	23.0	0.97	35.8*	1.8	20.6	0.98	27.7*	3.0	23.6	0.97	35.2*	23.6	35.8*
A722	WRDS	11.2	93	1.9	20.1	0.94	27.7	1.1	16.1	0.96	20.4	1.9	20.1	0.95	27.6	20.1	27.7
A723	WRDS	10.1	96	3.7	22.6	0.95	37.2*	1.6	19.4	0.97	25.7*	3.4	23.0	0.93	36.4*	23.0	37.2*
A724	WRDS	9.3	94	2.1	23.2	0.96	31.5	0.7	21.2	0.90	24.0*	1.8	23.5	0.96	30.6	23.5	31.5
A725	WRDS	9.4	91	2.4	24.9	0.95	34.2	1.7	19.9	0.97	26.4*	2.2	25.0	0.94	33.8	25.0	34.2
A726	WRDS	12.0	96	4.0	25.9	0.92	41.5*	2.3	18.1	0.94	27.0*	4.0	25.9	0.92	41.5*	25.9	41.5*
A727	WRDS	12.0	94	2.3	21.2	0.92	30.2	2.3	17.6	0.97	26.6*	2.2	21.6	0.94	30.2	21.6	30.2
A728	WRDS	11.2	91	3.6	25.1	0.90	39.2*	2.3	15.4	0.68	24.4*	3.5	25.3	0.90	39.0*	25.3	39.2*
A729	WRDS	10.5	97	2.2	25.5	0.95	34.0*	1.9	20.2	0.94	27.5*	2.2	25.5	0.95	34.0*	25.5	34.0*
A730	WRDS	10.1	92	2.5	23.7	0.95	33.3	3.0	20.8	0.96	32.7*	2.3	24.6	0.96	33.4*	24.6	33.4
A731	WRDS	11.7	95	2.4	21.5	0.90	30.9	1.6	19.5	0.99	25.7*	2.1	22.0	0.86	30.4	22.0	30.9
A732	WRDS	7.0	91	3.1	26.8	0.99	39.0*	2.4	21.6	0.89	30.9*	2.9	27.2	0.98	38.6*	27.2	39.0*
A733	WRDS	10.0	94	3.5	25.4	0.92	39.1*	1.4	18.0	0.94	23.4	3.5	25.4	0.92	39.1*	25.4	39.1*
A734	WRDS	9.6	92	3.0	24.9	0.97	36.8*	2.3	18.8	0.96	27.9*	2.9	25.1	0.95	36.4*	25.1	36.8*
A735	WRDS	11.3	97	2.8	23.5	0.88	34.5*	2.3	18.4	0.92	27.5*	2.9	23.7	0.91	34.9*	23.7	34.9*

* indicates the station is a member of the governing set of stations for a particular distribution (N, S, M or E)

Table C.2 (cont...) - Extreme distribution parameters of Class A INMET ASWS

INMET ID	DATA-SET	t_{tot} (yrs)	Obs. (%)	Non-Synoptic				Synoptic				Mixed Distribution				Envelope	
				a_N	U_N (m/s)	R_N^2	$G_{50,N}$ (m/s)	a_S	U_S (m/s)	R_S^2	$G_{50,S}$ (m/s)	a_M	U_M (m/s)	R_M^2	$G_{50,M}$ (m/s)	U_E (m/s)	$G_{50,E}$ (m/s)
A736	WRDS	10.1	93	2.1	22.3	0.98	30.7	2.4	18.0	0.94	27.4*	2.1	22.6	0.98	30.9	22.6	30.9
A737	WRDS	9.7	93	2.6	21.5	0.92	31.7	2.1	17.6	0.96	25.9*	2.4	21.9	0.91	31.3	21.9	31.7
A738	WRDS	11.4	96	2.7	21.4	0.96	31.8	1.2	16.0	0.93	20.9	2.7	21.4	0.96	31.8	21.4	31.8
A739	WRDS	11.2	97	2.6	19.7	0.96	29.7	1.2	14.8	0.98	19.4	2.6	19.7	0.96	29.7	19.7	29.7
A740	WRDS	11.4	98	1.7	24.5	0.96	31.0	1.8	17.3	0.85	24.3*	1.6	24.5	0.95	30.8	24.5	31.0
A741	WRDS	9.4	97	2.5	24.1	0.99	34.0*	2.2	20.8	0.96	29.5*	2.3	24.6	0.98	33.5*	24.6	34.0*
A742	WRDS	8.3	94	2.3	24.1	0.91	33.0	2.3	17.2	0.91	26.4*	2.1	24.2	0.91	32.6	24.2	33.0
A743	WRDS	8.9	98	2.7	25.4	0.79	36.2*	1.4	18.8	0.87	24.4	2.7	25.5	0.78	36.0*	25.5	36.2*
A746	WRDS	8.2	95	1.6	17.7	0.94	24.1	0.9	14.4	0.97	17.9	1.6	17.7	0.94	23.8	17.7	24.1
A747	WRDS	10.9	98	2.6	24.4	0.98	34.4*	1.1	18.2	0.99	22.4*	2.6	24.4	0.98	34.4*	24.4	34.4*
A748	WRDS	8.9	99	2.1	20.1	0.97	28.2	0.9	15.3	0.92	18.9	2.0	20.1	0.97	28.1	20.1	28.2
A749	WRDS	8.1	98	1.6	21.3	0.97	27.4	1.4	18.5	0.93	23.9	1.5	21.5	0.98	27.5	21.5	27.5
A750	WRDS	10.2	94	2.8	24.4	0.92	35.2	2.1	21.0	0.94	29.4*	2.5	24.8	0.89	34.5	24.8	35.2
A751	WRDS	10.4	96	4.3	25.3	0.95	42.0*	2.0	20.5	0.98	28.4*	4.1	25.6	0.94	41.4*	25.6	42.0*
A752	WRDS	5.0	84	3.5	27.7	0.97	41.3*	1.8	21.4	0.86	28.6*	3.1	27.9	0.97	40.2*	27.9	41.3*
A753	WRDS	9.5	97	4.1	23.1	0.87	39.0*	1.8	17.1	0.97	24.2*	4.0	23.2	0.86	38.8*	23.2	39.0*
A754	WRDS	8.6	93	3.8	25.2	0.98	40.1*	2.0	19.6	0.96	27.3*	3.6	25.4	0.97	39.6*	25.4	40.1*
A755	WRDS	6.0	95	1.8	24.0	0.96	31.1	1.4	18.6	0.98	24.0*	1.8	24.0	0.96	31.1	24.0	31.1
A756	WRDS	8.1	96	2.8	24.3	0.98	35.3*	3.3	19.3	0.95	32.2*	2.8	24.8	0.99	35.7*	24.8	35.7*
A757	WRDS	7.6	98	2.5	22.9	0.94	32.8*	2.1	18.8	0.95	26.9*	2.3	23.2	0.93	32.3*	23.2	32.8*
A758	WRDS	7.4	94	2.5	21.9	0.99	31.6	0.9	17.3	0.96	20.9	2.5	21.9	0.99	31.5*	21.9	31.6
A759	WRDS	5.8	94	2.0	24.2	0.96	32.2	1.3	20.7	0.97	25.8*	1.8	24.3	0.97	31.3	24.3	32.2
A760	WRDS	6.5	99	3.5	26.7	0.95	40.3*	1.7	19.5	0.91	26.3*	3.5	26.7	0.94	40.3*	26.7	40.3*
A761	WRDS	6.3	95	3.4	26.5	0.95	39.8*	1.7	20.1	0.88	26.8*	3.3	26.6	0.95	39.6*	26.6	39.8*
A801	WRDS	18.0	96	3.8	23.4	0.88	38.1*	1.1	19.9	0.99	24.3	3.7	23.5	0.86	37.8*	23.5	38.1*
A802	WRDS	13.9	92	3.0	22.6	0.99	34.4	2.6	23.3	0.97	33.5*	2.6	24.9	0.98	34.9	24.9	34.9
A803	WRDS	15.6	96	2.7	23.2	0.98	33.8	2.4	23.7	0.98	32.9*	2.1	25.4	0.95	33.4	25.4	33.8
A804	WRDS	13.2	91	3.3	24.7	0.98	37.5*	1.1	21.4	0.93	25.6	3.1	24.9	0.96	36.9*	24.9	37.5*
A805	WRDS	6.9	93	4.8	29.2	0.94	47.9*	2.0	22.2	0.89	29.9*	4.6	29.3	0.91	47.2*	29.3	47.9*
A806	WRDS	12.4	96	4.6	21.7	0.95	39.8*	1.6	19.0	0.96	25.3	4.0	22.5	0.91	38.3*	22.5	39.8*
A807	WRDS	12.5	91	2.4	21.2	0.94	30.6	1.7	19.1	0.93	25.8*	2.3	21.7	0.97	30.8	21.7	30.8
A808	WRDS	12.3	96	2.9	22.6	0.89	33.8	2.2	22.2	0.98	30.6	2.6	24.0	0.92	34.1	24.0	34.1
A809	WRDS	9.9	95	3.3	25.1	0.93	38.0*	1.4	22.1	0.98	27.5	3.1	25.4	0.91	37.4*	25.4	38.0*
A810	WRDS	11.3	95	4.6	26.1	0.94	44.2*	1.8	18.9	0.98	25.9	4.6	26.1	0.94	44.2*	26.1	44.2*
A811	WRDS	12.1	98	3.5	27.1	0.99	40.6*	2.6	27.9	0.96	38.1*	2.4	29.8	0.99	39.1*	29.8	40.6*
A812	WRDS	12.6	97	3.9	28.1	0.98	43.5*	2.8	24.6	0.96	35.8	3.6	29.1	0.98	43.1*	29.1	43.5*
A813	WRDS	11.0	95	3.0	25.9	0.98	37.8*	1.6	21.0	0.95	27.3*	3.0	26.0	0.98	37.5*	26.0	37.8*
A814	WRDS	8.6	96	4.3	23.5	0.94	40.4*	2.0	16.1	0.85	23.8	4.2	23.7	0.93	40.1*	23.7	40.4*
A815	WRDS	10.9	97	3.8	22.7	0.98	37.6*	2.1	23.4	0.99	31.4*	2.4	25.2	0.98	34.6	25.2	37.6*
A816	WRDS	9.5	95	4.5	29.7	0.98	47.4*	2.9	26.4	0.83	37.6*	4.4	30.7	0.98	47.9*	30.7	47.9*
A817	WRDS	11.4	96	3.2	23.5	0.89	36.2*	1.4	17.9	0.98	23.4*	3.2	23.5	0.89	36.2*	23.5	36.2*
A818	WRDS	11.4	96	2.2	22.5	0.98	31.2	1.7	17.9	0.97	24.5*	2.2	22.5	0.98	30.9	22.5	31.2
A819	WRDS	12.6	97	2.1	22.3	0.98	30.5	2.0	19.5	0.97	27.3*	2.0	22.7	0.98	30.5	22.7	30.5
A820	WRDS	10.6	95	3.6	28.3	0.98	42.5*	2.8	22.6	0.88	33.4*	3.3	28.8	0.98	41.9*	28.8	42.5*
A821	WRDS	11.6	98	2.8	24.3	0.97	35.2*	0.7	20.9	0.91	23.6*	2.7	24.4	0.97	35.0*	24.4	35.2*
A822	WRDS	6.5	93	2.6	24.7	0.99	34.8	1.4	18.7	0.96	24.2	2.5	24.7	0.99	34.6	24.7	34.8
A823	WRDS	6.0	96	2.0	20.6	0.97	28.4	2.2	20.6	0.96	29.0*	1.4	22.0	0.99	27.4	22.0	29.0
A824	WRDS	7.3	91	3.4	26.8	0.93	39.9*	1.4	21.5	0.97	26.8*	3.2	26.9	0.92	39.2*	26.9	39.9*
A825	WRDS	7.9	94	4.3	30.6	0.98	47.3*	1.5	22.0	0.93	28.0*	4.3	30.6	0.98	47.3*	30.6	47.3*
A826	WRDS	12.0	96	2.2	21.7	0.93	30.4	1.6	19.8	0.81	26.1	2.3	22.2	0.93	30.9	22.2	30.9
A827	WRDS	10.7	98	4.9	25.7	0.96	45.0*	2.7	23.2	0.91	33.7*	4.6	26.9	0.96	44.7*	26.9	45.0*
A828	WRDS	10.0	95	1.9	22.6	0.95	30.2	1.6	18.7	0.97	24.7	1.9	22.7	0.94	30.0	22.7	30.2
A829	WRDS	9.5	91	4.0	25.8	0.81	41.3*	2.5	30.3	0.94	40.1*	3.4	31.0	0.90	44.1*	31.0	44.1*
A830	WRDS	8.2	93	3.3	28.1	0.99	41.1*	1.6	21.0	0.97	27.2*	3.3	28.1	0.99	41.1*	28.1	41.1*
A831	WRDS	7.4	93	2.4	27.9	0.99	37.3*	1.9	22.4	0.97	29.9*	2.3	28.0	0.99	36.9*	28.0	37.3*
A832	WRDS	10.8	99	4.4	25.3	0.95	42.3*	1.5	19.7	0.87	25.5	4.3	25.4	0.95	42.1*	25.4	42.3*
A833	WRDS	9.4	92	4.3	26.1	0.96	42.8*	1.5	21.0	0.97	27.0*	3.9	26.5	0.96	41.6*	26.5	42.8*
A834	WRDS	10.0	97	4.4	24.6	0.94	41.9*	2.7	26.0	0.96	36.7*	3.4	27.8	0.94	40.9*	27.8	41.9*
A835	WRDS	11.5	93	1.6	24.6	0.92	31.0	2.4	20.2	0.93	29.7*	1.7	24.9	0.96	31.5	24.9	31.5
A836	WRDS	11.8	97	3.5	25.6	0.98	39.3*	1.8	22.6	0.97	29.7	3.1	26.2	0.97	38.2*	26.2	39.3*
A837	WRDS	10.8	96	3.6	29.6	0.98	43.7*	2.0	24.5	0.98	32.1*	3.5	29.8	0.98	43.4*	29.8	43.7*
A838	WRDS	6.7	95	2.1	21.8	0.96	29.9	1.8	21.1	0.94	28.2	1.6	22.8	0.93	29.2	22.8	29.9
A839	WRDS	12.3	98	3.6	28.6	0.90	42.8*	3.0	24.3	0.96	36.1*	3.2	29.5	0.89	41.9*	29.5	42.8*
A840	WRDS	12.2	97	2.3	26.2	0.95	35.2	2.0	22.6	0.98	30.4*	1.9	26.7	0.95	34.3	26.7	35.2
A841	WRDS	8.7	98	3.2	30.7	0.97	43.2*	1.9	24.8	0.99	32.0*	3.1	30.8	0.96	42.9*	30.8	43.2*
A842	WRDS	11.0	91	2.8	23.8	0.97	34.9	1.3	20.2	0.92	25.3*	2.7	24.0	0.97	34.5	24.0	34.9
A843	WRDS	8.1	96	4.7	30.1	0.93	48.3*	2.1	20.6	0.96	28.9*	4.6	30.1	0.92	48.1*	30.1	48.3*

* indicates the station is a member of the governing set of stations for a particular distribution (N, S, M or E)

Table C.2 (cont...) - Extreme distribution parameters of Class A INMET ASWS

INMET ID	DATA-SET	t_{tot} (yrs)	Obs. (%)	Non-Synoptic				Synoptic				Mixed Distribution				Envelope	
				a_N	U_N (m/s)	R_N^2	$G_{50,N}$ (m/s)	a_S	U_S (m/s)	R_S^2	$G_{50,S}$ (m/s)	a_M	U_M (m/s)	R_M^2	$G_{50,M}$ (m/s)	U_E (m/s)	$G_{50,E}$ (m/s)
A844	WRDS	11.9	98	3.6	28.3	0.95	42.4*	1.7	22.6	0.96	29.4*	3.5	28.4	0.95	42.1*	28.4	42.4*
A845	WRDS	10.7	94	5.3	30.4	0.92	51.1	4.1	42.5	0.96	58.6	4.0	42.6	0.95	58.4	42.6	58.6
A846	WRDS	8.2	94	2.3	26.8	0.97	35.9	1.7	21.9	0.99	28.4*	2.2	26.9	0.96	35.3	26.9	35.9
A847	WRDS	9.0	92	4.7	24.2	0.75	42.5*	1.8	19.2	0.97	26.2*	4.5	24.5	0.73	42.1*	24.5	42.5*
A848	WRDS	9.9	94	3.1	24.5	0.91	36.6	2.0	21.3	0.98	29.0*	2.9	25.0	0.90	36.1	25.0	36.6
A849	WRDS	6.4	94	3.3	25.2	0.95	37.9*	2.7	20.8	0.93	31.4*	3.1	25.8	0.98	38.0*	25.8	38.0*
A850	WRDS	9.5	95	3.5	26.4	0.91	39.9*	1.1	19.5	0.97	23.9	3.5	26.4	0.91	39.9*	26.4	39.9*
A851	WRDS	8.1	94	1.9	19.4	0.98	26.8	1.4	14.8	0.85	20.3	1.8	19.5	0.98	26.7	19.5	26.8
A852	WRDS	10.9	93	1.9	26.9	0.94	34.3	1.6	21.7	0.95	28.0*	1.8	27.0	0.95	34.0	27.0	34.3
A853	WRDS	7.7	97	3.3	28.4	0.95	41.1*	1.4	21.9	0.97	27.2*	3.2	28.4	0.95	41.0*	28.4	41.1*
A854	WRDS	7.1	97	3.4	24.7	0.96	38.0	1.6	19.5	0.99	25.8	3.1	24.8	0.93	37.0	24.8	38.0
A855	WRDS	9.5	92	3.5	26.4	0.95	40.1*	2.8	21.0	0.96	32.1*	3.4	26.7	0.97	40.1*	26.7	40.1*
A856	WRDS	9.7	95	2.3	24.5	0.95	33.5	1.7	21.1	0.98	27.8*	2.2	24.7	0.95	33.2	24.7	33.5
A857	WRDS	10.8	96	3.6	26.1	0.94	40.3*	2.1	22.8	0.92	30.9*	3.2	26.8	0.94	39.1*	26.8	40.3*
A858	WRDS	8.5	98	3.6	26.3	0.96	40.2*	1.5	26.5	0.91	32.5*	2.4	28.3	0.96	37.7*	28.3	40.2*
A859	WRDS	8.0	98	2.7	23.8	0.97	34.4	1.2	20.0	0.97	24.7	2.5	24.0	0.95	33.8	24.0	34.4
A860	WRDS	11.0	98	5.1	27.0	0.87	46.9*	1.1	19.8	0.88	24.1	5.1	27.0	0.87	46.9*	27.0	46.9*
A861	WRDS	7.9	90	3.0	24.3	0.94	35.9	1.1	16.7	0.97	21.1	3.0	24.3	0.94	35.9	24.3	35.9
A862	WRDS	6.5	95	3.6	26.9	0.96	41.0*	1.2	21.1	0.95	25.7*	3.5	27.0	0.94	40.5*	27.0	41.0*
A863	WRDS	7.8	95	3.7	24.9	0.96	39.5*	1.7	15.3	0.94	22.1	3.7	24.9	0.96	39.5*	24.9	39.5*
A864	WRDS	9.0	99	2.9	24.7	0.93	35.9*	1.6	20.2	0.96	26.4*	2.8	24.8	0.92	35.6*	24.8	35.9*
A865	WRDS	4.3	95	1.5	24.2	0.90	30.2	1.4	19.4	0.95	24.7	1.4	24.2	0.92	29.7	24.2	30.2
A866	WRDS	8.2	95	3.5	27.7	0.96	41.3*	1.2	29.1	0.96	33.6*	2.0	30.2	0.91	38.2*	30.2	41.3*
A867	WRDS	9.6	94	3.0	24.1	0.98	35.8*	3.1	20.4	0.79	32.3*	3.2	24.9	0.96	37.3*	24.9	37.3*
A868	WRDS	8.9	99	3.7	20.6	0.79	35.2*	1.7	17.7	0.94	24.2	3.4	21.0	0.75	34.5*	21.0	35.2*
A869	WRDS	6.8	92	3.1	25.3	0.98	37.5	2.0	19.4	0.91	27.1*	2.8	25.5	0.96	36.5	25.5	37.5
A871	WRDS	7.0	96	2.5	23.0	0.96	32.7	1.2	17.0	0.93	21.5	2.4	23.0	0.96	32.5	23.0	32.7
A872	WRDS	7.6	93	2.6	25.0	0.97	35.2*	2.0	22.1	0.92	29.9*	2.5	25.5	0.95	35.1*	25.5	35.2*
A873	WRDS	7.5	96	3.3	26.2	0.97	39.0*	1.7	18.2	0.96	24.7*	3.2	26.2	0.96	38.9*	26.2	39.0*
A874	WRDS	7.8	97	1.8	19.5	0.97	26.5	0.8	14.7	0.97	17.7	1.8	19.5	0.97	26.5	19.5	26.5
A875	WRDS	10.7	96	2.2	21.1	0.93	29.7	1.1	17.9	0.95	22.0	2.0	21.3	0.95	29.2	21.3	29.7
A876	WRDS	6.7	96	1.6	23.5	0.98	29.9	1.3	21.3	0.96	26.3	1.3	23.8	0.98	29.0	23.8	29.9
A878	WRDS	9.9	92	4.4	27.5	0.96	44.8*	2.3	25.9	0.96	34.8*	3.8	28.9	0.95	43.6*	28.9	44.8*
A879	WRDS	10.0	96	4.4	23.0	0.98	40.3*	2.2	21.8	0.91	30.2*	3.4	24.7	0.95	37.8*	24.7	40.3*
A880	WRDS	5.8	95	3.2	23.3	0.95	35.9	1.2	21.8	0.95	26.6	2.3	24.4	0.90	33.3	24.4	35.9
A881	WRDS	8.3	93	1.9	26.7	0.96	34.3	1.4	21.7	0.95	26.9	1.9	26.7	0.96	34.3	26.7	34.3
A882	WRDS	6.5	97	3.3	27.6	0.93	40.3*	1.5	20.5	0.96	26.3	3.2	27.6	0.92	40.2*	27.6	40.3*
A883	WRDS	6.2	96	3.3	23.8	0.90	36.5	0.9	19.7	0.93	23.3	3.0	24.0	0.87	35.7	24.0	36.5
A884	WRDS	5.5	98	2.6	25.4	0.95	35.4	1.6	17.8	0.92	24.0	2.5	25.4	0.94	35.3	25.4	35.4
A899	WRDS	9.7	96	3.2	27.5	0.99	39.9*	2.1	27.4	0.95	35.6*	2.2	29.3	0.96	37.9*	29.3	39.9*
A901	WRDS	13.4	91	1.9	19.5	0.92	26.7	1.6	16.3	0.85	22.4*	1.8	19.7	0.94	26.8	19.7	26.8
A902	WRDS	12.4	92	4.9	25.7	0.94	44.7*	1.7	17.8	0.96	24.5*	4.8	25.7	0.93	44.6*	25.7	44.7*
A903	WRDS	12.4	85	1.8	18.9	0.97	26.0	1.1	14.6	0.97	18.8	1.8	18.9	0.97	26.0	18.9	26.0
A904	WRDS	7.6	90	2.1	20.7	0.81	28.9	1.0	16.2	0.98	20.1*	2.1	20.8	0.80	28.8	20.8	28.9
A905	WRDS	10.4	93	3.1	20.1	0.95	32.3	2.0	18.2	0.90	26.0*	2.8	20.9	0.93	32.0	20.9	32.3
A906	WRDS	7.2	95	2.5	21.0	0.97	30.6*	1.2	15.1	0.98	19.8*	2.5	21.0	0.97	30.6*	21.0	30.6*
A907	WRDS	14.3	95	3.5	24.3	0.99	37.8*	1.8	16.9	0.94	23.8*	3.4	24.4	0.99	37.6*	24.4	37.8*
A908	WRDS	11.5	95	4.0	24.3	0.96	39.9*	1.0	16.6	0.98	20.6*	4.0	24.3	0.96	39.9*	24.3	39.9*
A909	WRDS	6.1	85	2.9	23.0	0.96	34.2	1.5	17.9	0.94	23.6	2.8	23.1	0.97	33.9	23.1	34.2
A910	WRDS	8.2	90	2.8	21.0	0.97	32.0*	1.8	14.3	0.78	21.2*	2.8	21.1	0.98	32.0*	21.1	32.0*
A912	WRDS	10.6	91	2.6	23.1	0.93	33.5	1.2	18.8	0.98	23.7*	2.6	23.2	0.93	33.3	23.2	33.5
A913	WRDS	11.1	95	4.0	22.9	0.99	38.7*	1.3	17.3	0.98	22.5*	4.0	23.0	0.99	38.5*	23.0	38.7*
A914	WRDS	9.8	92	1.8	19.4	0.97	26.4	1.7	14.9	0.88	21.5*	1.8	19.5	0.98	26.4	19.5	26.4
A915	WRDS	7.8	86	2.9	23.9	0.95	35.1*	1.6	17.1	0.90	23.2*	2.8	24.0	0.94	34.8*	24.0	35.1*
A916	WRDS	8.6	89	1.9	21.3	0.98	28.6	1.4	16.3	0.97	21.6*	1.9	21.3	0.98	28.6	21.3	28.6
A917	WRDS	9.1	88	2.1	20.8	0.98	28.9	1.8	16.2	0.80	23.0*	2.0	21.0	0.97	28.8	21.0	28.9
A918	WRDS	8.2	93	2.8	22.8	0.97	33.8*	1.2	15.6	0.99	20.3*	2.8	22.8	0.97	33.8*	22.8	33.8*
A919	WRDS	10.8	93	1.6	17.1	0.97	23.3	1.2	13.5	0.96	18.1*	1.5	17.1	0.97	23.2	17.1	23.3
A920	WRDS	8.3	89	2.0	20.3	0.94	28.1	1.2	14.0	0.95	18.6	2.0	20.3	0.94	28.1	20.3	28.1
A921	WRDS	8.1	90	2.5	21.3	0.98	31.2	0.9	15.4	0.95	18.9*	2.5	21.3	0.98	31.2	21.3	31.2
A922	WRDS	6.7	94	2.2	21.0	0.94	29.7	1.0	16.3	0.97	20.3*	2.2	21.0	0.93	29.6	21.0	29.7
A924	WRDS	7.9	87	1.7	19.4	0.93	26.2	1.0	13.8	0.97	17.9*	1.7	19.4	0.93	26.2	19.4	26.2
A925	WRDS	4.3	83	2.0	21.0	0.96	28.8	0.9	14.3	0.91	17.7*	2.0	21.0	0.96	28.8	21.0	28.8
A926	WRDS	8.4	96	2.8	22.4	0.89	33.5*	1.2	15.2	0.88	19.8*	2.8	22.4	0.89	33.5*	22.4	33.5*
A927	WRDS	6.6	95	3.0	21.9	0.77	33.8*	1.1	17.4	0.91	21.8*	2.9	22.1	0.75	33.6*	22.1	33.8*
A928	WRDS	7.8	97	2.9	21.4	0.90	32.9*	1.1	15.2	0.96	19.3*	2.9	21.4	0.90	32.9*	21.4	32.9*
A929	WRDS	8.8	87	3.2	24.6	0.96	36.9*	1.1	17.7	0.99	21.9*	3.2	24.6	0.96	36.9*	24.6	36.9*

* indicates the station is a member of the governing set of stations for a particular distribution (N, S, M or E)

Table C.2 (cont...) - Extreme distribution parameters of Class A INMET ASWS

INMET ID	DATA-SET	t_{tot} (yrs)	Obs. (%)	Non-Synoptic				Synoptic				Mixed Distribution				Envelope	
				a_N	U_N (m/s)	R_N^2	$G_{50,N}$ (m/s)	a_S	U_S (m/s)	R_S^2	$G_{50,S}$ (m/s)	a_M	U_M (m/s)	R_M^2	$G_{50,M}$ (m/s)	U_E (m/s)	$G_{50,E}$ (m/s)
A930	WRDS	8.5	94	2.7	21.4	0.95	31.8	1.3	14.8	0.97	19.7*	2.7	21.4	0.95	31.8	21.4	31.8
A931	WRDS	10.1	95	4.4	24.6	0.98	41.6*	1.2	18.7	0.96	23.5*	4.3	24.7	0.98	41.4*	24.7	41.6*
A932	WRDS	7.2	98	2.6	22.6	0.94	32.7	1.2	16.5	0.97	21.2	2.6	22.6	0.94	32.7	22.6	32.7
A933	WRDS	3.6	90	3.0	26.0	0.94	37.7*	1.9	21.9	0.96	29.4*	2.4	26.2	0.92	35.7*	26.2	37.7*
A934	WRDS	8.5	96	3.4	24.9	0.95	38.1*	1.8	19.0	0.88	26.2*	3.3	25.1	0.95	37.8*	25.1	38.1*
A935	WRDS	8.9	87	1.6	20.7	0.93	26.8	1.3	14.3	0.98	19.5	1.6	20.7	0.93	26.8	20.7	26.8
A936	WRDS	10.5	96	2.5	20.5	0.98	30.3	0.9	15.7	0.97	19.2*	2.5	20.5	0.98	30.3	20.5	30.3
A937	WRDS	9.3	97	3.2	22.1	0.96	34.6*	1.2	16.4	0.97	21.0*	3.2	22.1	0.96	34.5*	22.1	34.6*
A938	WRDS	9.7	94	4.4	20.8	0.96	38.2*	1.1	14.9	0.88	19.1*	4.4	20.9	0.96	38.0*	20.9	38.2*
A939	WRDS	10.2	94	4.2	23.6	0.96	39.9*	1.2	15.1	0.93	19.6*	4.2	23.6	0.96	39.9*	23.6	39.9*
A940	WRDS	7.8	93	2.8	21.3	0.85	32.3*	0.9	14.2	0.93	17.8*	2.8	21.3	0.85	32.3*	21.3	32.3*
A941	WRDS	6.4	91	1.9	20.2	0.99	27.5	0.6	14.5	0.93	16.7	1.9	20.2	0.99	27.5	20.2	27.5
F501	WRDS	5.3	98	3.2	25.3	0.94	37.8	1.4	25.2	0.94	30.6	1.9	26.9	0.82	34.2	26.9	37.8
U565	WRDS	3.9	96	3.2	22.4	0.93	35.1	2.1	23.5	0.94	31.8	2.4	24.9	0.93	34.1	24.9	35.1

* indicates the station is a member of the governing set of stations for a particular distribution (N, S, M or E)

APPENDIX D

EVENT CLASSIFICATION ALGORITHMS AND EXAMPLES

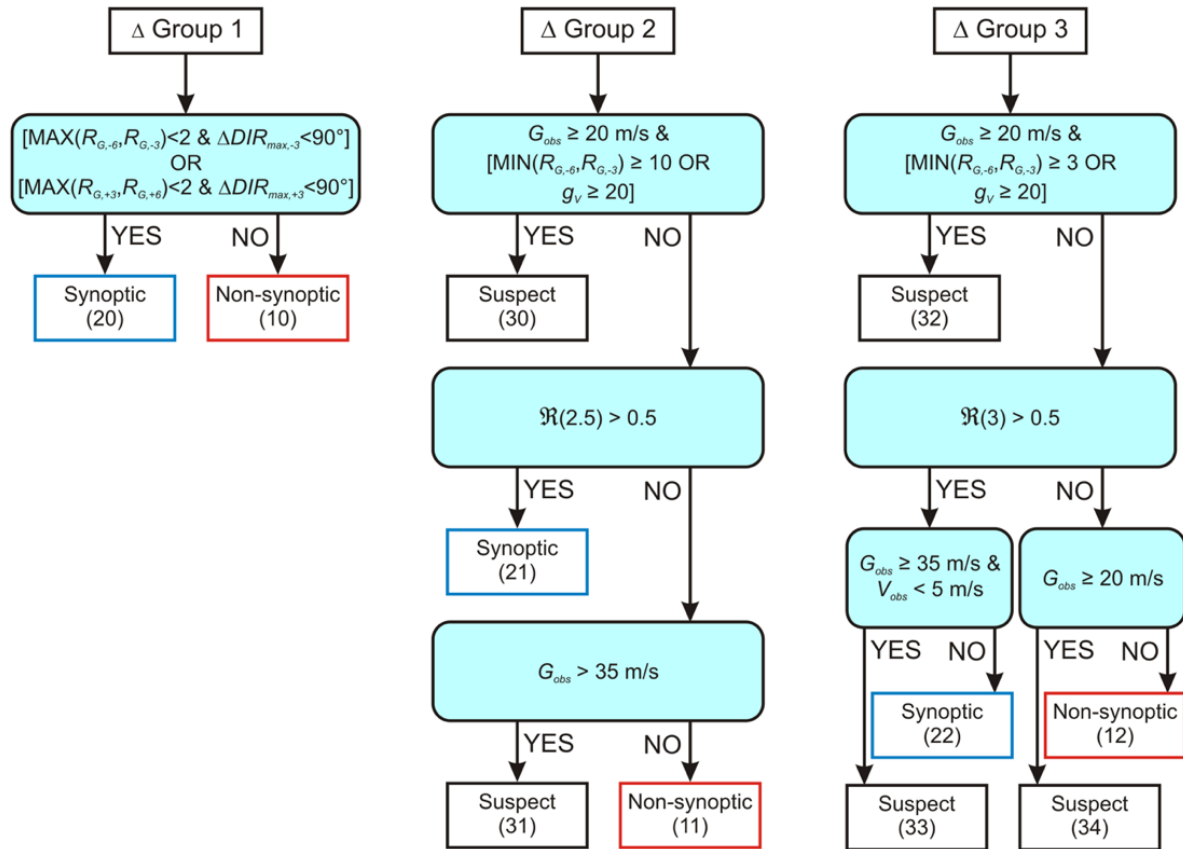


Figure D.1 – Extreme wind type classifying algorithm for INMET ASWS.

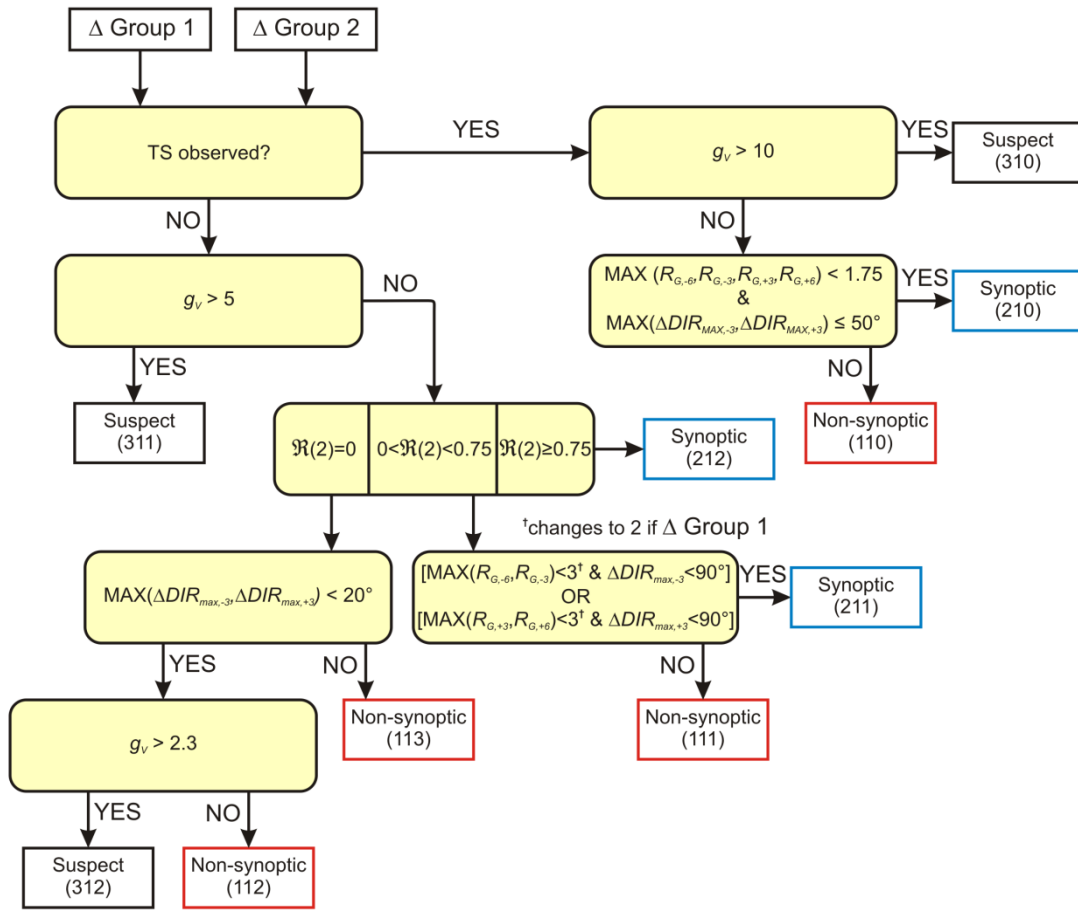


Figure D.2 – Extreme wind type classifying algorithm for aerodrome SWS with G_{obs} peak gust speed ($\Delta Groups$ 1 & 2 only).

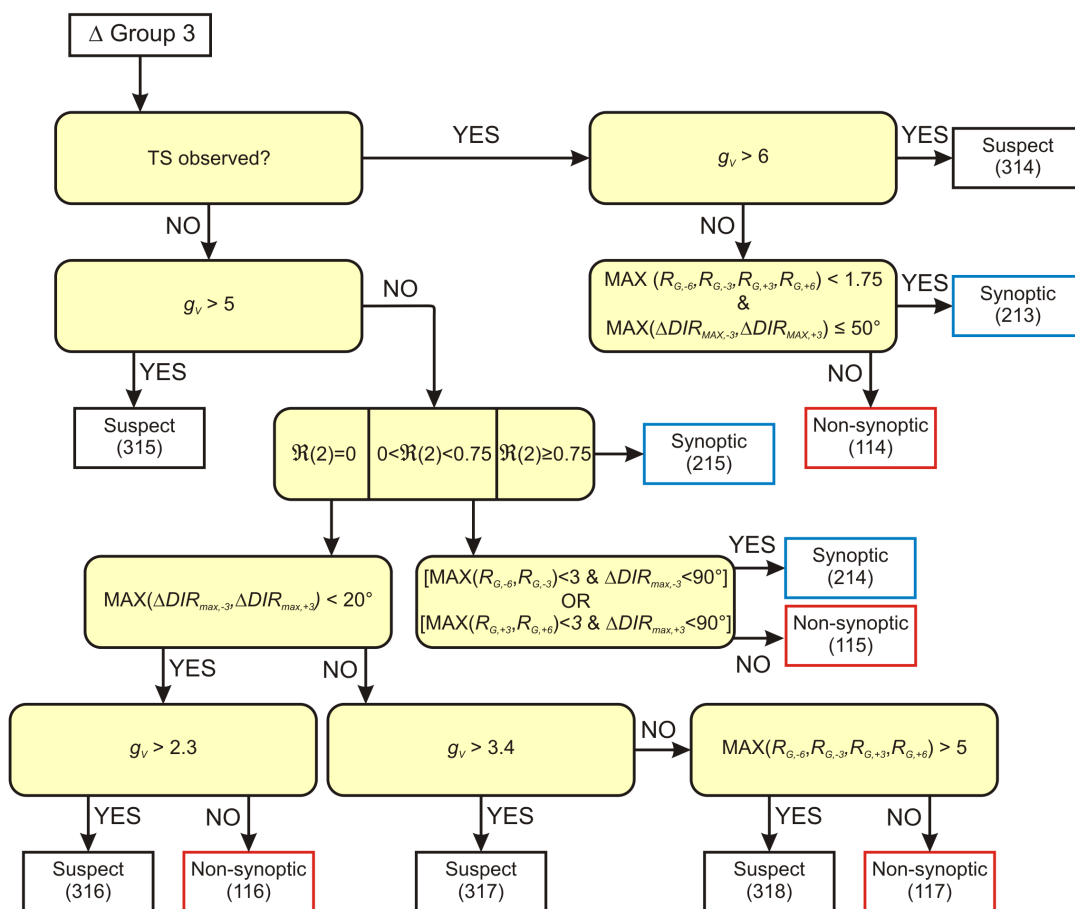


Figure D.3 – Extreme wind type classifying algorithm for aerodrome SWS with G_{obs} peak gust speed ($\Delta Group$ 3).

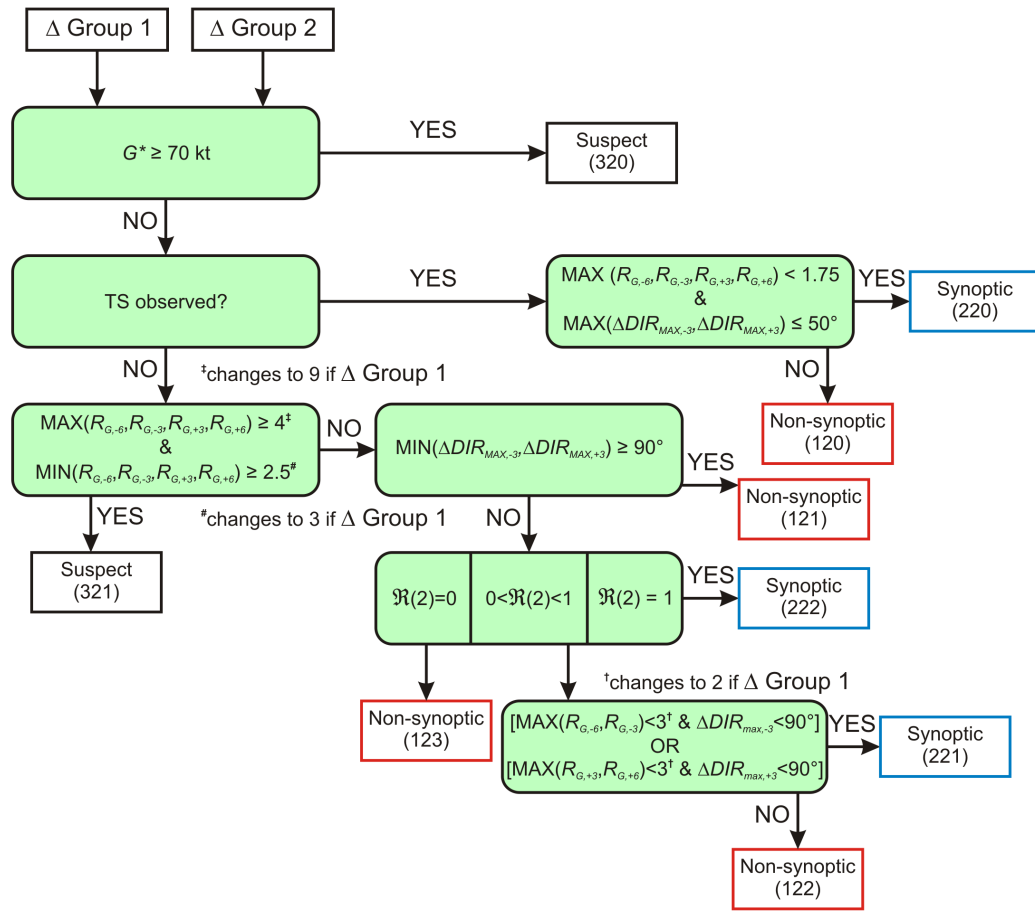


Figure D.4 – Extreme wind type classifying algorithm for aerodrome SWS with G^* (i.e. no G_{obs}) peak gust speed ($\Delta Groups$ 1 & 2 only).

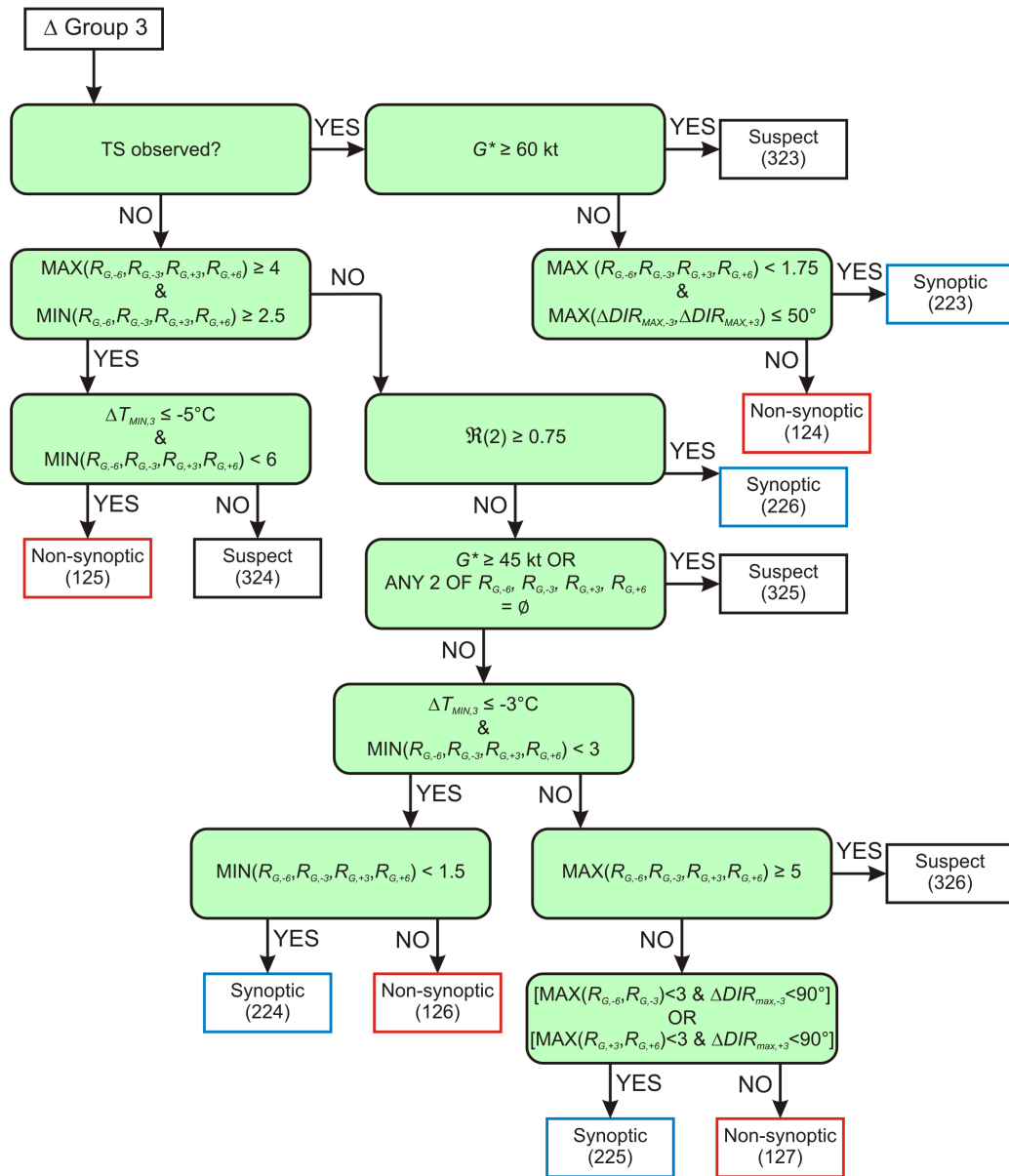


Figure D.5 – Extreme wind type classifying algorithm for aerodrome SWS with G^* (i.e. no G_{obs}) peak gust speed (Δ Group 3 only).

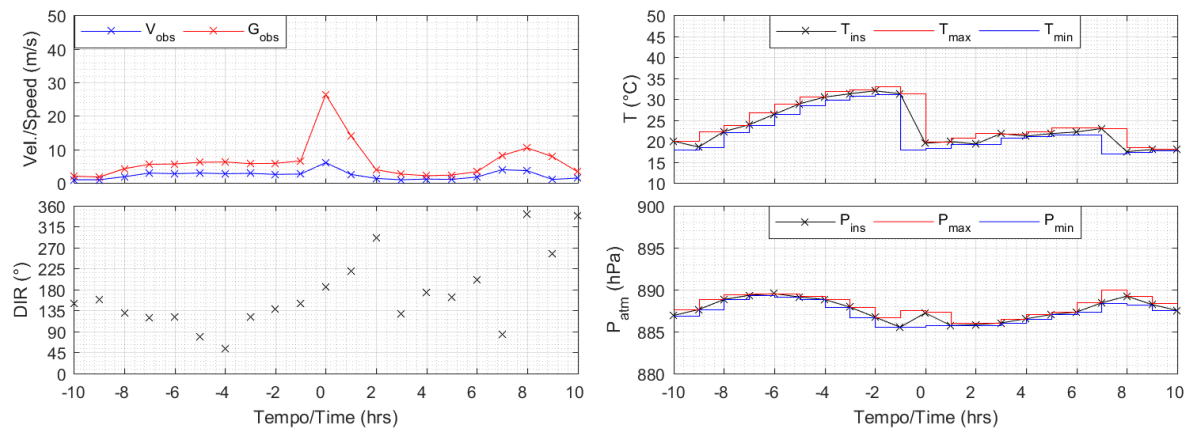


Figure D.6 – Manually classified as non-synoptic. Peak $G_{obs} = 26.4$ m/s at A001 – Brasília, DF, 01/10/2014, 18:00 UTC.

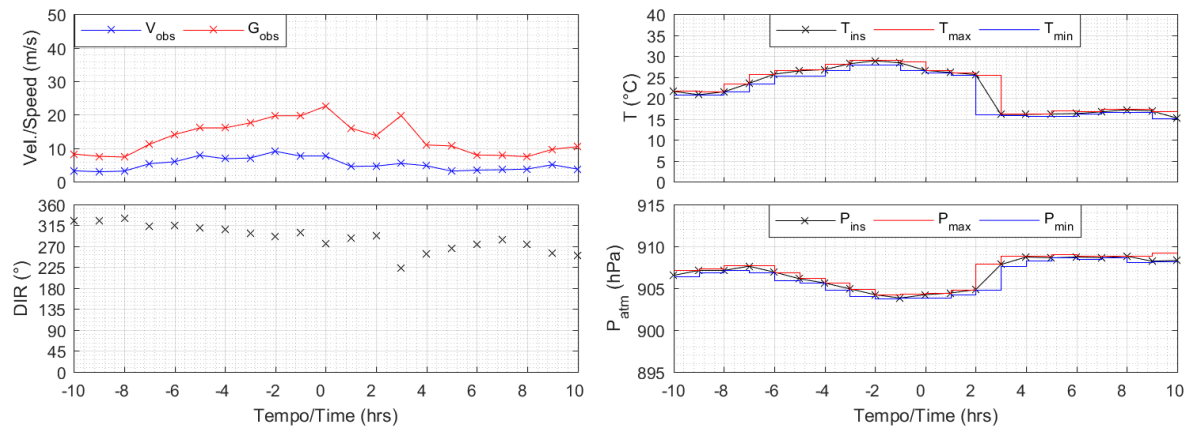


Figure D.7 – Manually classified as synoptic. Peak $G_{obs} = 22.6$ m/s at A807 – Curitiba, PR, 13/09/2016, 18:00 UTC.

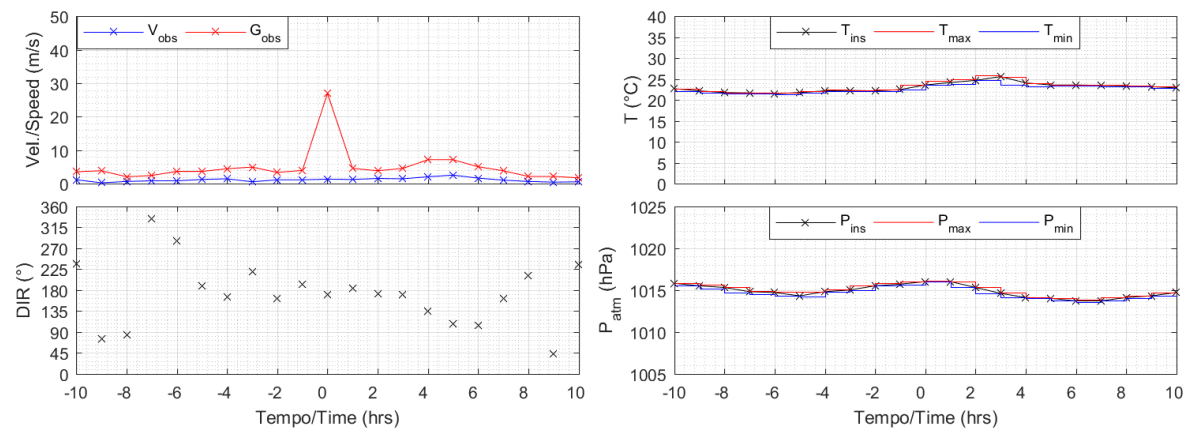


Figure D.8 – Manually classified as suspect. Peak $G_{obs} = 27.0$ m/s at A301 – Recife, PE, 06/07/2009, 12:00 UTC.

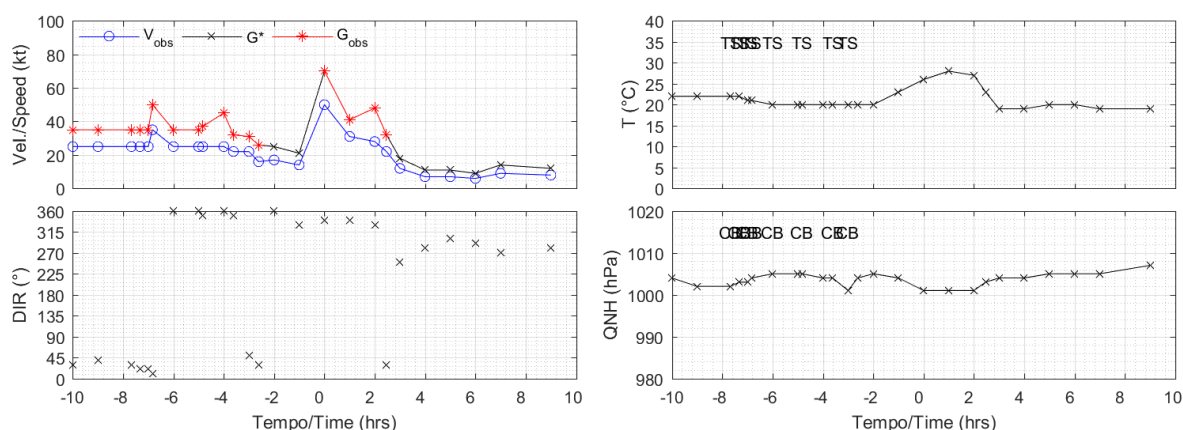


Figure D.9 – Manually classified as non-synoptic. Peak $G_{obs} = 70$ kt (36.0 m/s) at SULS – Punta del Este, Uruguay, 02/03/2013, 16:00 UTC.

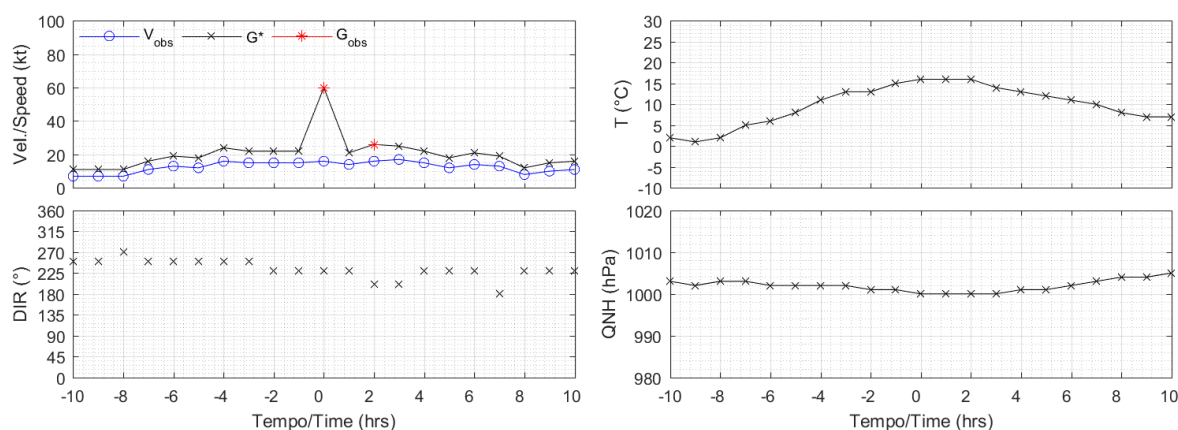


Figure D.10 – Manually classified as suspect. Peak $G_{obs} = 60$ kt (30.9 m/s) at SAWG – Río Gallegos, Argentina, 19/02/2012, 18:00 UTC.

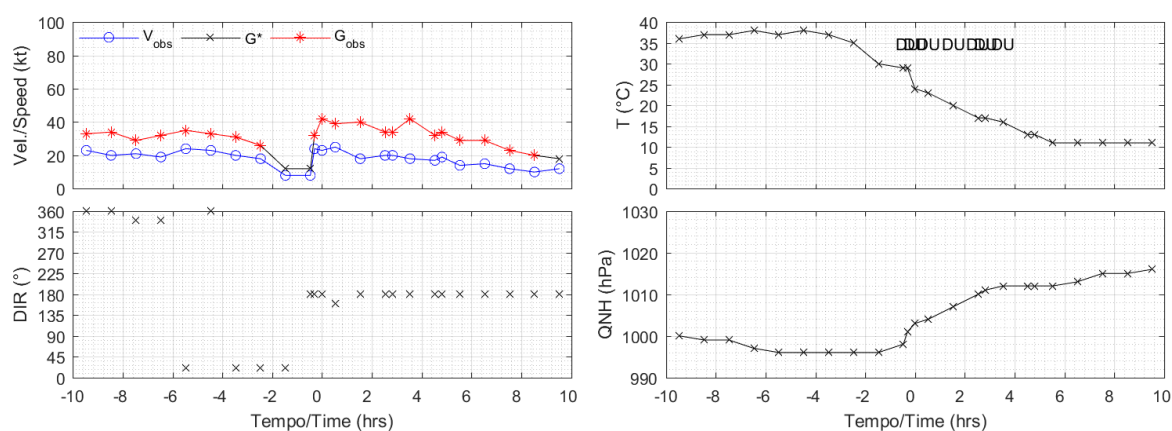


Figure D.11 – Manually classified as synoptic. Peak $G_{obs} = 42$ kt (21.6 m/s) at SACO – Córdoba, Argentina, 08/11/2010, 00:28 UTC.

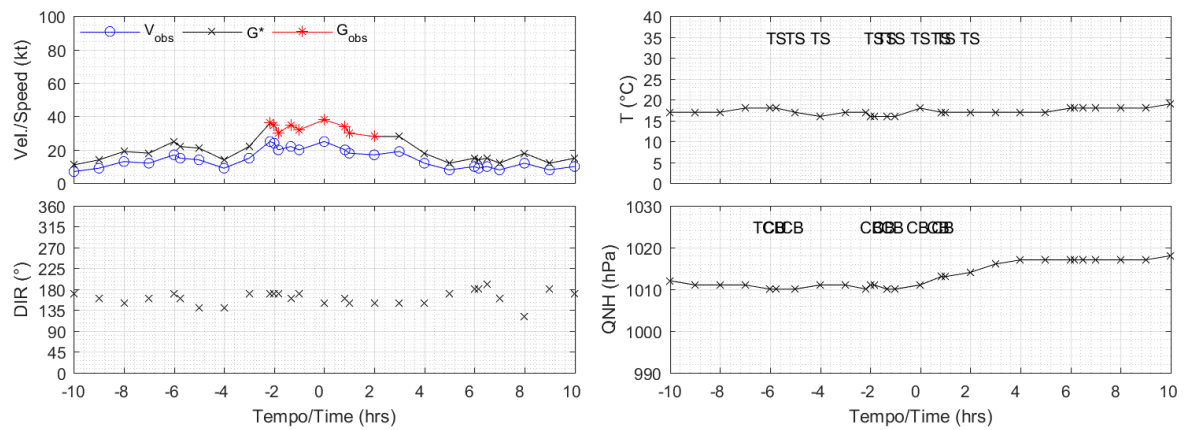


Figure D.12 – Manually classified as synoptic. Peak G_{obs} = 38 kt (19.5 m/s) at SBPA – Porto Alegre, RS, 03/05/2008, 09:00 UTC.

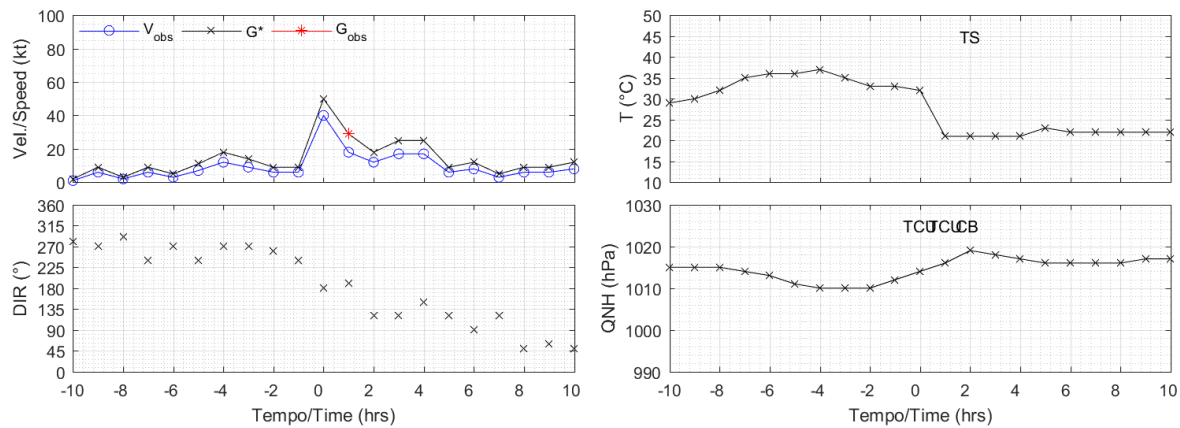


Figure D.13 – Manually classified as non-synoptic. Peak G^* = 50 kt (25.7 m/s) at SBSR – São José do Rio Preto, SP, 22/10/2015, 22:00 UTC.

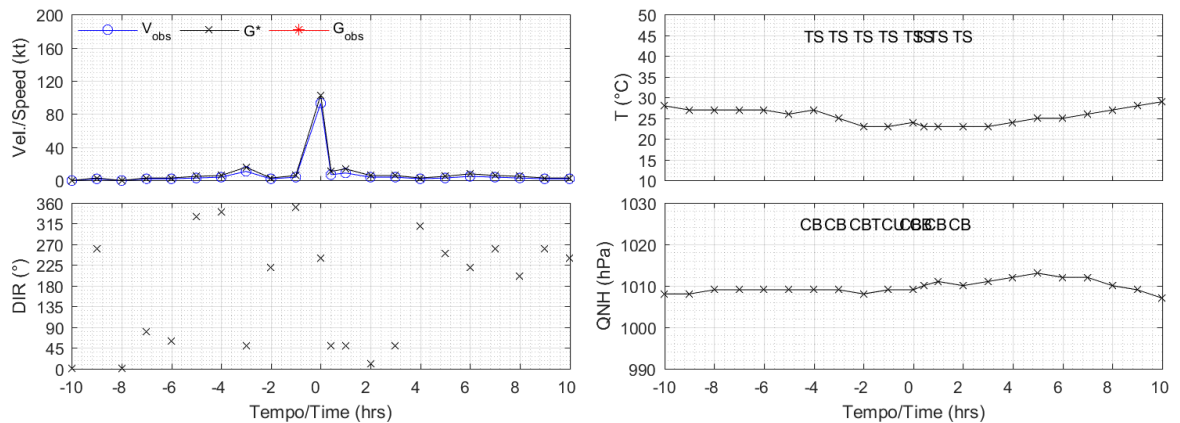


Figure D.14 – Manually classified as suspect. Peak G^* = 103 kt (53.0 m/s) at SBEG – Manaus, AM, 26/11/2015, 09:00 UTC.

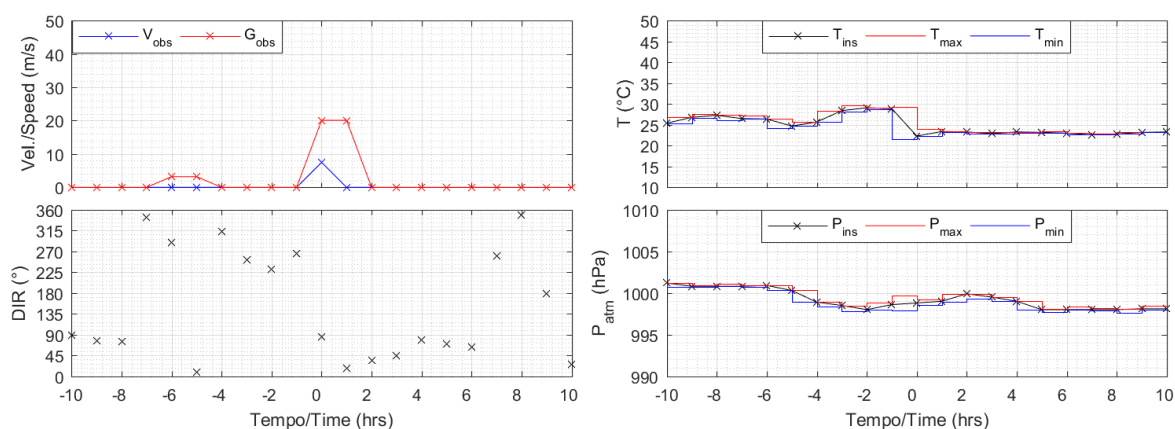


Figure D.15 – F&N event classified as suspect by INMET algorithm. Peak $G_{obs} = 20.1$ m/s at A830 – São Borja, RS, 03/02/2015, 22:00 UTC.

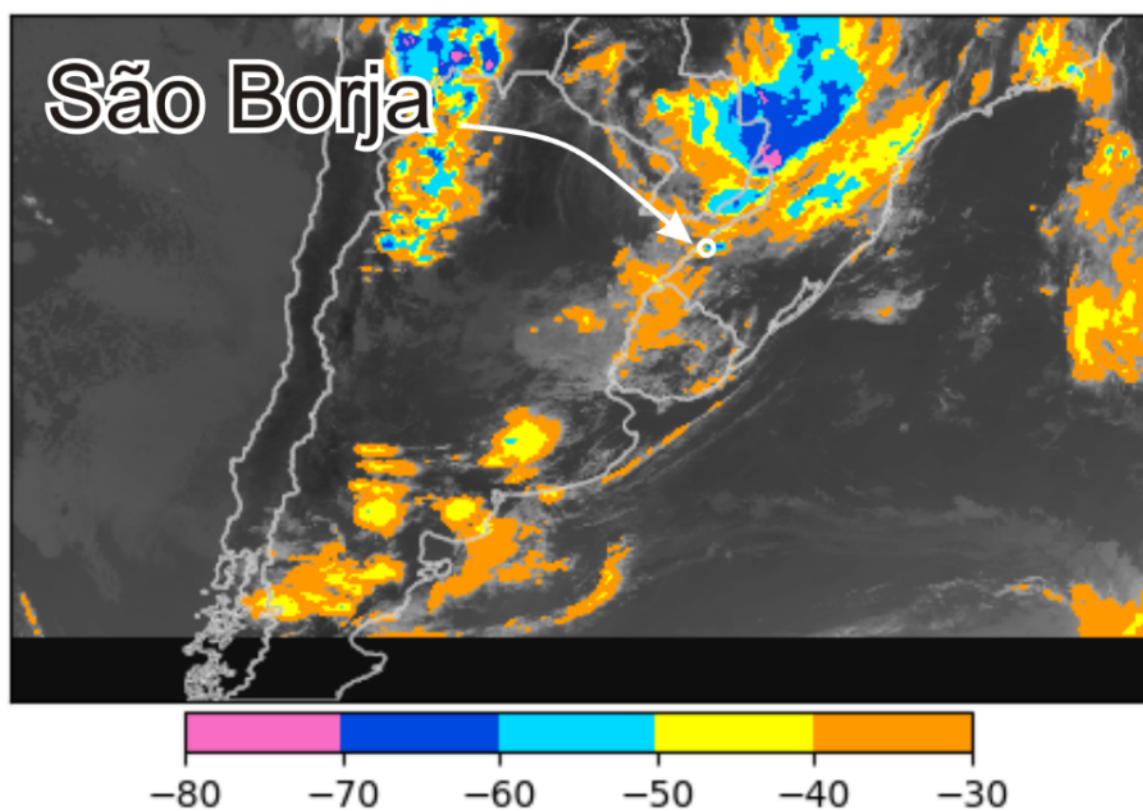


Figure D.16 – Infrared channel of GOES 12 satellite enhanced with brightness temperature data, T_B (°C), 03/02/2015, 22:08 UTC.

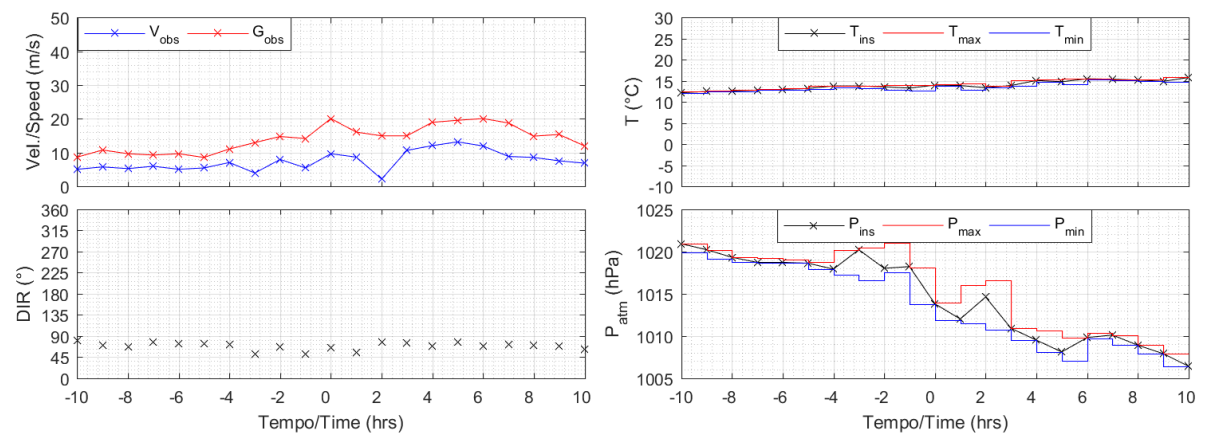


Figure D.17 – F&N event classified as synoptic by INMET algorithm. Peak $G_{obs} = 20.1$ m/s at A802 – Rio Grande, RS, 27/08/2011, 15:00 UTC.

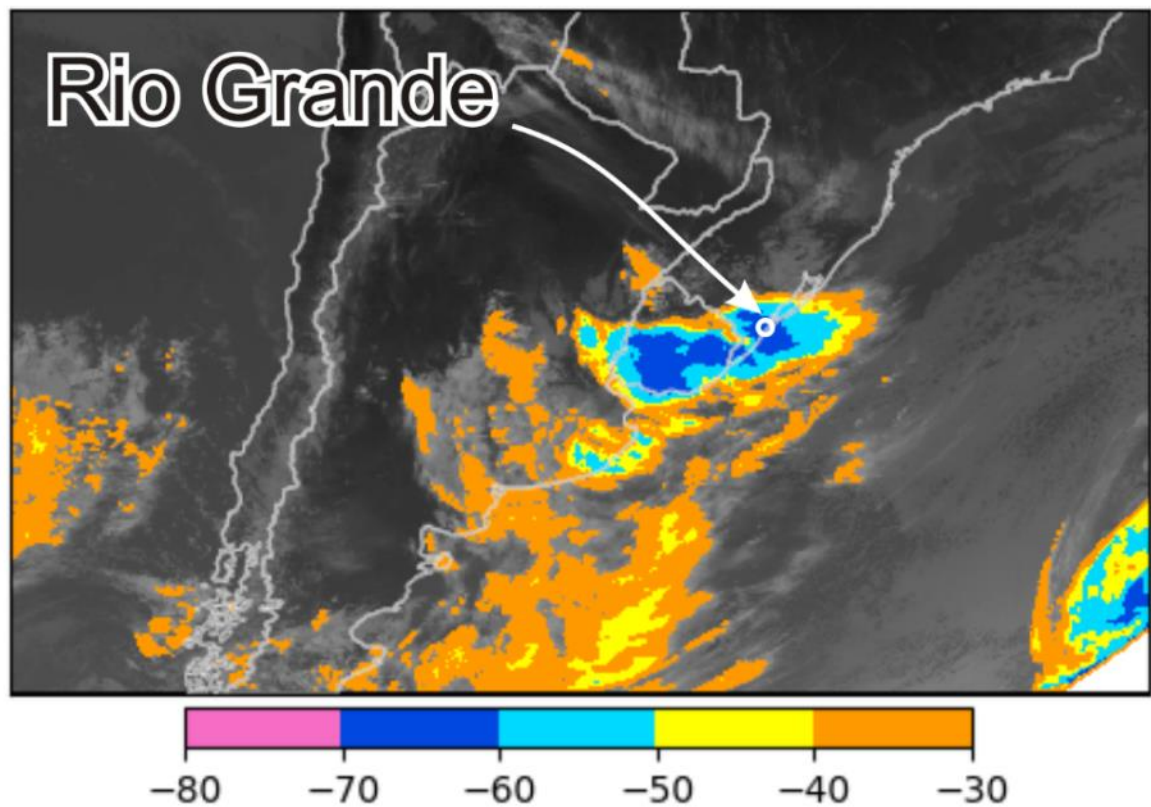


Figure D.18 – Infrared channel of GOES 13 satellite enhanced with brightness temperature data, T_B (°C), 27/08/2011, 14:45 UTC.

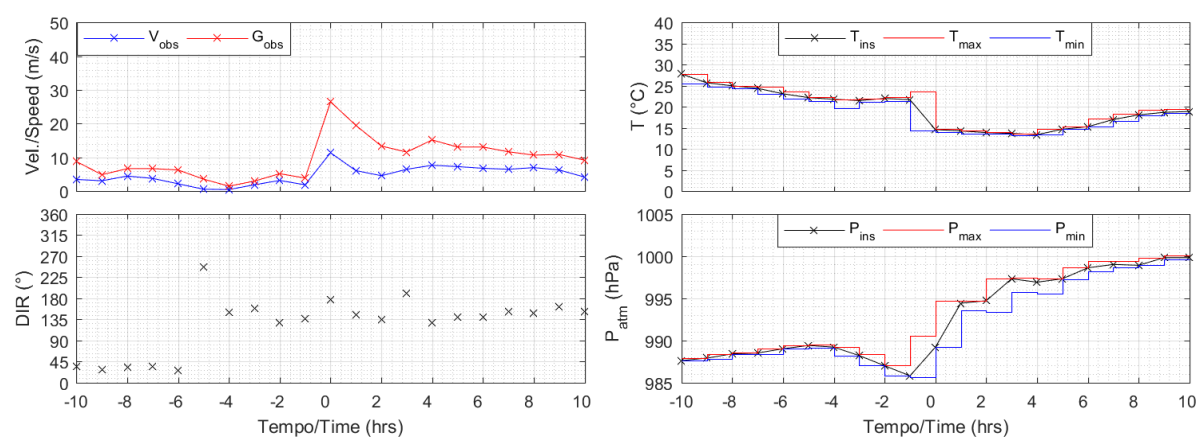


Figure D.19 – F&N event classified as synoptic by INMET algorithm. Peak $G_{obs} = 26.5$ m/s at A831 – Quaraí, RS, 24/10/2009, 08:00 UTC.

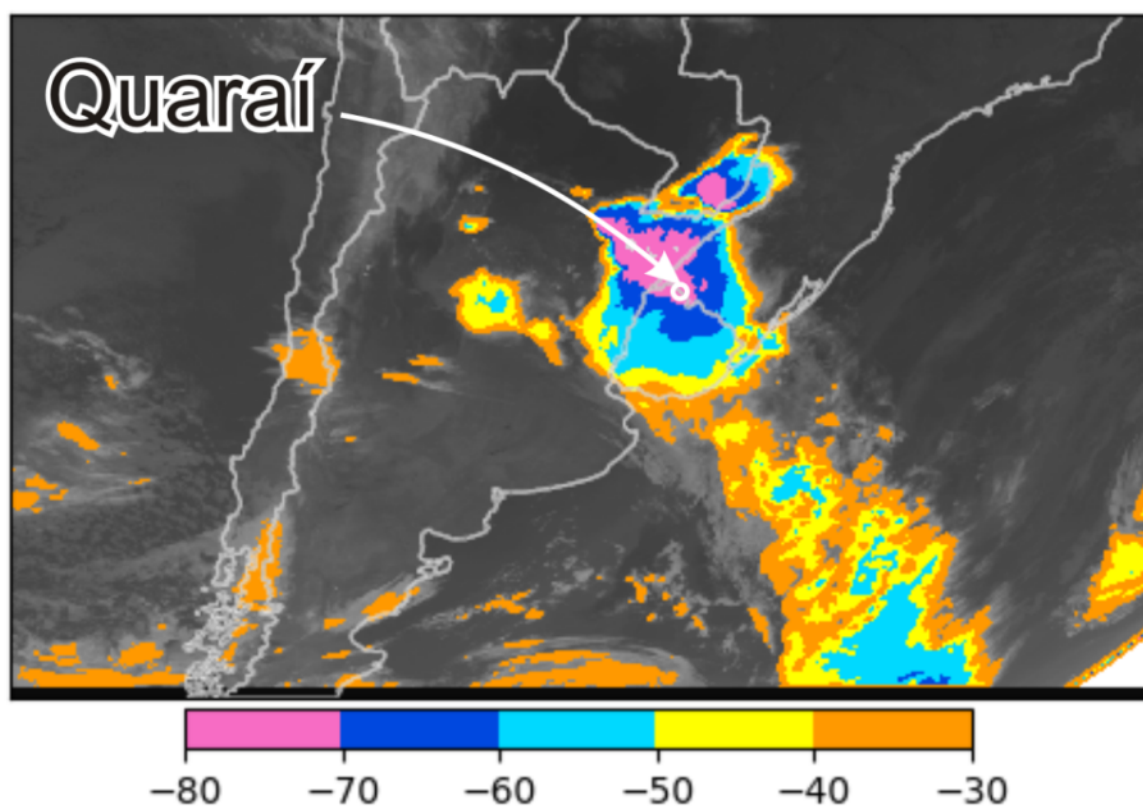


Figure D.20 – Infrared channel of GOES 12 satellite enhanced with brightness temperature data, T_B (°C), 24/10/2009, 08:09 UTC.

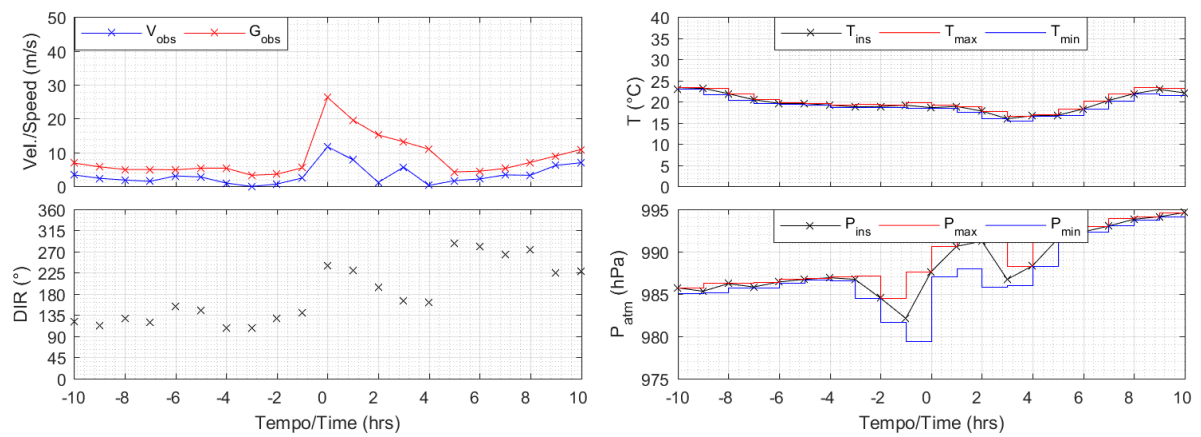


Figure D.21 – F&N event classified as non-synoptic by INMET algorithm. Peak $G_{obs} = 26.3$ m/s at A831 – Quaraí, RS, 15/10/2015, 06:00 UTC.

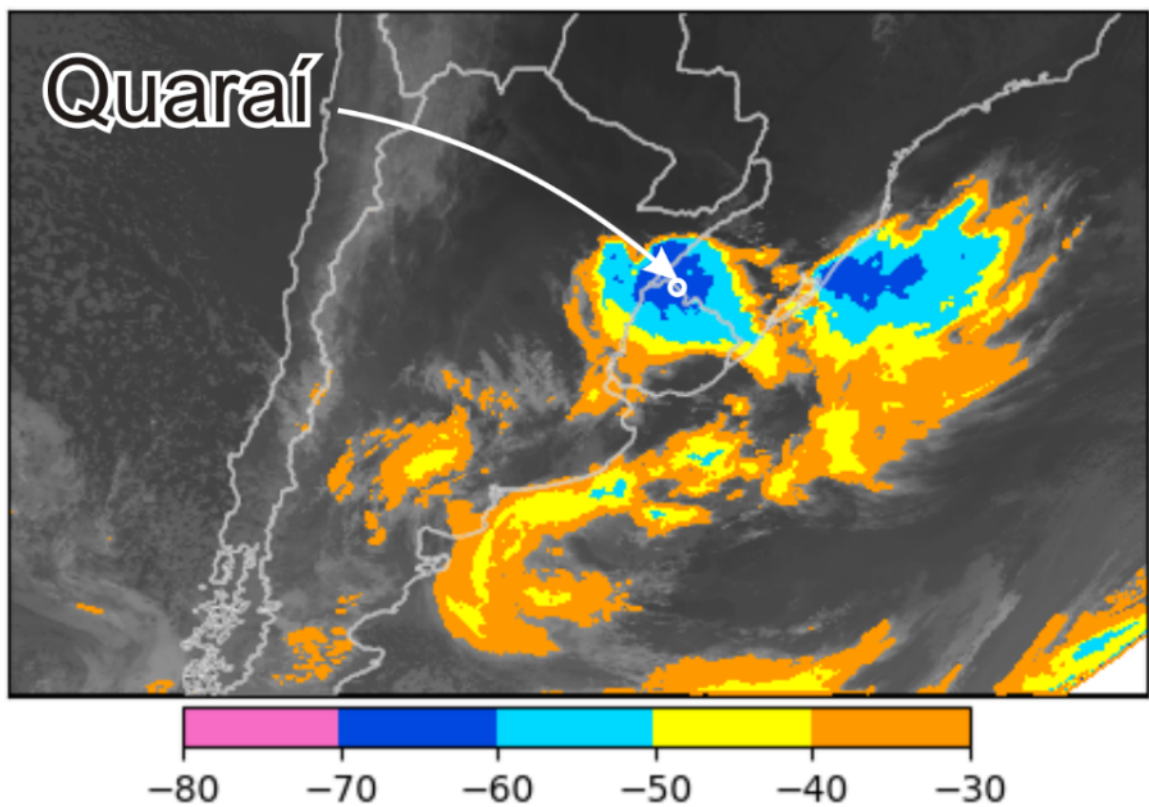


Figure D.22 – Infrared channel of GOES 13 satellite enhanced with brightness temperature data, T_B (°C), 15/10/2015, 05:45 UTC.

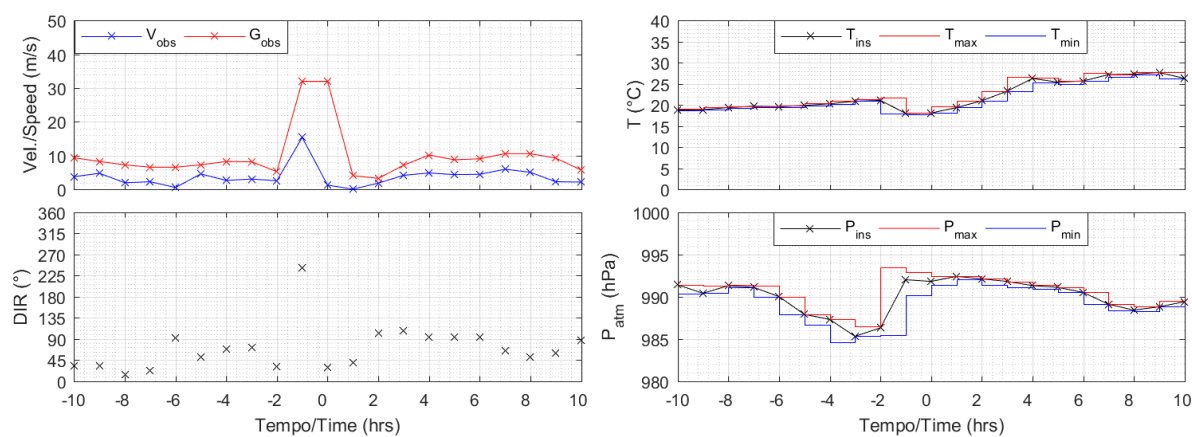


Figure D.23 – F&N event classified as non-synoptic by INMET algorithm. Peak $G_{obs} = 32.0$ m/s at A831 – Quaraí, RS, 16/10/2016, 11:00 UTC.

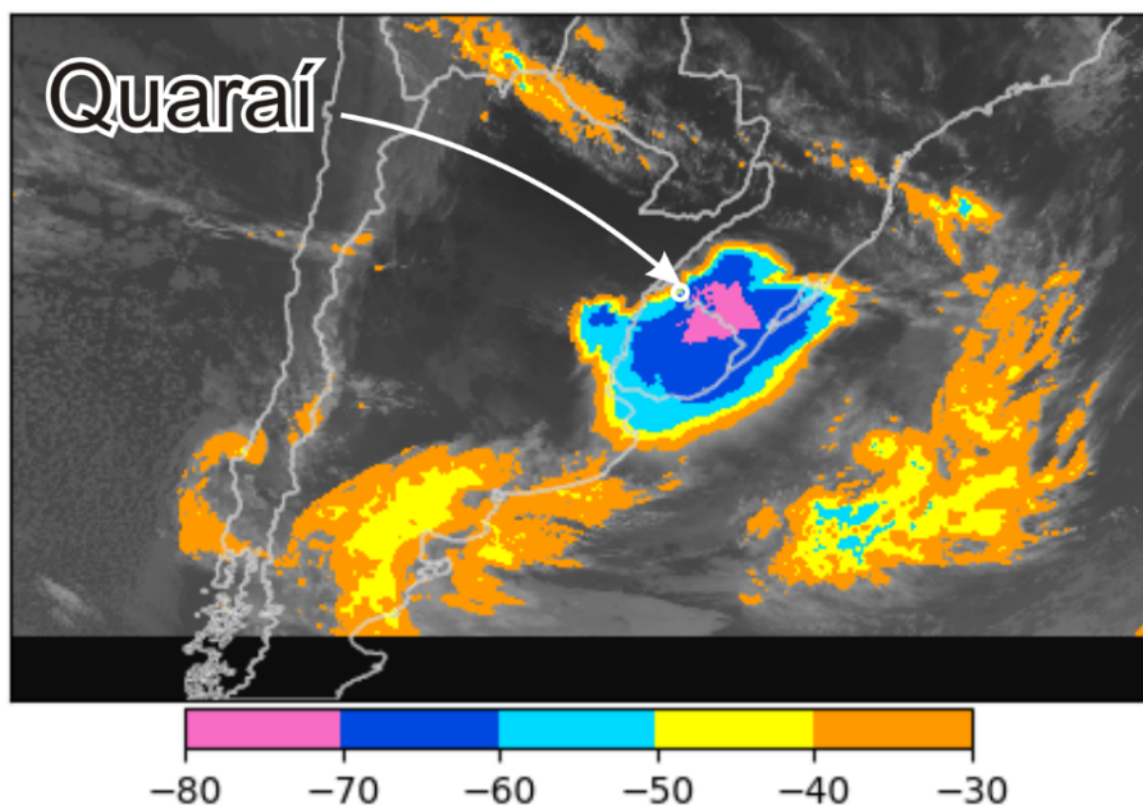


Figure D.24 – Infrared channel of GOES 13 satellite enhanced with brightness temperature data, T_B (°C), 16/10/2016, 11:08 UTC.

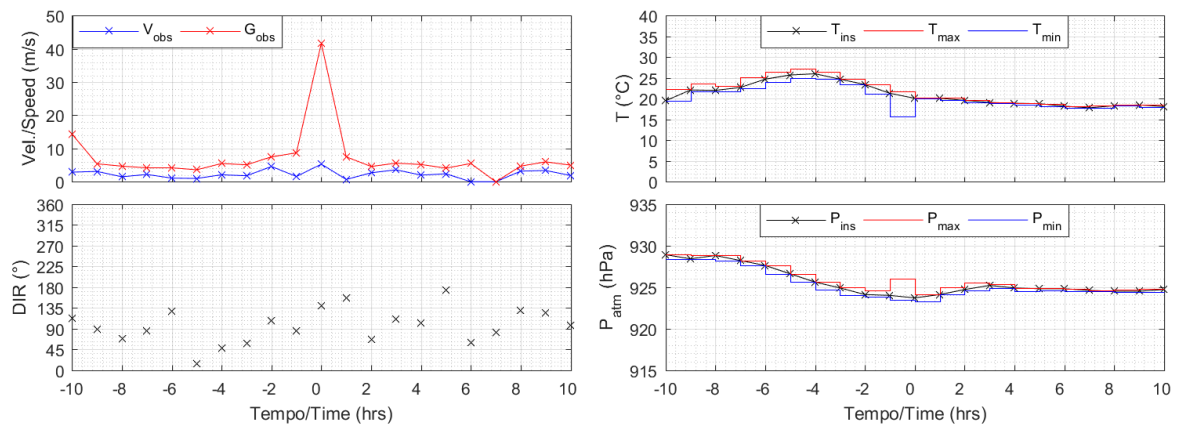


Figure D.25 – Event classified as non-synoptic by INMET algorithm. Peak $G_{obs} = 41.7$ m/s at A714 – Itapeva, SP, 27/11/2012, 21:00 UTC.

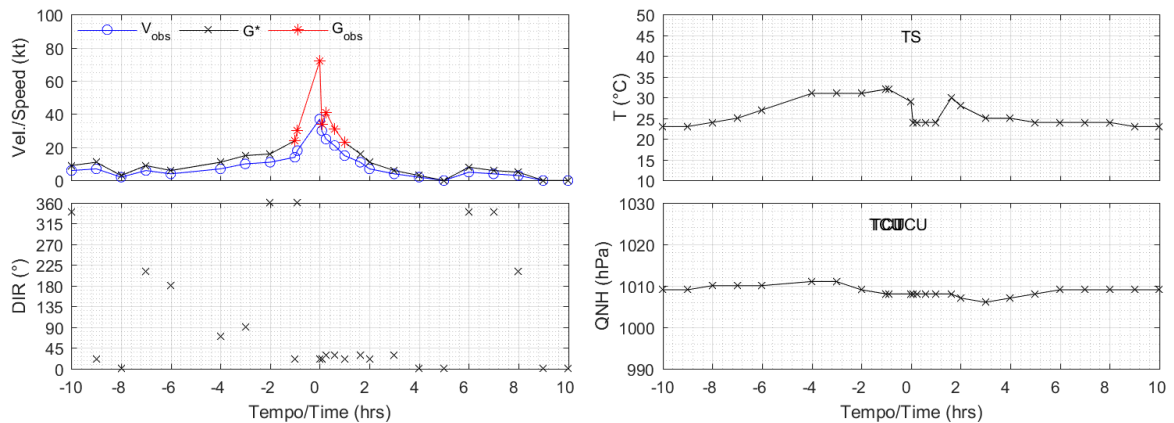


Figure D.26 – Event classified as non-synoptic by aerodrome algorithm. Peak $G_{obs} = 72$ kt (37.0 m/s) at SPQT – Iquitos, Peru, 15/05/2009, 19:00 UTC.

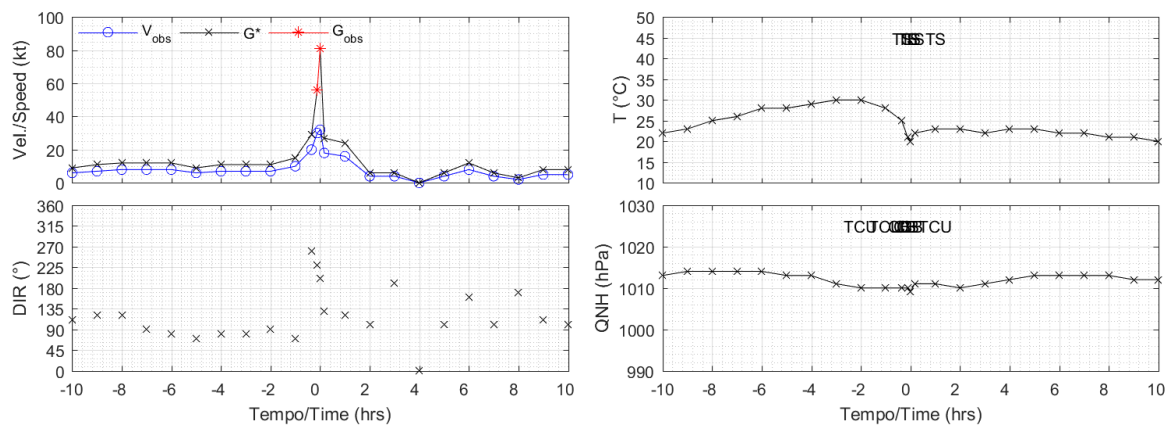


Figure D.27 – Event classified as non-synoptic by aerodrome algorithm. Peak $G_{obs} = 81$ kt (41.7 m/s) at SBLO – Londrina, PR, 20/11/2017, 20:00 UTC.

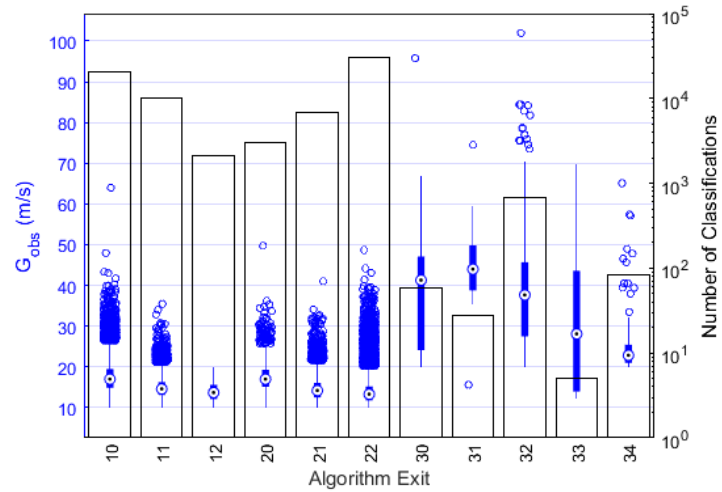


Figure D.31 – Frequency of occurrence and peak gust box plots for INMET algorithm exits (Figure D.1).

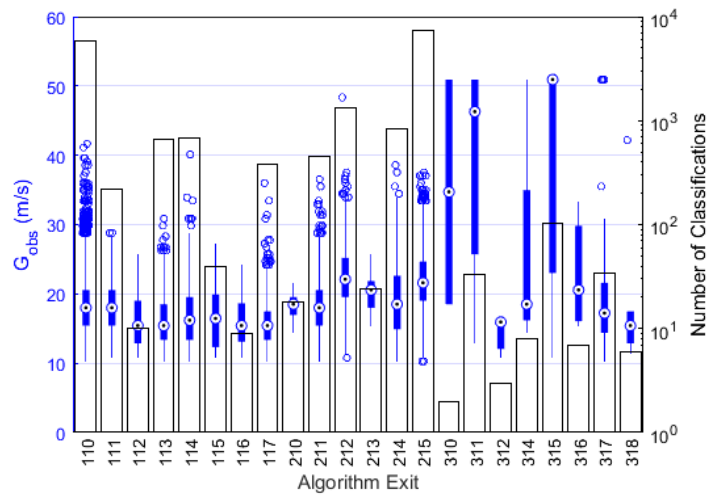


Figure D.32 – Frequency of occurrence and peak gust box plots for aerodrome SWS G_{obs} algorithm exits (Figure D.2 and D.3).

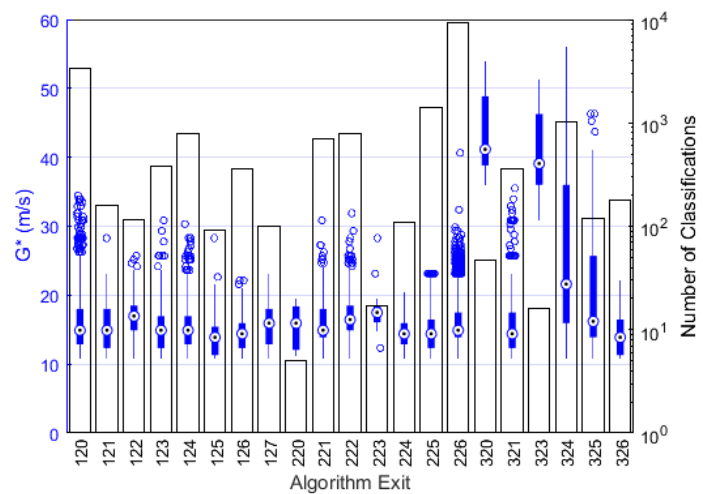


Figure D.33 – Frequency of occurrence and peak gust box plots for aerodrome SWS G^* algorithm exits (Figure D.4 and D.5).

APPENDIX E

COMPARISON OF EXTREME VALUE ANALYSES FOR SELECTED SWS

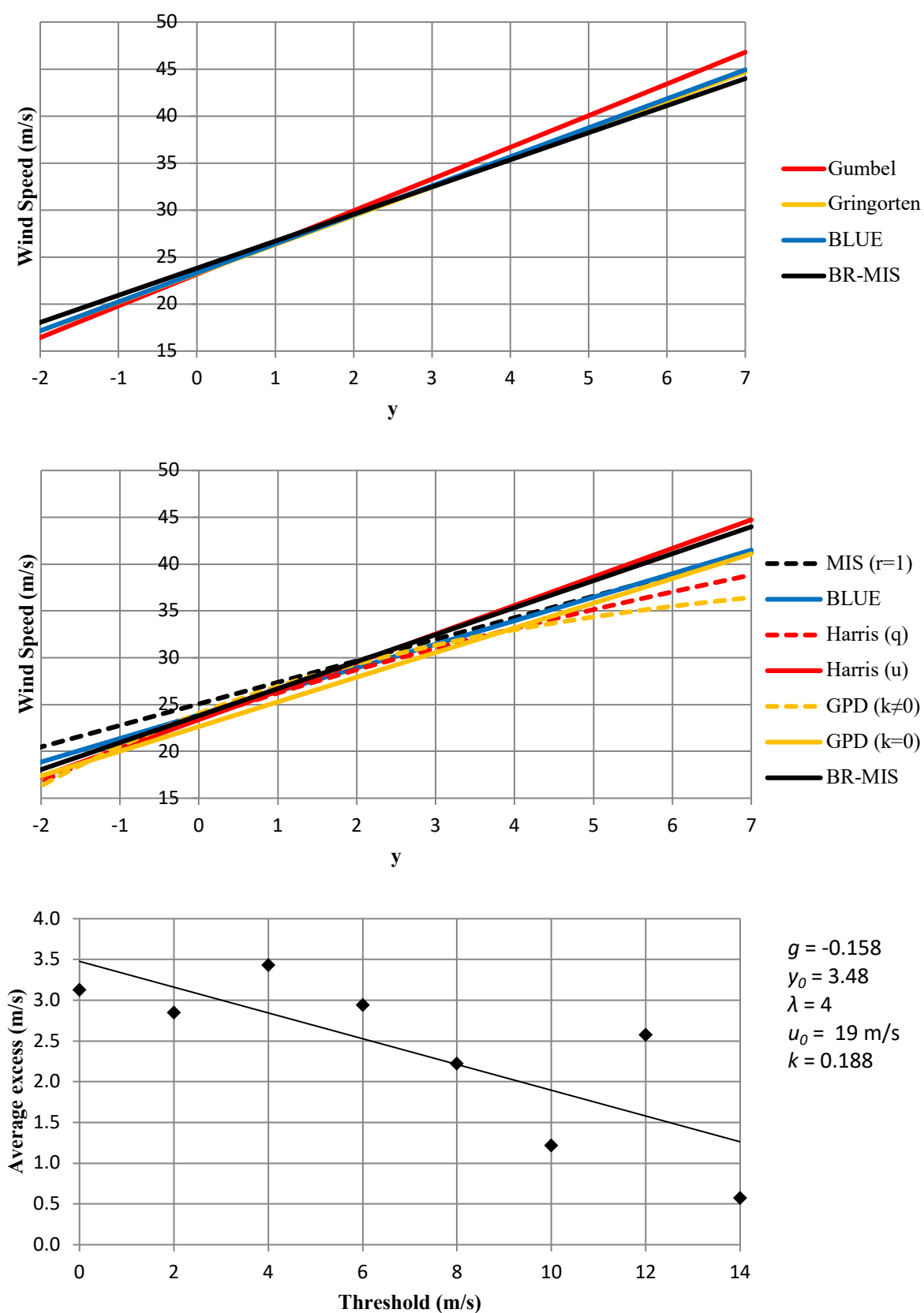


Figure E.1 – Extreme value distributions for non-synoptic winds at SBUR – Uberaba, MG, $t_{tot} = 27.9$, $M = 28$ years. Annual maximums (top); independent storms (middle); GPD (bottom).

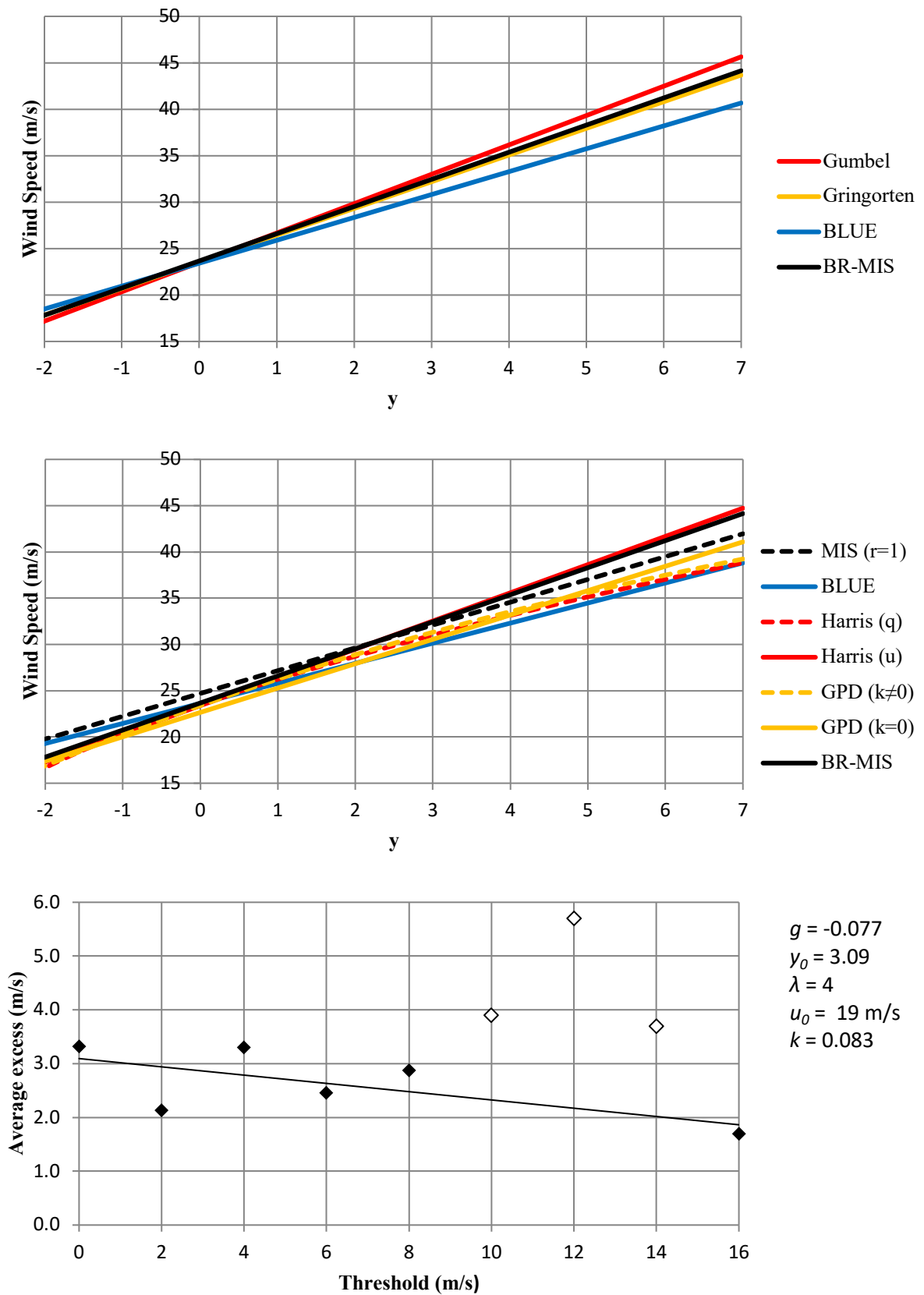


Figure E.2 – Extreme value distributions for non-synoptic winds at SBPA – Porto Alegre, RG, $t_{tot} = 21.3$, $M = 22$ years. Annual maximums (top); independent storms (middle); GPD (bottom).

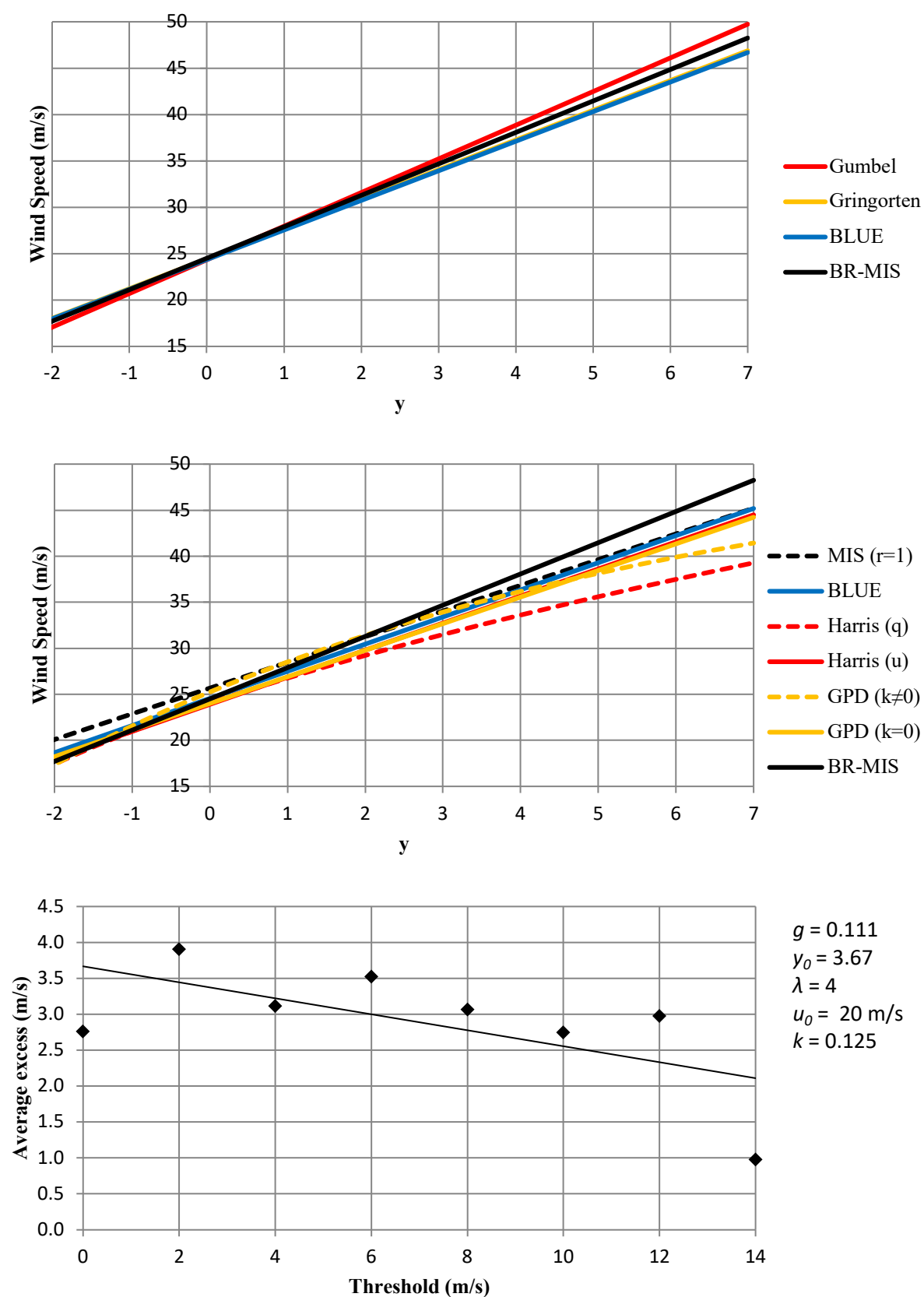


Figure E.3 – Extreme value distributions for non-synoptic winds at SBKP – Campinas, SP, $t_{tot} = 17.0$, $M = 17$ years. Annual maximums (top); independent storms (middle); GPD (bottom).

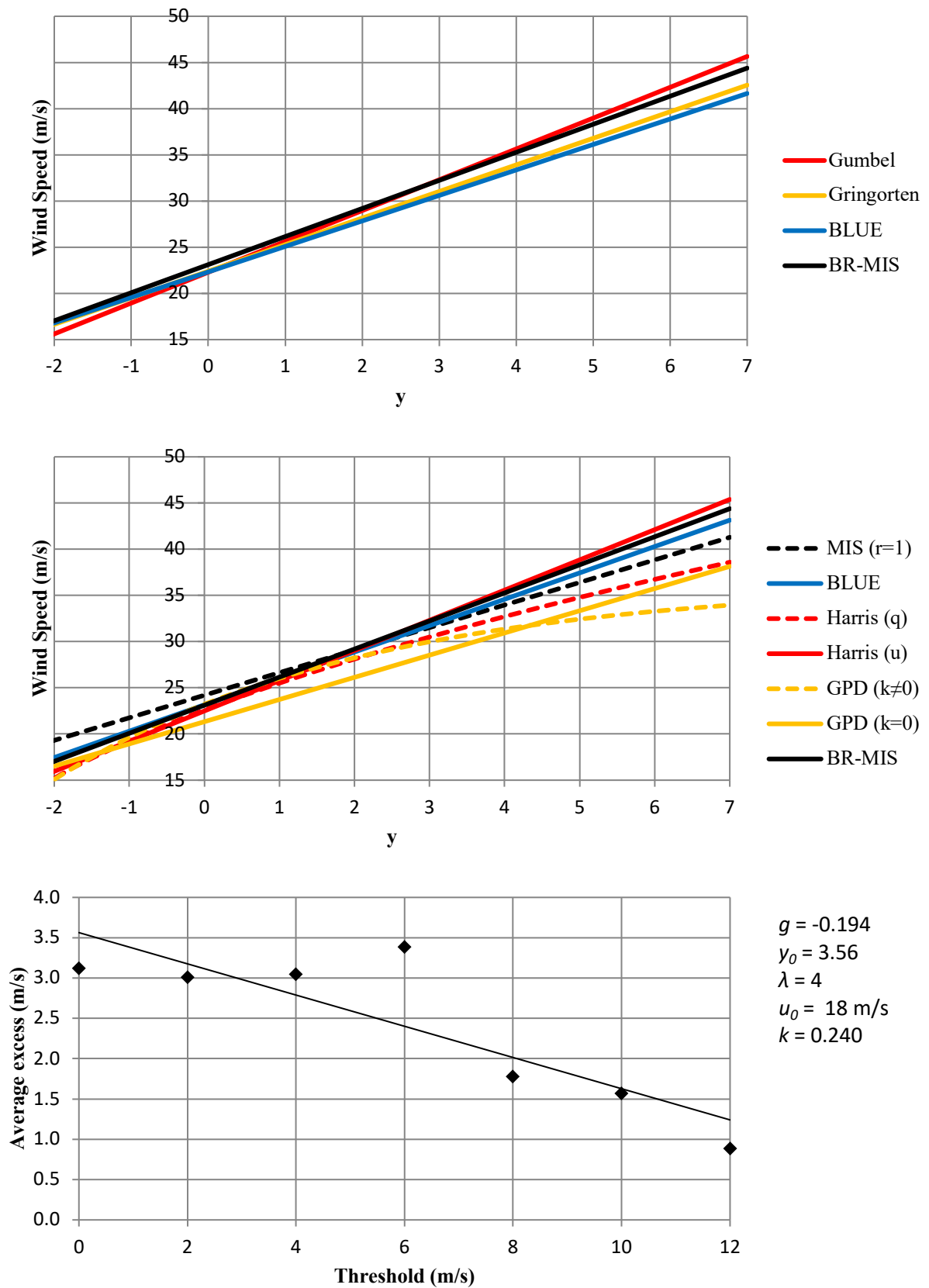


Figure E.4 – Extreme value distributions for non-synoptic winds at A502 – Barbacena, MG, $t_{tot} = 13.1$, $M = 13$ years. Annual maximums (top); independent storms (middle); GPD (bottom).

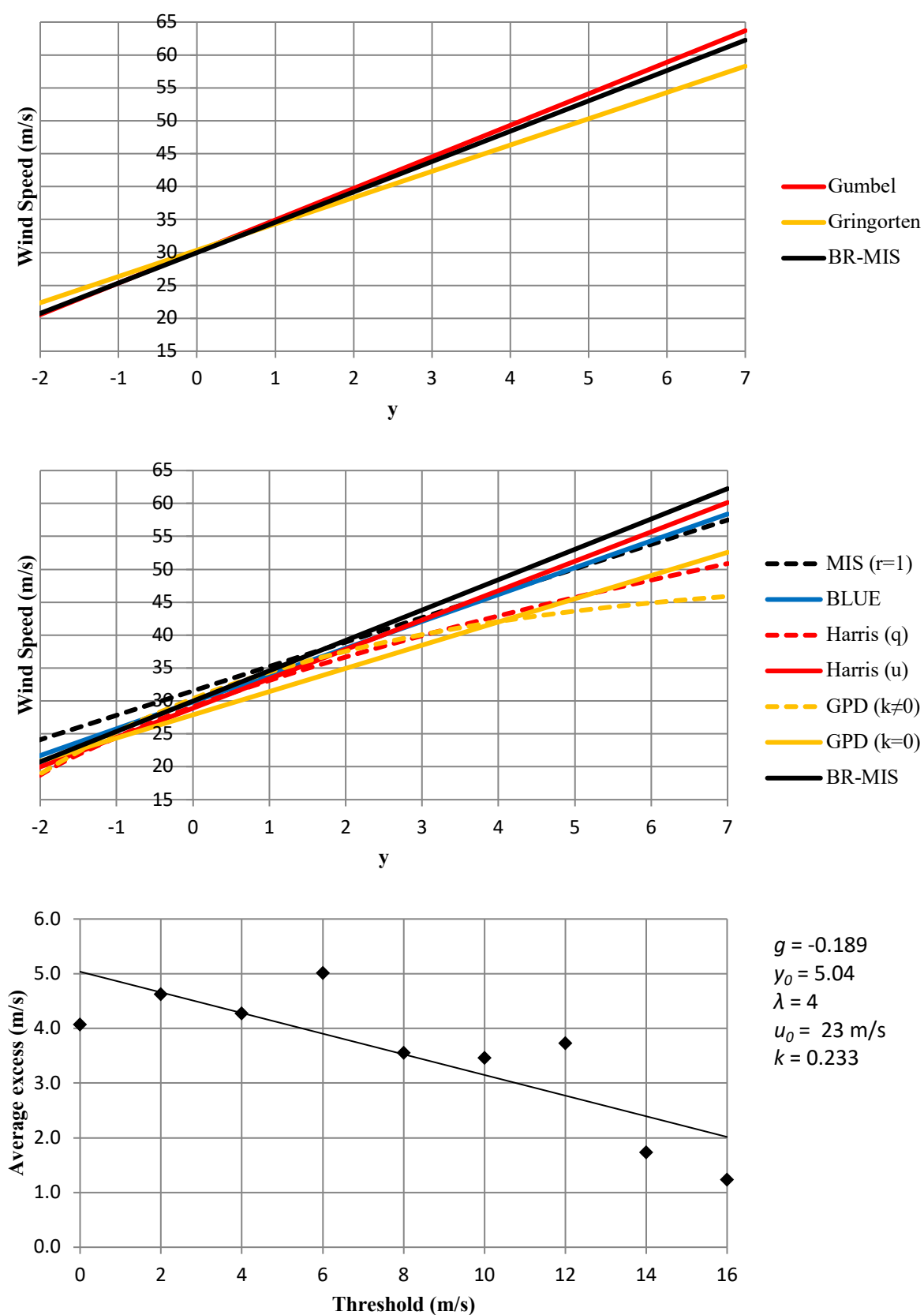


Figure E.5 – Extreme value distributions for non-synoptic winds at A816 – Novo Horizonte, SC, $t_{tot} = 8.3$, $M = 9$ years. Annual maximums (top); independent storms (middle); GPD (bottom).

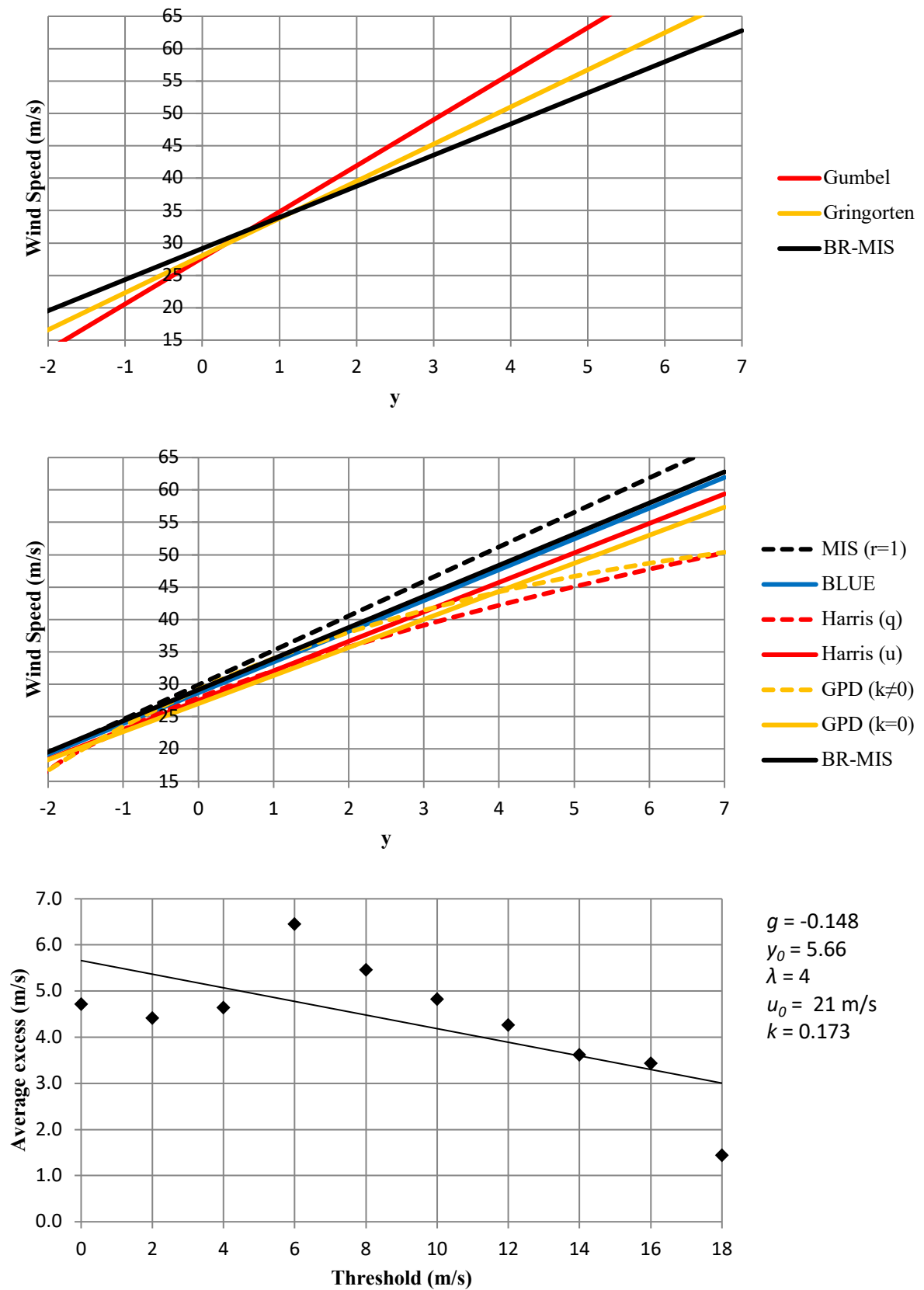


Figure E.6 – Extreme value distributions for non-synoptic winds at A805 – Santo Augusto, RS, $t_{tot} = 6.9$, $M = 7$ years. Annual maximums (top); independent storms (middle); GPD (bottom).

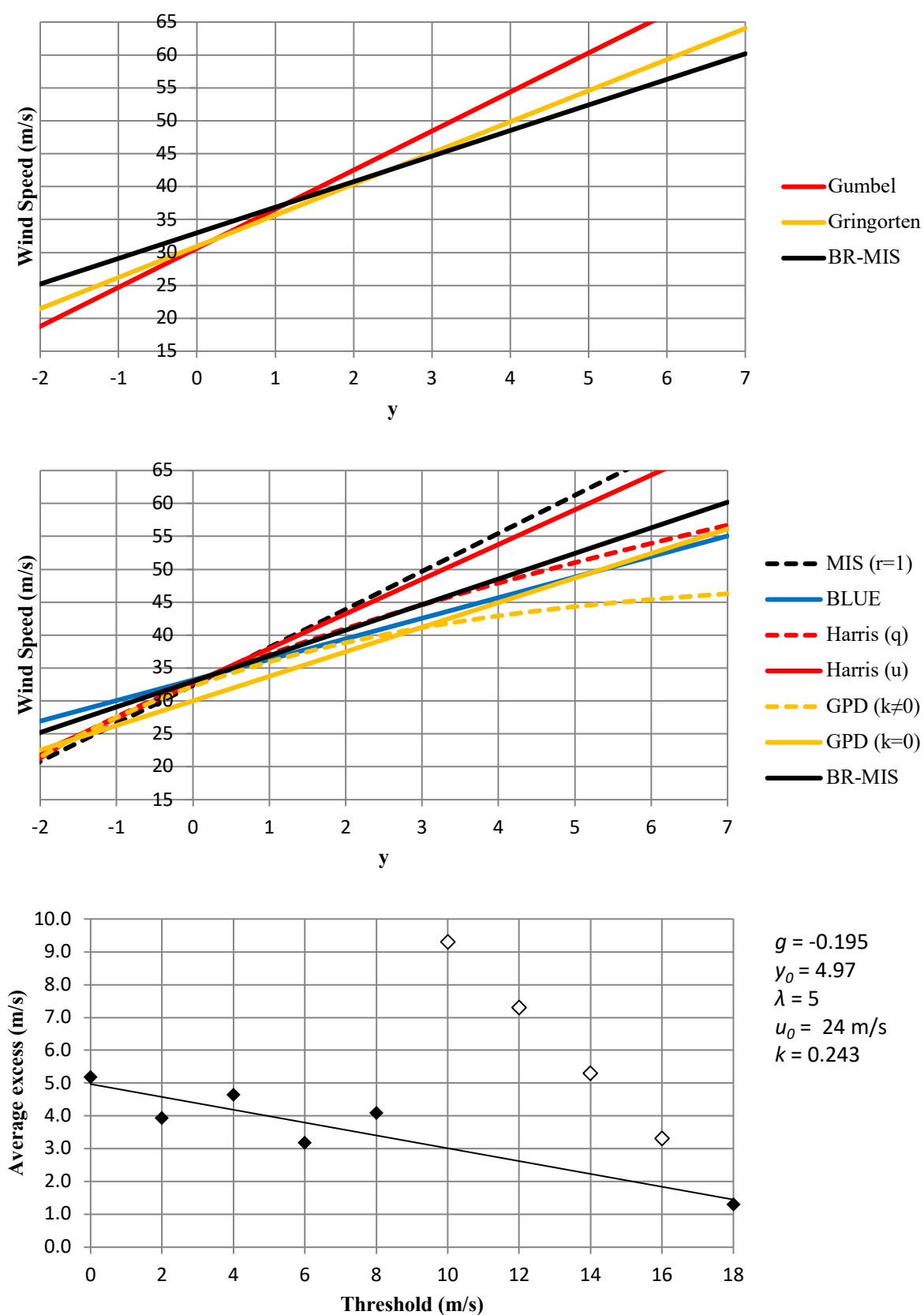


Figure E.7 – Extreme value distributions for non-synoptic winds at SBCH – Chapecó, SC, $t_{tot} = 4.1$, $M = 5$ years. Annual maximums (top); independent storms (middle); GPD (bottom).

APPENDIX F

ASSORTED TABLES

Table F.1 – Relevant b , p and F_r parameters for the calculation of terrain and height multiplier, S_2 . Table 21 of NBR 6123 (ABNT, 1988)

CAT	τ (s)	3	5	10	15	20	30	45	60	120	300	600	3600
I	b	1.10	1.11	1.12	1.13	1.14	1.15	1.16	1.17	1.19	1.21	1.23	1.25
	p	0.06	0.065	0.07	0.075	0.075	0.08	0.085	0.085	0.09	0.095	0.095	0.10
II	b	1.00	1.00	1.00	1.00	1.00	1.00	1.00	1.00	1.00	1.00	1.00	1.00
	p	0.085	0.09	0.10	0.105	0.11	0.115	0.12	0.125	0.135	0.145	0.15	0.16
	F_r	1.00	0.98	0.95	0.93	0.90	0.87	0.84	0.82	0.77	0.72	0.69	0.65
III	b	0.94	0.94	0.93	0.92	0.92	0.91	0.90	0.90	0.89	0.87	0.86	0.85
	p	0.10	0.105	0.115	0.125	0.13	0.14	0.145	0.15	0.16	0.175	0.185	0.20
IV	b	0.86	0.85	0.84	0.83	0.83	0.82	0.80	0.79	0.76	0.73	0.71	0.68
	p	0.12	0.125	0.135	0.145	0.15	0.16	0.17	0.175	0.195	0.215	0.23	0.25
V	b	0.74	0.73	0.71	0.70	0.69	0.67	0.64	0.62	0.58	0.53	0.50	0.44
	p	0.15	0.16	0.175	0.185	0.19	0.205	0.22	0.23	0.255	0.285	0.31	0.35

Table F.2 – Lieblein’s BLUE Coefficients for $M = 10$ (ESDU, 1990[a])

m (rank)	A_m	B_m	y
1	0.2229	-0.3478	-0.875
2	0.1623	-0.0912	-0.533
3	0.1338	-0.0192	-0.262
4	0.1129	0.0222	-0.012
5	0.0956	0.0487	0.238
6	0.0806	0.0661	0.501
7	0.0670	0.0770	0.794
8	0.0542	0.0828	1.144
9	0.0417	0.0836	1.606
10	0.0289	0.0779	2.351

Table F.3 – Lieblein’s BLUE Coefficients for $M = 20$ (ESDU, 1990[a])

m (rank)	A_m	B_m
1	0.1172	-0.2288
2	0.0946	-0.0951
3	0.0837	-0.0559
4	0.0757	-0.0322
5	0.0694	-0.0154
6	0.0637	-0.0029
7	0.0590	0.0067
8	0.0545	0.0142
9	0.0503	0.0206
10	0.0465	0.0256
11	0.0435	0.0292
12	0.0398	0.0328
13	0.0360	0.0353
14	0.0331	0.0372
15	0.0301	0.0384
16	0.0269	0.0392
17	0.0239	0.0394
18	0.0207	0.0389
19	0.0175	0.0377
20	0.0140	0.0352

Table F.4 – Saffir-Simpson Hurricane Wind Scale⁴²

Category	Sustained wind speeds	Types of damage
1	74-95 mph 64-82 kt 119-153 km/h 33-42 m/s	Very dangerous winds will produce some damage: Well-constructed frame homes could have damage to roof, shingles, vinyl siding and gutters. Large branches of trees will snap and shallowly rooted trees may be toppled. Extensive damage to power lines and poles likely will result in power outages that could last a few to several days.
2	96-110 mph 83-95 kt 154-177 km/h 43-49 m/s	Extremely dangerous winds will cause extensive damage: Well-constructed frame homes could sustain major roof and siding damage. Many shallowly rooted trees will be snapped or uprooted and block numerous roads. Near-total power loss is expected with outages that could last from several days to weeks.
3	111-129 mph 96-112 kt 178-208 km/h 50-57 m/s	Devastating damage will occur: Well-built framed homes may incur major damage or removal of roof decking and gable ends. Many trees will be snapped or uprooted, blocking numerous roads. Electricity and water will be unavailable for several days to weeks after the storm passes.
4	130-156 mph 113-136 kt 209-251 km/h 58-69 m/s	Catastrophic damage will occur: Well-built framed homes can sustain severe damage with loss of most of the roof structure and/or some exterior walls. Most trees will be snapped or uprooted and power poles downed. Fallen trees and power poles will isolate residential areas. Power outages will last weeks to possibly months. Most of the area will be uninhabitable for weeks or months.
5	157 mph or higher 137 kt or higher 252 km/h or higher 70 m/s or higher	Catastrophic damage will occur: A high percentage of framed homes will be destroyed, with total roof failure and wall collapse. Fallen trees and power poles will isolate residential areas. Power outages will last for weeks to possibly months. Most of the area will be uninhabitable for weeks or months.

⁴² <https://www.nhc.noaa.gov/aboutsshws.php>

APPENDIX G

MAPPED GENERAL WIND TRENDS

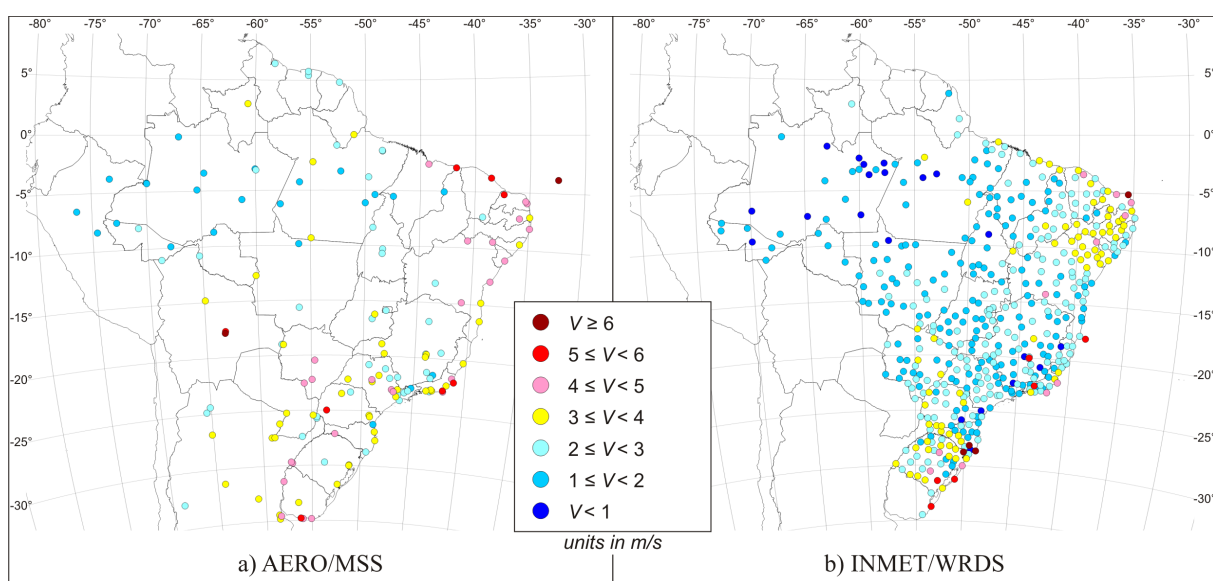


Figure G.1 – Average V wind speeds (m/s).

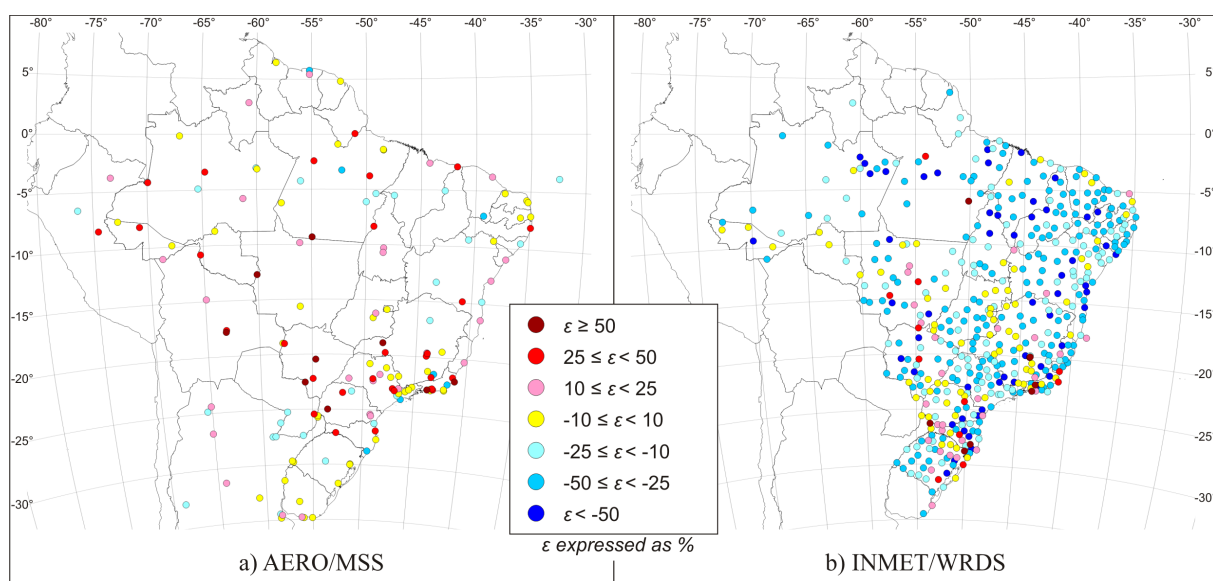


Figure G.2 – Average error, ε , between station monthly means, V_m , at stations and ECMWF ERA-Interim data.

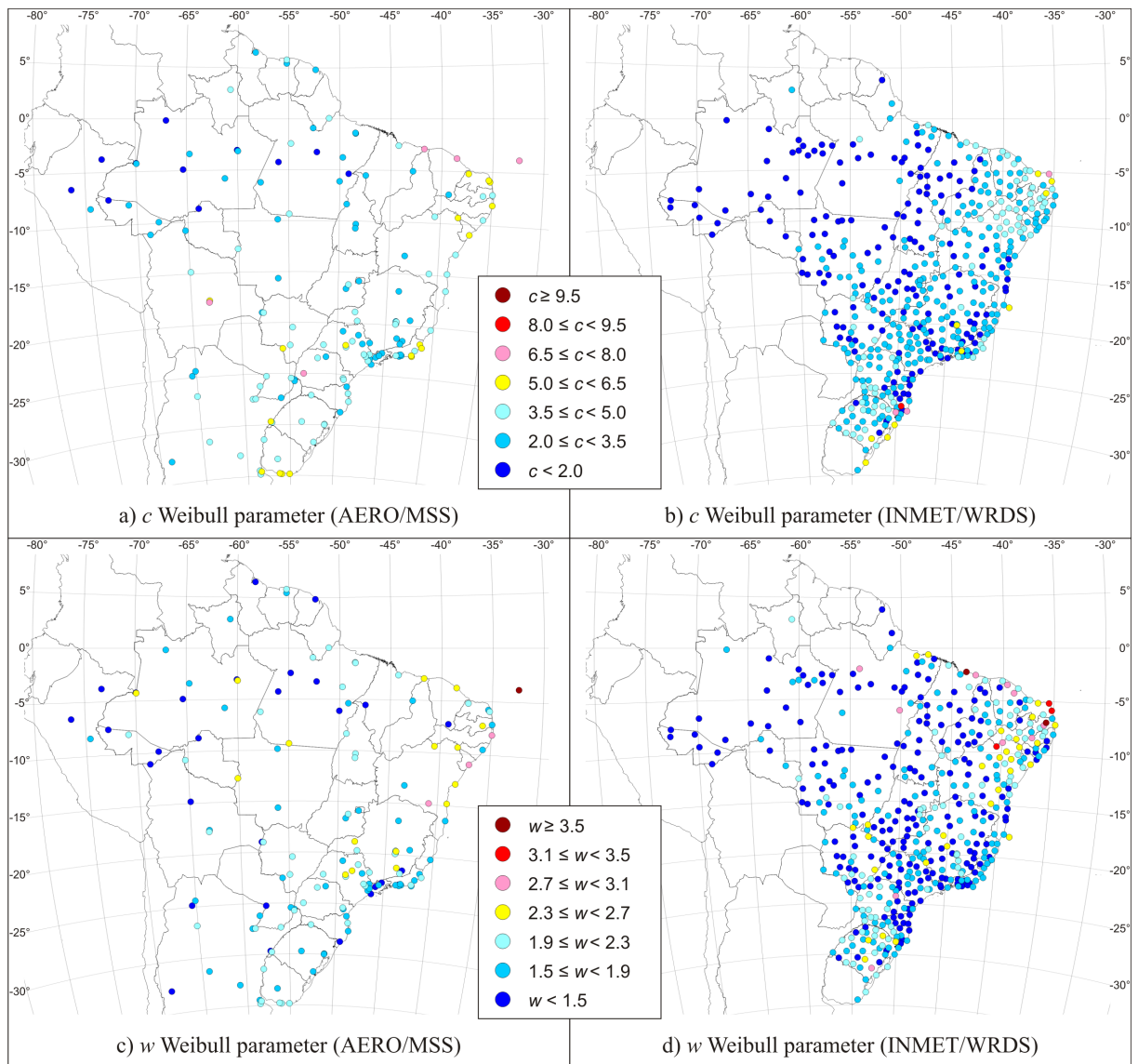


Figure G.3 – Parameters for Weibull model fitted to V_{cor} (m/s) parent distribution.

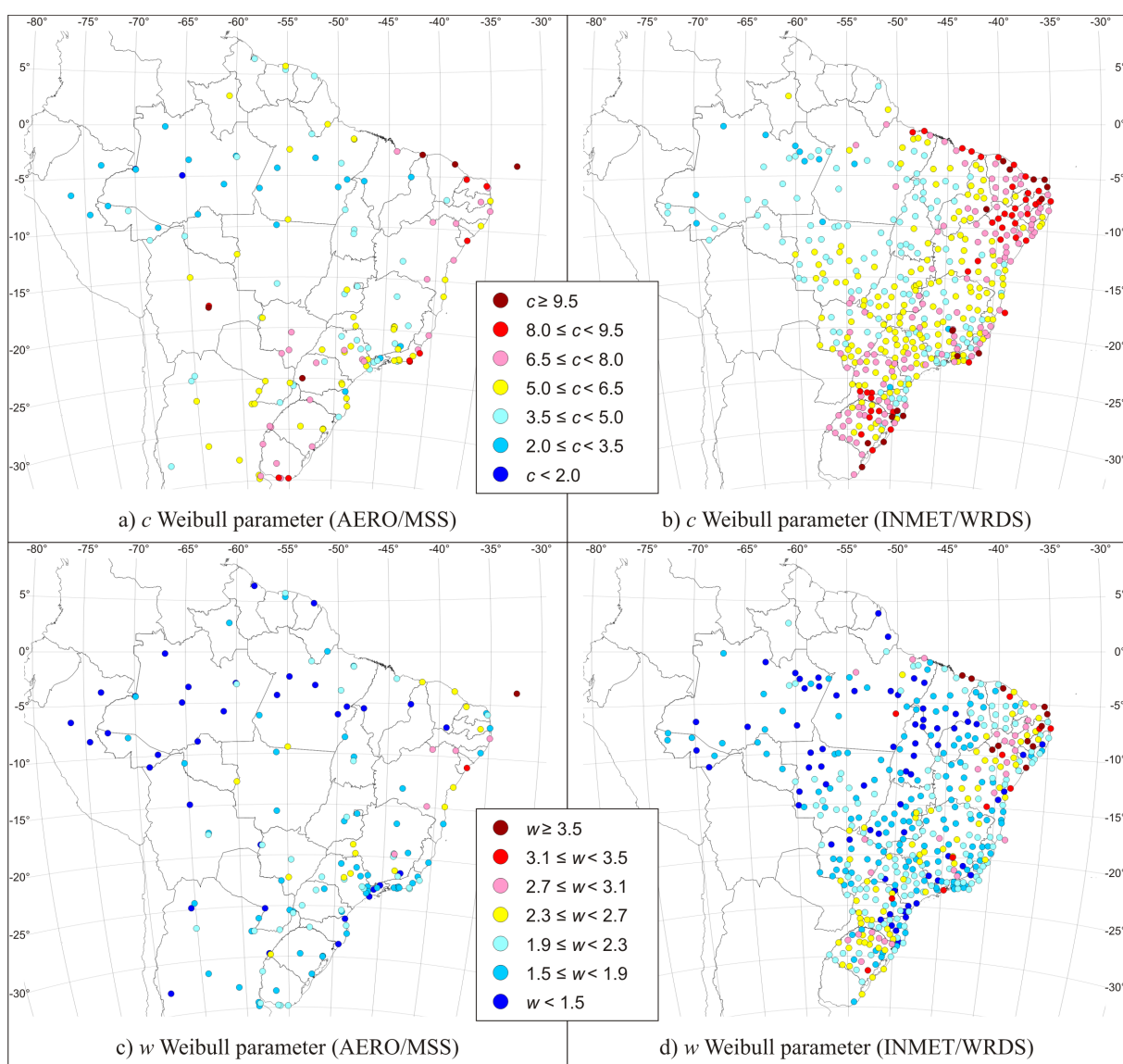


Figure G.4 – Parameters for Weibull model fitted to G_{cor} (m/s) parent distribution.

APPENDIX H

MAPPED EXTREME WIND TRENDS

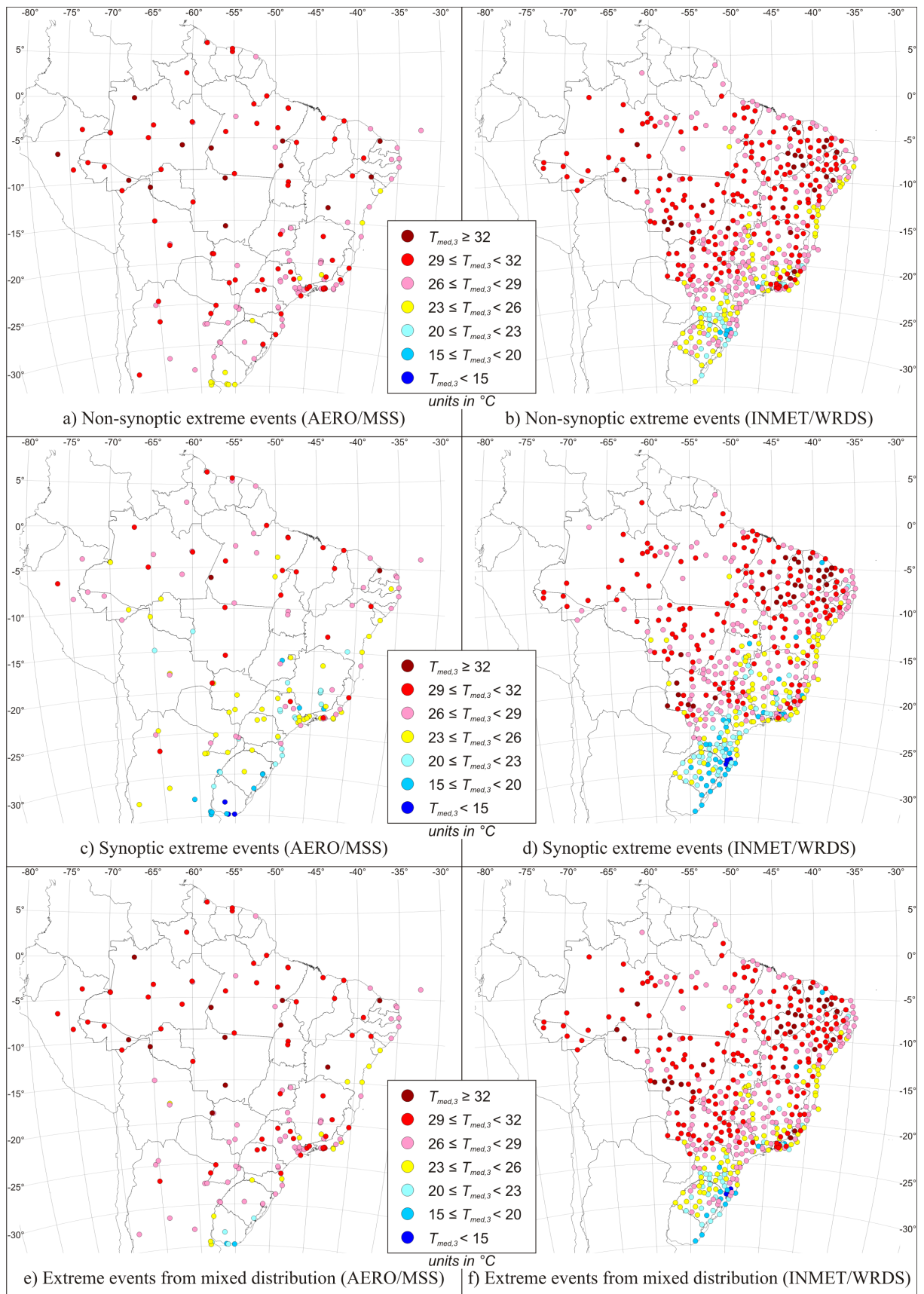


Figure H.1 – $T_{med,3}$ (°C) averaged over each set of extreme events (N_N , N_S and N_M).

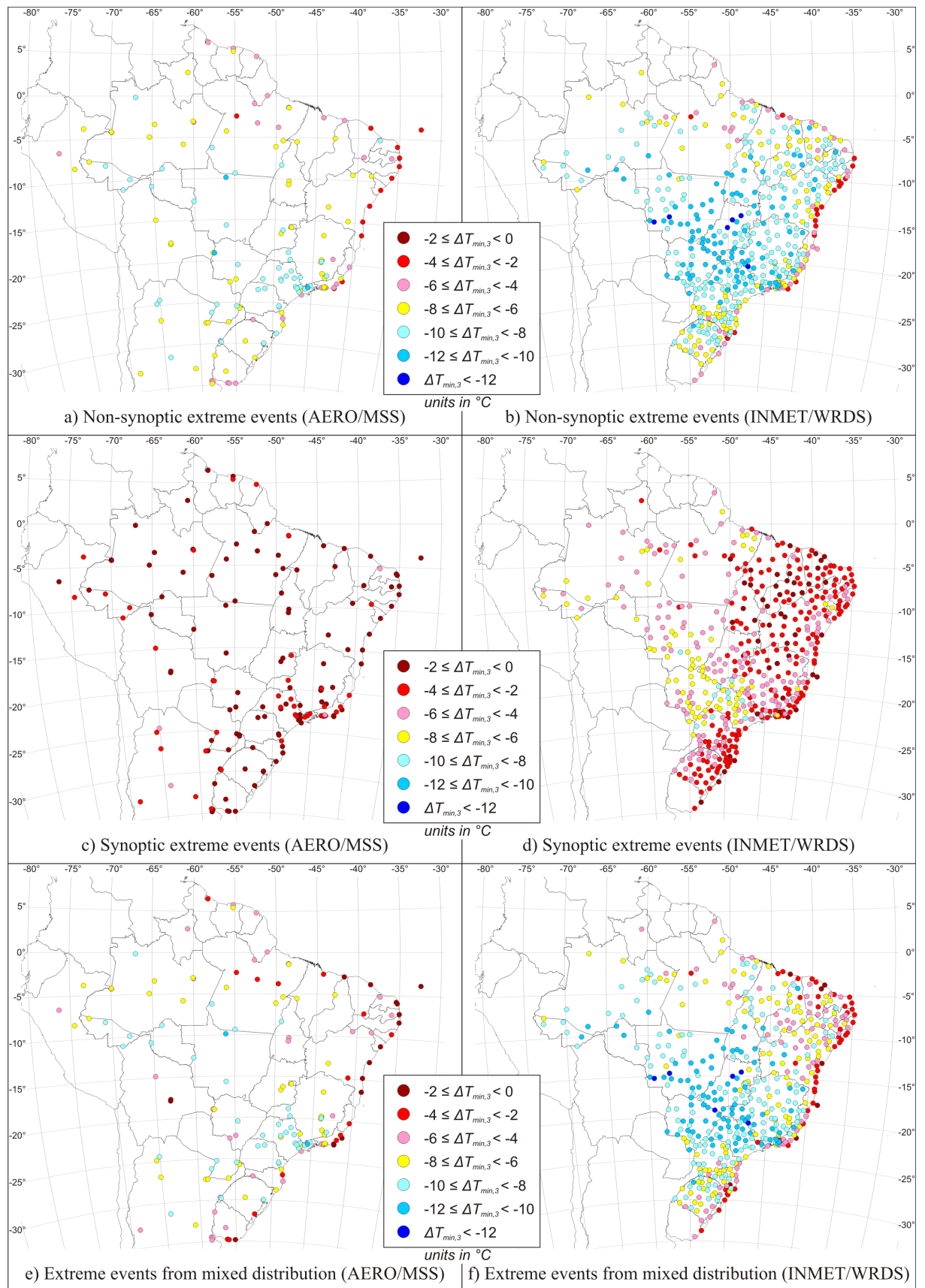


Figure H.2 $-\Delta T_{\min,3}$ ($^{\circ}\text{C}$) averaged over each set of extreme events (N_N , N_S and N_M).

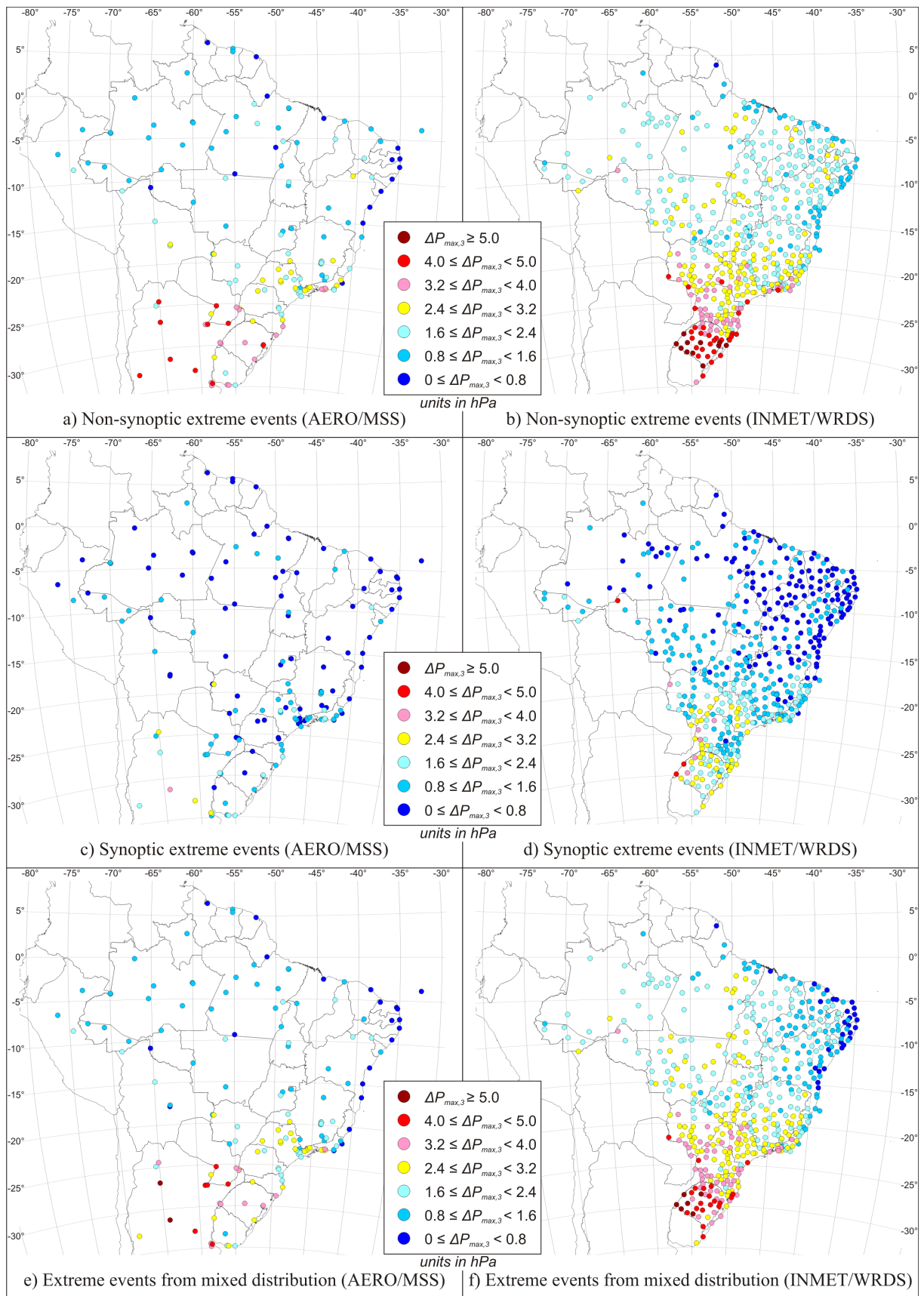


Figure H.3 $-\Delta Q_{max,3}$ and $\Delta P_{max,3}$ (hPa) averaged over each set of extreme events (N_N , N_S and N_M).

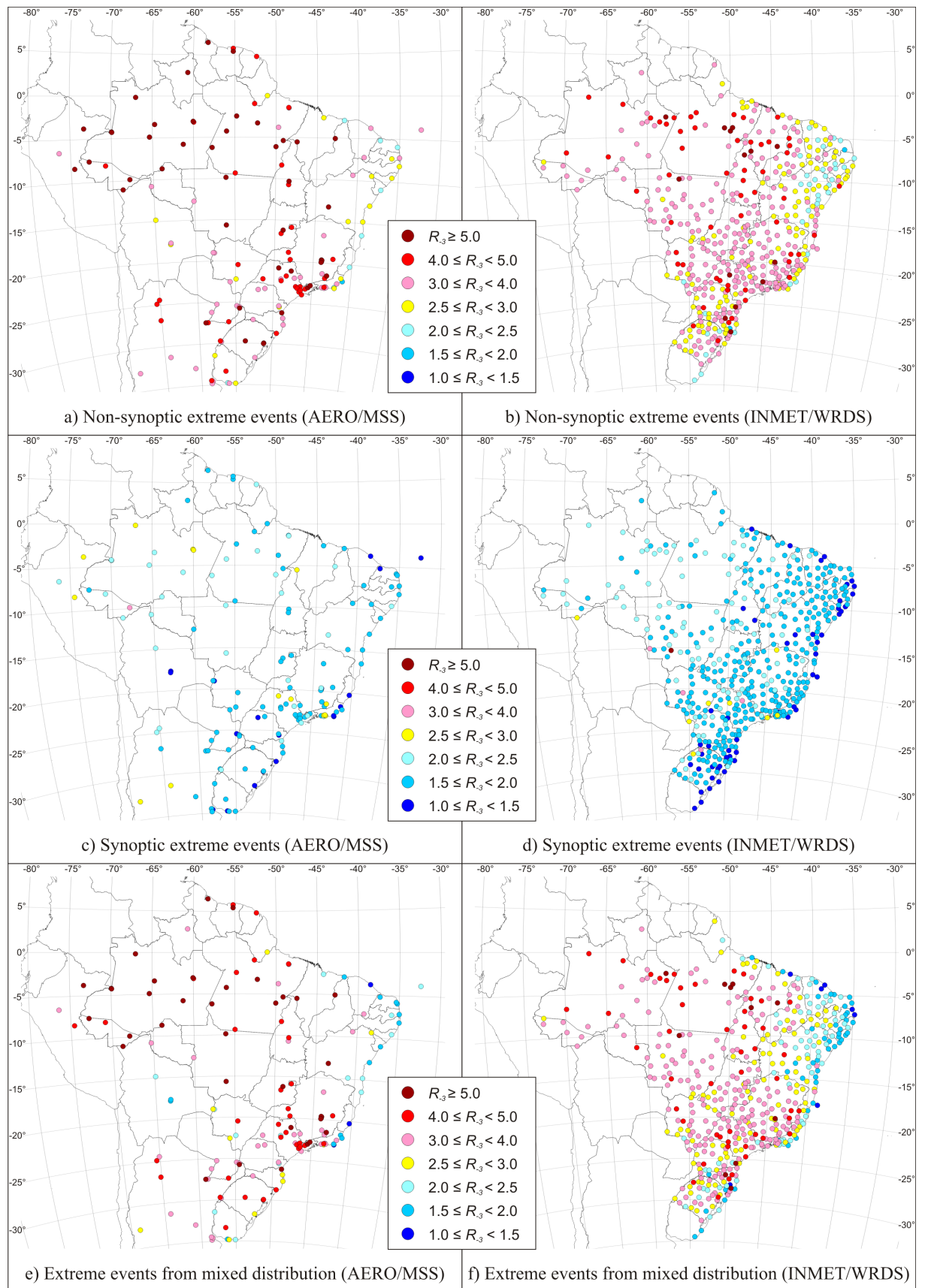


Figure H.4 – Peak ratio R_3 averaged over each set of extreme events (N_N , N_S and N_M).

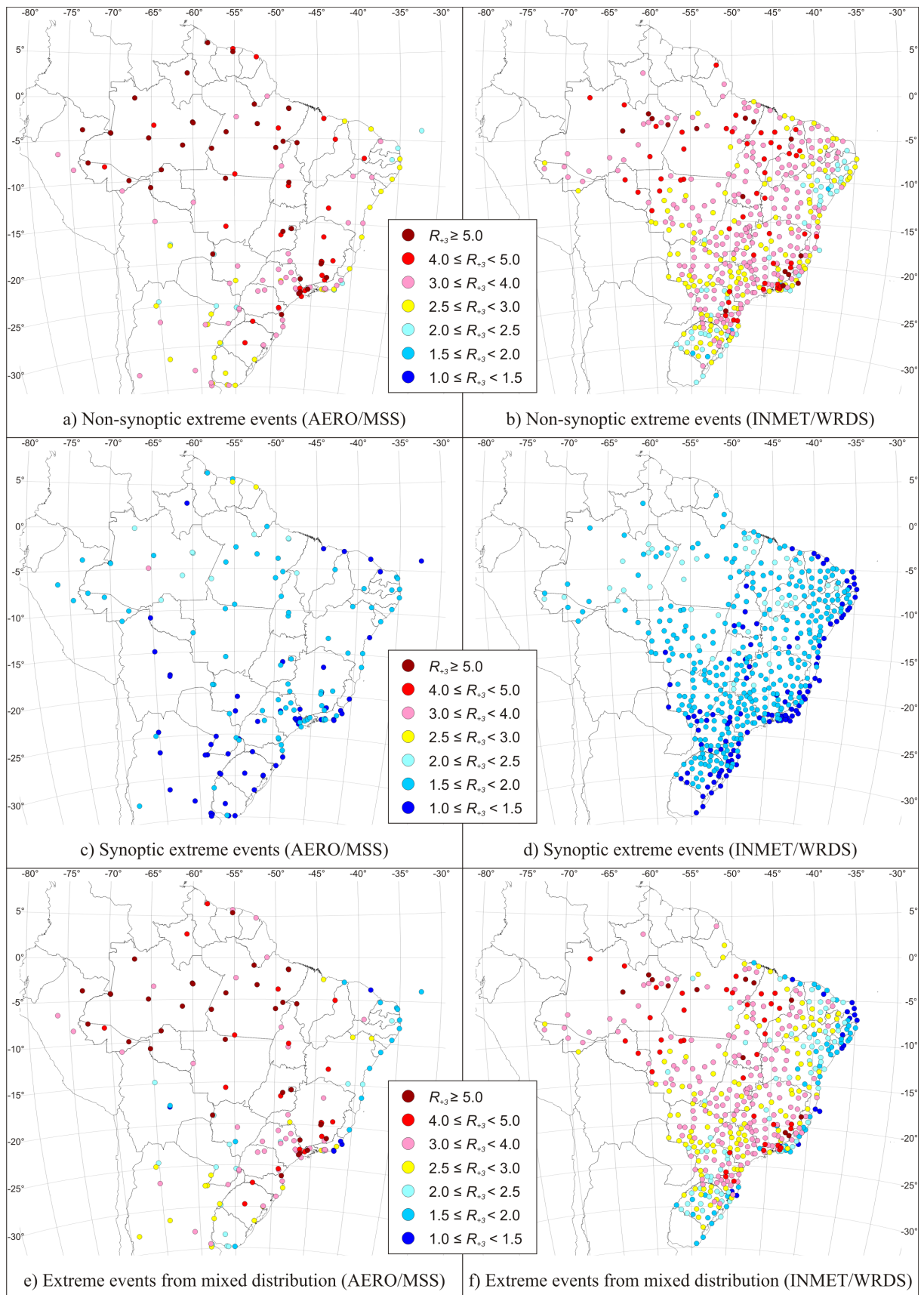


Figure H.5 – Peak ratio R_{+3} averaged over each set of extreme events (N_N , N_S and N_M).

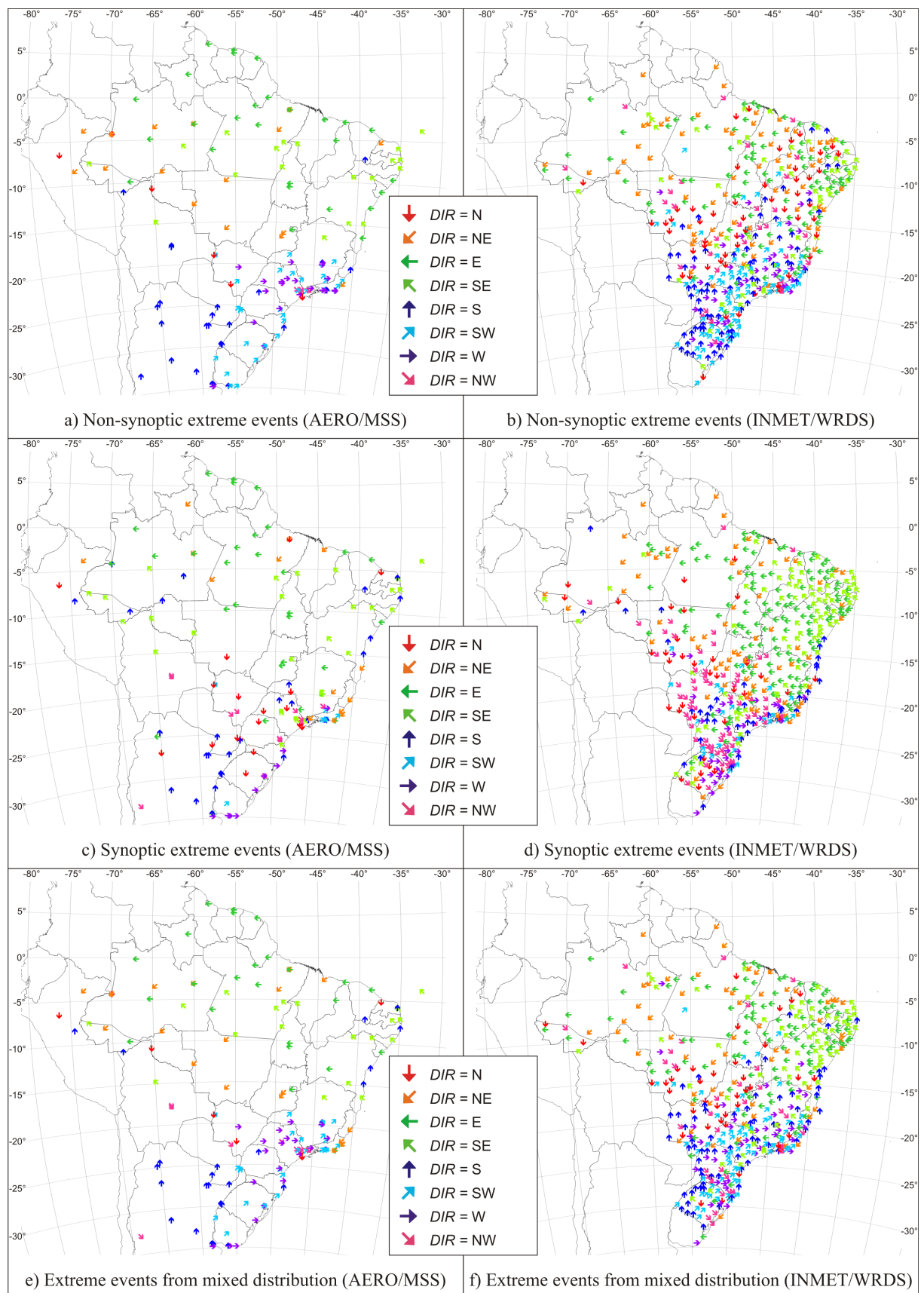


Figure H.6 – Predominant wind direction for each set of extreme events (N_N , N_S and N_M).

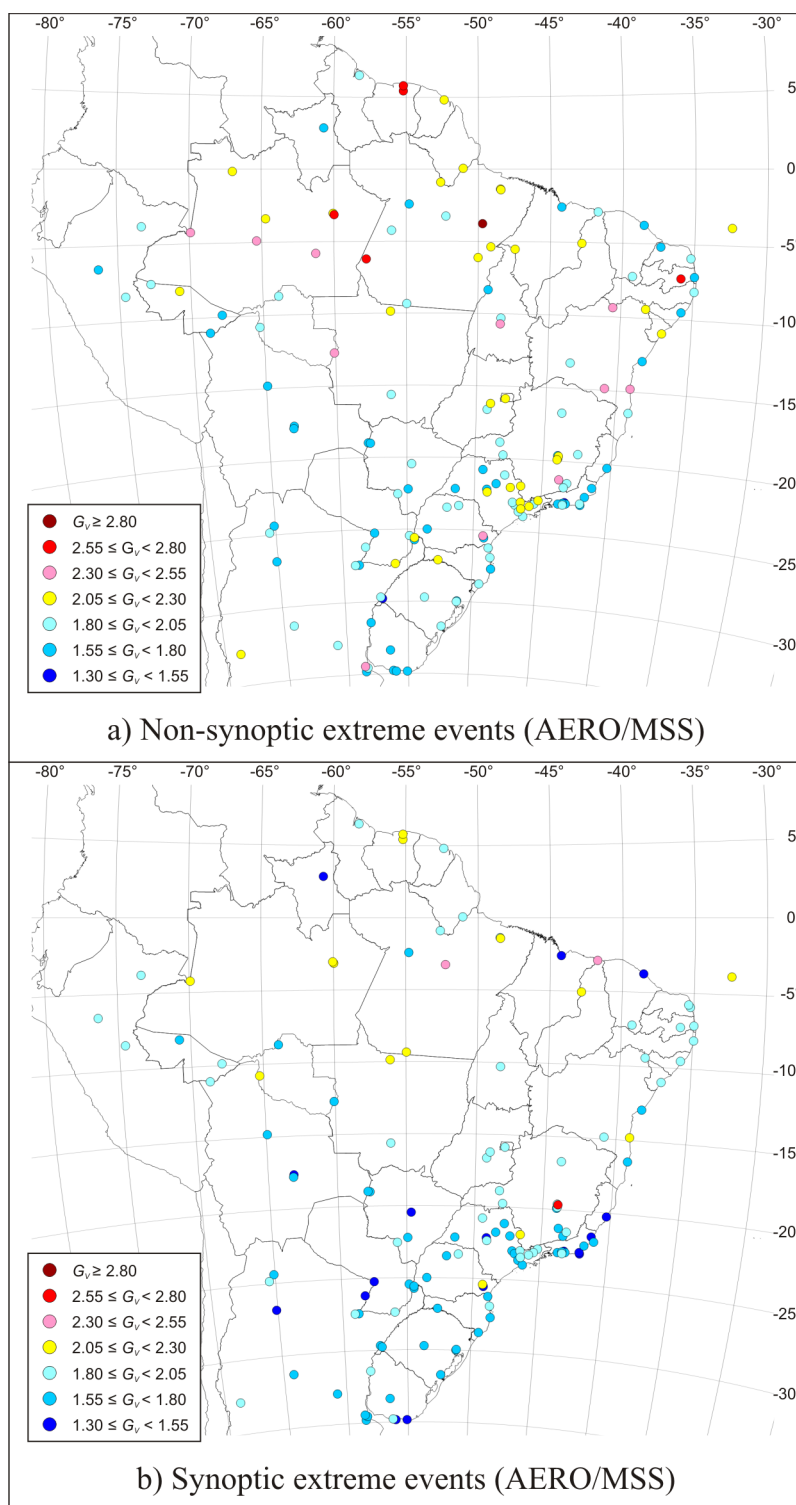


Figure H.7 – Average gust factor, G_v , for each set of extreme events (N_N and N_S).

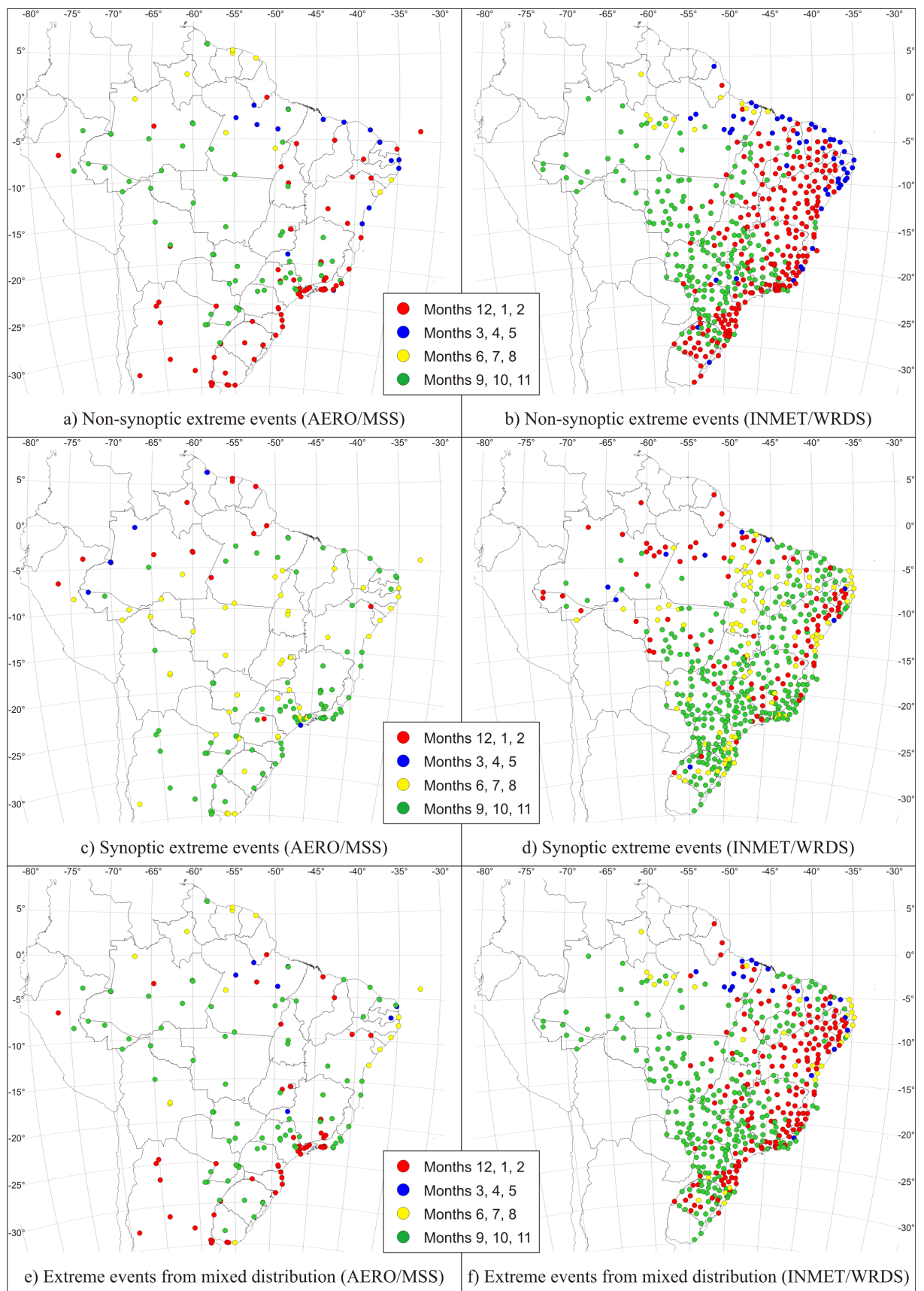


Figure H.8 – Predominant season (months of year) for each set of extreme events (N_N , N_S and N_M).

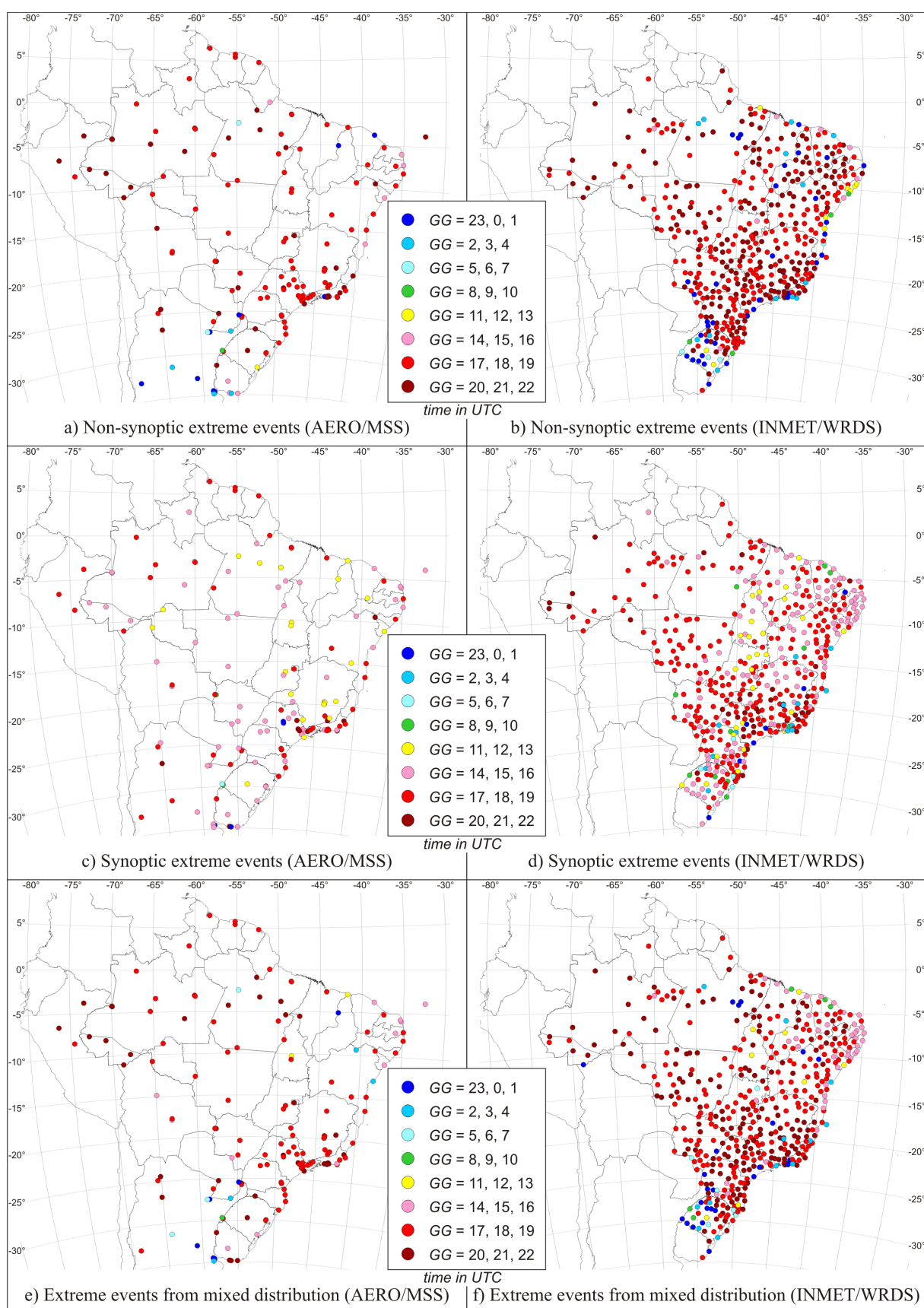


Figure H.9 – Predominant hour (UTC) for each set of extreme events (N_N , N_S or N_M).

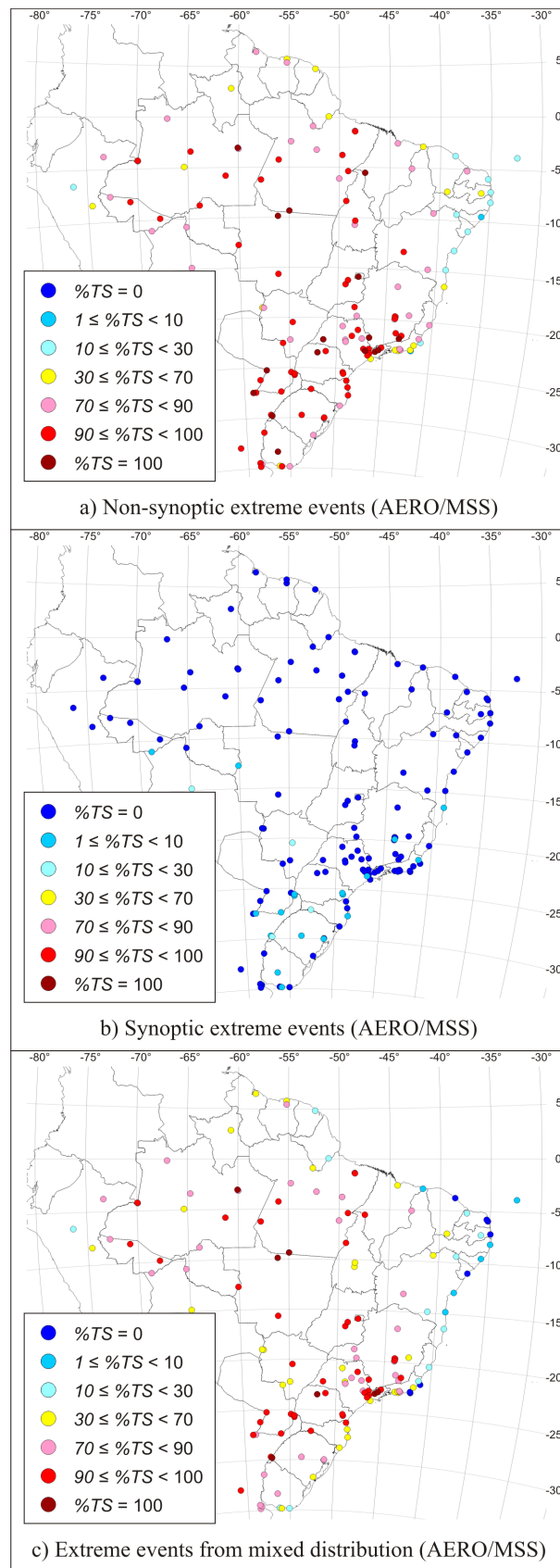


Figure H.10 – Percentage of events with thunderstorm observations (TS) for each set of extreme events (N_N , N_S or N_M).

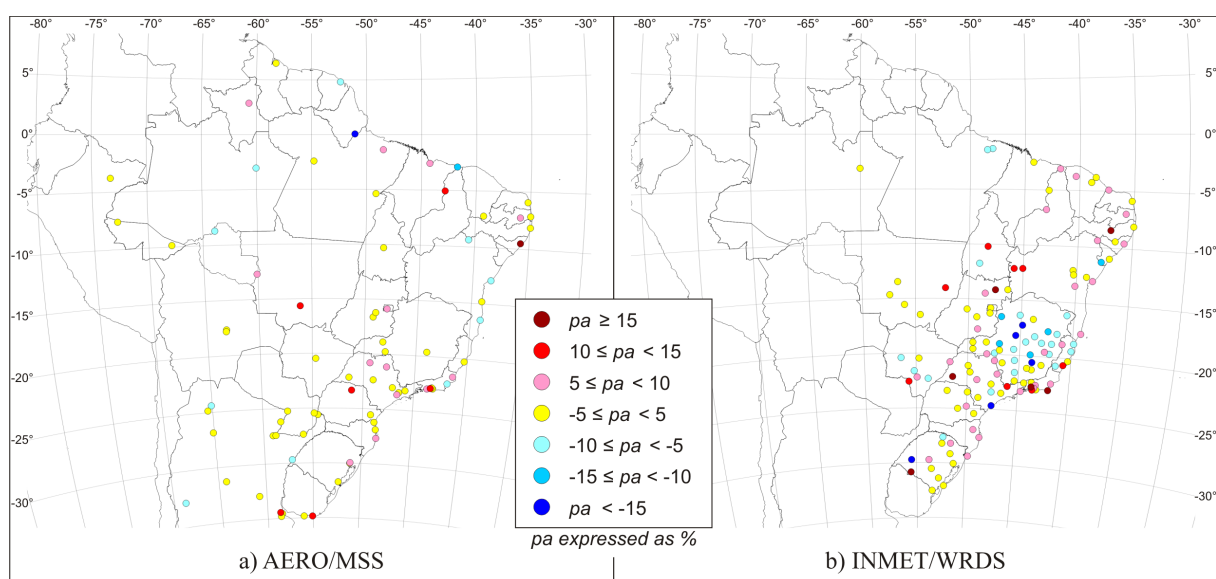
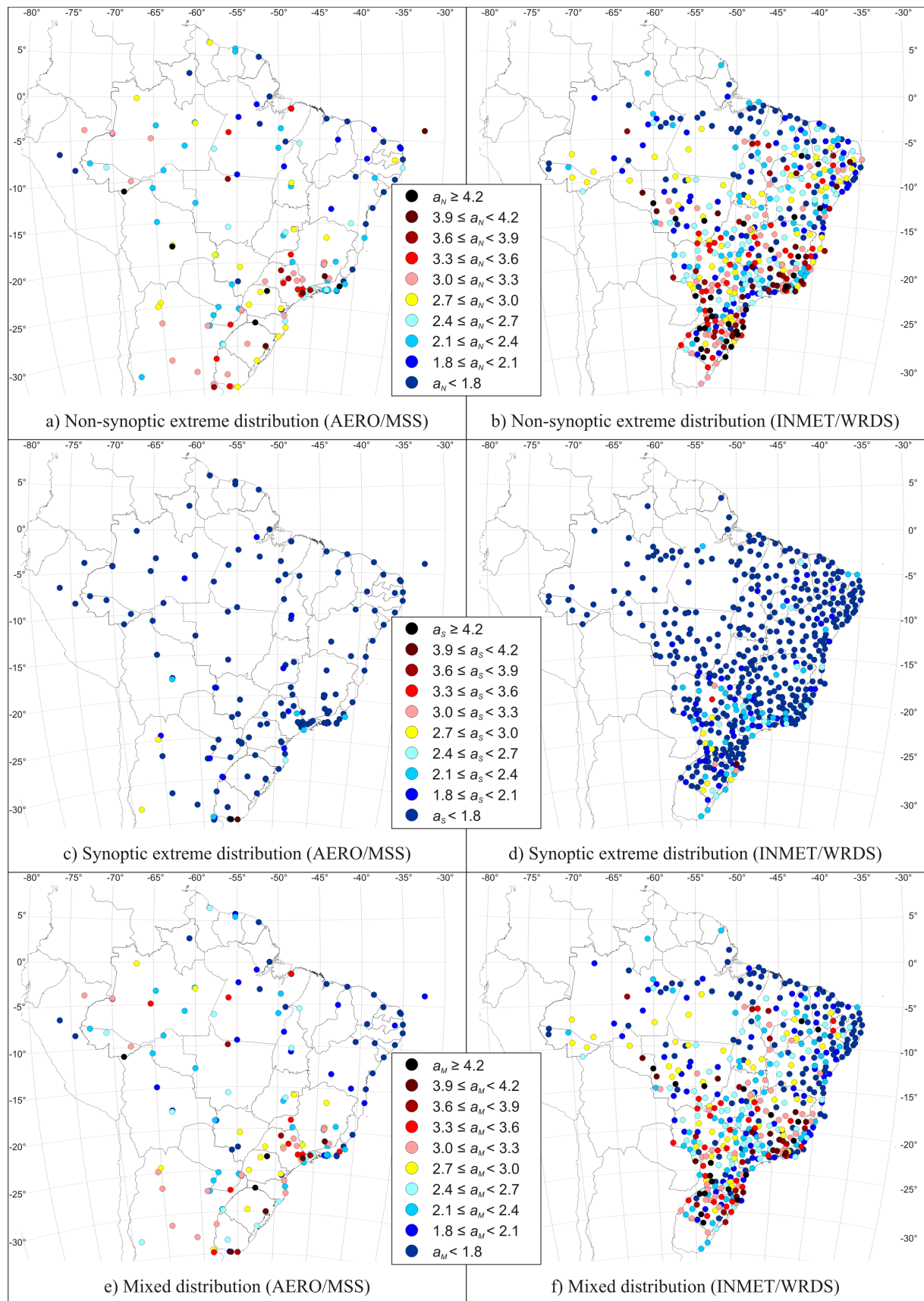
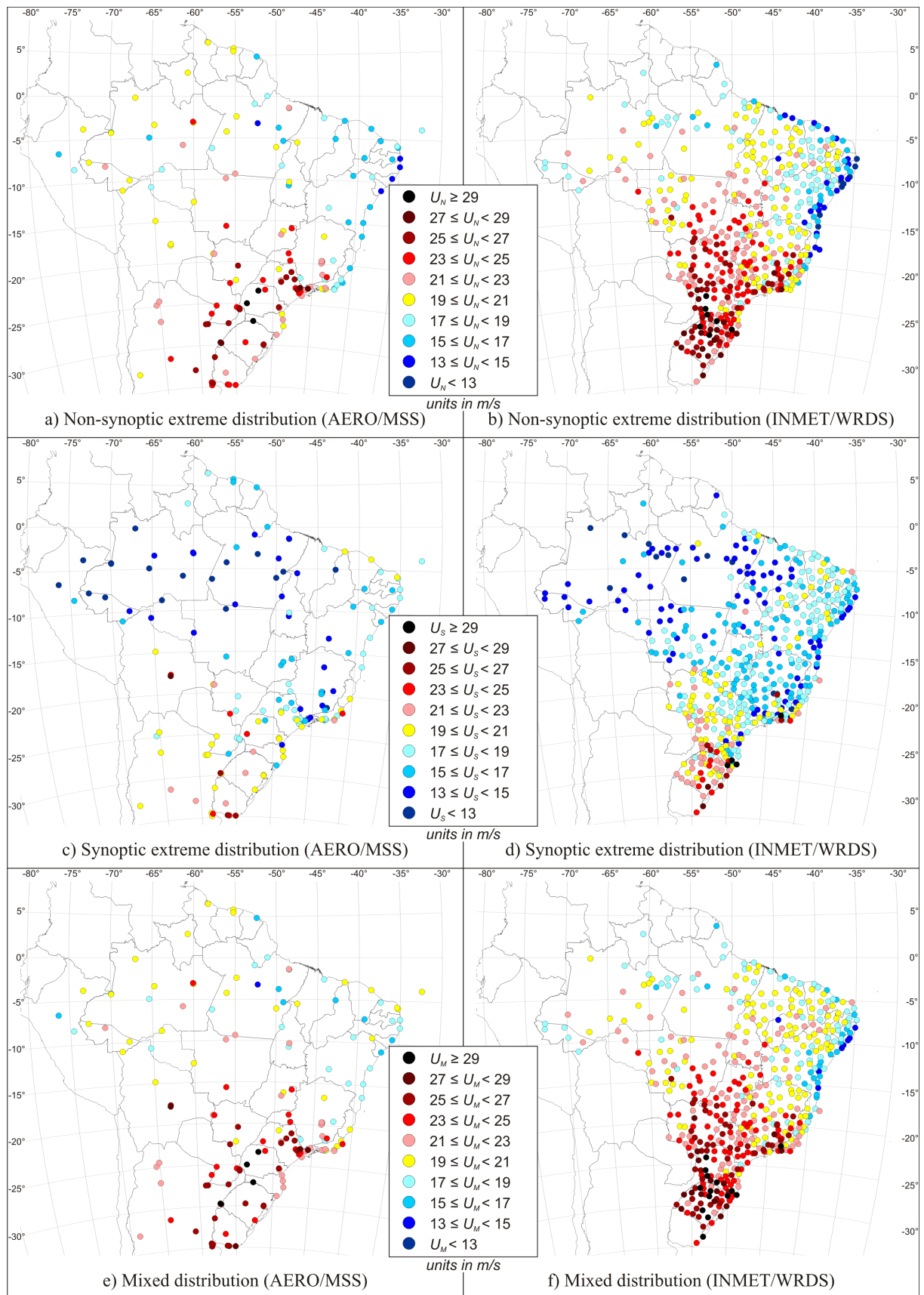
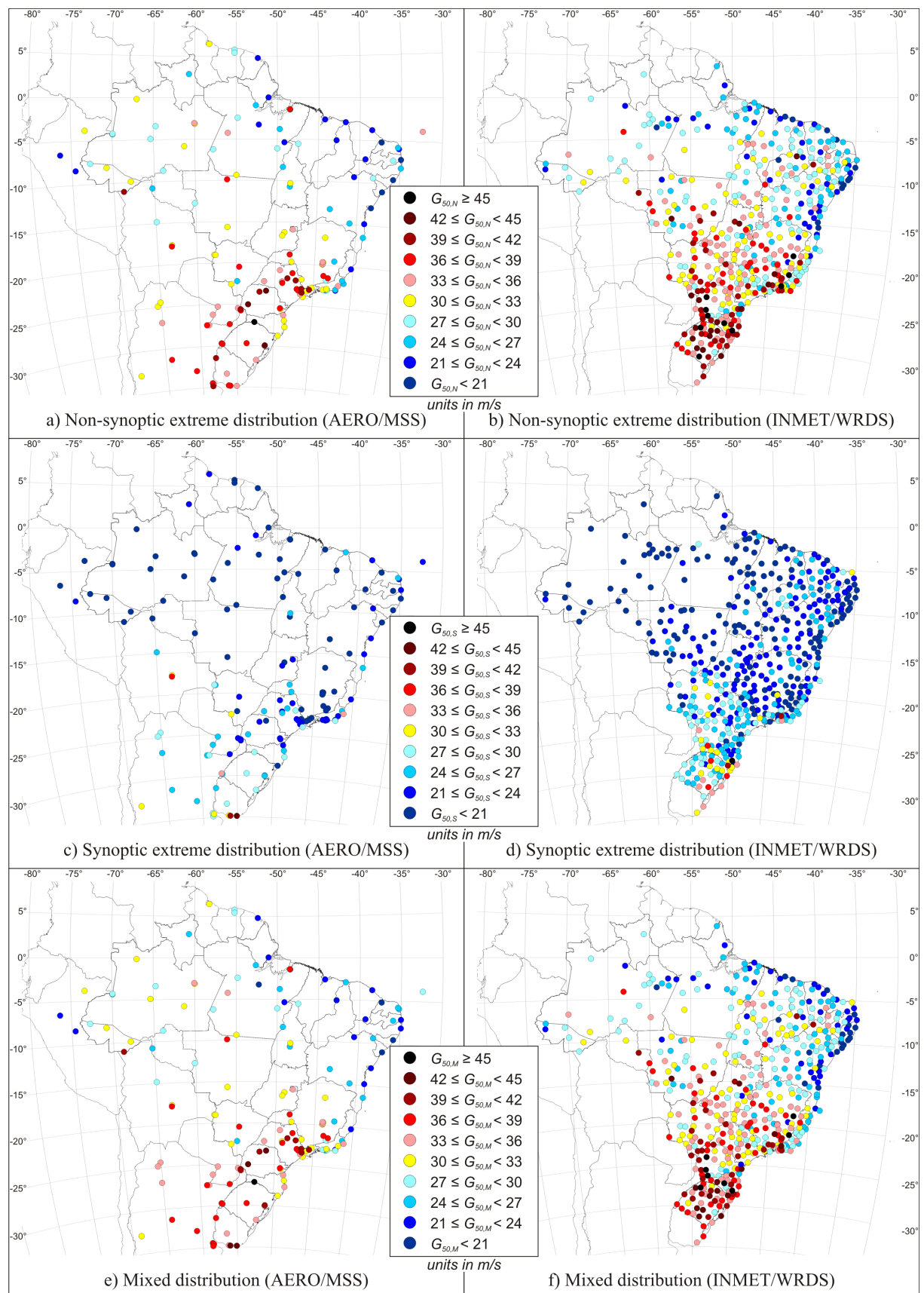


Figure H.11 – Annual growth rate of extreme wind events, pa (%).

Figure H.12 – Extreme distribution model parameter a .

Figure H.13 – Extreme distribution model parameter U (m/s).

Figure H.14 – 50-year return gust speed G_{50} (m/s).

APPENDIX I

ALTERNATIVE ZONE SOLUTIONS

A manual and iterative approach was undertaken to derive the regional wind climate models and their extents for both Type N and Type S winds. In order to maintain safety as the top priority, an averaging approach which considers all stations equally and smooths over the variations between stations in close proximity was rejected. Instead, the first step for each of the wind types was the identification of the most critical regions. For Type N winds this was western Paraná, western Santa Catarina, and north-western Rio Grande do Sul; for Type S winds this was coastal Rio Grande do Sul. The stations with the highest set of G_{50} in each region were selected to determine the representative climate model parameters. In the case of Zone N1 and S1, the most extreme zones for each wind type, seven SWS of $G_{50,N} \geq 46$ m/s and seven SWS of $G_{50,S} \geq 34$ m/s were selected to determine the respective wind climate models. An averaging scheme weighted by t_{tot} of each selected station determined the regional model parameters a , U and G_{50} , as represented by X in Equation I.1. Examples are given in Table I.1 and Table I.2 of the stations which contributed to the determination of a , U and G_{50} of Zones N1 and S1, both of which have $n = 7$ stations.

$$X_{zone} = \frac{\sum_{i=1}^n X_i \cdot t_{tot,i}}{\sum_{i=1}^n t_{tot,i}} \quad \text{I.1}$$

Table I.1 – Station contributions to Zone N1 wind climate model.

SWS (Dataset)	t_{tot} (years)	a	U (m/s)	G_{50} (m/s)
SBCH (MSS)	4.1	3.9	33.0	48.1
SBCH (PAS31-1)	3.9	3.4	33.7	47.1
SBCA (PAS31-1)	3.6	4.1	31.4	47.5
A843 (WDS)	7.7	4.7	30.1	48.5
A805 (WDS)	6.9	4.8	29.2	48.0
A816 (WDS)	8.3	4.5	30.4	48.0
A825 (WDS)	7.8	4.3	30.6	47.4
Total	42.3	4.4	30.8	47.9

Table I.2 – Station contributions to Zone S1 wind climate model.

SWS (Dataset)	t_{tot} (years)	a	U (m/s)	G_{50} (m/s)
A829 (WDS)	8.4	2.5	30.5	40.1
A811 (WDS)	10.6	2.6	28.3	38.3
A834 (WDS)	9.2	2.7	26.2	36.8
A812 (WDS)	11.2	3.0	24.8	36.3
A899 (WDS)	8.4	2.1	27.7	36.0
A878 (WDS)	8.8	2.3	26.1	35.0
A827 (WDS)	9.2	2.8	23.5	34.3
Total	65.8	2.6	26.7	36.7

Working outward from the most extreme zone, estimates of boundaries of the next zones were drawn. The same process was performed for the other zones at 3 m/s intervals, generating 7 zones for Type N and 6 zones for Type S winds. The contributing stations for each wind type are shown in c) of Figure I.1 and Figure I.2. Stations influenced by extreme topography were not considered in the determination of zone regional models, including A845 – Morro da Igreja, SC, A610 – Pico do Couto, RJ, and F501 – Cercadinha, MG. A minimum basic gust speed of 30 m/s for $R = 50$ years as proposed by Padaratz (1977) is to be maintained for Type N winds despite some regions, particularly the northeastern coastline, exhibiting lower basic wind speeds. Zone boundaries follow state boundaries where possible and are defined in Figure I.3 for Type N and Figure I.5 for Type S winds. Model parameters and return wind speeds are given in Table I.3 for Type N and Table I.4 for Type S winds. The return wind speeds of these tables are plotted in Figure I.4 for Type N and Figure I.6 for Type S winds.

Once the zone wind models of Table I.3 and Table I.4 were defined, comparisons were made between the individual station models and model of the zones in which they were located. Using U and G_{50} values as indicators, zones boundaries were adjusted from their original conceptions to reduce errors between station extreme distributions and their assigned zone, with alterations made for stations with higher t_{tot} . Data visualisation tools were utilized and include plots of station U vs a with return wind speeds, V_R , for each zone. Relevant plots are Figure I.7 for Type N and Figure I.8 for Type S winds. If a station's combination of U and a is above or to the right of a certain R line, the V_R wind speed for that station will be greater than that of the zone in which it's located. Each station's t_{tot} is also indicated. Stations which appear well beyond the R lines were investigated and many were identified to be subjected to topographic effects which could explain their outlier characteristics. Of the stations with more extreme characteristics and $t_{tot} > 10$ years, only A902 – Tangará da Serra, MT, for Type N and A839 – Passo Fundo, RS, for Type S, were located in flat terrain.

Differences between U and G_{50} of individual SWS and their zones, represented by $e(U)$ and $e(G_{50})$, were plotted against t_{tot} in Figure I.9 and Figure I.10 for U and G_{50} of Type N winds, and Figure I.11 and Figure I.12 for U and G_{50} of Type S winds. A positive difference indicates zone values greater than station values. From these tools the following adjustments were made:

- Northern cities of Manaus, AM, and Belém, PA, were re-classified from Zone N6 and N7 to Zone N5 respectively. Prior to the adjustment, SBEG – Manaus, with $t_{tot} = 15.9$

years, was approximately 15% above U of Zone N6, and SBBE – Belém, with t_{tot} of 15.6 years, was approximately 16% above U , and 22% above V_{50} of Zone N7.

- The southern region of Minas Gerais was re-classified as Zone N4 due to a grouping of SWS in Juiz de Fora and Barbacena which exhibited characteristics more extreme than Zone N5 for which they were originally classified. As such, Zone N5 was extended from São Paulo across southern Minas Gerais causing Zone N6 to break into two separate regions.
- Re-classification of Palmas, TO, from Zone S5 to Zone S4.
- Re-classification of the state of Roraima from Zone S6 to Zone S5.

The majority of inland Bahia SWS exhibit Type N characteristics closer to that of Zone N7 as opposed to Zone N6 as seen in Figure I.1. Discretion was used to re-classify this region from Zone N7 to Zone N6. A noticeable difference in G_{50} is observed at the border of Bahia (4th DISME) with its neighbouring states: Minas Gerais (5th DISME) to the south, Tocantins and Goiás (10th DISME) to the west, and Piauí and Pernambuco (3rd DISME) to the north. There is no known meteorological, topographical or geographical reason for these differences, suggesting administrative or operational reasons. The filtering of extreme wind events for both SADMET and Web sources of INMET data was previously identified in this study, however the whole extent of the practice remains unknown. Taking this into consideration, inland Bahia was re-classified as Zone N6 to best match its neighbouring states.

Discretion was also used in the extension of Zone S1 from coastal Rio Grande do Sul to the northern border of neighbouring Santa Catarina. Although not represented in data acquired along the coast of Santa Catarina, there are concerns that this region may be adversely affected by change in global climate. Two TCs have affected this region over the past 15 years have, include the destruction caused by TC Catarina when it made landfall in March of 2004, and the transition of subtropical cyclone Anita to TC in March of 2010 (Loredo-Souza, 2012). The first known subtropical cyclone to form on the Santa Catarina coast was observed in December of 2016, with observed winds reaching gusts of up to 64 kt at SBFL – Florianópolis. Further anecdotal evidence of the potential threat of climate change is the development of a rare tropical storm Iba off the coast of Bahia and Espírito Santo in March of 2019, and the development of subtropical cyclone Lexi in May of 2018 off the coast of Chile, the most western subtropical cyclone in the Southern Pacific Ocean.

The residuals, e (%), of U and G_{50} , the differences between individual SWS results and zonal models, are plotted against sampling periods in Figure I.9 and Figure I.10 for non-synoptic winds and Figure I.11 and Figure I.12 for synoptic winds. Figure I.9 to Figure I.12 reveal that stations with positive residuals, station U and G_{50} values greater than those of zone models, are restricted to those with $t_{tot} < 15$ years. There are few stations of $t_{tot} > 15$ years for which U or G_{50} are 5% or more than their zones, but all stations of $t_{tot} > 20$ years have differences of 5% or less in U and G_{50} when compared to their zones. In average terms, U is approximately 10% and 15% less at SWS than the proposed zones for Type N and S wind respectively. For G_{50} , mean SWS values are approximately 18% and 20% less at SWS than the proposed zones. For mean plus one standard deviation, U and G_{50} are equal to, or less than, those of proposed zone models, giving confidence in the proposed maps' ability to deliver security in regard to extreme wind speeds across Brazil.

The 50-year return gust speeds of Zone N5 and S1 are comparable to Australia's 50-year return gust speed for non-TC Region A (AS/NZS, 2011) of 36 m/s for $\tau = 3$ s (39 m/s for $\tau = 0.2$ s), while the highest non-TC gust speed for continental United States of 41 m/s (ASCE, 2016) is comparable to Zone N3 for 50-year return wind speed.

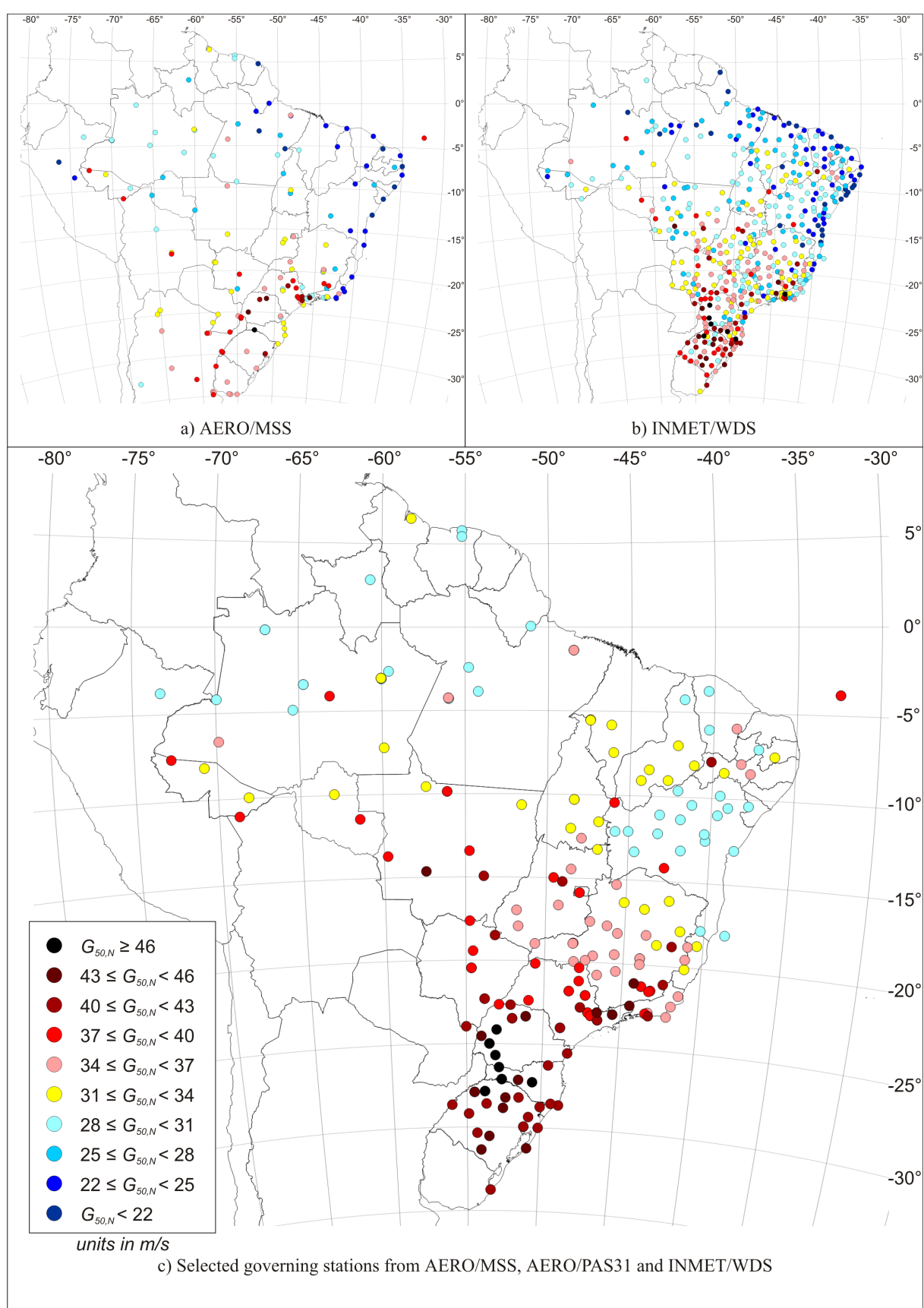


Figure I.1 – Non-synoptic extreme wind $R = 50$ -year return period homogenised gust speeds for individual stations.

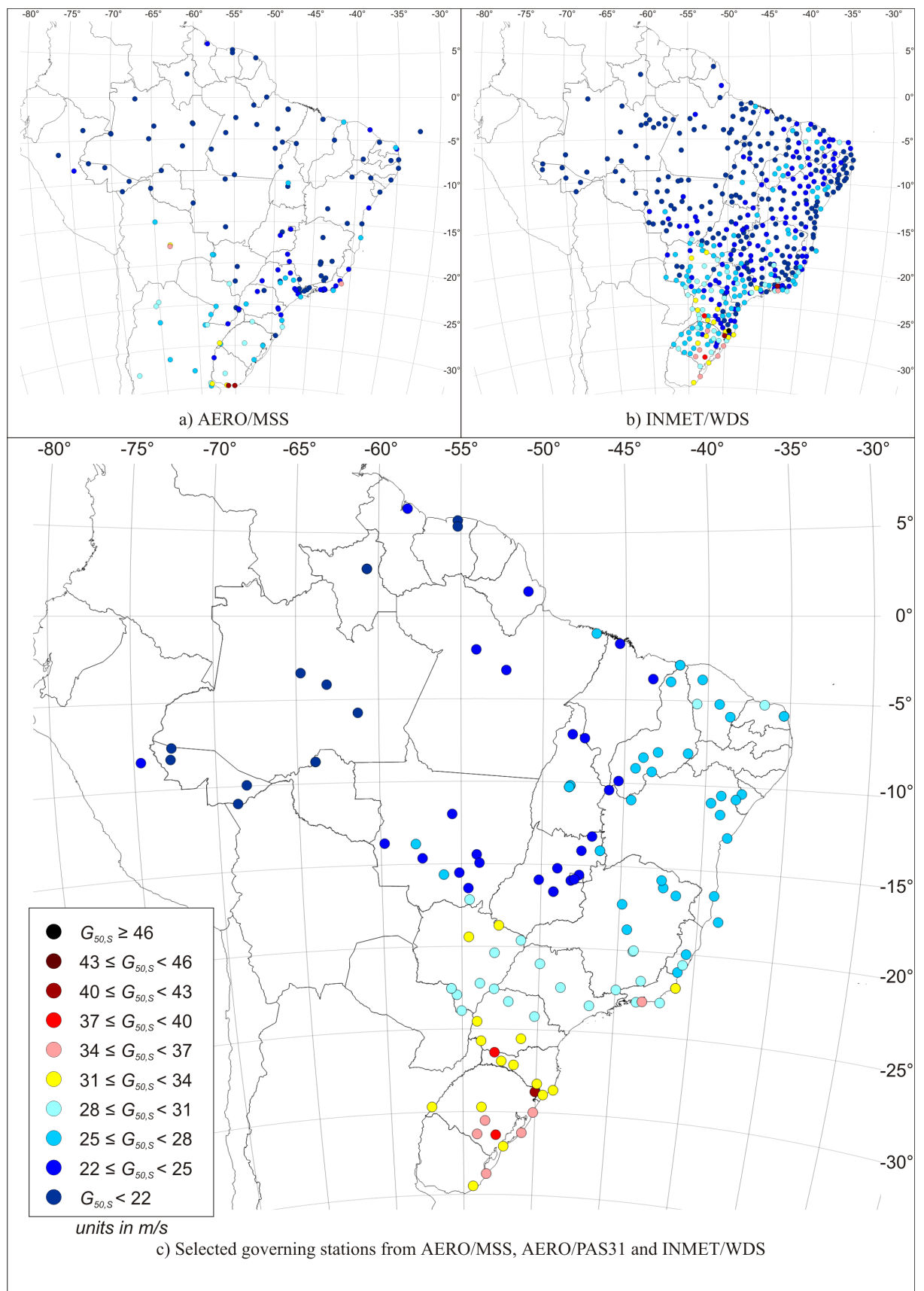


Figure I.2 – Synoptic extreme wind $R = 50$ -year return period homogenised gust speeds for individual stations.

R (years)	N1 (m/s)	N2 (m/s)	N3 (m/s)	N4 (m/s)	N5 (m/s)	N6 (m/s)	N7 (m/s)
1	31	28	27	25	23	21	19
10	41	38	36	33	30	27	25
100	51	48	45	42	38	35	32
1000	62	58	54	50	46	42	38

Modelo Climático para Ventos Extremos no Brasil/Brazilian Extreme Wind Climate



Figure I.5 – Definition of zones for Type S extreme winds (synoptic).

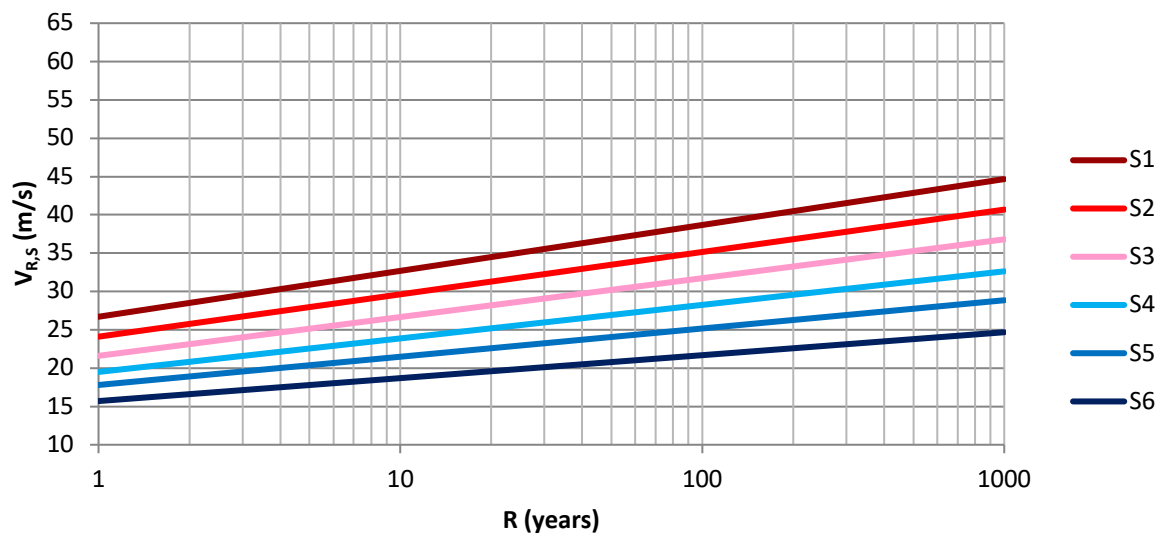


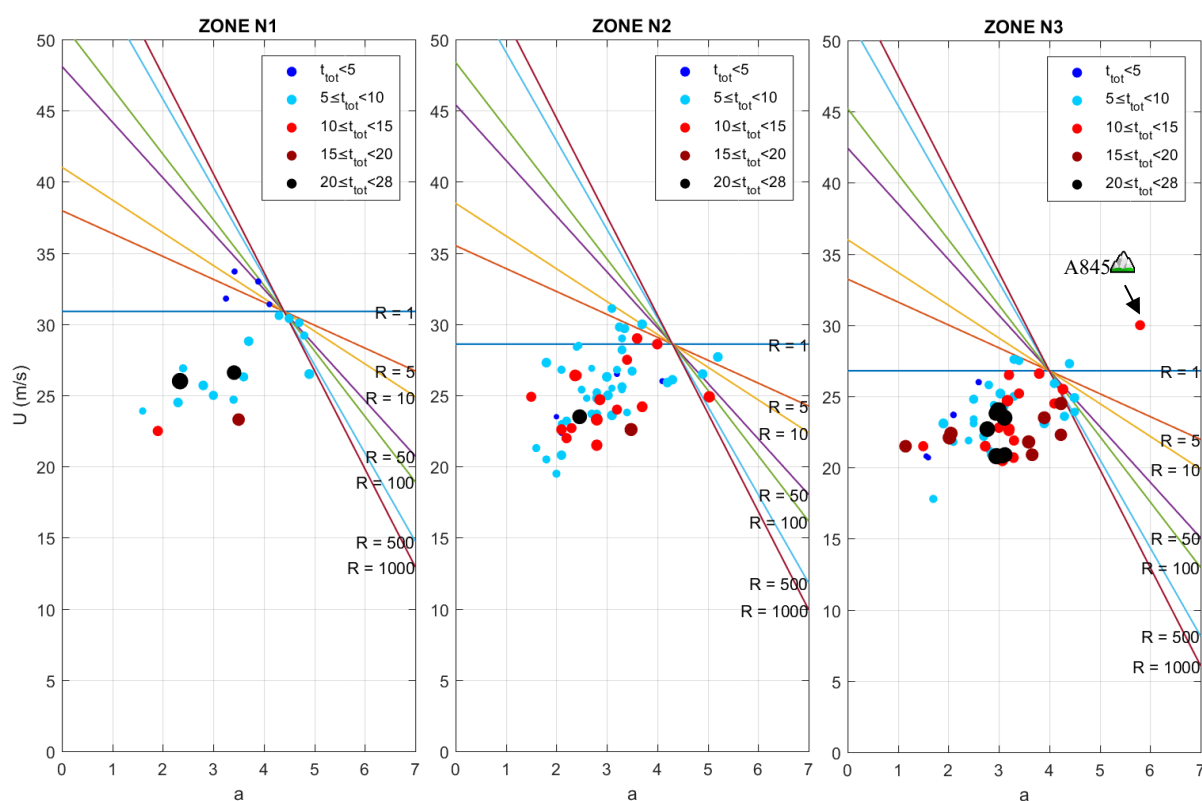
Figure I.6 – Type S (synoptic) wind speed as function of return period.

Table I.3 – Model parameters for Type N winds (non-synoptic) and basic wind speed, $V_{R,N}$.

Zone	U (m/s)	a	R (years)								
			1	5	10	20	50	100	200	500	1000
N1	30.9	4.4	31	38	41	44	48	51	54	58	61
N2	28.6	4.3	29	36	39	41	45	48	51	55	58
N3	26.8	4.0	27	33	36	39	42	45	48	52	54
N4	25.0	3.7	25	31	34	36	39	42	45	48	51
N5	23.0	3.4	23	28	31	33	36	39	41	44	46
N6	21.2	3.1	21	26	28	30	33	35	38	40	43
N7	19.5	2.7	20	24	26	28	30	32	34	36	38

Table I.4 – Model parameters for Type S winds (synoptic) and basic wind speed, $V_{R,S}$.

Zone	U (m/s)	a	R (years)								
			1	5	10	20	50	100	200	500	1000
S1	26.7	2.6	27	31	33	34	37	39	40	43	45
S2	24.1	2.4	24	28	30	31	33	35	37	39	41
S3	21.6	2.2	22	25	27	28	30	32	33	35	37
S4	19.5	1.9	20	23	24	25	27	28	30	31	33
S5	17.8	1.6	18	20	21	23	24	25	26	28	29
S6	15.7	1.3	16	18	19	20	21	22	23	24	25

Figure I.7 – Comparison of individual SWS and zone V_R for Type N winds.

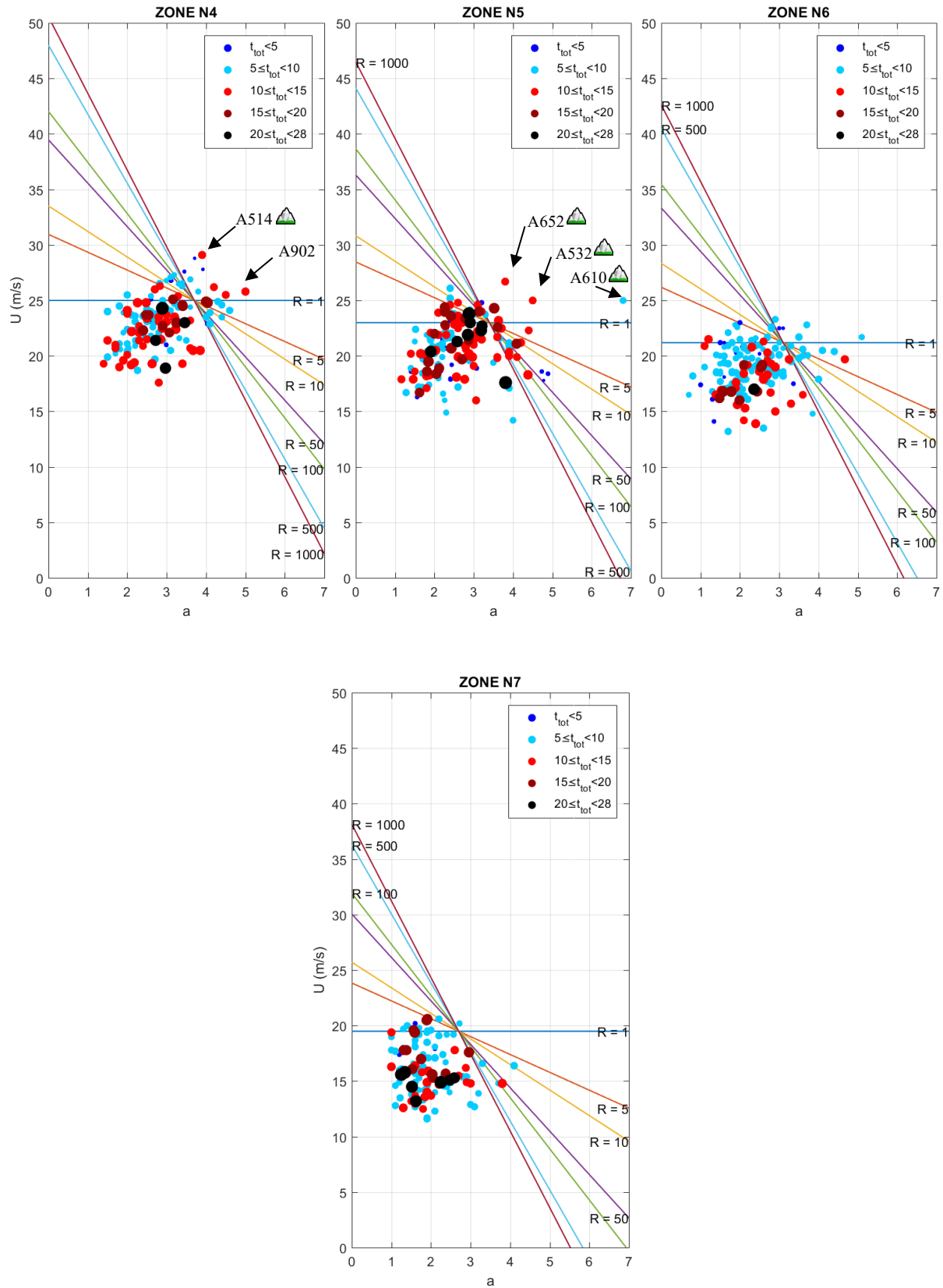


Figure I.7 (...cont) – Comparison of individual SWS and zone V_R for Type N winds.

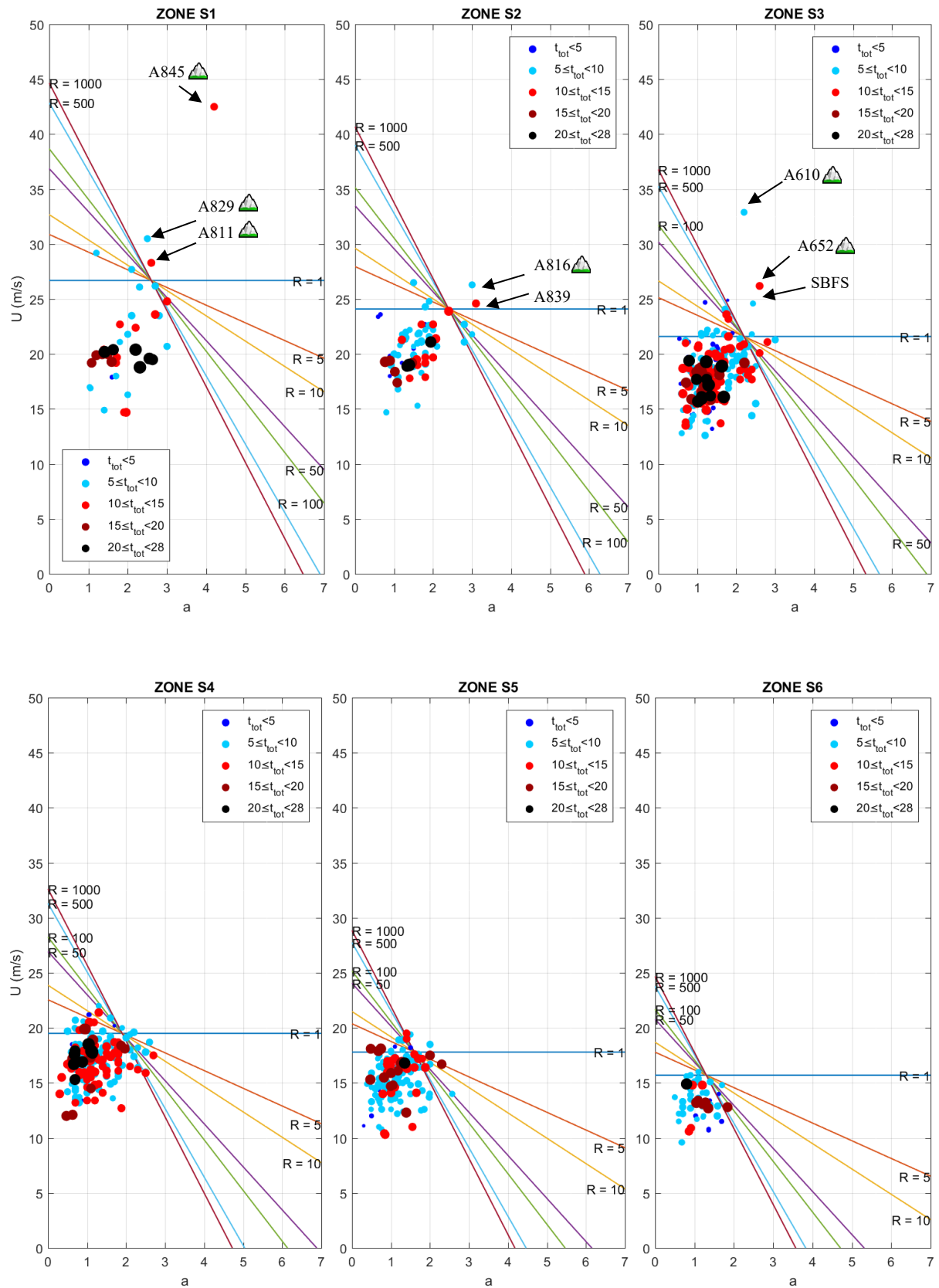


Figure I.8 – Comparison of individual SWS and zone V_R for Type S winds.

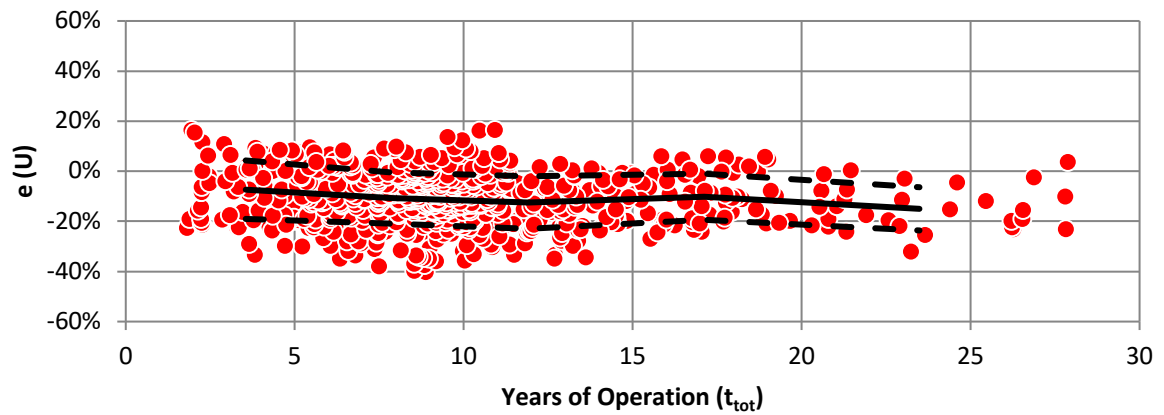


Figure I.9 – Residuals of U for Type N winds against sampling period t_{tot} (years).

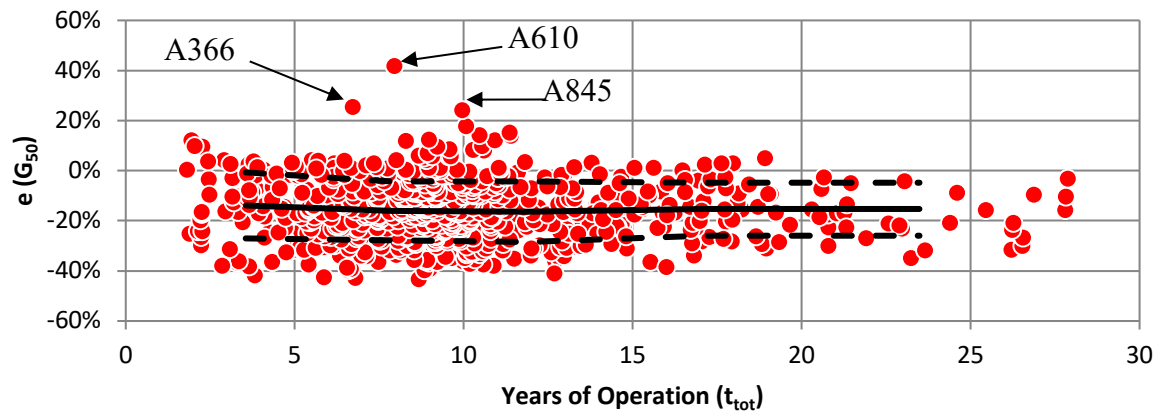


Figure I.10 – Residuals of G_{50} for Type N winds against sampling period t_{tot} (years).

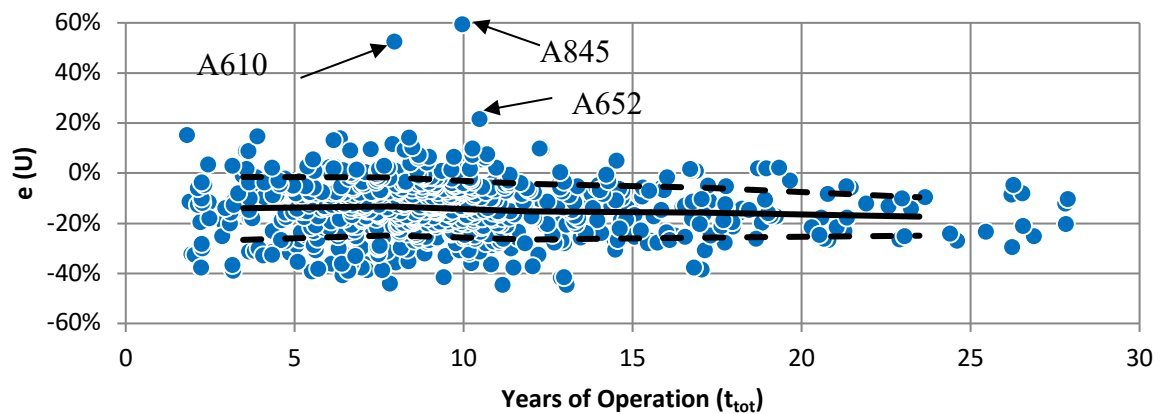


Figure I.11 – Residuals of U Type S winds against sampling period t_{tot} (years).

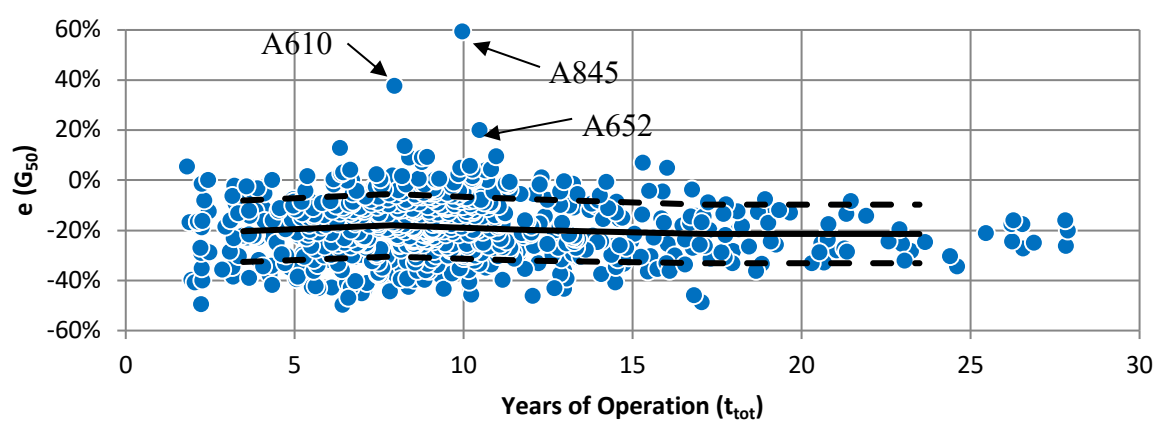


Figure I.12 – Residuals of G_{50} for Type S winds against sampling period t_{tot} (years).

APPENDIX J

LOCAL POLYNOMIAL REGRESSION SOLUTION

Commercial software package, MapViewer 8 by Golden Software, was employed to determine the isopleth contours fitted to discrete SWS scalar data (such as G_{50} , U , and e). The selected gridding method was local polynomial regression, also referred to as LOWESS (Locally Weighted Scatterplot Smoothing). Using a weighted least squares regression technique, scalars (Z_o) were determined at node locations (X_o , Y_o) within a grid of 100 x 100 equally spaced nodes. At each node, SWS were identified within a radius of $R = 3,000$ km for $4 \times 90^\circ$ sectors. A maximum of 16 SWS was permitted per sector, with N representing the total number of contributing SWS within the neighbourhood. The coordinates of each SWS are represented by (X_i , Y_i) and scalar data at this datum is represented by Z_i .

The weighted sum of the squared residuals, e_w , was determined by Equation J.1, with the weighting of each SWS represented by W_i . 1st, 2nd and 3rd order polynomials, $F(X,Y)$, were available for implementation, as shown in Equations J.2 to J.4. Model parameters (a to j) were determined by the minimization of e_w . The weighting of each SWS was determined by Equation J.5, which is a function of the normalised distance from the node under consideration (Equation J.6) and a user defined power, p_L . The closer the SWS to the node under consideration, the larger the weighting assigned to its scalar.

$$e_w = \sum_{i=1}^N W_i [F(X_i, Y_i) - Z_i]^2 \quad \text{J.1}$$

1st order:

$$F(X, Y) = a + bX + cY \quad \text{J.2}$$

2nd order:

$$F(X, Y) = a + bX + cY + dXY + eX^2 + fY^2 \quad \text{J.3}$$

3rd order:

$$F(X, Y) = a + bX + cY + dXY + eX^2 + fY^2 + gX^2Y + hXY^2 + iX^3 + jY^3 \quad \text{J.4}$$

$$W_i = (1 - R_i)^{p_L} \quad \text{J.5}$$

$$R_i = \sqrt{\left(\frac{X_i - X_o}{R}\right)^2 + \left(\frac{Y_i - Y_o}{R}\right)^2} \quad \text{J.6}$$

Software users have the option of selecting the search radius, R , number of grid nodes for both orthogonal directions, number of search sectors, maximum number of datum per search sector, the order of local polynomial $F(X,Y)$ and power, p_L . With the exception of $F(X,Y)$ and p_L , controls were set at, or near to, the recommended default settings. A sensitivity study was performed for the governing set of SWS for non-synoptic 50-year return wind speeds, $G_{50,N}$, in order to determine the most appropriate combination of polynomial order and power to be applied to the weightings.

Solutions for 1st order polynomials are shown in Figure J.1, 2nd order polynomials in Figure J.2 and 3rd order polynomials in Figure J.3. Six different values of p_L were plotted for each of the polynomial orders from 2 to 12 at intervals of $p_L = 2$. The $G_{50,N}$ values for each of the individual SWS can be found mapped in Figure 8a) at listed in table format in Appendix C *Extreme Distributions of SWS*.

The 18 (3x6) solutions were assessed in a qualitative manner in order to determine the most appropriate combination of $F(X,Y)$ and p_L . It was determined that solutions provided by 1st order polynomials were too general (smooth) and did not adequately represent western Paraná, Santa Catarina and Rio Grande do Sul, the region home to the most extreme non-synoptic wind speeds. Although this region was adequately captured by the 3rd order polynomials, particularly for $p_L \geq 6$, the regions in the northwest of Pará and northwest of Amazonas appear unstable with sharp gradients which are not representative of the input data. For the 2nd order schemes, only those with $p_L \geq 6$ satisfactorily represented the southwestern region of the country. A significant number of highly localised contours were produced for $p_L = 10$ and 12, which was undesirable. Although two such regions were produced for the 2nd order polynomial with $p_L = 8$, this combination was selected as the optimal case due to the smoother contour lines and larger region of $G_{50,N} \geq 45$ m/s when compared to the $p_L = 6$ case.

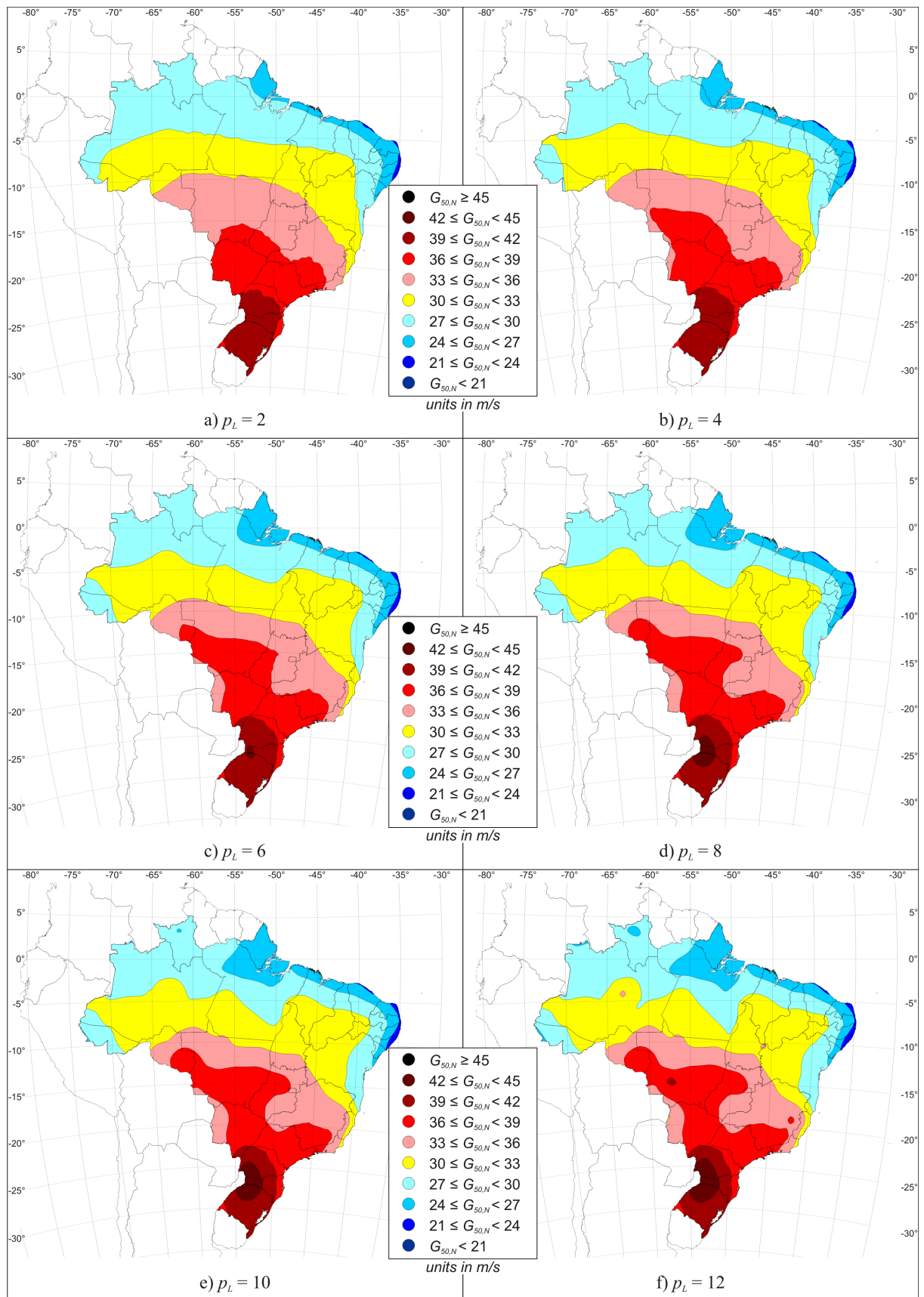


Figure J.1 – Solutions for governing $G_{50,N}$ using 1st order polynomial and varying p_L .

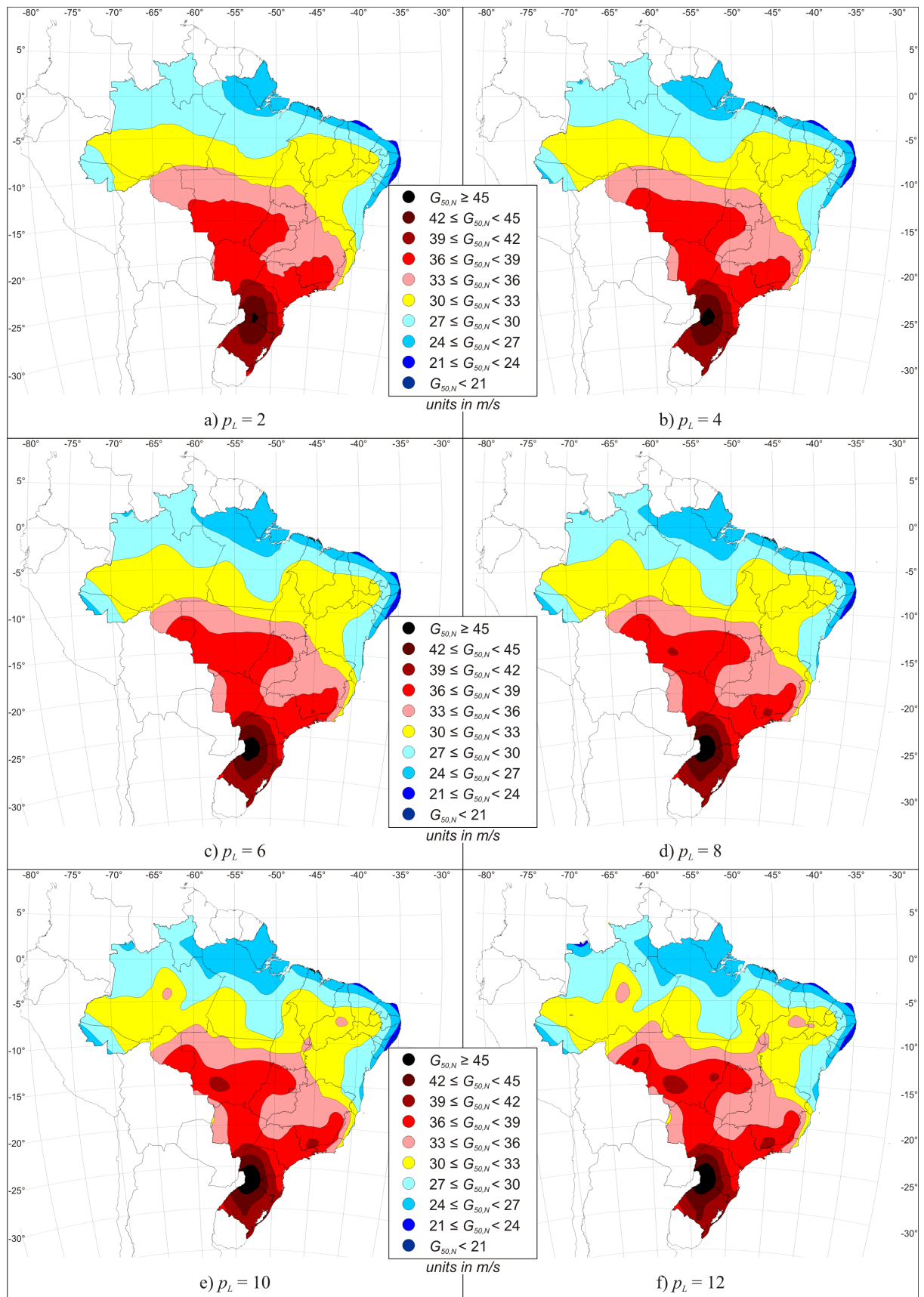


Figure J.2 – Solutions for governing $G_{50,N}$ using 2nd order polynomial and varying p_L .

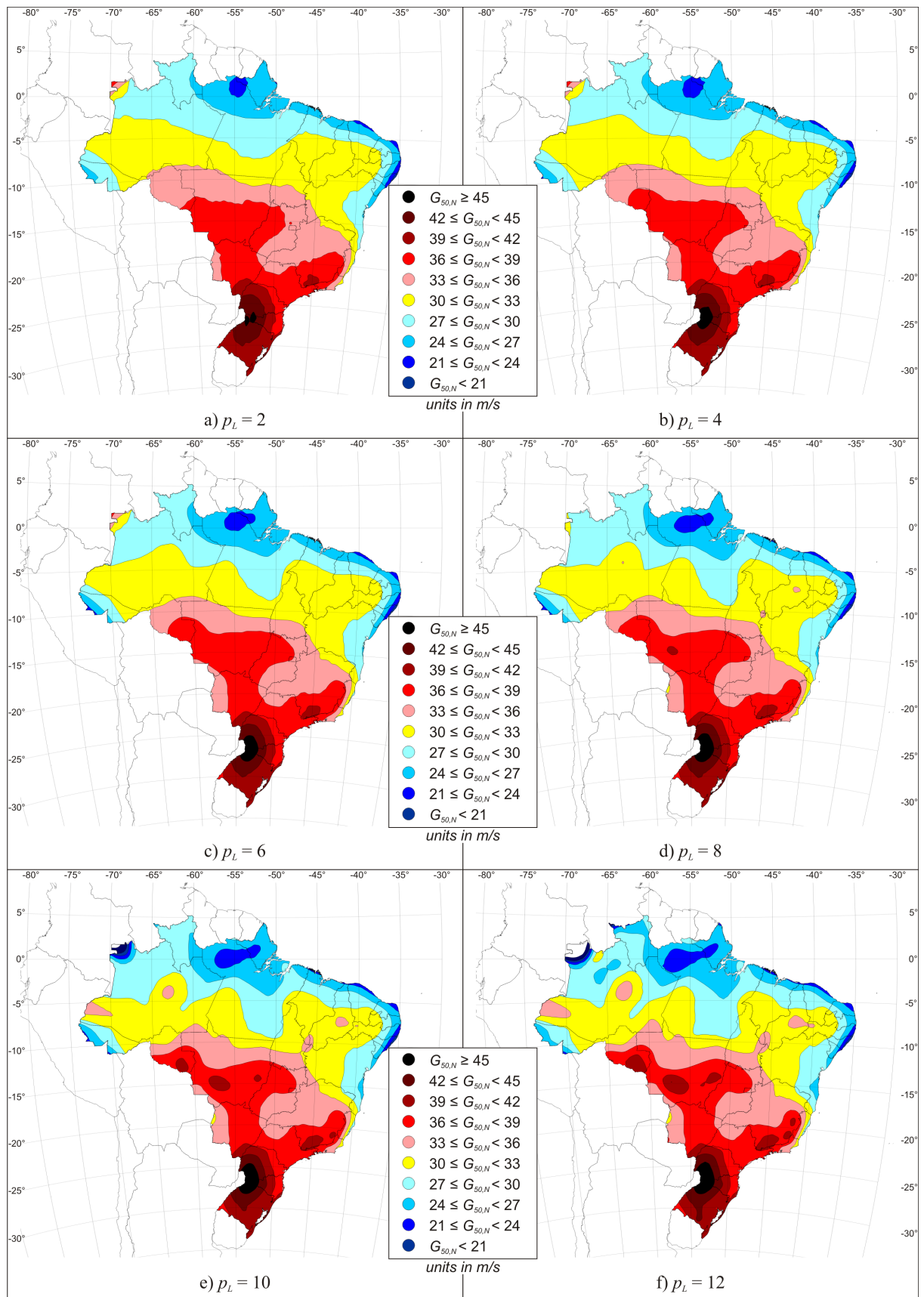


Figure J.3 – Solutions for governing $G_{50,N}$ using 3rd order polynomial and varying p_L .

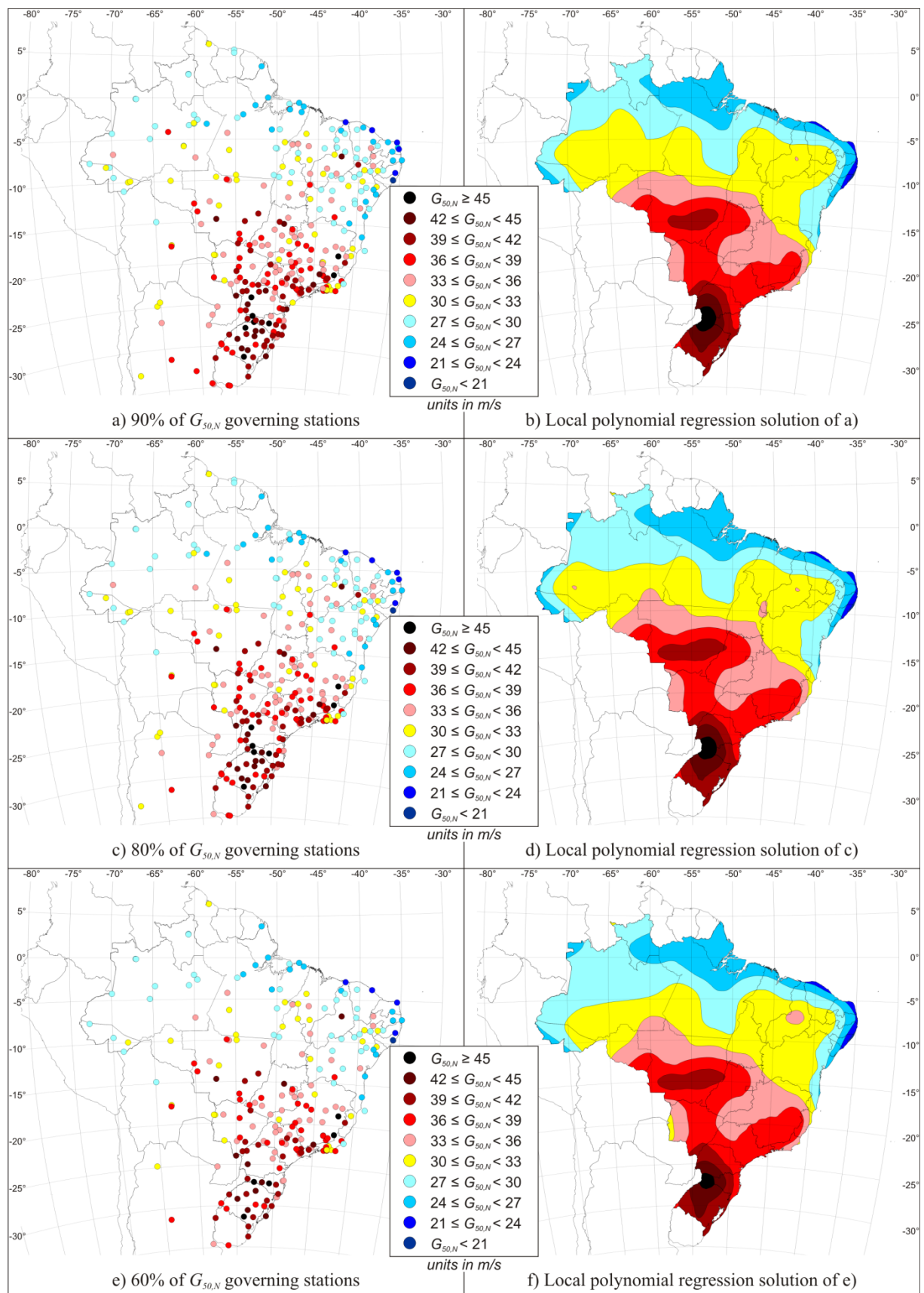


Figure J.4 – Solutions of $G_{50,N}$ for reduced number of governing stations.

APPENDIX K

DETERMINATION OF PROBABILISTIC FACTOR S_3

S₃ of NBR 6123 (ABNT, 1988)

The following steps generate Table K.1 and Equation 2.12 which define the ratio between a wind speed with a certain annual probability of exceedance or mean recurrence interval, V_R , and the basic velocity, V_0 , which is defined for $R_L = R_P = 50$ years. P_L , the probability of exceedance over a lifetime R_L years for a given annual probability of non-exceedance, P , is defined in Equation K.1, which is expanded in Equation K.2 to show the relationship with return period, R_P .

$$P_L = 1 - P^{R_L} \quad \text{K.1}$$

$$P_L = 1 - \left(1 - \frac{1}{R_P}\right)^{R_L} \quad \text{K.2}$$

The mathematical definition of S_3 is shown in Equation K.3.

$$S_3 = \frac{V_R}{V_0} \quad \text{K.3}$$

V_0 must first be defined in terms of its Fréchet distribution. Equation 2.10 is re-arranged to present X as a function of P as shown in Equation K.4. Equation 2.11 is then substituted into Equation K.4 to create Equation K.5, and solved for $R_P = 50$ and $\gamma = \gamma_{mp} = 6.369$, giving V_0 as a function of β as shown in Equation K.6.

$$X = \beta [-\ln(P)]^{-1/\gamma} \quad \text{K.4}$$

$$V_R = \beta \left[-\ln \left(1 - \frac{1}{R_P} \right) \right]^{-1/\gamma} \quad \text{K.5}$$

$$V_0 = 1.845\beta \quad \text{K.6}$$

P_L is defined as per Equation K.1 and is re-arranged in Equation K.7.

$$P = [1 - P_L]^{1/R_L} \quad \text{K.7}$$

Returning to Equation K.4 and substituting in $P(X)$ from Equation K.7 gives Equation K.8, which is then simplified to the familiar form of Equation K.9.

$$V_R = \beta [-\ln([1 - P_L]^{1/R_L})]^{-1/\gamma} \quad \text{K.8}$$

$$V_R = \beta \left[-\frac{\ln(1 - P_L)}{R_L} \right]^{-1/\gamma} \quad \text{K.9}$$

Substituting V_R and V_0 from Equations K.6 and K.9, respectively, gives Equation K.10 which is equal to Equation 2.12 once $\gamma = \gamma_{mp} = 6.369$ is substituted.

$$\frac{V_R}{V_0} = 0.54 \left[-\frac{\ln(1 - P_L)}{R_L} \right]^{-1/\gamma} \quad \text{K.10}$$

In the special case of $R_P = R_L$, as R_L tends to ∞ , P_L tends to 0.63 due to the special limit case shown in Equation K.11. For $P_L = 0.63$, both R_P and R_L are replaced by the mean recurrence interval, R . Different to R_P , R can be defined for periods equal to, or less than, 1 year.

$$\lim_{x \rightarrow \infty} \left(1 - \frac{1}{x} \right)^x = \frac{1}{e} \quad \text{K.11}$$

Table K.1 – NBR 6123 S_3 factors (ABNT, 1988).

R_L (years)	P_L					
	0.10	0.20	0.50	0.63	0.75	0.90
2	0.86	0.76	0.64	0.60	0.57	0.53
10	1.10	0.98	0.82	0.78	0.74	0.68
25	1.28	1.13	0.95	0.90	0.85	0.79
50	1.42	1.26	1.06	1.00	0.95	0.88
100	1.58	1.42	1.18	1.11	1.06	0.98

Table K.2 – Minimum permitted values of probabilistic factor, S_3 (ABNT, 1988).

Group	Description	S_3
1	Buildings whose total or partial failure could affect security or assistance to people after a destructive storm (hospitals, fire stations, security forces, communication centres, etc.)	1.10
2	Hotels, residences, commerce and industry with high occupation rates	1.00
3	Buildings and industrial complexes with low occupation rates (deposits, silos, rural buildings, etc.)	0.95
4	External sealants (roofs, glazing, sealing panels, etc.)	0.88
5	Temporary structures and Group 1-3 structures during construction phase	0.83

Proposed Updated S_3

Gumbel form (Type I) of GEVD ($k=0$):

$$P(X) = \exp \left[-\exp \left(-\frac{X - U}{a} \right) \right] \quad \text{K.12}$$

Re-organisation of Equation K.12:

$$X = U - a \cdot \ln[-\ln(P)] \quad \text{K.13}$$

For $P = 1 - 1/R_P$ and $X = V_R$:

$$V_R = U - a \cdot \ln \left[-\ln \left(1 - \frac{1}{R_P} \right) \right] \quad \text{K.14}$$

Substituting Equation 7.2, $U = 7a$, into Equation K.14:

$$V_R = a \left\{ 7 - \ln \left[-\ln \left(1 - \frac{1}{R_P} \right) \right] \right\} \quad \text{K.15}$$

For $R_P = 50$, $V_R = V_0$:

$$V_0 = a \left\{ 7 - \ln \left[-\ln \left(1 - \frac{1}{50} \right) \right] \right\} \quad \text{K.16}$$

$$V_0 = 10.9a \quad \text{K.17}$$

Substituting Equation K.7 into Equation K.15:

$$V_R = a \left\{ 7 - \ln \left[\frac{-\ln(1 - P_L)}{R_L} \right] \right\} \quad \text{K.18}$$

Substituting Equation K.18 and Equation K.17 into Equation K.3 removes variable a :

$$S_3 = \frac{1}{10.9} \left\{ 7 - \ln \left[\frac{-\ln(1 - P_L)}{R_L} \right] \right\} \quad \text{K.19}$$

Table K.3 – Wind speeds for various mean recurrence intervals, V_R , in m/s ($P_L = 0.63$).

V_0	R (years)														
	1	2	5	10	15	20	25	50	100	150	200	250	500	700	1000
30	19	21	24	26	27	28	28	30	32	33	34	34	36	37	38
31	20	22	25	26	28	28	29	31	33	34	35	36	38	39	40
32	21	23	25	27	29	29	30	32	34	35	36	37	39	40	41
33	21	23	26	28	29	30	31	33	35	36	37	38	40	41	42
34	22	24	27	29	30	31	32	34	36	37	38	39	41	42	43
35	22	25	28	30	31	32	33	35	37	39	40	40	42	44	45
36	23	25	28	31	32	33	34	36	38	40	41	41	44	45	46
37	24	26	29	32	33	34	35	37	39	41	42	43	45	46	47
38	24	27	30	32	34	35	36	38	40	42	43	44	46	47	49
39	25	28	31	33	35	36	37	39	42	43	44	45	47	49	50
40	26	28	32	34	36	37	38	40	43	44	45	46	49	50	51
41	26	29	32	35	37	38	38	41	44	45	46	47	50	51	52
42	27	30	33	36	37	39	39	42	45	46	47	48	51	52	54
43	28	30	34	37	38	39	40	43	46	47	49	49	52	53	55
44	28	31	35	38	39	40	41	44	47	49	50	51	53	55	56
45	29	32	36	38	40	41	42	45	48	50	51	52	55	56	57
46	30	32	36	39	41	42	43	46	49	51	52	53	56	57	59

APPENDIX L

MAPPED RESIDUALS OF CONTOUR SOLUTIONS

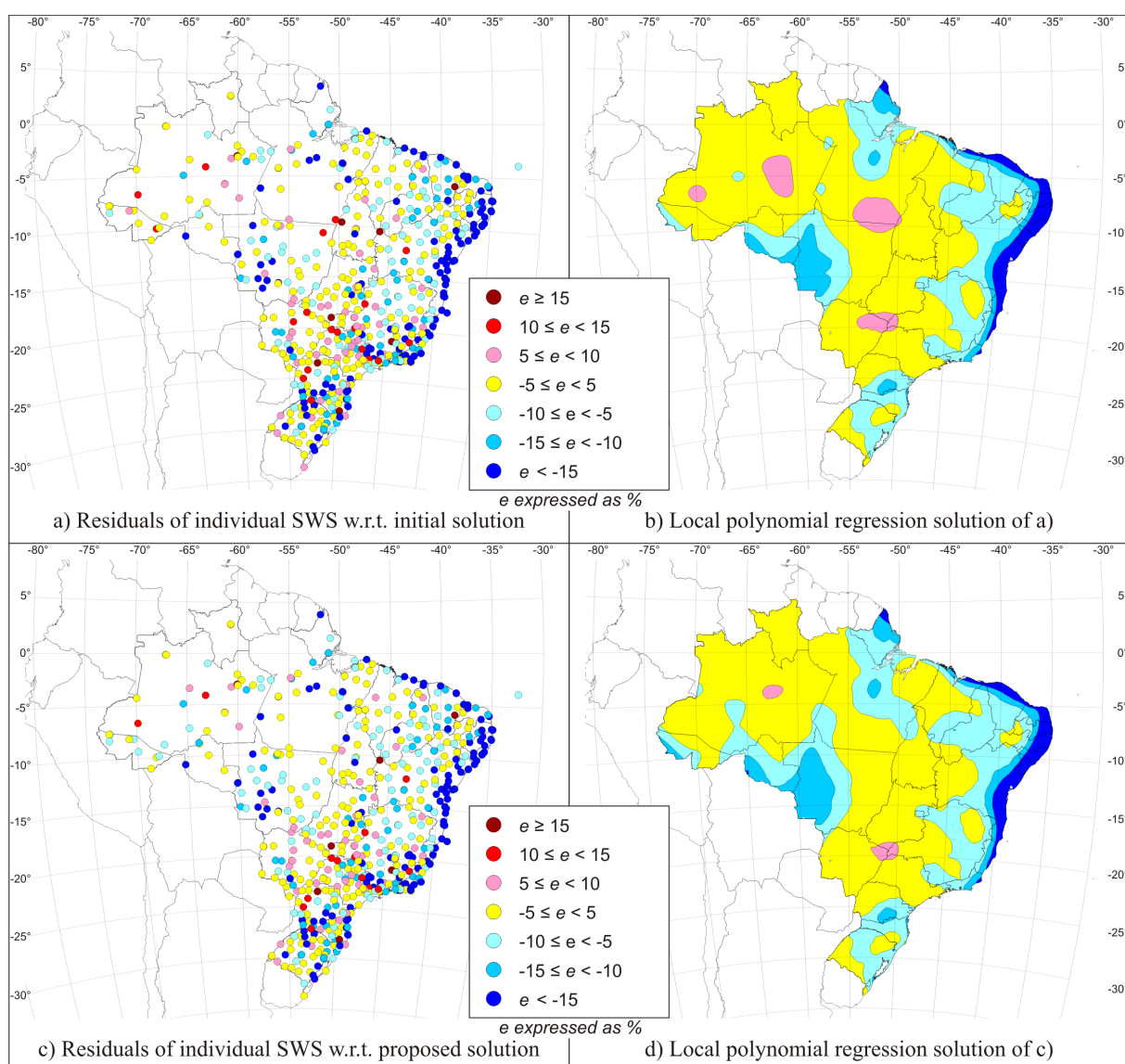


Figure L.1 – Residuals of U_N for all SWS.

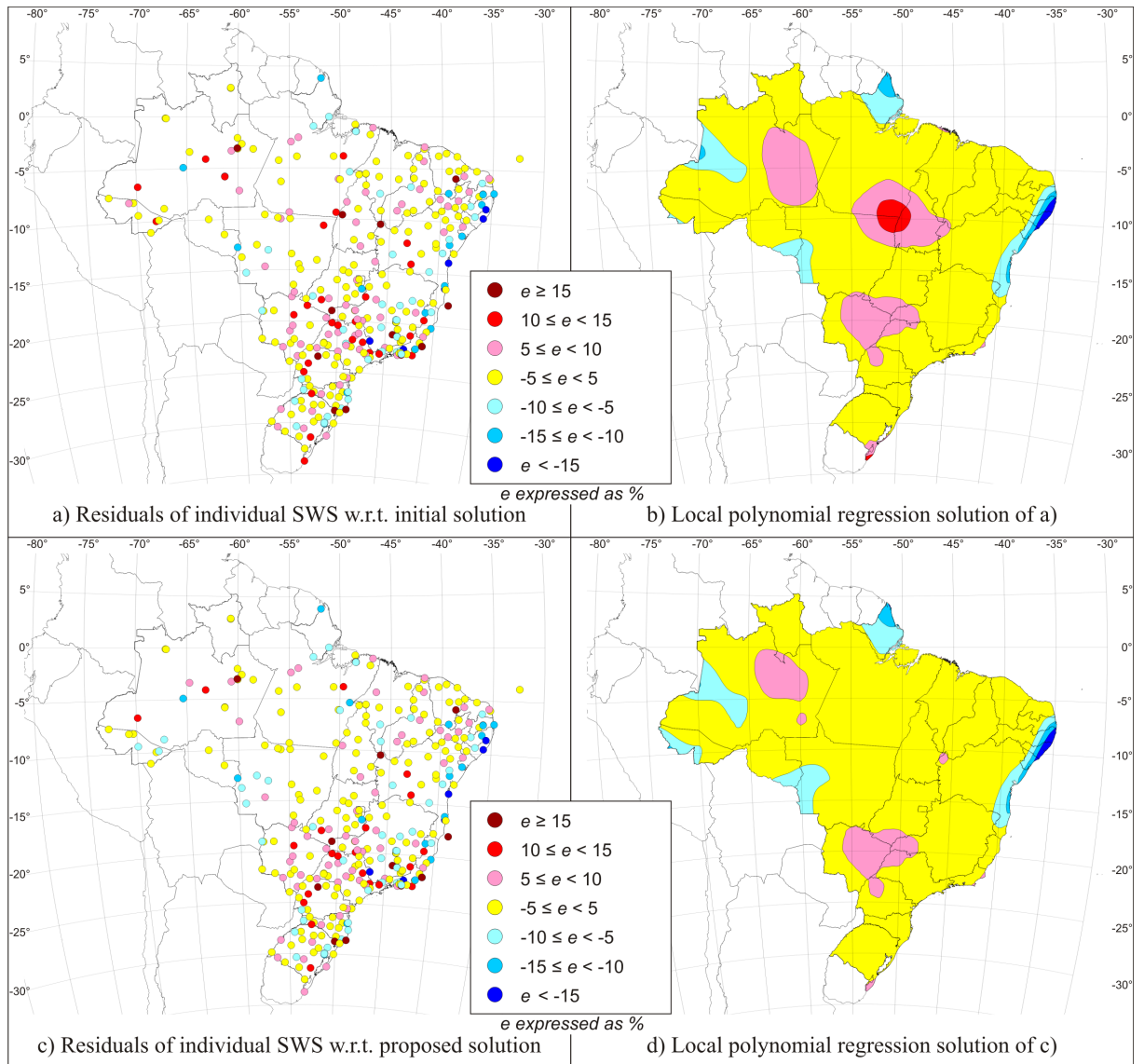


Figure L.2 – Residuals of U_E for governing SWS.

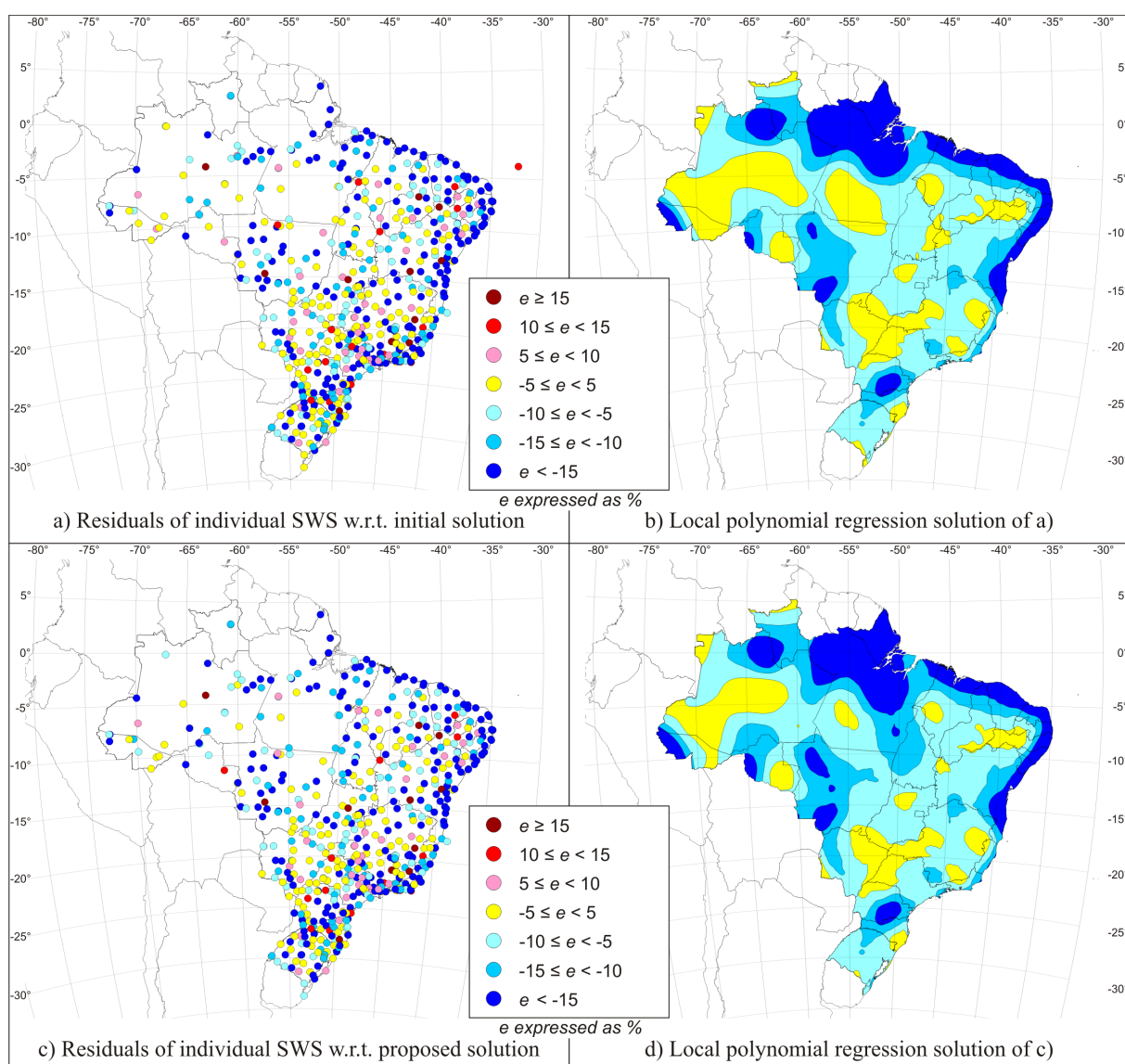


Figure L.3 – Residuals of $G_{50,N}$ for all SWS.

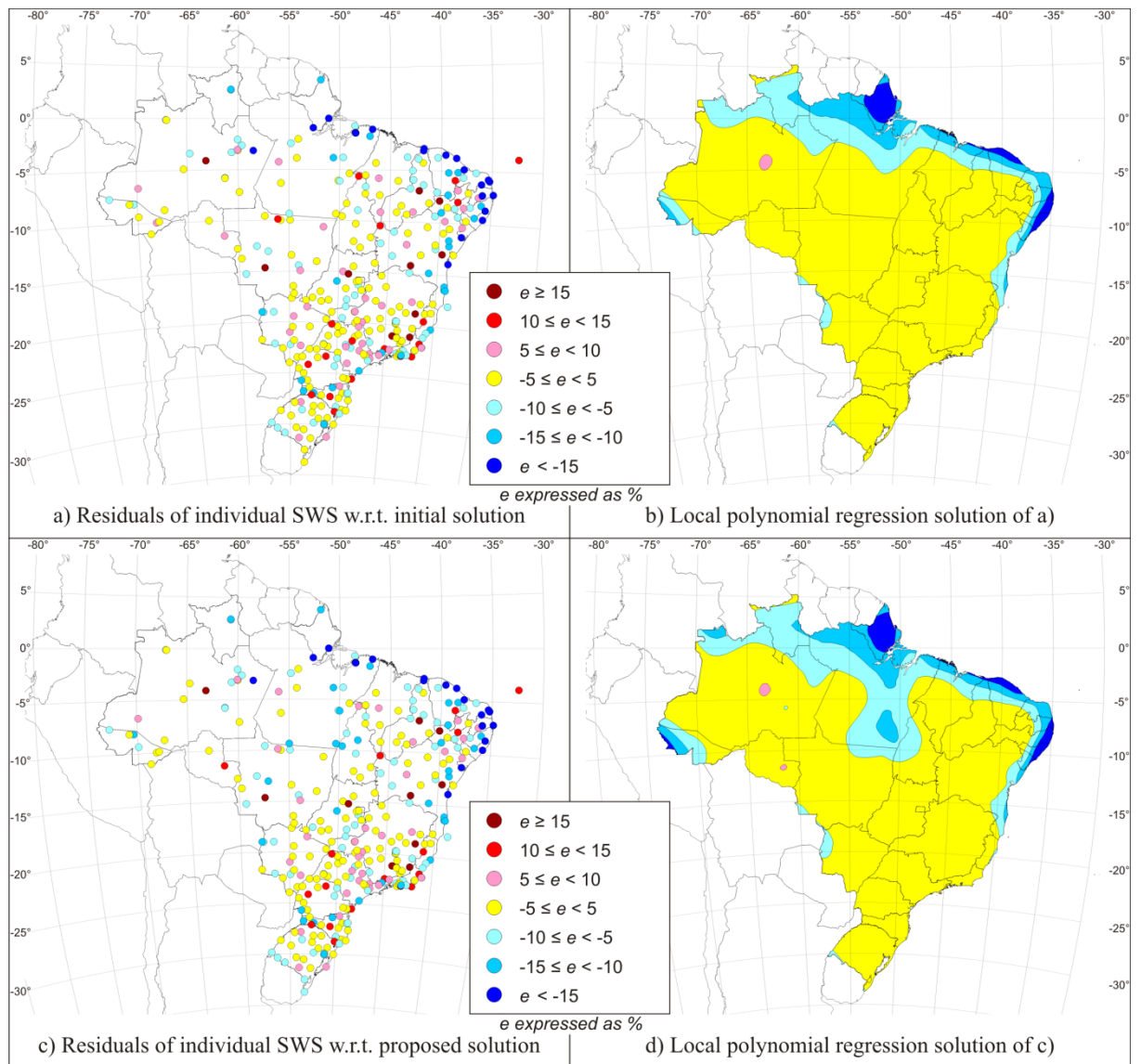


Figure L.4 – Residuals of $G_{50,E}$ for governing SWS.

APPENDIX M

GUIDE TO WINDYTIPS.COM

Observed Data

Time-series of all observed data

1. Predominant wind direction, DIR ($^{\circ}$)
 - For PSEC-46, direction of maximum daily V_{obs} (all anemometers)
2. Observed 10-minute mean wind speed, V_{obs} (kt or m/s)
 - Observations greater than 100 kt or 50 m/s are plotted at 100 kt or 50 m/s
 - For PSEC-46, daily maximum V_{obs} (all anemometers)
3. Observed peak gust speed, G_{obs} (kt or m/s)
 - Observations greater than 100 kt or 50 m/s are plotted at 100 kt or 50 m/s
 - For PSEC-46, daily maximum G_{obs} (all anemometers)
4. Observed temperature, T ($^{\circ}\text{C}$)
 - For PSEC-46, daily maximum and minimum T
 - For WRDS, spurious data manually deactivated in grey
5. Observed atmospheric pressure (hPa)
 - QNH for AERO datasets (adjusted to mean sea level)
 - For PSEC-46, daily maximum and minimum QNH
 - P_{atm} for INMET datasets
 - For WRDS, spurious data manually deactivated in grey
6. Number of observations per year
 - For MSS, data origin is given (RM = Redemet METAR/SPECI; WM = WeatherUnderground METAR/SPECI; NM = NCEI/NCDC METAR/SPEC; WS = WeatherUnderground SYNOP; NS = NCEI/NCDC SYNOP)
 - For MSS, displayed is the number of wind data fields manually extracted
 - For PAS-31, anemometer label typically in reference to runway heading
 - For PSEC-46, number of days per year (%)
 - For NCEI/NCDC, data origin is given ($SPECI$; $METAR$; MIX = Combination of METAR/SPECI and SYNOP; $SYNOP$; BRA = Dataset from Brazil; $AUTO$ = Automatic station)
 - For WRDS, data origin is given (WEB = INMET website; $RESTR.$ = Restricted INMET; $DISME$; $SADMET$)
 - For RESTR. and SADMET, classification of G_{obs} given (\emptyset = no gust observation; OK = gust observation present)

Processed Data

Processed time-series of wind data (active periods in heavier, bold colours; deactivated data greyed or fainter in colour)

1. Most frequent wind sector per month
2. Monthly mean wind speeds, V_m (m/s)
 - ECMWF ERA-Interim data from nearest inland co-ordinate (—)
 - Homogenised 10-minute mean V_{cor} of Surface Weather Station – SWS (—)
 - *Dif. Tot.* = mean net difference over sampling period of SWS to ECMWF
 - *Dif. Abs.* = mean absolute difference over sampling period of SWS to ECMWF
3. Normalised monthly mean wind speeds, V_m/V_{clim}
 - V_{clim} is the mean wind speed for each of the 12 months of the year
 - Separate V_{clim} are calculated for ECMWF and SWS data
4. Temporal distribution of most 100 extreme wind events and trend
 - Columns representing number of events per month (N_{ev})
 - Threshold gust speed for the top 100 events is given and unique for each SWS
 - Annual growth rate of extreme wind events, pa (%), is given (blue for overall decrease; red for increase)
5. Percentage of month with valid wind data observations, $Obs.$ (%)
 - Percentage of monthly even-numbered V_{obs} (—) i.e. 2, 4, 6 kt... (high percentage indicates biased or conventional observing procedures)
6. Classification of homogenised gust time-series, G_{cor} (m/s)
 - No classification (•)
 - Peak event gust, non-synoptic (▲)
 - Peak event gust, synoptic (●)
 - Suspect peak - discarded (X)

Station Trends

Daily and monthly trends

1. Observation frequency per hour of the day. Frequency is relative to the hour of the day with most observations.
2. Seasonal average 10-minute mean wind speeds per hour of the day, $V_{cor,m}$.
3. Time above G_{cor} threshold (defined by top 100 extreme events) per season and 3-hr period of the day (± 1 -hr of hour shown). $t_{ext,rel}$ is relative to the 3-hour period with the most time.
4. Predominant wind sector per month of the year.
5. Average homogenised 10-minute mean wind speed per month of the year, V_{clim} (m/s).
6. Average maximum monthly homogenised gust speed per month of the year, $G_{max,clim}$ (m/s).

Parent Distribution

Probability density and cumulative distribution function

1. Probability density of V_{cor} at 2 m/s intervals (based on time per interval normalised by total sampling time of station, t_{tot}).
2. Cumulative distribution function of V_{cor} with fitted parameters w and c for Weibull distribution.
3. PDF histogram of G_{cor} at 2 m/s intervals (based on time per interval normalised by total sampling time of station, t_{tot}).
4. Cumulative distribution function of G_{cor} with fitted parameters w and c for Weibull distribution.

Extreme Distributions

Extreme value distributions using BR-MIS (Brazilian Method of Independent Storms) as defined in Section 6.6 *Development of BR-MIS extreme value analysis*

1. Non-Synoptic Extreme Distribution

- Set of extreme non-synoptic wind events (▲)
- Fitted linear model to non-synoptic wind events (—)
- Standard deviation (--X--) according to using methodology of ESDU 87034 (1990[a])
- a_N – scale factor of non-synoptic wind model
- U_N – mode of non-synoptic wind model
- R_N^2 – correlation coefficient of fitted non-synoptic model
- N_N – total number of non-synoptic events identified
- r_N – average number of extreme non-synoptic events per year

2. Synoptic Extreme Distribution

- Set of extreme synoptic wind events (●)
- Fitted linear model to synoptic wind events (—)
- Standard deviation (--X--) according to using methodology of ESDU 87034 (1990[a])
- a_S – scale factor of synoptic wind model
- U_S – mode of synoptic wind model
- R_S^2 – correlation coefficient of fitted synoptic model
- N_S – total number of synoptic events identified
- r_S – average number of extreme synoptic events per year

3. Mixed Extreme Distribution (no separation by wind type)

- Set of extreme wind events (◆)
- Fitted linear model to mixed distribution (—)
- Standard deviation (--X--) according to using methodology of ESDU 87034 (1990[a])
- Fitted linear model to non-synoptic wind events (—)
- Fitted linear model to synoptic wind events (—)

- Fitted combined model to envelope of non-synoptic and synoptic models (—)
- a_M – scale factor of mixed model
- U_M – mode of mixed model
- R_M^2 – correlation coefficient of fitted mixed model
- N_M – total number of extreme events
- r_M – average number of extreme events per year
- t_{tot} – total number of years of valid observations

Directionality

Directional polar plots (North = 360°, East = 90°, South = 180°, West = 270°) against G_{cor} (m/s) or percentage of time above threshold for certain probability of non-exceedance, P .

1. Polar plot of G_{cor} (m/s) vs DIR (°) time-series
 - No classification (•)
 - Peak event gust, non-synoptic (▲)
 - Peak event gust, synoptic (●)
2. Overall directional distribution of time (%)
 - Entire time-series, $P = 0$
 - Percentage of time with calm conditions, $G_{cor} = 0$ (m/s).
 - Percentage of time with variable or unknown wind direction, $DIR = \emptyset$.
3. Directional distribution of time (%) with G_{cor} above threshold defined by $P = 0.5$
4. Directional distribution of time (%) with G_{cor} above threshold defined by $P = 0.9$
5. Directional distribution of time (%) with G_{cor} above threshold defined by $P = 0.99$
6. Directional distribution of time (%) with G_{cor} above threshold defined by $P = 0.999$
7. Directional distribution of time (%) with G_{cor} above threshold defined by $P = 0.9999$
8. Directional distribution of time (%) with G_{cor} above threshold defined by top 100 extreme events.

Event Trends

Parametric trends for the set of extreme winds (N_M – mixed distribution), non-synoptic winds (N_N) and synoptic winds (N_S).

1. Parameters used in classification of wind types

- Mean values
 - Gust factor, G_V
 - Peak ratios, R_{-6} , R_{-3} , R_{+3} , R_{+6}
 - Mean temperature before peak gust, $T_{med,3}$ (°C)
 - Largest decrease in temperature over hour of peak gust, $\Delta T_{min,3}$ (°C)
 - Largest increase in atmospheric pressure over hour of peak gust,
 - For AERO SWS $\Delta Q_{max,3}$ (hPa)
 - For INMET ASWS $\Delta P_{max,3}$ (hPa)
- Predominant
 - Wind sector of peak gust (% of set of extremes)
 - Season of the year
 - Time of the day (UTC)
- Percentage of extreme events with thunderstorm (TS) observed

2. Time-series of wind speed (normalised by peak gust speed) ± 10 hours from peak gust

- Each hourly x is an average of all data within ± 30 mins
- Gust speed, G_{cor} , averaged over set of extreme events ($-x-$)
- Standard deviation of G_{cor} for set of extreme events ($---x---$)
- 10-minute mean speed, V_{cor} , averaged over set of extreme events ($-x-$)
- Standard deviation of V_{cor} for set of extreme events ($---x---$)

3. Time-series of wind sector

- Represented as a percentage of all extreme wind events within the particular time-interval
- The larger the ball (\bullet), the higher the percentage of observations in wind sector for the corresponding time-interval

4. Time-series of temperature ± 10 hours from peak gust

- Temperature, T (°C), averaged over set of extreme events ($-x-$)

- Standard deviation of T for set of extreme events (---X---)
5. Time-series of atmospheric pressure ± 10 hours from peak gust
 - Atmospheric pressure, P_{atm} or QNH (hPa), averaged over set of extreme events (—X—)
 - Standard deviation of atmospheric pressure for set of extreme events (---X---)

Classifications

Information on classifications of extreme wind events.

1. Number of classifications per algorithm exit to achieve minimum N_N and N_S values for extreme value analysis. Algorithms paths and exits defined in Appendix D
 - Red bar = non-synoptic classification
 - Blue bar = synoptic classification
 - Black bar = suspect peak
2. Maximum, minimum and average peak gusts per classification exit
3. Manual overwrite classifications (most 30 extreme events are analysed verified manually)

Isolated Events

Time-series of key parameters, summary parameters and classifications of extreme wind events.

1. Event summary details and parameters

- Event ranking, date, time and source of peak observation
- Peak values of the event
 - Peak observed gust, G_{obs} , or equivalent gust G^* if no gust observed (kt or m/s)
 - Peak observed 10-minute mean, V_{obs} (kt or m/s)
 - Peak factor, $G_V = G_{obs}/V_{obs}$, or $G_V = []$ if no gust observed
 - Peak gust corrected to height of $z = 10$ m, CAT II according to height/terrain multiplier F_G (refer to metadata), G_{cor}
 - Peak 10-minute mean corrected to height of $z = 10$ m, CAT II according to height/terrain multiplier F_V (refer to metadata), V_{cor}
- Peak ratios
 - R_{-6} , ratio of peak G_{cor} to the average speed over the previous 6 hours
 - R_{-3} , ratio of peak G_{cor} to the average speed over the previous 3 hours
 - R_{+3} , ratio of peak G_{cor} to the average speed over the next 3 hours
 - R_{+6} , ratio of peak G_{cor} to the average speed over the next 6 hours
 - For WRDS, R_G refers to G_{cor} ratios and R_V refers to V_{cor} ratios
- Change in temperature and pressure
 - Mean temperature before peak gust, $T_{med,3}$ (°C)
 - Largest decrease in temperature over hour of peak gust, $\Delta T_{min,3}$ (°C)
 - Largest increase in atmospheric pressure over hour of peak gust,
 - For AERO SWS $\Delta Q_{max,3}$ (hPa)
 - For INMET ASWS $\Delta P_{max,3}$ (hPa)
 - Severity of change in temperature and pressure, $\Delta Group$
 - $\Delta Group$ 1= severe
 - $\Delta Group$ 2= intermediate
 - $\Delta Group$ 3= weak
- Wind direction
 - Wind direction of peak gust

-
- $\Delta DIR_{max,-3}$ largest change in direction over the previous 3 hours
 - $\Delta DIR_{max,+3}$ largest change in direction over the next 3 hours
 - For MSS and PAS31 datasets, thunderstorm (TS) observed within ± 1 hr of peak gust
 - Event classification
 - NON-SYNOPTIC,
 - SYNOPTIC, or
 - SUSPECT
 - (with algorithm exit number)
 - For MSS, METAR/SPECI or SYNOP meteorological report of peak gust is displayed
2. Time-series of wind data (m/s), time-scale in minutes from time of peak gust
 - G_{obs} (—X—) or G^* (—X—)
 - V_{obs} (—X—)
 - G_{cor} (—X—) or G^*_{cor} (—X—)
 - V_{cor} (—X—)
 3. Time-series of wind direction, DIR , ($^\circ$), time-scale in minutes from time of peak gust
 - $DIR = 0$ and $V_{obs} = 0 \rightarrow$ calm conditions
 - $DIR = 0$ and $V_{obs} \neq 0 \rightarrow$ variable or invalid wind direction
 4. Time-series of temperature ($^\circ\text{C}$)
 - For PAS31 and MSS,
 - T , instantaneous temperature (—X—)
 - For WRDS,
 - T_{max} , maximum temperature of previous hour (—X—)
 - T_{min} , minimum temperature of previous hour (—X—)
 - T_{ins} , instantaneous temperature on hour (—X—)
 5. Time-series of atmospheric pressure (hPa)
 - For PAS31 and MSS,
 - QNH , instantaneous atmospheric pressure (—X—)
 - For WRDS,
 - P_{max} , maximum atmospheric pressure of previous hour (—X—)
 - P_{min} , minimum atmospheric pressure of previous hour (—X—)
 - P_{ins} , instantaneous atmospheric pressure on hour (—X—)
-